Straw and Coal Ash Rheology

Becerra, Signe V.r.v.

Publication date:
2001

Document Version
Early version, also known as pre-print

Straw and Coal Ash Rheology

by

Signe Vargas

Ph.D. Thesis

March 2001

Combustion and Harmful Emission Control
Department of Chemical Engineering
Technical University of Denmark
2800 Lyngby
Denmark

Preface

The present thesis is the result of a Ph. D. study carried out at the Department of Chemical Engineering at the Technical University of Denmark (DTU) in the period August 1996 to March 2001. Professor Kim Dam-Johansen and Research Associate Professor Flemming J. Frandsen have supervised the project.

The project was funded by a DTU-scholarship, the EU Joule project *Prediction of Ash and Deposit Formation for Biomass Co-combustion* - contract No. JOR3-CT98-0198 and The Danish Energy Research Programme project *Effektiv og ren anvendelse af biomasse til produktion af el og varme. Fase III i et langsigtet strategisk forskningsprojekt* - contract No. 1323/99-0001.

The Combustion and Harmful Emissions Control (CHEC) Research Centre is financially supported by the Danish electricity consortia, ELSAM (The Jutland-Funen Electricity Consortium) and ELKRAFT (The Zealand Electricity Consortium), STVF (The Danish Technical Research Council) and the Nordic Energy Research Programmes.

I wish to give my thanks to Mr. John Vahle and the staff at our workshop, in particular Mr. Per Kirkegaard, who have shown outstanding collaboration and patience with the numerous technical problems related to the experimental setup. They made me feel less alone with my problems.

I also wish to thank my supervisors, especially Dr. Flemming J. Frandsen, for their support and trust in me when times were tough.

Finally, I thank my family. My husband and children for being who they are, and for being patient with me. My mother for taking days off to nurse the girls when they were ill. And my sister for helping out with the sometimes very annoying English compositions.

Lyngby, 30 March 2001

Signe Vargas

Summary

Traditionally, Danish power plants operate on coal and on a smaller scale also on natural gas and fuel oil. But in recent years, focus has been moved towards sustainable energy resources such as sun, wind and biomass, mostly straw. Straw has a cellular structure that includes both potassium and chlorine, but the bales also contain soil impurities. In plants where straw is co-combusted with coal, potassium is bound up as aluminum - potassium silicates.

Ash deposits on heat transfer surfaces influences the turn-over of power and heat production, and they are the main reason for unplanned shut-downs of power plants. The viscous behaviour of fly ashes strongly affects the tendency towards deposit formation and strength build-up in deposits, and this is the motive for the present work.

A comprehensive literature review has acted to sum up the state of the art on the rheological properties of high-temperature melts of coal ashes and other silicates. Structural aspects are considered together with measurements and model predictions of the temperature dependence of the viscosity of silicate melts of varying composition. Experimental determinations of the viscosity-temperature relationship for silicate melts with two, three, four, five and six components as well as multi-component silicates composed of the oxides SiO_2, Al_2O_3, Fe_2O_3, FeO, CaO, MgO, Na_2O, K_2O, Li_2O, MnO, TiO_2 and B_2O_3 are cited in 58 tables (listed by publication year and author) and 105 figures (listed by composition).

A rotational viscometer with a maximum temperature of 1700°C was purchased for the experimental determination of the viscosity of ashes from the co-combustion of coal and straw. Several changes have been made to the design, but now the viscometer has been calibrated, and a measurement series has been carried out for pre-treated ashes from a pilot plant co-combusting straw and coal. The viscosity vs temperature relationship has been modelled for the ash-composition concerned.

Resumé

Alle ældre danske kraftværker er enten kul- eller halmfyrede, men inden for de senere år er fokus blevet flyttet til vedvarende energikilder såsom sol, vind og biomasse (mest halm). Halmstrå er opbygget af celler, der indeholder både kalium og klor, men halmballer er også forurenet med jordpartikler. Når halm samfyres med kul, bindes kalium som aluminium-kaliumsilikat.

Askebelægninger på hedeflader påvirker rentabiliteten af strøm- og varmeproduktion, og dannelsen af belægninger er den hyppigste årsag til akutte anlægs-nedlukninger. Tendensen til belægningsdannelse og styrkeopbygning i belægninger påvirkes i betydelig grad af flyveaskepartiklernes viskositet, og dette forhold er motivationen for nærværende projekt.

Et omfattende litteraturstudium har medvirket til at skabe overblik over det arbejde, der er blevet foretaget inden for studiet af kulaskers og andre silikaters rheologiske højtemperatur-egenskaber. Studiet inddrager strukturelle aspekter, målinger og modellering af silikatsmelters viskositet - temperatur forhold. Experimentelle bestemmelser af viskositet - temperatur forholdet for silikater med to, tre, fire, fem og seks komponenter og multi-komponent silikater bestående af oxiderne SiO_2, Al_2O_3, Fe_2O_3, FeO, CaO, MgO, Na_2O, K_2O, Li_2O, MnO, TiO_2 og B_2O_3 citeres i 58 tabeller (listet efter publiceringsår og forfatter) og 105 figurer (listet efter sammensætning).

Et rotationsviskosimeter med en maksimaltemperatur på 1700°C er blevet indkøbt for at muliggøre den eksperimentelle bestemmelse af viskositeten af asker fra kul - halm samfyring. Det har været nødvendigt at lave flere ændringer på det oprindelige design, men viskosimeteret er nu kalibreret, og en måleserie er blevet gennemført på en forbehandlet askeprøve fra en kul - halm samfyret pilot-opstilling, ligesom askeviskositetens temperaturafhængighed er blevet modelleret.

Table of contents

Chapter 1
Introduction

1.1 Background

Traditionally, Danish power plants operate on coal and on a smaller scale also on natural gas and fuel oil. But in recent years, focus has been moved towards sustainable energy resources such as sun, wind and biomass. Currently, the Danish energy consortia combust 1.2 M tonnes of straw (mainly the cereal straw types: wheat, rye, oat and barley), and 0.2 M tonnes of wood chips on a yearly basis. However, the conversion from fossil fuels towards biomass is not easy, and with the new initiatives, know-how on the combustion of straw and wood chips has to be built up.

Figure 1.1 Avedøre combined heat and power plant (CHP) near Copenhagen, Denmark.

The main concern is straw because it is a more troublesome fuel than wood chips, and because the total mass for combustion is six times higher than that of wood chips. In the following, only the combustion of straw will be discussed. The most common straw type in Denmark is wheat straw.

Straw can be combusted either alone or together with another fuel. In the nineties, Danish studies were made to test pure straw combustion and co-combustion with coal. Technologies

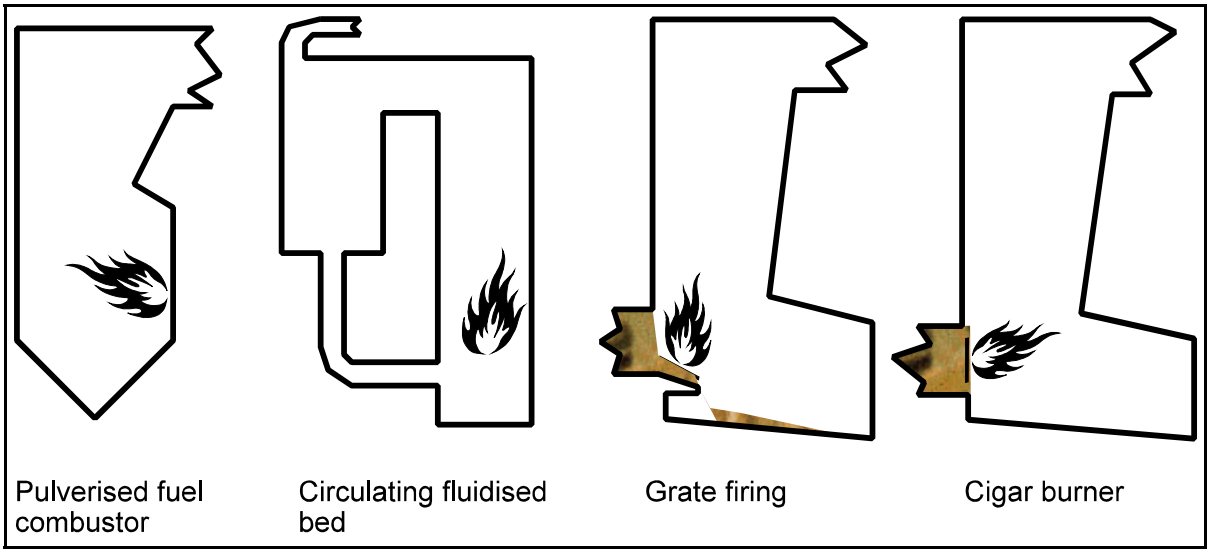

Figure 1.2 Some combustor types that have been tested for straw combustion in Denmark.

such as pulverised fuel combustion, fluidised bed combustion, grate firing, and cigar burning were taken into consideration. For combined heat and power plants (CHP), grate fired boilers with effects of up to 30 MW_e seem to have taken the lead, but co-combustion with coal in pulverised fuel combustors will probably gain more interest in the years to come.

When straw is used for energy production, the ash content is typically in the range 2 - 7 weight-% on a dry fuel basis,[1]. For bituminous coals, the ash content can go as high as 15-20%,[2] and for coals of lower rank, the ash content may be even higher. The composition of straw ash differs from that of coal ash, mainly in the low content of aluminum and iron and the high content of potassium, see Table 1.1. The data listed for cereal straws is based on an average composition, but as for bituminous coals, there is a wide variation in composition.

Table 1.1 Ash composition for bituminous coals and cereal straws.

	Bituminous coal ash[3]	**Cereal straw ash[1]**
Component	**Weight-%**	**Weight-%**
Ash content in fuel	5 - 20	2 - 7
SiO_2	40 - 60	38
Al_2O_3	20 - 35	0.2
Fe_2O_3	2 - 15	0.3
CaO	0 - 10	12
MgO	0 - 4	3
K_2O	0 - 4	30
Na_2O	0 - 1	1
Cl	< 0.5	9

Coal is a fossil fuel, it consists mainly of carbon, hydrogen, nitrogen and sulphur, but it also contains minerals that are either located as discrete inclusions or bound to the carbon-matrix. Straw on the other hand has a cellular structure that includes both potassium and chlorine, but the plants also contain soil impurities.[4]

Upon the combustion of coal, the mineral fraction is hardly affected by volatilisation. Instead silicate ash particles are formed as the other components are volatilised.

When wheat straw is combusted, most potassium and almost all chlorine are released to the gas phase, and some potassium is bound to the silicate phase.[5] Re-condensation upon cooling in the convective section causes the resulting fly ash to become a composite of silicates and salts. The salts readily deposit on the surfaces of the plants, either by condensation onto the cooler surfaces or by sticking. The salt-bound deposits lower the heat transfer through the

walls, and enhance chlorine-induced corrosion.[6]

Figure 1.3 KCl-containing deposit from the straw-fired Masnedø CHP, Denmark.[6]

In co-fired plants, potassium is bound up as potassium - aluminum silicates and K_2SO_4; chlorine leaves the system primarily as HCl.[7] The need to predict the fate of these silicates has been the basis of this project. Chapter 2 and Appendix B describe how viscosity is a key-factor in the prediction of silicate behaviour in a combustion system. But the viscosity of silicate melts at temperatures well above 1000°C are difficult to determine, and as a result, the general predictability of viscosity as a function of temperature and composition is not very good.

Appendix A is a literature review on the scientific knowledge that has been accumulated over many years of studying the rheological properties of high-temperature melts of coal ashes and other silicates. A short summary of the content of the article is given in Chapter 3, and a definition of viscosity has been extracted for presentation at the end of this chapter.

Rheological studies have been focussed mainly on limited compositional ranges of interest to the combustion of specific coal types. Hence certain compositional intervals have been studied thoroughly. Mathematical models have been developed, that enable the prediction of viscosity as a function of composition and temperature for these limited composition intervals. However, the ash compositions of interest to straw-containing combustion include ashes with a major content of potassium (> 5%), and no studies have been made on this subject in the past. Therefore, a high-temperature viscometer was purchased for the purpose of studying the rheological properties of ashes from the co-combustion of straw and coal.

Chapter 4 contains a short summary of the process that lead to the purchase of an ME 1700 - RV 20 apparatus from the German company Haake, and Chapter 5 contains a detailed description of the setup.

The run-in of the setup has been difficult and time-consuming, and it is only just now, that the viscometer is ready for use. Changes made to the setup are described in Chapter 5, and some of the valuable experiences are outlined in Chapter 6.

Chapter 7 presents the experimental viscosity determinations for an ash sample from the co-combustion of coal and straw, and the results are compared the viscosity predictions of several mathematical models. Chapter 8 concludes the thesis with a summary and ideas for

further work.

1.2 Definition of viscosity

Viscosity is a non-equilibrium property,[8] a measure of the resistance of a fluid towards motion. It can be related to the tendency of a fluid to dissipate energy (produce entropy)[9] due to internal fluid friction,[8] or it can be considered to be a momentum conductivity analogous to thermal conductivity in conductive heat transfer, and to the diffusion coefficient in diffusive mass transfer.[10] Unlike the electrical conductance of silicate melts, where the charge is transferred above all by cations, the transport of momentum in viscous flow is provided mostly by anions.[11]

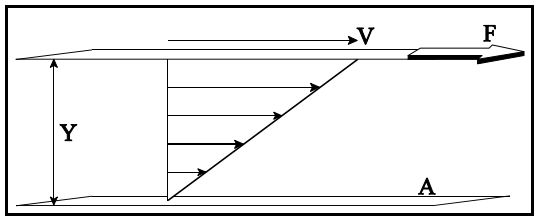

Figure 1.4 Schematic depiction of viscosity. V = velocity of the upper plane, F = force driving the upper plane, Y = distance between the lower and upper planes, A = Surface area of each plane.[26]

Isaac Newton first defined *dynamic* or *absolute viscosity* [N·s/m^2] as the ratio of shear stress, τ [kg/s^2·m], to shear rate, $\dot{\gamma}$ [s^{-1}].[12,13]

$$\eta \equiv \frac{\tau}{\dot{\gamma}} \tag{1.1}$$

The concept of viscosity can be visualised as in Fig 1.4. A fluid is entrained between two parallel planes of area A; the lower plane is fixed while the upper plane is moved at a constant velocity, v. After reaching steady state, the velocity distribution of the fluid will be linear (assuming laminar flow), and the viscosity may be expressed as the force, F [N], per unit area of plate, A [m^2], divided by the velocity gradient (ie the ratio of the velocity of the upper plate, v [m/s], and the distance, Y [m], between the planes):[14]

$$\frac{F}{A} = \eta \cdot \frac{v}{Y} \tag{1.2}$$

The dimension of viscosity is thus mass per time and length. The SI-unit, Pa·s, will be used in this thesis, and the following conversion factors may be applied:[8,15]

$$1Pa \cdot s = 1\frac{N \cdot s}{m^2} = 1\frac{kg}{m \cdot s} = 10P(oise) = 0.672\frac{lb_m}{ft \cdot s} = 0.020886\frac{lb_f \cdot s}{ft^2} \tag{1.3}$$

1.2.1 Newtonian fluid

Newtonian fluids obey Newton's law of viscosity, ie shear force per unit area is proportional to the local velocity gradient:[14]

$$\tau = \mu \cdot \dot{\gamma} \quad (1.4)$$

The expression in Eq (1.4) is analogous to that of Eq (1.2) except that here, the general term for viscosity, η, has been substituted by the viscosity coefficient, μ,[15] a term used extensively for Newtonian fluids. Gasses and most simple liquids are Newtonian [14] and when the viscosity of a liquid is quoted as a single number in a handbook, the liquid is assumed Newtonian, and the number is the viscosity coefficient.[15]

Other flow types for more complex fluid systems (where the viscosity varies as a function of shear rate and sometimes also time) are described in the review article, but these fluids are often just referred to as non-Newtonian fluids.

Chapter 2
Applications for viscosity data

2.1 Introduction

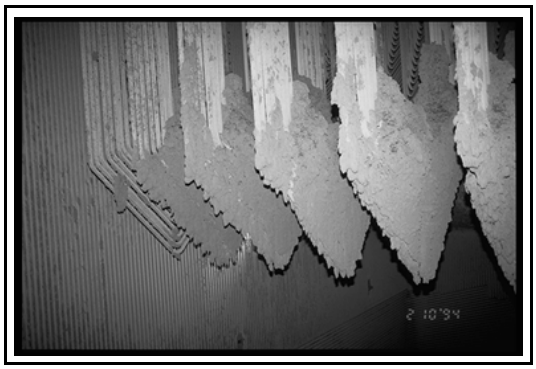

Figure 2.1 Heavy deposits on the superheaters at the pulverised fuel combustor Amagerværket CHP (near Copenhagen, Denmark) after coal combustion.

The formation of deposits on the heat-transfer surfaces of power plants seriously affects the performance of the plants, because the deposits insulate the hot flue gas from the water/steam cycle on the other side of the wall. Mathematical modelling is used to improve the understanding of the underlying processes that lead to deposit formation, and it is thus a tool for the optimization of operating parameters.

Boiler manufacturers use mathematical models to simulate the performance of planned plants as a function of input fuel composition, plant dimensions and operating parameters. Once built, operators use mathematical models to predict the effect of a change in fuel composition on the operation of the plant, or the effect of a shift in load on operating conditions and output performance.

It is of crucial importance for the construction and operation of gasifiers to know whether the ash will be slagging or solid. But unlike standard boilers, the atmospheric conditions in a gasifier are reducing, and this affects the ash viscosity because the oxidation level and structural coordination of some species in the ash are affected by the atmosphere.

The importance of the predictability of the viscosity of fly ash particles in combustion systems is the subject of this chapter. It is strongly related to the pronounced role played by viscosity in mathematical models such as those described above.

2.2 Deposit build-up

As described in Chapter 1, ash particles are formed when a solid fuel is fed to a combustion system. Depending on the combustion technology and the characteristics of the fuel, a smaller or larger fraction of the ash leaves the system as bottom ash and the rest forms small air-born particles of varying composition and size (1 - 20 μm), the so-called fly ash particles.[16] When

straw is combusted without previous pulverisation, pieces of char of up to several centimetres in length may also be carried with the flue gas, but this subject is out of the scope of this text.

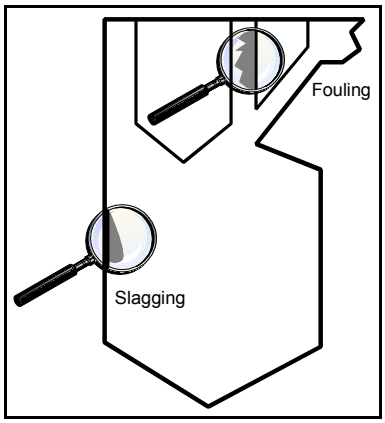

Figure 2.2 Deposit types.

Depending on the operating conditions, the fly-ash particles may form deposits on heat-transfer surfaces. This is highly undesirable, since the deposits insulate the hot flue gas from the water/steam cycle, thereby reducing the effectiveness of the energy-conversion process. In the boiler section, temperatures may be so high that a glassy deposit is formed, this is called slagging. In the convective section, temperatures and radiation are lower, and the deposits will maintain the visual aspect of individual particles, this is called fouling.

The mechanisms that lead to deposit formation are subject to continued studies. But in a system, were no salts are available in the gas phase for condensation, only fly ash particles that are carried through the system with the flue gas are available for deposit formation. Whether or not a given fly ash particle will deposit on the surface is a function of the system fluid dynamics, the particle composition, density, size and temperature and the surface material, temperature and shape.

An important point to consider when evaluating the tendency towards deposit formation is whether particles will get into physical contact with the surface. The flow is deviated when the flue gas approaches a surface. Fig 2.3 shows how smaller particles are carried with the gas away from the surface. The inertia of the larger particles causes them to continue on their forward path and thus impact onto the surface. Surfaces that cause a strong deviation of the flue gas, and surfaces that experience a heavy gas flow are more prone to deposit build up than more protected surfaces.

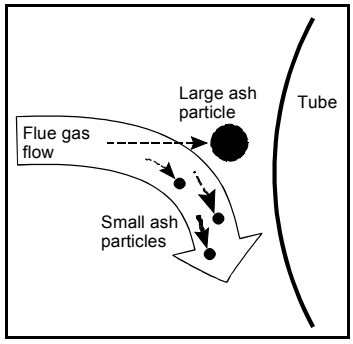

Figure 2.3 Inertial impaction.

The sticking tendency of an impacting particle depends on the size, shape, velocity, density and stickiness of the particle and on the characteristics of the surface. A clean tube collects only sticky particles, and a particle with a high momentum will have a tendency to bounce off.

If a particle deposits on the surface, it will solidify as long as the deposit is thin, because the metal temperature is lower than that of the flue gas. But as the deposit thickness and surface temperature

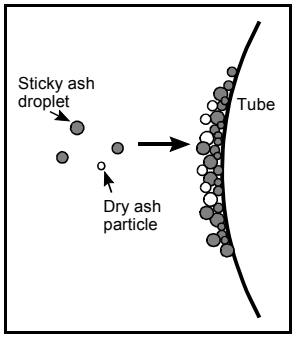

Figure 2.4 Deposit build-up on a tube wall.

increase, some particles remain sticky on the surface after cooling to the instantaneous surface temperature, thereby causing an increase in the capture efficiency, see Fig 2.4.[17]

The probability of retention in a dry deposit of an impacting particle depends on its stickiness. For deposition to occur, the kinetic energy of the fly-ash particle has to be consumed by the energy of viscous deformation.[18] Two scenarios exist. For silicate-particles, the stickiness depends on the viscosity of the silicate, but for particles with both a silicate phase and a salt phase, the stickiness is related to the melt percentage of the particle. Different approaches to the determination of the stickiness tendency of impacting silicate particles have been proposed, two of which will be outlined below.

In 1990, Walsh et al formulated a simple mathematical expression to account for observed influences of ash composition and temperature on deposition rate. The sticking probability of particles, p_{stick}, was determined by viewing the incoming and deposited particles as liquid and supercooled liquid droplets. The authors assumed that for droplets of similar surface energies per unit area and small equilibrium contact angles, viscosity determines the extent to which the droplets are deformed and the area over which contact is established in a collision between an incoming droplet and a droplet already bonded to the surface of a deposit. The larger the contact area developed between them before the incoming droplet comes to rest, the more likely it will remain attached to the deposit. Based on this argument, Walsh et al assumed the sticking probability to be inversely proportional to viscosity for viscosities higher than a reference viscosity, η_{ref}, defined as the viscosity at which droplets become perfectly sticky.[17,19]

$$\begin{aligned} p_{stick}(T,comp) &= \frac{\eta_{ref}}{\eta} \quad , \quad \eta > \eta_{ref} \\ &= 1 \quad , \quad \eta \le \eta_{ref} \end{aligned} \tag{2.1}$$

In 1992, Beér et al proposed an even simpler expression by assuming that all particles with viscosities lower than the critical viscosity value, η_{ref}, will stick to the tube surface on impaction; those of higher value will bounce off.[18]

$$\begin{aligned} p_{stick}(T,comp) &= 0 \quad , \quad \eta > \eta_{ref} \\ &= 1 \quad , \quad \eta \le \eta_{ref} \end{aligned} \tag{2.2}$$

A graphical comparison of the two models is given in Fig 2.5. The models predict that deposits will not form, if all particles have viscosities higher than η_{ref}. But if a sticky surface has been formed, even dry particles can contribute to the growth of the deposit, but because

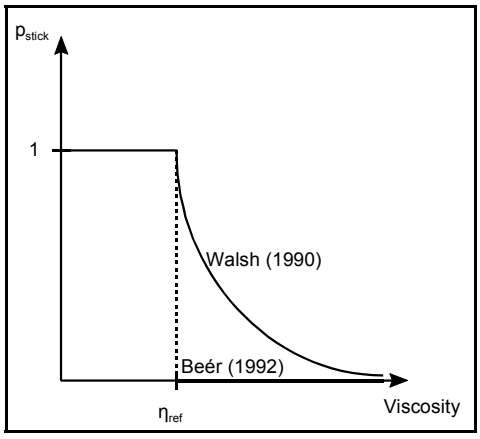

Figure 2.5 Graphical comparison of the predictions of the p_{stick} models presented in the text.[17, 18]

they are dry, they will not give rise to a new sticky spot. As the deposit grows, the surface temperature increases, and more and more deposited particles maintain their stickiness, thus the surface is roughened by the deposit, thereby causing an increased entrapment of the impacting particles. On the other hand, a large deposit will also be more prone to shedding in large cakes due to its own weight and structure, and this last point will be the subject of the next section: Deposit strength.

Walsh et al (1990) estimated the net mass fraction, f_{dep}, of impacting particles depositing as a sum of three separate contributions:

1. Incoming sticky particles that collide with sticky or non-sticku particles on the surface to form deposits.
2. Incoming particles (sticky or non-sticky) that collide with sticky particles on the surface to form deposits.
3. Non-sticky particles that collide with non-sticky particles on the surface and remove some of these particles from the deposit by erosion.

The resulting expression is:

$$f_{dep} = p(T_g) + \left(1 - p(T_g)\right) \cdot p_s(T_s) - k_e \left(1 - p(T_g)\right)\left(1 - p_s(T_s)\right) \tag{2.3}$$

where p(T) is the sticking probability for incoming particles at temperature T, T_g and T_s are the gas and surface temperatures, respectively, k_e is the erosivity of try ash towards its own deposits, and p_s is the sticking probability for the particles exposed on the surface. The authors suggested that this particle-by-particle accumulation of deposit should be combined with an expression to account for the shedding of larger pieces of deposit.[17]

Three years later, Richards et al proposed the use of Eq (2.3) in a slightly altered formulation that includes N particles of different compositions.

$$f_{dep} = \sum_{i=1}^{N} \left(p_i(T_{ps}) + \left[1 - p_i(T_{ps})\right] \cdot p_s(T_s) \right) \tag{2.4}$$

where $p_i(T_{ps})$ is the sticking probability of particles of composition i, T_{ps} is the particle temperature on impaction, $p_s(T_s)$ is the sticking probability of the deposit surface, and T_s is the temperature of the deposit surface.[20]

As mentioned above, the fly ash particles in a combustion system vary both in size and composition. If a fuel gives rise to many fly ash particles with a viscosity lower than η_{ref}, deposits will build up faster than if the particles are generally dry.

Different approaches have been used to estimate the value of η_{ref}. Senior and Srinivasachar

(1995) used laboratory experiments by Wibberley and Wall (1982) on sodium-silica glass particles to calculate that the particles in the experiments produced deposits when the estimated particle viscosities were between 10^5 and 10^7 Pa·s.[21,22] But they also mentioned that more recent laboratory experiments by other scientists, using soda-lime-silica glass spheres showed that the criteria for sticking were dependent on particle kinetic energy and viscosity. They concluded that the critical viscosity for conditions of interest in utility boilers fired with bituminous coals is between 10^5 and 10^8 Pa·s. Differences in sticking coefficients observed in laboratory coal experiments can therefore be attributed to composition-based differences in ash particle viscosities.[21]

Boow (1969) determined viscosities by measuring the rate of penetration into melts of a $Pt_{80}Rh_{20}$ penetrator. He found that slags with viscosities exceeding 10^4 to 10^7 Pa·s will not readily cohere.[23]

2.2 Deposit strength

As already mentioned, deposits tend to shed when they reach a certain size. The continuous flue gas flow past the deposit exercises a pressure that erodes the deposit, and soot blowing is installed in different parts of the system to keep surfaces clean by a combination of direct mechanical action and a more indirect thermal action caused by the local cooling (and hence shrinkage) of the area that is soot blown. The internal strength of a deposit determines if it has the capacity to grow big. If no strength builds up, the deposit is easily swept off the surface.

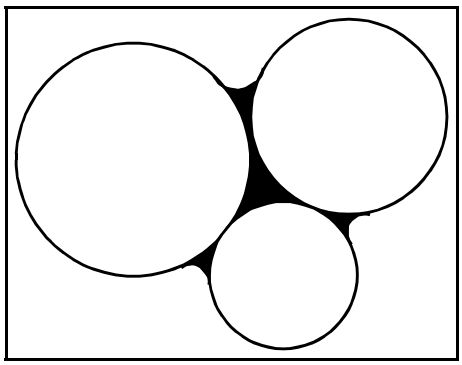

Figure 2.6 Sintering by viscous necking.

According to Sarofim and Helble (1993), deposit strength is often more important to boiler operation than the rate of deposition. They identified two mechanisms that affect deposit strength. The first was sintering of particles by solid state diffusion and viscous necking (flow sintering) of adjacent particles (Fig 2.6) at a rate determined by viscosity and inversely proportional to particle radius. The second was bonding of particles by chemical deposition or reaction.[16]

2.2.1 Sintering

When powders of metals, ionic crystals or glasses are heated to temperatures near their melting points, the powder particles weld together and the density of the compact changes: this process is known as sintering. Sintering is a process that reduces the surface area of the powder particles, and the driving force arises from the excess free energy of the surface of the powder over that of the solid material, ie the surface tension.[24]

Mackenzie and Shuttleworth (1949) developed a model for the shrinkage of closed pores. They considered pores of radius r_1 surrounded by a spherical shell of the real incompressible material, out to a radius, r_2. From r_2 outwards, the material has the density of the porous material as a whole. A graphical representation of the parameters is given in Fig 2.7. For the sintering of a material with a Newtonian (ie shear independent) viscosity, they found the rate of pore shrinkage to be equal to:

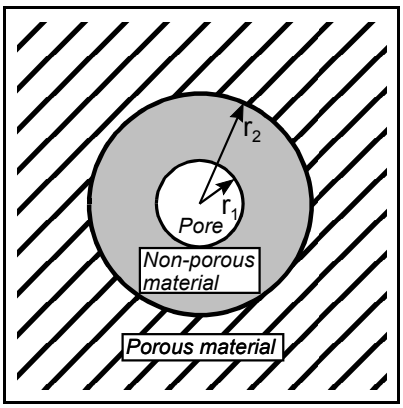

Figure 2.7 Graphical representation of the theoretical basis of the Mackenzie - Shuttleworth model.

$$\frac{dr_1}{dt} = -\frac{\gamma}{2\eta}\frac{1}{\rho_{rel}} \qquad (2.5)$$

where t = time, γ = surface tension and ρ_{rel} = density of the porous material relative to that of the non-porous material.[24]

Senior (1997) expanded the Mackenzie - Shuttleworth model for the purpose of modelling the sintering of coal ash deposits from approx 50% to 0% porosity. The equation presented by her was:

$$\frac{\varepsilon(t)}{\varepsilon_0} = e^{-3t\gamma/2r_0\eta} \qquad (2.6)$$

where ε_0 and $\varepsilon(t)$ = deposit porosity initially and at time t and r_0 = initial pore radius.[25]

A non-sintered, porous deposit does not possess much strength, and it is easily swept off the surface. Sintering causes the deposit to consolidate and build up internal strength that makes it more solid and more difficult to remove mechanically. Eq (2.6) shows that the rate of sintering is strongly influenced by the viscosity: dry particles will not sinter together whereas sticky particles will.

2.3 Deposit shedding

In addition to the above-described shedding mechanisms that affect deposits of individual particles that stick together, glassy slags may form in the boiler-section. Here temperatures are sometimes sufficiently high to cause slags of some compositions to run down the sides of the boiler. Wet-bottom plants are designed for this to happen, but in all other cases it is an undesired phenomenon for two reasons. The first is that a relatively large wall area can be covered with such wet deposits, thus affecting the heat transfer to the vaporising water on the other side of the wall, and the other is that molten oxides may be chemically very aggressive, and they can act to corrode the wall metal although the action occurs through a thin layer of

solid deposit.

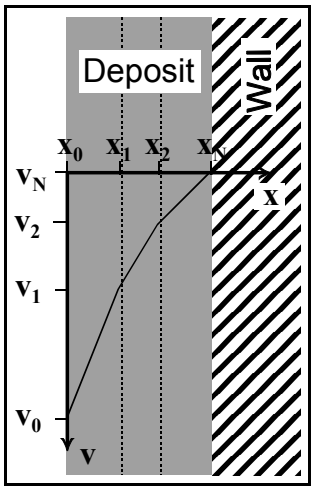

Figure 2.8 Schematic representation of Eq (2.7).

Appendix B contains an outline of the mathematical description of the flow down a plane vertical surface of a thick film of uniaxially varying composition and temperature. The resulting model divides a film of constant thickness, D, into N layers of constant composition and temperature, ie constant viscosity, η, and density, ρ. As is the case for most condensed phases, the densities of silicate melts of constant composition are close-to temperature invariant, in which case the model simplifies to:

$$v - v_n = \frac{\rho \cdot g}{2 \cdot \eta_n}(x_n^2 - x^2) \qquad (2.7)$$

Where: $n \in [1; N]$, $x \in [x_{n-1}; x_n]$, $x_N = D$, $v_N = 0$

where n = current layer number, x = distance from deposit surface, v = linear velocity and g = gravitational acceleration.

If combustion conditions give rise to low-viscosity slag deposits, these may run down the walls of the boiler. The temperature gradient through such a deposit will cause the slag layers close to the wall surface to be solid, and it will be the outer layer of the deposit that causes the running.

2.4 Summary

Ash viscosity affects many processes concerning deposit formation and shedding, but the effect can be more or less pronounced.

- Particle sticking probability: $p_{stick} \propto 1/\eta$
- Deposit sintering: $\ln \varepsilon \propto -1/\eta$
- Liquid flow: $v \propto \eta$

so for the particle sticking probability and the liquid flow, a measurement error of an order of magnitude, $\eta_{meas} = \eta / 10$, will mean an estimation error in the same range of magnitude, whereas for deposit sintering, the same error will cause the sintering rate to be over-estimated by a factor 10. This calculation clearly shows the importance of precise viscosity measurements and models.

Chapter 3
Literature review

A literature review has been published in Progress in Energy and Combustion Science, Vol 27(3) 2001, pp 237-429, under the title *Rheological Properties of High-Temperature Melts of Coal Ashes and other Silicates*. The authors are Signe Vargas, Flemming J. Frandsen and Kim Dam-Johansen.

The article in its full version is supplied as Appendix A, but a short summary of the contents is given in this chapter. A short definition of viscosity has already been given in Chapter 1.

3.1 Viscometer types

Five different experimental approaches to the measurement of high temperature viscosity are presented in the article.

3.1.1 Capillary viscometer

A liquid drains or is forced through a fine-pore tube, and the viscosity is determined from the measured flow, applied pressure, and tube dimensions, see Fig 3.1. Absolute viscosities are difficult to measure with capillary viscometer, but the instrument can also be calibrated, facilitating greatly its use.[26] Above 1200°C complications arise in the selection of a suitable crucible and capillary material in terms of dimensional stability and corrosion resistance (NB: $\eta \propto r^4$).[27]

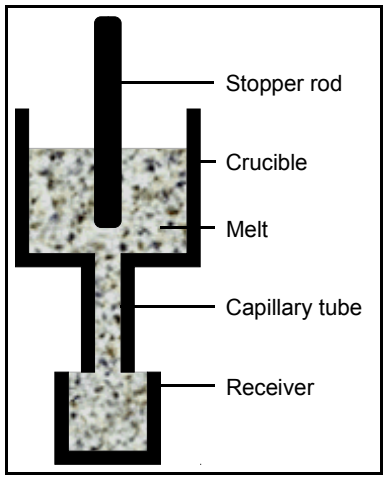

Figure 3.1 Schematic drawing of a capillary viscometer.[26]

3.1.2 Falling body viscometer

Measurement range: $\log_{10} \eta \in [-2 , 6]$.

Fig 3.2 is a schematic drawing of a falling sphere viscometer. The body can also be cylindrical, and the tube in which the body falls can be inclined instead of vertical.[9] The body can either fall due to gravity or it can be dragged upwards through the melt.[27]

English (1924) criticised the method of using a small sphere suspended by a very fine thread over a light, well-balanced, free-running pulley, where the sphere is partly counterbalanced so as to

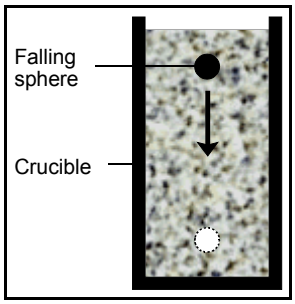

Figure 3.2 Schematic drawing of a falling sphere viscometer.[26]

control the rate of fall. He found it to be difficult to produce consistent results owing to the fact that, no matter how fine the thread or wire supporting the sphere, there was always a drag caused by the passage of the thread through the liquid under test.[28]

3.1.3 Rotational viscometer

Measurement range: $\log_{10} \eta \in [2 , 13]$.

Rotational viscometers are primary instruments [9] and with corrections for gaps and end effects, very accurate measurements are possible.[29] Usually, the instrument is calibrated with liquids of known viscosity, but absolute determination is possible.[26,30]

Fig 3.3 shows a schematic drawing of a rotating cylinder viscometer where the inner cylinder is rotated and the outer cup is fixed. Three variations of the principle are possible:[30]

i. Inner cylinder rotates and outer cup is fixed
ii. Inner cylinder is fixed and outer cup rotates
iii. Both inner cylinder and outer cup rotate

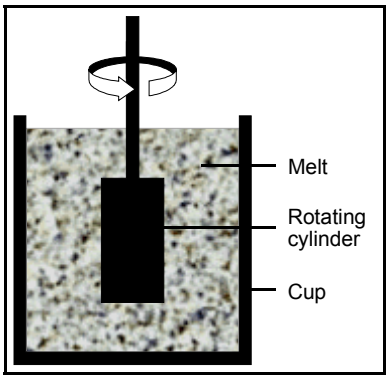

Figure 3.3 Schematic drawing of a rotating cylinder viscometer.[26]

An evaluation of the three principles against each other has not been found in the literature. However, the centering of the inner cylinder is of great importance in all three cases,[30] and this may be the reason why the first principle is most commonly used in practice.

3.1.4 Rod elongation viscometer

Measurement range: $\log_{10} \eta \in [7 , 13.5]$.

The rod elongation viscometer measures the elongation velocity of a filament of known length and radius loaded by a known mass.[30]

3.1.5 Squeeze film viscometer

Measurement range: $\log_{10} \eta \in [-5, (7)]$.

In the squeeze film rheometer, the sample to be tested is retained between two horizontal plates and is compressed axially by driving the plates together as depicted in Fig 3.4.[31] This method is also known as the parallel plates method.[32]

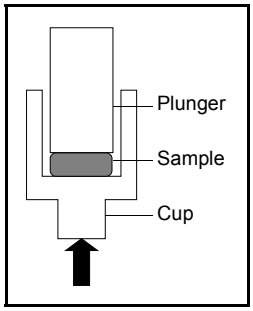

Figure 3.4 Schematic drawing of a squeeze film viscometer.[31]

3.2 Experimental results

Experimental data has been produced for almost a century, but the elder measurements can be considered no more than indicative due to insufficient apparatus calibration and the inappropriate choice of sensor material.

3.2.1 General comments

The presence of an inordinately high amount of any single component, such as SiO_2, CaO and Fe_2O_3, in the ash should serve as a warning to look for abnormal slag behaviour.[33]

Most materials decrease in viscosity as temperature increases. The dependence is logarithmic and can be substantial, up to 10% change per degree K.[26]

3.2.2 Error sources

3.2.2.1 Temperature

General for all high-temperature viscometers is that more errors are made and more disagreements over viscosity results arise due to incorrect or drifting temperature that for any other reason.[26]

3.2.2.2 Composition

While the composition of the ash may be an inadequate predictor of viscosity, the composition of the resulting slag may be an important parameter.[34]

3.2.2.3 Atmosphere

The choice of atmosphere seriously affects the viscous behaviour of some silicate melts. For example, the oxidation state of iron changes depending on atmosphere and this affects viscosity.

The value of viscosity measurements on silicate melts is restricted if they are not performed under a controlled atmosphere.[35] In practical combustion systems, the atmosphere can be highly reducing (eg gasifiers), mildly reducing (eg low-NO_x combustion systems) or highly oxidising (eg post-combustion zone of conventional coal-fired boilers) The flow properties of slags must be predicted under all these atmospheres to accurately understand the impact of ash on combustion systems.

3.2.2.4 Phase separation

Non-uniformity of the melt due to the formation of crystals which are not detected may result in misleading results.[36]

The possibility of the simultaneous existence of more than one liquid phase may not be

completely ruled out.[36]

3.2.2.5 Sensor material

The choice of sensor material is of great importance to the quality of the measurements.[37]

If the detecting parts of apparatus are made of graphite, the properties of slags may be changed by suspension of flaky carbon in the slag or by the chemical reaction between slag and carbon. This contamination is avoided using platinum.[38]

According to J. P. Hurley, the contamination of coal ash slags by alumina crucibles usually mounts to a few weight-percent.[39]

The sample contamination caused by the use of Mo sensors has been registered to 10 - 20 ppmw Mo in some samples.[37]

3.2.2.6 Errors related to specific measurement techniques

Experiences with two rotational viscometers and a squeeze film viscometer are cited.

3.2.3 Cited experimental results

A list of compositional systems sums up all the measurements that are reported in the review article. The list contains important information about the experimental techniques employed and measurement accuracies. The experimental viscosity results are tabulated in 58 tables in chronological order of publication (log η [Pa·s] vs temperature, T [K]) and graphically represented as a function of compositional regime in 105 figures (η [Pa·s] vs temperature, T [K]).

The compositional system comprises the species: SiO_2, Al_2O_3, FeO_x, CaO, MgO, Na_2O, K_2O, Li_2O, MnO, TiO_2, B_2O_3, NaCl and KCl.

3.3 Structure of silicate melts and glasses

3.3.1 Random network theory

Zachariasen's experiments in 1932 on X-ray diffraction from silicate glass at room temperatures formed the basis for the modern view of the silicate melts as organised in a three-dimensional random network in which each silicon is tetrahedrally surrounded by four oxygens and each oxygen is bonded to two silicons.[40,41]

In this view, molten SiO_2 is organised tetrahedrally in six-membered rings as illustrated in Fig 3.5. These rings are a product of the tetrahedral network structure, and they form the borders

of five-sided dices. In the midst of these dices there is ample room for interstitial atoms such as alkali ions. These atoms can also enter the network, breaking bonds and loosening the structure.

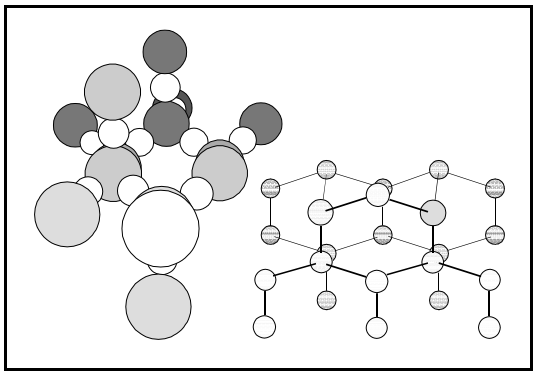

Figure 3.5 Spacial arrangement of SiO_2-network according to the network theory. (Left image: Si = big circles, O = small circles. Right image: Only Si-atoms depicted.)

Silicate melts can be described by dividing the components into basic and acidic oxides. Parallel to the Brønsted definition for aqueous solutions of an acid as a substance capable of donating a proton, a base in an oxide melt can be defined as a substance capable of donating an anion (oxygen); thus basic oxides act as oxygen donators (network modifiers) and acid oxides as receptors (network formers).

Based on acidity, the components in a silicate melt may be arranged in three groups as either network formers, network modifiers or amphoterics. Network formers are cations that always occupy a tetrahedral position and as such act as building blocks in the network. Network modifiers, on the other hand, are cations that have a disruptive effect on the network. Amphoterics can act as either network formers or modifiers according to their coordination number in the melt. When combined with modifier ions which balance their charge, they form stable metal-oxygen anion groups that can fit into the silicate. However, if insufficient modifier ions are present in the melt, amphoteric cations will act as modifier ions themselves.[21,38,42-45]

- Network formers: Si^{4+}, Ge^{4+}, Ti^{4+}
- Network modifiers: Na^{+}, K^{+}, Mg^{2+}, Ca^{2+}, Fe^{2+}, Cr^{3+}, Ti^{4+}, V^{5+}, Ba^{2+}, Sr^{2+}
- Amphoterics: Al^{3+}, Fe^{3+}, B^{3+}, Zn^{2+}

Fig 3.6 gives a representation of some of the effects of the different network components. The top-image shows a SiO_2 network where silicon atoms are organised in a tetrahedral structure through oxygen bonds (long-range order is absent)[5]. If an alkaline earth oxide, MO (eg CaO), is introduced, a loosening of the network structure will be the result, as shown in the bottom left corner. In case an alkali oxide, M_2O (eg Na_2O), is introduced, the result will be a bond rupture as shown in the bottom right corner.

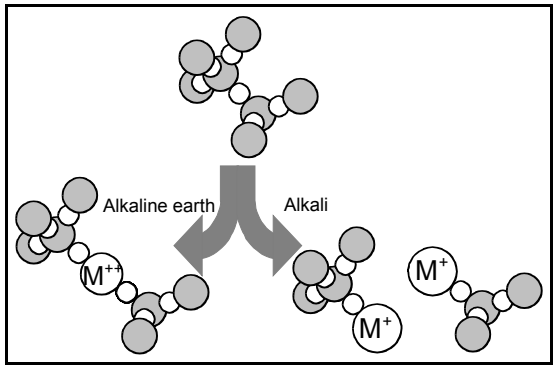

Figure 3.6 According to the network theory, an alkaline earth metal can weaken the silica network by lengthening a bond between two silicon atoms, whereas an alkali metal will break the bond.

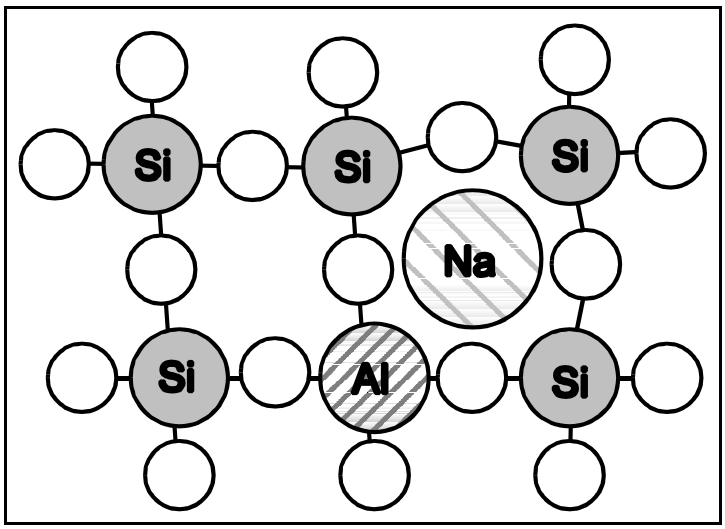

Figure 3.7 Aluminum demands charge stabilisation to enter the silica network in tetrahedral coordination. (Si = dark circles, O = white circles, Al = darkly hatched circle, Na = lightly hatched circle).[52]

Aluminum is categorised as an amphoteric in the network theory; it can act as either a network former or a network modifier. It can be tetrahedrally coordinated when charge balanced by a basic oxide, see Fig 3.7.

Iron plays an important, and complex, part in the strucural properties of silicate melts. This part is dominated by two main features, each influenced by several aspects of the prevailing conditions, and both intimately linked to each other:

- Oxidation level
  - Atmosphere
  - Concentration of other species in the melt
  - Temperature
- Coordination
  - Atmosphere
  - Concentration of other species in the melt
  - Temperature
  - Melt acidity

Iron can occur both as a network modifier (ferrous iron, Fe^{2+}) and as an amphoteric (ferric iron, Fe^{3+}),[46,47] and it is of great structural importance to know the distribution of iron between the two oxidation states.

It is beyond doubt that the coordination of iron affects viscosity. However, structural investigations do not give a clear answer to the coordinational properties of the two oxidation states of iron.

3.4 Crystallisation

The presence of suspended solid matter seriously affects the viscosity of silicate melts, as indeed it affects the viscosity of any other type of melt.

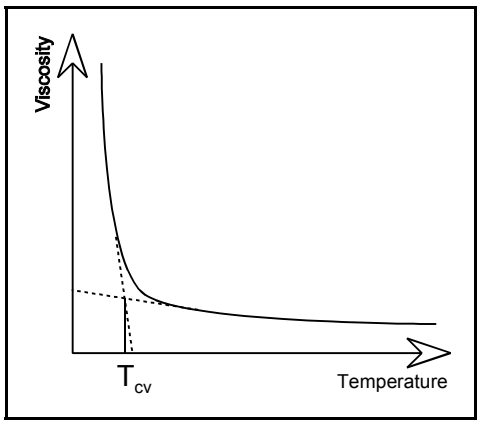

Figure 3.8 Graphical definition of the temperature of critical viscosity, T_{cv}.

- Viscosity increases sharply with the appearance of solids in the melt.
- Non-Newtonian behaviour is commonly observed in crystal - melt slushes.
- At concentrations higher than a certain limit, the measurement signal will be disturbed by the interference of solid particles.[12]

The temperature of critical viscosity, T_{cv}, indicates a point of often very abrupt change in the viscosity-temperature relationship. It is often assumed that T_{cv} marks the division between crystal-affected viscosities and viscosities not affected by the presence of crystals; this point is called the critical viscosity, see Fig 3.8.

3.5 Liquid mixture models

The term *liquid mixture* comprises mixtures of different oxides that are either completely or partially liquid.

Completely molten silicate melts are Newtonian liquids as opposed to melts with a certain amount of crystals. Therefore the following review of existing models found in the literature can be divided into models for Newtonian and non-Newtonian systems.

3.5.1 Generalised models for Newtonian fluids

Newtonian fluids, for which viscosity is independent of shear rate, represent the most simple flow type, and therefore they are also the most closely examined. Fortunately, completely molten silicates are usually categorised as Newtonian, although for high shear rates (beyond the focus of this text), the flow may deviate from Newtonian behaviour.

Table 3.1 Generalised models for Newtonian fluids (a, b and c are composition-specific adjustable parameters).

Model	Year	Definition
Arrhenius (Eyring)	1887	$\log \eta = a + \frac{b}{T}$
Vogel - Fulcher - Tammann	1921	$\log \eta = a + \frac{b}{T - c}$
Grunberg	1949	$\ln \eta = x_1 \cdot \ln \eta_1 + x_2 \cdot \ln \eta_2 + 2 x_1 x_2 a$, x_i = molar concentration

Doolittle	1951	$\eta = a \cdot e^{-b \cdot V_m / V_f}$, V_m = volume occupied by molecules, V_f = Free volume
Williams - Landel - Ferry	1955	$\log\left(\frac{\eta}{\eta_{ref}}\right) = \frac{-a \cdot (T - T_{ref})}{b + (T - T_{ref})}$, $\eta_{ref} = \eta(T_{ref})$
Weymann	1962	$\log \eta = a + \log T + \frac{b}{T}$
Adam - Gibbs	1965	$\log \eta = a + \frac{b}{T \cdot S_c(T)}$, $S_c = f(T)$
Seetharaman - Du Sichen	1994	$\log \eta = a + \frac{E_A}{T}$, $E_A = f(T)$
Model coupling theory	-	Still under development

3.5.2 Models for completely molten silicates

The models constructed for the estimation of the viscosity of silicate melts all attempt to relate viscosity to temperature and a simplified melt composition.

Existing models for the estimation of the silicate melt viscosities can be classified as follows:

- Models based on the Arrhenius equation relating viscosity to temperature
  - Shaw (1972), Watt - Fereday (1963), S^2 (1944)
- Models based on the Weymann equation relating viscosity to temperature
  - Kalmanovitch - Frank (1988), Streeter (1984), Urbain (1981), Riboud (1981)
- Models based on the Vogel - Fulcher - Tammann equation relating viscosity to temperature
  - Lakatos (1972)
- Models relating viscosity to composition
  - Bottinga - Weill (1972)
- Unclassified models
  - Sage - McIlroy (1959), Reid - Cohen (1944)

All the models are the result of an empirical fitting of data, and they all apply to Newtonian liquids only, ie completely molten systems. They have all been developed for a limited compositional interval, and should only be used outside this interval with precaution.

An example of the performance of most of the models can be found in Chapter 7. For that particular composition, the predictions of the Urbain model turned out to be outstanding.

In the article, the overall performances of the models are evaluated by taking the average deviation found for seven measurement-series. This procedure lead to the following ranking

of the models in order of decreasing ability to reproduce experimental results: Bottinga - Weill, Reid, Riboud, Sage, Kalmanovitch - Frank, S^2, Urbain, Watt - Fereday, Shaw, Lakatos, Streeter.

On the basis of the conducted test, it is not possible to indicate a model that performs better than all the others for all compositions considered. Each model was developed on the basis of some experimental studies of melts of a given range of compositions, and this point should be carried in mind when selecting a model for the estimation of viscosities of a test-sample.

3.5.2.1 Senior and Srinivasachar

A model by Senior and Srinivasachar (1995) was not presented in the review article. For the sake of completeness it will be lined out in the following.[21]

The model is designed to predict viscosity of silicates containing 35 to 99% SiO_2 with Al_2O_3, Fe_2O_3, FeO, CaO, MgO, Na_2O, K_2O and TiO_2, and it is special in the sense that it focusses on a higher viscosity range than other models (10^4 - 10^8 Pa·s). The model is based on 134 data sets for viscosities greater than 10^4 Pa·s, and 294 sets for viscosities less than 10^4 Pa·s, a grand total of 2925 viscosity measurements.

The model is divided into two parts, a low-viscosity part and a high-viscosity part. The low-viscosity part is a reformulation of the Urbain model, based on the Weymann expression:

$$\log(\frac{\eta}{T}) = A + \frac{10^3 \cdot B}{T} \tag{3.1}$$

For the determination of the composition-dependent variables A and B, a number of auxiliary variables have to be calculated and combined with the fitted b-values in Table 3.2.

Table 3.2 Fitted values of coefficients for compositional dependence of B.

	High temperature	**Low temperature**		**High temperature**	**Low temperature**
$\mathbf{b_0}$	-224.98	-7563.46	$\mathbf{b_6}$	-957.94	-46484.8
$\mathbf{b_1}$	636.67	24431.69	$\mathbf{b_7}$	3366.61	146008.4
$\mathbf{b_2}$	-418.70	-17685.4	$\mathbf{b_8}$	-2551.71	-104306.0
$\mathbf{b_3}$	823.89	32644.26	$\mathbf{b_9}$	387.32	21904.63
$\mathbf{b_4}$	-2398.32	-103681.0	$\mathbf{b_{10}}$	-1722.24	-68194.8
$\mathbf{b_5}$	1650.56	74541.33	$\mathbf{b_{11}}$	1432.08	48429.31

First N is defined as the molar concentration of SiO_2 in the melt:

$$N = SiO_2 \tag{3.2}$$

The quantity α is calculated as the ratio of mole fraction of CaO to the sum of the molar fractions of CaO and Al_2O_3:

$$\alpha = \frac{CaO}{CaO + Al_2O_3} \tag{3.3}$$

Now B can be calculated by combination of N, α and Table 3.2:

$$B = b_0 + b_1 a + b_2 a^2 + N(b_3 + b_4 a + b_5 a^2) + N^2(b_6 + b_7 a + b_8 a^2) + N^3(b_9 + b_{10} a + b_{11} a^2) \tag{3.4}$$

Then the ratio of non-bridging oxygens to tetrahedral oxygens (NBO/T) is given by:

$$\frac{NBO}{T} = \frac{CaO + MgO + FeO + Na_2O + K_2O - Al_2O_3 - Fe_2O_3}{½ \cdot (SiO_2 + TiO_2) + Al_2O_3 + Fe_2O_3} \tag{3.5}$$

Coefficient A is calculated by use of B and NBO/T. A different scheme is used for high and low temperatures. For high temperatures, A_H is given as:

$$A_H = -3.81629 - 0.46341 \cdot B - 0.35342 \cdot NBO / T \tag{3.6}$$

For low temperature, the choice of expression depends on the value of NBO/T (An error in the article text was identified and corrected):

$$A_L = \begin{cases} -1.982 - a \cdot B & , \quad 1.3 \le NBO / T \\ 1.478718 - a \cdot B - 2.662091 \cdot NBO / T & , \quad 0.2 \le NBO / T < 1.3 \\ 8.223 - a \cdot B - 36.3835 \cdot NBO / T & , \quad 0.0 \le NBO / T < 0.2 \\ 8.223 - a \cdot B & , \quad NBO / T < 0.0 \end{cases} \tag{3.7}$$

where a = 0.902473.

To select the appropriate coefficients, at each temperature the viscosity is calculated using both the high and the low temperature coefficients and the *highest* value is used.

The authors conclude that the new model performs better than the Kalmanovitch model for viscosities in the range 10^4 to 10^9 Pa·s, but the Kalmanovitch model is best at viscosities less than 100 Pa·s. At low temperatures, viscosities greater than 10^9 Pa·s, neither model describe viscosity well. They also encounter problems in predicting the viscosity of high-iron glasses and glasses containing no modifier ions.

The model will be applied together with the models from the review article for the measurement series in Chapter 7.

An overview of all the models is given in table 3.3.

Table 3.3 Structure of the temperature-dependence of viscosity in mathematical models. Please refer to the above for a more comprehensive presentation of the Senior - Srinivasachar model and Appendix A for all other models. A, B and C are composition-independent values that are fixed for each model.

Name	Year	Model structure
S^2	1963	$\log \eta = A \cdot \varsigma^2 + \frac{B}{T} - C$, where ς = f(comp.)
Watt - Fereday	1963	$\log \eta = A \frac{m}{(T-B)^2} + C$, where m = f(comp.)
Bottinga - Weill	1972	$\log \eta = \sum_i x_i \cdot D_i - 1$, where i = species no "i"
Shaw	1972	$\log \eta = \alpha \cdot \left(\frac{A}{T} - B \right) + C$, where α = f(comp.)
Lakatos	1972	$\log \eta = a + \frac{b}{T-c}$, where a, b, c = f(comp.)
Urbain	1981	$\eta = a \cdot T \cdot e^{\frac{A \cdot b}{T}}$, where a, b = f(comp.)
Riboud	1981	$\eta = a \cdot T \cdot e^{\frac{A \cdot b}{T}}$, where a, b = f(comp.)
Kalmanovitch - Frank	1984	$\eta = a \cdot T \cdot e^{\frac{A \cdot b}{T}}$, where a, b = f(comp.)
Senior - Srinivasachar	1995	$\log\left(\frac{\eta}{T} \right) = a + \frac{A \cdot b}{T}$, where a, b = f(comp.)

3.5.3 Generalised models for non-Newtonian fluids

The term non-Newtonian fluid covers a wide range of fluids: time-independent flow types except those with a shear-rate independent viscosity as well as all time-dependent flow types. For silicate melts, non-Newtonian flow can be caused by two different mechanisms both related to phase separation:

- The appearance of crystals in the melt
- Separation of the melt into two or more immiscible liquids

The mathematical description of time-dependent flow types is very complex and not very well understood, so Table 3.4 concentrates on time-independent non-Newtonian fluids, relating shear stress, τ, to shear rate, $\dot{\gamma}$, through a number of parameters that are explained in the review article.

Table 3.4 Models for time-independent, non-Newtonian fluids (a, b = composition-dependent constants).

Model	**Definition**
Power law or Ostwald - de Waele	$\tau = a \cdot \dot{\gamma}^{b}$
Bingham plastic	$\tau - \tau_0 = a \cdot \dot{\gamma}$
Herschel - Bulkley	$\tau - \tau_0 = a \cdot \dot{\gamma}^{b}$
Casson	$\tau^{1/2} - \tau_0^{1/2} = \eta_\infty^{1/2} \cdot \dot{\gamma}^{1/2}$
Meter or if $\eta_\infty = 0$: Ellis	$\eta - \eta_\infty = (\eta_0 - \eta_\infty)(1 - \lvert \tau / \tau_{1/2} \rvert \cdot \alpha^{-1})$
Williamson	$\eta - \eta_\infty = \frac{\tau_{"0"}}{c + \dot{\gamma}}$

3.5.4 Liquid-solid mixtures

The modelling of the viscosity of condensed phases is a non-trivial task that involves the determination of crystal fraction and crystal shape and on the basis of these: viscosity calculation.

As is often the case, the most simple models are the oldest ones. The concept of some of the simpler models are presented in Table 3.5. An exact description of the parameters used is given in the article text.

Table 3.5 Models relating the effective viscosity of a liquid-solid mixture, η_e, to the volume fraction of particles, θ (a, b = constants).

Model	**Year**	**Definition**
Einstein	1906	$\frac{\eta_e - \eta}{\eta} = a \cdot \theta$
Vand	1948	$\eta_e = \eta \cdot (1 + a \cdot \theta + b \cdot \theta^2)$
Roscoe	1952	$\eta_e = \eta \cdot (1 - a \cdot \theta)^{-5/2}$
Sherman	1968	$\ln \frac{\eta_e}{\eta} = \frac{a \cdot D_m}{(\theta_{max}/\theta)^{1/3} - 1} - b$, D_m = mean particle diameter
Shaw	1969	$\log\left(\frac{\eta_e(T)}{\eta_0(T_0)}\right) \approx 0.1 \cdot (T - T_0)$
Quemada	1982	$\eta_{e,0} = \eta \cdot \left(1 - \frac{\theta}{\theta_{max}}\right)^{-2}$, θ_{max} = maximum packing fraction

Chapter 4
The purchase of a high-temperature viscometer

4.1 To build or to buy

To perform high-temperature viscosity-measurement is like walking down a narrow path filled with unfathomable holes. This was the bottom line of what everyone told us and what we read in the literature (and what we were soon to discover ourselves). Nevertheless, we were determined to find a way to perform precise viscosity-measurements on silicate melts. The objective was clear: All mathematical models accounting for the behaviour of ashes in a thermal fuel conversion system depend strongly on the predictability of ash viscosity - will the fly ash particles and/or deposits be solid, sticky or even flowing?

We soon discovered that basically two paths were viable; either to buy a viscometer or to build one ourselves. The advantages and disadvantages of each of these options seemed clear: If we decided to build the instrument ourselves, costs would be kept down, but it would be a time-consuming job. A pre-fabricated high-temperature viscometer on the other hand would be expensive, but we would be able to start measurements much sooner.

4.1.1 Viscometer technology

A literature review on the experimental apparatuses applied by scientists around the world for viscosity-measurements reveals that the rotational viscometer is by far the most commonly used.[48]

Table 2 in Appendix A shows how the rotational viscometer out passes all other techniques with a measurement range that reaches from low viscosities (100 Pa·s in the table, but the accurate number is probably more like 1 Pa·s) where the substance is liquid to high viscosities (10^{13} Pa·s) for which the substance is practically solid. In addition to this, the rotational principle is used in most existing instruments applied for the range of viscosities that reaches down to the liquid end of the scale, whereas rod elongation and squeeze film viscometers are predominant in the high-viscosity end.

On this basis, I decided to focus on rotational viscometers for our set-up.

Some month were spent investigating the two alternatives, and ultimately the choice stood between the following products:

4.1.2 The pre-fabricated product

The only ready-to-use apparatus is produced by the German company Haake. Basically it consists of a vertical tube-furnace and a viscometer. As can be visualized from Figs 4.1 and 4.2, the viscometer is placed centralized on an arm above the furnace, and it is fitted with a bob on a long stick that reaches down into the furnace. The container cup is centralized both vertically and horizontally inside the furnace by a pedestal that stands on a bottom-plate under the furnace. This bottom plate also serves to close the low-end extreme of the furnace and thus allow for a controlled test-atmosphere.

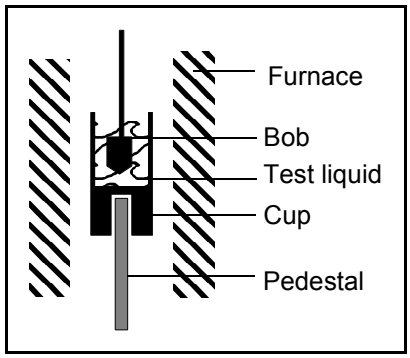

Figure 4.1 Schematic representation of the placement of a viscometer sensor inside a tube furnace.

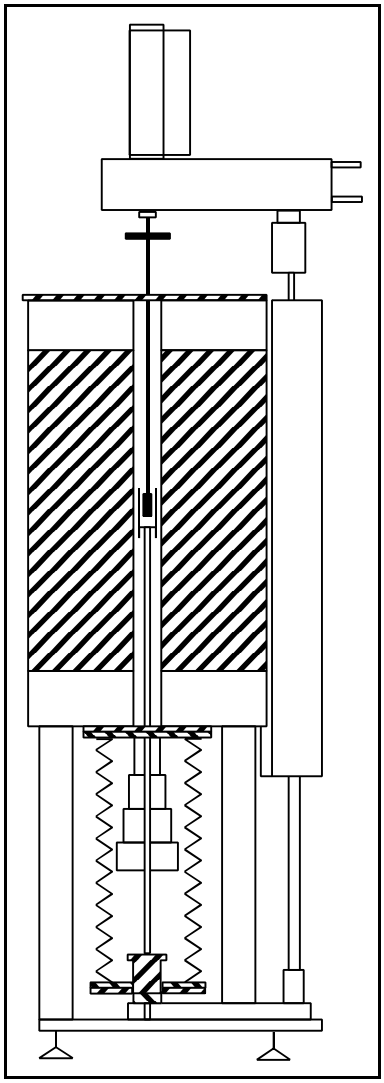

Figure 4.2 Schematic depiction of the Haake ME 1700 - RV 20.

The set-up was developed some time ago, and the user-interface is somewhat outdated in the sense that it does not allow for the extend of automation that would be expected for a newly developed apparatus. But the set-up does allow for computerized control of the viscometer and on-line registration of viscosities and temperatures.

During a sales-demonstration in the company's headquarters in Karlsruhe, Germany, we were demonstrated a recently developed apparatus, but it was observed that the performance of this instrument was not acceptable - there were too many bugs - why it was decided to consider only the purchase of the older, well-tested model.

4.1.3 The home-made product

The Danish company Struers Kebo Lab (now Merck Eurolab) negociates both Brookfield viscometers and Carbolite furnaces.

The American company Brookfield produces a line of viscometers for use at temperatures around room temperature. The products are parallel to those of Haake, and they are on the same cost level. Likewise, these instruments can be controlled from a computer.

Another American company, Carbolite, produces a large

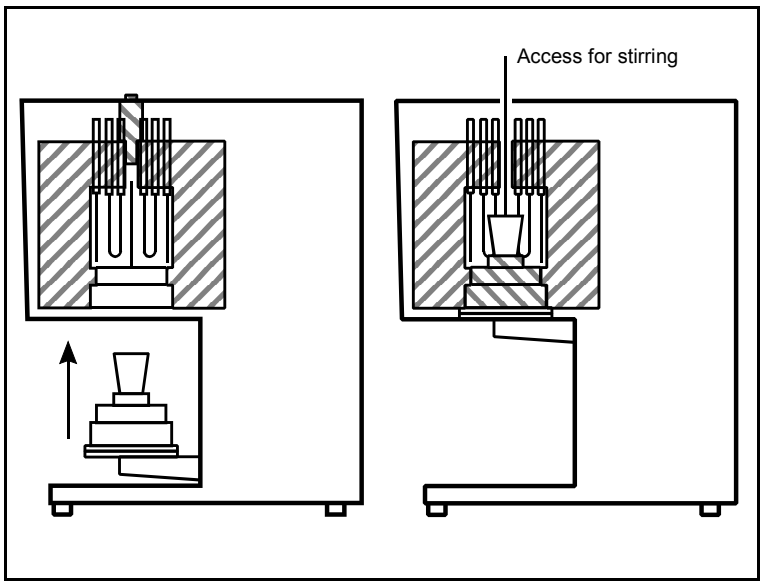

Figure 4.3 Carbolite BLF furnace: Loading and stirring.

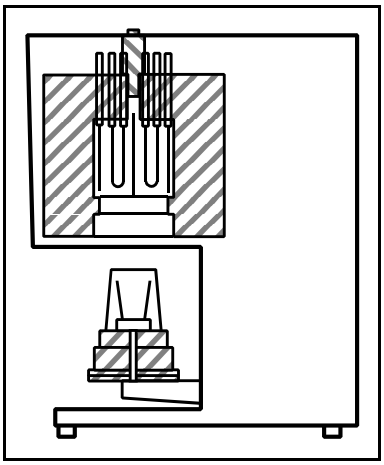

Figure 4.4 Atmosphere control in a Carbolite BLF furnace.

variety of furnaces, reaching from small lab-ovens to high-temperature furnaces. A chamber furnace was proposed, Fig 4.3.

The furnace is bottom loaded which reduces the operator-exposure to heat radiation in comparison to side or top-loaded furnaces. The top of the furnace can be kept open to give access for the viscometer spindle, Fig 4.3.

A problem with this set-up is to keep a controlled atmosphere in and around the crucible. The proposed solution is an alumina-crucible turned upside down to cover the sample-container combined with a gas inlet through the bottom plate, see Fig 4.4. A hole in the alumina crucible would allow for the passage of the viscometer spindle, but this hole would have to be big enough to permit the entry of the bob.

In short, it would probably be possible to construct a set-up that combines the viscometer and the furnace in a neat way, but it is insecure whether or not it would be possible to assure an adequate atmosphere around the test-sample.

Simultaneous, computerized compilation of coherent temperatures and viscosities would demand the installation of a computer program supplied by an external manufacturer.

4.2 The choice

The pros and contras of the two alternatives ended up being.

Table 4.1 Advantages and disadvantages of a pre-fabricated viscometer and a home-made viscometer.

	Advantages	**Disadvantages**
Pre-fabricated (Haake)	Existing and tested instrument and sensor design with guaranteed high-precision functionality Possible to maintain a controlled atmosphere in the test zone. Has already been used for similar sample types by several independent laboratories around the world Existing software integrates furnace and viscometer High degree of automation Short installation time High support level: Whole set-up produced by the same company and specially trained technical support in Denmark	Expensive acquisition
Home made (Struers)	Cheap individual components	Unclear precision level Uncertain degree of automation, hence possible high operation-costs Long installation time Low support-level: Different personnel in Struers to handle viscometer and furnace and an external company to handle the software, not to mention thermocouples and other accessories.

4.3 Conclusions

The main argument speaking for the home-made viscometer is the low equipment-price. The pre-fabricated apparatus is probably superior in terms of installation-time, operation-cost, precision-level and support-level.

So: we bought the Haake ME 1700 RV 20, and the setup is shown in Fig 4.5.

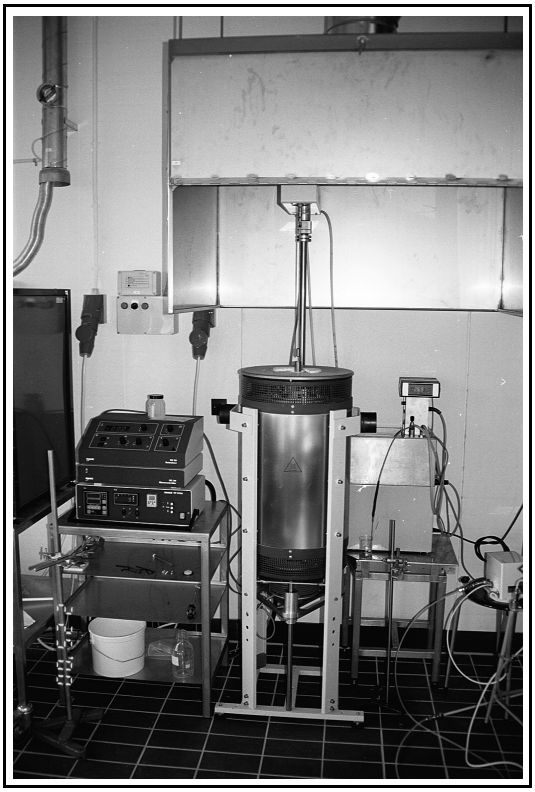

Figure 4.5 High-temperature viscometer setup at the Technical University of Denmark.

Chapter 5
Experimental setup

5.1 Introduction

A technical description of the experimental setup for viscosity determination on high temperature melts is given in this chapter.

5.2 Key data

Company:	Haake, Karlsruhe, Germany
Product specification:	Viscometer: Rotovisco RV20
	Controller: Rheocontroller RC20
	Furnace: ME 1700, TP 1700
Date of purchase:	December 1997
Temperature limit:	T_{max} = 1700°C
Heating capacity:	4.4 kW
Viscosity range:	0.005 - 10^6 Pa·s
Maximum rotational speed:	500 rpm

5.3 Theory

RV20 is a rotational viscometer. The liquid is contained in an outer cylinder, a cup, and an inner cylinder, a spindle, is rotated at a steady speed in the liquid, see Fig 5.1.

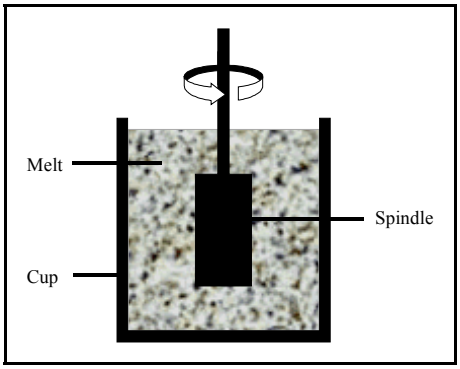

Figure 5.1 Rotational viscometer.

Viscosity, η, [Pa·s] is given as the ratio of shear stress, τ, [Pa] to shear rate, D, [s^{-1}].

$$\eta = \frac{\tau}{D} \tag{5.1}$$

Newtonian liquids, are defined as liquids for which viscosity is independent of shear rate. For all other liquids η = f(D).

5.4 The apparatus

The viscometer and the furnace interact strongly in the setup, and thus it will not be possible to describe the two sub-systems entirely independently. A complete schematic drawing of the setup is given in Fig 5.2.

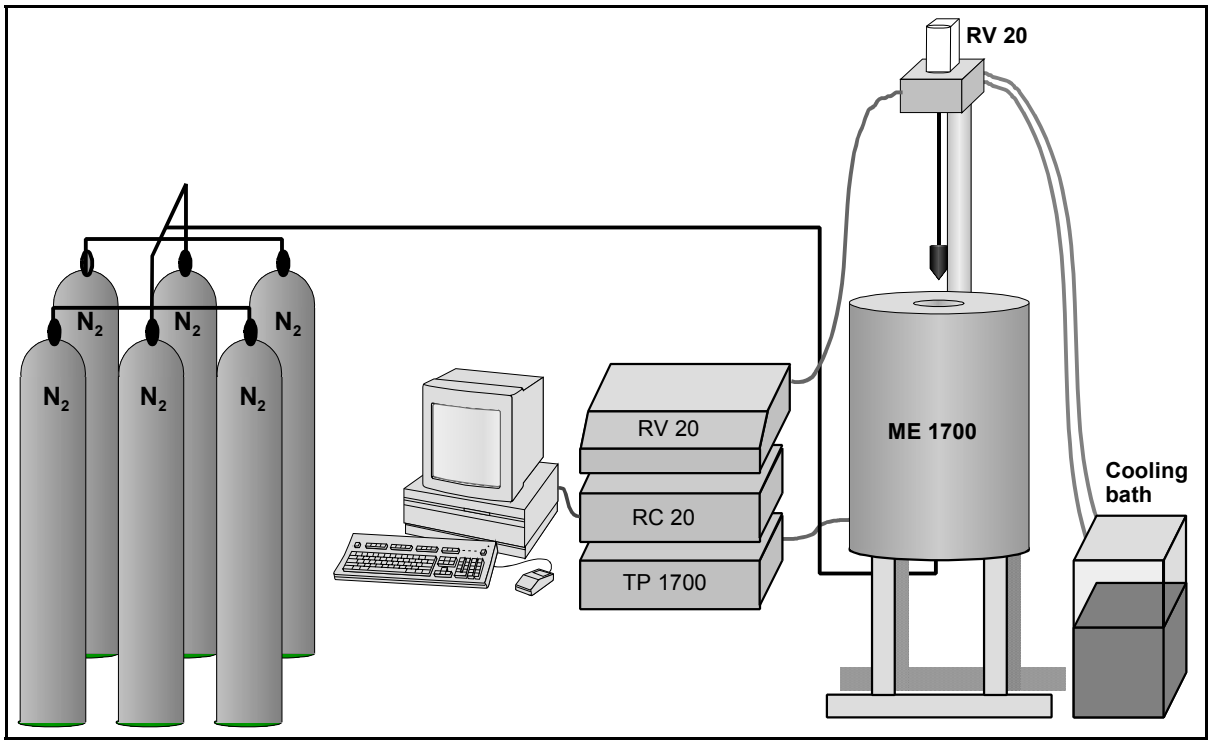

Figure 5.2 Complete setup used for viscosity measurements.

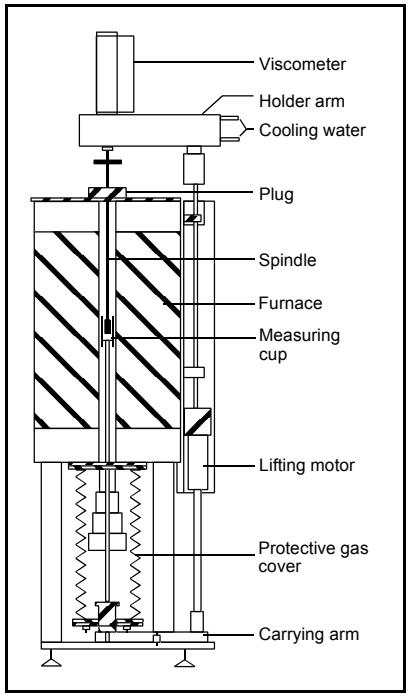

Figure 5.3 ME 1700.

5.5 Furnace

The ME 1700 furnace is basically a vertical tube furnace with a maximum temperature of 1700°C. A schematic drawing of the complete setup with furnace and viscometer is shown on Fig 5.3.

The furnace is equipped with six heating elements made of chromium - lanthanium oxide. In two groups of three, these rods are serial coupled while the two groups are parallel coupled, see Fig 5.4. Due to the cost of more than EUR 1300 per rod, they are changed individually upon breakage.

The furnace is fitted with a protective inner ceramic tube for two reasons: one is to allow for the establishment of an inert atmosphere in the furnace, and the other is to prevent any waste material from the measuring cup from damaging the heating elements. The ceramic tube has the side-effect of lowering the test-temperature approx 50°C. A description of possible leakages related to this protective tube is given at the end of the chapter.

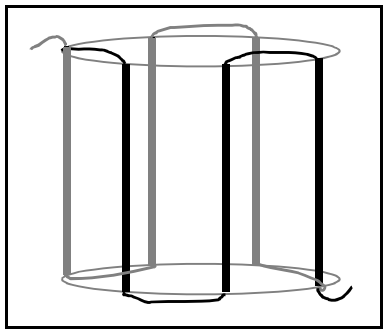

Figure 5.4 Electrical connection of rod heaters.

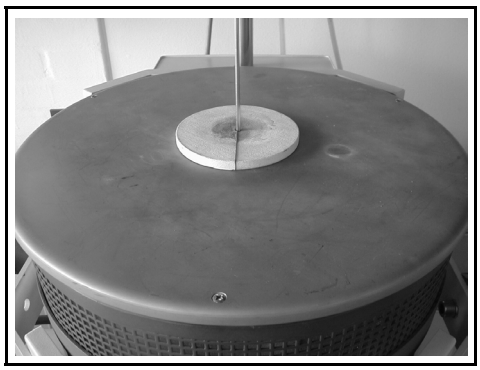

Figure 5.5 Ceramic plug..

The hole at the top of the furnace should be covered with a ceramic plug during operation. The plug consists of two half-circles that, when joined, have the shape of a circle with a little hole in the middle for the spindle, see Fig 5.5.

As depicted in Fig 5.3, the measuring cup is placed on top of an alumina pedestal of length 785 mm. The pedestal in turn is placed on a moveable carrying arm under the furnace. The pedestal is a rod with two parallel holes. A Pt/Rh-thermocouple is mounted at the top of the pedestal, and its two legs run through the holes in the pedestal down to the carrying arm, where they are led through a hole in the socket and are connected to a temperature display, “Th 2" in Fig 5.7. Since the pedestal reaches from the cold bottom plate to the hot-zone of the furnace, it experiences severe thermal shocks when moved vertically, and this causes frequent fractures.

The carrying arm of the ME 1700 was not sufficiently stable to control the horizontal movements of the pedestal, so a steering aid was constructed. It consists of three vertical tubes that maintain the carrying arm in a horizontal position at all vertical positions, see Fig 5.6.

A holder for the viscometer is positioned above the furnace. It is moved vertically in coordination with the carrying arm. Measures have been taken to prevent reheating of the viscometer during operation:

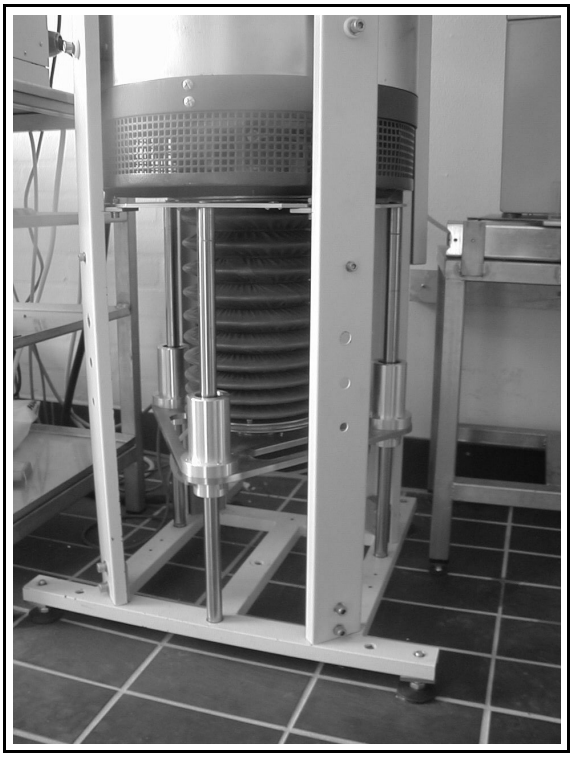

Figure 5.6 Furnace with improved steering.

- The spindle is mounted in the viscometer via a joint with a radiation shield
- The holder is water-cooled. Experience has shown that 5°C water should be used since the viscometer will otherwise be overheated during operation.

5.6 TP 1700

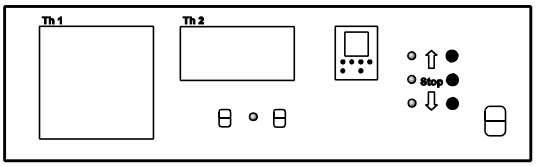

Figure 5.7 TP 1700.

The TP 1700 controller box is used to operate the ME 1700, see Fig 5.7. Buttons on the right hand side of the controller box control vertical movements of the pedestal: In the top position, the tip of the pedestal almost reaches the top of the furnace to allow for placement and removal of the measuring cup. In its lowest position, the arm is locked in a cone-funnel arrangement. In this position, the pedestal ensures vertical and horizontal centralisation of the measuring cup in the furnace.

5.7 Temperature programming

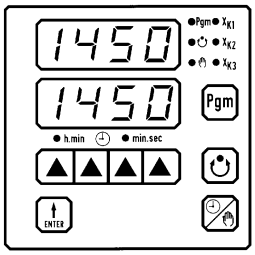

Figure 5.8 Displays and controls for TP 1700.

The furnace temperature is controlled via a program controller in the TP 1700 controller box (Fig 5.8). The box enables both manual and automatic temperature control.

The set-point temperature is displayed as the lower temperature in Fig 5.8, and the actual temperature of the furnace is displayed as the upper temperature. This temperature is measured on the outside of the ceramic tube, and it will be approximately 50°C higher than the temperature measured just under the measuring cup, primarily due to a temperature-gradient through the ceramic tube.

5.7.1 Example of automatic operation

Before programming, the desired temperature-curve should be marked in graphical and tabular form as shown in Figs 5.9 and 5.10 because direct programming of the controller box can be rather confusing.

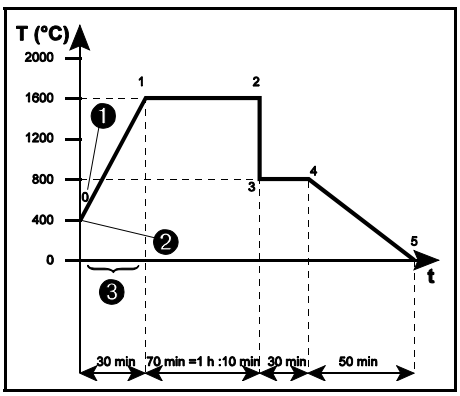

Figure 5.9 Graphical representation of temperature-curve in example.

Fig 5.9 shows an example of a graphical representation of a temperature-curve. First a 30 min ramp from 400°C to 1200°C where a steady temperature is kept for 70 minutes. Then a step to 800°C, where temperature is

kept constant for 30 minutes. At last a ramp down to 0°C in 50 minutes. The numbers 1 through 3 in dark circles in Fig 5.9, indicate points that can be re-found in the table in Fig 5.8.

With Fig 5.9 in hand, it is a relatively easy task to enter the necessary data in the table. The result is given in Fig 5.10. Only section numbers, set-point temperatures and section times should be filled in, operating contacts 1 and 2 are self-programming.

	❶ Section Sc-. Pr-.		❷ Setpoint SETP		❸ Section time TIME h:min min:sec		Operating Contact 1 Out 1		Operating Contact 2 Out 2	
Pgm → ENTER →	0		400		0.30		On		OFF	
	1		1600		1.10		OFF		On	
	2		1600		0.00		OFF		OFF	
	3		800		0.30		OFF		On	
	4		800		0.50		OFF		On	
	5		0		0.00		OFF		OFF	→ Pgm

Figure 5.10 Tabular representation of temperature-curve in example.

The main point to bear in mind when programming the TP 1700 is that in a given section, a set-point temperature is given as well as the time interval to the next set-point temperature. Thus the time given in the last section of a program is irrelevant to the program (ie the time in section 5 of the example program).

5.8 Viscometer

The RV 20 measuring head is placed in a holder arm over the furnace as shown in Figs 5.2 and 5.3. From this position, it measures the viscosity of the test melt by use of the concentric cylinders principle where an inner cylinder, the spindle, is brought to rotate in the test-liquid which in turn is kept in a measuring cup (Fig 5.1). The control parameter for the rotation of the spindle can be chosen to be either torque or rotational speed, the latter is used by us since it ensures a constant deformation of the test liquid.

Operation of the viscometer head is performed through the RV 20 control box in Figs 5.2 and 5.11. The A-section of Fig 5.11 is the display where readings of the actual rotational speed and torque can be obtained (the temperature reading is not valid). The B-section is the rotational speed control, the C-section is the damping of the torque signal display, and torque measuring range is chosen in the D-section, where also the zero can be adjusted.

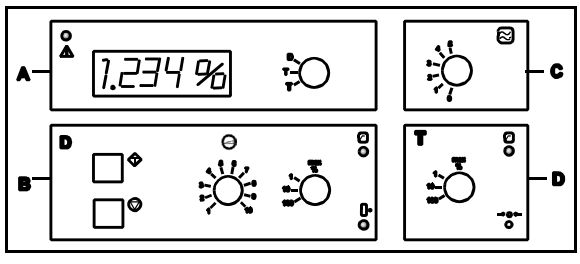

Figure 5.11 Control box for the RV 20.

5.9 Computerised measurements

A computer is connected to the setup through the RC 20 control box in Fig 5.2. The RC 20 is connected to the RV 20 control box and the TP 1700 control box, which allows for data sampling of both viscosities and temperatures.

A computer program reads coherent values of melt temperature, measured in a hole under the measuring cup ("Th 2" in Fig 5.7), and rotational speed and torque. It is possible to control the RV 20 from the computer program, but temperatures must still be set with the TP 1700.

The computer program uses calibrated sensors. The operator enters two calibration constants to define each sensor, and the program then calculate the resulting viscosity, so that the output from the program consists of pairs of temperature and viscosity, plus rotational speed and torque if desired.

5.9.1 Sensor constants

As mentioned in the introduction to this chapter, viscosity is defined as:

$$\eta \equiv \frac{\tau}{D} \tag{5.2}$$

where η = viscosity, [Pa·s], τ = shear stress [Pa] and D= shear rate [s^{-1}].

The shear stress is linearly linked to the torque at the rotor, M_d:

$$\tau \propto M_d \tag{5.3}$$

Thus τ can easily be calculated from the %τ-value on the viscometer control box (A is a geometric factor):

$$\tau = A \cdot \%\tau \tag{5.4}$$

In a similar manner, the shear rate, D, can be calculated using the %D-value on the viscometer control box (M is a geometric factor):

$$D = M \cdot \%D \tag{5.5}$$

For the setup used with the ME 1700, constants A and M can not be calculated from geometric considerations, so they should both be estimated experimentally. The procedure used, is given below.

Combination of equations (2), (4) and (5) leads to the following result:

$$\eta = \frac{\tau}{D} = \frac{A}{M} \cdot \frac{\%\tau}{\%D} \tag{5.6}$$

Equation (6) clearly shows that only one geometrical factor is needed to evaluate viscosity from rotational measurements. The equation also shows that only a single factor *can* be estimated. This leaves the user with the frustrating experience of having to assign values to *two* geometrical factors without having data for more than *one* factor.

Ideally, each set of viscometer sensors (cups and spindles) should be calibrated before use. The principle of calibration is as follows. Viscosity is independent of shear rate for Newtonian liquids, so a graphical representation of shear stress, τ, vs shear rate, D, ie a flow curve, results in a straight line through origo. If the line does not pass through the origo, it is due to an unsatisfactory zero-calibration. At high shear rates, the line will deviate from linearity due to frictional heating of the test liquid.

The absolute torques, τ, and shear rates, D, are not known, but pairs of $\%\tau$- and %D-values can be obtained by measuring $\%\tau$ at different shear rates with a speed ramp. The fraction of $\%\tau$ to %D is found to be the coefficient of inclination of the $\%\tau$-to-%D-line, α.

In accordance with equation (6), the proportionality constant, A/M, is then given as:

$$\frac{A}{M} = \frac{\eta}{\alpha} = \frac{\eta}{\frac{\%\tau}{\%D}} \tag{5.7}$$

Both A and M should be assigned values in the viscometer software, and the choice of values is optional as long as the fraction between the two is kept constant, ie A/M = 0.01: A = 1 and M = 100 or A = 0.01 and M = 1.

In order to have complete control of the rotational speed actually used during a measurement, it was chosen to keep M = 1 for all applications and calibrate only the A-factor. In this way, the %D-value that appears on the display of section A in Fig 5.11 during initial testing to determine an appropriate rotational speed (ie an appropriate torque) is the same that is used as input to the computer software.

Two types of calibration can be performed. At room temperature the sensors are calibrated in a standard oil and at elevated temperatures a standard glass is used. In principle, the two types of calibration are identical, they are just carried out under different conditions. Stretching of the spindle by thermal expansion does not give rise to major errors (< 5%). But in reality, a deviation in the range of 50% is seen as mentioned in Chapter 6. As a consequence, calibration should be carried out in standard glass only.

5.9.2 Sensor dimensions

Since the sensors are calibrated manually, the dimensions can be picked freely, as long as the spindle head is completely immersed in the liquid during measurements and the bottom of the

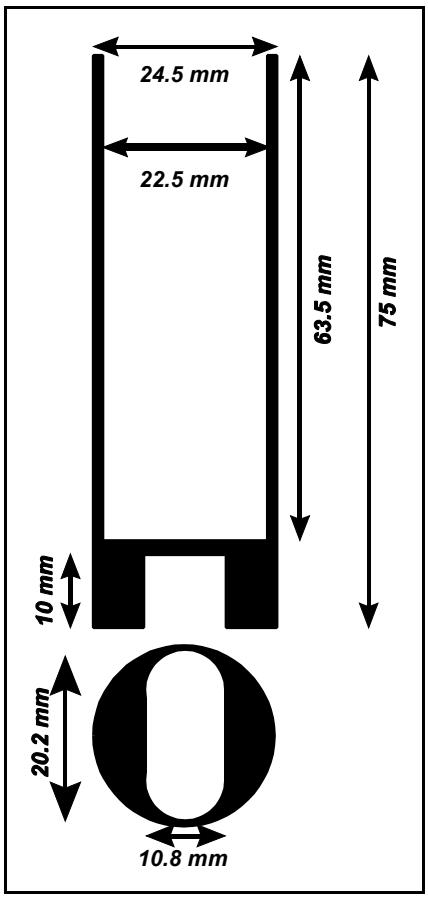

Figure 5.12 Molybdenum cup.

spindle is kept at a distance from the bottom of the measurement cup to avoid end effects. We have chosen to maintain the vertical dimensions proposed by the manufacturer, and the only parameter that we vary is the diameter of the spindle head.

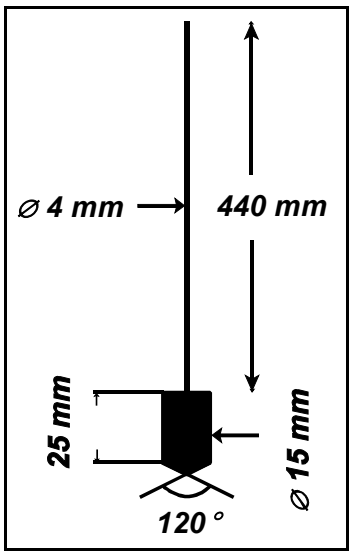

Figure 5.13 Molybdenum spindle.

A large spindle head is adequate for measurements in melts with low viscosities, and visa versa. Since we attempt to cover a large viscosity interval in our measurements, a choice in between is preferred. But the material cost plays in on this decision.

Chapter 6 contains a detailed evaluation of material choice for the sensors. In this chapter, it will just be mentioned that molybdenum (Mo) and rhodium-enforced platinum ($Pt_{80}Rh_{20}$) are used. When Mo is used, it happens in a protective atmosphere of N_2, while $Pt_{80}Rh_{20}$ is used in air.

Molybdenum sensors are produced at our own workshop from bars. The dimensions are shown in Figs 5.12 and 5.13.

The material use is more critical for $Pt_{80}Rh_{20}$ sensors since both components are extremely expensive, and the sensors have to be manufactured externally. Therefore

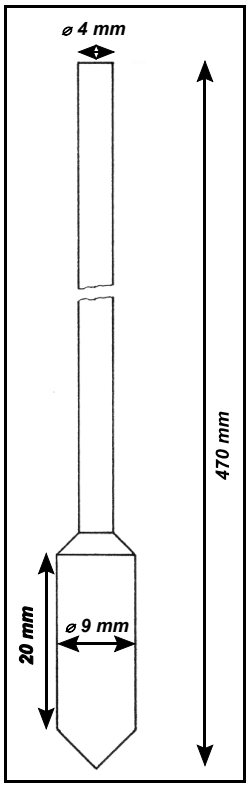

Figure 5.15 $Pt_{80}Rh_{20}$ spindle.

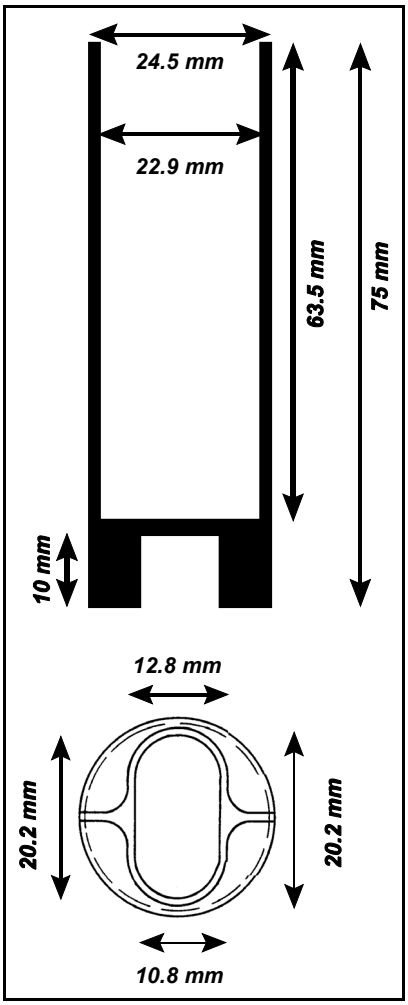

Figure 5.14 $Pt_{80}Rh_{20}$ cup.

all excessive material is removed from the cup (Fig 5.14), and the spindle dimensions are smaller (Fig 5.15).

5.10 Atmosphere

Measurements under oxidising conditions are most relevant to deposit behaviour in combustion systems since the walls of full-scale boilers are kept in an oxidising atmosphere. On the other hand, the individual ash-particles may experience local reducing conditions during combustion, and gasifiers are operated under-stoichiometrically and will thus have reducing conditions even at the walls.

As indicated by Fig 5.2, measurements can be conducted in a controlled atmosphere because atmosphere of the test-zone is kept isolated by the protective tube and the gas cover. The chimney effect (that is caused by the tendency of hot air to rise) will cause the test-zone to be filled with the gas that is supplied through the bottom plate. At present, only N_2 is used, in order to keep a non-oxidising atmosphere in the test-zone when molybdenum is used as a sensor material. But in the future, the setup enables the mixing of combustion-relevant atmospheres - IF the present leakage-problem caused by an insufficient gasket fitting is solved, see below.

5.10.1 Leakages

The main reasons for leakages are:

- *Broken protective tube*
  If the protective tube has been polluted with glass, cooling and heating will cause thermal tensions to arise in the border area between glass and tube material due to differences in thermal expansion. This may cause the tube to break locally.
  A broken protective tube will allow for the penetration of false air, and the tube should therefore be replaced.

- *Misplaced protective tube*
  The protective tube stands on a gasket in a metallic fitting. Upon placement of the tube, care should be taken for the tube to enter into the fitting. In this position, the top end of the protective tube will be located slightly below the top plate of the furnace when cold and the two will meet in the hot state.
  If the tube stands on the fitting, the chimney effect will cause the entry of false air because it has a sucking effect (local pressures of < 1 atm). But even when the tube is in place, the entry of some false air can not be prevented because the gasket does not keep all air out. An enhanced compression of the gasket will result if the tube end is

rounded mechanically.

- *Gaps in the bellow section*
  The main purpose of the bellow is to prevent the entry of false air to the furnace. But gaps may appear in this section. In the original setup, only three screws were used to keep the gas cover firmly attached to the bottom plate. An additional three screws have been added as it was otherwise not possible to keep the fitting air-tight. We have not experienced any problems in that section since.

As described above, it is not possible to gain complete control of the test-atmosphere at the moment because false air enters the test-zone under the protective tube. As described in Chapter 6, the oxygen-level can only be kept low by maintaining a high N_2-flow rate through the system, a flow that in turn affects the quality of temperature measurements because it introduces a temperature gradient over the test-zone.

Chapter 6
Practical aspects

6.1 Introduction

In the past century, much effort has been put into the measurement and modelling of the viscosity of silicate melts as a function of temperature, composition and atmosphere, but the work has been focussed on the narrow composition intervals of interest to each investigator. Whenever an ash composition falls outside these intervals, the accuracy of the existing mathematical models decreases strongly. The mathematical modelling of deposit formation is, however, affected by the lack of generally applicable data on the viscosity of ashes from coals and biomass of varying origin and composition.

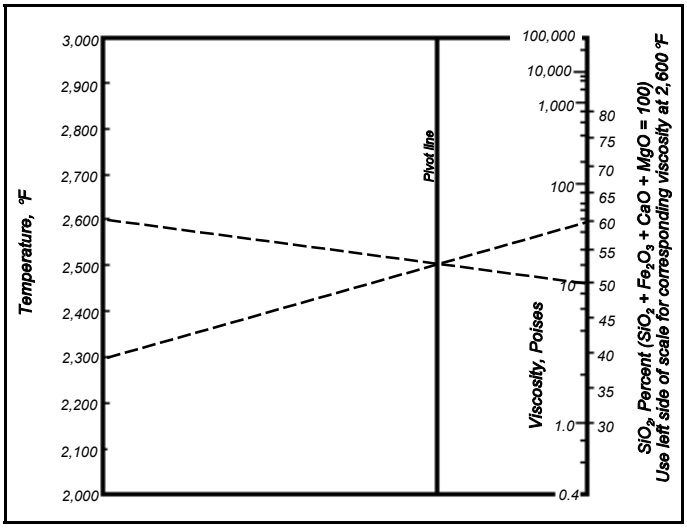

Figure 6.1 Nomogram suggested by Reid and Cohen in 1944 for the prediction of the viscosity of coal ash slags (Reproduced by permission of the publisher).[53] A detailed description of the nomogram can be found in Appendix A.

The introduction of straw for heat and power production poses great challenges on the Danish energy consortia. Straw differs strongly from coal in chemical and physical composition, and it contains high levels of chlorine. The viscous behaviour of ash compositions like those that arise from the co-combustion of straw with coal has not been studied in the past, but a high-temperature viscometer has been bought for the investigation of these ashes, see Chapter 4.

6.2 Viscometer

As described in Chapter 4, at the time when we decided to buy a high-temperature viscometer, the only product in the marked was the TP 1700, RV 20 from the German company Haake. A unit was bought in faith that a tested setup would be relatively easily to run in. We were to become wiser, and that is the subject of this chapter: To share some of our acquired skills in hope that this will be of help to other scientists in similar situations. A detailed description of the apparatus can be found in Chapter 5.

6.3 Sensor material

The sensor is the only part of the apparatus that is in direct contact with the ash melt. For a concentric cylinders viscometer, the sensor is composed of a crucible and a spindle.

The sensor material should be chosen with great care in order to optimise test conditions. A single material can not be pointed out as being the best choice in all conditions, it is a trade-off situation.

Basically, there are three alternatives: Graphite, platinum and molybdenum. Other materials such as porcelain and alumina, Al_2O_3, do not comply with standards such as shape stability and resistance to the chemically very aggressive oxide melts that result from the heating of ashes.

6.3.1 Graphite

Graphite is often chosen as a sensor material due to the cost efficiency of the material. The price that is payed is a deterioration in measurement accuracy since graphite is attacked by the oxide melt.

Cost:	The most cost-efficient material.
Atmosphere:	Can be used in non-oxidising environments only, as it will otherwise burn up.
Temperature:	Can be used even at high temperature.
Interactions with melt:	Graphite has a highly reducing effect on oxide melts, which leads to the reduction of iron oxide to metallic iron, especially if oxygen is present in the atmosphere, because it will advance the process.
	Graphite slowly dissolves in the melt, and concentrations up to a few percent can be found at the end of a test-run.

According to a data sheet from the German producer of equipment for thermal analysis, Netzsch, a series of conditions should be avoided when using graphite-crucibles. Examples relevant to this subject are molten metals, sulphur and SO_3 and nitrous gases (NO, NO_2).[49]

6.3.2 Platinum

Platinum should be alloyed with rhodium to improve the strength characteristics of the metal, but a side-effect is an increased brittleness. $Pt_{90}Rh_{10}$ is often used for historical reasons, but $Pt_{80}Rh_{20}$ is even harder, hence this is the material used by us.

Cost:	Both platinum and rhodium are very high-priced ($Pt_{80}Rh_{20}$: EUR 15/g). Manufacturing is also expensive (Cup: EUR 1300, Spindle (⌀ 9 mm): EUR 700)
Atmosphere:	Can be used under oxidising and inert conditions, but not in reducing atmospheres due to alloy formation with free metal, see below.
Temperature:	At temperatures exceeding 1400°C, $Pt_{80}Rh_{20}$ becomes increasingly soft, and even after cooling to room temperature, the spindle is prone to deformation. Fig 6.2 shows the fracture of a spindle that had been exposed to a maximum temperature of 1460°C and a maximum viscosity of 2000 Pa·s. The rotation of the softened material resulted in a twisted cross-section, and finally fracture.
Interactions with melt:	Pt is very stable under non-reducing conditions, and it will not interact with the melt. Residual carbon in the ash will reduce iron to free iron. The iron in turn will alloy with the platinum to form regions of relatively low-melting composition, and hence cause pit-corrosion of the crucible (Figs 6.3 and 6.4).

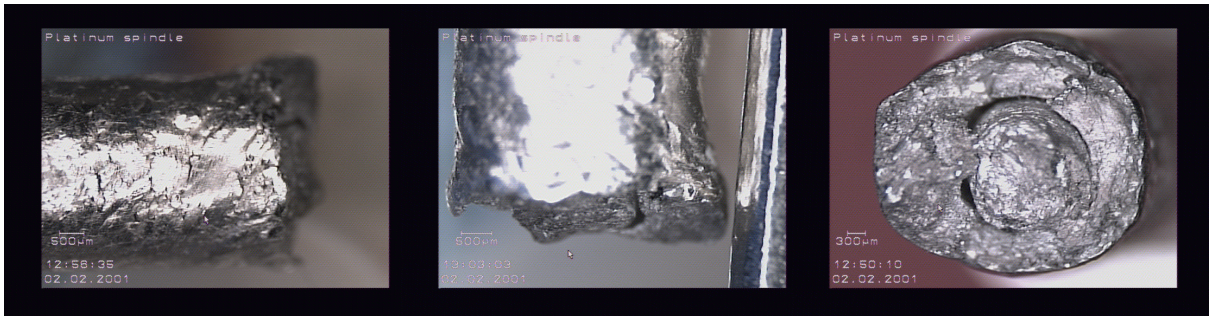

A Side view, focussed on surface. **B** Side view focussed on fracture. **C** End view.

Figure 6.2 Spindle fracture after heating to 1460°C (10 Pa·s), cooling to 1000°C (2000 Pa·s) and subsequent reheating to 1350°C where the fracture happened. The spindle had at that time been rotating at a slow rate for Approx. 24 h.

According to Netzsch, a series of conditions should be avoided when using platinum-crucibles. Some of these are, reducing atmospheres, a series of metals incl Fe, K, Na, Si (alloy formation), HCl with an oxidizing agent, halogens, KCl, NaCl, $MgCl_2$, alkali carbonates and alkali sulphates.[49]

Figure 6.3 Pit corrosion of a platinum crucible exposed to 1600°C in air with an ash melt containing 3% Fe_2O_3 and residual carbon.

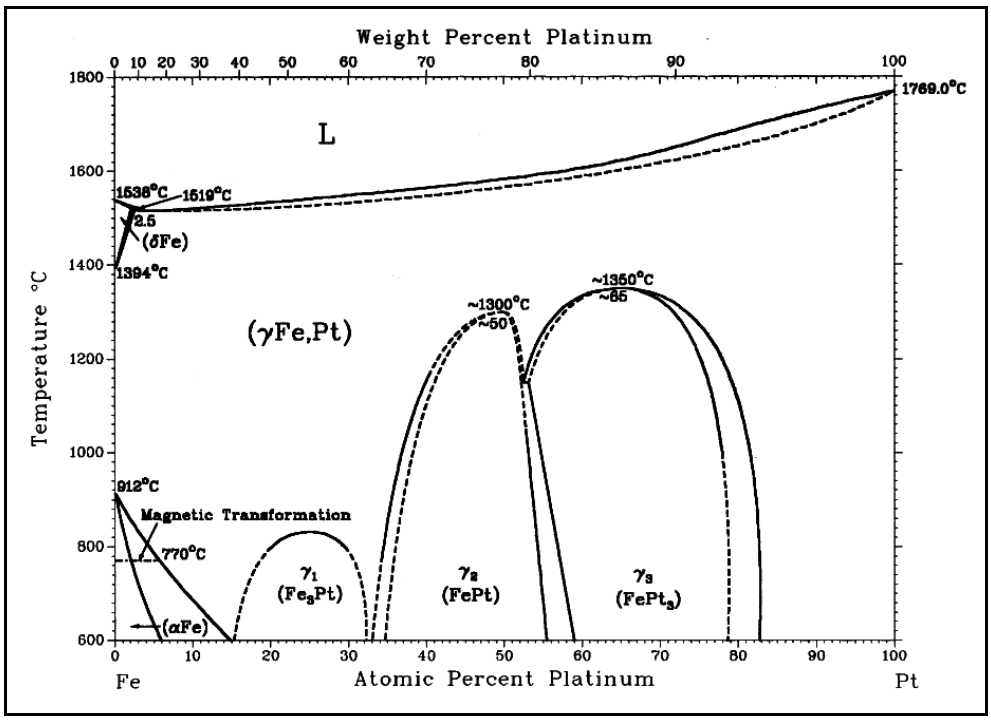

Figure 6.4 Fe-Pt Phase diagram, Reproduced from *Binary Alloy Phase Diagrams, 2nd edition* by permission of ASM International. Please refer to a textbook on the subject for at description of the use of phase diagrams.

6.3.3 Molybdenum[50]

Cost:	Molybdenum is quite expensive, but much cheaper than platinum. Approximate material price: Cup: EUR 50, spindle (⌀ 15 mm): EUR 35.		
Atmosphere:	Air, O_2:	T > 400°C:	Oxidation to MoO_3
		T > 600°C:	Sublimation
	Ammonia:	T > 1100°C:	Nitriding possible
	CO_2:	T > 1200°C:	Oxidation
	CO:	T > 1400°C:	Oxidation
	Hydrocarbons:	T > 1100°C:	Carburation
	H_2, dry (≤ 0.5 g H_2O/Nm^3):		Stable
	H_2, moist (≥ 0.6 g H_2O/Nm^3):	T > 1400°C:	Oxidation / reduction with ablation in the hot regions and deposition in the cold regions
	N_2:		Stable
	Noble gasses:		Stable
Temperature:	No softening observed at 1700°C		

Interactions with melt:	Molten glass	T < 1700°C:	Stable
	Molten iron		Unstable (over months)
	Boron:	T > 1600°C:	Boride formation
	Carbon:	T > 1100°C:	Carbide formation
	Phosphorus:	T < 2000°C:	No reaction
	Sulphur:	T > 440°C:	Sulphide formation
	Chlorine:	T > 450°C:	Unstable

Even low concentrations of oxygen will cause oxidation of molybdenum, and to some extent the resulting oxide will mix with the molten ash and cause progressive pollution of the melt on a ppm level. The expected lifetime of a molybdenum sensor is limited to a maximum of some 10 measurements, depending on factors such as oxygen concentration, temperature and measurement time.

Molybdenum can be bought in sticks and shaped by a well-equipped workshop. But it is not very workable and a list of concerns should be kept in mind. The experience of our workshop is presented below.

Molybdenum is shape stable during mechanical handling, it neither shrinks nor grows. When turned, it is soft and even more ductile than copper; but unlike most ductile materials it produces short turnings. When turned, it wears down the cutting edge some 25 times faster than stainless steel - after just two turnings, the roll is gone. Molybdenum has a very loose texture and it tends to get torn. It is like working stainless steel with a broken cutting edge. A smooth surface is best made using a turning velocity 30-40 times higher than would be used with stainless steel; but the rate of feed should be kept low (approx 50 mm/min).

The use of a cooling medium greatly facilitates turning. Water is the best choice at high turning velocities and oil at low. However, the metal surface appears to suck up the liquid, and residual oil will cause smoke production upon heating. It is thus a good idea to remove the last turning without cooling.

The workability of molybdenum is not affected by the thickness of the turnings. It wears down the cutting edge to remove all excess material with thin turnings, but on the other hand it is not possible to produce a smooth surface with thick turnings because the tendency towards fretting is enhanced. On the other hand, polishing with a cloth is very profitable.

Drilling is more difficult than turning. When drilled, the material feels hard instead of soft, a bit like cast iron, just softer. It is difficult to remove the turnings and the driller burns up fast.

The addition of just a droplet of drilling oil or water facilitates the job.

6.4 Calibration

Sensors can be calibrated in oil, at room temperature, and/or in glass at elevated temperatures. The latter is the most time consuming but also the most accurate method due to the temperature level used. A deviation in the range of 50% is observed if the two methods are compared, ie determination of instrument constants in standard oil and subsequent verification in standard glass (Fig 6.5). So, unfortunately the calibrations in standard oil can only be used to compare sensors of identical dimensions and material and to detect deformations. Apparatus calibration should be carried out in standard glass only.

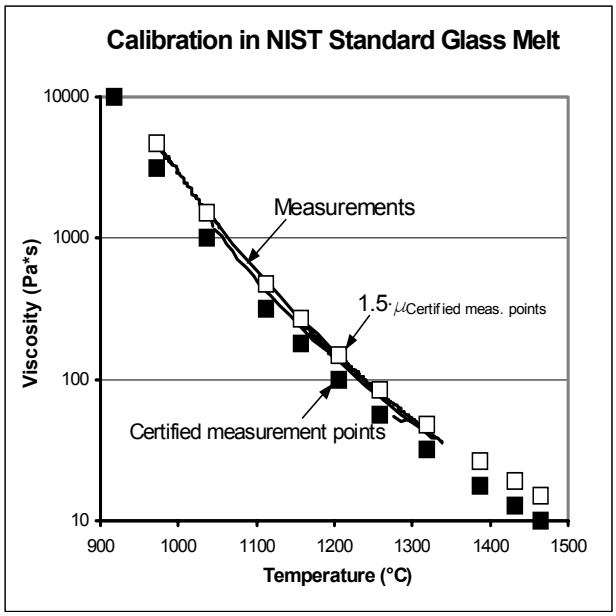

Figure 6.5 Reproduction of the certified measurement points of the NIST standard glass SRM 710a, soda-lime-silica, with sensors calibrated in standard oil at 20°C.

6.4.1 Standard oil

The standard oil should have a viscosity in the range of interest, but the oil should not be too viscous since this complicates the pouring into and out of the crucible. A choice of approx 20 Pa·s seems adequate.

Standard oils are very temperature sensitive. The 20 000 AW standard oil from the German Institute of Calibration (Deutscher Kalibrierdienst) varies 10% in viscosity for a temperature change of just 1°C.

Calibration in a standard oil should be carried out in a thermostated bath. The first step is to obtain the desired temperature inside the crucible. For that purpose, a thin thermocouple is inserted into the crucible so that the measurement point is placed at the level of the spindle head. The thermocouple should be placed against the crucible wall in order to avoid unnecessary interference with the spindle. The spindle is then set to rotate at a slow rate (approx 25 rpm depending on sensor dimensions) to ensure thermal equilibrium but avoiding frictional heating of the oil. The bath temperature can now be adjusted to give the desired oil temperature.

Once the temperature is set, the thermocouple can be removed, and a slow rotational speed

ramp can be made. This ramp will be linear for slow speeds, but it will deviate from linearity at high speeds, and thus it will indicate the rotational speed at which frictional heating starts influencing the measurements.

The result of this manoeuvre will not only be a calibration of the sensor but it will also give an indication of a good choice of rotational speed for the measurement. The latter will most probably result in a trade-off situation between frictional heating and the mechanical advantages of a high rotational speed, see below.

6.4.2 Standard glass

A standard glass is used for sensor calibration. A speed ramp identical to the one described for the standard oil is used at a melt temperature for which the viscosity is known. Subsequently, it should be possible to reproduce the other certified measurement points. If this is not the case, a variety of possible reasons can be investigated:

- Is the spindle head completely submerged in the test liquid?
- Is the spindle properly centred?
- Is the rotational speed adequate?
- Is the flow laminar?
- Are the instrument constants correct or should the sensor be tested in a standard oil?
- Is the temperature reading correct?

6.5 Sensor cleaning

Both standard glass and ash melts tend to stick to the sides of the crucibles and spindles. The following two methods are known to do the job of cleaning.

- Concentrated HF is nasty but effective. It dissolves the silicon matrix and leaves the glass with a spongy consistence. But it should be handled with great care.

- Another more delicate way of cleaning platinum crucibles is to heat up the crucible with some Na_2CO_3 (if too much is used, the platinum is attacked) to 1180°C and leave it to react for approx 10 minutes. Then the melt is poured out and the crucible is cooled in water. It is now possible to remove much of the residual melt with a brush and hot water. The last melt is removed by leaving the crucible in diluted H_3PO_4 (1:5) and placing it in a ultrasound bath for a couple of hours.
- Alternatively 5 g $Li_2B_4O_7$ can be used per gram of melt, two different heating stages have been proposed, either 950°C or 1200 - 1300°C for 15 min, and complete cleaning in HCl or HNO_3.

6.6 Rotational speed

Some care should be taken in the choice of rotational speed. An inadequate choice will affect the quality of the measurements or even the measurability of some samples.

6.6.1 Measurement accuracy

If a rotational speed near the capacity limits of the viscometer is chosen, the accuracy of measurements is affected. The applied torque should not be less than 5% of the measurement range.

6.6.2 Self centring

A general point of concern with a high-temperature viscometer is the length of the spindle. A long spindle is more unstable than a short spindle. A high rotational speed will be an advantage for the self-centring of the spindle.

6.6.3 Frictional heating

Excessive rotational speeds cause frictional heating of the test liquid, as can be visualised in Fig 6.6 where the graphs deviate from linearity at high rotational speeds (pronounced at %D > 20), and they should therefore be avoided.

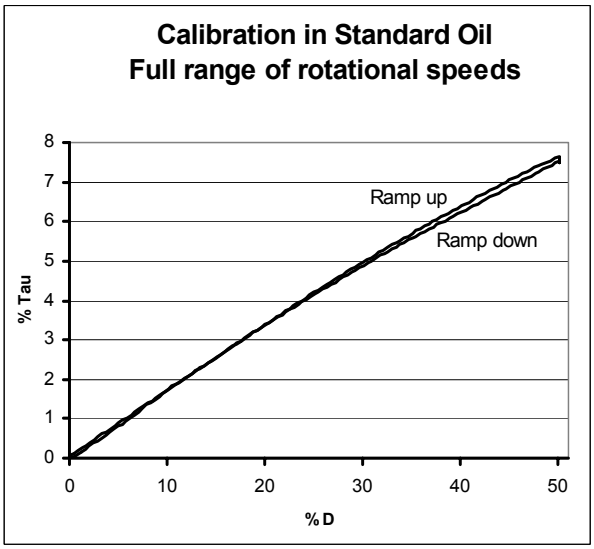

A Full range of rotational speeds.

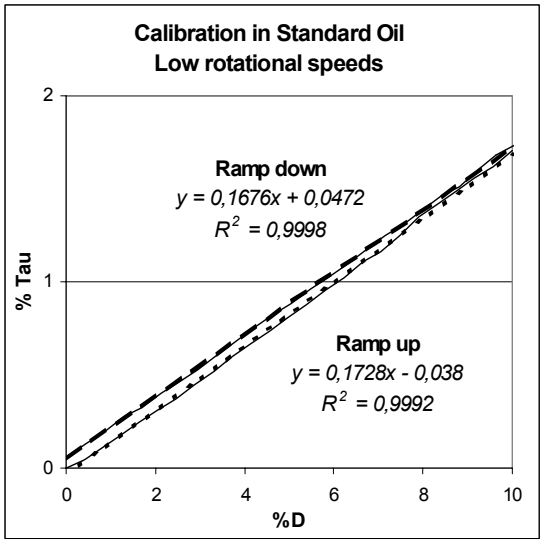

B Low rotational speeds.

Figure 6.6 Viscosity vs rotational speed for the20 000 AW standard oil from Deutscher Kalibrierdienst.

6.7 Gas flow

The use of graphite or molybdenum sensors demands a flow of a non-oxidising gas, eg N_2. This flow will in turn affect the measurements. The effect of gas flow rate on the measured temperature and the melt temperature has been tested for the Haake ME 1700 with the setup

shown in Fig 6.7. The oxygen concentration is measured near the crucible and temperature is measured both under the crucible, T_{bottom}, and in the melt, T_{top}.

Fig 6.8 shows the results of the test run. The concentration of oxygen in the furnace decreases strongly with increasing nitrogen flow, but an uncertainty is introduced in the temperature measurement at high gas flows.
Due to an inevitable leakage in the ME 1700, a substantial gas flow rate is needed to keep the oxygen-level low when using molybdenum sensors. Any oxygen present in the test zone will attack the molybdenum, but the rate of attack can be kept low with a high nitrogen flow rate. At such high flow rates, an underestimation of approx 20°C is introduced in the temperature reading.The divergence in the temperature reading will cause a measurement error of some 50% depending on the characteristics of the test melt.

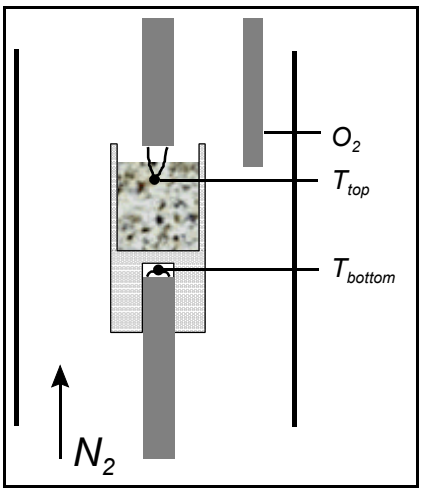

Figure 6.7 Setup used for simultaneous measurements of Tempera-ture under cup, T_{bottom}, temperature in glass melt, T_{top}, and oxygen concentration in the furnace for the Haake ME 1700.

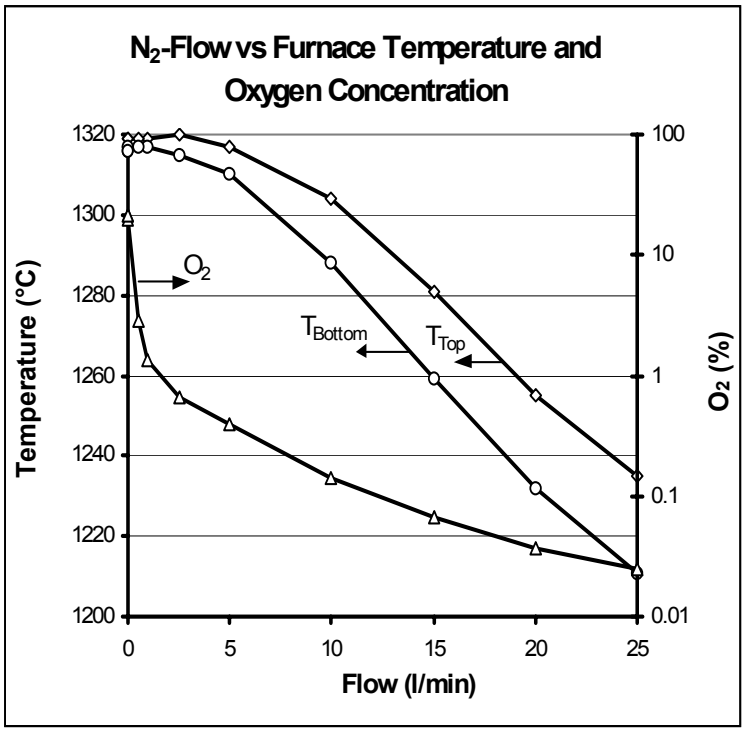

Figure 6.8 Nitrogen flow vs Temperature under cup, T_{bottom}, temperature in glass melt, T_{top}, and oxygen concentration in the furnace measured near the crucible for the Haake ME 1700.

6.8 Ash pretreatment

The ash demands pretreatment before the measurement crucible can be filled with test material.

- Washing is needed if the ashes contain salts as do ashes from co-combustion with straw or pure straw combustion. The salts can be damaging to the sensor material and cause boil-up.
- Residual carbon can not be avoided for any solid fuel ashes. If present, it will cause --

boil-up of the ash upon heating, and reduction of the resulting melt.

- The density of fly ash is very low, and it thus shrinks considerably upon melting. This will call for numerous re-fillings of the crucible if pre-melting is bypassed.

In summary, a maximum of three pre-treatments are needed for each test sample.

6.8.1 Washing

Danish wheat straw contains potassium, chlorine and sulphur that evaporate during combustion and re-condense on the fly ash particles upon cooling. The result is a salt layer on the fly ash particles consisting mainly of KCl and K_2SO_4. If the straw is co-fired with coal, other elements are introduced such as calcium and maybe sodium. This in turn will result in the formation of salts such as $CaSO_4$, Na_2SO_4 and NaCl.

Viscosity measurements on fly ash melts are only useful if the conditions experienced by the particles in the hot-zone of the combustor can be reproduced, because this is the only location where the particles are heated to temperatures high enough for softening of the silicate-matrix to occur.

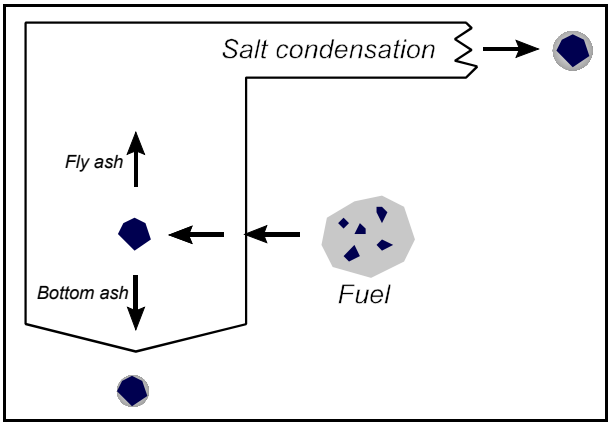

Figure 6.9 Schematic representation of the fate of fuel ash in a pulverised fuel combustion system.

The alkali-containing salt layer on the fly ash particles will interfere with the experiment if it is not removed prior to heating. Washing in water partly removes alkali salts, but $CaSO_4$ has a low solubility in water. The sulphur that is bound to calcium will vaporise upon pre-melting due to thermal decomposition.

The procedure that we have followed for washing is: repeated dissolutions in boiling, ultra-clean water (pH = 4), stirring, sedimentation and centrifuging if necessary and decantation. The decanted liquid is filtrated (pore-size 0.45 μm), and the material on the filter is re-fed to the ash. After 4 - 6 repetitions, the wash water is analysed for K, Na and Ca by ion chromatography, and the result is used to decide if more washing is needed. After washing, the ash is dried at 105°C for 24 h. A later analysis of anions in the wash water gives an idea of the composition of the salts that were washed out.

6.8.2 Combustion of residual carbon

Complete combustion is often not practically obtainable, minor amounts of residual carbon will be found in the ash. This carbon will burn upon heat-up of the ash, and if the container is tall like the crucibles for viscosity-testing, this will result in the entrapment of gas-bubbles

(especially if the ash starts to melt). Eventually the ash will expand out of the crucible and stain the surroundings.

If all residual carbon is not removed prior to melting, it will reduce any iron present in the ash. The reduction will probably follow a reaction scheme like the one proposed by Bryant et al. (2000):[51]

$$FeO_{(l)} + C_{(s)} \rightarrow Fe_{(l)} + CO_{(g)}$$

If a platinum crucible is used, the free iron will cause corrosion of the platinum because areas of low-melting Pt-Fe alloy are formed, see Figs 6.3 and 6.4.

Residual carbon can be burnt-off in a furnace at 900°C where no other species will leave the system. At higher temperatures, the ash may partly start to melt. Shallow porcelain dishes can be used to ensure a large sample surface. A slow air flow over the crucible will speed up the process, but the temperature should be kept high for some hours depending on the ash characteristics and the experimental conditions.

6.8.3 Pre-melting

Ashes should be pre-melted because the melt is Approx 10 times more dense than the ash, so a large volume of ash is needed to produce the necessary sample-volume for a viscosity measurement (20 ml, 50 g). It is a good idea to cover the crucible with a lid to avoid staining of the furnace surroundings caused by unsuspected boil-up of the ash. Melting directly in the test-crucible demands repeated re-fillings of the crucible as the material melts.

The choice of crucible material comes into question for this pre-treatment as well as for the measurement stage. Platinum crucibles can be used in air, which is very convenient if the pre-melt furnace is not air-tight. But the crucibles soften at high temperatures, and the lid comes to behave like a sticky sheet of paper. Molybdenum can only be used if the furnace enables atmosphere control.

The pre-melt furnace must be big enough to hold a crucible that can contain the necessary sample size. It must also be able to reach a top-temperature of at least 1600°C, since many ashes are very viscous at lower temperatures, and thus do not homogenise at an acceptable rate. A chamber furnace can hold large items and the crucible can be removed quite fast, ie the glass does not have time to cool down. This latter point is rather important as will be made clear in the next paragraph. But the heating elements are generally unprotected in a chamber furnace, and this is unwise when working with ashes. A tube furnace can be fitted with an inner tube that protects the heating elements and enables atmosphere control; and things can be pulled out of a tube furnace in a matter of seconds. But the round dimensions

pose limitations on the shape of the pre-melt crucible.

A major concern with pre-melting is to get the sample out of the crucible in which it was melted. If the ash has a low viscosity, it can be poured out of the crucible; and if the melt solidifies before it has been removed completely, it can just be re-heated. If, on the other hand, the ash is relatively viscous (for instance of a consistency like chewing gum), it can be a tedious task to get the melt out of the crucible.

The ash can be poured out onto a brass plate or into a large bucket of water. The result of the first procedure will be a large lump of glass whereas the latter will result in a granulate that can easily be filled into the viscometer crucible.

6.9 Measurement procedure

The furnace is heated to a temperature for which the test glass is completely liquid. This enables the entry of the spindle head into the melt. It is important that the spindle head is completely submerged into the melt.

Radiation from the furnace will eventually cause overheating of the viscometer. Thus the holder arm should be cooled with 5°C cooling water through the fittings on the back of the arm. Overheating of the viscometer results in an unstable output from the device.

The rotational speed of the spindle is adjusted to keep the torque above 5% of the total measurement range.

The TP 1700 is programmed to give a desired test run, and the computer is programmed to start with a slow velocity ramp to the end rotational velocity (1 - 2 h), then it will keep this velocity for as long as the program runs, and it will end with a velocity ramp down to 0 s^{-1}. If a large temperature interval is covered in the test run, it may be a good idea to change to a lower rotational speed for lower temperatures. An example of such a procedure is described in Chapter 7 for a measurement series.

Optimal operation of the viscometer is invariably a product of experience. Whether or not to use temperature ramps or steps and whether or not to vary the rotational speed of the spindle are questions that can not be answered. However the following guidelines should be followed:

- If possible, avoid torques under 5% of the total measurement range.
- Make sure that the melt has reached isothermal conditions before the measurement is registered, ie test for stable reading.

- Test for Newtonian behaviour by varying the rotational speed, in particular at high viscosities where crystallisation can occur.

It is a good idea to follow the decreasing temperature ramp with a similar increasing ramp either in the same test run or just after. This will result in an end-temperature at which the melt has a low viscosity that will enable the lifting of the spindle from the melt.

6.9.1 Reproduction of measurement

The reproducibility of measurements should be tested on a regular basis by two separate methods:

- Same pre-melting batch - Parallel measurement runs
- Different pre-melting batches - Parallel measurement runs

On the basis of such tests the measurement reproducibility should be estimated. Notice should be taken that the reproducibility may vary with composition. In addition, reproducibility will probably be lower for samples taken from power plants than for pure, lab-mixed oxide melts.

6.10 Summary

In this chapter, different practical aspects of the measuring of silicate melt viscosities in general and ash melt viscosities in particular have been described.

The choice of sensor material is a trade-off between the inertness and softness of $Pt_{80}Rh_{20}$ and the hardness and O_2-intolerance of molybdenum. The use of graphite or ceramic material for sensors is not advisable. Viscometers using concentric cylinders should be calibrated in standard glass, but a standard oil can be useful for detecting changes in sensor dimensions. Measurements should be conducted with as low a rotational speed as allowed by the limitations in the apparatus accuracy. Whenever a gas flow is used, the implications on measurement uncertainty should be investigated. Temperature deviations in the range of 20°C are very possible.

Fly ashes from the thermal conversion of straw will have a high salt-content. The salts can be washed out in water. Ashes from the combustion of any solid fuel contain residual carbon. This can be burnt off at 900°C. The last stage in ash pretreatment is an advisable pre-melting of the ash in a large separate crucible.

Care should be taken to reproduce measurements on a regular basis. Both from the same pre-melted batch, and from parallel pre-melting batches.

Chapter 7
Measurements

7.1 Introduction

Chapter 6 gives a generalised description of the calibration procedure and ash pretreatment. This chapter describes the concrete procedure used to calibrate platinum sensors as well as the pretreatment given to an ash and the following viscosity measurement routine. At the end of the chapter, the measurements are compared with modelled temperature - viscosity relationships.

7.2 Temperature reading

The thermocouples have been calibrated at the temperatures 900, 1100, 1300, 1500 and 1650°C at the Risø National Laboratory in Denmark. According to the certificate, the thermocouples have a slight tendency towards overestimating temperature in the range 1 - 3°C, with the highest deviation at 1300°C.

According to the gas flow rate test described in Chapter 6, there is no notable temperature difference between the melt and the test position under the cup when no gas flow is used, so the total uncertainty on the temperature is thus that of the thermocouple.

7.3 Calibration

The $Pt_{80}Rh_{20}$-sensors all have identical dimensions, so the calibration of one sensor can be generally used for all sensors of the same type (dimensions and material).

Calibration was carried out in a standard glass from the American National Institute of Standards and Technology (NIST). It is a soda - lime - silica glass with 11 certified measurement points, four of which are listed in Table 7.1.

Table 7.1 Certified measurement points for the standard reference material 710a (soda-lime-silica) from NIST.

Log_{10} Viscosity (Pa·s)	1.00 ± 0.015	2.00 ± 0.008	3.00 ± 0.11	4.00 ± 0.016
Temperature (°C)	1464	1205	1037	918

Three measurement runs were made in the same batch of glass. Each measurement run was initiated with a 1 hour ramp to the final rotational speed, and this ramp was used to determine if the zero-adjustment should be corrected. The software conducts its own zero-adjustment at the beginning of each test run, but ideally this should be done with the clean spindle hanging freely in the air above the melt. Because the measurement runs were performed on the same test sample, the spindle would be covered with glass if lifted out of the melt, so instead it was just left in the melt during zero-adjustment, and thus the result could not be relied. Nevertheless, it was only for the last test run that zero-correction was necessary, as shown in Fig 7.1. As a result of the zero-correction, all %Tau readings of this test run were corrected: $\%Tau_{correct} = \%Tau_{reading} - 0.1199$.

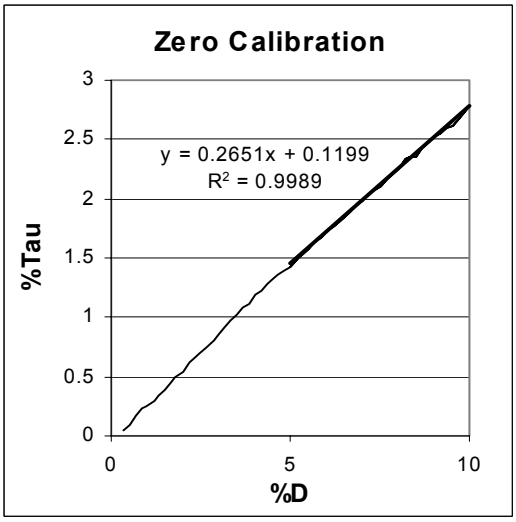

Figure 7.1 Determination of zero-correction on %Tau-values for test run # 3.

The corrected measurement values were used to calculate a viscosity estimate according to the procedure outlined in Chapter 5:

$$\eta_{est} = A_{est} \cdot \frac{\%Tau}{\%D} \quad , \quad M = 1 \tag{7.1}$$

The resulting estimated viscosity graph was compared with the certified values from Table 7.1, and the result is given in Fig 7.2.

Generally spoken, spindle heads with small diameter are used for the measurement of high viscosities and visa versa because in this way the measurement limits of the viscometer are shifted. When a smaller spindle head is applied, the force needed to rotate the spindle at a given speed in a fluid with a given viscosity decreases, all other things equal.

Because of the relatively small diameter of the $Pt_{80}Rh_{20}$ spindle head, it was chosen to put most weight on the high viscosities, ie the certified points actually used for the calibration were those with viscosities around

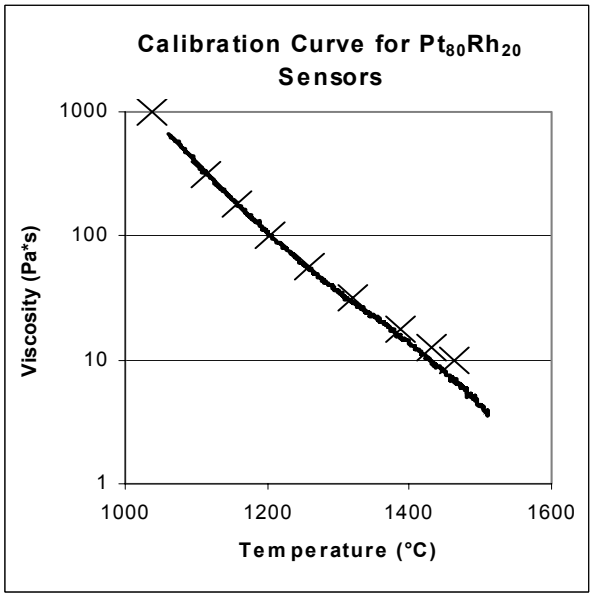

Figure 7.2 Best calibration fit for Pt_{80} Rh_{20} sensor in NIST standard glass. (A , M) = (84 , 1)

100 Pa·s (Fig 7.2). The way the measured graph starts to deviate from the certified points at higher temperatures can very well be explained by the fact that the applied torques in the measurement series 1350°C - 1510°C were in the range 0.5 - 2.7 %Tau, ie less than the suggested 5% of the total measurement range, even though a high rotational speed of 50 rpm was used. A higher rotational speed was not an option, since it would cause frictional heating of the melt sample.

On basis of Eq 7.1 and Fig 7.2, the apparatus constants for the $Pt_{80}Rh_{20}$ sensors are: A = 84 Pa·s and M= 1.

7.4 Ash description

The test ash was the result of a test run where 75% hard coal and 25% Danish wheat straw were combusted in a 0.5 MW_{th} down-fired pilot scale combustor at the Institut für Verfahrenstechnik und Dampfkesselwesen, IVD (Institute of process Engineering and Power Plant Technology) of the University of Stuttgart, Germany. The ash was received as a part of a current EU Joule project on the *Prediction of Ash and Deposit Formation for Biomass Co-combustion* under contract no. JOR3-CT98-0198. The ash analysis that was supplied with the sample is listed in Table 7.2.

Table 7.2 Ash analysis for test sample, supplied by IVD. A.R. = As received.

Cl % A.R.	**N % A.R.**	**C % A.R.**	**S % A.R.**	**H % A.R.**	**Moisture % A.R.**	**Volatiles % A.R.**	**Ash % A.R.**	**Fixed C % A.R.**
0.23	0.09	3.98	1.13	0.21	1.01	5.84	92.58	0.58
SiO_2	**Al_2O_3**	**Fe_2O_3**	**MgO**	**CaO**	**Na_2O**	**K_2O**	**TiO_2**	**P_2O_5**
65.6	9.9	5.0	1.7	5.3	0.3	6.3	0.4	1.2

7.5 Ash pretreatment

According to the ash analysis in Table 7.2, the ash contains 0.23% chlorine and 4.56% residual carbon along with other volatile species, so both washing and carbon burn-off are compulsory pretreatments.

7.5.1 Washing

The ash was washed six times in ultra-clean water. According to ion chromatography, practically all KCl was removed by this procedure, see Fig 7.3. Minor amounts of calcium and sodium were also removed, probably bound up as $CaSO_4$ and NaCl, but these

concentrations were much smaller than those of KCl. The removal of NaCl is a desired effect whereas the loss of calcium is an undesired side-effect that will probably cause a minor shift towards higher viscosities for the resulting ash melt as compared to the desired ash melt composition.

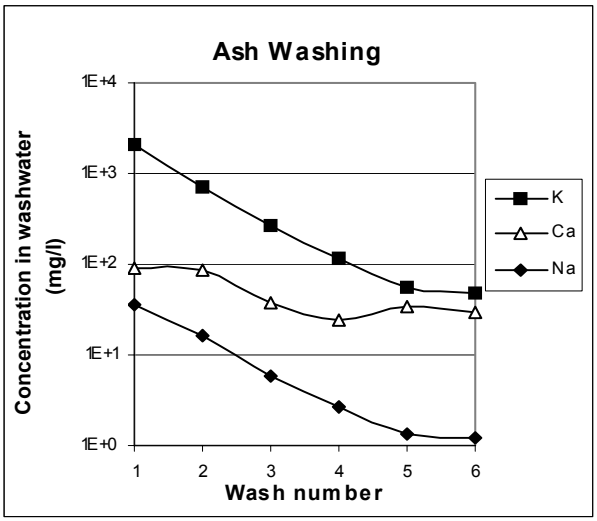

Figure 7.3 Cation concentrations in wash water.

7.5.2 Carbon burn-off

The ash was placed in small rectangular porcelain dishes, that were pushed into a tube furnace. The furnace was then heated to 900°C for 5 hours, and after cooling to approx 250°C, the dishes were removed, and the ash collected in a container. The procedure was repeated until all ash had been treated.

Weighing of the dishes with ash prior to and after heat treatment showed a mass loss of 6.5%. This result can not be directly compared with Table 7.2 since the ash has been washed.

7.5.3 Melting

Due to the fact that there was no furnace available for pre-melting, the sample was melted directly into the sensor crucible by approx 25 re-fillings. The ash behaved nicely, no expansion was observed, indicating that all salts and residual carbon had been removed from the ash. As the temperature of the sample increased, the ash would shrink to form a freely standing cone inside the crucible foregoing melting.

7.6 Viscosity measurements

Viscosity was measured in four consecutive runs. This procedure was chosen because the Haake software is not very stable. For no apparent reason, the software sometimes stops sampling in the middle of a measurement run, and it seems to be extremely sensitive to speed ramps. Hence for each measurement series, a ramp up to the final rotational speed is applied, and the rotational speed is then fixed for the rest of the measurement run. Finalising the measurements, a final speed ramp down to zero is programmed, but not always supported by the software.

Due to these technicalities, it is an advantage to break up the desired temperature range into smaller section for which a steady rotational speed can be applied. The velocities that were used for this measurement are stated in Table 7.3.

Table 7.3 Technical data for ash viscosity measurements.

Measurement run #	**1**	**2**	**3**	**4**	**5**
Temperature (°C)	1570 - 1364	1364 - 1305	1315 - 1163	1160 - 1329	1364 - 1564
Rotational speed (rpm)	25	2.5	0.25	0.5	10
% Torque	7 - 100	10 - 24	2 - 34	69 - 3	41 - 3

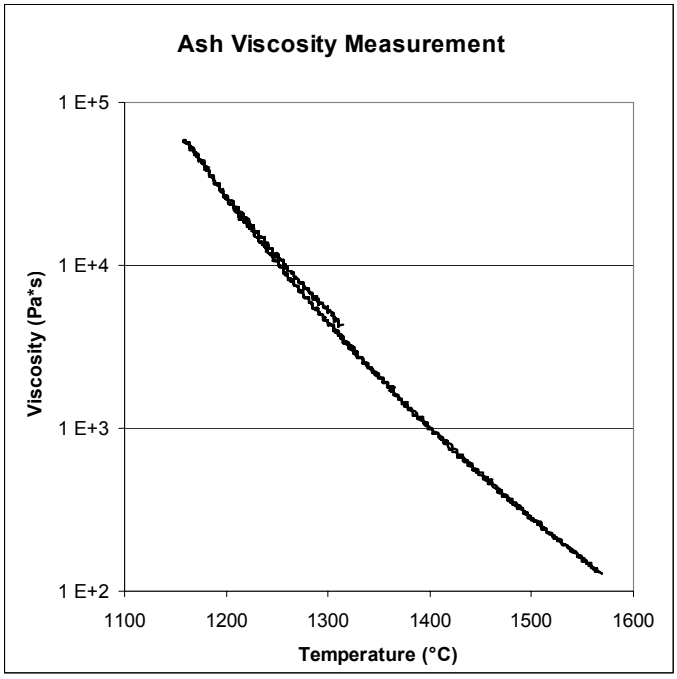

Figure 7.4 Result of Ash viscosity measurements.

The result of the measurements is presented in Fig 7.4. All measurements are in accordance except measurement run # 3 that for unknown reasons overestimates viscosity. Since both measurements performed before and after run # 3 are in accordance, the results of measurement run # 3 will be ruled out. Table 7.4 presents the data in a tabulated form, as they have been extracted directly from the data sets.

Table 7.4 Tabulated data from the individual measurement runs.

Measurement run # 1	**T (°C)**	**Viscosity (Pa·s)**	**Standard Deviation**	**# Points**
	1569	129	3.9	10
	1549	158	2.3	13
	1525	207	1.6	5
	1500	274	2.2	7
	1476	371	4.4	8
	1452	498	8.0	13
	1427	693	7.0	7
	1398	1029	14.1	9
	1373	1439	19.9	9
	1364	1666	4.5	27

Measurement run # 2

T (°C)	Viscosity (Pa·s)	Standard Deviation	# Points
1359	1841	33.9	15
1349	2090	19.6	4
1325	2996	24.7	5
1310	3852	57.3	9

Measurement run # 4

T (°C)	Viscosity (Pa·s)	Standard Deviation	# Points
1163	54639	806.8	11
1173	45531	732.8	12
1197	27457	635.3	15
1227	15974	316.5	14
1251	10232	197.5	15
1276	6607	124.7	15
1300	4452	64.1	11
1325	2981	45.2	13

Measurement run # 5

T (°C)	Viscosity (Pa·s)	Standard Deviation	# Points
1364	1694	23.6	8
1378	1375	27.3	7
1403	985	15.3	6
1427	717	15.2	8
1452	521	8.0	6
1476	383	4.1	4
1500	281	4.3	6
1525	213	1.9	4
1549	161	1.9	4
1564	137	1.1	4

A more useful summary table is found studying closely the graph in Fig 7.4. The result is given in Table 7.5:

Table 7.5 Temperature - vs viscosity. By visual examination of the graphical representation.

Temperature (°C)	1175	1200	1225	1250	1275	1300	1325	1350
Viscosity (Pa·s)	44,000	26,000	16,500	10,500	6,700	4,500	3,025	2,075
Temperature (°C)	1375	1400	1425	1450	1475	1500	1525	1550
Viscosity (Pa·s)	1,425	1,010	725	525	380	280	210	157.5

7.7 Model performances

The mathematical models dated later than 1960 presented in chapter 3 and appendix A for completely molten silicates (Chapter 11, sections 2 and 3), are tested on the studied ash melt below, with the exception of the Streeter model that is not generally applicable. A short summary of the final structure of each model is given in Table 7.6.

Table 7.6 Structure of the temperature-dependence of viscosity in mathematical model. Please refer to chapter 3 and Appendix A for a more comprehensive presentation of the models.

Name	**Year**	**Model structure**
S^2	1963	$\log\eta = 4.468 \cdot 0.84536^2 + \frac{12650}{T} - 8.44$
Watt - Fereday	1963	$\log\eta = \frac{0.5844 \cdot 10^7}{(T-423)^2} - 1.3324$
Bottinga - Weill	1972	$\log\eta = 0.76 \cdot D_{SiO_2} + 0.05 \cdot D_{FeO} + 0.03 \cdot D_{MgO} + 0.05 \cdot D_{CaO} + (0.09 + 0.01) \cdot D_{NaAlO_2} + 0.02 \cdot D_{CaAl_2O_4} - 1$, Table D.1
Shaw	1972	$\log\eta = 1.4682 \cdot \left(\frac{10^4}{T} - 1.5\right) - 3.78$
Lakatos	1972	$\log\eta = -2.7128 + \frac{5730.0}{T - 511.02}$
Urbain	1981	$\eta = 1.24 \cdot 10^{-11} \cdot T \cdot e^{\frac{41.37 \cdot 10^3}{T}}$
Riboud	1981	$\eta = 3.51 \cdot 10^{-10} \cdot T \cdot e^{\frac{32.27 \cdot 10^3}{T}}$
Kalmanovitch - Frank	1984	$\eta = 6.46 \cdot 10^{-12} \cdot T \cdot e^{\frac{41.37 \cdot 10^3}{T}}$
Senior - Srinivasachar	1995	$\log(\frac{\eta}{T}) = -11.66 + \frac{16.84 \cdot 10^3}{T}$, High-temperature region

The models are applied to the studied ash by a re-calculation of the composition in which all chlorine is assumed tied up to potassium as KCl, and sulphur is assumed to leave the system without depleting the melt from any other cation. The resulting composition is listed in Table 7.7.

Table 7.7 Recalculated ash composition minus KCl.

Oxide	Mole-%	Weight-%
SiO_2	75.90	68.78
Al_2O_3	6.75	10.38
Fe_2O_3	2.18	5.24
CaO	6.57	5.56
MgO	2.93	1.78
Na_2O	0.34	0.31
K_2O	4.41	6.26
TiO_2	0.35	0.42
P_2O_5	0.59	1.26

On basis of the recalculated ash composition, it is possible to model the viscosity - temperature relationship, and the result can be found in Fig 7.5. As it is easily visualised, the Urbain model manages a prediction of the measured data that is better than any of the other models.

7.8 Summary

The $Pt_{80}Rh_{20}$ sensor design has been calibrated: (A , M) = (84 , 1). The calibration routine revealed that viscosities below 100 Pa·s should be measured with a sensor spindle with a bigger head diameter.

The test ash was washed and heated to 900°C, whereby practically all chlorine and residual carbon was removed. Subsequently the viscosity - temperature relationship was determined, and tabulated in Table 7.5.

The temperature accuracy has been estimated to ± 3°C. With a tendency towards overestimations.

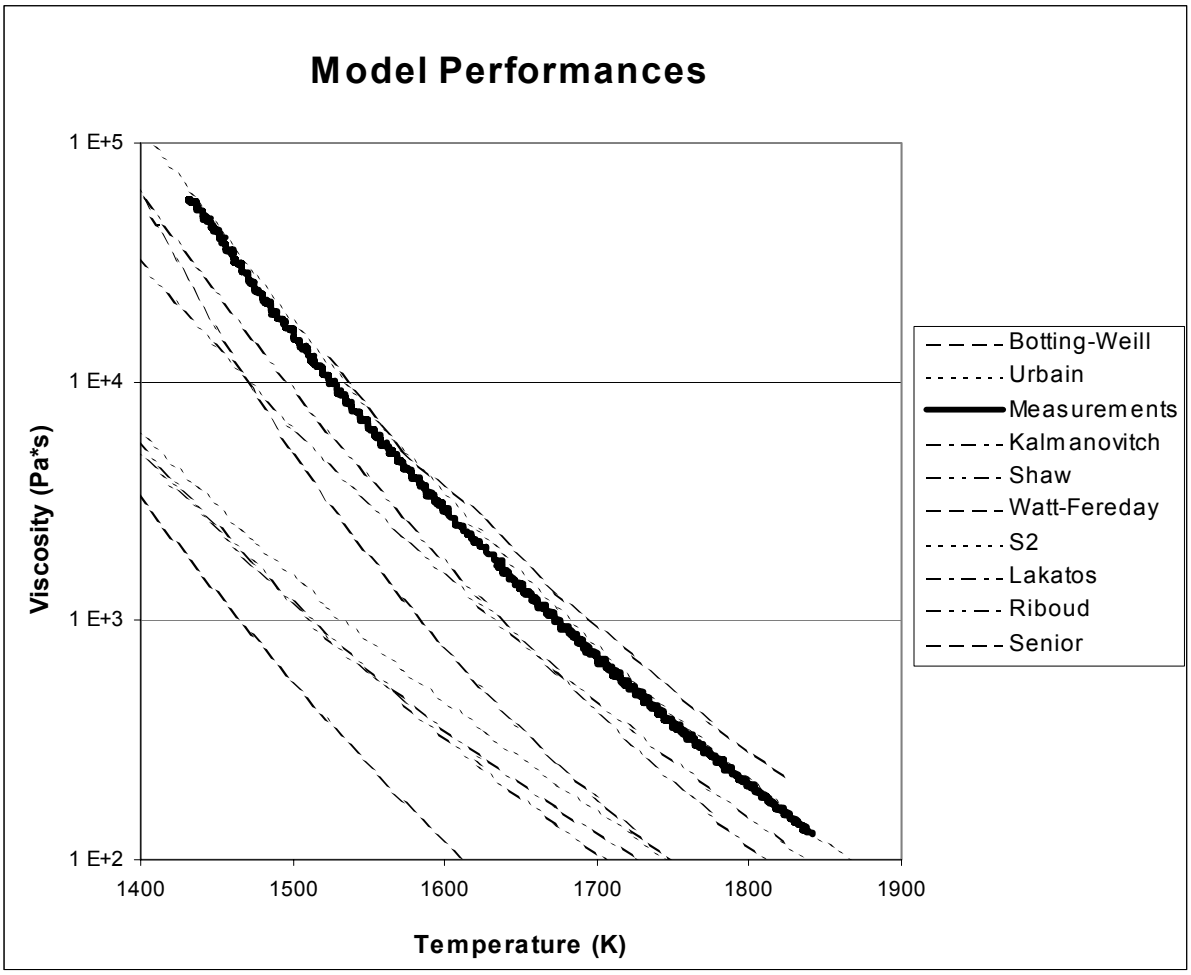

Figure 7.5 Performance of mathematical models on studied ash. The models are listed in the same order as they appear on the chart.

The standard deviations on viscosity lies in the range: $\frac{St.Dev.}{Viscosity} \in [0.003 ; 0.03]$, with an average value of 0.014.

The best viscosity prediction is obtained with the Urbain model.

Chapter 8
Conclusion and further work

8.1 Conclusion

Ash deposits on the heat transfer surfaces are the main reason for unplanned shut-downs of power plants. Not only do they insulate the water and steam on the inside of the tubes from the hot flue gas on the outside (Fig 8.1), but they also cause wear-out of the system. The estimated daily capital loss of the shut-down of a large power plant exceeds EUR 100 000, and the insulating effect of deposits can seriously affect the economy of the plant. Therefore the economic incentive towards minimisation of deposit formation is large.

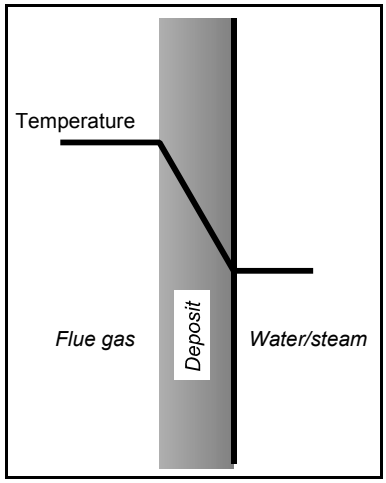

Figure 8.1 Temperature drop through a deposit.

The viscous behaviour of fly ashes strongly affects the tendency towards deposit formation and deposit sintering, so the predictability of ash viscosity as a function of composition and temperature is a point of strong interest. However, the experimental determination of the viscosity of high-temperature melts is difficult, and only limited compositional ranges have been studied thoroughly. Mathematical models exist for some of these compositional ranges, but they should only be applied for ashes that fall outside these ranges with the greatest of care.

The experimental results are listed in tables by publication year and author as well as in tables by composition with the most simple systems first. All melts contain SiO_2, but the other oxides present are listed below. "+" = SiO_2, These oxides PLUS one of the oxides listed in the parenthesis, separated by ",".

- Binary: Al_2O_3, FeO_x, CaO, MgO, Na_2O, K_2O, Li_2O, MnO
- Ternary: Al_2O_3 + (CaO, MgO, Na_2O, K_2O, MnO)
  FeO_x + (CaO, MgO, Na_2O, K_2O)
  CaO + (MgO, Na_2O, MnO, TiO_2)
  MgO + Na_2O
  Na_2O + (K_2O, TiO_2)
  K_2O + TiO_2
- Quaternary: Al_2O_3 + FeO_x + (CaO, Na_2O)
  Al_2O_3 + CaO + (MgO, Na_2O, MnO, TiO_2, $CaCl_2$, $MgCl_2$, $NaCl$)

FeO_x + CaO + MgO

- Quinternary: Al_2O_3 + FeO_x + CaO + MgO
  Al_2O_3 + CaO + MgO + Na_2O
- Sexternary: Al_2O_3 + CaO + MgO + Na_2O + K_2O

- Multi-component: Only major components cited, ie mole fractions > 5%

  Al_2O_3, CaO, Na_2O
  Al_2O_3 + (FeO_x, CaO, Na_2O,)
  FeO_x + MgO
  CaO + (MgO, Na_2O)
  MgO + Na_2O
  Na_2O + B_2O_3
  Al_2O_3 + FeO_x + CaO
  Al_2O_3 + CaO + (MgO, Na_2O)
  Al_2O_3 + CaO + Na_2O + K_2O

The temperature intervals covered by each measurement series varies from 600 K to as much as 3000 K for pure SiO_2, and different measurement methods have been applied by different authors with the weight lying on rotational viscometers for low viscosities and rod deformation for high viscosities. Most measurements were conducted in air, but the effect of other atmospheres was also considered in some studies.

The introduction of straw as a fuel poses new challenges on viscosity determination. Straw contains up to 2 weight-% potassium, and with a total ash content in the range of 2 - 7 weight-%, this component comes to affect the ash viscosity strongly in co-combustion with coal. The full-scale measurements of coal-straw co-firing performed by Laursen (1998) clearly show an effect. She varied the fuel straw-fraction in three steps (0, 10 and 20 % straw on a energy basis), this caused the K_2O-content in the fly ash to rise from 2% to 5% on a weight basis.[7]

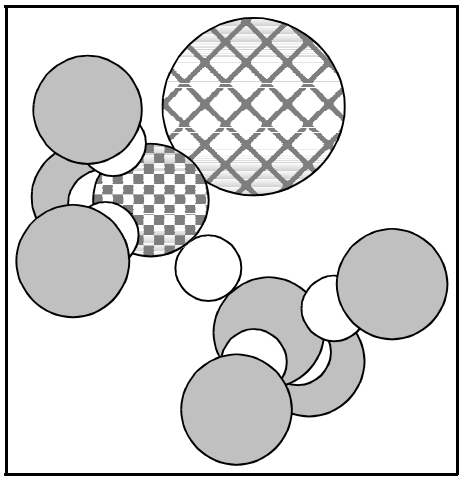

Figure 8.2 Charge stabilisation for Fe^{3+} in tetrahedral coordination in the silica network. (Si = Dark circles, O = White circles, Fe = Circles with dark squares, Other cation = Circle with dark grid).

The major components of ashes from the co-combustion of coal and straw are: SiO_2, Al_2O_3, Fe_2O_3, CaO, MgO, K_2O and Na_2O. Each of these oxides interacts in a complex way with the other components of the ash, and this fact severely complicates the prediction of viscosity.

The most plausible structural model for ash melts is the network model. The model predicts a three-dimensional

network of which the structural backbone of ash-melts is silicon dioxide. SiO_2 form at tetrahedral structure and Si^{4+} is a so-called network former. Both Al^{3+} and Fe^{3+} can enter this structure if they are charge stabilised by low-valence cations (see Fig 8.2); but the effect of Al^{3+} and Fe^{3+} is amphoteric: in the case of a lack of charge stabilising ions, they will act to break up the tetrahedral structure and thus decrease the viscosity of the melt at a given temperature. The effect of Ca^{2+}, Mg^{2+}, K^+ and Na^+ is to create ruptures in the tetrahedral network and thus cause a decrease in viscosity. These elements are therefore categorised as network modifiers.

A viscometer with a maximum temperature of 1700°C has been purchased in order to study the effect of composition on the rheological behaviour of the thermal conversion of straw and/or coal (Fig 8.3). Although fully developed from the manufacturer, Haake, the viscometer could not be set to work right away because the apparatus did not live up to the expectations that we had been induced by the sellers. Three years have passed from the date of purchase (December 1997), and run-in of the apparatus has only just been finished (March 2001). The reasons for this are numerous: when one problem was solved, two others seemed to appear. An improved vertical steering is among the biggest changes made to the system, and even today it is not possible to maintain a controlled atmosphere in the test zone.

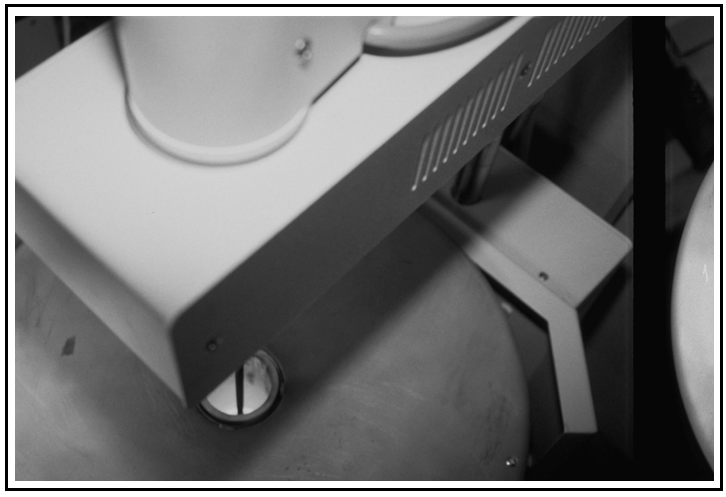

Figure 8.3 Haake viscometer seen from the top.

In short the design of the Haake setup could be improved strongly. It is inadequate for the intended high-temperature use.

- It will be extremely difficult to fix the leakage under the protective tube because of the local high temperature. No flexible gasket can stand these temperatures, and the tube does not have enough mass to press it together for airtightness. The original four screws were highly insufficient to ensure an airtight joint between the bellow and the bottom plate, and this should have been corrected long before the shipment of the apparatus.
- Likewise, it is incomprehensible why the setup was constructed with a movable arm to support a 3/4 m long pedestal that should be positioned with a millimetre top-precision instead of a sturdy steering.

- And finally, the choice of a long, thin and delicate ceramic pedestal is inadequate because it does not support the thermal shock experienced on the threshold between the furnace and the bellow section.

Sensors of platinum-rhodium and molybdenum have been found to be useful for high-precision viscosity measurements. $Pt_{80}Rh_{20}$ is used in oxidising atmospheres; the high level of rhodium addition has been chosen because of the improved material strength, but it introduces some brittleness into the material, however the material softens at higher temperatures, and should not be used over 1600°C. Molybdenum does not soften, but it is only stable in non-oxidising environments so it can not be used with a leaking system.

A measurement series has been carried out with success. In spite of a content of potassium oxide of more than 6 weight-%, the measured viscosity-temperature relationship was predicted with great precision by the Urbain model.

8.2 Further work

The viscometer has now been fully installed, and it is ready to use. Experimental determinations of ash viscosities can be made as well as investigations on oxide-mixtures prepared in the laboratory, and a full experimental procedure should be developed, when sufficient experience has been gained.

Investigations in controlled atmospheres is another subject of interest. It is generally acknowledged, that atmosphere plays a role for the rheological behaviour of ash melts, but it is a subject that has not been studied very profoundly. However, before such studies can be realised, all leakages should be fixed, and this will not be an easy task.

The ultimate goal of the experiments is the development of an adequate mathematical model that can easily be used by people who need to predict the temperature-dependence of the viscosity of a given ash. It is not realistic to think that a model that is generally applicable for a wide range of compositions can be condensed in a simple mathematical expression like the ones presented in this thesis, maybe a more viable road would be a model complex that makes use of interpolation between experimental results. For such a model it would also be possible to include data on the formation of crystals in the melt.

Bibliography

1. Sander, B. *Biomass Bioenerg* **12(**3), pp. 177-83 (1997).
2. Hurst, H.J., Novak, F., Patterson, J.H. *Fuel* **78** pp. 439-44 (1999).
3. Unsworth, J.F., Barratt, D.J., Roberts, P.T. *Coal Quality and Combustion Performance* (1991).
4. Jensen, P.A., Frandsen, F., Dam-Johansen, K., Sander, B. *Energ Fuel* **14**(6), pp. 1280-5 (2000).
5. Dam-Johansen, K., Hu, G., Sander, B., Lærkedal, L., and Jensen, P.A. Biomass Gasification and Pyrolysis (1997).
6. Hansen, L.A. Deposit Formation at Masnedø CHP, Technical University of Denmark, Lyngby, CHEC.Report No. 9821 (1998).
7. Andersen, K.H. *Deposit Formation during Coal-Straw Co-Combustion in a Utility PF-Boiler,* Department of Chemical Engineering, Technical University of Denmark, Lyngby (2001).
8. Reid, R.C., Prausnitz, J.M., Poling, B.E. ch. 9, Viscosity. *The properties of gases and liquids,* 4th ed ; Sun B, Fleck GH, (Eds), pp. 388-490, McGraw-Hill, Singapore (1988).
9. Kestin, J., Wakeham, W.A. ch. 4, The measurement of viscosity. *Transport properties of fluids, Thermal conductivity, viscosity, and diffusion coefficient,* ; Ho CY (Ed), pp. 73-147, Hemisphere publishing corporation, New York (1988).
10. *Perry's chemical engineers' handbook,* 6th ed; Perry RH, Green DW, Maloney JO, (Eds), chs. 3 + 5, Viscosity, pp. 3-278-82, McGraw-Hill Book Co, Singapore (1984).
11. Danek, V., Licko, T., Panek, Z. *Silikáty* **29** pp. 291-9 (1985).
12. De Jong, B.H.W.S. Glass. *Ullmann's Encyclopedia of Industrial Chemistry,* 5th ed ; Arpe H-J, Biekert E, Davis HT et al. (Eds), pp. 365-432, Würzburg (1990).
13. Clark Jr, S.P. ch. 12, Viscosity *Handbook of Physical Constants,* ; Clark Jr SP (Ed), pp. 291-300, The Geological Society of America (1966).
14. Bird, R.B., Stewart, W.E., Lightfoot, E.N. *Transport phenomena,* John Wiley & sons, Inc, Singapore (1960).
15. White, F.M. Ch. 3-1, Properties of a fluid. *Viscous fluid flow,* 2nd ed; Beamesderfer L, Morriss JM, (Eds), pp. 15-27, McGraw Hill, Simgapore (1991).
16. Sarofim, A.F. and Helble, J.J. The impact of ash deposition on coal fired plants, June 20-25 1993, pp. 567-582 (1994).
17. Walsh, P.W., Sayre, A.N., Loehden, D.O., Monroe, L.S., Beér, J.M., Sarofim, A.F. *Prog Energ Combust* **16** pp. 327-46 (1990).
18. Beér, J.M., Sarofim, A.F., Barta, L.E. *J I Energy* **65** pp. 55-62 (1992).
19. Harb, J.N., Zygarlicke, C.J., Richards, G.H. *J I Energy* **66** pp. 91-8 (1993).
20. Richards, G.H., Slater, P.N., Harb, J.N. *Energ Fuel* **7** pp. 774-81 (1993).

21. Senior, C.L., Srinivasachar, S. *Energ Fuel* **9** pp. 277-83 (1995).
22. Wibberley, L.J., Wall, T.F. *Fuel* **61** pp. 93-9 (1982).
23. Boow, J. *Fuel* **48**(2), pp. 171-8 (1969).
24. Mackenzie, J.K., Shuttleworth, R. *Proc Phys Soc (London)* **B62,** 12-B, pp. 833-52 (1949).
25. Senior, C.L. *Energ Fuel* **11**(2), pp. 416-20 (1997).
26. Kirk, R.E., Othmer, D.F. *Encyclopedia of chemical technology. Recycling, oil to silicon*, 4th ed; Kroschwitz J, Howe-Grant M, (Eds), *Rheological measurements*, pp. 347-404, John Wiley & Sons, USA (1997).
27. Mills, K.C. *Viscosities of Molten Slags*, National Physical Laboratory (1992).
28. English, S. *J Soc Glass Technol* **8** pp. 205-51 (1924).
29. Bacon, L.R. *J Franklin I* **221**(1322-18) pp. 251-73 (1936).
30. Scholze, H., Kreidl, N.J. ; Uhlmann CR, Kreidl NJ, (Eds), *Volume 3 Viscosity and Relaxation,* Academic Press Inc. New York (1986).
31. Stanmore, B.R., Budd, S. *Fuel* **75**(12) pp. 1476-9 (1996).
32. Shiraishi, Y., Meister, R. *J Phys, C9* **12**(43) pp. 447-50 (1982).
33. Jones, E.E., Lindsey, J.S. *Miner Metall Proces*, pp. 60-4 (1987).
34. Schobert, H.H., Diehl, E.K., Streeter, R.C. *DOE/METC* **82**(24) pp. 415-3 (1982).
35. Urbain, G., Bottinga, Y., Richet, P. *Geochim Cosmochim Acta* **46** pp. 1061-72 (1982).
36. Machin, J.S., Yee, T.B., Hanna, D.L. *J Am Ceram Soc* **35**(12) pp. 322-5 (1952).
37. Urbain, G. *J Mater Edu* **7**(6) pp. 1007-78 (1985).
38. Kato, M., Minowa, S. *Transactions of the Iron and Steel Institute of Japan ISIJ* **9** pp. 31-8 (1969).
39. Hurley, J.P., Kay, J.P. *Personal communication* (1998).
40. Shartsis, L., Spinner, S., Capps, W. *J Am Ceram Soc* **35**(6) pp. 155-60 (1952).
41. Lillie, H.R. *J Am Ceram Soc* **22**(11) pp. 367-74 (1939).
42. Urbain, G. *Steel Res* **3** pp. 111-6 (1987).
43. Kalmanovitch, D.P. and Frank, M. *Mineral Matter and Ash Deposition from Coal*, pp. 89-101 (1988).
44. Nowok, J.W. and Benson, S.A. *Inorganic Transformations and Ash Deposition During Combustion*. 1991 March 10-15, pp. 405-424 (1991).
45. Brown Jr., G.E., Farges, F., Calas, G., ch. 9, X-ray scattering and x-ray spectroscopy studies of silicate melts. *Structure, dynamics and properties of silicate melts,* Stebbins J.F., McMillan P.F., Dingwell D.B., (Eds), pp. 317-410, Mineralogical Society of America, Washington, D.C (1995).
46. Mysen, B.O., Virgo, D., Scarfe, C.M., Cronin, D.J., *Am Mineral* **70** pp. 487-98 (1985).
47. Nowok, J.W. *Energ Fuel* **9** pp. 534-9 (1995).
48. Vargas, S., Frandsen, F., Dam-Johansen, K. *Prog Energ Combust* **27**(3) pp. 237-429 (2001).

49. *Compatibility of Calibration Substances with Various Crucible Materials - Chemical Behavior of Platinum, Aluminum Oxide and Graphite Crucibles*, Compatibility 12/96.Selb/Bavaria, Germany Netzsch-Gerätbau GmbH (1996).
50. Molybdenum, 530 DEF 12.97 VV.Austria Plansee (1997).
51. Bryant, G.W., Browning, G.J., Gupta, S.K., Lucas, J.A., Gupta, R.P., Wall, T.F. *Energ Fuel* **14** pp. 326-35 (2000).
52. Bottinga, Y., Weill, D.F. *Am J Sci* **272** pp. 438-75 (1972).
53. Reid, W.T., Cohen, P. *T ASME* **66** pp. 83-97 (1944).

PERGAMON

Progress in Energy and Combustion Science 27 (2001) 237–429

PROGRESS IN ENERGY AND COMBUSTION SCIENCE

www.elsevier.com/locate/pecs

Rheological properties of high-temperature melts of coal ashes and other silicates

S. Vargas*, F.J. Frandsen, K. Dam-Johansen

Department of Chemical Engineering, Technical University of Denmark, 2800 Lyngby, Denmark

Received 19 January 1999; accepted 15 July 2000

Abstract

This paper reviews the 20th century advances within the field of the measurement and the prediction of the rheological properties of high-temperature ($T > 1000$ K) silicate melts at atmospheric pressure with a focus on coal ashes and other melts of compositions relevant to coal ashes.

Theoretical considerations are represented firstly by a synopsis of definitions and flow-regimes and secondly by an outline of the ruling network theory and the notations used therein. The influence of different cations on viscosity is discussed thoroughly.

Experimental points include a listing of the most common apparatus for viscosity measurements on high-temperature liquids and a summary of existing experimental data. Viscosity vs temperature is reported in tables as well as graphically for melts composed of major amounts of one or more of the species: SiO_2, Al_2O_3, FeO_x, CaO, MgO, Na_2O, K_2O, Li_2O, MnO, TiO_2, B_2O_3. For each experimental source, relevant information is listed (apparatus, sensor material, atmosphere).

With a basis in both theory and experimental data, general equations for liquids, are presented, relating viscosity to temperature and/or concentration of dispersed solids, as are more specific mathematical models, relating the viscosity of silica melts and glasses to temperature and composition.

Keywords: Silicates; Viscosity; Coal ash

Contents

* Corresponding author. Tel.: +45-252-835; fax: +45-88-2258.
E-mail address: sv@kt.dtu.dk (S. Vargas).

0360-1285/01/$ - see front matter
PII: S0360-1285(00)00023-X

1. Introduction

The objective of this paper is to review the knowledge that has been accumulated during the past century to provide the best possible basis for the elaboration of a precise and accurate mathematical model on viscosity estimation for silicate melts.

The rheological properties of silicate melts is an area of vast interest to all industries and sciences dealing with SiO_2-containing material at temperatures beyond 1000 K. For the art of glass making, the viscous properties of the glass are decisive for the workability of the glass.

In the production of pure metals, metallurgists continuously search for the most efficient methods for the removal of silicate slags, and the subject is also of interest to the cement industry.

Geologists studying magmas, i.e. naturally occurring molten rock material generated under Earth's crust, are concerned with silicate melts (although often at extreme pressures) with much the same composition as the coal ashes, which are of great interest to power producers.

Even though the effect of pressure on melt viscosity is an important subject for geologists, the subject is not included in this paper.

The authors of this review occupy themselves with the solution of problems related to the combustion of solid fuels such as coal and biomass (e.g. straw and wood) in utility boilers, and thus the subjects most relevant to these systems will be the focus of this review.

Very briefly, boilers operate as follows. Fuel is continuously transported to the furnace where it is combusted, and the resulting flue gas is transported through a channel to the stack. Both in the furnace and in the following channel, heat is removed through tubes that act as walls or hang from the sides. Inside these tubes water is first vaporised and subsequently overheated to a pressure that operates one or more turbines.

Most fuels consist of a series of elements that will leave the system in a vaporised state with the flue gas (C, H, N, O) and an ash fraction that will partly vaporise in the hot section of the boiler but will eventually end up as either fly-ash particles that are carried along with the flue gas or as deposits on the heat transfer surfaces, i.e. the tubes.

Nomenclature

Symbols

a	Constant
b	Constant
A	Area of plane (m^2)
c	Constant
d	Constant
	Diameter
D	Bottinga–Weill model constant
E	Energy
F	Force (N)
g	Gravitational acceleration (m/s^2)
G	Grunberg parameter
k	Constant
L	Length (m)
m	Mass (kg)
	Slope constant
N	Number of observations
p	Pressure ($kg/m\ s^2$)
P	Probability
r	Radius (m)
R	Bond length (m)
R_0	Bond valence parameter (m)
t	Time (s)
T	Temperature (K)
V	Volume (m^3)
v	Velocity (m/s)
x	Mole fraction
Y	Distance between parallel planes (m)
z	Constant
α	Constant
$\dot{\gamma}$	Shear rate (s^{-1})
η	Viscosity ($N\ s/m^2$)
θ	Volume fraction solids
μ	Viscosity coefficient for Newtonian fluids ($N\ s/m^2$)
v	Kinematic viscosity (m^2/s)
v_i	Intrisic viscosity
ρ	Density (kg/m^3)
ς	Silica ratio
τ	Shear stress ($kg/s^2\ m$)
τ_0	Yield stress ($kg/s^2\ m$)
T	Torque (N m)
φ	Fluidity ($m^2/N\ s$)
ω	Angular velocity (s^{-1})

Subscripts

a	Absolute
	Amphoteric
A	Activation
c	Configurational
cryst	Crystal
cv	Critical viscosity
e	Effective
	Jumping
i	Inner
	Enumerator
f	Free
ff	Fraction free
g	Glass transition
	Glass former
h	Hemisphere
l	Liquidus
liq	Liquid
m	Molecular
	Glass modifier
	Mean
max	Maximum
mix	Mixing
mixt	Mixture
o	Outer
	True liquid state
p	Isobar
pl	Plastic
r	Residual slag
ref	Reference
s	Cone softening
T	Temperature
v	Hole
0	Zero shear (yield)
	Initial uniform
"0"	Pseudo yield
∞	Infinite
η	Viscosity

Silicate melts and glasses are created from the ash-part of the fuel, and it is largely the behaviour of these ashes that determines the appropriateness of a given fuel for combustion. Sticky or even molten particles will easily stick on surfaces, and the resulting deposits will act as insulation that inhibits the heat-flow from flue gas to water or steam. Furthermore, deposits may be corrosive, and the resulting tube leaks must be prevented since they are highly destructive due to the high pressure water-vapour inside the tubes. Tube surfaces will also be eroded by the fly-ash passing by with the flue gas. Thus in a series of ways, the behaviour of the fuel ash is crucial to the optimisation of the boiler design and operation.

A given fuel is problematic if it forms low-melting ashes. This can be handled in one of several ways. Either the fuel can be blended with another fuel or an additive can be used in order to improve the ash-characteristics. Another possibility is to keep operation temperatures low. In any case, the objective is to avoid the creation of molten slags inside the furnace and thereby avoid the build-up of extensive deposits.

If a fuel forms low-melting slags upon combustion, this will seriously affect the maximum operation temperature of the boiler and thus the overall efficiency of the process just as it will increase maintenance costs. In fact, ash-related problems are the main reason for unscheduled shut-downs of utility-boilers.

Thus knowledge of ash-performance is important both for those who design new boilers and for those who operate them — the profitability of a plant may depend on it. The slags formed inside boiler furnaces are silicates, and the flow-characteristics of these silicate melts are the subject of this paper. The ultimate objective of the extensive investigations that are made within the subject is to gain sufficient insight into the structural characteristics of silicate melts in order to be able to define a mathematical model capable of predicting the viscosity of any silicate melt as a function of the prevailing conditions such as temperature, pressure and atmosphere. Such a model will greatly simplify the optimisation of plant design and the daily operation of existing plants as will it be a powerful tool for those who investigate processes that involve the viscous behaviour of silicates.

The first section of the paper is devoted to the outline of experimental work. After a brief, general introduction to rheology, the most common apparatus employed in high-temperature viscosity measurements on silicates are described physically as well as mathematically, then attention is turned to existing experimental data found in the literature. Appendix B contains a list of experimental measurements performed on different chemical systems. For each reference, experimental conditions (apparatus, sensor material, atmosphere) are noted. Appendix C contains tabulated values for all of the works mentioned in Appendix A expressed as viscosity ($\log \eta$ (Pa s)) vs temperature (T (K)) (see Figs. C1–C105). In Appendix D, the same data is reported graphically.

Since it is difficult, expensive and time-consuming to produce measurements on silicate melts, there is a demand for accurate mathematical models capable of predicting viscosity as a function of temperature and composition. But experience has shown that the elaboration of a high-accuracy model calls for theoretical considerations on the interactions between the different components in the melt, thus both experimentally and theoretically related subjects are discussed in this paper.

Reflections on the structural composition of silicate melts are presented with a focus on the network theory. The effect of alkali, alkaline earth, aluminium, iron and titanium oxides on the structure and viscosity of silicate melts is discussed just as is the influence of atmosphere.

When crystallisation occurs upon cooling of a silicate melt, the effect on viscosity is vast. Some guidelines are given on the prediction of the effect of crystals in the melt, and various definitions of critical viscosity are given.

In the last section, predictive models are presented for liquids of different flow-types. The performance of the models for silicate melts is investigated by testing the model predictions against experimental data reported in the literature by different authors.

2. Definitions and dimensions

Viscosity is a non-equilibrium property [1], a measure of the resistance of a fluid towards motion. It can be related to the tendency of a fluid to dissipate energy (produce entropy) [2] due to internal fluid friction [1] or it can be considered an analogue of momentum conductivity to thermal conductivity in conductive heat transfer and to the diffusion coefficient in diffusive mass transfer [3]. Unlike the electrical conductance of silicate melts, where the charge is transferred by cations, the transport of momentum in viscous flow is provided mostly by anions [4].

Newton first defined *dynamic* or *absolute viscosity* (N s/m^2) as the ratio of shear stress, τ (kg/s^2 m) to shear rate, $\dot{\gamma}$ (s^{-1}) [5,6].

$$\eta \equiv \frac{\tau}{\dot{\gamma}} \tag{1}$$

The concept of viscosity can be visualised as in Fig. 1. A fluid is entrained between two parallel planes of area A; the lower plane is fixed while the upper plane is moved at a constant velocity, v. After reaching steady state, the velocity distribution of the fluid will be linear (assuming laminar flow), and the viscosity may be expressed as the force, F (N), per unit area of plate, A (m^2), divided by the velocity gradient (i.e. the ratio of the velocity of the upper plate, v (m/s), and the distance, Y (m), between the planes) [7] Appendix B

$$\frac{F}{A} = \eta \cdot \frac{v}{Y} \tag{2}$$

The dimension of viscosity is thus mass per time and length. The SI-unit, Pa s, will be used in this paper, and the following conversion factors may be applied [1,8]:

$$1\ \text{Pa s} = 1\frac{\text{N s}}{\text{m}^2} = 1\frac{\text{kg}}{\text{m s}} = 10\ \text{P(poise)} = 0.672\frac{\text{lb}_\text{m}}{\text{ft s}} = 0.020886\frac{\text{lb}_\text{f}\ \text{s}}{\text{ft}^2} \tag{3}$$

Table 1 contains a list of the viscosities of some common

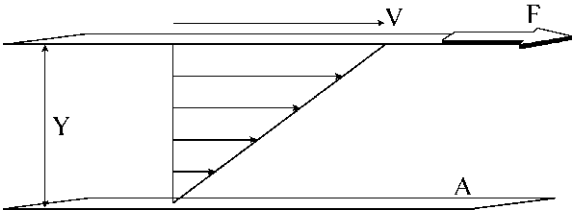

Fig. 1. Schematic depiction of viscosity. V = velocity of the upper plane, F = force driving the upper plane, Y = distance between the lower and upper planes, A = surface area of each plane [11].

Table 1
Approximate viscosities for some well known materials at room temperature [9]

Material	$\log_{10}\eta$ (Pa s)
Ideal fluid	$-\infty$
Water	−3
Machine oil	−1
Heavy oil	0
Glycerol	1
Glass	>18

substances [9]. An *ideal* or *perfect liquid* is a hypothetical fluid (gas or liquid) which offers no resistance to shear, i.e. has $\eta = 0$ [3].

To conclude this section, a few terms that are closely related to viscosity will be defined: kinematic viscosity, v (m^2/s), is the ratio of the viscosity to the density of a fluid. Fluidity, φ ($m^2/(N\,s)$), is the reciprocal of viscosity [10], and plastic viscosity is defined as [11,12]

$$\eta_{pl} \equiv \frac{d\tau}{d\dot{\gamma}}, \qquad d\dot{\gamma} > 0 \tag{4}$$

3. Classification of flow types

A study on the rheological properties of a fluid requires the evaluation of flow type. Each flow type has one or more parameters to be determined before the rheological properties of the fluid are well defined, and each flow type has a set of mathematical models fit for the description of the fluid. An oversimplification of flow type will leave the researcher unable to account for the behaviour of the fluid.

The main classification of liquid flows concerns the time-dependence of flow characteristics. If a liquid that is subjected to a given stress for a period of time continues to show the same viscosity, then the liquid has a time-independent flow type.

3.1. Time-independent flow types

Fig. 2 shows the flow-curves for the four classes of time-independent flow types.

Newtonian fluids obey Newton's law of viscosity, i.e. shear force per unit area is proportional to the local velocity gradient [7]

$$\tau = \mu \cdot \dot{\gamma} \tag{5}$$

The expression in Eq. (5) is analogous to that of Eq. (1) except that here, the general term for viscosity, η, has been substituted by the viscosity coefficient, μ [8], a term used extensively for Newtonian fluids. Gases and most simple liquids are Newtonian [7] and when the viscosity of a liquid is quoted as a single number in a handbook, the liquid is assumed to be Newtonian, and the number is the viscosity coefficient [8].

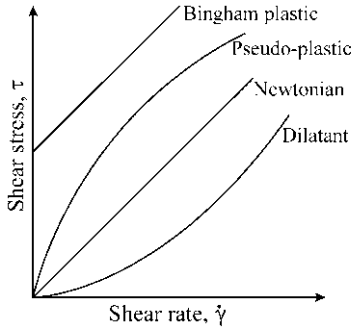

Fig. 2. Flow types for which viscosity can be described independently of the history of the fluid [5,11].

Pseudo plastics or *shear-thinning materials* [8] include the majority of non-Newtonian fluids, e.g. polymeric solutions or melts and suspensions of paper pulp and pigment [3]. The decrease of viscosity with increasing rate of deformation can usually be attributed to the breakdown of a structure at the colloidal or molecular level [5]. If the thinning effect is very strong, the fluid is termed *plastic* [8].

A *Bingham plastic* is an idealised material which requires a finite shear stress to initiate flow, the so-called yield stress, τ_0. Once flowing, shear stress depends linearly on shear rate, i.e. viscosity decreases with shear rate but plastic viscosity is constant, independent of shear rate [3]. As opposed to all the other flow-types here mentioned that are true fluids, Bingham plastics are yielding fluids with a flow-curve that is not differentiable at zero shear rate [5].

Dilatant or *shear-thickening* [8] *materials* exhibit rheological behaviour opposite to that of pseudo-plastics [3]. Examples of dilatant materials are suspensions with a high concentration of solids and with a relatively uniform particle-size distribution [5].

3.2. Time-dependent flow types

This group includes all those materials for which shear stress changes with duration of shear. Excluded are changes which might be produced through mechanical breaking or destruction of particles or molecular bonds [3].

Thixotropic fluids have decreasing viscosities with time of shear [5]. This is due to a structural breakdown of the fluid [3]. If the flow curve is measured in a single experiment in which the shear rate is steadily increased at a constant rate from zero to some maximum value and then decreased at the same rate to zero shear rate, a hysteresis loop as the one shown in Fig. 3 is observed [5]. If shear rate is kept constant at a given value, viscosity will decrease to a minimum after some time [3]. Examples of such fluids are mayonnaise, drilling muds, paints and inks [3].

Rheopectic fluids are rarely observed [5], but the effect is

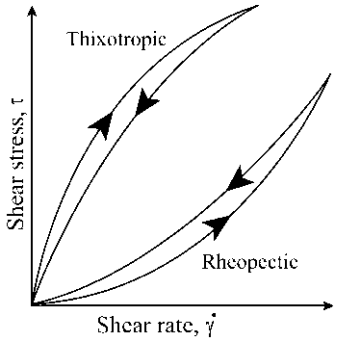

Fig. 3. Flow types for which viscosity depends on the history of the fluid [5,11].

opposite to that of thixotropic fluids. An example is gypsum suspensions in water [3].

4. High-temperature viscometers

Viscometers, viscosimeters or rheometers are the names most commonly used for the apparatus applied to experimental viscosity determinations.

Most viscometers are designed for use at room temperature ±100 K, and a series of instruments exist which operate with high accuracy at these temperatures. At measurement temperatures above 1000 K, material choice strongly restricts the variables of freedom available to the designer.

The focal point of this paper is silicate liquids. These exist mainly at temperatures exceeding 1000 K, and therefore the proceeding section will focus on viscosity measurement methodologies fit for high-temperature use.

Viscometers can be classified according to their ability to perform absolute viscosity measurements, i.e. direct measurement with no use of calibration factors established through measurements on standardised liquids [13].

Likewise viscometers which are most often used for accurate work are categorised as primary instruments. Whereas less accurate, but often more simple, instruments are categorised as secondary [2].

A brief introduction to the principles behind some viscometers that are adequate for measurements at high temperatures is given below. The list is not exhaustive since methods such as the needle penetration are not included.

4.1. Capillary viscometer

Capillary viscometers have been used as a primary instrument for viscosity measurements for well over a century. Although great care has often been taken in the design of such instruments, the evaluation of viscosity has sometimes been carried out with the aid of inadequate working equations, leading to inaccurate experimental results, despite the high precision of the measurements [2].

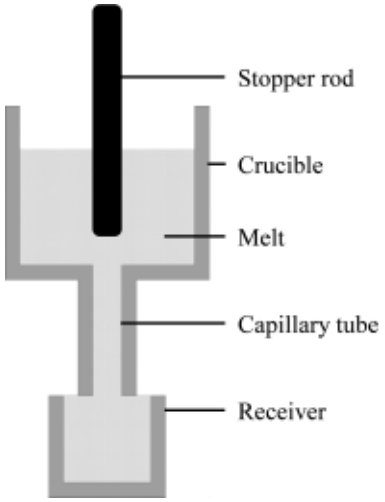

Fig. 4. Schematic drawing of a capillary viscometer [11].

A schematic drawing of a capillary viscometer is given in Fig. 4. A liquid drains or is forced through a fine-pore tube, and the viscosity is determined from the measured flow, applied pressure, and tube dimensions. The basic equation is the Hagen–Poiseuille expression, where η is the viscosity (Pa s), r the radius of capillary (m), Δp the pressure drop through capillary ([kg/m s^2], V the volume of liquid (m^3) that flows in time t (s) and L the length of capillary (m) [11]:

$$\eta = \frac{\pi r^4 \Delta p t}{8\, VL} \tag{6}$$

Kerstin and Wakeham (1988) present a discussion of the theoretical aspects of the capillary viscometer, and the article contains references to complete theoretical treatments [2].

Absolute viscosities are difficult to measure with a capillary viscometer, but the instrument can also be calibrated, facilitating greatly its use [11]. Above 1200°C complications arise in the selection of a suitable crucible and capillary material in terms of dimensional stability and corrosion resistance (NB: $\eta \propto r^4$) [14].

4.2. Falling body viscometer

The falling body viscometer can be used for absolute viscosity measurements [13]. However, the method is secondary [2].

Fig. 5 is a schematic drawing of a falling sphere viscometer. The body can also be cylindrical, and the tube in which the body falls can be inclined instead of vertical [2]. The body can either fall due to gravity or it can be dragged upwards through the melt [14]. Viscosity is calculated on the basis of Stokes law for a freely falling sphere (η is the viscosity (Pa s), r the radius (m), g the gravitational acceleration (m/s^2), ρ the density (kg/m^3), v the velocity of sphere

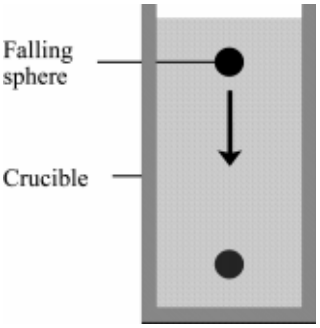

Fig. 5. Schematic drawing of a falling sphere viscometer [11].

(m/s)) [2]:

$$\eta = \frac{2r^2 g(\rho_{\text{sphere}} - \rho_{\text{liquid}})}{9v} \tag{7}$$

References to literature containing more thorough theoretical treatments of the method can be found in Kerstin and Wakeham (1988) [2].

English (1924) criticised the method of using a small sphere suspended by a very fine thread over a light, well-balanced, free-running pulley, where the sphere is partly counterbalanced so as to control the rate of fall. He found it to be difficult to produce consistent results owing to the fact that, no matter how fine the thread or wire supporting the sphere, there was always a drag caused by the passage of the thread through the liquid under test [15].

4.3. Rotational viscometer

Rotational viscometers are primary instruments [2] and with corrections for gaps and end effects, very accurate measurements are possible [13]. Usually, the instrument is calibrated with liquids of known viscosity, but absolute determination is possible using the Margules equation (η is the viscosity (Pa s), T the torque (N m), r_o and r_i the radii of outer and inner cylinders (m), L the depth of penetration (m), ω the angular velocity (s^{-1})) [9,11]:

$$\eta = \frac{T(r_o^2 - r_i^2)}{4\pi L\omega r_o^2 r_i^2} \tag{8}$$

Fig. 6 shows a schematic drawing of a rotating bob viscometer where the inner cylinder is rotated and the outer cup is fixed. Three variations of the principle are possible [9]:

(i) inner cylinder rotates and outer cup is fixed;
(ii) inner cylinder is fixed and outer cup rotates;
(iii) both inner cylinder and outer cup rotate.

An evaluation of the three principles against each other has not been found in the literature. However, the centring of the inner cylinder is of great importance in all three cases [9], and this may be the reason why the first principle is most commonly used in practice.

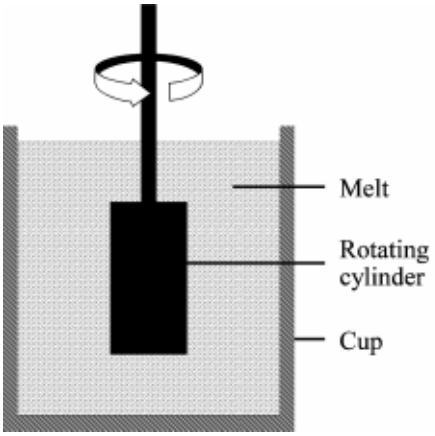

Fig. 6. Schematic drawing of a rotating cylinder viscometer [11].

4.4. Rod elongation viscometer

The rod elongation viscometer measures the elongation velocity, v (m/s), of a filament of length L (m), and radius r (m) loaded by mass m (kg) by means of the equation (g is gravitational acceleration (m/s^2)) [9]

$$\eta = \frac{Lmg}{3\pi r^2 v} \tag{9}$$

4.5. Squeeze film rheometer

In the squeeze film rheometer, the sample to be tested is retained between two horizontal plates and is compressed axially by driving the plates together as depicted in Fig. 7 [16]. This method is also known as the parallel plates method [17].

4.6. Choice of viscometer for high-temperature measurements

The choice of viscometer depends on factors such as

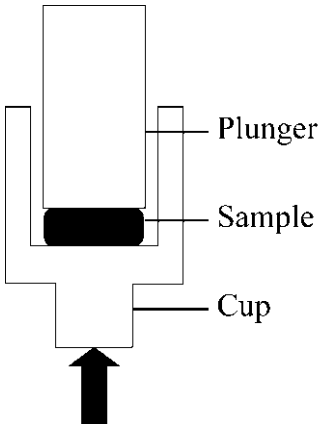

Fig. 7. Schematic drawing of a squeeze film rheometer [16].

Table 2
Measurement ranges for some viscometers [9,16,20]

Viscometer type	Measurement range $\log_{10} \eta$ (Pa s)
Falling sphere viscometer	−2–6
Rotating cylinder viscometer	2–13
Rod elongation viscometer	7–13.5
Squeeze film rheometer	5–(7)

operation cost, measurement duration and precision requirements. Table 2 indicates the rotational viscometer as being the most flexible with regard to measurement range.

In 1924, Washburn and Shelton [18] wrote that the peculiar difficulties associated with the measurement of the viscosity of molten glass over a wide temperature range arise from the simultaneous presence of the following conditions:

- a very wide viscosity range;
- poor heat conducting properties of the liquid;
- invariable presence of small bubbles in the liquid;
- the very high temperatures at which the experiments must be carried out.

The only method adaptable to all the above-mentioned conditions is that of the rotational viscometer [18].

Urbain and Boiret (1990) stress the superiority of the rotational viscometer over other devices for high-temperature measurements on liquid silicates [19], and Urbain et al. (1982) conclude that this method gives the best results for viscosities ranging from 10^{-2} to 10^{4} Pa s [20].

The capillary viscometer is conventionally used for common liquids of low viscosity; but measuring glass in this manner is very difficult and, therefore, rare [9]. Stanmore and Budd (1996) recommend the use of this for measurements on coal ashes of interest to fouling [16].

5. Experimental results

Experimental data have been produced for almost a century, but the oldest measurements can be considered no more than qualitative due to insufficient apparatus calibration and the inappropriate choice of sensor material.

Appendix A contains a list of compositional systems for which measurements are reported in this paper. The list contains important information about the experimental techniques employed and measurement accuracies.

Appendices B and C contain the experimental viscosity results as tabulated values (log η (Pa s) vs temperature, T (K)) and graphically (η (Pa s) vs temperature, T (K)).

Most viscometers used for the production of the data reported in Appendices A–C are described in a preceding section of this paper.

The experimental data reported are by no means exhaustive, though comprehensive. It has been left for the reader to decide what data to trust, but guides have been laid out in the form of the information given about the experimental results employed.

5.1. Sources of error

5.1.1. Temperature

General for all high-temperature viscometers is that more errors are made and more disagreements over viscosity results arise due to incorrect or drifting temperature than for any other reason [11].

5.1.2. Composition

A comparison of the compositions of low-rank coal ashes produced by the ASTM procedure, the so-called high-temperature ash, and the solidified slag from a viscosity test showed significant differences for some elements. Based on a combination of this observation and viscosity measurements, Schobert et al. (1982) state that while the composition of the ash may be an inadequate predictor of viscosity, the composition of the resulting slag may be an important parameter [21].

Traditionally, power generating facilities have attempted to predict the severity of coal as deposition by calculating empirical indices based upon the overall ash composition of the coal. While suitable for narrow ranges of coal-boiler combinations, these indices are less accurate predictors when extrapolated to other coals or operating conditions. This can be attributed to their use of overall ash composition, when in fact deposition is initiated and propagated by individual ash particles with varying compositions and sizes [22].

5.1.3. Atmosphere

As it will be pointed out repeatedly in the rest of the paper, the choice of atmosphere seriously affects the viscous behaviour of some silicate melts. For example, the oxidation state of iron changes depending on atmosphere and this affects viscosity. This point becomes extraordinarily important since glasses containing large amounts of iron oxide are often found in practical combustion systems. Uncontrolled atmosphere during measurement of viscosity can cause errors.

5.1.4. Phase separation

The possibility of erroneous results resulting from phase separation is considered by Machin et al. (1952) [23]:

- Non-uniformity of the melt due to the formation of crystals which are not detected may result in misleading results.
- Upon cooling of the slag, a clear glass does not always result. In this case the crystalline phases and the glassy phase probably differ in composition. Thus, remelting of the sample may not result in a uniform glass.

- The possibility of the simultaneous existence of more than one liquid phase may not be completely ruled out.

5.1.5. Sensor material

The choice of sensor material is of great importance to the quality of the measurements [24].

If the detecting parts of apparatus are made of graphite, the properties of slags may be changed by suspension of flaky carbon in the slag or by the chemical reaction between slag and carbon [25]. Hofmaier (1968) states that in earlier studies, reactions between the silicates and the graphite sensors were the main cause for the considerable measurement errors that were made at times [26].

In a study on low-rank coal slags, Streeter et al. employ a rotating bob viscometer for viscosity measurements. In the earlier tests, the slag was melted in crucibles of vitreous carbon. It soon became evident that iron oxides in the slag were being reduced by reaction with the carbon crucible, as small pools of molten iron invariably settled from the slag during the carbon-crucible tests. Consequently, the carbon crucibles were eventually replaced with high-purity alumina crucibles. Thereafter, metallic iron was only rarely observed in the slag. On the other hand, varying degrees of attack on the alumina crucible by the slag were observed. Generally, dissolution of Al_2O_3 by the slag was slight, but in a few cases noticeable thinning of the crucible walls occurred [27].

According to Hurley, the contamination of coal ash slags by alumina crucibles usually amounts to a few weight-percent in acid slags, but can me much higher (10–15%) in basic slags [28].

Contamination of the test material can be avoided using platinum [25], but this material should not be used with iron-containing materials in reducing atmospheres [21].

Slags derived from low-rank coals are exceptionally corrosive. Alumina crucibles are attacked, presumably by alkali, and vitreous carbon crucibles are attacked or destroyed by CO_2 or SO_3 outgassing from the slag. Carbon can also reduce iron compounds to metallic iron, and the melting of some ashes in nickel crucibles produces green melts. Some ashes are capable of destroying zirconium crucibles [21]. Unfortunately, the atmospheric conditions used to produce these results were not stated in the cited paper.

Hofmaier (1968) states that although many studies on silicate melt viscosities have been carried out, only more recent studies employing molybdenum or tungsten sensors should be regarded as trustworthy [26]. The sample contamination caused by the use of Mo sensors has been registered to 10–20 ppm w/w Mo in some samples [24]. But molybdenum is only stable under non-oxidising conditions at elevated temperatures. In air, molybdenum will oxidise at temperatures over 400°C and sublimation will start at 600°C.

In a study on the system SiO_2–Al_2O_3–FeO–CaO–MgO, Vorres et al. (1986) used alumina crucibles in a rotating cylinder viscometer because, as they noted, although alumina is not a suitable material for long-term containment of these slags at elevated temperatures, the amount of dissolution was insignificant for the 24 h exposure time without slag motion with respect to the crucible [29].

5.1.6. Errors related to specific measurement techniques

Seki and Oeters (1984) found the main errors of their rotational viscometer measurements to be created by the following [30]:

- errors in the temperature (the recorded temperature is not the actual temperature in the melt);
- eccentricity between the crucible and the torsion body;
- eccentricity between the crucible axis and the rotational axis;
- errors in the immersion depth;
- thermal expansion influences.

Washburn et al. (1924) found that although some improvements in the temperature control of their rotational viscometer could perhaps have been made, the two principal factors which limited the accuracy of the results were [18]

- errors in the calibration curve for the apparatus (performed at 298 K) and
- contamination of the glass by the porcelain crucibles employed.

Shiraishi and Meister (1982) state the three main sources of error in their squeeze film rheometer measurements to be [17]

- resolution of the computer measurements (only signal changes over a certain limit can be registered);
- volume expansion of the sample;
- non-cylindrical deformation of the sample.

6. Structure of silicate melts and glasses

An inevitable first step in any attempt to predict the viscosity of silicate melts is to strive to understand the fundamental structural aspects of the melt, i.e. how do different components affect the overall structure, and what is the effect of changing the temperature?

In this section, we will try to give a comprehensive view of how researchers imagine the organisation of atoms in silicate melts. The section also contains a number of parameters that are used to represent the structural influence on the viscosity of melts.

First, why are glasses and melts treated in the same fashion?

In the first chapter of his book from 1960, Morey defines a glass as an inorganic substance in a condition which is continuous with, and analogous to, the liquid state of that substance. As the result of a reversible change in viscosity during cooling, the substance has attained so high a degree

of viscosity as to be for all practical purposes rigid [31]. This assumption appears to be reasonable for highly viscous liquids in which diffusion rates are slow relative to the quench rates used to produce the glass [32].

Glass is an amorphous solid, and, considering the tendency of most glasses to precipitate crystals under proper conditions, the substance may be thought of as a supercooled liquid or supersaturated solution [33]. However, structural studies of molten silicates performed with X-ray scattering, X-ray absorption spectroscopy, vibrational spectroscopy and NMR have shown significant difference in local and medium-range structure for some compositions as compared to the corresponding glasses. So the assumption that the structure of a glass is the same as that of its melt is not always true [34].

Whereas the property of a liquid is uniquely determined by temperature (and pressure) the property of a glass also depends on thermal history [9]. At temperatures below the glass transition temperature, T_g, the time needed for structural stabilisation of the liquid upon temperature changes or physical deformation is so large that equilibrium can not be assumed to be reached immediately.

Caution should be taken when quenching silicate melts to glass without concern for thermal history. It may be possible to produce significantly different structures by quenching depending on the degree of superheating and thermal treatment above the liquidus. These effects seem to occur more readily in relatively depolymerised melts [29] i.e. low-acidity melts with loosened structures.

In the rest of this paper, silicate glass will be thought of as a supercooled liquid, and we will not treat it separately, but simply consider it a special case of silicate melts.

Now, let us turn to the structural considerations that are the main topic of this section. Silicate melts are substances in which the nearest neighbours of each atom are organised as in a crystal, whereas the more distant atoms are not as well organised [26]. They are classified as Newtonian fluids, however, at high rates of motion, non-Newtonian behaviour may be seen [35].

Urbain (1985) gives a historical review of the development of the structural models used to describe silicate melts [24], which is given in a short form below.

In 1934, Schenck et al. published the classical molecular model. The initial postulate was the existence, in the liquid phase, of "free-molecule-like" species such as: SiO_2, CaO, $2FeO–SiO_2$, $3CaO–Fe_2O_3$, etc. — a clear extrapolation to the liquid of definite compounds of the solid state. The model is reported to cause unavoidable complexity when used in practice.

The ionic concept was introduced by Flood et al. in 1952 [24]. It postulates the existence in silicate melts of different ions:

- Simple cations: Na^+, K^+, Ca^{2+}, etc.
- Simple anions: O^{2-}, S^{2-}, F^-, etc.
- Complex anions: SiO_4^{4-}, PO_4^{3-}, etc.

The model was reported to provide a good description of the thermodynamic properties of liquid silicates and a reasonable estimate for mixtures and complex melts [24].

Just one year later, in 1953, Flory et al. published the polymerisation model. Statistical considerations were applied to the distribution of bonds between the structural units, thus, allowing a calculation of the fractions of monomer, dimer, etc. [24]. In 1955, Bockris and co-workers proposed the existence of discrete units ($Si_3O_9^{6-}$, $S_4O_{12}^{8-}$, $Si_6O_{15}^{6-}$, $Si_8O_{20}^{8-}$, $Si_9O_{21}^{6-}$) that could exist in liquid silicate melts. The authors' interpretation of the spatial arrangement of the silicon and oxygen atoms in the ions is depicted in Fig. 8 [36].

6.1. Crystallite model

One of the first theories of silicate glass structure is attributed to Frankenheim (1835) who postulated that glasses are made up of very small crystals which are referred to as crystallites [34].

In the crystallite model, a glass is composed of units which have a crystalline-like order bonded together in a random fashion by regions of lesser order. A multi-component glass may be an essentially heterogeneous structure consisting of several types of crystallites, generally corresponding to the structures of the appropriate liquidus phases. This is in contrast to the random network model (see below), in which the glass structure is homogeneous with only a minimal amount of crystal-like ordering.

In 1958, Porai and Koshits proposed a modified crystallite model in which discrete crystallites do not occur. In this model there are spatial fluctuations in the degree of medium-range order in the glass network for simple network glasses like vitreous SiO_2. The more highly ordered regions may have atomic arrangements that approach those of crystals, and these regions are envisioned as being interconnected by less-ordered regions. The total volume fraction of the ordered regions is estimated to be less than 80%, and one could think of them as being precursors to nuclei of crystals [34].

6.2. Random network model

Zachariasen's experiments in 1932 on X-ray diffraction from silicate glass at room temperatures formed the basis for the modern view of the silicate melts as organised in a three-dimensional random network in which each silicon is tetrahedrally surrounded by four oxygens and each oxygen is bonded to two silicons [33,37].

In this view, molten SiO_2 is organised tetrahedrally in six-membered rings as illustrated in Fig. 9. These rings are a product of the tetrahedral network structure, and they form the borders of five-sided dices. In the midst of these dices there is ample room for interstitial atoms such as alkali ions.

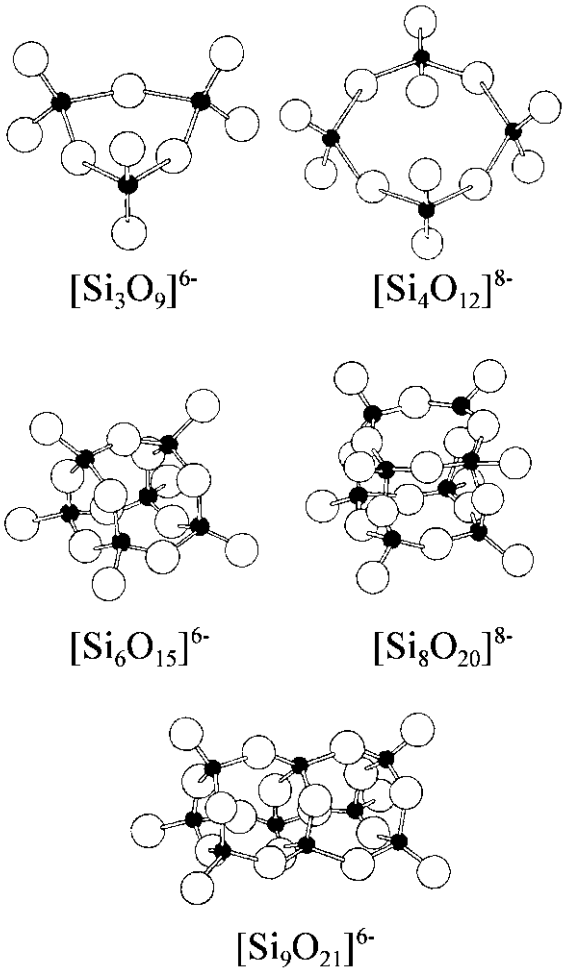

Fig. 8. Spatial arrangement of discrete silicon-oxide units proposed by Bockris et al. (1955) [36].

These atoms can also enter the network, breaking bonds and loosening the structure.

Silicate melts can be described by dividing the components into basic and acidic oxides. Parallel to the Brønsted definition for aqueous solutions of an acid as a substance capable of donating a proton, a base in an oxide melt can be defined as a substance capable of donating an anion (oxygen); thus basic oxides act as oxygen donators (network modifiers) and acid oxides as receptors (network formers). Therefore viscosity decreases with increasing basicity. This concept is typically represented by the base-to-acid ratio [30,38,39]

$$\frac{\text{Base}}{\text{Acid}} = \frac{Na_2O + K_2O + CaO + MgO + FeO}{SiO_2 + Al_2O_3 + Fe_2O_3 + TiO_2} \quad (10)$$

where SiO_2 etc. denote molar fractions. A more theoretical approach to the subject of acidity is given below in Section 7.3.

The definition of the base-to-acid ratio has changed with time. According to Bryers (1982), a base-to-acid ratio was first proposed by Nicholls, Selvig and Ricketts in 1932 containing only the acids TiO_2 and Al_2O_3 and with Fe_2O_3 on the base-side instead of FeO [40]. Only some of the many different formulations that have been attempted will be presented here.

Quon et al. (1985) and others include only ferric iron (Fe^{3+}) in the equation, classified as a base. Furthermore, they construct the equation on a weight basis of oxides [39,41]. Van der Colf and Howat (1979) also base their equation on weight ratios, but they did not include neither Al_2O_3 nor TiO_2 in the equation although they were present in the melt under investigation (only the melt components: SiO_2, CaO and MgO were included) [42]. None of the

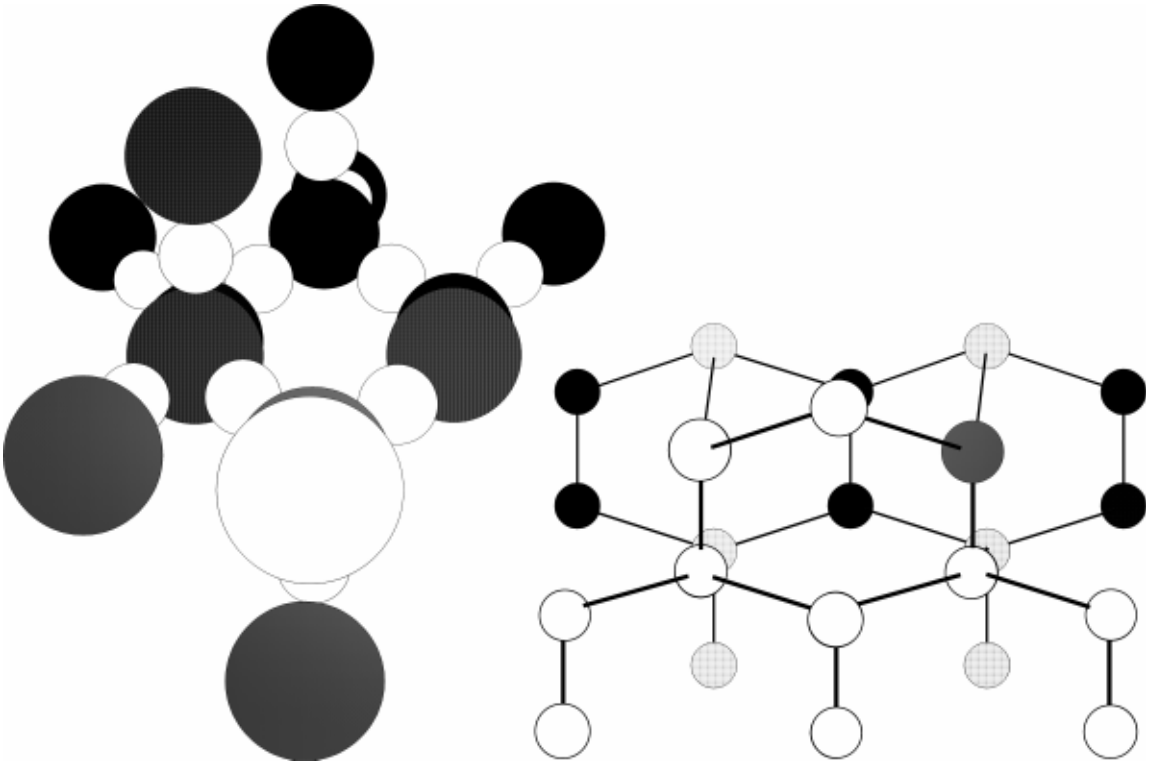

Fig. 9. Spatial arrangement of SiO_2-network according to the network theory (left image: Si = big circles, O = small circles, right image: only Si-atoms depicted).

authors evaluated the appropriateness of their choice of basis.

Bryers (1982) relates that in 1958, Majumdar found the base-to-acid ratio to correlate better with fusibility data for coal ashes when the concentrations of the constituents were expressed on a molar basis [40].

Based on acidity, the components in a silicate melt may be arranged in three groups as either network formers, network modifiers or amphoterics. Network formers are cations that always occupy a tetrahedral position and as such act as building blocks in the network. Network modifiers, on the other hand, are cations that have a disruptive effect on the network. Amphoterics can act as either network formers or modifiers according to their coordination number in the melt. When combined with modifier ions, which balance their charge, they form stable metal-oxygen anion groups that can fit into the silicate. However, if insufficient modifier ions are present in the melt, amphoteric cations will act as modifier ions themselves [25,34,43–46].

- Network formers: Si^{4+}, Ge^{4+}, Ti^{4+}.
- Network modifiers: Na^{+}, K^{+}, Mg^{2+}, Ca^{2+}, Fe^{2+}, Cr^{3+}, Ti^{4+}, V^{5+}, Ba^{2+}, Sr^{2+}.
- Amphoterics: Al^{3+}, Fe^{3+}, B^{3+}, Zn^{2+}.

It should be noted that while ferrous iron, Fe^{2+}, is grouped as a network modifier, ferric iron, Fe^{3+}, is an amphoteric. The reasons for this distinction will be discussed in Section 9.4.

Fig. 10 gives a representation of some of the effects of the different network components. The top-image shows a SiO_2 network where silicon atoms are organised in a tetrahedral structure through oxygen bonds (long-range order is absent) [5]. If an alkaline earth oxide, MO (e.g. CaO), is introduced, a loosening of the network structure will be the result, as shown in the bottom left corner. In case an alkali oxide, M_2O (e.g. Na_2O), is introduced, the result will be a bond rupture as shown in the bottom right corner. A more thorough treatment of some of the most commonly encountered network modifiers is given later.

The role of phosphorus is not well established. Urbain (1987) and Senior and Srinivasachar (1995) assign it as a network former [43,45], while Kalmanovitch and Frank (1988) appoint it to be a network modifier [44]. Mysen (1988) argues that the solution of phosphorus in highly polymerised aluminosilicate melts results in depolymerisation of the melt while in depolymerised melts, phosphorus dissolves as a phosphate complex, most likely PO_4^{3-} and extracts metal cations, preferentially calcium, from the silicate network in the process. This results in a net polymerisation [47].

It appears that the average Si–O bond length in molten

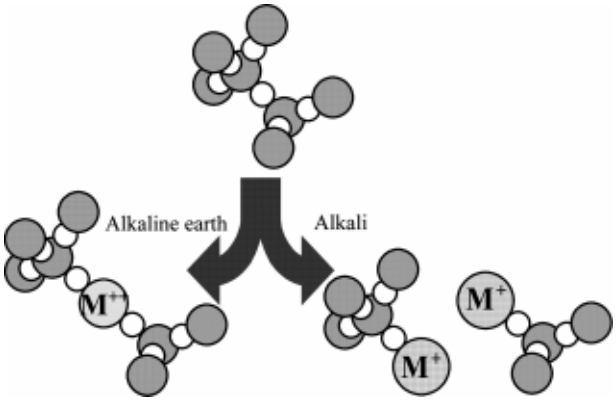

Fig. 10. According to the network theory, an alkaline earth metal can weaken the silica network by lengthening a bond between two silicon atoms, whereas an alkali metal will break the bond.

silicates changes little with temperature or pressure. However, the Si–O bond length increases in alkaline earth and alkali silicates in the series Ca, Mg, K, Na and Li [48].

In Ullmann's Encyclopaedia of Industrial Chemistry (1990), MgO is listed as an amphoteric oxide [5]. However, in other references MgO is uniformly listed as a network modifier, and as such it is also listed above [43–45].

7. Structural parameters

7.1. Ionisation potential

The ionisation potential of an atom is a measure of how strongly an electron is bound to the atom [49,50].

- The first ionisation potential of an atom is the energy required to remove an electron from the neutral atom to an infinite distance.
- The second ionisation potential of an atom is the energy required to remove an electron from the singly charged atom to an infinite distance.

According to Hess (1980), the value of the ionisation potential of the cation should be a good measure of the state of polymerisation of a melt. In general, melts containing cations of high ionisation potential should be more polymerised than melts containing cations of low ionisation potential. The ionisation potential of the cation is an important, but certainly not the only, property that must be considered in the analysis of melt structure. It has been demonstrated that both the size and the charge of the cation strongly influence the structures of ionic compounds [51].

7.2. Electronegativity

Electronegativity is a measure of the relative ability of an atom in a molecule to attract electrons to itself. It is considered to be a combination of the ionisation potential and the electron affinity of the atom. Electronegativities can be used to predict the nature of the bonding that a compound will have. The electronegativity of each atom depends not only upon the structure of the atom under consideration but also upon the number and nature of the atoms to which it is bonded, so each cationic element will have a range of electronegativities, each related to a combination of charge and coordination. For the scientist, the concept of electronegativity is useful but inexact, and there is no simple method of measurement [52,53].

Based on spectrographical measurements of silicate minerals from a schist (13 biotite ($K(Mg,Fe,Al)_3(Si,Al)_4O_{10}(OH)_2$), 13 hornblende ($Ca_2(Mg,Fe,Al)_5(Si,Al)_8O_{22}(OH)_2$) and 8 chlorite ($(Fe,Mg,Al)_3(Si,Al)_2O_5(OH)_4$) analyses), Nickel (1954) found that elements with similar electronegativities behave in a structurally similar fashion. Thus, the electronegativities of the elements can be used to predict their distribution among the minerals in which they occur. The minor elements fall into groups having similar electronegativities and these behave according to the major element they most resemble: cobalt, nickel, chromium, titanium and vanadium are iron-like; manganese, zirconium and scandium are more similar to magnesium [53]. Nickel based these conclusions on electronegativity values obtained from Fyfe (1951) [52].

Several electronegativity scales have been proposed, but none of these are very sensitive; they give only a rough grouping of cations. Although the ionisation potential is not a true measure of the electronegativity, it probably is related to it. Consequently, Hess (1980) assumes that an ordering of cations according to their ionisation potentials should be the same as ordering obtained from their true electronegativities [51].

7.3. Ionic potential

The concept of ionic potential (ratio of ionic charge to ionic radius (Å)) can be used to differentiate slag constituents

on the basis of their ability to attract a common anion (oxide ions in these systems). The strongest acids attract anions most strongly or are most able to effectively compete for anions to complete a regular close packed coordination. The bases are not able to compete for anions, and serve primarily as oxide ion donors.

This type of model involves the formation of large polymers by the acids, and polymer breaking by the bases. In the presence of a large amount of a very strong acid, SiO_2, some acidic constituents such as Al_2O_3 and Fe_2O_3, behave with an amphoteric character. Ferric iron (Fe^{3+}) behaves as a weak acid while ferrous iron (Fe^{2+}) is classified as a weak base. Thus, in a more oxidising environment, the system has a more acidic or highly polymerised character than in less oxidising environments, all other things being equal [29,54]. Temperature too plays a role on the oxidation state of iron. In a silicate melt in an oxidising atmosphere at temperatures near T_{cv} iron is primarily present as Fe^{3+} while at higher temperatures (above 1500°C) there will be considerable amounts of Fe^{2+} in the same melt and same atmosphere.

7.4. Field strength

Cationic field strength is defined as cation charge divided by cation–anion distance. Among network modifiers, those with the highest cationic field strength are most effective in reducing viscosity. A quantifiable distinction can be made between the three categories of atoms [5]:

- Network formers (acids): Field strength 1.4–2 N/m.
- Amphoterics: Field strength 0.5–1.0 N/m.
- Network modifiers (bases): Field strength 0.1–0.4 N/m.

The ranges for each category are but guidelines and a given cation may have a field strength that lies between two categories. In that case, a clear grouping is not possible.

It should be born in mind that a given cation may have different values of field strength depending on the coordination in which it appears, i.e. the ionic radius of magnesium depends on whether it appears in four-, five- or six-fold coordination. A list of cationic field strengths can be found in Table 1 of Brown Jr. et al. (1995) [34].

7.5. Bond valence

Pauling defined bond valence as the ratio of valence to the coordination number; but Brown et al. (1995) found that the bond valence of a M–O bond can also be calculated as a function of bond length, R (Å), and the bond valence parameter of the cation M, R_0 (Å):

$$\text{Bond valence} = \exp\left(\frac{(R_0 - R)}{0.37}\right) \tag{11}$$

where the R_0-values for an element vary as a function of the cation's valence but not as a function of coordination number. The explicit way of accounting for cation valence and coordination in Pauling's original definition is replaced by an implicit way, namely through the R_0 and R-values in Eq. (11).

Brown et al. (1995) tabulated both R (at 298 and 1773 K) and R_0 together with the related bond valences for a range of cations [34].

A classification of cations into network formers and modifiers is possible on the basis of bond valences. Two sets of guidelines have been proposed:

- Hess (1991) [55]
  Network former: Bond valence >0.75
  Network modifier: Bond valence <0.75
- Brown et al. (1995) [34]
  Network former: Bond valence $\in [0.75; 1.25]$
  Network modifier: Bond valence <0.75 or
  bond valence >1.25

Brown et al. (1995) found the introduction of an upper limit on the bond valences of network formers necessary, because it provided a more stringent definition of network modifier in that a cation–oxygen bond with bond valence >1.25 cannot share oxygens with SiO_4-tetrahedra. In contrast, cation polyhedra with M–O bond valences <0.75 can share oxygens with SiO_4-tetrahedra and thus can be embedded in the tetrahedral network.

In principle, the bond-valence model should be useful in developing constraints for medium-range structures around any cation, but it has found greatest use for highly charged cations that form bonds of high bond valence because such cations place the greatest constraints on possible atomic arrangements [34].

7.6. Oxygen

The notation of bridging and non-bridging oxygen bonds (BO and NBO) is described in Fig. 11. A BO is linked to two silicon atoms, while a NBO is only linked to one silicon atom.

A tectosilicate composition is one where the structure is fully polymerised, i.e. all the oxygens are stoichiometrically constrained to form bridging bonds between tetrahedral cations [56].

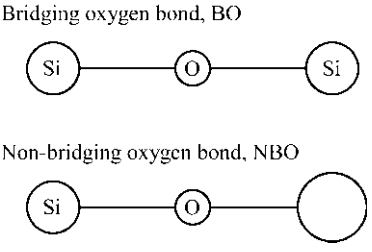

Fig. 11. A bridging oxygen atom (BO) is bonded to two silicon atoms. A non-bridging oxygen atom (NBO) is only bonded to one silicon atom.

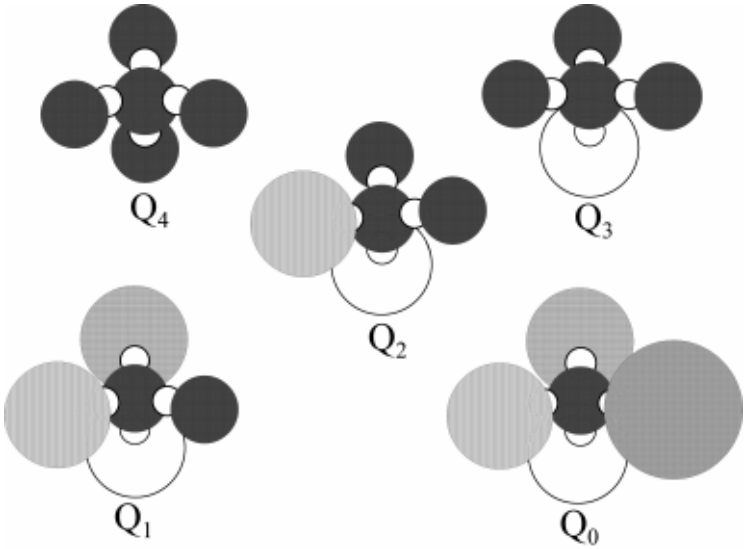

Fig. 12. The Q designation accounts for the number of bridging oxygens per silicon atom (Si = dark circles, O = white circles, all other circles = other atoms).

Senior and Srinivasachar (1995) define the ratio of NBO to BO (NBO/BO) [45]. Close examination of the expression indicates that the right hand side of the original expression should be divided by 2, which has been done below

$$\frac{\mathrm{NBO}}{\mathrm{BO}} = \frac{\mathrm{CaO} + \mathrm{MgO} + \mathrm{FeO} + \mathrm{Na_2O} - (\mathrm{Al_2O_3} + \mathrm{Fe_2O_3})}{\mathrm{SiO_2} + \mathrm{TiO_2} + 2(\mathrm{Al_2O_3} + \mathrm{Fe_2O_3})} \tag{12}$$

where the quantities CaO etc. denote molar fractions of oxides in the melt. In this equation, alumina and ferric oxides are assumed to be network formers, charge-stabilised by bases. The proceeding explanation of the construction of the ratio is based on considerations made in subsequent sections.

On the right hand side of the equation the numerator (denominator) corresponds to 2·NBOs (2·BOs). Addition of one network modifying oxide creates two NBOs. One basic oxide molecule stabilises one Al_2O_3 or Fe_2O_3 molecule in tetrahedral coordination in the network, creating four BOs and cancelling two NBOs.

The relationship between the NBO-to-BO ratio and the O-to-Si ratio can be derived through a series of structural considerations. The total number of oxygen atoms in the melt is given as the sum of NBO and BO

$$\mathrm{O} = \Sigma\mathrm{O} = \mathrm{NBO} + \mathrm{BO} \tag{13}$$

Each silicon atom can accommodate four oxygen atoms. If all oxygen atoms are NBOs, the relationship is four NBOs to one silicon atom; if they are all BOs, the relationship is two BO to one silicon atom. Thus the total number of silicon atoms in the melt is

$$\mathrm{Si} = \frac{\mathrm{NBO}}{4} + \frac{\mathrm{BO}}{2} \tag{14}$$

By rearrangement of these two equations, an alternative formulation of the NBO-to-BO ratio appears [57]

$$\frac{\mathrm{NBO}}{\mathrm{BO}} = \frac{2\cdot(\mathrm{O/Si} - 2)}{4 - \mathrm{O/Si}} \tag{15}$$

7.7. Q designation

Q designation is used in the structural description of glasses and melts [5]. It is based on the presence of BO and NBO. The designations are as follows, Fig. 12 [5]:

1. Each silicon atom is coordinated tetrahedrally to four oxygen atoms.
2. If all oxygen atoms in a tetrahedron are connected to two silicon atoms, the local environment around the silicon atom is designated Q_4. All four Si–O bonds of the tetrahedron are, therefore, bridging bonds.
3. The local silicon environments are designated Q_3, Q_2, Q_1 and Q_0 if three, two, one or zero oxygen atoms are connected to two silicon atoms. In Q_3 there are three BO and one NBO, and for Q_0, all Si–O bonds are NBO.

8. Flow

Stebbin et al. (1995) state that local bond breaking such as the breaking of the strong Si–O bonds is the primary control on flow in molten $K_2Si_4O_9$ and $(Na_2O)_{0.4}(SiO_2)_{0.6}$, and they claim that alternative mechanisms, such as the relative

motion of large molecular units (e.g. chains or sheets) or of coherent domains (e.g. silica-like clusters) involving the breaking primarily of weak bonds to network-modifying cations along domain boundaries, seem to be ruled out. They also infer that a lowering of the silica content tends to decrease viscosity both because a smaller proportion of the bonds broken during flow are strong Si–O bonds and also because NBO linkages are weakened by increasing interactions among network modifying cations and BOs [58].

Conductivity and viscous flow are probably positively correlated with the strength of bonds between tetrahedrally coordinated cations and oxygen. Since increasing bond length is associated with a decreasing inter-tetrahedral angle, a lowering of the inter-tetrahedral angle will enhance diffusivity and conductivity and lower viscosity [47].

Because viscosity is a measure of the resistance to flow of a certain volume of melt, not of a given number of atoms, such factors as the number of ions and the number of network linkages per unit volume should be taken into account, as well as the relationship between polarising tendencies, ionic volumes etc., when the effects of individual cations on viscosity are considered in detail [59].

The importance of this aspect can be illustrated by the work of Hochella and Brown (1984). They found, that the viscosity of the compositional series of melts albite ($NaAlSi_3O_8$)–jadeite ($NaAlSi_2O_6$)–nepheline ($NaAlSiO_2$) differ over two orders of magnitude not because of significant structural change, but because the concentration of Si–O–Si linkages gives way to $Si-O\langle^{Al}_{Na}$ linkages within an apparently similar framework structure. This indicates that melts of magmatic composition can undergo compositional changes that dramatically affect their viscosities without resulting in a structural change of the melt [32].

Most materials decrease in viscosity as temperature increases. The dependence is logarithmic and can be substantial, up to 10% change per degree Kelvin [11].

9. The cations

In the following the role of different species on the structure and viscosity of silicate melts will be summarised. The species chosen for investigation are mainly the ones most frequently encountered in silicate melts and glasses of relevance to combustion systems.

- Alkali metals: Li, Na, K
- Alkaline earth metals: Mg, Ca
- Aluminium
- Iron
- Titanium

The chemical composition of coal ashes varies within wide ranges, but SiO_2 as the major component is often encountered in concentrations ranging between 40 and 65 wt%. Al_2O_3 is generally the second-most concentrated species with concentrations ranging between 20 and 35 wt%. Iron-oxide and CaO are encountered in concentrations up to 20 and 15 wt%. MgO is rarely found in concentrations major than 5 wt%, and oxides such as K_2O and TiO_2 are found in concentrations that do not exceed a few wt%. Li_2O is not present in coal ashes at more than trace-level, but it is included in the presentation for the sake of completeness. Phosphorus is found in most low-temperature coal-ashes but it is of no significance to high-temperature deposits. Numerous other oxides can also be found in coal ashes, but in concentrations less than 1 wt%.

Each section will concentrate firstly on the effect of the species in a binary silicate melt and secondly on the effect of the species in silicate melts of higher order.

As a general rule, the presence of an inordinately high amount of any single component, such as SiO_2, CaO or Fe_2O_3, in the ash should serve as a warning to look for abnormal slag behaviour [60].

9.1. Alkali metals, Li, Na, K

Alkali metals are classified as network modifiers. In alkali silicates (crystalline as well as vitreous) the structural feature most crucial to viscosity is the appearance of NBO. The solution of an alkali metal oxide into the silica network leads to the transformation of a BO bond to a NBO bond [61]:

$$\equiv Si–O–Si\equiv + M_2O \rightleftarrows \equiv Si–O^-M^+ + M^+O^-–Si\equiv \quad (16)$$

In Q-notation this becomes

$$2Q_4 + M_2O \rightleftarrows 2Q_3 \quad (17)$$

The resulting loosening, or depolymerisation, of the tetrahedral network sharply decreases the liquidus temperature as well as viscosity [5,9]. The effect is illustrated for Na_2O in Fig. 13.

Binary alkali silicates are completely miscible in the liquid state [62], but viscosity increases rapidly when the alkali concentration decreases to below about 10 mol%, see Fig. 13. For such low concentrations the structure consists essentially of a three-dimensional silica network with cations randomly distributed in the interstices. On addition of alkali to more than 10 mol% the structure collapses to one consisting of Si–O rings with cations randomly distributed between the anion units [62]. This postulate is supported by density measurements, showing an almost constant specific volume up to about 12 mol% from where the specific volume increases sharply upon further addition of alkali oxide [26].

Small additions of sodium oxide enhance the crystallisation of SiO_2, and for low Na_2O ($<20\%$) silicate glasses, glass–glass phase separation occurs [9].

The viscosity of a binary silicate melt depends on the size of the alkali cations. The smaller the radius of the

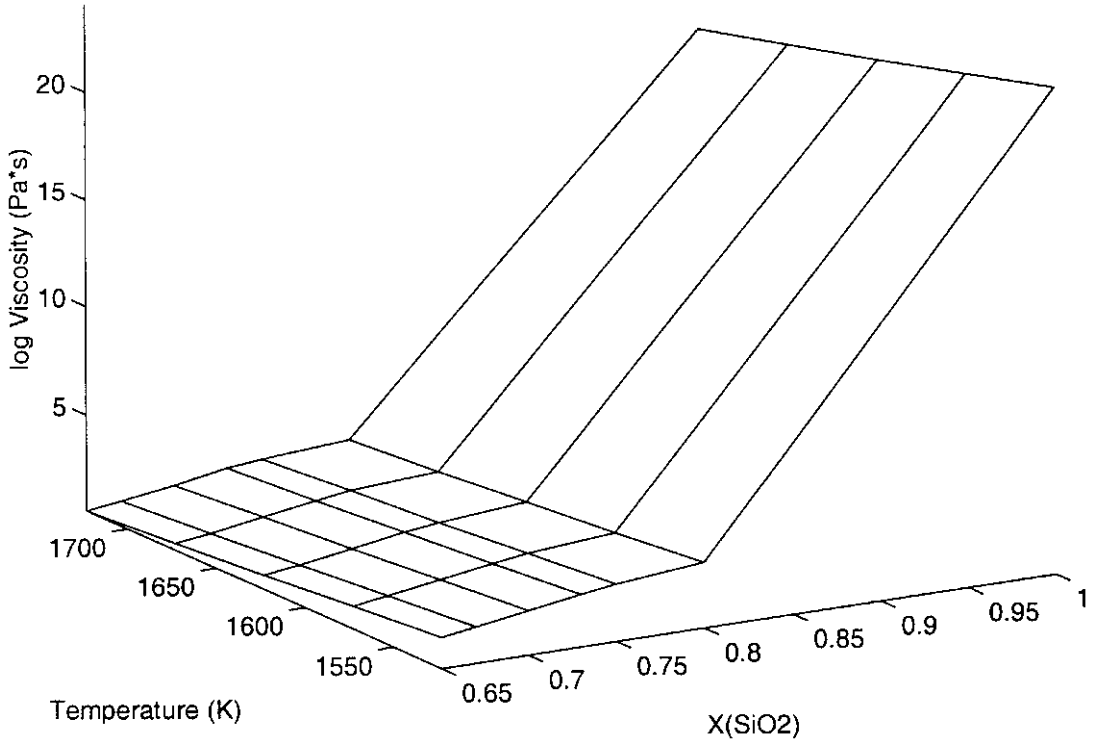

Fig. 13. Viscosity depicted as a function of temperature and mole fraction SiO_2, $x(SiO_2)$, for the system SiO_2–Na_2O [20,36].

monovalent cation (corresponding to a higher field strength) the more attraction the non-bridging oxygen experiences from the cation. This becomes manifest in a decrease of viscosity in the series $\eta(\mathrm{Li}) > \eta(\mathrm{Na}) > \eta(\mathrm{K})$ at temperatures below 900 K and alkali concentrations in the range of 17–40 wt% [59]. At high temperatures (low viscosities) the mobility of the cation becomes more important and the series is reversed, i.e. $\eta(\mathrm{K}) > \eta(\mathrm{Na}) > \eta(\mathrm{Li})$ [9,59]. De Jong and Brown (1980) have shown that, for the group IA elements of the periodic table, H–K, K^+ forms the weakest bond with the bridging oxygen in a model $H_6Si_2O_7$ dimer molecule, while Na^+, Li^+ and H^+ form progressively stronger bonds [32].

X-ray and infrared spectroscopy studies have revealed that binary glasses are characterised by the formation of micro-heterogeneity, i.e. division into regions of varying silica content. This tendency is restrained when one alkali oxide is replaced by another (i.e. a second alkali oxide is introduced at the expense of the original alkali oxide), and the glass becomes more homogeneous [63].

Another property of the binary silica–alkali mixtures is that the thermal expansivity over the range 25–1300°C increases with alkali content [37].

In binary as well as multi-component acidic melts, the addition of Na_2O not only depresses viscosity, it also lengthens the glass, i.e. it dampens the temperature effect on viscosity at temperatures below T_{cv} (see Fig. 14) [64]. However, according to Hurley, the effect is instrument-dependent, and it does not appear for melts measured with a rotating bob viscometer [28].

Based on measurements in the system SiO_2–FeO_x–Na_2O in the temperature range 673–923 K, Klein et al. (1981) found that for otherwise identical conditions, viscosity decreases with increasing Na_2O content and decreasing SiO_2 content [65,66].

In melts containing more than one alkali species, many properties, though rarely viscosity, exhibit spectacular maxima or minima. The mixed alkali effect results in enhanced stability of the intermediate compound which again results in the development of maxima in enthalpy, free energy, electrical conductivity, and chemical durability when one alkali component is replaced by others at a definite optimum ratio of oxides. The magnitude of the effect depends on the difference in ionic radii, on the total content of ion-conducting oxides, and on the type of the glass-forming system [9,47,63].

When Na_2O is replaced by K_2O in glasses of the system SiO_2–Na_2O–K_2O (while keeping the concentration of silica constant), a minimum effect on viscosity is observed when the total alkali oxide content exceeds 10 mol%. The effect is observed in chemically heterogeneous glasses, and an increase in the difference between the ionic radii leads to a weakening of the effect [63,67].

A point to bear in mind when working with alkali-

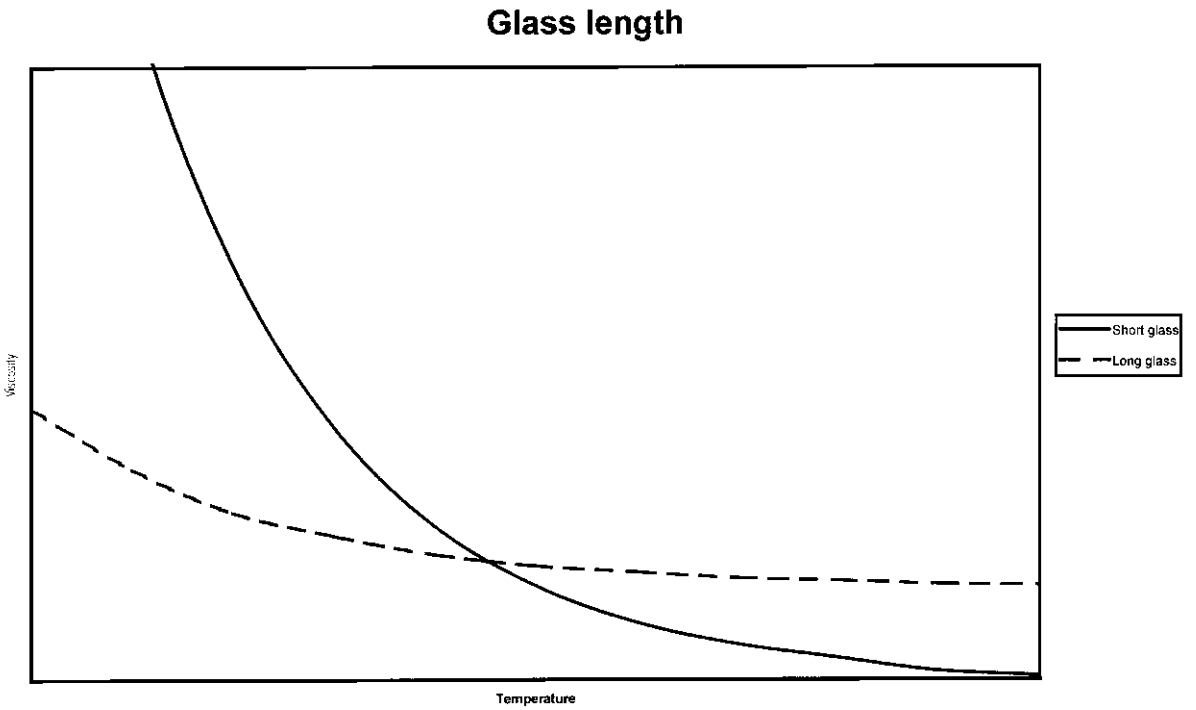

Fig. 14. The influence of a change in temperature on viscosity is increased when a glass is shortened.

containing silicate melts is that when the temperature of a liquid increases, the composition is subject to changes due to preferential volatilisation of species. The alkalis typically have the higher vapour pressures in these systems, and therefore the acidity can be expected to slightly increase as a result of this volatilisation [29] leading to a rise in viscosity.

9.2. Alkaline earth metals, Mg, Ca

Although alkaline earth metals are classified as network modifiers, their structural role is of an amphoteric nature, i.e. Nickel (1954) found magnesium to occupy octahedral sites in the schist-minerals hornblende, biotite and chlorite [53].

In general, alkaline earth oxides, MO, tend to decrease viscosity by one of two mechanisms. Eq. (17) corresponds to a divalent atom covalently linked between two silica tetrahedra.

$$\equiv\text{Si–O–Si}\equiv + \text{MO} \rightleftarrows \equiv\text{Si–O–M–O–Si}\equiv \quad (18)$$

Eq. (19) shows an M^{2+}-atom held in close proximity to the oxygen atoms due to their electric charges. It is an ionic linkage with more or less free M^{2+}-ions [59]:

$$= \text{Si–O–Si} = + \text{MO} \rightleftarrows 2(= \text{Si–O}^{-}) + \text{M}^{2+} \quad (19)$$

The nature of the actual mechanism is most likely to be a mixture of the two mechanisms here cited.

For the alkaline earth–silica system there is a sharp increase in viscosity below about 20 mol% of the alkaline earth oxide. With the addition of alkaline earth oxide to silica, Si–O bonds are broken and the cations are randomly distributed throughout the lattice, giving rise to two major effects:

- weak points in the silica network introduced by the rupture of Si–O bonds;
- a general loosening of the lattice owing to the polarising effect of the cation that weakens the Si–O bonds near the metal ion.

As for the alkali oxides, the theory is supported by density measurements showing strong influence of alkaline earth oxide concentration on the specific volume of the melt for concentrations greater than 20 mol% [26,36,68].

The individual alkaline earth oxides differ in their effect on viscosity. Nowok et al. (1991) state that among the alkaline earth metals, Ba most powerfully reduces viscosity, followed by Sr, Ca and Mg [46].

The effect of alkaline earth metals on the structure of silicate melts is not quite as simple as the grouping of the elements as network modifiers could indicate. CaO and BaO have cations sufficiently large to accommodate six or higher coordination with oxygen. But MgO tends to decrease its coordination from six to four at higher temperatures, causing an abnormal η–T correlation [9], as indicated by data produced by Bockris et al. in 1955 (Fig. 15). A sudden

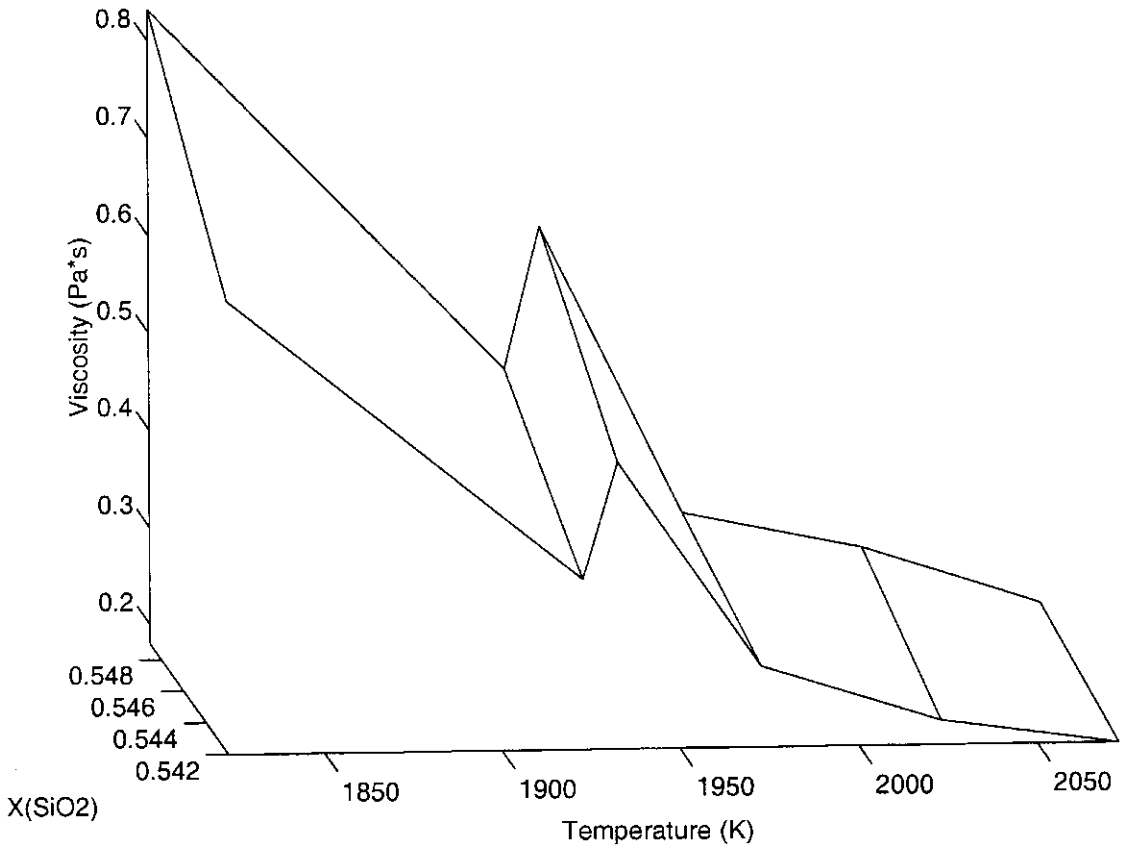

Fig. 15. Effect of temperature and mole fraction of SiO_2 on the viscosity of SiO_2–MgO melts: The shift from coordination six to four for magnesium causes an abnormal viscosity–temperature relationship [36].

decrease is registered in the viscosity of binary melts when lowering the temperature of the melt by 10° from 1933 to 1923 K.

At high silica concentrations, alkaline earth silicates tend to separate into two liquids [62]; this trend is shown in the binary phase diagram for SiO_2 and CaO (Fig. 16), where two liquids are formed at concentrations between 73 and 98 wt% SiO_2 and temperatures above 1698°C [69].

The addition of CaO to SiO_2 introduces NBOs in the network, resulting in a strong negative effect on viscosity. At high temperatures, viscosity decreases as more CaO is added, but at low temperatures the effect is reversed and the addition of calcium reinforces the structure of the melt as it coordinates the NBOs. In the terminology used by glass manufacturers, CaO shortens the glass, i.e. it pronounces the effect of temperature on viscosity. This effect is illustrated in Fig. 17, where it can be observed that the temperature–viscosity graphs will cross for different levels of CaO-addition.

MgO has an even stronger shortening effect on binary glasses than CaO; the addition of magnesium oxide to a given SiO_2–MgO glass will cause the viscosity of the resulting glass to increase more rapidly with decreasing temperatures than it did for the original glass. The effect is closely related to the bond strength of this species to oxygen.

MgO has relatively small Mg^{2+} ions which may assume the coordination of four as MgO_4 tetrahedra or can be housed in interstices as octahedral coordination. Part of the Mg will thus enter the glass structure as MgO_4 building units in addition to acting as modifiers in interstices or bridge linkages [59,70].

The effect of adding CaO to an alkali silicate is similar to what is observed when adding CaO to pure SiO_2. The low-temperature shortening of the glass causes a sharp viscosity-increase with decreasing temperatures [9]. El-Badry et al. (1981) found that for ternary mixtures with SiO_2 and Na_2O, the effect of temperature on viscosity is most pronounced when the third oxide is CaO, followed by SrO, BaO and MgO [59].

Ba is the only alkaline earth metal that monotonically depresses viscosity with increasing concentration. Sr also shows this effect at high temperatures, but at low temperatures the effect is reversed. Mg displays an ambivalent effect similar to that of Ca [59].

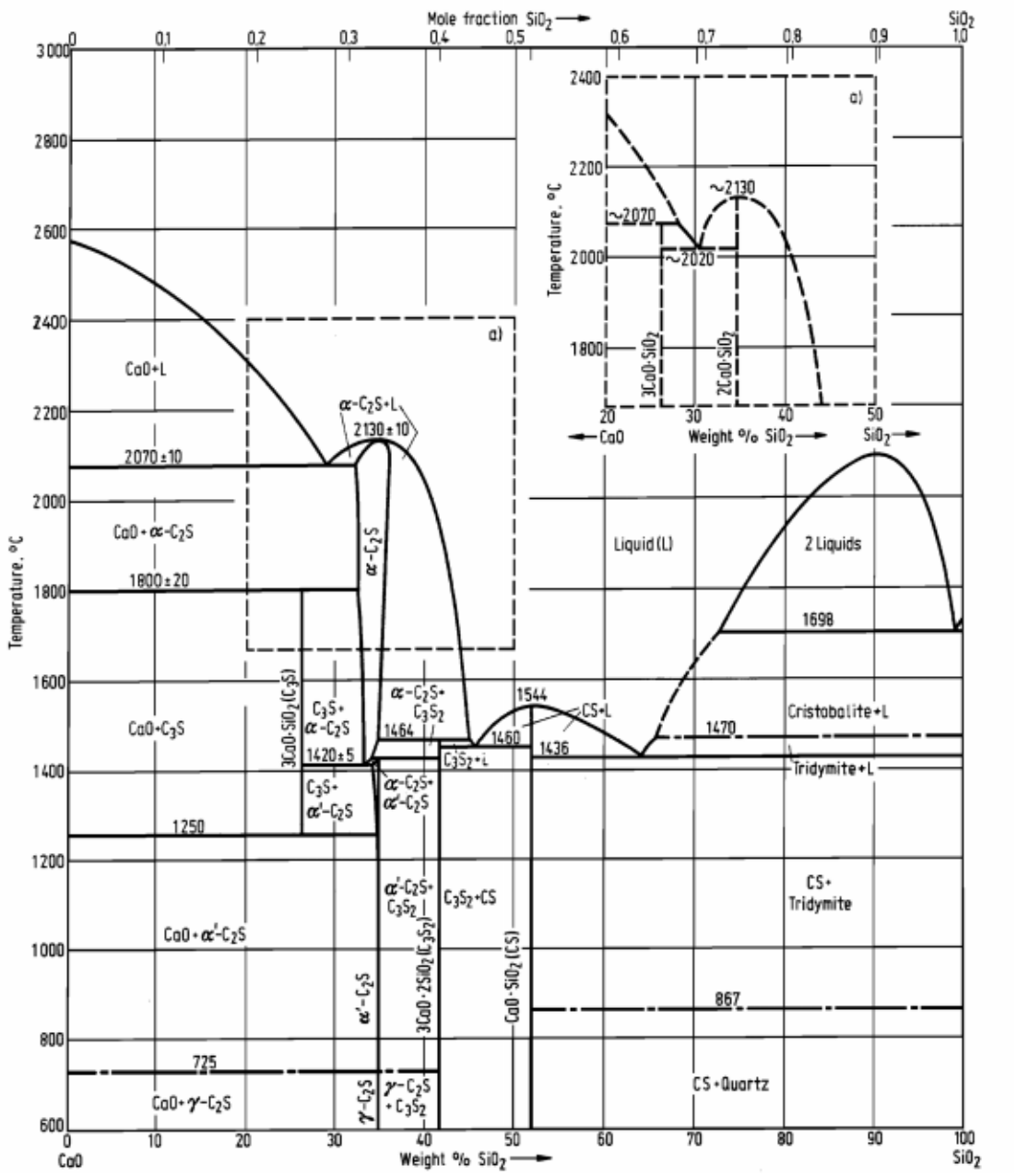

Fig. 16. Phase diagram SiO_2–CaO. Abbreviations C and S used for CaO and SiO_2, thus e.g. $C_3S = 3CaO{\cdot}SiO_2$. Redrawn after Obst, Fix, Trömel, Heinke, Rankin, Wright, Muan, Osborn and Ol'shanskii [69] (by permission of the publisher).

When ternary melts are created by replacing some of the CaO in a binary SiO_2–CaO glass with MgO, minima of viscosity are obtained, and the glass shortens [9].

Aluminium-containing silicates often exhibit particular characteristics due to the amphoteric character of aluminium. Since coal ash slags almost always contain aluminium and silicon oxides, an understanding of the behaviour of aluminosilicate melts is necessary for predicting the viscosity of slags in practical combustion systems.

In 1964, Riebling studied the SiO_2–Al_2O_3–MgO system and found a gradual formation of MgO_6 octahedra from MgO_4 tetrahedra to accompany the substitution of MgO for Al_2O_3 in melts containing 50 mol% SiO_2 [71]. In a

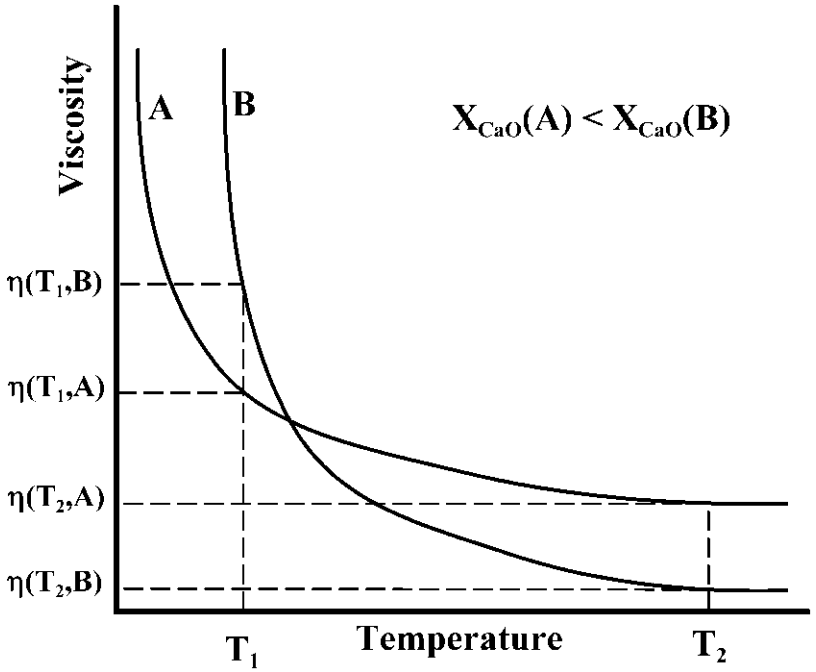

Fig. 17. SiO_2–CaO:CaO shortens the glass.

study on the system SiO_2–Al_2O_3–CaO–MgO, Yakushev et al. (1977) found that a variation in the CaO content from 40 to 58% has a significant effect on the viscosity and on the initial solidification temperature of the slags. The addition of CaO to the slag with a constant ratio of the remaining components affects viscosity in a similar way as additions of magnesium oxide — the viscosity of slags in the homogeneous state is decreased and T_{liq} rises [72].

Examination of the system SiO_2–Al_2O_3–Na_2O–K_2O–CaO–MgO revealed that further addition of CaO made the melt viscosity more sensitive to temperature changes over the whole temperature range from 800 to 1700 K, while MgO had that effect only at the high end of the temperature-range [73].

Observations of various natural glasses indicate that magnesium occupies octahedral sites in these glasses [53].

9.3. Aluminium

Aluminium is categorised as an amphoteric in the network theory; it can act as either a network former or a network modifier. It can be tetrahedrally coordinated when charge balanced by a basic oxide.

The introduction of aluminium into a pure SiO_2-network will lead to a weakening of the structure [35] and an increased friability; the reduction in viscosity is substantial: at a concentration of 10 wt% Al_2O_3 and temperatures in the range of 2000–2500 K, the viscosity reduction is about two orders of magnitude as compared to pure SiO_2, and it amounts to three orders of magnitude at 18 wt% Al_2O_3 [74].

When Al_2O_3 is introduced into an alkali and/or alkaline earth oxide-containing silicate glass in lower concentration than the alkali and alkaline earth oxide ($Al_2O_3 < M_2O + MO$), then, for a wide range of compositions, NBOs are eliminated because the trivalent aluminium engages basic oxide for charge stabilisation when it is incorporated into the SiO_2-network (Fig. 18). The result is an increase in viscosity until the concentration of aluminium oxide balances that of the sum of the alkali and alkaline earth oxide. In this case, aluminium acts as a network former, occupying tetrahedrally coordinated sites with charge-balancing alkali or alkaline earth cations [68,75].

Bottinga and Weill (1972) argue that aluminium oxide should not be considered an isolated species when studying

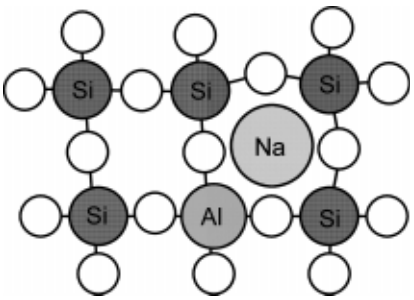

Fig. 18. Aluminum demands charge stabilisation to enter the silica network in tetrahedral coordination (Si = dark circles, O = white circles, Al = darkly hatched circle, Na = lightly hatched circle) [68].

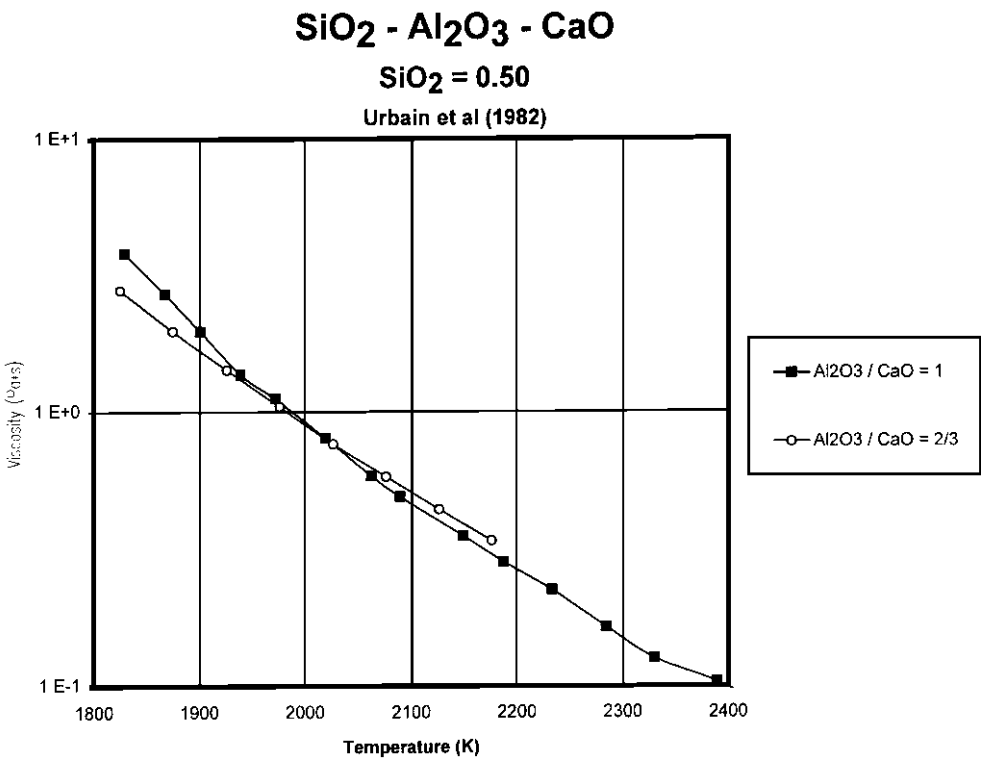

Fig. 19. The effect of the Al_2O_3–CaO ratio on viscosity for $x_{SiO_2} = 0.5$ [20].

the compositional effects on the viscosity of a silicate melt. They believe that Al_2O_3 combines preferentially with K_2O to form $KAlO_2$, and that an excess of Al_2O_3 is further combined with Na_2O, BaO, SrO, CaO, MgO and MnO in that order until all Al_2O_3 is used up. According to the authors, the sequence corresponds to the order of stability suggested by viscosity measurements. A more viscous melt coincides with a more stable melt, all other things being equal. For example, if potassium is added to an aluminosilicate melt, a higher viscosity results than if instead an equal amount of sodium had been added [68].

Viscosity will decrease when more Al_2O_3 is added to the melt than can be balanced by the alkali and alkaline earth oxides present ($Al_2O_3 > M_2O + MO$). Studies by NMR techniques have revealed that excess aluminium, lacking charge-balancing cations, will occupy five-, six- or even higher coordination sites, resulting in a weakly network modifying behaviour. This is particularly noticeable in the absence of alkali [9,75–78].

The role played by aluminium in silicate melts is not quite as simple as the proceeding could lead one to believe. For instance, the effect of the coordination of aluminium on viscosity is not clear. Based on a Raman spectroscopic study on liquid jadeite ($NaAlSi_2O_8$), Urbain, Bottinga and Richet (1982) concluded that, although a change in aluminium coordination from four to six fold is believed to cause a decrease in viscosity as a result of an increase in the concentration of NBOs in the melt, the observed viscosity decrease in aluminosilicate melts with increasing pressure can not be explained in this way [20].

The effect of temperature on the coordination of aluminium is not clear. Urbain, Bottinga and Richet (1982) produced results that are in contradiction with the anticipation that aluminium should become more tetrahedrally coordinated at higher temperatures [20].

According to the general theory on the amphoteric role played by aluminium in silicate melts, an addition of Al_2O_3 that equals the total amount of alkali and alkaline earth oxide ($Al_2O_3 = M_2O + MO$) should result in all aluminium being in tetrahedral coordination. Results from the study by Urbain, Bottinga and Richet (1982) contradict this simple concept by showing a higher viscosity for a ternary melt with $Al_2O_3/CaO = 2/3$ than for one with $Al_2O_3/CaO = 1$ ($SiO_2 = 0.5$) for temperatures exceeding 2000 K (Fig. 19) [20]. These observations are indirectly confirmed by Stein and Spera (1993), who found the introduction of Na and Al in a 1:1 molar ratio into molten SiO_2 to produce irregular intra-tetrahedral network distortion. In addition, they observed a net reduction of intra-tetrahedral bond strength due to both the greater Al–O bond length and the polarising effects of six-membered ring hole filling by Na. These microscopic features give rise to a decrease in both viscosity and its temperature derivative [35].

Potanin et al. (1976) experimentally found that for the

system SiO_2–Al_2O_3–CaO, viscosity increases sharply with increasing concentrations of silica and alumina at temperatures below 1550°C and melt concentrations of about 50% Al_2O_3 and 40% CaO [79].

There appears to be a relationship between an increasing polymerisation of the silicate structure and an increasing tendency for aluminium to replace silicon [53]. Studies on viscosity–temperature relationships for fully polymerised alkali and alkaline-earth aluminosilicate liquids define a trend of decreasing viscosity with increasing field strength or decreasing basicity of the network-stabilising (alkali or alkaline-earth) cation [56].

Although the structural role of aluminium is variable, experimental data suggest that aluminium is in no case capable of creating Al–O–Al bonds due to their inherent electrostatic instability. Aluminium is distributed exclusively in Si–O–Al bonds [57,76,80].

In 1965, Lacy proposed a network forming index, R, as the ratio of the molecular percentage of non-bridging oxygens, NBO, to network forming cations, Si, Al [81].

$$R = \frac{\text{NBO}}{\text{Si} + \text{Al}} \tag{20}$$

Piwinskii and Weed (1980) experimentally found the viscosity of some multi-component melts of to decrease with increasing values of R [81].

This section will be concluded with a couple of observation of special importance to specific areas:

- Glass makers make use of the fact that Al_2O_3 in small quantities, suppresses phase separation, this counteracts the tendency of Na_2O to enhance the crystallisation of SiO_2 [9].
- Most melts of geological interest have compositions such that the sum of alkali and alkaline earth oxides exceeds Al_2O_3 on a molar basis [68]. This is also true for the bulk composition of many coal ashes and slags from practical combustion systems, whereas the individual ash particles may vary significantly in composition, as evidenced for a couple of ash slags by Nowok (1994) [82].

9.4. Iron

Iron plays an important, and complex, part in the structural properties of silicate melts. This part is dominated by two main features, each influenced by several aspects of the prevailing conditions, and both intimately linked to each other:

- oxidation level
  - atmosphere
  - concentration of other species in the melt
  - temperature
- coordination
  - atmosphere
  - concentration of other species in the melt
  - temperature
  - melt acidity

9.4.1. Oxidation level

Iron can occur both as a network modifier (ferrous iron, Fe^{2+}) and as an amphoteric (ferric iron, Fe^{3+}) [41,83], and it is of great structural importance to know the distribution of iron between the two oxidation states. It is for this purpose that the $Fe^{3+}/\sum$Fe-ratio has been defined as the ratio of molar concentration of ferric ion to the total molar concentration of iron (i.e. "Fe" $= x_{Fe}$ and $\sum \text{Fe} = \text{Fe} + \text{Fe}^{2+} + \text{Fe}^{3+}$). The ratio is a function of temperature, pressure and atmosphere [83].

The degree of polymerisation of a silicate melt depends on the $Fe^{3+}/\sum$Fe-ratio, and viscosity measurements on silicate melts are of limited value, if this ratio is not known [20]. Therefore, Schobert et al. (1982) propose that tests run in different atmospheres should be supplemented by characterisation of the iron by such techniques as Mössbauer or XPS (X-ray photon spectroscopy) [21].

There is a general tendency for the $Fe^{3+}/\sum$Fe-ratio to increase with the alkali and alkaline earth oxide content of the melt [41,76].

Seki and Oeter (1984) studied the effect of parameters such as Fe-oxidation state, CaO/SiO_2, and atmosphere on the viscosity of melts in the system SiO_2–FeO_x–CaO [30]. Fig. 20 shows that for all other conditions constant:

- $Fe^{3+}/\sum$Fe decreases with increasing temperatures;
- An increase in CaO/SiO_2 leads to a increase in $Fe^{3+}/\sum$Fe;
- An increase in total Fe-content (i.e. a decrease in SiO_2 and CaO) leads to a decrease in $Fe^{3+}/\sum$Fe for $CaO/SiO_2 = 1.5$, and an increase in $Fe^{3+}/\sum$Fe for $CaO/SiO_2 = 0.7$.

In a study on the system SiO_2–FeO_x–Na_2O, Dingwell and Virgo (1987) found a decrease in the $Fe^{3+}/\sum$Fe-ratio to cause a strong, non-linear reduction of the viscosity of oxidised melts. They also found the effect to depend distinctly on the composition of the melt [84]. In another study on the same system, the oxidation state of iron was found to become important in glasses containing more than 10 mol% FeO_x. For these glasses there is a major effect of the choice of atmosphere on the melting-behaviour of the glass. On the basis of these observations, it was concluded that at concentrations exceeding 10 mol% FeO_x, Fe^{3+} may behave like Al^{3+} and Fe^{2+}, like an alkaline earth [65,66].

A study on the SiO_2–Fe_2O_3–MO/M_2O system revealed that Cs gives the highest viscosities for a given melt in the temperature and compositional range of the study, followed by Rb, K, Na, Ba, Sr, Ca, Mg and Li with the lowest viscosity [56].

The molar volume of glasses appears to increase with increasing $Fe^{3+}/\sum$Fe-ratio, and for each composition there is an approximately linear relationship. If the molar volume is a reflection of the packing efficiency of the glass structure,

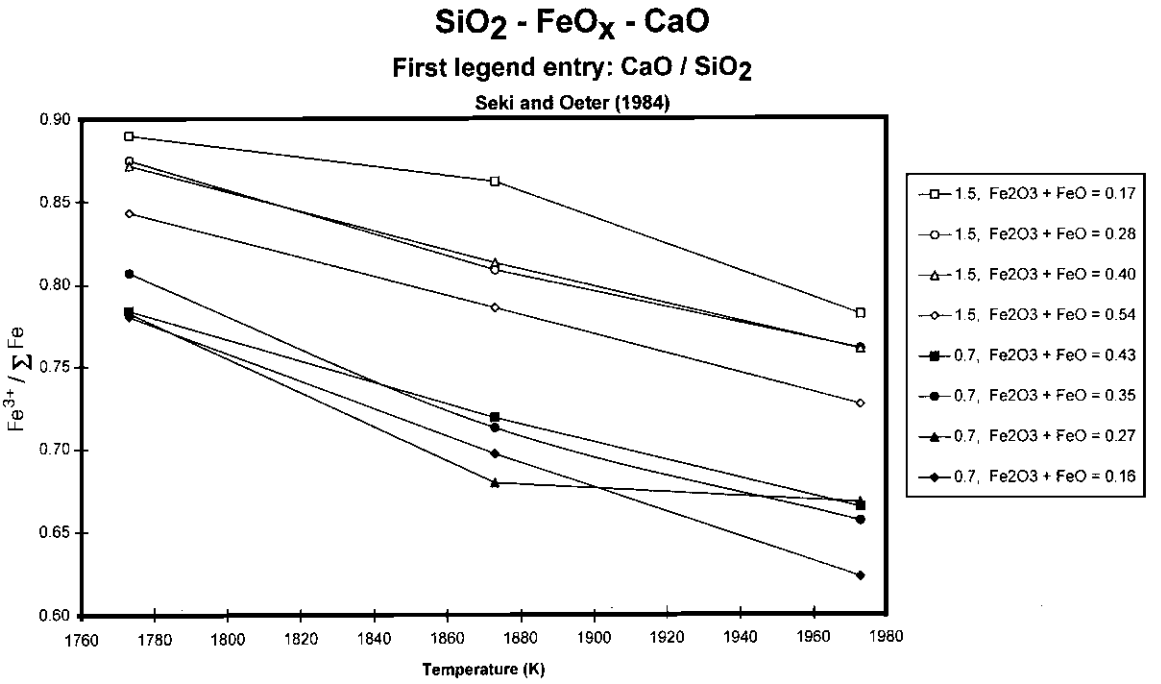

Fig. 20. Effect of temperature on the $Fe^{3+}/\sum Fe$-ratio in the system SiO_2–FeO_x–CaO, atmosphere: air [30].

then the reduced glasses may have Fe^{2+} packed into holes in the structure, while oxidised glasses may have Fe^{3+} acting to open up the structure. The trends observed in the calculated molar volume are in line with the higher viscosities in oxidised glasses [66].

Temperature also has an effect on the oxidation level of iron. In 1993, Nowok et al. reported the results of some ^{57}Fe Mössbauer-spectra performed on a Beulah lignite-slag (North Dakota, USA), consisting mainly of SiO_2 and CaO and containing 5 mol% Fe_2O_3. They found 96% of the iron to be present as Fe^{3+} at 1400°C as compared to 88% at 1500°C. On this basis, they concluded that below 1400°C nearly all iron exists as ferric iron in air [76].

9.4.2. Coordination

It is beyond doubt that the coordination of iron affects viscosity. However, structural investigations do not give a clear answer to the coordinational properties of the two oxidation states of iron. By analogy to crystals, Klein et al. (1983) suggest that, typically, divalent iron is surrounded by four or six oxygens, while trivalent iron is more commonly surrounded by six oxygens [66]. In contradiction to this, Nowok (1995) writes that investigations on alkali and iron-bearing silicate and aluminosilicate melts have shown that Fe^{3+} is tetrahedrally coordinated by oxygen (in analogy to Al^{3+}, the charge deficiency of the Fe^{3+} ion is compensated by an alkali ion) and Fe^{2+} is octahedrally coordinated. He also writes that he did not find the same clear trend for alkaline melts [41].

Fig. 21 contains a schematic drawing of Fe in tetrahedral and octahedral coordination with SiO_4^{4-}-tetrahedra. If iron molecules are to be bonded to tetrahedrally coordinated silicon atoms, a charge deficit in the range of 1–4 will arise. Thus, the structure needs charge-stabilisation by positively charged atoms [41]. This charge stabilisation has been illustrated in Fig. 22, where a sodium ion stabilises a ferric ion in tetrahedral coordination.

In all of its coordinations, iron can participate in the formation of complexes. According to Bodnár et al. (1978), the Fe^{3+} cation may build complex $Fe_xO_y^{2-}$ anions with oxygen in homogeneous melts (probably mostly FeO^{2-} and $Fe_2O_5^{2-}$, see Fig. 23), thus complicating the structure of the melt and increasing viscosity [70].

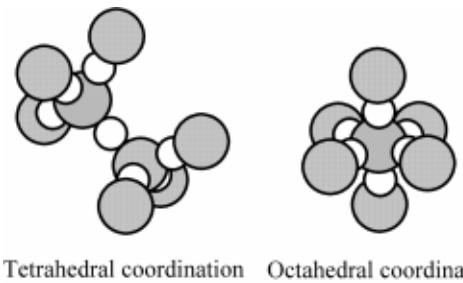

Fig. 21. Iron in tetrahedral and octahedral coordination in the silica network (Si = dark circles, O = white circles, Fe = circles with dark squares).

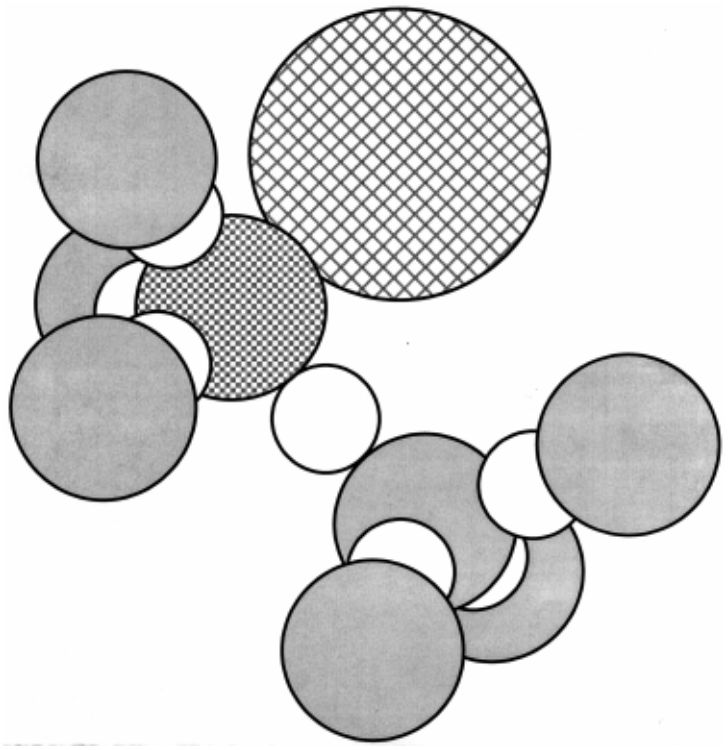

Fig. 22. Charge stabilisation for Fe^{3+} in tetrahedral coordination in the silica network (Si = dark circles, O = white circles, Fe = circle with dark squares, other atom = circle with dark grid).

9.4.3. General observations

According to studies performed by Dingwell and Virgo (1987) on glasses of the system SiO_2–FeO_x–Na_2O, ^{57}Fe Mössbauer spectra of quenched melt samples indicate that a transition of ferric iron from tetrahedral to non-tetrahedral coordination with decreasing $Fe^{3+}/\sum Fe$, results in a minimum in bulk polymerisation, which corresponds closely to a region of iron-invariant viscosity [84].

Danek et al. (1985) found the viscosity of melts in the system SiO_2–FeO_x–CaO to increase with increasing SiO_2-content and with decreasing temperature. The melt viscosity was generally decreased by the addition of iron oxides, indicating that not only calcium but also iron cations reduce the polymerisation of the silicate anions [4] in an oxidising atmosphere, see Fig. 24 for $SiO_2/CaO = 1$.

In a study on the system SiO_2–Al_2O_3–FeO_x–Na_2O, Klein et al. (1983) found indication that the combination

Fig. 23. Iron-oxide anions, claimed to exist in silicate melts [70].

(Fe + Al) acts to increase viscosity more than Fe alone decreases viscosity. They concluded that this supports the idea that $(NaFe^{3+}O_4)^{4-}$, see Fig. 25, behaves like $NaAlO_4$ or SiO_2 [66].

9.5. Titanium

In coal slags, titanium is rarely present in excess of several weight percent TiO_2, and the TiO_2-content of magmatic rocks rarely exceeds 2 wt% [47].

The structural role played by titanium in a silica network seems to be complex. It is only superficially understood, and at this moment, it is not possible to predict whether titanium will enter a network as a modifier or as a network former. Mysen (1988) argues that physical, chemical and thermodynamic properties of titanium-bearing silicate melts generally is consistent with a polymerising role of Ti^{4+} in the melts [47].

The most straightforward scenario for the network forming activity of titanium is the simple Ti^{4+} substitution for Si^{4+}. However, titanium may also enter the silica network of a partially depolymerised silicate melt in an octahedral form, tetrahedrally coordinated by oxygen with four bridging (BO) and two non-bridging (NBO) oxygens.

The network modifying activity of titanium may be described in analogy with alkaline and alkaline earth oxides.

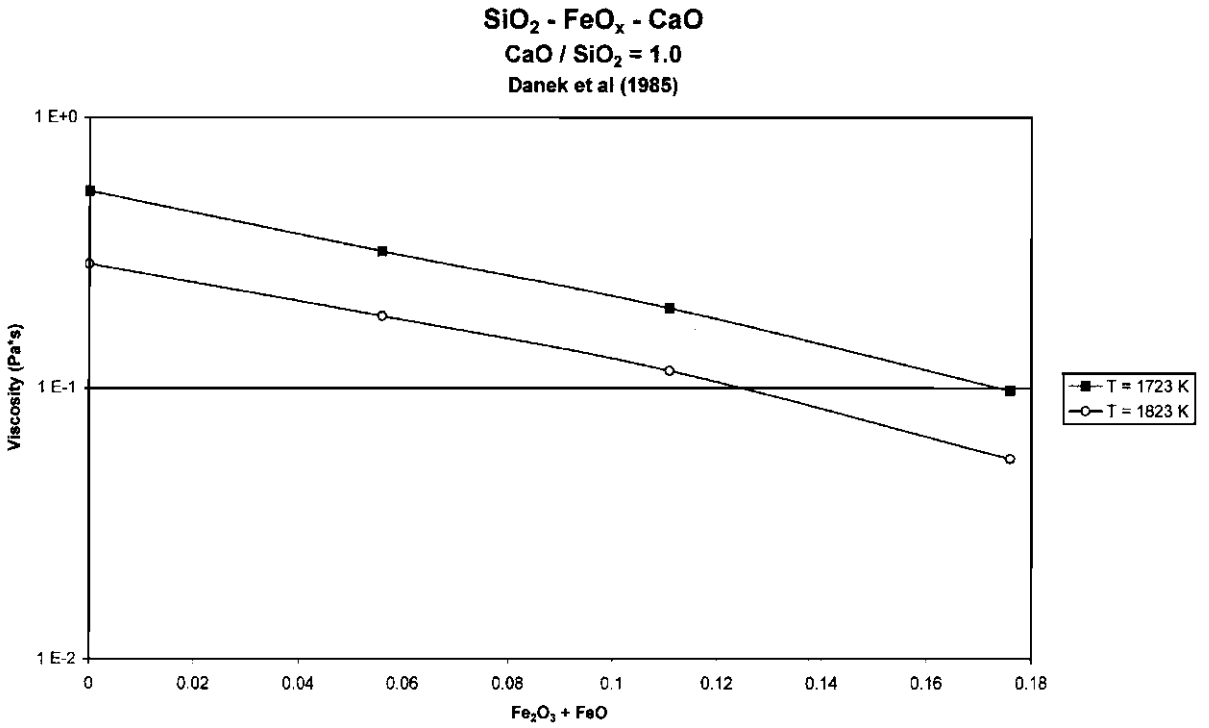

Fig. 24. Effect of Fe addition to a melt of equimolar concentration of SiO_2 and CaO[4].

In this case the oxygen ions of TiO_2 are used to depolymerise the silica network, e.g.

$$2[\equiv Si–O–Si\equiv] + TiO_2 \rightarrow 4[\equiv Si–O^-] + Ti^{4+} \quad (21)$$

For the purpose of this schematic representation it is irrelevant whether the coordination state of Ti^{4+} with oxygen is six-fold or some other number.

The third possible structural function appears if some of the Ti^{4+}-cations form TiO_2 clusters with Ti^{4+} in octahedral or tetrahedral coordination. Like in the previous case, the coordination number of titanium embedded in such clusters does not affect the polymerisation degree of the silicate network [85].

The structural role of TiO_2 depends on chemical composition and temperature. Both octahedral and tetrahedral coordinations of Ti are found in partially depolymerised SiO_2–Na_2O–TiO_2 glasses by XPS. For low contents, Ti is octahedrally coordinated, but with increasing concentrations the coordination number decreases. Abrupt changes in the viscosity vs temperature relationship for this system at concentrations above 10 mol% TiO_2 probably indicates the change of coordination number in this region, Fig. 26 [85]. However, a different investigation performed on the same system indicates that the shift occurs at 3–4 mol% TiO_2 [86].

Alkali titanium silicates have lower viscosities than the alkaline earth titanium silicate liquids, and also the partial molar volume of TiO_2 is alkali-cation specific. In general, much larger values are observed for the alkali-containing liquids than for the alkaline earth titanium silicates and pure TiO_2 liquid. This suggests that Ti has a lower coordination number in the alkali titanium silicates [87].

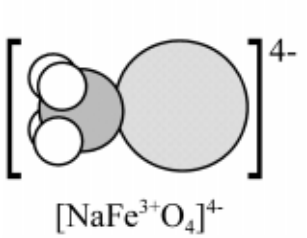

Fig. 25. According to Klein et al. (1983), the $NaFe^{3+}O_4^{4-}$-anion behaves like $NaAlO_4$ [66].

9.6. Atmosphere

The value of viscosity measurements on silicate melts is restricted if they are not performed under a controlled atmosphere [20]. In practical combustion systems, the atmosphere can be highly reducing (e.g. gasifiers), mildly reducing (e.g. low-NO_x combustion systems) or highly oxidising (e.g. post-combustion zone of conventional coal-fired boilers) The flow properties of slags must be predicted

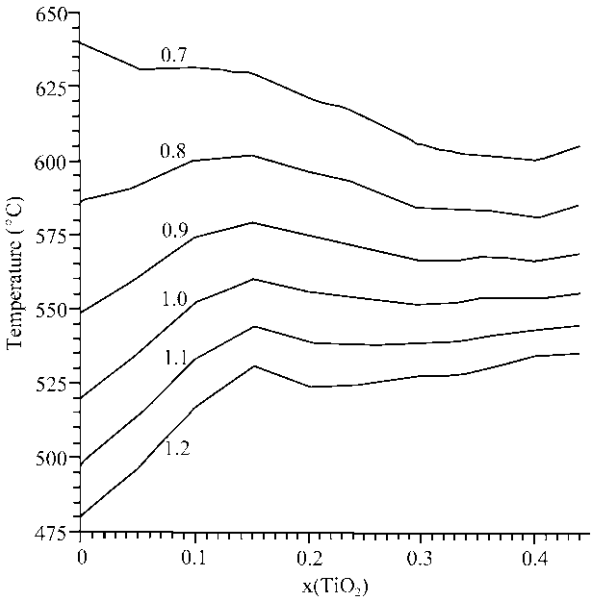

Fig. 26. Temperature depicted as functions of molar fraction of TiO_2 for constant values of viscosity, log η in Pa s [85] (by permission of the publisher).

under all these atmospheres to accurately understand the impact of ash on combustion systems.

When using an atmosphere of carbon dioxide, dissolution of CO_2 in the melt can occur to some extent. However, the solubility of CO_2 in vitreous melts has been found to be very low (window glass is reported to dissolve only 0.0017 wt% CO_2 at 1300°C and $P_{CO2} = 1$ atm), and on this basis it can be assumed that the solubility of CO_2 in silicate melts — probably as CO_3^{2-} — is generally low [88]. Furthermore, it appears to have a minimal effect on viscosity [89].

The viscosity of iron-containing silicate melts is lower if measured under reducing conditions than oxidising because of the reduction of tetrahedrally coordinated Fe^{3+} to octahedrally coordinated Fe^{2+} [41,46].

Dingwell (1989) reported the redox effect on viscosity to range between 2 and 4 Pa s when changing between oxidising and reducing atmospheres, i.e. the effect is substantial for low-viscosity fluids. Among the ternary systems tested, the largest effect of atmosphere should be expected for alkali ferro-silicate melts [56].

Klein et al. (1981) performed low-temperature viscosity measurements (673–923 K) on samples in the system SiO_2–FeO_x–Na_2O. Each sample was pre-melted in air to form oxidised samples, in forming gas (N_2/H_2 (95/5 vol%)) to form mildly reduced samples, and in forming gas with carbon in the batch to form strongly reduced samples. Four glasses containing 20 mol% Na_2O, 2, 5, 10 and 20 mol% FeO_x and the rest SiO_2 were tested under all three melting conditions, and the results are shown in Figs. 27–30. While the two glasses with low iron content (Figs. 27 and 28) show little effect on viscosity of oxidation state, the glasses with 10 and 20 mol% FeO_x (Figs. 29 and 30) show a large effect. The glass with 20 mol% FeO_x shows

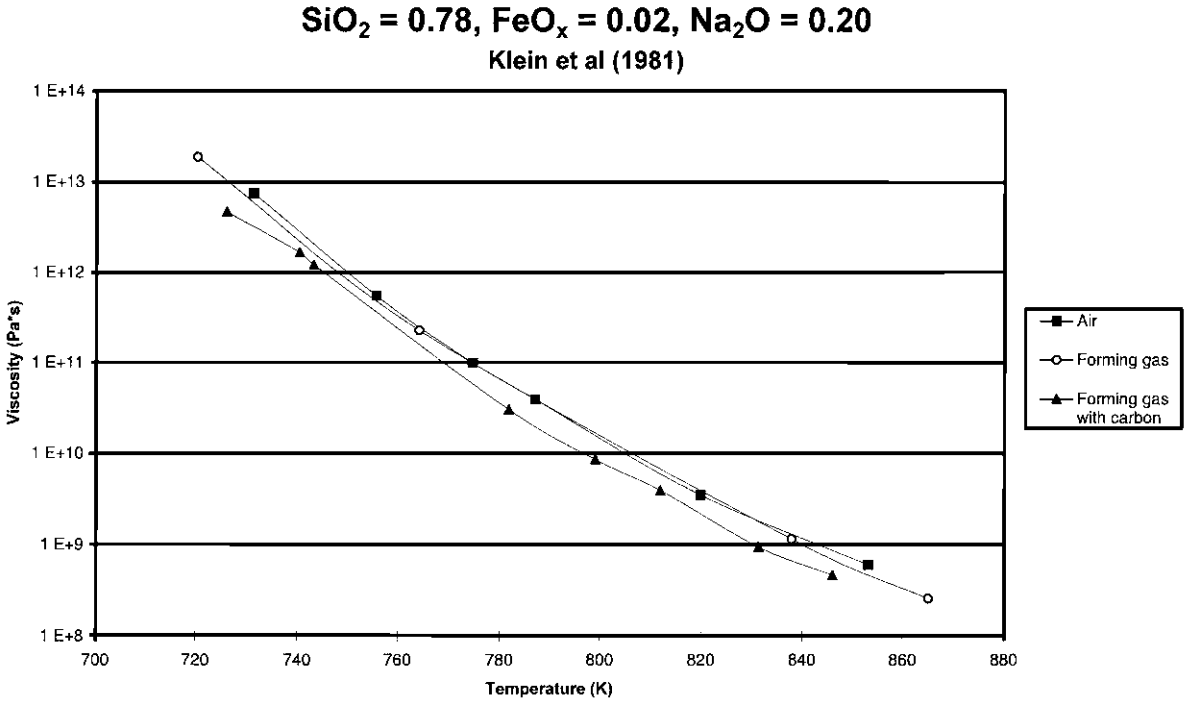

Fig. 27. The effect of atmosphere on viscosity for $FeO_x = 0.02$ [65].

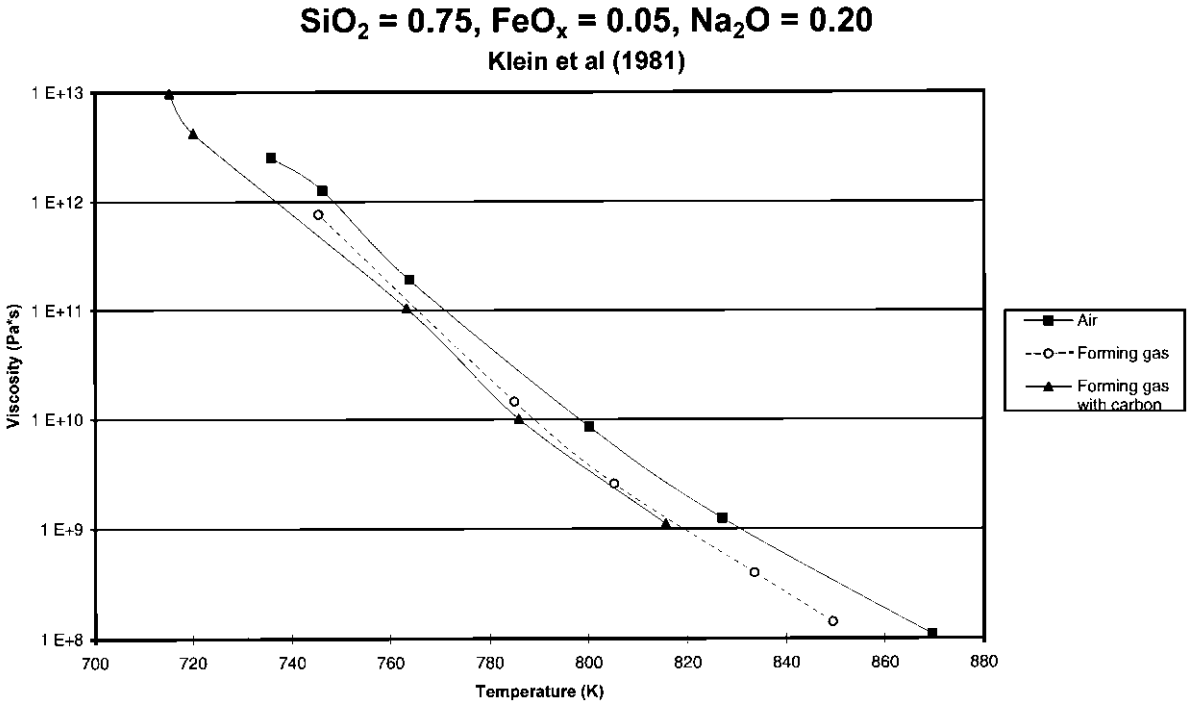

Fig. 28. The effect of atmosphere on viscosity for $FeO_x = 0.05$ [65].

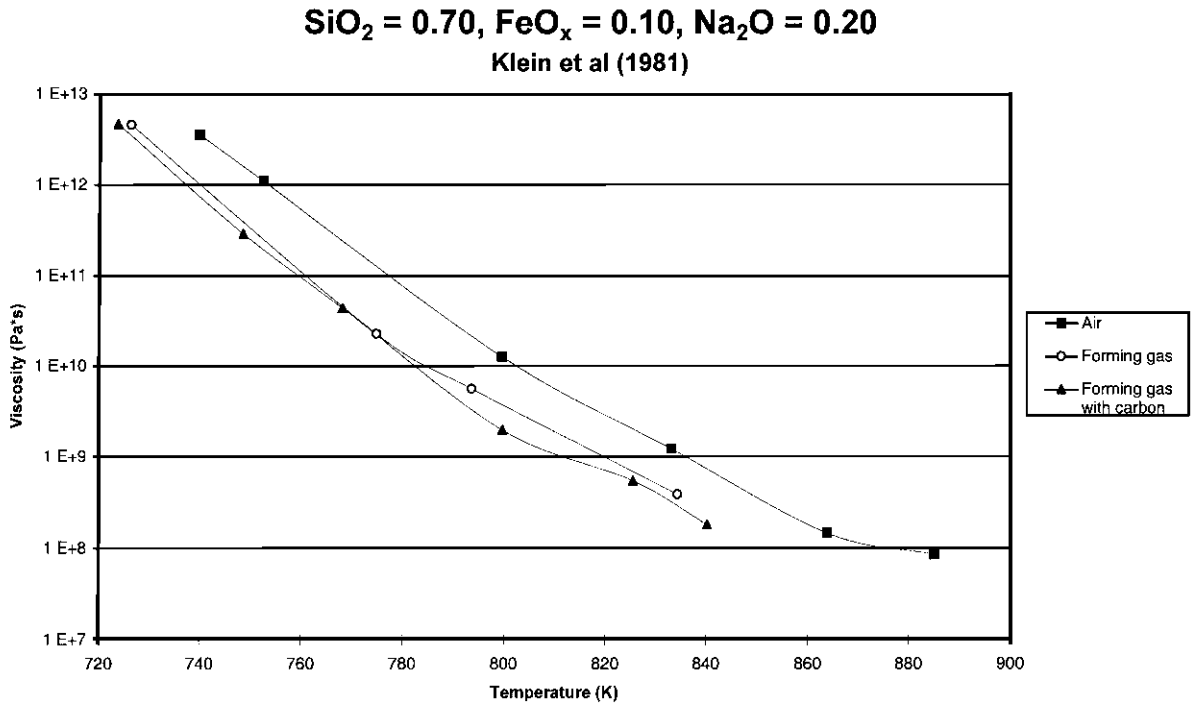

Fig. 29. The effect of atmosphere on viscosity for $FeO_x = 0.10$ [65].

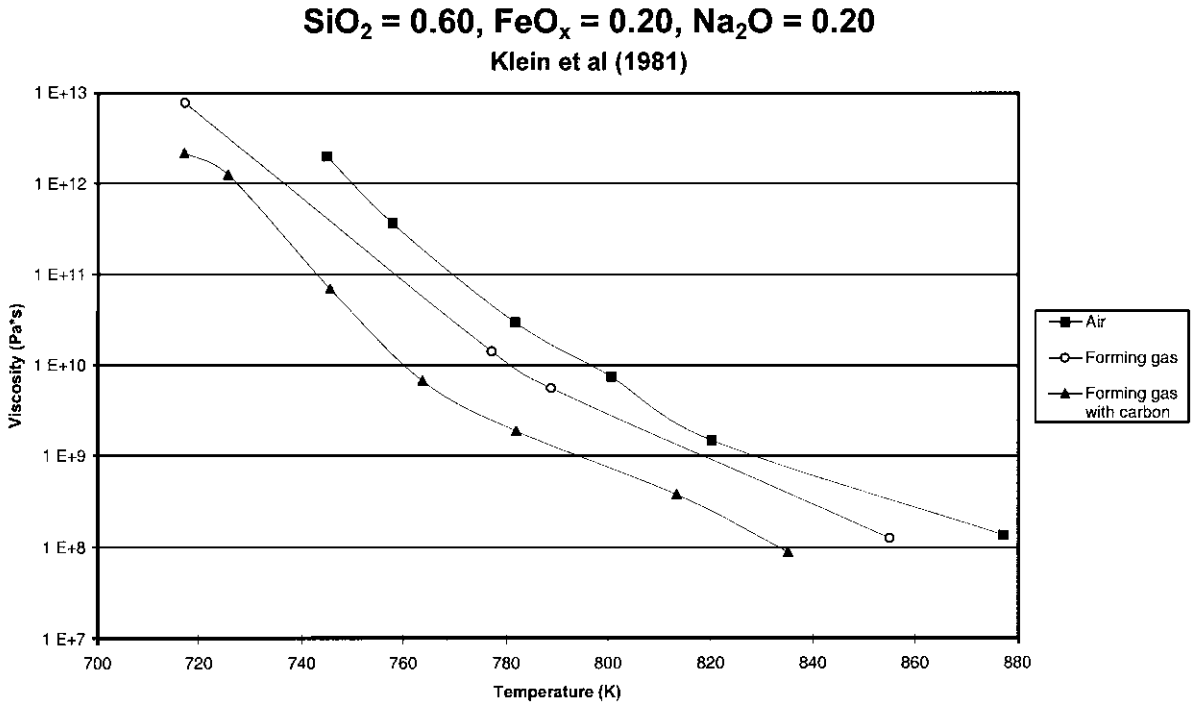

Fig. 30. The effect of atmosphere on viscosity for $FeO_x = 0.20$ [65].

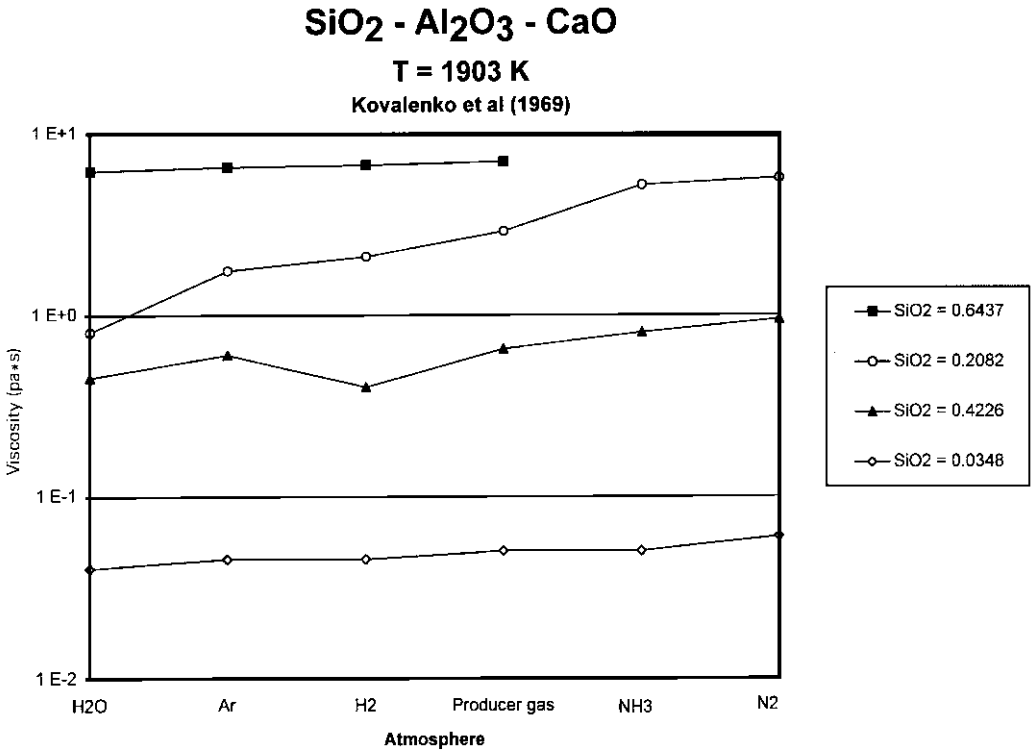

Fig. 31. At 1903 K, the choice of atmosphere affects the viscosity of melts of the system SiO_2–Al_2O_3–CaO [90].

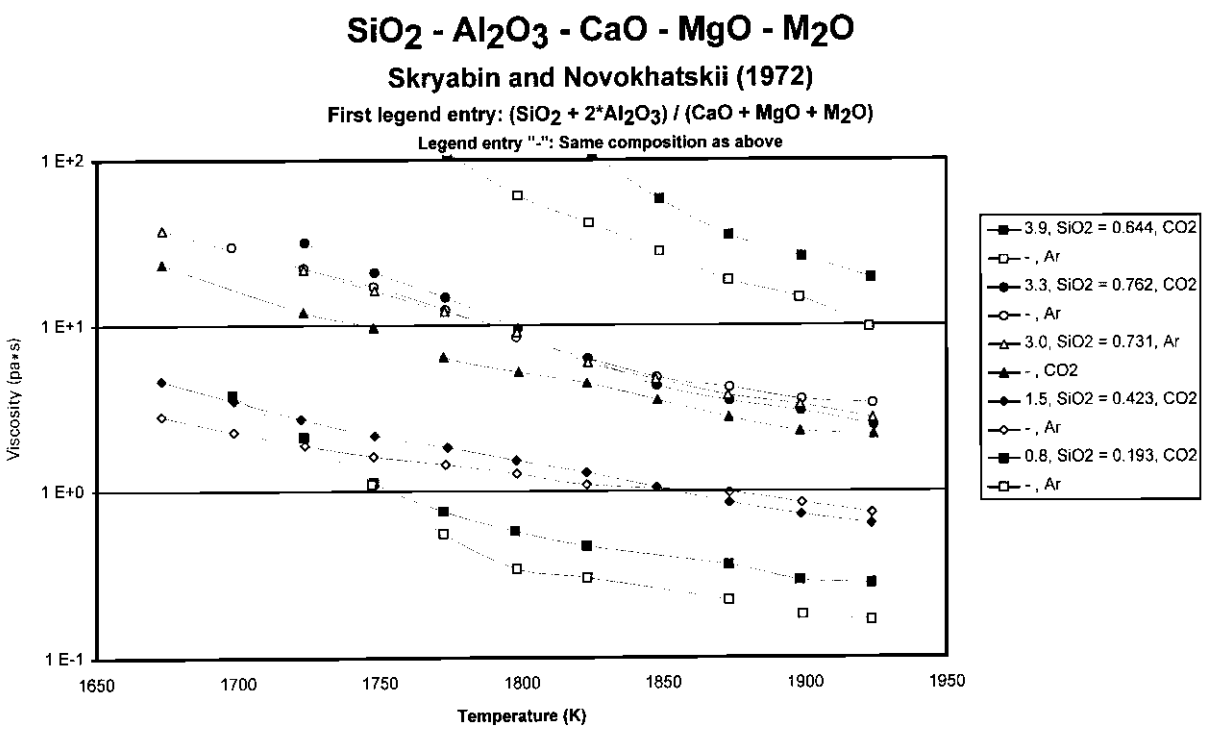

Fig. 32. Viscosity as a function of temperature, atmosphere and silica content. For four out of five compositions in the figure, a higher viscosity is observed in an atmosphere of CO_2 than in argon [88].

an order of magnitude increase in viscosity from the reduced to the oxidised sample [65].

Two years later, the system SiO_2–Al_2O_3–FeO_x–Na_2O was studied by Klein et al. (1983) under similar conditions as those just mentioned, and temperatures ranging from 750 to 1000 K. They found the following dependency of oxidational state of iron (i.e. "Fe" $= x_{Fe}$, $\sum Fe = Fe + Fe^{2+} + Fe^{3+}$) on atmosphere [66]:

1. oxidising conditions: $Fe^{2+}/\sum Fe < 0.25$;
2. mildly reducing atmosphere: $Fe^{2+}/\sum Fe > 0.27$;
3. strongly reducing atmosphere: $Fe^{2+}/\sum Fe > 0.50$.

In a study of the effect of atmosphere on melt viscosities in the system SiO_2–Al_2O_3–CaO at 1903 K, Kovalenko et al. (1969) found the following general trend shown in Fig. 31. An atmosphere of N_2 gave the highest viscosities, followed by NH_3, a producer gas of unspecified composition, H_2, Ar and air saturated with H_2O [90].

The viscosities of fused commercial glasses are affected by an atmosphere of CO_2 in different manners. As illustrated in Fig. 32, the viscosity of an optical glass (indicated by circles) is increased by a factor of 1.5–2 when changing from an atmosphere of Ar to CO_2 at 1700 K. Likewise, the viscosity of a window glass (indicated by triangles) is reduced by a factor of 1.5. Measurements performed on three ternary melts containing SiO_2, Al_2O_3 and CaO unanimously showed an atmosphere of CO_2 to give higher viscosities than argon, Fig. 32 [88].

The effect of atmosphere on the viscosity of coal slags has been studied by Hurley et al. (1996). They conducted parallel measurements in air, air +10% water vapour and a reducing atmosphere of $H_2/CO/CO_2$ (31/45/24 vol%) in a rotational viscometer. As shown in Fig. 33, they found an atmosphere of air to produce the highest viscosities, followed by air and H_2O and with the reducing atmosphere producing the lowest viscosities [91].

For a Baukol-Noonan (North Dakota, USA) lignite slag, the effect of a transition from reducing to oxidising conditions at 1300°C was found to increase the viscosity by 11 Pa s — more than a doubling [92].

10. Crystallisation

10.1. Crystallisation

The presence of suspended solid matter seriously affects the viscosity of silicate melts, as indeed it affects the viscosity of any other type of melt.

- viscosity increases sharply with the appearance of solids in the melt;
- non-Newtonian behaviour is commonly observed in crystal–melt slushes;

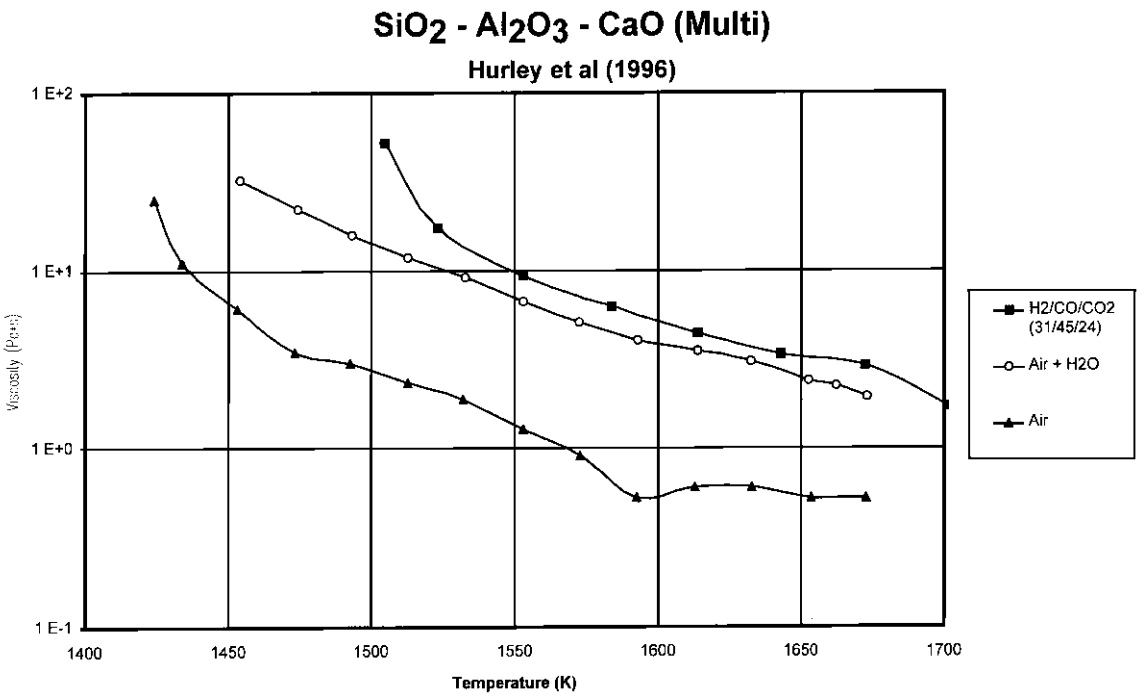

Fig. 33. The effect of atmosphere on the viscosity of a melt of composition (molar fraction): $SiO_2 = 0.43$, $Al_2O_3 = 0.13$, $Fe_2O_3 = 0.03$, $CaO = 0.27$, $MgO = 0.11$, $Na_2O = TiO_2 = P_2O_5 = 0.01$ [91].

- at concentrations higher than a certain limit, the measurement signal will be disturbed by the interference of solid particles [5].

Sharp rheological changes have been observed to take place at crystal volume fractions in the range 25–55 vol%, and for irregular shapes the limit may be as low as 5% [93,94].

Lava is fluid rock that issues from a volcano or fissure, and it is rarely encountered with more than about 55% phenocrysts (relatively large crystals that are prominent in some types of igneous rock). The cutoff is abrupt, and it is likely that the viscosity of the magma encounters a locking point upon which the viscosity increases so much that the magma becomes essentially a solid. The lavas define a limit of crystallinity that decreases with increasing silica content at a rate of 4.08 vol% per wt% silica [95].

10.1.1. Indices

Some characteristic temperatures for the solidification and melting of silicate melts are given in Table 3. In general, an index of the crystallising properties of a slag should indicate not only whether a slag is capable of crystallising under a given set of conditions but also whether or not crystallisation is likely [96].

The glass-forming tendency of a melt is related to the viscosity at the liquidus temperature, i.e. the liquidus viscosity [97].

Watt (1969) did not find any useful relation between the ash fusion temperature of a coal slag and its crystallisation properties [96].

10.1.2. Crystallisation process

In 1990, De Jong postulated that the crystallisation process occurs in two steps upon the cooling of a melt:

(i) crystal nuclei formation;
(ii) nucleus growth.

The total rate of crystallisation of an undercooled liquid is defined as the sum of the rates of these two steps [5]. Nucleation studies of silicate melts indicate that the rate of crystal growth increases with increasing undercooling, reaches a maximum, and then decreases with further undercooling due to the increase in viscosity [5].

In undercooled liquids, heterogeneous nucleation (i.e. nucleation at interfaces) is the dominant nucleation process. It occurs at places such as the air–liquid interface, interfaces with particles or gas bubbles, the liquid container walls, and boundaries between immiscible regions [5].

The rate of formation of crystals upon cooling may be — and frequently is — different from the dissolution rate for the crystals during heating [98]. For example, coal slags of low silica ratio have often been found to crystallise readily — and once formed, the crystals are not always readily resorbed on heating [99].

Table 3
Characteristic temperatures [9,96,103,105,106,159,160]

Name	Symbol	Definition
Liquidus temperature	T_l	Maximum temperature at which liquid and solid phase can coexist
Crystal remelting temperature	T_j	Temperature at which the viscosity curve of the slag on reheating rejoins the curve corresponding to the fully liquid conditions ($T_j \approx T_l - 30$ K)
Flow temperature	T_{80}	Temperature at which slag has sufficient fluidity to allow free flow ($\eta = 8$ Pa s = 80 P)
Normal slag removal temperature	T_{200}	Recommended temperature for easy slag-tapping from a furnace ($\eta = 20$ Pa s = 200 P)
Slag removal temperature	T_{250}	Temperature corresponding to the maximum viscosity at which slag can be tapped from a furnace ($\eta = 25$ Pa s = 250 P)
Temperature of critical viscosity	T_{cv}	See text
Solidus temperature	T_s	Lowest temperature at which liquid and solid phase can coexist
Glass transition temperature	T_g	Temperature at which $\eta = 10^{12}$ Pa s for conventional glasses or Temperature at which the rate of change of the melt structure with cooling becomes too slow to maintain equilibrium at the given cooling rate
Annealing temperature		Temperature at which $\eta = 10^{12.7}$ Pa s

Many slags are very reluctant to crystallise and can often be cooled to a hundred degrees or more below the liquidus temperature without serious risk of crystallising within a certain time limit [96]. In some cases the minor oxides such as K, Ti and P may promote the nucleation process [82].

- In glasses containing four or more components, even small proportions of alumina prevent the formation of a crystalline phase upon cooling [100].
- Mixed alkali systems exhibit a lower critical cooling rate than either of the single alkali systems [97]. This means, that crystallisation is bypassed even at relatively slow cooling rates and a glass is obtained.

10.1.3. Crystal shape and size distribution

The nature (shape, size distribution and composition) of the solid phase that is formed under experimental conditions is determined more by kinetic factors, i.e. the rate of crystallisation, than by considerations of phase equilibria [96,101]. The size distribution of crystals, for instance, is a direct result of the effective undercooling at which the melt crystallises [101].

According to Cashman (1990), the shapes of the crystals in a melt can be quantified by Fourier analysis or fractal analysis [101].

10.1.4. Composition of crystal and melt

The phases resulting from crystallisation are not always those which are expected on the basis of the corresponding normalised phase equilibrium diagrams [29].

As a rule of thumb, all minor oxides such as K, Ti and P are assumed to remain in the solution; but in some cases they may be incorporated into crystalline phases as chemical defects, if they match some crystallographic rules such as the formation of solid solution [82].

Iron is a fluxing agent in coal-ash slags, so if iron precipitates out of the slag, the viscosity of the slag may increase significantly [98].

10.2. Critical viscosity

The separation of a solid phase upon cooling of a melt has a vast effect on the rheological behaviour of the sample, and therefore it is a subject of major importance for all those concerned with silicate melts.

T_{cv} indicates a point of often very abrupt change in the viscosity–temperature relationship. It is often assumed that T_{cv} marks the division between crystal-affected viscosities and viscosities not affected by the presence of crystals; this point is called the critical viscosity, see Fig. 34. Because, in general, the absolute viscosity of a melt at the critical viscosity is of minor interest, whereas the temperature where it occurs is more important, the critical point is generally

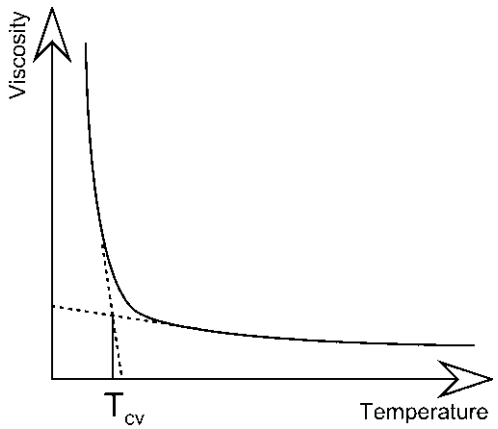

Fig. 34. Graphical definition of the temperature of critical viscosity, T_{cv}.

Table 4
Temperature of critical viscosity

Authors	Year	Definition
Mills and Broadbent [134]	1993	The temperature below which there is very rapid rise in viscosity
Nowok, Hurley and Stanley [76]	1993	Roughly the temperature at which the composition of slag is changed from a one-phase to a two-or-more-phase mixture
Singer (editor) [103]	1991	The temperature at which solid phases begin to crystallize and separate out from the liquid
Nowok and Benson [46]	1991	The temperature at which the stoichiometries of the melt components mimic those of the crystalline phases that appear at the liquidus point
Do		The temperature at which the flow properties change from being those of a Newtonian fluid to those of a non-Newtonian fluid
Vorres et al. [29]	1986	Transition from a system which has a significant amount of liquid phase to one in which the system is predominantly solid phases. Often the temperature and phase compositions of this transition correlate well with a eutectic
Watt [96]	1969	The temperature at which crystallisation is likely to interfere with flow
Corey [102]	1964	The division between between fluid and and plastic viscosities. It is the point where internal yield stress is first developed in the slag upon cooling
Reid and Cohen [125]	1944	The viscosity during the gradual cooling of a slag where there is a sudden transition from liquid to plastic flow, as evidenced by an abrupt increase in viscosity

considered in terms of the temperature of critical viscosity, T_{cv} [102]. In the Soviet literature, T_{cv} was referred to as the temperature of the true liquid state, T_0 [103].

- $T < T_{cv}$: viscosity varies strongly with temperature ($|\partial\eta/\partial T|$high);
- $T > T_{cv}$: viscosity varies weakly with temperature ($|\partial\eta/\partial T|$low).

But the relationship between crystallisation and T_{cv} is not yet clear, although several authors have attempted a definition, see Table 4 [29,46,76,96]. Hurley proposes that heated stage X-ray diffraction studies should be carried out to prove the frequent assumption that T_{cv} is the temperature below which the viscosity is affected by the presence of crystals [28].

In 1959, Sage and McIlroy alleged that viscosity measurements at $T < T_{cv}$ (defined as the point where the first crystallisation occurs) are no longer true viscosities, but they do give an apparent viscosity which can be used as a measure of flow characteristics [104].

Corey (1964) found the T_{cv} of coal ash slags to decrease between 40 and 270 K when shifting from oxidising to reducing conditions [102]. This observation is in accordance with the melting point for ashes being lower under reducing than under oxidising conditions.

Hurley et al. (1996) found that the addition of magnesium to a Powder River Basin (USA) coal slag increases T_{cv} from approximately 1250°C to around 1350°C and the addition of aluminium raises T_{cv} to 1330°C [91]. The definition of T_{cv} used in this study was the same as the one illustrated in Fig. 34.

Relations of the temperature of critical viscosity to other properties of the melt are listed below. They are all empirical correlations, relating T_{cv} to easily achievable characteristics of the sample such as composition and, for coal, the ASTM ash fusion test.

The ASTM ash fusion test is a test often performed on coal ashes (ASTM standard D 1857-87): In this test, a cone is produced, 19 mm in height and 6.4 mm in width at each side of the base which is an equilateral triangle. The deformation of the cone is observed upon continuous heating at 8 K/min. The outcome of the test is a set of characteristic temperatures shown in Fig. 35.

The term *major components* is used in the Watt model and several times later in the paper. It indicates the oxides of major concentration in the mixture. A concentration limit of 5% either on a weight- or a mole-basis is generally used.

None of the relations should be considered more than

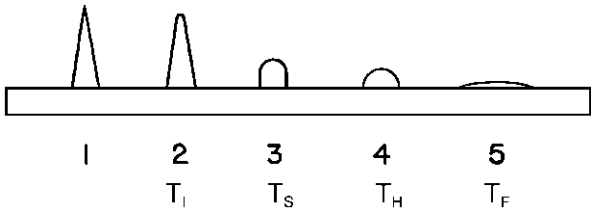

Fig. 35. The four characteristic temperatures of the ASTM ash fusion test (D 1857-87).

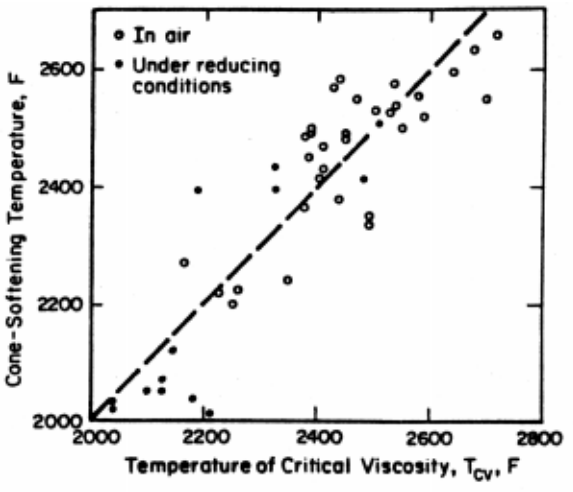

Fig. 36. The relationship between the cone-softening temperature and the temperature of critical viscosity [102] (by permission of the publisher).

indications of T_{cv}, and much work still remains to be done before a trustworthy model can be generated.

10.2.1. Corey (1964)

Corey strived to relate T_{cv} — defined as the transition of the melt from a Bingham plastic to Newtonian flow — to the cone-softening temperature, T_s — defined as the temperature at which the cone has fused down to a lump with height = width, Fig. 35.

Fig. 36 shows T_{cv} vs T_s for a number of ashes tested under oxidising and reducing atmospheres. The points seem to crowd around the broken line ($T_{cv} = T_s$) with considerable deviations; but as it can be seen in Table 5, the mean deviation is negligible.

For the slags tested under reducing conditions, T_{cv} was higher than T_s in the low-temperature range, but the data in Fig. 36 does not indicate any apparent effect of oxidation state on the T_{cv} vs T_s relationship: a change in the state of oxidation of a coal ash slag seems to have similar effect on the temperature of critical viscosity and on the cone-softening temperature [102].

Table 5
Temperature of critical viscosity vs cone softening temperature [102]

	Air	Reducing atmosphere
T_{cv} > cone softening temperature	18 slags	10 slags
T_{cv} > cone softening temperature	1 slag	1 slags
T_{cv} > cone softening temperature	16 slags	3 slags
Maximum temperature difference	170 K	110 K
Mean temperature difference	6 K[a], 3 K[b]	17 K[a]

[a] Calculated as the average of differences.
[b] As reported by Corey [102].

Procedure: Corey

(i) Perform ASTM ash fusion test under the conditions of interest;
(ii) Estimate T_{cv} as: $T_{cv} = T_s$.

In 1982, Bryers tested T_{cv} against T_s for a number of other ashes, and he also found the correlation to be reasonably good [40].

10.2.2. Sage and McIlroy (1959)

In a study of a large number of slags from slag tap furnaces operating at 10–15% excess air, the slags were found to have an average ferric percentage (Fe^{3+}/(Fe^{3+} + Fe^{2+} + Fe)) of 20 mol%, and Sage and McIlroy found the hemispherical temperature in a reducing atmosphere, T_h (K), to be an adequate guide for T_{cv} (K) — defined as the temperature where the cooling (η vs T)-curve deviates from being logarithmic due to commenced precipitation of solids [104]:

$$T_{cv} = T_h + 111 \text{ K} \quad (22)$$

The hemispherical temperature of coal ash is defined according to the ASTM ash fusion test as the temperature at which the cone has fused down to a hemispherical lump (height = 1/2 × width), Fig. 35.

Deviations from Eq. (22) may partly be due to variations in ferric oxidation level [104].

Procedure: Sage and McIlroy

(i) Perform ASTM ash fusion test in a reducing atmosphere;
(ii) Calculate T_{cv} according to Eq. (22).

10.2.3. Watt (1963)

With the temperature of critical viscosity defined as the

temperature at which the viscosity of a slag begins to rise sharply upon cooling as a consequence of the formation of crystals, T_{cv} was found to be related to coal ash slag composition. Based on results from 63 coal ash slags, T_{cv} (K) was estimated with a standard deviation of approximately 54 K (standard deviation of experimental determinations ≈37 K):

$$T_{cv} = 3263 - 1470\cdot\frac{SiO_2}{Al_2O_3} + 360\cdot\left(\frac{SiO_2}{Al_2O_3}\right)^2 - 14.7\cdot(Fe_2O_3 + CaO + MgO) + 0.15\cdot(Fe_2O_3 + CaO + MgO)^2 \quad (23)$$

where the individual components are expressed on a weight basis ($SiO_2 + Al_2O_3 + Fe_2O_3 + CaO + MgO = 100\%$) [105,106].

All major components of a typical coal ash slag are represented in the equation and all minor components are neglected, so the validity of the model is probably limited to melts with the above-mentioned major components. The choice of atmosphere may influence the performance of the equation (atmosphere not reported in the papers).

Procedure: Watt

(i) Recalculate:
$SiO_2 + Al_2O_3 + Fe_2O_3 + CaO + MgO = 100$ wt%.
(ii) Calculate T_{cv} according to Eq. (23).

10.2.4. Marshak and Ryzhakov (1969)

Singer (1991) presents a model for Soviet coals proposed by Marshak and Ryzhakov [103]. However, the reference given by Singer does not contain the model.

T_{cv} (K) of a coal ash — defined as the temperature where log η vs T deviates from linearity probably due to the onset of crystallisation — is related to the cone-softening temperature of the ash, T_s (K), according to the Soviet standard, please refer to Fig. 35 [103].

$$T_{cv} = 0.75\cdot T_s + 548\ \text{K} \quad (24)$$

Procedure: Marshak and Ryzgajiv

(i) Perform ash fusion test according to Soviet standard.
(ii) Calculate T_{cv} according to Eq. (24).

11. Liquid mixture models

The term *liquid mixture* comprises mixtures of different oxides that are either completely or partially liquid.

Completely molten silicate melts are Newtonian liquids as opposed to melts with a certain amount of crystals. Therefore the following review of existing models found in the literature can be divided into models for Newtonian and non-Newtonian systems. For the Newtonian fluids, the review will concentrate firstly on general equations and secondly on detailed models applicable to the silica system, and for the non-Newtonian fluids, there will be a general introduction to models for non-Newtonian systems followed by a review of existing models for liquid–solid mixtures.

- Newtonian fluids
  - General
  - Silicate melts
- Non-Newtonian fluids
  - General
  - Liquid–solid mixtures

Silicate melts containing minor amounts of solid phase can also perform as Newtonian fluids, but due to the intimate relationship with more dense solutions, all models relating to the two-phase solid–liquid system will be presented in the section devoted to the non-Newtonian flow regime.

Most of the models are based on theoretical considerations concerning flow mechanisms and compositional influences on structure, but they fall back on empirical testing of their performance.

The viscosity of a liquid mixture is usually a non-linear function of composition and is very difficult to predict [5]. According to El-Badry et al. (1981), experience has shown that in the range from 10 to about 10^{11} Pa s, the viscosity of silicate glass depends only on temperature and composition. In the range from 10^{11} to 10^{14} Pa s and higher, it is also time dependent [59].

11.1. Generalised models for Newtonian fluids

Newtonian fluids, for which viscosity is independent of shear rate, represent the most simple flow type, and therefore they are also the most closely examined. Fortunately, completely molten silicates are usually categorised as Newtonian, although for high shear rates (beyond the focus of this text), the flow may deviate from Newtonian behaviour.

Over the past century, a series of equations has been developed relating the viscosity of an arbitrary mixture to temperature or some temperature-dependent characteristics.

All the equations contain one or more composition-specific constants that require optimisation by the user.

The first models that will be presented all relate viscosity to temperature for a given mixture with a given set of composition-specific parameters. As opposed to this, the last models relate the viscosity of a mixture to the viscosity of the individual mixture components rather than temperature.

11.1.1. Arrhenius (1887)

The Arrhenius model is often used for silicate melts as well as for other liquids. It is an approximation of a more complete equation derived by Eyring and inspired by observations made by Arrhenius in 1887 [107,108]

On a molecular scale, viscous flow involves relative movements of the structural elements of the liquid. Two

conditions must be realised for such displacement:

- an energetic condition: the jumping probability, Pe;
- a geometric condition: the probability that there is a hole to jump to, Pv.

So the fluidity of a liquid, Φ, i.e. the inverse of viscosity, can be expressed as

$$\Phi = \frac{1}{\eta} \propto Pe \cdot Pv \tag{25}$$

Based on this expression, it is possible to obtain an expression between viscosity and temperature using only two parameters

$$\log \eta = \log a + \frac{b}{T} \tag{26}$$

where a and b are composition-specific constants and T the temperature on an absolute scale, (K or °R, $T(°R) = 1.8 \cdot T(K)$) [11,24,109].

Richet et al. (1986) experimentally found the constant b to depend on temperature, $b = b(T)$, for the substances examined [110].

The model is also referred to as the Andrade model [1]; however, the origins of this model is quite different: Where the Arrhenius model is based on the concept of activation energy, the basis for the Andrade model includes a specific volume term [109,111].

In view that the relationship between $\log \eta$ and $1/T$ is often not linear, Wang and Porter (1995) proposed a reformulation of the b-constant in the Arrhenius model for polymer-systems. b is calculated in terms of temperature and composition-related parameters: volume expansion coefficient and T_g, and an adjustable parameter [109].

11.1.2. Vogel–Fulcher–Tammann (1921)

The VFT-model was proposed independently by Vogel, Fulcher and Tammann. It contains three composition-specific constants, a, b and c [1,5,73]

$$\log \eta = a + \frac{b}{T - c} \tag{27}$$

The model is generally accepted to give an adequate representation of the temperature dependence of silicate melts [5,24]. The level of performance is probably due to the introduction of a third adjustable parameter in the equation, which increases not only the performance of the model, but also the amount of experimental data needed to fit the parameter values.

Urbain (1985) stated that the VFT-model gives a good fit with experimental results for silicates under the following three conditions [24]:

- liquid silicates at temperature above liquidus (single liquid phase in thermodynamic equilibrium): $T > T_l$;
- supercooled liquids: $T_g < T < T_l$;
- glasses: $T < T_g$.

11.1.3. Doolittle (1951)

The empirical equation can be written in several alternative ways, here three are given [109,112–115]

$$\eta = a \cdot e^{-bV_m/(V-V_m)} = a \cdot e^{-bV_m/V_f} = a \cdot e^{-b/V_{ff}} \tag{28}$$

where a and b are composition-specific fitting constants, V the total volume, V_m the volume "occupied" by the molecules, V_f the free volume or free space ($V_f = V - V_m$) and V_{ff} the fraction free volume ($V_{ff} = V_f/V_m$).

According to the definition of the terms as originally presented by the author, the free-space, V_f, in a liquid is considered to be that space seemingly arising from the total thermal expansion of the liquid without change of phase. Relative free-space is therefore the fractional increase in volume resulting from expansion.

- V_f = volume of free-space per gram of liquid at any temperature;
- V_m = volume of 1 g of liquid extrapolated to absolute zero without change of phase;
- V = volume of 1 g of liquid at any temperature [112].

The equation can also be obtained through simplifications of the free volume theory, developed by Cohen and Turnbull in 1959. The basic assumption of this model is that atoms are confined to cells defined by their nearest neighbours. These cells can be liquid or solid-like, depending on whether their volume is larger or smaller than the critical volume (approximately equal to the atomic volume) [107].

Other models relating viscosity to free volume are described by Cohen and Grest (1979), Cranmer and Uhlmann (1981) and Scholze and Kreidl (1986) [9,110,116]. But it would require too much space to present all of these models in this paper.

11.1.4. Williams–Landel–Ferry (1955)

The WLF-model contains two composition-specific constants a and b

$$\log\left(\frac{\eta}{\eta_{ref}}\right) = \frac{-a(T - T_{ref})}{b + (T - T_{ref})} \tag{29}$$

where T_{ref} is a reference temperature and $\eta_{ref} = \eta(T_{ref})$. In general, the WLF-equation holds over the temperature range T_g to (T_g + 100 K) [11,109], where T_g is the glass transition temperature that characterises the amorphous phase. It is defined as the temperature, or narrow range of temperatures, below which the phase is in a glassy state, and above which it is rubbery [117].

11.1.5. Adam–Gibbs (1965)

Another model of similar appearance as the Arrhenius model is the Adam–Gibbs model. It is the result of a generalisation and extension of an earlier work by Gibbs and DiMarzio (1958) on the configurational entropy theory [107,118].

$$\log \eta = a + \frac{b}{T \cdot S_c(T)} \tag{30}$$

where a and b are the composition-specific constants, T the absolute temperature and S_c the configurational entropy calculated from the following equation [118]:

$$S_c(T) = S_c(T_{ref}) + \int_{T_{ref}}^{T} \frac{\Delta C_p}{T} dt \tag{31}$$

where T_{ref} is a reference temperature and ΔC_p the configurational heat capacity, a measure for structural changes in the material defined as the difference between liquid and glassy phase states [110]

$$C_{p,c} = \Delta C_p = C_{p,liq} - C_{p,glass} \tag{32}$$

Configurational heat capacity can be calculated as the difference of heat capacities between the glassy state at the fictive reference temperature T_{ref} and the melt at the temperature T. $S_c(T_{ref})$ can be calculated according to the scheme [118,119]

$$S_c(T_{ref}) = S_{c,cryst} + \int_0^{T_f} \frac{C_{p,cryst}}{T} dT + \Delta S_f + \int_{T_f}^{T_{ref}} \frac{C_{p,liq}}{T} dT + \int_{T_{ref}}^{0} \frac{C_{p,gas}}{T} dT \tag{33}$$

where T_f and ΔS_f are the temperature and the entropy of fusion of the crystal, $S_{c,cryst}$ the configurational entropy of the crystal, $C_{p,cryst}$, $C_{p,liq}$ and $C_{p,gas}$ the heat capacities of the crystalline, liquid and glassy phases of the substance. If the temperature data are not available, T_{gas} or the temperature at which the viscosity is 10^{12} Pa s can be used instead. It is here assumed that the misfit with Eq. (1) in Richet (1984) is due to a misprint in the latter paper [118,119].

11.1.6. Weymann (1962)

Eq. (25) can be used as a basis for the deduction of the Weymann model as well as the Arrhenius model [24].

The model is also known as the Frenkel model. It extends the Arrhenius model by including an extra absolute temperature term [20,120]

$$\log \eta = \log a + \log T + \frac{b}{T} \tag{34}$$

This model has proven successful in the description of the temperature dependence of silicate melt viscosities, and together with the Arrhenius model it will be referred to in the next section. Different versions exist of the above mentioned equations, but the heart of the equations remains unchanged.

The construction of a complete mathematical model relating viscosity directly to the composition of the mixture has been attempted. However, these models also tend to fall back on the optimisation of a series of composition-dependent constants.

Irving (1977) tested 25 mathematical models for binary mixtures on 318 systems, and he found the following classification scheme to be appropriate

(i) additive equations: $f(\eta) = x_1 \cdot f(\eta_1) + x_2 \cdot f(\eta_2)$ no adjustable constants;
(ii) parabolic equations: $f(\eta) = x_1 \cdot f(\eta_1) + x_2 \cdot f(\eta_2) + 2x_1x_2C$ one adjustable constant;
(iii) equations with mixture density;
(iv) free-volume equations;
(v) kinematic viscosity equations;
(vi) equations with other parameters;
(vii) unclassified equations.

He concluded that the usefulness of the models of Classes (iii)–(vi) is greatly reduced by the fact that they require knowledge of constants that are not readily available [121].

11.1.7. Seetharaman–Du Sichen (1994)

A modelling scheme for estimating the viscosities of multi-component metallic and ionic melts at high temperatures was attempted. In the model, viscosity is expressed by the Arrhenius equation, and the activation energy, E_A, is described as a sum of pure component contributions and a mixing term

$$E_A = \sum x_i \cdot E_{A,i} + E_{A,mix} \tag{35}$$

where x_i is the molar fraction of species i. A series of assumptions is made in the model, but nevertheless, a number of parameters have to be fitted [111,122,123]. The model will not be described in detail in this paper since it will not be used below. Thorough descriptions are given in the references.

11.1.8. Grunberg

The Grunberg equation relates the viscosity of a mixture of two liquids to the viscosity of the parent liquids (pure components or mixtures) at the same temperature.

$$\ln \eta = x_1 \ln \eta_1 + x_2 \ln \eta_2 + 2x_1x_2G \tag{36}$$

The equation requires knowledge of the parent liquid viscosities, η_1 and η_2, and the value of the adjustable parameter, G [1,121].

In the above-mentioned study on models for binary mixtures, Irving (1977) found the best descriptive equation with the widest applicability for organic liquids and yet possessing comparative simplicity to be the Grunberg equation [121].

11.1.9. Model coupling theory (MCT)

The MCT is an example of a general atomic theory that has not yet been fully developed and therefore can not be applied to complicated liquids. Like the free volume and configurational entropy theories, it strives to explain the occurrence of the glass transition. An inevitable by-product of each of these theories is an expression for the viscosity as a function of temperature.

The point of departure of the MCT is that the number density of the atoms or molecules in the liquid increases when the temperature decreases, i.e. the structure of the liquid becomes more compact.

Due to this densification of the structure, more and more particles are trapped for increasing time intervals in cages formed by their nearest neighbours; the particles can not easily move because the neighbouring particles are in the way. Because of this effect, the viscosity increases with decreasing temperature, and eventually the glass transition takes place when the translations of the particles are virtually frozen [107].

Born and Green (1949) have suggested that the expression for liquid viscosity should consist of two parts, namely one corresponding to interatomic forces and another to thermal motion. The interatomic forces are characterised by the thermodynamic state of the liquid, and the thermal motion could reasonably be expected to be a function of the thermal entropy of the system. While enthalpy is a direct reflection of the interatomic bonding and thereby the ordering in the system, entropy represents the extent of disorder in the system [123].

An alternative approach is to classify mixtures according to their content of polar, non-polar and aqueous components [121].

11.2. Models for completely molten silicates

The models constructed for the estimation of the viscosity of silicate melts all attempts to relate viscosity to temperature and a simplified melt composition.

Existing models for the estimation of the silicate melt viscosities can be classified as follows:

(i) models based on the Arrhenius equation relating viscosity to temperature (Shaw (1972), Watt–Fereday (1963), S^2 (1944));
(ii) models based on the Weymann equation relating viscosity to temperature (Kalmanovitch–Frank (1988), Streeter (1984), Urbain (1981), Riboud (1981));
(iii) models based on the Vogel–Fulcher–Tammann equation relating viscosity to temperature (Lakatos (1972));
(iv) models relating viscosity to composition (Bottinga–Weill (1972));
(v) unclassified models (Sage–McIlroy (1959), Reid–Cohen (1944)).

All the models are the result of an empirical fitting of data, and they all apply to Newtonian liquids only, i.e. completely molten systems.

In the following, a description of each of the models will be given in chronological order. For each model, a viscosity-estimate will be calculated for the system:

Melt: Molar basis: 62.5% SiO_2, 6.25% Al_2O_3, 12.5% CaO, 12.5% MgO, 6.25% Na_2O;
Weight-basis: 62.7% SiO_2, 10.6% Al_2O_3, 11.7% CaO, 8.4% MgO, 6.5% Na_2O.

A melt of this composition was studied by Scarfe and Cronin (1986) [124] (see Appendices), and they measured the viscosity at 1623 K to be 32.8 Pa s. This measurement has not been reproduced and can therefore not be verified. Tables 6–20 give the estimated viscosity calculated by different procedures.

11.2.1. Reid–Cohen (1944) [125]

From measurements on coal-ash slags, Reid and Cohen prepared a nomogram by which the viscosity of a slag can be predicted graphically at any temperature above that of the critical viscosity.

They found that a plot of $|d\eta/dT|$ against η on logarithmic paper gave a straight-line relationship, indicating that

$$\eta^{-z} = a \cdot T - b \tag{37}$$

For viscosity measured in Pa s and T in K, the values of z and a were reported to be $z = 0.1614$ and $a = 1.18 \cdot 10^{-3}$. Constant b is composition-dependent.

It was found desirable to omit Al_2O_3 from the slag composition and recalculate so that (SiO_2 + Equiv.Fe_2O_3 + CaO + MgO) = 100 wt%.

The total alkali content in the slags never exceeded 2.5 wt%; thus they were not considered in the modelling.

The equivalent Fe_2O_3 is a recalculation of the total iron content to Fe_2O_3 performed on a weight basis.

$$\text{Equiv.}Fe_2O_3 = Fe_2O_3 + 1.11FeO + 1.43Fe \tag{38}$$

1 g of Fe_2O_3 contains the same amount of iron atoms as 1/1.11 g FeO or 1/1.43 g Fe, so the Equiv. Fe_2O_3 designates the weight represented by Fe-oxide if all iron were bound as Fe_2O_3.

Plotting the SiO_2 content on this basis against viscosity resulted in better agreement with experiments than when Al_2O_3 was included.

The nomogram is shown in Fig. 37. Scale C shows the relationship between the SiO_2 content of the slag and its viscosity given in poise at 2600°F (1700 K) and it can be used directly to determine the liquid viscosity at this

Table 6
Calculated example

Reid–Cohen (1944)	
Composition (excl Al_2O_3 and Na_2O) (weight-basis)	75.7% SiO_2, 14.1% CaO, 10.2% MgO
Temperature	2462°F
Estimated viscosity	1200 P = 120 Pa s

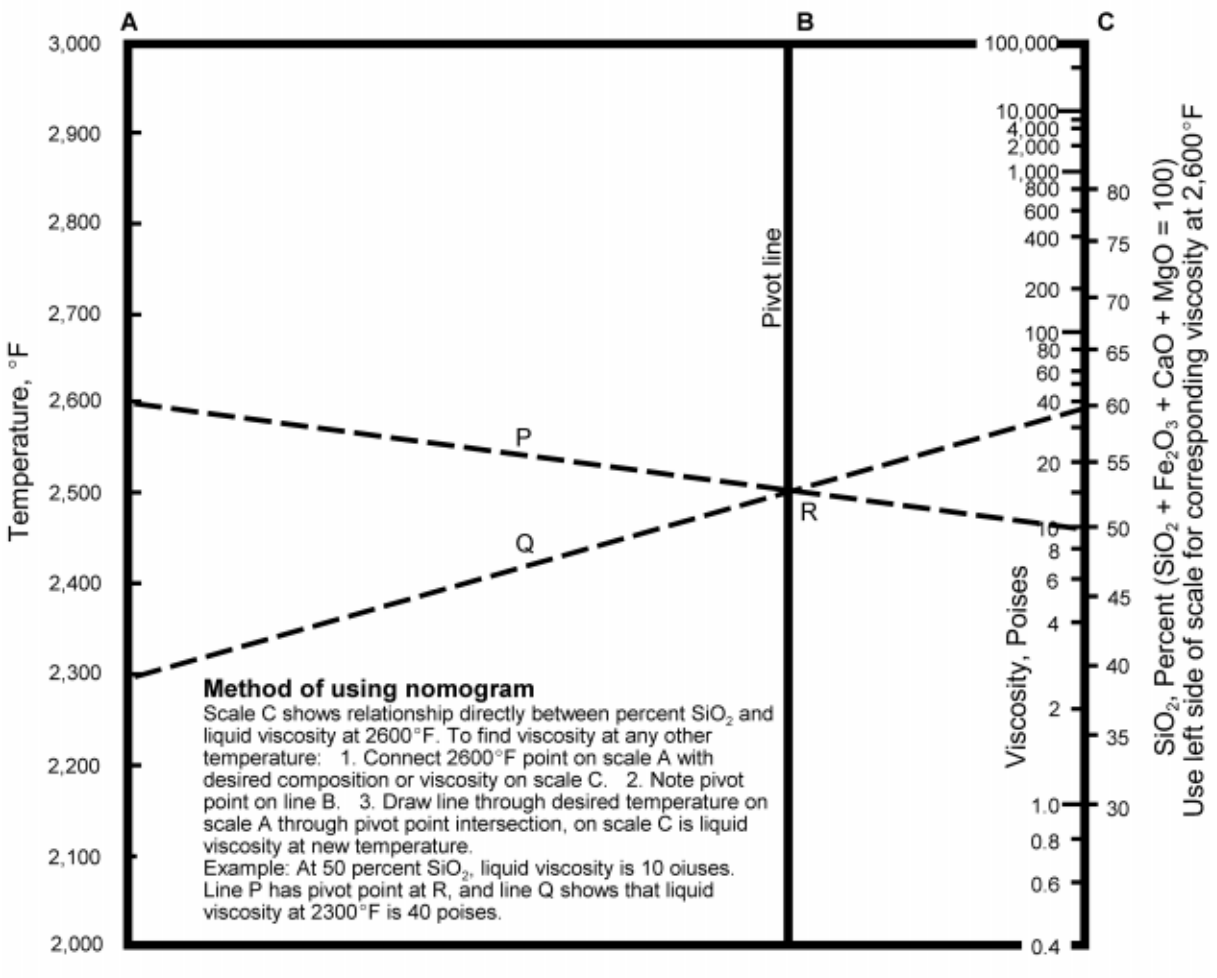

Fig. 37. Nomogram relating viscosity to composition and temperature according to the Reid–Cohen model [125] (by permission of the publisher).

temperature. To convert to other temperatures shown on scale A, pivot line B must be used as illustrated on the nomogram.

The authors suggest that for slags containing more than 3 wt% MgO and less than 5 wt% CaO, or where the alkalies exceed 2.5 wt%, the predictions of the model should be applied with reservations.

Procedure: (Reid–Cohen)

(i) Recalculate composition:
$(SiO_2 + \text{Equiv.}Fe_2O_3 + CaO + MgO) = 100$ wt% (Eq. (37))

(ii) Use nomogram to find temperature–viscosity relationship

11.2.2. Sage–McIlroy (1959) [104]

The authors present the model as a minor part of a paper, and they just state that it is based on experimental data. These data probably comprise both pure coal ashes and chemically altered coal ashes, all of which were probably composed chiefly of silicon, aluminium, iron and calcium, with smaller amounts of titanium, magnesium, sodium, potassium and other trace elements [104].

Table 7
Calculated example

Sage–McIlroy (1959)	
Composition	67.1% SiO_2,
(excl Na_2O)	11.4% Al_2O_3,
(weight-basis)	12.5% CaO, 9.0% MgO
Silica ratio (ς)	75.7%
Temperature	2462°F
Estimated viscosity	1300 P = 130 Pa s

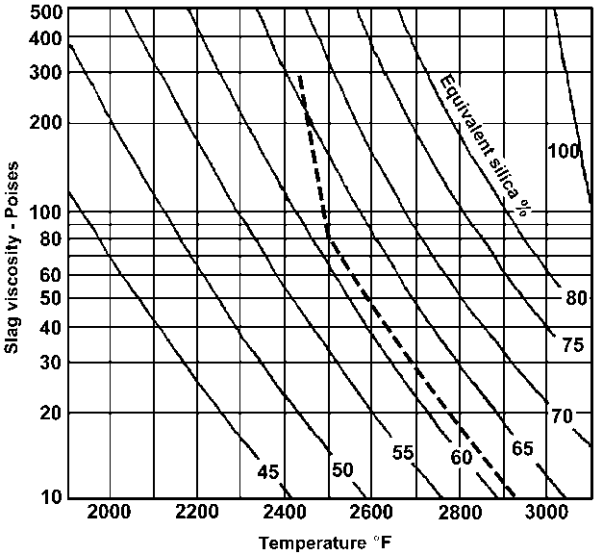

Fig. 38. Graph relating the viscosity of a slag to its temperature and composition according to the Sage–McIlroy model [104] (reproduced from Sage and McIlroy (1959)).

The silica ratio, ς, is calculated on a weight-basis

$$\varsigma = \frac{100 \cdot SiO_2}{SiO_2 + Equiv.Fe_2O_3 + CaO + MgO} \quad (39)$$

A family of logarithmic curves was established by Sage and McIlroy showing the viscosity–temperature relationship for a range of silica ratios, Fig. 38. The graphs are only valid for completely molten silicates, but a broken line in Fig. 38 indicates how the viscosities of partly crystallised melts can be estimated. If T_{cv} falls below 250 P, extending a line upward at a 10° slope gives a reasonable approximation of the temperature–viscosity relationship up to 250 P.

Procedure: (Sage–McIlroy)

(i) Calculate silica ratio, ς (Eqs. (37) and (38))
(ii) Find appropriate temperature–viscosity curve

11.2.3. Modified silica ratio, S^2 (1963)

As it is the case for the Reid–Cohen model, the S^2-model is also based on studies of coal ash slags, containing silicon, aluminium, iron, calcium and magnesium as major components. Minor components such as the alkali oxides are not considered in the model.

Table 8
Calculated example

S^2 (1963)	
Composition (excl Na_2O) (weight-basis)	67.1% SiO_2, 11.4% Al_2O_3, 12.5% CaO, 9.0% MgO
Silica ratio (ς)	75.7%
Temperature	1623 K
Estimated viscosity	82 Pa s

The model relates the viscosity–temperature characteristics of wholly liquid slags with their chemical composition, and it is based on a recalculation of the compositional analysis of the slag in which all Fe is assumed present in the mixture as Fe_2O_3 (see Eq. (38))

$$SiO_2 + Al_2O_3 + Equiv.Fe_2O_3 + CaO + MgO = 100\ wt\% \quad (40)$$

The silica ratio is calculated according to Eq. (38), and viscosity (Pa s) is modelled as a function of the silica ratio, ς, and temperature (K)

$$\log \eta = 4.468\left(\frac{\varsigma}{100}\right)^2 + 1.265 \cdot \frac{10^4}{T} - 8.44 \quad (41)$$

The relationship is a mathematical reformulation of the nomogram elaborated by Reid and Cohen in 1944 [105], and all constants have been fitted from experimental data.

The correlation was calculated from data from determinations on 62 samples of slags that covered the following range of chemical compositions:

- SiO_2: 31–59 wt%
- Al_2O_3: 19–37 wt%
- Equiv.Fe_2O_3: 0–38 wt%
- CaO: 1–37 wt%
- MgO: 1–12 wt%
- $Na_2O + K_2O$: 1–6 wt%
- Silica ratio (ς): 45–75
- SiO_2/Al_2O_3: 1.2–2.3

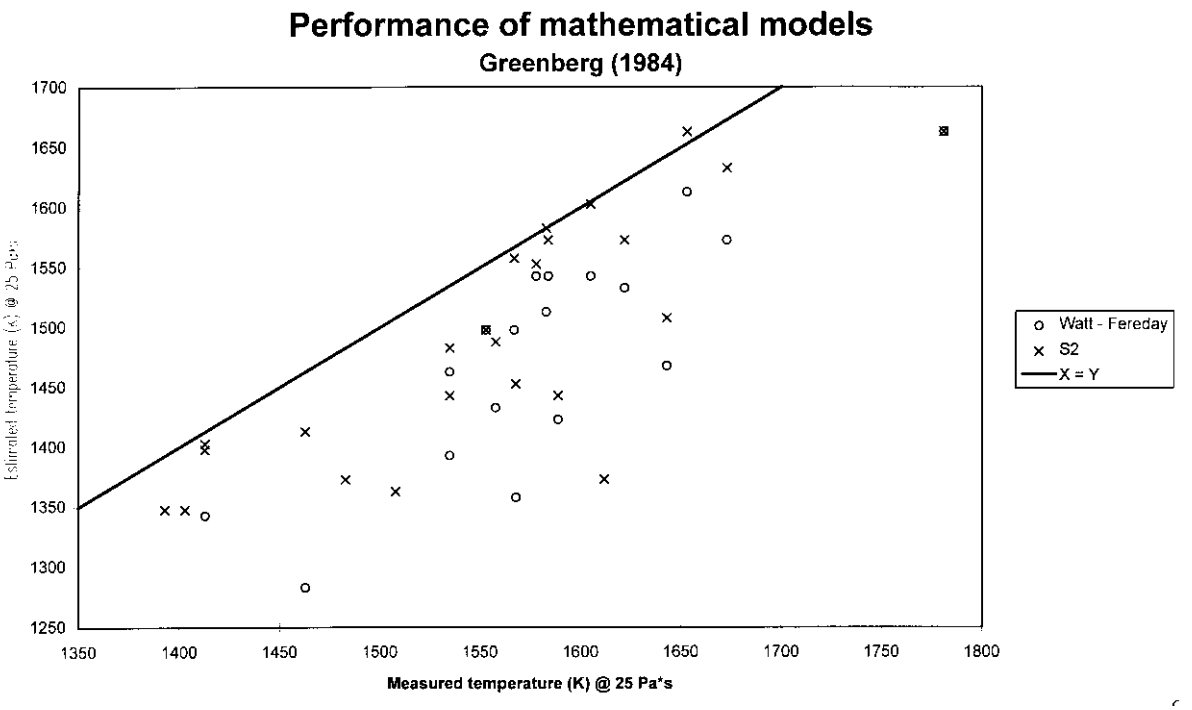

Fig. 39. The performance of the Watt–Fereday and the S^2-models tested against measured values [126].

Procedure: (S^2)

(i) Recalculate composition (Eqs. (39) and (37))
(ii) Calculate silica ratio, ς (Eq. (38))
(iii) Calculate viscosity as a function of temperature (Eq. (40))

The performance of the S^2-model has long been surpassed by those of other models. Greenberg (1984) tested the model on a variety of natural and synthetic coal slags. Fig. 39 shows the measured and predicted temperatures for a viscosity of 25 Pa s depicted against each other for a series of compositions. The model tends to underestimate viscosity, and the average temperature difference is $(T_{meas} - T_{est})_{mean} = 66$ K [126].

11.2.4. Watt–Fereday model or slope and intercept model (1963)

The model was originally launched as the slope and intercept model, but nowadays it is generally referred to as the Watt–Fereday model after the authors. The basis of the model is a recalculation of the composition identical to that of the S^2 model, Eq. (39). The two parameters, m and c, should be calculated from the species concentrations in weight percent:

$$\text{Slope: } m = 0.00835 \cdot SiO_2 + 0.00601 \cdot Al_2O_3 - 0.109 \quad (42)$$

$$\text{Intercept: } c = 0.0415 \cdot SiO_2 + 0.0192 \cdot Al_2O_3 + 0.0276 \cdot Fe_2O_3 + 0.0160 \cdot CaO - 4.92$$

Table 9
Calculated example

Watt–Fereday (1963)	
Composition	67.1% SiO_2,
(excl Na_2O)	11.4% Al_2O_3,
(weight-basis)	12.5% CaO, 9.0% MgO
Slope (m)	0.52
Intercept (c)	−1.71
Temperature	1623 K
Estimated viscosity	78 Pa s

to enable the estimation of viscosity (Pa s) as a function of temperature (K)

$$\log \eta = \frac{m \cdot 10^7}{(T - 423)^2} + c \quad (43)$$

The model was derived for British coal ashes on the basis of measurements on 113 ashes all lying within the following compositional limits.

- SiO: 30–60 wt%
- Al_2O_3: 15–35 wt%
- Fe_2O_3: 3–30 wt%
- CaO: 2–30 wt%
- MgO: 1–10 wt%
- Silica ratio (ς): 40–80
- SiO_2/Al_2O_3: 1.4–2.4

Procedure: Watt–Fereday

(i) Recalculate composition: (SiO_2 + Equiv.Fe_2O_3 + CaO + MgO) = 100 wt% (Eq. (37))
(ii) Calculate constants m and c (Eq. (41))
(iii) Determine viscosity as a function of temperature (Eq. (42))

The model is frequently used for modelling the low-temperature behaviour of silicate melts [127,128]. Jones and Lindsey (1987) and Quon et al. (1985) all found the model to overestimate the viscosity of multi-component slags [39,60]. The results of Greenberg (1984) are in accordance with this, Fig. 39; he found the model to underestimate the temperature for a viscosity of 25 Pa s for all compositions tested, $(T_{meas} - T_{est})_{mean} = 180$ K [126].

Due to a misprint, the model is erroneously cited in a paper by Hoy et al. (1965) and in a paper by Quon et al. (1984) [105,129]. In the paper by Hoy and co-workers, the second term in the expression for c is given as "$0.001923 \cdot Al_2O_3$", i.e. ten times less than above cited [105].

Bomkamp (1976) attempted a modification of the Watt–Fereday equations for calculating the constants m and c to account for the MgO-content [39]:

$$\text{Slope: } m = 0.0104291 \cdot SiO_2 + 0.0100297 \cdot Al_2O_3 - 0.296285$$

$$\text{Intercept: } c = 0.0154148 \cdot SiO_2 - 0.0388047 \cdot Al_2O_3 - 0.0167264 \cdot Fe_2O_3 - 0.0089096 \cdot CaO - 0.012932 \cdot MgO + 0.04678 \quad (44)$$

Procedure: Bomkamp

(i) Recalculate composition: (SiO_2 + Equiv.Fe_2O_3 + CaO + MgO) = 100 wt% (Eq. (37))
(ii) Calculate constants m and c (Eq. (43))
(iii) Determine viscosity as a function of temperature (Eq. (42))

Table 10
Calculated example

Bomkamp (1976)	
Composition (excl Na_2O) (weight-basis)	67.1% SiO_2, 11.4% Al_2O_3, 12.5% CaO, 9.0% MgO
Slope (m)	0.52
Intercept (c)	0.41
Temperature	1623 K
Estimated viscosity	10,100 Pa s

Quon et al. (1985) found the Bomkamp modification to over-estimate viscosities by as much an order of magnitude for some melts [39].

11.2.5. Bottinga–Weill (1972)

Bottinga and Weill found it to be easier to build up mathematical relations from synthetic systems than to reduce analytically the magmatic systems, for which the model was intended, largely because of the relative abundances of data [130].

The prediction of the viscosity of anhydrous silicate liquids is approached by means of tabulated constants, D_i, for each species in the melt. D_i values are given for different levels of SiO_2 content and for temperatures in the range 1473–2073 at 50 K intervals (Appendix D).

$$\log \eta = \sum_i x_i \cdot D_i - 1 \quad (45)$$

Viscosity is evaluated in Pa s, and x_i indicates the individual species molar fractions. It was recommended that for all major components present ($x_i > 5$ mol%) only the D_i-values actually listed in the tables of Appendix D should be used.

The model was proposed for natural magmatic liquids, i.e. molten rock found beneath Earth's crust. Since most melts of geological interest have compositions such that the sum of the concentrations of MO and M_2O oxides exceeds that of Al_2O_3 on a molar basis, it is assumed that aluminium predominantly exists in tetrahedral coordination. Based on observations performed by others, Bottinga and Weill made the assumption that Al_2O_3 combines with other oxides to form $KAlO_2$, $NaAlO_2$, $BaAl_2O_4$, $SrAl_2O_4$, $CaAl_2O_4$, $MgAl_2O_4$ and $MnAl_2O_4$ in the order of preference stated here, until all aluminium is used [68].

The authors only had very few data available on the viscosity of iron-containing silicate liquids, and the measurements were all in the low-Fe_2O_3 range with poor control of oxidation state. In the model, equimolar amounts of Fe^{3+} and Fe^{2+} are assumed to have roughly the same influence on viscosity; accordingly all Fe^{3+} should be converted to Fe^{2+} in the model.

Since no data are available on the effect of $KAlO_2$ on viscosity, the assumption $D_{KAlO_2} = D_{NaAlO_2}$ should be used for purposes of calculation. No data exists for D_{NaAlO_2} in the composition range $0.35 < x_{SiO_2} < 0.45$. Fortunately most rock systems in this range also tend to have only

Table 11
Calculated example

Bottinga–Weill (1972)	
Composition (molar basis)	62.5% SiO_2, 12.5% $NaAlO_2$, 12.5% CaO, 12.5% MgO
Temperature	1623 K
Estimated viscosity	33 Pa s

relatively minor amounts of alkali metals, so the authors found it acceptable to use the equivalent D_{NaAlO2} constants for the composition range $0.45 < x_{SiO_2} < 0.55$.

Whenever D_i-constants are lacking for certain minor MO-components, the arithmetic average of the D_{MO}-values listed in Appendix D should be used.

When values of D_{TiO_2} are not accessible, the approximation $D_{TiO_2} = D_{CaO}$ should be used.

Procedure: Bottinga–Weill

(i) Recalculate composition according to compositional list in tables (Appendix D) and following the guidelines outlisted above
(ii) Select table according to SiO_2-content (Appendix D)
(iii) Calculate viscosity at the two neighbouring temperatures and intrapolate

The model performs well on some geological samples [20,131], but it is not suitable for the evaluation of melts with high contents of aluminium.

The authors estimate all the above approximations to be valid to within $\log \eta \pm 1$.

11.2.6. Shaw (1972) [130]

Based on the compilation of data and the calculations of Bottinga and Weill, Shaw (1972) discovered that the viscosities of multi-component anhydrous silicate liquids could be estimated more easily and with equal accuracy without the use of extensive tables.

When the Bottinga–Weill model was published, Shaw was investigating additivity relations for the a and b constants in the Arrhenius equation, Eq. (25). He attempted to fit the viscosity data for compositions of the rock-system using methods of multiple regression analysis.

The first of two principal assumptions used to define an empirical model of average behaviour was that viscosity curves for multi-component silicate liquids intersect the reference curve for pure SiO_2-melt at a characteristic set of temperature and viscosity suggested by the averages of the binary intersections. Or in other words: No matter what chemical system is simulated, the ($\log \eta$ vs $10^4/T$)-curve will intersect the SiO_2-curve in an invariant point with coordinates (c_T, c_η). This principle is shown graphically in Fig. 40 (where the invariant point has been designated the coordinates mentioned below and the second point on the SiO_2-graph is the intercept of the two measured graphs in Fig. C.1)

Table 12
Constants for the calculation of α in the Shaw model

Metal oxide	α_i^0
K_2O, Na_2O, Li_2O	1.2
MgO, FeO	1.5
CaO, TiO_2	2
"AlO_2"	2.9

Table 13
Calculated example

Shaw (1972)	
Composition	See Table 14
$\alpha = \frac{x_{SiO_2} \cdot \sum(x_i \cdot \alpha_i^0)}{1 - x_{SiO_2}} = \frac{0.588 \cdot 0.824}{1 - 0.588} = 1.176$	
$\log \eta = \alpha \cdot \frac{10^4}{T} - c_T \cdot \alpha + c_\eta$	
$= 1.176 \cdot \frac{10^4}{T} - 1.5 \cdot 1.176 - 3.78 = \frac{11765}{T} - 5.54$	
Temperature	1623 K
Estimated viscosity	51 Pa s

Mathematically, the consequence of this assumption is that the a-parameter in the Arrhenius equation is fixed by the value of the slope in a ($\log \eta$ vs $10^4/T$)-plot. Physically, of course, this also implies a systematic relationship between a and b. Thus, the temperature dependence of viscosity is given by an equation of the form (T measured in K, and η in Pa s)

$$\log \eta = \alpha \cdot \frac{10^4}{T} - c_T \cdot \alpha + c_\eta \quad (46)$$

where α is a characteristic slope for a given multi-component mixture, and c_T and c_η the coordinates of the invariable point. A study of binary and multicomponent data lead to the adoption of the weighed means $c_T = 1.50$ and $c_\eta = -3.78$.

According to Shaw, the operations required to test and apply the empirical model are as outlined below.

Procedure: Shaw

(i) convert the chemical analysis to a value for the mean slope, α
  (a) convert the chemical analysis to moles of the appropriate oxides in Table 12 and calculate the corresponding mole fractions
  (b) multiply the values of α_i° in Table 12 by the total mole fraction of each α_i° category
  (c) sum the products and multiply by $x_{SiO2}/(1 - x_{SiO2})$ giving the mean value of the slope
(ii) derive viscosity versus temperature (Eq. (45))

Table 14
Calculation sheet for the Shaw model example

Constituent	Moles	x_i	α_i^0	$x_i \cdot \alpha_i^0$
SiO_2	0.625	0.588	–	–
"AlO_2"	0.125	0.118	2.9	0.341
CaO	0.125	0.118	2.0	0.235
MgO	0.125	0.118	1.5	0.176
Na_2O	0.063	0.059	1.2	0.071
Total	1.0625	11	–	0. 824

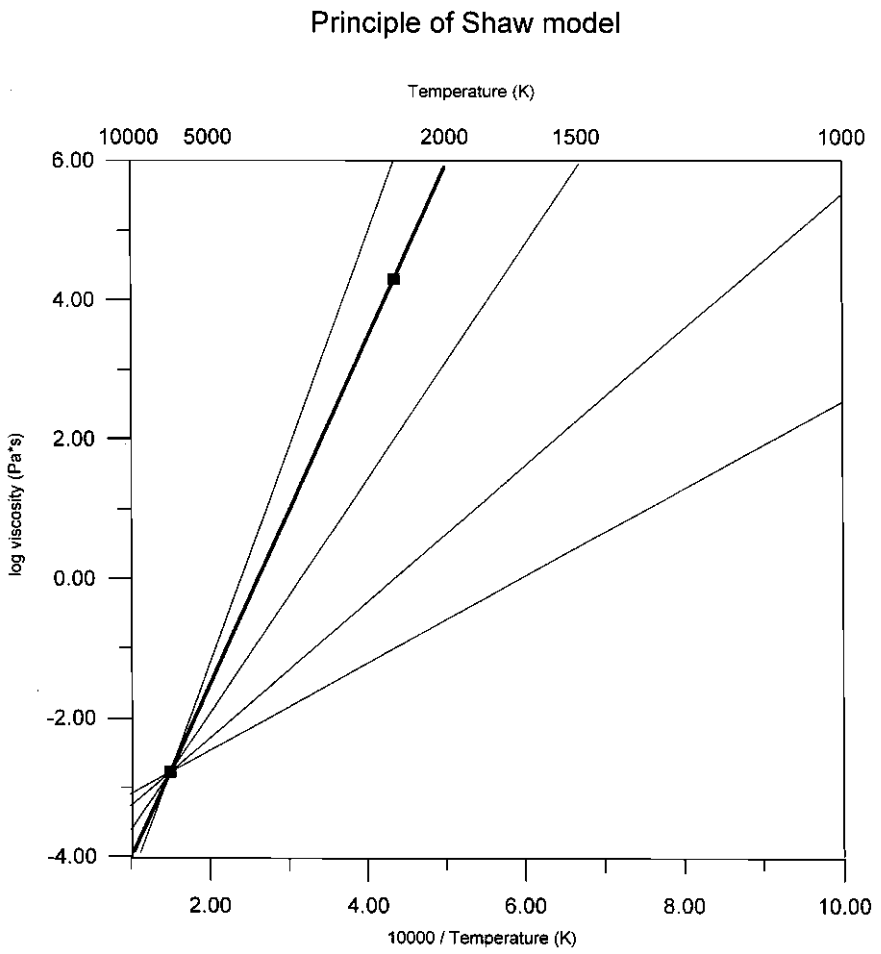

Fig. 40. According to the predictions of the Shaw model, a linear relationship exists between log η and $1/T\,(\mathrm{K}^{-1})$ through the invariant point at the bottom left corner. The thick line indicates the behaviour of pure SiO_2 through the invariant point and the intercept of two measured graphs in Fig. C.1. All dashed lines indicate possible relationships for other compositions.

Shaw tested the performance of the model on data that had not been used for the development of the model. He concluded that

1. Predicted viscosities may not reproduce experimental data at viscosities above approximately 10^7 Pa s, where calculated values may be too low in many cases.
2. The model predicts the viscosity of melts that are not exposed to any thermal or compositional gradients. Thus predictions must inevitably fail unless they are referred to a limiting equilibrium condition or take special account of sample history.

As a general remark, Shaw stated that it appeared that both his own model and the Bottinga–Weill model more often than not tend to deviate towards values higher than the measured viscosities [130].

According to Urbain (1985), no physical background for the relationship between constants a and b employed by Shaw has been clearly deduced [24].

11.2.7. Lakatos (1972)

Based on viscosity–temperature measurements on 30 different laboratory-prepared compositions in the

Table 15
Calculated exmple

Lakatos (1972)	
Composition (moles per mole SiO_2)	Al_2O_3: 0.1, CaO: 0.2, MgO: 0.2, Na_2O: 0.1
A	−3.57
B	5831
C	530
Temperature	1623 K
Estimated viscosity	58 Pa s

SiO_2–Al_2O_3–Na_2O–K_2O–CaO–MgO system, Lakatos et al. (1972) chose to fit the experimental data with a model based on the Vogel–Fulcher–Tamann (VFT) equation. Compositions in the following ranges were used:

- SiO_2: 0.61–0.77 molar fraction
- Al_2O_3: 0–0.05 molar fraction
- CaO: 0.09–0.14 molar fraction
- MgO: 0–0.10 molar fraction
- Na_2O: 0.10–0.15 molar fraction
- K_2O: 0–0.06 molar fraction

Although the curve of deviations showed a systematic S-shaped form, independent of measuring techniques, apparatus, and viscosity range, indicating that the VFT-equation is not descriptive of the real relationship, it was decided to use it because of its simplicity and general acceptance.

The VFT-equation expressed the viscosity–temperature relationship as

$$\log \eta = a + \frac{b}{T - c} \tag{47}$$

with viscosity η in Pa s, temperature T in K, and a, b, c composition-specific constants. The VFT-equation was optimised for minimum temperature deviations by least squares techniques, as the deviations of log viscosities were not normally distributed. There is no direct method to optimise this form of equation, so the VFT-equation was first transformed into a form that allowed for multiple regression analysis of two independent variables.

The three equations for calculating the VFT-constants for glass compositions were found to be

$$a = 1.5183 \cdot Al_2O_3 - 1.6030 \cdot CaO - 5.4936 \cdot MgO + 1.4788 \cdot Na_2O - 0.8350 \cdot K_2O - 2.4550 \tag{48}$$

$$b = 2253.4 \cdot Al_2O_3 - 3919.3 \cdot CaO + 6285.3 \cdot MgO - 6039.7 \cdot Na_2O - 1439.6 \cdot K_2O + 5736.4$$

$$c = +294.4 \cdot Al_2O_3 + 544.3 \cdot CaO - 384.0 \cdot MgO - 25.07 \cdot Na_2O - 321.0 \cdot K_2O + 471.3$$

The symbols Na_2O, K_2O, CaO, MgO and Al_2O_3 represent the molar fraction of each species per mole SiO_2, i.e. Na_2O = mole Na_2O/mole SiO_2.

Procedure: Lakatos
Recalculate concentration of species: Al_2O_3, CaO, MgO, Na_2O, K_2O to basis moles per mole SiO_2
Calculate constants a, b and c (Eq. (47))
Calculate viscosity as a function of temperature (Eq. (46))

The performance of the model was tested on data produced on three glasses of similar compositions as used in the investigation by another laboratory. Calculated values showed good agreement with measured viscosities for one glass. For the other two glasses, significant deviations were found at high temperatures, although agreement at lower temperatures was somewhat better.

The authors suggest that rectification of the parameter-fitting with more experimental data may improve the model [73].

11.2.8. Urbain (1981)

The Weymann relation is the basis of this model. By studying approximately 60 different compositions of ternary SiO_2–Al_2O_3–MO and SiO_2–Al_2O_3–M_2O mixtures (where MO and M_2O, respectively, represent the bi-and monovalent oxides), all lab-prepared, Urbain et al. (1981) worked out a model for the estimation of the viscosity of ceramics, and subsequently they tested the model performance on natural minerals of multi-component composition [132].

First, the species in the liquid are grouped according to the oxygen content as glass formers, glass modifiers or as amphoterics

$$x_g = SiO_2 + P_2O_5 \tag{49}$$

$$x_m = FeO + CaO + MgO + Na_2O + K_2O + MnO + NiO + 2(TiO_2 + ZrO_2) + 3CaF_2$$

$$x_a = Al_2O_3 + Fe_2O_3 + B_2O_3$$

Then α is calculated

$$\alpha = \frac{x_m}{x_m + x_a} \tag{50}$$

Now the parameter b (K) is calculated by combination of four parabolic equations in α with the molar ratio of silica, SiO_2

$$b_0 = 13.8 + 39.9355\ \alpha - 44.049\alpha^2$$

$$b_1 = 30.481 - 117.1505\alpha + 129.9978\alpha^2$$

$$b_2 = -40.9429 + 234.0486\alpha - 300.04\alpha^2 \tag{51}$$

$$b_3 = 60.7619 - 153.9276\alpha + 211.1616\alpha^2$$

$$b = b_0 + b_1 \cdot SiO_2 + b_2 \cdot SiO_2^2 + b_3 \cdot SiO_2^3$$

Table 16
Calculated example

Urbain (1981)	
(x_g, x_m, x_a)	(0.6250, 0.3125, 0.0625)
α	0.833
(b_0, b_1, b_2, b_3)	(16.5, 23.1, −54.3, 79.1)
b	29.1 K
a	3.40×10^{-10} Pa s/K
Temperature	1623 K
Estimated viscosity	33 Pa s

and the parameter a (Pa s/K) is given from b as

$$-\ln a = 0.2693 \cdot b + 13.9751 \quad (52)$$

Finally, viscosity (Pa s) is computed as a function of temperature (K) according to the Weyman equation:

$$\eta = a \cdot T \cdot e^{(b \cdot 10^3)/(T)} \quad (53)$$

The choice of temperature is restricted to the range of existence of the liquid

- $T \geq T_m$ or T_l for stable liquids,
- $T > T_g$ for supercooled liquids,

where T_m, T_l, T_g are melting, liquidus and glass transition temperatures [24].

Procedure: Urbain

(i) Recalculate composition according to oxides present in Eq. (48)
(ii) Calculate grouping constants x_m, x_a (Eq. (48))
(iii) Calculate constant α (Eq. (49))
(iv) Calculate constants b_1, b_2, b_3, b_4 and subsequently b (Eq. (50))
(v) Calculate constant a (Eq. (51))
(vi) Derive viscosity as a function of temperature (Eq. (52))

In a paper from 1985, Urbain gives system-specific constants for the derivation of the b-constant for a range of binary and ternary systems, derived on the basis of less than ten melts per system [24]

- SiO_2–Al_2O_3 /CaO
- Al_2O_3–CaO
- SiO_2–Al_2O_3–MO (M = Mg, Ca, Mn)

Mills (1992 and 1993) tested the Urbain model extensively on mixtures of few components as well as multicomponent mixtures. The model was able to predict viscosities to within an order of magnitude, and often the predicted viscosities differed by less than a factor two from the experimental results. Thus, the results indicate that the model is capable of describing trends in the viscosity–composition relationship [14,134].

Senior (1995) states that the Urbain relationship can describe viscosity at high temperatures, i.e. for viscosity less than 10^2–10^3 Pa s [45].

Vargas et al. (1997) found the model to give reasonable but not very accurate predictions of the viscosities of high-rank coal ashes, i.e. the predictions could deviate from the experimental results with an order of magnitude, but not with five orders of magnitude [135].

Experiments performed on three melts of olivine type ($FeCaSiO_4$) show an increase in b with an increase in the ratio Fe^{3+}/Fe^{2+} [24], and Mills (1984) argues that Fe_2O_3 behaves more like a modifier than an amphoteric, and therefore it should be moved from x_a to x_m with a factor 3 to account for the oxygen content of 1.5 per iron-atom [133].

Urbain continued his work on the model after the publication in 1981. In 1987, he proposed new sets of constants for the relationship between a and b, and in 1990, he proposed even more system-specific improvements together with Boiret. In the following, the proposed constants have been assigned the characters c and d

$$-\ln a = c \cdot b + d \quad (54)$$

- Ionic melts: $c = 0.29$, $d = 13.87$
- Network liquids, e.g. SiO_2, B_2O_3 and GeO_2: $c = 0.207$, $d = 12.591$

  The borderline between the two sets of values depends on the slag composition, but it is generally located in the range $x_C \in [0.85; 0.90]$, $C \in (SiO_2, BO_{3/2}, GeO_2)$ [43].
- SiO_2–Al_2O_3: $c = 0.247$, $d = 14.33$
- SiO_2–Be_2O_3: $c = 0.232$, $d = 10.978$
- SiO_2–PbO: $c = 0.414$, $d = 14.425$ [19]

Deletter et al. (1984) established a similar model for feldspar melts. The data used correspond to silica contents higher than 0.5 mole fraction and to equal proportions of alumina and modifier ions. These two conditions constitute an important limitation of the model [136].

11.2.9. Riboud (1981)

An experimental study of the CaO–Al_2O_3–SiO_2–CaF_2 system was used as a basis for a reevaluation of the Urbain model (a in Pa s/K; b in K):

$$\ln a = -35.76Al_2O_3 + 1.73(FeO + CaO + MgO + MnO) + 7.02(Na_2O + K_2O) + 5.82CaF_2 - 19.81 \quad (55)$$

$$b = 68.833Al_2O_3 - 23.896(FeO + CaO + MgO + MnO) - 39.159(Na_2O + K_2O) - 46.356CaF_2 + 31.140$$

where all concentrations are calculated as molar fractions. Some uncertainty exists concerning the formulation of the third term in the expression for b; Riboud and co-workers present the equation twice in their paper, but with a different order of the digits in the third term: 39,519 ($Na_2O + K_2O$) and 39,159 ($Na_2O + K_2O$) [120].

Table 17
Calculated example

Riboud (1981)	
(x_g, x_m, x_a)	(0.6250, 0.3125, 0.0625)
α	0.833
a	6.37×10^{-10} Pa s/K
b	27.02 K
Temperature	1623 K
Estimated viscosity	18 Pa s

The equation was tested on continuous casting slags by the authors, and it was found to apply over the entire compositional range studied [120]:

- SiO_2: 27–56 wt%
- Al_2O_3: 0–12 wt%
- CaO: 8–46 wt%
- Na_2O: 0–22 wt%
- CaF_2: 0–18 wt%

Procedure: Riboud

(i) Recalculate composition according to species present in Eq. (54)
(ii) Calculate constants a and b (Eq. (54))
(iii) Derive viscosity as a function of temperature (Eq. (52))

Riboud et al. (1981) found computed viscosity to be in good agreement with the measured values for 22 industrial continuous casting slags [120]; but Mills (1984) found the Urbain model to be marginally better for coal gasification slags [134].

11.2.10. Streeter (1984)

Based on viscosity measurements on 17 Western US lignite and subbituminous coal slags within the compositional range:

- SiO_2: 0.25–0.70 molar fraction
- Al_2O_3: 0.08–0.27 molar fraction
- Fe_2O_3: 0–0.09 molar fraction
- CaO: 0.08–0.33 molar fraction
- MgO: 0.04–0.13 molar fraction
- Na_2O: 0–0.11 molar fraction
- Minor constituents ($x_i < 5\%$) : K_2O, TiO_2, P_2O_5, SO_3

Streeter, Diehl and Schobert proposed a correction term to the Urbain equation.

$$\ln \eta = \ln a + \ln T + \frac{10^3 \cdot b}{T} - \Delta \tag{56}$$

where

$$\Delta = m \cdot T + c \tag{57}$$

The evaluation of Δ was divided into three groups according to the silica-content of the melt, i.e. the b value in the Urbain expression, Eq. (49) — all concentrations in molar fractions.

- High-silica slags ($b > 28$):
  $F = SiO_2/(CaO + MgO + Na_2O + K_2O)$
  $10^3 \cdot m = -1.7264 \cdot F + 8.4404$
  $c = -1.7137(10^3 \cdot m) + 0.0509$
- Intermediate-silica slags ($24 < b < 28$):
  $F' = b \cdot (Al_2O_3 + FeO)$
  $10^3 \cdot m = -1.3101 \cdot F' + 9.9279$
  $c = -2.0356(10^3 \cdot m) + 1.1094$
- Low-silica slags ($b < 24$):
  $F'' = CaO/(CaO + MgO + Na_2O + K_2O)$
  $10^3 \cdot m = -55.3649 \cdot F'' + 37.9186$
  $c = -1.8244(10^3 \cdot m) + 0.9416$

Procedure: Streeter

(i) Recalculate composition according to species present in Eq. (48)
(ii) Calculate grouping constants, x_m, x_a (Eq. (48))
(iii) Calculate constant α (Eq. (49))
(iv) Calculate constants b_1, b_2, b_3, b_4 and subsequently b (Eq. (50))
(v) Calculate constant a (Eq. (51))
(vi) Classify as high-, intermediate- or low-silica (see above)
(vii) Calculate constants F, m and c (see above)
(viii) Derive correction, Δ (Eq. (56))
(ix) Derive viscosity as a function of temperature (Eq. (55))

Vargas et al. (1997) tested the model on high-silica coal ashes that generally deviated from the compositional range for which the model was developed in their low contents of CaO and MgO. They found the model predictions to deviate from the experimental results with several orders of magnitude in some cases, and in one case, a positive $d\eta/dT$ was obtained [135].

11.2.11. Kalmanovitch–Frank (1988)

Using the original Urbain model as a basis, experimental data from Machin (glasses of the system SiO_2–Al_2O_3–CaO–MgO) was used for refinement of the model. A new

Table 18
Calculated example

Streeter (1984)	
Classification	High-silica slag
F	2
10^3 m	4.99
c	−8.5
Δ	−0.4
Temperature	1623 K
Estimated viscosity	49 Pa s

Table 19
Calculated example

Kalmanovitch–Frank (1988)	
(x_g, x_m, x_a)	(0.6250, 0.3125, 0.0625)
α	0.833
(b_0, b_1, b_2, b_3)	(16.5, 23.1, −54.3, 79.1)
b	29.1 K
a	2.06×10^{-10} Pa s/K
Temperature	1623 K
Estimated viscosity	20 Pa s

relationship between a and b was determined:

$$-\ln a = 0.2812 \cdot b + 14.1305 \quad (58)$$

Procedure: Kalmanovitch–Frank

(i) Recalculate composition according to oxides present in Eq. (48)
(ii) Calculate grouping constants, x_m, x_a (Eq. (48))
(iii) Calculate constant α (Eq. (49))
(iv) Calculate constants b_1, b_2, b_3, b_4 and subsequently b (Eq. (50))
(v) Calculate constant a (Eq. (57))
(vi) Derive viscosity as a function of temperature (Eq. (52))

The authors found the model to agree with experimental data for British coals ash slags including some with additives, and for Illinois #6 and Pittsburgh #8 coal ashes [44]. But in general the performance of the model has not been able to demonstrate a better fit than the Urbain model.

Srinivasachar et al. (1992) state that the Kalmanovitch–Frank model does not predict viscosity well at low temperatures where $\eta > 10^3$ Pa·s [22]. Nevertheless, Harb et al. (1993) chose this model for the prediction of low-temperature viscosities for Western US coals [137].

11.2.12. Summary

Table 20 contains a list of the measured and calculated viscosities in the above examples, where viscosity was calculated for a sample from the system SiO_2–Al_2O_3–CaO–MgO at 1623 K. Intervals around the measurement point can be used to judge the accordance between measurement and estimates. A logarithmic scale is used to obtain a close-to linear relationship between viscosity and temperature, and thereby ensure equal weighing of the high-temperature and the low-temperature end of the scale. The Bottinga–Weill and the Urbain models fall within the immediate vicinity of the measurement value, the Streeter and the Shaw models fall within ±0.2, Lakatos and Riboud: ±0.3, S^2 and Kalmanovitch–Frank: ±0.4, Reid–Cohen and Sage–McIlroy: ±0.6, and far-off readings are obtained with the Watt–Fereday and the Bomkamp models; i.e. all models developed 1972 or later, with the exception of the Bomkamp model, lie within an interval: log $\eta \pm 0.4$.

All the older models tend to overestimate the viscosity at 1623 K while the newer models are evenly distributed around the measurement point.

The calculated example was a quite uncomplicated test of the models against a single experimental result. According to the network theory, aluminium occurs as a network former in the melt due to the high content of modifier oxides (CaO, MgO, Na_2O). The melt does not contain any oxides with an amphoteric behaviour that would probably have given rise to major discrepancies.

Table 20
Measured and estimated viscosities for the system 62.5% SiO_2 — 6.25% Al_2O_3 — 12.5% CaO — 12.5% MgO — 6.25% Na_2O at $T = 1623$ K

Model	Year	Viscosity (Pa s)
Measured value [124]	1986	32.81
Reid–Cohen	1944	120
Sage–McIlroy	1959	130
S^2	1963	82
Watt–Fereday	1963	78
Bomkamp	1976	10,100
Bottinga–Weill	1972	33
Shaw	1972	51
Lakatos	1972	58
Urbain	1981	33
Riboud	1981	18
Streeter	1984	49
Kalmanovitch–Frank	1988	20

11.3. Discussion

In the above presentation of models for silicate melts, the viscosity predictions of a mixture at a single temperature were produced as an example and the results are summarised in Table 20. A more complete comparison of model predictions and experimental results has also been carried out, and the results are presented in the following.

Together with six other compositions, the model predictions of the viscosity of the mixture over a wide range of temperatures are presented in Figs. 41–47. The systems are examples of experimental results reported in Appendices A–D. They were chosen to represent compositions from binary to multi-component systems, as well as systems with and without iron. For the sake of completeness, a number of reproductions of similar compositions are included, and no two measurements were produced by the same authors. Most measurements are from the eighties, however, one set of data was produced in 1959.

Some models can not be used for all compositions and temperatures, so for some systems, the results from these models are either incomplete or absent. The results are presented in order of increasing compositional complexity in the following; and it is important to bear in mind, that although the measurements in general are the most trustworthy, also they can be erroneous.

11.3.1. SiO_2–FeO_x

Figs. 41 and 42 show results from the SiO_2–FeO_x system with low silica contents. The high viscosity measured at the lowest temperature in the system studied by Williams et al. (1983) [138] indicates that the temperature of critical viscosity is located somewhere between the two lowest measurement temperatures.

For both mixtures, the models exhibit a tendency to overestimate viscosity, most pronounced compared to the

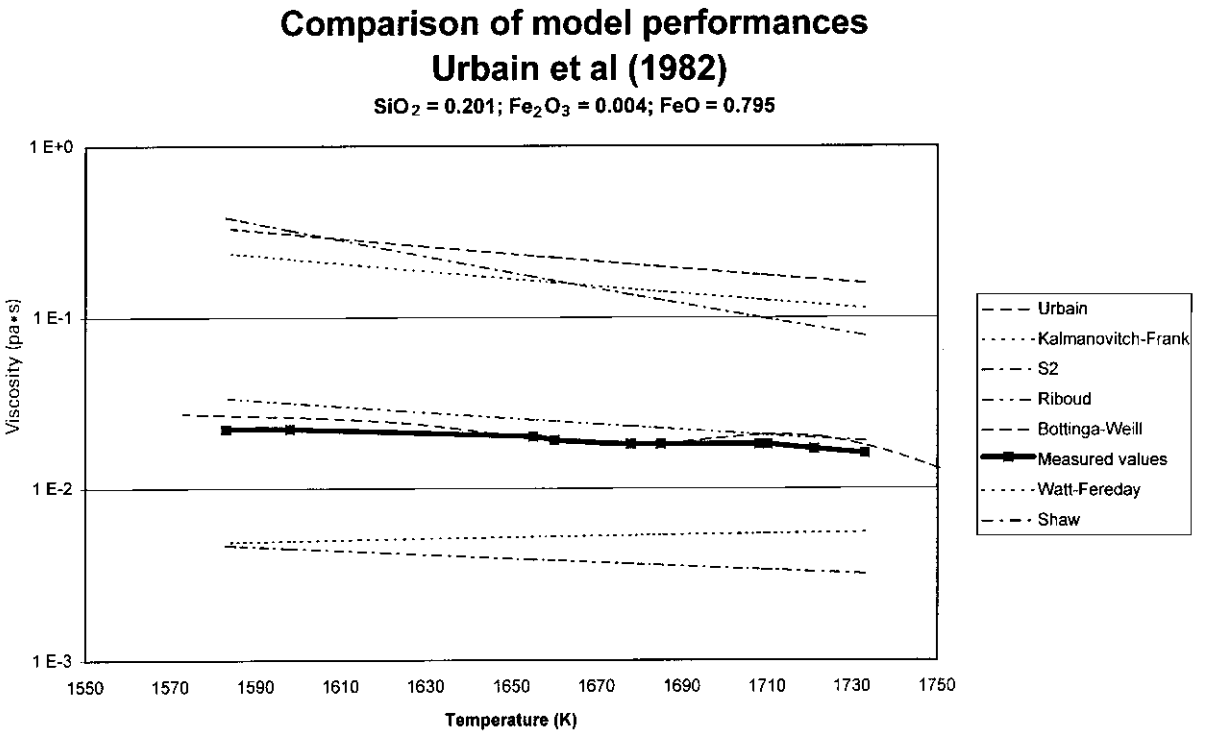

Fig. 41. Graphical comparison of experimental results obtained by Urbain et al. (1982) [20] and predictions produced by mathematical models for the same chemical composition.

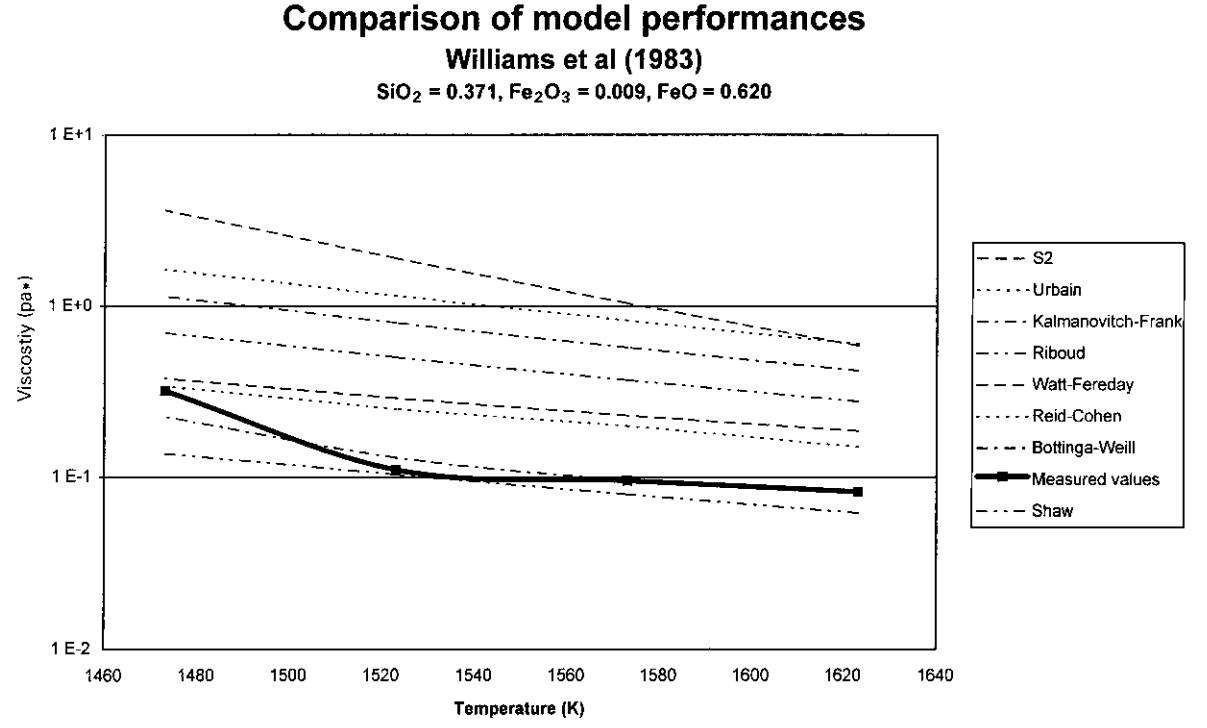

Fig. 42. Graphical comparison of experimental results obtained by Williams et al. (1983) [138] and predictions produced by mathematical models for the same chemical composition.

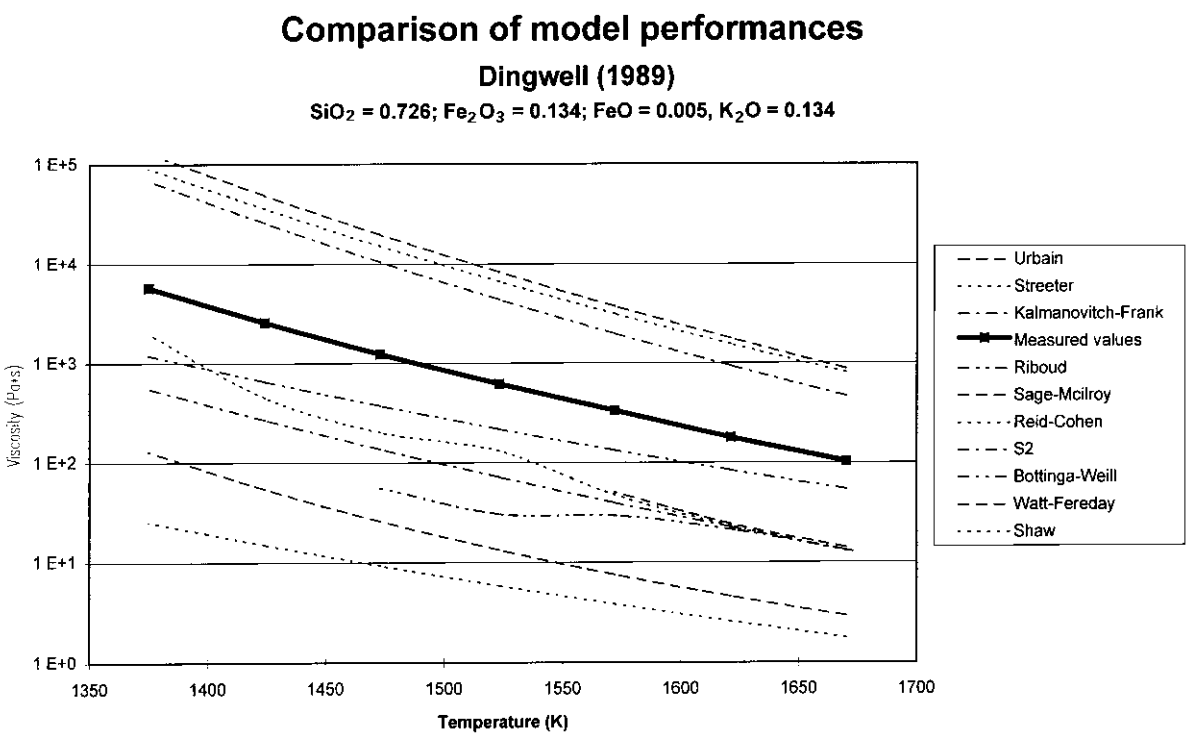

Fig. 43. Graphical comparison of experimental results obtained by Dingwell (1989) [56] and predictions produced by mathematical models for the same chemical composition.

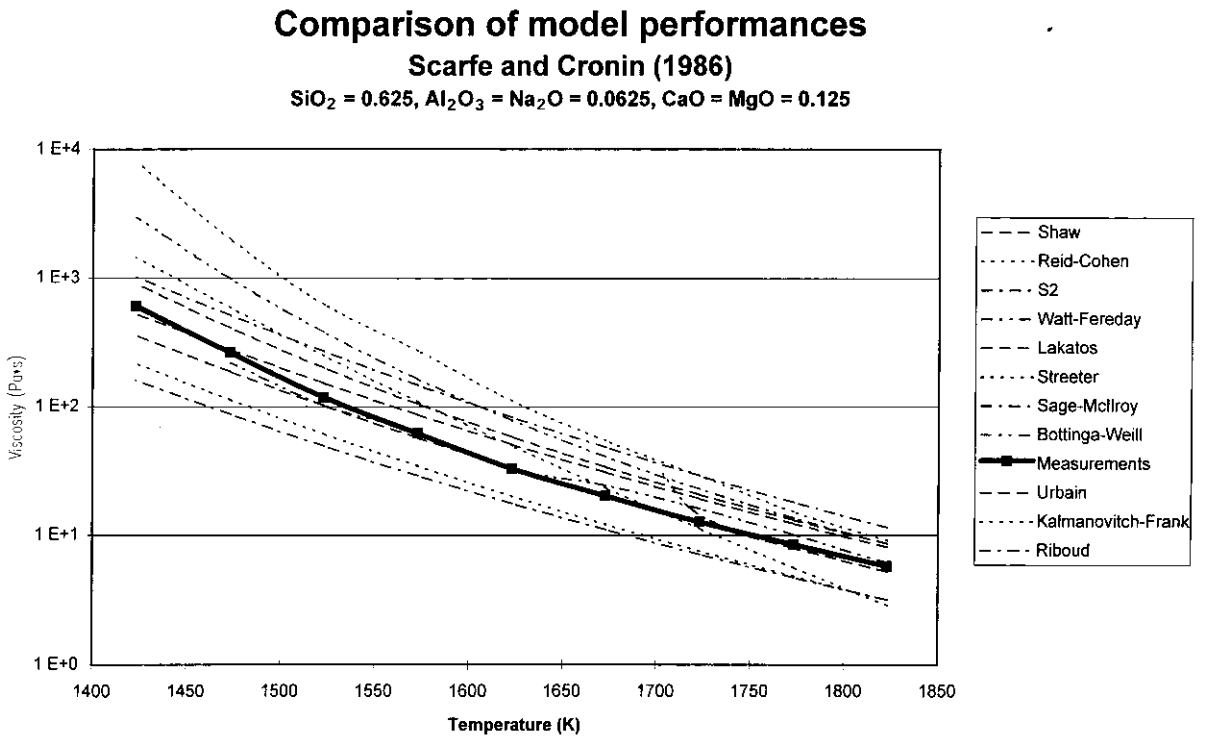

Fig. 44. Graphical comparison of experimental results obtained by Scarfe and Cronin (1986) [124] and predictions produced by mathematical models for the same chemical composition.

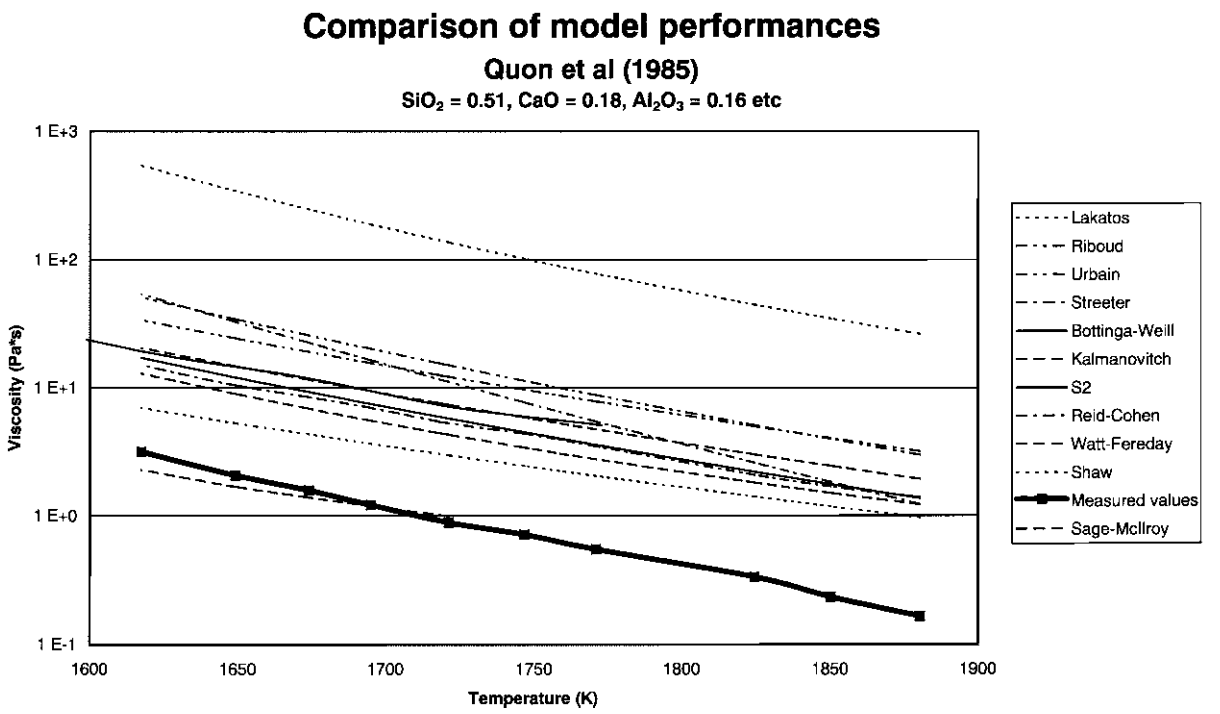

Fig. 45. Graphical comparison of experimental results obtained by Quon et al. (1985) [39] and predictions produced by mathematical models for the same chemical composition.

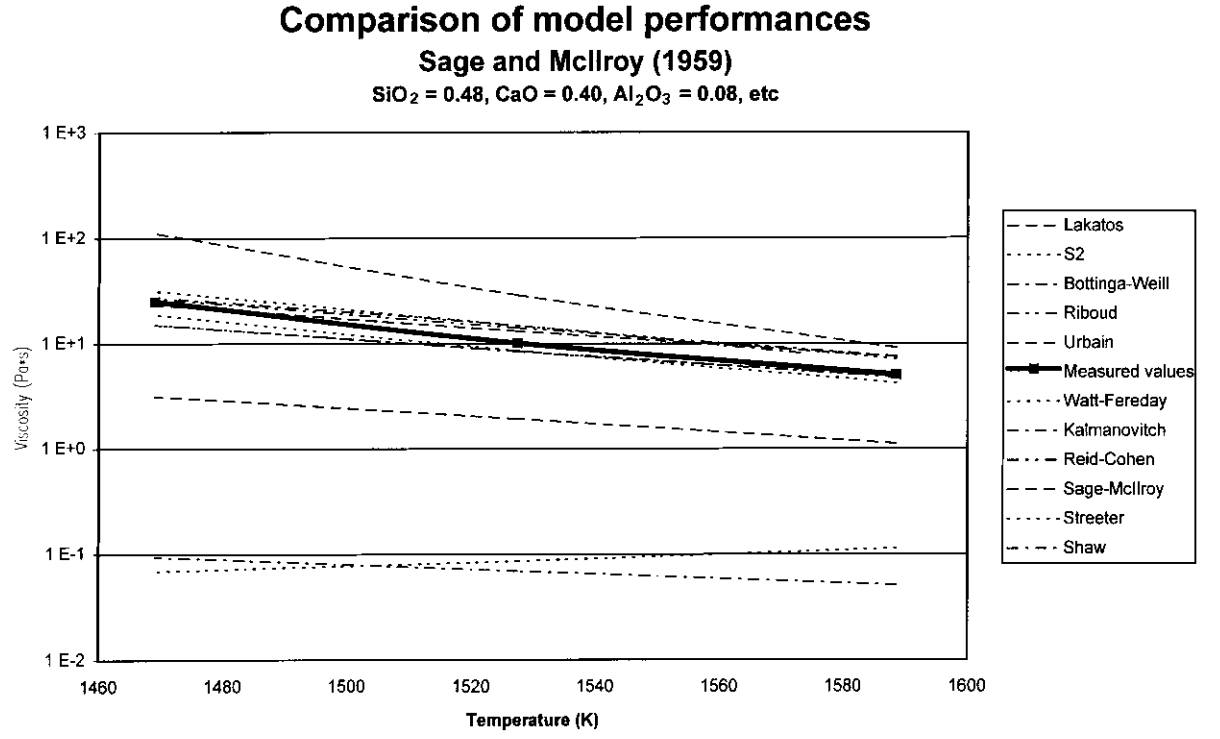

Fig. 46. Graphical comparison of experimental results obtained by Sage and McIlroy (1959) [104] and predictions produced by mathematical models for the same chemical composition.

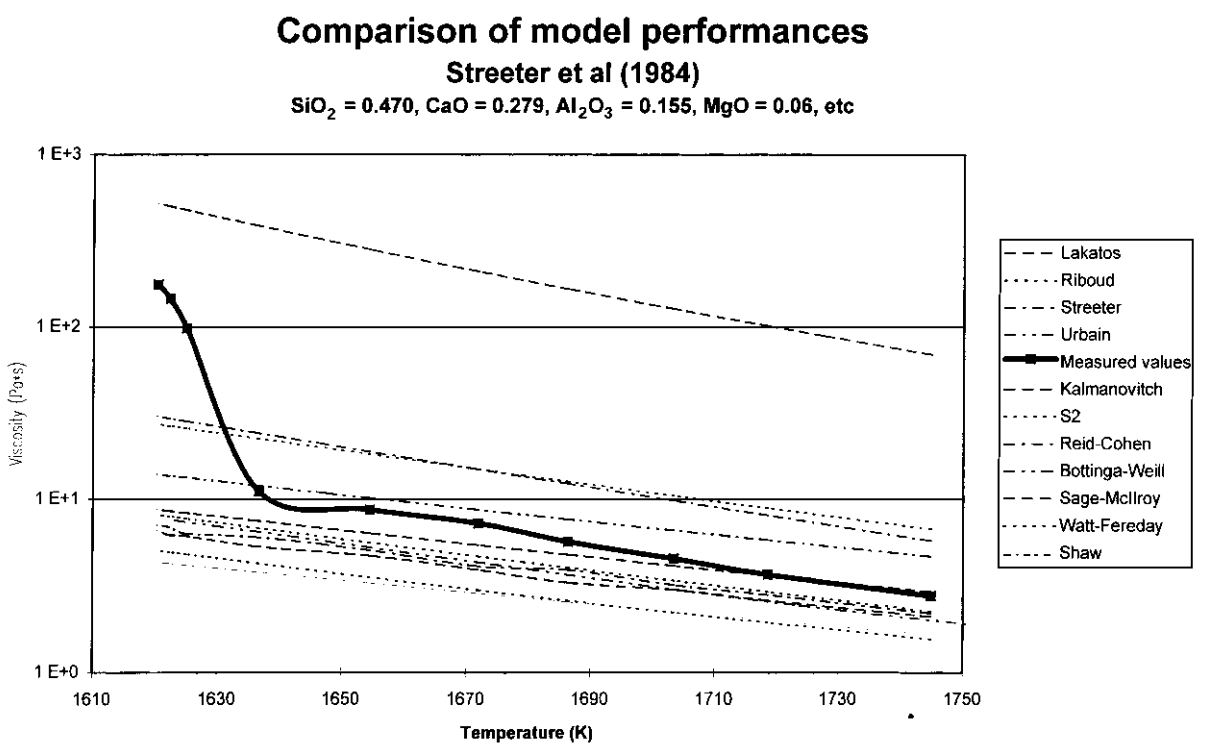

Fig. 47. Graphical comparison of experimental results obtained by Streeter et al. (1984) [27] and predictions produced by mathematical models for the same chemical composition.

Williams et al. measurements, Fig. 42. The Bottinga–Weill model gives the best prediction of the viscosity of both mixtures (within $\log\eta \pm 0.1$ (Fig. 41) and $\log\eta \pm 0.2$ (Fig. 42)). The Riboud model reproduces the measurements by Urbain et al. to within $\log \eta \pm 0.2$ (Fig. 41), and the Shaw model manages a reproduction of the Williams et al. measurements that is only slightly inferior to the Bottinga–Weill model, but still within $\log \eta \pm 0.2$ (Fig. 42). It should be mentioned that only the three lowest viscosities for the Williams et al. measurements have been included in the evaluation.

By visual examination, all models appear to reproduce the inclination of the viscosity–temperature graph, except the S^2 model, that clearly overestimates the temperature dependence for both mixtures and the Watt–Fereday model that underestimates the temperature-dependence in Fig. 41.

11.3.2. SiO_2–FeO_x–K_2O

The measurements performed by Dingwell (1989) [56] on a mixture in the SiO_2–FeO_x–K_2O system are presented in Fig. 43.

No model is capable of predicting the measured viscosities to within a level of uncertainty that comes anywhere near the one observed for the other measurements in this test; they all give results that are either too high or too low. The model that comes closest is the Riboud model that reproduces the experimental results to within $\log \eta \pm 0.7$.

All models that overestimate the viscosity also overestimate the inclination of the graph; and most models that underestimate the viscosity underestimate the inclination. Only the Reid–Cohen model shows a good estimate of the inclination.

11.3.3. SiO_2–Al_2O_3–CaO–MgO–Na_2O

The complete temperature range for the mixture used as an example in the preceding section is shown in Fig. 44.

In no point does the Bottinga–Weill model exceed the $\log \eta \pm 0.1$ interval, but viscosity at the lowest measurement temperature could not be calculated using this model. The Shaw model reproduces measurements to within $\log \eta \pm 0.2$. The Urbain model is the one that reproduces the measured viscosities best at the high-temperature end, but it deviates at the low-temperature end, leading to an overall $\log \eta \pm 0.3$. Only the three viscosities at the high-temperature end can be estimated using the Sage–McIlroy model without making use of extrapolation.

Visually, all the models seem to reproduce the slope of the viscosity–temperature relationship well at the high-temperature end. At the low-temperature end the result is more variable: some models (Reid–Cohen, Watt–Fereday) overestimate the influence of temperature on viscosity;

Table 21
Evaluation of model performances calculated as sums of squares

Model\graph	Urbain	Williams	Dingwell	Scarfe	Quon	Sage	Streeter	Average
Bottinga	0.01	0.02	0.50	0.02	0.34	0.03	0.07	0.14
Kalmanovitch	0.29	0.45	0.33	0.10	0.29	0.08	0.03	0.22
Lakatos				0.07	0.69	0.28	0.59	0.41
Reid		0.18	0.29	0.21	0.25	0.08	0.07	0.18
Riboud	0.03	0.34	0.18	0.12	0.38	0.08	0.14	0.18
S^2	0.29	0.61	0.36	0.11	0.26	0.08	0.06	0.25
Sage				0.17	0.04	0.44	0.09	0.19
Shaw	0.22	0.05	0.77	0.05	0.17	1.27	0.14	0.38
Streeter			0.39	0.09	0.33	1.23	0.13	0.44
Urbain	0.33	0.54	0.43	0.03	0.36	0.07	0.06	0.26
Watt	0.18	0.22	0.62	0.84	0.22	0.06	0.13	0.32

others seem to slightly underestimate it (Riboud, Kalmanovitch–Frank, Urbain, Shaw, S^2).

11.3.4. SiO_2–Al_2O_3–CaO (multi)

Fig. 45 (Quon et al., 1985) and Fig. 46 (Sage and McIlroy, 1959) show the results for two mixtures of the multi-component system with SiO_2, CaO and Al_2O_3 as the major components in the mentioned order. The mixtures were chosen because the graphs are located in extension of each other on a viscosity vs temperature plot, indicating similar rheological properties for the two mixtures in the molten state.

Nevertheless the model performances are quite distinct in the two cases. The results produced by Quon et al. (1985) (Fig. 45) are only reproduced properly by the Sage–McIlroy model (log $\eta \pm 0.2$). All other models overestimate the viscosity, although the general picture is a good reproduction of the temperature dependence.

The reproducibility of the Sage and McIlroy (1959) measurements is much higher (Fig. 46). Most models manage rather good estimates of viscosity (S^2: log $\eta \pm$ 0.1; Watt–Fereday, Bottinga–Weill (one point only), Urbain, Riboud: log $\eta \pm 0.2$), only the proper Sage–McIlroy model and the Shaw, the Lakatos and the Streeter models do not perform well.

Although the overall performance of the estimates is good, the temperature dependence is not always well-described. The Streeter model fails to reproduce the inclination of the temperature dependence in both cases; for the composition studied by Sage and McIlroy, the model even predicts a positive temperature–viscosity relationship. The Lakatos model overestimates the temperature dependence as compared to the measurements by Sage and McIlroy.

11.3.5. SiO_2–Al_2O_3–CaO–MgO (multi)

The last mixture that has been tested is the complex system studied by Streeter et al. (1984) [27] with four major components (SiO_2, CaO, Al_2O_3 and MgO), Fig. 47. The temperature of critical viscosity, T_{cv}, seems to be located somewhere around 1630 K; thus the model performances should only be evaluated on basis of the six high-temperature measurements where the rheological properties of the mixture are not influenced by the presence of crystals in the melt.

The model performances vary from log $\eta \pm 0.2$ (Kalmanovitch–Frank, S^2) to log $\eta \pm 0.5$ with the only model standing out as performing markedly poorer than the others being the Lakatos model with log $\eta \pm 0.1.6$.

As far as can be interpret by the somewhat wave-like shape of the log η–temperture graph, the temperature dependence appears to be well described by all the models.

A mathematical resumé of the above evaluations is given in Table 21. Here the sums of squares are used to obtain a number that can be related to the performance of the model. The sums are calculated as

$$SS = \frac{\sqrt{\sum_{i=1}^{N} (\log \eta_{\mathrm{est},i} - \log \eta_{\mathrm{meas},i})^2}}{N} \tag{59}$$

where N is the number of observations.

Whenever a model did not perform an estimate of the full temperature range, only the viscosities actually estimated are used. For the graph in Fig. 47 (Streeter et al., 1984), the four low-temperature measurements are excluded, as they show signs of crystallisation in the melt, causing a pronounced temperature dependence. The same could be the case for the lowest measurement temperature in Fig. 42 (Williams et al., 1983), thus only the three high-temperature measurements have been included in the evaluation.

The overall performances of the models are evaluated by taking the average deviation found for each measurement-series. This procedure leads to the following ranking of the models in order of decreasing ability to reproduce experimental results: Bottinga–Weill, Reid, Riboud, Sage,

Table 22
Models for the description of non-Newtonian behavior

Model	Definition
Power law or Ostwald–de Waele [3,11]	$\tau = c\cdot\dot{\gamma}^{d}$
Bingham plastic [5,11,12]	$\tau - \tau_0 = c\cdot\dot{\gamma}$
Herschel–Bulkley [5,11]	$\tau - \tau_0 = c\cdot\dot{\gamma}^{d}$
Casson [5,140,161,162]	$\tau^{1/2} - \tau_0^{1/2} = \eta_\infty^{1/2}\cdot\dot{\gamma}^{1/2}$
Meter or if $\eta_\infty = 0$: Ellis [11]	$\eta - \eta_\infty = (\eta_0 - \eta_\infty)/(1 + \lvert\tau/\tau_{1/2}\rvert\alpha^{-1})$
Williamson [141]	$\eta - \eta_\infty = \tau_{\text{“0”}}/(c + \dot{\gamma})$

Kalmanovitch–Frank, S^2, Urbain, Watt–Fereday, Shaw, Lakatos, Streeter.

On the basis of the conducted test, it is not possible to indicate a model that performs better than all the others for all compositions considered. Each model was developed on the basis of some experimental studies of melts of a given range of compositions, and this point should be carried in mind when selecting a model for the estimation of viscosities of a test-sample.

The value of a test as the one conducted above is not so much the resulting ranking of the models against each other on the basis of an overall performance as it is a hint on what model may be an adequate choice for the prediction of the viscosity of a given composition. Also it gives a clear view of the importance of ensuring that the sample is completely molten at the temperature in question.

11.4. Generalised models for non-Newtonian fluids

The term non-Newtonian fluid covers a wide range of fluids: time-independent flow types except those with a shear-rate independent viscosity as well as all time-dependent flow types. For silicate melts, non-Newtonian flow can be caused by two different mechanisms both related to phase separation:

- The appearance of crystals in the melt
- Separation of the melt into two or more immiscible liquids

The mathematical description of time-dependent flow types is very complex and not very well understood, so the following will concentrate only on time-independent non-Newtonian fluids.

Malkin (1995) proposed a classification scheme for non-Newtonian fluids relating the reasons for the non-linearity [139]

(i) weak, stationary, geometrical non-linearity
explained by large elastic deformations
(e.g. rubbers)
(ii) strong, kinetic, physical non-linearity
explained by changes in inherent structure of a material
caused by deformations (e.g. colloid suspensions)
(iii) rupture, phase, thermodynamic non-linearity
explained by phase or relaxation transitions induced by
deformation (e.g. deformation-induced crystallisation
in cured rubbers)

Table 22 contains a list of mathematical models for the description of time-independent, non-Newtonian fluids. Each of the models will be discussed below.

11.4.1. Power law

Widely used as a model for non-Newtonian fluids. It works for many solutions and can describe Newtonian ($d = 1$), shear-thinning ($d < 1$), and shear-thickening ($d > 1$) flow-types [8,11]. However, the law is empirical and must fail for both high and low shear rates [5].

11.4.2. Hershel–Buckley model

An extension of the power law where a yield stress term, τ_0, is included [11].

11.4.3. Bingham plastics

Exhibit a yield stress. That is, the shear stress τ must exceed a certain yield value, τ_0, before the fluid deforms and flows. Subsequently, the flow curve is linear [5].

11.4.4. Casson equation

Was originally intended for suspensions of pigments in oil media where the particles form chain-like groups, the dimensions of which control the viscosity of the suspension [140].

11.4.5. Meter model

Has the following four parameters: $\eta_0 = \eta(\dot{\gamma} = 0)$; $\eta_\infty = \eta(\dot{\gamma} = \infty)$; $\tau_{(1/2)} = \tau([\eta_0 + \eta_\infty]/2)$; $\alpha = 1/d$. For shear thickening fluids, η_∞ is usually set equal to zero [5].

11.4.6. Williamson model

Has proven useful in the description of paints. The constant c determines the curvature of the shear–stress curve and $\tau_{\text{“0”}}$ is a pseudo yield stress as shown in Fig. 48 [11,141].

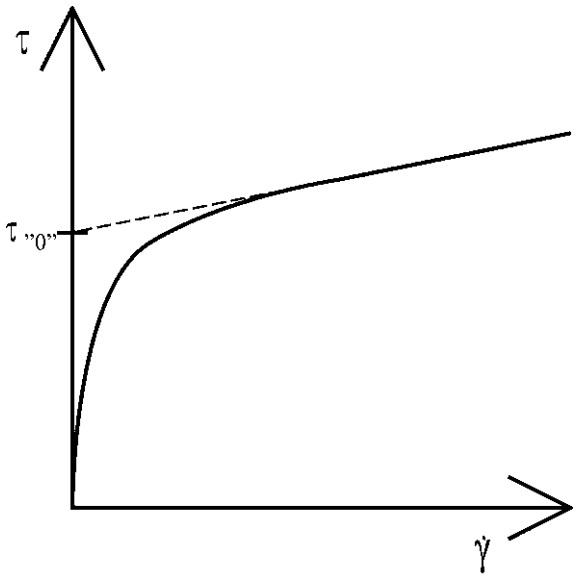

Fig. 48. Graphical definition of the pseudo yield stress, $\tau_{\text{"0"}}$, used in the Williamson model [141].

11.5. Liquid–solid mixtures

The modelling of the viscosity of condensed phases is a non-trivial task that involves the determination of crystal fraction and crystal shape and on the basis of these: viscosity calculation. A comprehensive model that allows for the simple determination of viscosity on the basis of composition, temperature and atmospheric data without any need for laboratory-tests would be an ideal — but unfortunately also unrealistic — solution to the needs of scientists and technicians. A more realistic scheme is the experimental determination of crystal fraction and shape supported by phase diagrams followed by a mathematical modelling of viscosity.

Considerable effort has been made to derive generally acceptable viscosity equations with few adjustable parameters. These equations are often used as a basis for system-specific models. The reason for non-Newtonian flow behaviour in silicate systems is usually the precipitation of solids, and special attention is given to liquid–solid mixtures in this section.

Empirical models for the prediction of silicate melt viscosities exclusively deal with completely molten samples, and the application of these models to partially solidified samples can be fraught with difficulties [93].

Weed et al. (1984) found that the non-Newtonian behaviour of molten silicate suspensions such as magmas and slags appears to arise from the increasing concentration of suspended crystals in the melt. In order to understand the flow behaviour of molten silicates containing suspended crystals, the rheological properties of the systems should be known as a function of volume fraction of the suspended crystalline phases at appropriate temperatures, oxygen fugacities and melt compositions [142].

When modelling fluid flow in silicate system, power law behaviour should be considered when the suspended crystal concentration exceeds approximately 20 vol% [142]. A generally recognised theory is the existence of four contributions to the stress required to maintain flow in a solution or dispersion

$$\text{Stress} = \text{Thermodynamic} + \text{Thermal(Brownian)} + \text{Hydrodynamic} + \text{Inertial} \quad (60)$$

It can be argued with some justification that the rheology will only be significantly different from that of the dispersion medium, i.e. the pure liquid, when the thermodynamic contribution to the stress parameter, i.e. particle interaction, dominates the others [143].

Numerous attempts have been made to model the viscosity of particle-containing suspensions and slurries, some very simple and others very complex. A few examples of models are mentioned here, but only six of them will be presented below.

- Dilute suspension
  - Convex body: Allen et al. (1996) [144]
  - Soft sphere: Buscall (1992) [143], Shaw (1969) [12]
  - Rigid sphere: Roscoe (1952) [12,145], Einstein (1906) [146]
  - Indefinite: Sherman (1968) [94], Vand (1948) [147]
- Dense slurry: Quemada (1982) [148], Sengun and Probstein (1989) [149]

Soft particles are useful in the modelling of colloidal suspensions. The particles interacting via soft repulsive potential have an effective, shear-dependent collision diameter. The viscosity of the suspension equals that of a suspension of hard particles with that diameter [143].

Usually, asymmetric particles are modelled as ellipsoids characterised by the ratio of the long axis to the short axis [146].

As is often the case, the simplest models are the oldest ones. The concept of some of the simpler models mentioned above will be presented in the following sections.

11.5.1. Einstein (1906)

At the start of the century, Einstein derived the following relation for the relative increase in the viscosity of an infinitely dilute solution of spherical particles

$$\frac{\eta_e - \eta}{\eta} = 2.5\theta \quad (61)$$

where η_e is the effective viscosity of the solution, η the pure

solvent viscosity and θ the volume fraction of particles [146,150–152].

The equation was derived in 1906 [150]. However, the results of this deduction were erroneous due to a calculation-error, which was corrected in 1911 [151].

For non-spherical particles, the equation can be written

$$\frac{\eta_e - \eta}{\eta} = \nu_i \cdot \theta \tag{62}$$

- Rigid spheres: $\nu_i = 2.5$ (Einstein) [151]
- Elongated particles: $\nu_i > 2.5$
- Soft or liquid spheres: $\nu_i < 2.5$ [153]

where ν_i is known as the intrinsic viscosity [146].

11.5.2. Roscoe (1952)

Based on the Einstein model, Roscoe derived a model relating the viscosity of a suspension of spheres of very diverse sizes to the concentration of spheres. He claimed the equation to be valid for all concentrations.

The suspension can be described as follows:

- A small volume-concentration, θ_1, of very small spheres of diameter d_1
- A small volume-concentration, θ_2, of small spheres of diameter $d_2 \gg d_1$
- Total concentration: $\theta = \sum \theta_i$

In some papers, this type of size-distributions is known as serial sizes.

On adding another set of spheres, all the other spheres are much smaller than the new set, and the original suspension can be regarded as a homogeneous liquid in its flow around new spheres. This assumption leads to Eq. (62) [12,145,152,154]

$$\eta_e = \eta(1 - \theta)^{-5/2} \tag{63}$$

The Einstein model can be derived from the Roscoe model through a Taylor series evolution about $\theta = 0$.

Based on work by Vand, where the importance of collisions between spheres and the amount of liquid effectively frozen between the spheres was pointed out, Roscoe calculated the effect of this freezing as resulting in an increase in the effective concentration by a factor 1.35. This lead him to propose a relationship of the following form for suspensions of high concentrations of uniform spheres [153,154]

$$\eta_e = \eta(1 - c \cdot \theta)^{-5/2} \tag{64}$$

where c is a constant:

- Suspensions of uniform spheres: $c = 1.35$ [154]
- Magmas with $\theta = 0.6 : c = 1.67$ [94]

Roscoe claims that the validity of Eq. (63) is not affected by the fact that aggregates are not strictly spherical.

The model is not in accordance with the Einstein model in the lower concentration-limit unless a value of $c = 1$ is used, and Roscoe states that the model is not valid for suspensions of spheres of nearly equal sizes (size ratio 1.17:1).

11.5.3. Vand (1948)

This model takes into account the hydrodynamic interaction between spheres and neglects Brownian motion [147]. As for the Einstein and Roscoe models, the effective viscosity of the system, η_e, is a function of the viscosity of the pure liquid, η, and the volume fraction solid phase, θ.

$$\eta_e = \eta \cdot (1 + c \cdot \theta + d \cdot \theta^2) \tag{65}$$

where c and d are constants. Vand states that the resulting mixture viscosity depends on the shapes of the solid assemblies (disks, spheres or rods).

For rigid, non-solvated spheres without mutual forces and without Brownian motion, the following constants were derived from theory: $c = 2.5$ and $d = 7.349$. [128,147,153]

11.5.4. Sherman (1968)

Sherman developed a viscosity model for emulsions based on a combination of theoretical considerations and laboratory experiments:

$$\ln\left(\frac{\eta_e}{\eta}\right) = \frac{\alpha \cdot D_m}{(\theta_{max}/\theta)^{1/3} - 1} - k \tag{66}$$

where η_e and η are the viscosities of the solution and the pure solvent, respectively, α and k the constants, D_m the mean particle diameter in microns, θ the concentration by volume of solids and θ_{max} the maximum concentration which can be attained by the solids [94,155].

Different values have been applied for the constants of Eq. (66):

- Sherman (1968): $\alpha = 0.036$, $k = 0.15$ [155]
- Murase (1985): $\alpha = 0.019$, $k = 0$
- Pinkerton and Stevenson (1992): $\alpha = 0.011$, $\theta_{max} = 1$ and $k = 0.15$ [94]

Sherman claims that the model is not valid for heterodisperse systems. He finds that presumably its form will vary with the degree of inhomogeneity of the system, and that α will decrease as the size distribution becomes broader.

The model was developed for emulsions with spherical solid-phase particles, and Sherman assumed that his suspensions behaved as Newtonian fluids. In addition, the maximum particle size used in Sherman's original experiments was only 5 μm. Owing to the exponential dependence of apparent viscosity on particle size, unrealistically high apparent viscosities will be calculated using this method for particle sizes >100 μm even at low crystal concentration [94].

11.5.5. Shaw (1969)

Based on his experimental studies of the cooling behaviour of tholeiitic (i.e. a basalt) crystal–liquid suspensions, Shaw (1969) affirmed that basaltic suspensions of crystals in silicate liquid can be considered to differ from the predictions of the Einstein–Roscoe model mainly for three reasons: during crystallisation

- temperature decreases;
- the silicate liquid changes towards a more viscous composition;
- the crystals are not absolutely rigid.

Instead he found the simple equation:

$$\log\left[\frac{\eta_e(T)}{\eta_0(T_0)}\right] \approx 0.1(T - T_0) \tag{67}$$

to describe the behaviour of the systems in focus in the Newtonian region. η_e is the effective viscosity of the suspension, T_0 an initial uniform temperature (the minimum melting temperature in $\theta = 1$) corresponding to an initial uniform viscosity, η_0 [12].

The data produced on other igneous rocks by Murase and McBirney (1973) support the Shaw relation [156].

11.5.6. Quemada (1982)

Non-Newtonian behaviour is observed in concentrated suspensions, $\theta > 0.3$, of colloidal particles, with a Newtonian plateau for viscosity at very low shear, $\eta_{e,0}$.

Taking θ_{max} as an effective maximum packing fraction, a hard sphere model for zero shear viscosity can be written [148,157]:

$$\eta_{e,0} = \eta \cdot \left(1 - \frac{\theta}{\theta_{max}}\right)^{-2} \tag{68}$$

Ponton et al. (1996) state an effective maximum packing fraction of: $\theta_{max} = 0.64$ [158].

12. Concluding remarks

The preceding sections of this paper have all been devoted to practical and theoretical considerations on viscosity estimation and prediction. Special attention has been paid to melts with Newtonian behaviour.

Many measurements have been performed by numerous researchers over the last century, but it is difficult to know how much confidence to place in them. Often the experimental conditions are not thoroughly presented or the experimental method employed is not completely trustworthy:

- over-simplified mathematical relations are used to correlate the measured properties with viscosity, leading to incorrect recordings;
- unsuitable measurement method is used where steady-state has not yet been reached (temperature, viscosity) when measurement is recorded;
- reported composition does not correspond to the composition of the melt actually analysed;
- instrumental problems
  - exactness of dimensions,
  - accuracy of temperature measurements,
  - choice of sensor material (see below);

To obtain exact viscosity measurements, it is crucial to avoid contamination of the melt by the sensor material, i.e. the material that is in direct contact with the melt. When graphite and alumina are used, contamination in the range of several weight-percents can been observed. Hurley reports that contamination in the range of 10–15% alumina has been observed when analysing basic slags with a rotational viscometer [28]. Better materials are as follows:

- *Platinum–rhodium.* A good — though expensive — material that can withstand even an oxidising atmosphere, but it should not be used when iron is present in the melt and it becomes increasingly soft at higher temperatures.
- *Tungsten.* A very resistant material though extremely difficult to shape.
- *Molybdenum.* Easy to mould with ordinary tools. Causes contamination on a parts-per-million scale in reducing and neutral atmospheres; however, as for platinum, the softening of molybdenum at higher temperatures can present a practical problem.

The most accurate method for viscosity measurements at temperatures in excess of 1000 K today is the rotational method, where a liquid is kept between two cylinders, one of which is brought to rotate at a given speed. The viscosity is then related to the torque used to maintain the rotational speed of the cylinder. The rotational viscometer is a primary instrument, i.e. it can be used for absolute viscosity measurements, but for normal use, the apparatus is calibrated with a standard solution.

The major properties affecting high-temperature viscosity measurements are:

- atmosphere;
- temperature;
- sample composition.

The choice of experimental atmosphere influences the observed viscosity. In particular iron-containing melts are very sensitive to the surrounding atmosphere. Iron will be oxidised from its ferrous, Fe^{2+}, to its ferric, Fe^{3+}, state when the atmosphere is changed from reducing to oxidising conditions; the result is an elevation of viscosity. In one experiment a doubling of viscosity was observed at a given temperature.

If either temperature or composition of a given sample is changed, the effect on viscosity can be drastic; therefore it is crucial to ensure a precise and accurate temperature measurement during testing.

The composition of a sample can be subject to changes during heat-up due to the selective evaporation of some species; thus the most correct composition will be the one observed after finishing the test, and the measurements should be conducted from high temperatures downwards.

When a set of experimental data is published, the following information should always be provided for completeness.

1. setup description incl accuracy and precision data and information on how this was obtained;
2. reproducibility data;
3. exhaustive description of test procedures incl the pretreatment of the test material;
4. test atmosphere;
5. sensor material and dimensions;
6. melt composition as measured after the completion of the test-run with belonging information on how it was obtained;
7. iron oxidation state;
8. tabulated measurement data.

The compositional effects on silicate melt viscosity are not understood in detail, although it appears that the network theory describes the general picture quite well with its grouping of the individual oxides according to their effect on the silica network. The effect of some oxides appears to be quite simple; they act as either network formers or modifiers, while others seem to play less clear-cut roles.

Silicon dioxide is the dominant network former, and the addition of other oxides to SiO_2 will always lead to a decrease in viscosity, all other things being equal.

The alkali oxides can all be classified as network formers whereas the alkaline earth oxides play more complex structural roles depending on the overall composition of the melt, although predominantly as network modifiers.

Aluminum oxide is a network former if charge stabilisation is available, otherwise it acts as a network modifier.

The role played by ferric iron oxide, Fe_2O_3, resembles that of aluminum; whereas ferrous iron oxide, FeO, is of a network-modifying nature.

Titanium oxide plays a not very-well understood structural role in silicate melts, but it seems to behave amphoterically dependent on the composition of the melt.

Many attempts have been made to model the dependence of the viscosity of a given melt on temperature and composition. Eleven models have been outlined together with information on the compositional ranges on which they were based. As a rule, a model should not be trusted outside the range of compositions for which it was elaborated.

In order to conduct a trustworthy test on model performance, it is compulsory to base it on well-documented measurement data. This requirement could not be met in this paper, since the documentation level of much of the available data is insufficient. Some composition-intervals have been studied by various scientists, and comparison of data can give hints on measurement accuracy in these cases; but in other cases, only one scientist has studied a composition regime, and in these cases it is often impossible to know whether or not to trust the given data.

Nevertheless, a minor test on model performance has been carried out for silicate melts in the concentration range $x_{SiO2} \in [0.20; 0.75]$. The eleven models were tested at temperatures in the range 1550–1900 K with measured viscosities in the range 0.01–10,000 Pa s with limited success. The models are capable of predicting viscosity only within several orders of magnitude of the reported measurements.

A ranking of the models based on their overall performances is as follows (best model first): Bottinga–Weill (1972), Reid (1944), Riboud (1981), Sage (1959), Kalmanovitch–Frank (1988) S^2 (1963) Urbain (1981), Watt–Fereday (1963), Shaw (1972), Lakatos (1972), Streeter (1984). As apparent from the above, this ranking is by no means valid as a general tool. It should not be used to choose one model over another. It is just the result of a testing on six different viscosity vs temperature measurement-runs on mixtures of varying compositions. For some compositions all the models performed well and for others they were all far off. No attempt was made to maintain testing within the compositional ranges for which the models were intended.

The valid way to select a model is to choose one that performs well on mixtures of similar compositions as the one in question, preferably one that was based on a compositional interval that includes the mixture in question.

All the models are based on the network theory, but they depend largely on experimental observations of varying reliability, and it seems that major improvements are not obtainable as long as this path is followed. Instead a more fundamental understanding of the compositional effects on viscosity is essential to permit a more exact mathematical modelling scheme. But a thorough study should be performed to check the consistency of all experimental data to be employed in any theoretical work. It can be observed from the plots of viscosity vs temperature in Appendix C that for even very simple systems, the data reported by different researchers are not always in harmony with one another.

All existing mathematical models for the prediction of the viscosity of silicates are intended for use with completely molten samples. If a given mixture is not completely molten it will most likely not exhibit Newtonian behaviour, and viscosity determination will have to depend on experimental procedures, either fully or partially. If the crystal fraction and shape are known, simple models exist that can give an indication of the overall viscosity of the mixture.

Appendix A

The most important information concerning the experimental conditions used to produce the viscosity data reported in each paper is pointed out in the table of this appendix.

The individual works are ordered according to the compositions of the chemical mixtures studied. The table is initiated with two studies on pure SiO_2 followed by binary, ternary, quartenary and quinary mixtures (presented in reverse chronological order and secondly in alphabetical order of authors). The components are organised as follows: SiO_2, Al_2O_3, FeO_x, CaO, MgO, Na_2O, K_2O, Li_2O, MnO, TiO_2, B_2O_3, XCl_x.

All mixtures containing more than six components are categorised as multi-component mixtures and organised separately according to the scheme described above.

Some studies comprise mixtures composed of different chemical components. The conditions for these studies are presented under each chemical composition in the table, i.e. the study conducted by Hofmaier (1968) contains measurements on both pure SiO_2 and on multi-mixtures with SiO_2, Al_2O_3 and CaO as the major components; thus the experimental conditions are outlined in both categories in the table.

The table contains the following information:

i. oxides and chlorides present in the test material;
ii. publication year;
iii. authors;
iv. types of viscometers used applied in study;
v. experimental accuracy as reported by the authors (no evaluation has been performed on the credibility of the values reported);
vi. sensor material, i.e. material used on parts that are in direct contact with the test material (Example: bob and spindle in a rotational viscometer);
vii. atmosphere in contact with the test material;
viii. significant comments made by the author or comments relating to the data treatment performed to produce the tabulated values of Appendix B;
ix. number of table where the data is presented in Appendix B (Table A1).

Table A1

Mixture	Year	Author	Viscometer type								Accuracy (as reported by authors)	Sensor material	Atmosphere	Comments	Table
			Rotational	Falling body	Electric vibration	Rod elongation	Rod bending	Isothermal deformation	Squeeze film	Penetrating rod					
SiO_2		Urbain et al.	X					X			η: ±20% (Rot)/10% (Iso), $T > 1873$ K: $T \pm 4.5$ K, $T < 1875$ K: $T \pm 10$ K, Composition: ±1 g/g	Mo/W	Vacuum or Ar	Rotational: η: $<10^4$ Pa s, Isothermal deform. η: $>10^7$ Pa s	B28
	1968	Hofmaier	X									Mo/W	Ar	Time-independent flow	B46
SiO_2–Al_2O_3	1982	Urbain et al.	X					X			η: ±20% (Rot)/10% (Iso), $T > 1873$ K: $T \pm 4.5$ K, $T < 1875$ K: $T \pm 10$ K, Composition: ±1 g/g	Mo/W	Vacuum or Ar	Rotational: η: $<10^4$ Pa s, Isothermal deform. η: $>10^7$ Pa s	B28
SiO_2–FeO_x	1983	Williams et al.	X									Fe		Some measurements: Calcia-stabilised Zr crucibles	B25
	1982	Urbain et al.	X					X			η: ±20% (Rot)/10% (Iso), $T > 1873$ K: $T \pm 4.5$ K, $T < 1875$ K: $T \pm 10$ K, Composition: ±1 g/g	Mo/W	H_2/CO_2/Ar	Rotational: η: $<10^4$ Pa s, Isothermal deform. η: $>10^7$ Pa s	B28
	1978	Bodnár et al.	X								η: ±12%, T: ±10 K	Fe crucible, Pt bob	N_2	Whenever necessary, an average FeO_x molar weight used, R-values in paper assumed erroneous	B35
	1978	Shiraishi et al.	X								T: ±2% (K), η: ±3%, Comp: ±4 g/g, Err_{tot}: [ ]%, Scatter: 5%	Fe	Ar-atmosphere deoxidised by Ca-metal	Iron oxide in equilibrium with Fe(s)	B36
SiO_2–CaO	1985	Danek et al.	X								T: ±5 K	Pt crucible, $Pt_{60}Rh_{40}$ bob			B15
	1982	Urbain et al.	X					X			η: ±20% (Rot)/10% (Iso), $T > 1873$ K: $T \pm 4.5$ K, $T < 1875$ K: $T \pm 10$ K, Composition: ±1 g/g	Mo/W	Vacuum or Ar	Rotational: η: $<10^4$ Pa s, Isothermal deform. η: $>10^7$ Pa s	B28
	1977	Yakushev et al.			X							Mo			B37
	1954	Machin and Yee	X									Pt			B50
	1948	Machin and Yee	X									Pt		Some data included in previous paper	B53
SiO_2–MgO	1982	Urbain et al.	X					X			η: ±20% (Rot)/10% (Iso), $T > 1873$ K: $T \pm 4.5$ K, $T < 1875$ K: $T \pm 10$ K, Composition: ±1 g/g	Mo/W	Vacuum or Ar	Rotational: η: $<10^4$ Pa s, Isothermal deform. η: $>10^7$ Pa s	B28
	1955	Bockris et al.	X									Mo			B49
SiO_2–Na_2O	1996	Liska et al.	X	X				X			η: ±Pa s			Glass PS1: $T = 897$ K NOT 917 K	B4
	1981	El-Badry et al.				X					T: ±0.01 K				B30
	1981	Klein et al.					X						Air, N_2/H_2 (95/5) (with or without C in batch)	$T_{max} = 923$ K (crystallisation)	B31
	1971	Shvaiko-Shvaikovskaya et al.		X							η: ±0.1 Pa s, Comp. mean deviation: ±0.15 mol%	Pt			B40
	1970	Taylor and Rindone					X								B41
	1969	Nemilov													B45
	1967	Meiling and Uhlmann	X						X			PtRh (Rotational)	Air	Rotational: $\eta < 10^6$ Pa s, Squeeze film $\eta > 10^5$ Pa s	B47
	1955	Bockris et al.	X									Mo			B49
	1952	Shartsis et al.		X								Pt			B52

(*continued on next page*)

Table A1 (*continued*)

Mixture	Year	Author	Viscometer type								Accuracy (as reported by authors)	Sensor material	Atmosphere	Comments	Table
			Rotational	Falling body	Electric vibration	Rod elongation	Rod bending	Isothermal deformation	Squeeze film	Penetrating rod					
	1939	Lillie	X								Comp: ±0.1 g/g, T: ±4 K, η: ±0.25 Pa s	PtRh	Air		B55
	1924	Washburn et al.	X								Accuracy: 20% (<100 Pa s) or 10% (>100 Pa s), Precision: 5%	Porcelain		Mostly only content of major components reported. Crystallisation possible at low-end temp. Stott (1925) finds observations useless, possibly due to non-homogeneities in glass	B58
SiO_2–K_2O	1981	El-Badry et al.				X					T: ±0.01 K				B30
	1969	Nemilov													B45
	1955	Bockris et al.	X									Mo			B49
	1952	Shartsis et al.		X								Pt			B52
SiO_2–Li_2O	1981	El-Badry et al.				X					T: ±0.01 K				B30
	1969	Nemilov													B45
	1955	Bockris et al.	X									Mo			B49
	1952	Shartsis et al.		X								Pt			B52
SiO_2–MnO	1982	Urbain et al.	X					X			η: ±20% (Rot)/10% (Iso), $T > 1873$ K: T ± 4.5 K, $T < 1875$ K: T ± 10 K, Composition: ±1 g/g	Mo/W	Vacuum or Ar	Rotational: η: $<10^4$ Pa s, Isothermal deform. η: $>10^7$ Pa s	B28
	1979	Segers et al.	X								η: ±4% (Pa s), T: ±6 K	$Pt_{80}Rh_{20}$	Ar		B34
SiO_2–Al_2O_3–CaO	1992	Tanigushi		X		X					log η: ±0.1 (body)/0.05 (rod)	Pt (falling body)		Falling body: $\eta < 10^4$ Pa s, Rod elongation: $\eta > 10^7$ Pa s	B8
	1984	Seki and Oeters	X									$Pt_{82}Rh_{18}$	Air or CO_2		B21
	1983	Scarfe et al.	X								Accuracy: 5%, Precision: 1%, T: ±1 K	Pt crucible, $Pt_{90}Rh_{10}$ cylinder	Air	Measurements during cooling, but heating gave same results	B24
	1982	Urbain et al.	X					X			η: ±20% (Rot)/10% (Iso), $T > 1873$ K: T ± 4.5 K, $T < 1875$ K: T ± 10 K, Composition: ±1 g/g	Mo/W	Vacuum or Ar	Rotational: η: $<10^4$ Pa s, Isothermal deform. η: $>10^7$ Pa s	B28
	1972	Skryabin and Novokhaskii			X						η: ±5% (P)	ZrO_2 crucible, Pt shaft	Ar, CO_2		B39
	1969	Boow								X		SiO_2		Grouped components: Average molar weight used	B42
	1969	Kato and Minowa		X							η: ±15% (Pa s)	Pt	Air	Large chlorine loss	B43
	1969	Kovalenko et al.			X							H_2O: Al_2O_3, All others: Mo	Air, H_2O, H_2, N_2, NH_3, a producer gas		B44
	1948	Machin and Yee	X									Pt		Some data included in previous paper	B53
	1945	Machin and Hanna	X									Pt			B54
SiO_2–Al_2O_3–MgO	1982	Urbain et al.	X					X			η: ±20% (Rot)/10% (Iso), $T > 1873$ K: T ± 4.5 K, $T < 1875$ K: T ± 10 K, Composition: ±1 g/g	Mo/W	Vacuum or Ar	Rotational: η: $<10^4$ Pa s, Isothermal deform. η: $>10^7$ Pa s	B28
	1954	Machin and Yee	X									Pt			B50

Table A1 (*continued*)

Mixture	Year	Author	Viscometer type								Accuracy (as reported by authors)	Sensor material	Atmosphere	Comments	Table
			Rotational	Falling body	Electric vibration	Rod elongation	Rod bending	Isothermal deformation	Squeeze film	Penetrating rod					
SiO_2–Al_2O_3–Na_2O	1993	Stein and Spera	X								η: ±1 Pa s, T: ±3 K				B5
	1986	Scarfe and Cronin	X								Accuracy: 5%, Precision: 1%, T: ±1 K	$Pt_{90}Rh_{10}$			B13
	1983	Klein et al.					X						Air, N_2/H_2 (95/5) (+ or − C in batch)	Fe^{3+}/Fe by titration, Air: Assumption Fe^{3+}/Fe constant for constant Al + Fe	B23
	1982	Urbain et al.	X					X			η: ±20% (Rot)/10% (Iso), $T > 1873$ K: $T \pm 4.5$ K, $T < 1875$ K: $T \pm 10$ K, Composition: ±1 g/g	Mo/W	Vacuum or Ar	Rotational: η: $<10^4$ Pa s, Isothermal deform. η: $>10^7$ Pa s	B28
	1970	Taylor and Rindone					X								B41
	1967	Meiling and Uhlmann	X						X			PtRh (rotational)	Air	Rotational: $\eta < 10^6$ Pa s, Squeeze film $\eta > 10^5$ Pa s	B47
SiO_2–Al_2O_3–K_2O	1982	Urbain et al.	X					X			η: ±20% (Rot)/10% (Iso), $T > 1873$ K: $T \pm 4.5$ K, $T < 1875$ K: $T \pm 10$ K, Composition: ±1 g/g	Mo/W	Vacuum or Ar	Rotational: η: $<10^4$ Pa s, Isothermal deform. η: $>10^7$ Pa s	B28
SiO_2–Al_2O_3–MnO	1982	Urbain et al.	X					X			η: ±20% (Rot)/10% (Iso), $T > 1873$ K: $T \pm 4.5$ K, $T < 1875$ K: $T \pm 10$ K, Composition: ±1 g/g	Mo/W	Vacuum or Ar	Rotational: η: $<10^4$ Pa s, Isothermal deform. η: $>10^7$ Pa s	B28
SiO_2–FeO_x–CaO	1985	Danek et al.	X								T: ±5 K	Pt crucible, $Pt_{60}Rh_{40}$ bob			B15
	1984	Seki and Oeter	X									$Pt_{82}Rh_{18}$	Air or CO_2		B21
	1982	Urbain et al.	X					X			η: ±20% (Rot)/10% (Iso), $T > 1873$ K: $T \pm 4.5$ K, $T < 1875$ K: $T \pm 10$ K, Composition: ±1 g/g	Mo/W	H_2/CO_2/Ar	Rotational: η: $<10^4$ Pa s, Isothermal deform. η: $>10^7$ Pa s	B28
	1985	Mysen et al.	X								Accuracy: 5% (Pa s), Precision: 1% (Pa s)	Pt crucible, $Pt_{90}Rh_{10}$ cylinder	Air	Fe^{3+}/Fe by Mössbauer	B16
	1983	Williams et al.	X									Fe		Some measurements: Calcia-stabilised Zr crucibles	B25
	1978	Bodnár et al.	X								η: ±12%, T: ±10 K	Fe crucible, Pt bob	N_2	Whenever necessary, an average FeO_x molar weight used, R-values in paper assumed erroneous	B35
SiO_2–FeO_x–MgO	1989	Dingwell	X								η: ±5% (Pa s)	$Pt_{80}Rh_{20}$	Air		B10
	1983	Williams et al.	X									Fe		Some measurements: Calcia-stabilised Zr crucibles	B25
SiO_2–FeO_x–Na_2O	1988	Dingwell and Virgo	X								T: ±2 K, log η: ±6%	$Pt_{80}Rh_{20}$		Fe^{3+}/Fe by Mössbauer	B11
	1985	Mysen et al.	X								Accuracy: 5% (Pa s), Precision: 1% (Pa s)	Pt crucible, $Pt_{90}Rh_{10}$ cylinder	Air	Fe^{3+}/Fe by Mössbauer	B16
	1983	Klein et al.					X						Air, N_2/H_2 (95/5) (+ or − C in batch)	Fe^{3+}/Fe by titration, Air: Assumption Fe^{3+}/Fe constant for constant Al + Fe	B23
	1981	Klein et al.					X						Air, N_2/H_2 (95/5) (with or without C in batch)	$T_{max} = 923$ K (crystallisation)	B31

(*continued on next page*)

Table A1 (*continued*)

Mixture	Year	Author	Viscometer type								Accuracy (as reported by authors)	Sensor material	Atmosphere	Comments	Table
			Rotational	Falling body	Electric vibration	Rod elongation	Rod bending	Isothermal deformation	Squeeze film	Penetrating rod					
SiO_2–FeO_x–K_2O	1989	Dingwell	X								η: ±5% (Pa s)	$Pt_{80}Rh_{20}$	Air		B10
SiO_2–CaO–MgO	1992	Tanigushi		X		X					log η: ±0.1 (body)/0.05 (rod)	Pt (falling body)		Falling body: $\eta < 10^4$ Pa s, Rod elongation: $\eta > 10^7$ Pa s	B8
	1983	Scarfe et al.	X								Accuracy: 5%, Precision: 1%, T: ±1 K	Pt crucible, $Pt_{90}Rh_{10}$ cylinder	Air	Measurements during cooling, but heating gave same results	B24
	1982	Urbain et al.	X					X			η: ±20% (Rot)/10% (Iso), $T > 1873$ K: T ± 4.5 K, $T < 1875$ K: T ± 10 K, Composition: ±1 g/g	Mo/W	$H_2/CO_2/Ar$	Rotational: η: $<10^4$ Pa s, Isothermal deform. η: $>10^7$ Pa s	B28
	1954	Machin and Yee	X									Pt			B50
	1952	Machin et al.	X									Pt		All data with no MgO in previous paper	B51
SiO_2–CaO–Na_2O	1981	El-Badry et al.				X					T: ±0.01 K				B30
	1924	Washburn et al.	X								Accuracy: 20% (<100 Pa s)/10% (>100 Pa s), Precision: 5%	Porcelain		Mostly only content of major components reported. Crystallisation possible at low-end temp. Stott (1925) finds observations useless, possibly due to non-homogeneities in glass	B58
SiO_2–CaO–MnO	1979	Segers et al.	X								η: ±4% (Pa s), T: ±6 K	$Pt_{80}Rh_{20}$	Ar		B34
SiO_2–CaO–TiO_2	1992	Dingwell	X								η: ±5% (Pa s)	$Pt_{80}Rh_{20}$	Air	Composition analysed post-test	B7
SiO_2–MgO–Na_2O	1981	El-Badry et al.				X					T: ±0.01 K				B30
SiO_2–Na_2O–K_2O	1969	Nemilov													B45
SiO_2–Na_2O–TiO_2	1996	Liska et al.	X	X				X			η: ±1 Pa s				B4
	1992	Dingwell	X								η: ±5% (Pa s)	$Pt_{80}Rh_{20}$	Air	Composition analysed post-test	B7
SiO_2–K_2O–Li_2O	1969	Nemilov												Glass #31 ($X_{SiO_2} = 0.7$; $X_{K_2O} = 0.3$): Three lowest T: +100 K	B45
SiO_2–K_2O–TiO_2	1992	Dingwell	X								η: ±5% (Pa s)	$Pt_{80}Rh_{20}$	Air	Composition analysed post-test	B7
SiO_2–Al_2O_3–FeO_x–CaO	1969	Kato and Minowa		X							η: ±15% (Pa s)	Pt	Air	Large chlorine loss	B43
SiO_2–Al_2O_3–FeO_x–Na_2O	1983	Klein et al.					X						N_2/H_2 (95/5) (some with C in the melt), Air	Fe^{3+}/Fe by titration, Air: Assumption Fe^{3+}/Fe constant for constant Al + Fe	B23

Table A1 (*continued*)

Mixture	Year	Author	Viscometer type								Accuracy (as reported by authors)	Sensor material	Atmosphere	Comments	Table
			Rotational	Falling body	Electric vibration	Rod elongation	Rod bending	Isothermal deformation	Squeeze film	Penetrating rod					
SiO_2–Al_2O_3–CaO–MgO	1992	Taniguchi		X		X					log η: ±0.1 (body)/0.05 (rod)	Pt (falling body)		Falling body: $\eta < 10^4$ Pa s, Rod elongation: $\eta > 10^7$ Pa s	B8
	1983	Scarfe et al.	X								Accuracy: 5%, Precision: 1%, T: ±1 K	Pt crucible, $Pt_{90}Rh10$ cylinder	Air	Measurements during cooling, but heating gave same results	B24
	1977	Yakushev et al.			X							Mo			B37
	1969	Kato and Minowa		X							η: ±15% (Pa s)	Pt	Air	Large chlorine loss	B43
	1954	Machin and Yee	X									Pt			B50
	1952	Machin et al.	X									Pt		All data with no MgO in previous paper	B51
	1945	Machin and Hanna	X									Pt			B54
SiO_2–Al_2O_3–CaO–Na_2O	1981	Cranmer and Uhlmann	X				X				T: ±1 K				B29
SiO_2–Al_2O_3–CaO–MnO	1969	Kato and Minowa		X							η: ±15% (Pa s)	Pt	Air	Large chlorine loss	B43
SiO_2–Al_2O_3–CaO–TiO_2	1969	Kato and Minowa		X							η: ±15% (Pa s)	Pt	Air	Large chlorine loss	B43
SiO_2–Al_2O_3–CaO–XCl_2, X = {Ca, Mg, Na}	1969	Kato and Minowa		X							η: ±15% (Pa s)	Pt	Air	Large chlorine loss	B43
SiO_2–Al_2O_3–Na_2O–K_2O	1982	Urbain et al.	X					X			η: ±20% (Rot)/10% (Iso), $T > 1873$ K: T ± 4.5 K, $T < 1875$ K: T ± 10 K, Composition: ±1 g/g	Mo/W	Vacuum or Ar	Rotational: η: $<10^4$ Pa s, Isothermal deform. η: $>10^7$ Pa s	B28
	1924	Washburn and Shelton	X								Accuracy: 20% (<100 Pa s) or 10% (>100 Pa s), Precision: 5%	Porcelain		Mostly only content of major components reported. Crystallisation possible at low-end temp. Stott (1925) finds observations useless, possibly due to non-homogeneities in glass	B58
SiO_2–FeO_x–CaO–MgO	1983	Williams et al.	X									Fe		Some measurements: Calcia-stabilised Zr crucibles	B25
	1978	Bodnár et al.	X								η: ±12%, T: ±10 K	Fe crucible, Pt bob	N_2	Whenever necessary, an average FeO_x molar weight used, R-values in paper assumed erroneous	B35
SiO_2–Al_2O_3–FeO_x–CaO–MgO	1978	Bodnár et al.	X								η: ±12%, T: ±10 K	Fe crucible, Pt bob	N_2	Whenever necessary, an average FeO_x molar weight used, R-values in paper assumed erroneous	B35
SiO_2–Al_2O_3–CaO–MgO–Na_2O	1986	Scarfe and Cronin	X								Accuracy: 5%, Precision: 1%, T: ±1 K	$Pt_{90}Rh_{10}$			B13
SiO_2–Al_2O_3–CaO–MgO–Na_2O–K_2O	1972	Lakatos et al.	X				X				T: ±5 K	$Pt_{90}Rh_{10}$ crucible (rotational)		Rotational: $\eta < 10^5$ Pa s, Rod bending: $\eta > 10^7$ Pa s	B38

(*continued on next page*)

Table A1 (*continued*)

Mixture	Year	Author	Viscometer type							Accuracy (as reported by authors)	Sensor material	Atmosphere	Comments	Table
			Rotational	Falling body	Electric vibration	Rod elongation	Rod bending	Isothermal deformation	Squeeze film	Penetrating rod				
Multi-component mixtures (organised according to major components ($X_i > 0.05$))													The major components are not always the same for all compositions in a study, but then the dominant components are used, or the work is cited in several places.	
SiO_2–Al_2O_3	1997	Goto et al.		X							Pt			B1
	1987	Jones and Lindsey	X										At melting: S outgassed	B12
	1984	Hochella and Brown	X											B19
	1984	Quon et al.	X								Mo			B20
	1980	Piwinskii and Weed	X							T: ±2 K				B32
	1982	Shiraishi and Meister							X	T: ±1 K	Mullite ($Al_6Si_2O_{13}$)			B27
	1969	Boow								X	SiO_2		Grouped components: Average molar weight used	B42
SiO_2–CaO	1979	Krauss			X						Mo	Neutral or red		B33
	1924	Washburn and Shelton	X							Accuracy: 20% (<100 Pa s) or 10% (>100 Pa s), Precision: 5%	Porcelain		Mostly only content of major components reported. Crystallisation possible at low-end temp. Stott (1925) finds observations useless, possibly due to non-homogeneities in glass	B58
SiO_2–Na_2O	1924	English	X								Porcelain crucible and rod, IrPt bob	Air	Calibrated at room temperature, Grouped components: Average molar weight used	B57
	1924	Washburn and Shelton	X							Accuracy: 20% (<100 Pa s) or 10% (>100 Pa s), Precision: 5%	Porcelain		Mostly only content of major components reported. Crystallisation possible at low-end temp. Stott (1925) finds observations useless, possibly due to non-homogeneities in glass	B58
SiO_2–Al_2O_3–FeO_x	1969	Boow								X	SiO_2		Grouped components: Average molar weight used	B42
	1959	Sage and McIlroy	X								PtRh crucible	H_2/N_2 (varying conc to control Fe oxidation)	Arithmetic mean of Fe oxidation level used when interval reported	B48
SiO_2–Al_2O_3–CaO	1996	Hurley et al.	X								Al_2O_3 crucible, Bob: $Pt_{90}Rh_{10}$(ox)/Mo(red)	Air, Air + 10% H_2O, H_2/CO/CO_2 (31/45/24)		B2
	1996	Hurst et al.	X								Mo	N_2	$Fe^{3+}/Fe^{2+} \approx 0.1$ for several slags	B3
	1987	Jones and Lindsey	X										At melting: S outgassed	B12
	1985	Quon et al.	X								Mo		Weight-basis assumed	B17
	1984	Streeter et al.	X								C or Al_2O_3 crucible, Mo bob	H_2/N_2 (20/80)		B22
	1982	Shiraishi and Meister							X	T: ±1 K	Mullite ($Al_6Si_2O_{13}$)			B27
	1968	Hofmaier	X							η: ±2.6% (Pa s)	Mo or W	Ar	Time-independent flow	B46
	1959	Sage and McIlroy	X								PtRh crucible	H_2/N_2 (varying conc to control Fe oxidation)	Arithmetic mean of Fe oxidation level used when interval reported	B48

Table A1 (*continued*)

Mixture	Year	Author	Viscometer type								Accuracy (as reported by authors)	Sensor material	Atmosphere	Comments	Table
			Rotational	Falling body	Electric vibration	Rod elongation	Rod bending	Isothermal deformation	Squeeze film	Penetrating rod					
SiO_2–Al_2O_3–Na_2O	1993	Stein and Spera	X								η: ±1 Pa s, T: ±3 K			Composition: Post-run	B6
	1986	Scarfe and Cronin	X								Accuracy: 5%, Precision: 1%, T: ±1 K	$Pt_{90}Rh_{10}$			B13
	1959	Sage and McIlroy	X									PtRh crucible	H_2/N_2 (varying conc to control Fe oxidation)	Arithmetic mean of Fe oxidation level used when interval reported	B48
	1924	English	X									Porcelain cruc/rod, IrPt bob	Air	Grouped components: Average molar weight used	B57
SiO_2–FeO_x–MgO	1986	Vorres et al.	X									Al_2O_3 crucible, Mo bob	$H_2/CO_2/N_2$ or Ar		B14
SiO_2–CaO–MgO	1986	Scarfe and Cronin	X								Accuracy: 5%, Precision: 1%, T: ±1 K	$Pt_{90}Rh_{10}$		One composition reported previously by Scarfe et al. (1983)	B13
SiO_2–CaO–Na_2O	1972	Lakatos et al.	X				X				T: ±5 K	$Pt_{90}Rh_{10}$ crucible (rotational)		Rotational: $\eta < 10^5$ Pa s, Rod bending: $\eta > 10^7$ Pa s	B38
	1925	English	X									Porcelain crucible and rod, IrPt bob	Air	Calibrated at room temperature, 2 glasses in previous paper	B56
	1924	English	X									Porcelain crucible and rod, IrPt bob	Air	Calibrated at room temperature	B57
	1924	Washburn and Shelton	X								Accuracy: 20% (<100 Pa s) or 10% (>100 Pa s), Precision: 5%	Porcelain		Mostly only content of major components reported. Crystallisation possible at low-end temp. Stott (1925) finds observations useless, possibly due to non-homogeneities in glass	B58
SiO_2–MgO–Na_2O	1925	English	X									Porcelain crucible and rod, IrPt bob	Air	Calibrated at room temperature	B56
	1924	English	X									Porcelain crucible and rod, IrPt bob	Air	Calibrated at room temperature, Grouped components: Average molar weight used	B57
SiO_2–Na_2O–B_2O_3	1924	English	X									Porcelain crucible and rod, IrPt bob	Air	Calibrated at room temperature, Grouped components: Average molar weight used	B57
SiO_2–Al_2O_3–FeO_x–CaO	1987	Jones and Lindsey	X											At melting: S outgassed	B12
	1984	Streeter et al.	X									C or Al_2O_3 crucible, Mo bob	H_2/N_2 (20/80)		B22
	1969	Boow								X		SiO_2		Grouped components: Average molar weight used	B42
	1959	Sage and McIlroy	X									PtRh crucible	H_2/N_2 (varying conc to control Fe oxidation)	Arithmetic mean of Fe oxidation level used when interval reported	B48

(*continued on next page*)

Table A1 (*continued*)

Mixture	Year	Author	Viscometer type								Accuracy (as reported by authors)	Sensor material	Atmosphere	Comments	Table
			Rotational	Falling body	Electric vibration	Rod elongation	Rod bending	Isothermal deformation	Squeeze film	Penetrating rod					
SiO_2–Al_2O_3–CaO–MgO	1991	Nowok and Benson	X										CO/CO_2 (60/40)		B9
	1987	Jones and Lindsey	X											At melting: S outgassed	B12
	1986	Vorres et al.	X									Al_2O_3 crucible, Mo bob	$H_2/CO_2/N_2$ or Ar		B14
	1985	Schobert et al.	X									C or Al_2O_3 crucible, Mo or $Pt_{90}Rh_{10}$ bob	H_2/N_2 (20/80), N_2, Air	Hysteresis observed, Gas-inlet: 500 ml/min, Error in Table 1 of paper: First four columns are all Baukol–Noonan ashes	B18
	1984	Streeter et al.	X									C or Al_2O_3 crucible, Mo bob	H_2/N_2 (20/80)		B22
	1982	Schobert et al.	X									Graphite	Reducing		B26
	1982	Shiraishi and Meister							X		T: ±1 K	Mullite ($Al_6Si_2O_{13}$)			B27
	1980	Piwinskii and Weed	X								T: ±2 K				B32
	1959	Sage and McIlroy	X									PtRh crucible	H_2/N_2 (Varying conc to control Fe oxidation)	Arithmetic mean of Fe oxidation level used when interval reported	B48
SiO_2–Al_2O_3–CaO–Na_2O	1987	Jones and Lindsey	X											At melting: S outgassed	B12
	1985	Schobert et al.	X									C or Al_2O_3 crucible, Mo or $Pt_{90}Rh_{10}$ bob	H_2/N_2 (20/80), N_2, Air	Gas-inlet: 500 ml/min, Error in Table 1 of paper: First four columns are all Baukol–Noonan ashes	B18
	1984	Streeter et al.	X									C or Al_2O_3 crucible, Mo bob	H_2/N_2 (20/80)		B22
	1982	Schobert et al.	X									Graphite	Reducing		B26
	1969	Boow								X		SiO_2		Grouped components: Average molar weight used	B42
	1972	Lakatos et al.	X				X				T: ±5 K	$Pt_{90}Rh_{10}$ crucible (rotational)		Rotational: $\eta < 10^5$ Pa s, Rod bending: $\eta > 10^7$ Pa s	B38
SiO_2–CaO–Na_2O–K_2O	1972	Lakatos et al.	X				X				T: ±5 K	$Pt_{90}Rh_{10}$ crucible (rotational)		Rotational: $\eta < 10^5$ Pa s, Rod bending: $\eta > 10^7$ Pa s	B38
	1972	Skryabin and Novokhaskii			X						η: ±5% (P)	ZrO_2 crucible, Pt shaft	Ar, CO_2		B39

Appendix B

The tables are presented in chronological order, new publications first, and secondarily in alphabetical order. Species concentrations are reported in mole fractions, temperatures in kelvin (K) and viscosities in $\log_{10} \eta$ (Pa s).

All numbers are reported with identical, high numbers of signficance to improve the uniformity of the data presentation (the reader is encourgaged to refer to Appendix A for experimental error levels). Mole fractions are reported with four decimals, temperatures with none and viscosities with three decimals.

All graphical data has been recorded semi-automatically using a simple PC program.

The data in each table is arranged in order of rising complexity of the mixtures (number of components) and with mixtures containing the components listed at the left end of the table first, i.e. data of the system SiO_2–Al_2O_3 is presented before data of the system SiO_2–FeO_x. Data of a given compositional system is listed in the order of decreasing contents of SiO_2. If two mixtures contain identical amounts of SiO_2, the content of the next component present will decide.

The temperature–viscosity data is listed in two or four rows. Four rows are used when repeated experiments have been conducted on the same mixture, or just in order to save space.

A description of the experimental conditions of each table can be found in Appendix A (Tables B1–B58).

Table B1
Goto et al. (1997) [75]

SiO_2	Al_2O_3	Fe_2O_3	CaO	MgO	Na_2O	K_2O	TiO_2	MnO	T	log η	T	log η
0.8115	0.0967	0.0110	0.0194		0.0201	0.0332	0.0075	0.0007	1873	2.760	1753	3.370
									1833	2.920	1713	3.590
									1793	3.100	1673	3.850
0.7942	0.1055	0.0213	0.0112	0.0260	0.0209	0.0207	0.0001	0.0001	1873	2.400	1673	3.520
									1823	2.650	1623	3.870
									1773	2.920	1573	4.190
									1723	3.220		
0.7873	0.1136	0.0128	0.0204		0.0225	0.0349	0.0078	0.0006	1873	2.590	1713	3.440
									1833	2.730	1673	3.710
									1793	2.950	1633	4.100
									1753	3.180		
0.7844	0.1090	0.0134	0.0309	0.0131	0.0330	0.0136	0.0020	0.0006	1873	2.480	1723	3.280
									1823	2.730	1673	3.610
									1773	3.000	1623	3.920
0.7769	0.1285	0.0123	0.0200		0.0205	0.0336	0.0077	0.0006	1873	2.340	1753	3.000
									1853	2.420	1733	3.110
									1833	2.550	1713	3.260
									1813	2.640	1693	3.420
									1793	2.750	1673	3.550
									1773	2.850	1653	3.680
0.7635	0.1427	0.0123	0.0199	0.0002	0.0202	0.0331	0.0075	0.0006	1873	2.220	1813	2.570
									1853	2.310	1793	3.000
									1833	2.420	1753	3.190
0.7550	0.1434	0.0132	0.0319	0.0122	0.0311	0.0130	0.0001	0.0001	1873	2.090	1773	2.600
									1823	2.330	1723	2.880
0.7550	0.1343	0.0204	0.0441	0.0121	0.0150	0.0157	0.0033	0.0001	1873	1.860	1723	2.670
									1823	2.090	1673	2.900
									1773	2.350	1623	3.290
									1723	2.640	1573	3.770

Table B2
Hurley et al. (1996) [91]

SiO_2	Al_2O_3	Fe_2O_3	CaO	MgO	Na_2O	TiO_2	P_2O_5	Atm	T	log η	T	log η
0.4271	0.1349	0.0253	0.2736	0.1067	0.0149	0.0124	0.0051	Air	1673	−0.282	1532	0.271
									1654	−0.282	1513	0.364
									1633	−0.224	1493	0.475
									1613	−0.224	1473	0.536
									1593	−0.282	1453	0.781
									1573	−0.048	1434	1.043
									1553	0.103	1424	1.398
								Air + H_2O	1673	0.288	1553	0.822
									1662	0.350	1533	0.959
									1653	0.378	1513	1.072
									1632	0.486	1493	1.199
									1614	0.545	1474	1.343
									1593	0.605	1454	1.508
									1572	0.705		
								$H_2/CO/CO_2$	1702	0.235	1584	0.792
									1672	0.464	1553	0.966
									1643	0.526	1523	1.236
									1614	0.644	1505	1.712

Table B3
Hurst et al. (1996) [163]

SiO_2	Al_2O_3	Fe_2O_3	CaO	MgO	Na_2O	K_2O	TiO_2	Mn_3O_4	P_2O_5	SO_3	T	log η
0.6725	0.1720	0.0462	0.0615	0.0174	0.0014	0.0042	0.0178	0.0003	0.0046	0.0010	1773	1.820
											1673	2.326
0.6216	0.0541	0.0021	0.3093	0.0038	0.0005	0.0017	0.0030		0.0002	0.0036	1773	0.544
											1673	0.982
0.6027	0.1687	0.0426	0.1372	0.0200	0.0001	0.0060	0.0151	0.0003	0.0042	0.0018	1773	0.845
											1673	1.346
0.5635	0.0576	0.0022	0.3634	0.0038	0.0005	0.0018	0.0027		0.0002	0.0042	1773	0.322
											1673	0.690
0.5596	0.1601	0.0389	0.1954	0.0183	0.0014	0.0055	0.0141	0.0002	0.0040	0.0023	1773	0.556
											1673	1.021
0.5437	0.2148	0.0081	0.1778	0.0127	0.0118	0.0020	0.0158		0.0004	0.0129	1773	0.924
											1673	1.508
0.4738	0.1895	0.0083	0.2866	0.0144	0.0096	0.0018	0.0133	0.0001	0.0004	0.0022	1773	0.398
											1673	0.863
0.4179	0.1683	0.0070	0.3676	0.0139	0.0086	0.0015	0.0119	0.0001	0.0003	0.0029	1773	0.079
											1673	0.763
0.3693	0.1504	0.0061	0.4365	0.0137	0.0079	0.0013	0.0109	0.0001	0.0003	0.0036	1773	0.079
											1673	0.505

Table B4
Liska et al. (1996) [86]

SiO_2	Na_2O	TiO_2	T	log η	T	log η	T	log η	T	log η
0.7633	0.2264	0.0103	1679	0.840	1024	4.740	1565	1.390	943	8.370
			1573	1.110	883	7.480	1517	1.590	933	8.730
			1523	1.300	873	7.720	1467	1.800	923	9.120
			1474	1.500	863	7.960	1418	2.060	903	9.870
			1426	1.720	854	8.200	968	7.630	893	10.210
			1377	1.960	844	8.470	960	7.930	884	10.590
			1325	2.230	834	8.770	952	8.190		
			1276	2.520	824	9.070				
			1226	2.850	814	9.440				
			1174	3.240	804	9.820				
			1124	3.670	793	10.210				
			1074	4.170	784	10.610				
0.7626	0.2128	0.0246	1676	0.910	1034	4.720	1565	1.220	933	8.080
			1575	1.080	985	5.440	1514	1.420	923	8.400
			1530	1.260	904	7.390	1464	1.640	914	8.670
			1480	1.460	894	7.630	1417	1.880	904	8.980
			1432	1.670	884	7.870	1365	2.150	894	9.300
			1381	1.920	875	8.150	1318	2.450	884	9.670
			1333	2.180	865	8.420	953	7.550	874	10.060
			1284	2.480	854	8.750	943	7.800	864	10.450
			1235	2.810	845	9.070				
			1183	3.200	835	9.430				
			1133	3.640	825	9.800				
			1084	4.130	815	10.170				
0.7592	0.2408		1683	0.850	1107	3.720	1591	1.120	934	7.350
			1644	0.980	1058	4.210	1547	1.290	926	7.550
			1593	1.160	1008	4.800	1497	1.500	915	7.820
			1541	1.330	984	5.130	1446	1.720	905	8.080
			1501	1.350	845	8.160	1399	1.960	897	8.350
			1458	1.520	835	8.430	1349	2.240	886	8.700
			1407	1.760	826	8.720	1300	2.550	876	9.030
			1359	1.990	815	9.050	1250	2.890	867	9.360
			1308	2.270	806	9.370	1201	3.290	857	9.710
			1260	2.550	795	9.780	1149	3.970	847	10.050
			1210	2.900	785	10.190	1098	4.540	837	10.460
			1158	3.280			1049	5.090		

Table B5
Stein and Spera (1993) [35]

SiO_2	Al_2O_3	Na_2O	T	log η	T	log η
0.8311	0.0853	0.0836	1573	5.533	1448	6.880
			1548	5.804	1423	7.140
			1523	6.097	1398	7.452
			1498	6.358	1373	7.739
			1473	6.630		
0.7801	0.1111	0.1088	1573	5.103	1448	6.369
			1548	5.255	1423	6.642
			1523	5.525	1398	6.881
			1498	5.760	1373	7.254
			1473	6.102	1348	7.500
0.7411	0.1306	0.1283	1573	4.686	1423	6.127
			1548	4.806	1398	6.447
			1523	5.078	1373	6.775
			1498	5.327	1353	7.050
			1473	5.593	1333	7.317
			1448	5.858		
0.7300	0.1349	0.1351	1623	4.365	1623	4.471
			1573	4.816	1598	4.663
			1548	4.998	1573	4.848
			1523	5.228	1548	5.037
			1498	5.532	1523	5.294
			1473	5.835	1498	5.580
			1448	6.063	1473	5.859
			1433	6.202	1453	6.057
			1423	6.325	1433	6.254
			1413	6.427	1413	6.500
			1403	6.566	1393	6.689
0.6950	0.1538	0.1512	1573	4.530	1423	5.887
			1548	4.702	1398	6.188
			1523	4.945	1373	6.431
			1498	5.107	1348	6.764
			1473	5.290	1323	7.138
			1448	5.573		
0.6723	0.1604	0.1673	1493	4.928	1523	4.562
			1473	5.153	1498	4.758
			1453	5.380	1473	4.947
			1433	5.557	1448	5.216
			1413	5.807	1423	5.495
			1393	6.028	1398	5.762
			1373	6.257	1373	6.055
			1353	6.475	1353	6.374
			1333	6.781	1333	6.656
			1323	6.915	1313	6.900
			1313	7.035	1298	7.207
			1303	7.189		
0.6554	0.1705	0.1742	1548	4.391	1398	6.003
			1523	4.519	1373	6.260
			1498	4.842	1348	6.580
			1473	5.051	1333	6.702
			1423	5.704		
0.6179	0.1858	0.1963	1533	4.249	1553	4.151
			1503	4.512	1533	4.275
			1473	4.830	1503	4.575
			1423	5.340	1473	4.836
			1373	5.977	1423	5.348
			1333	6.505	1373	5.949
					1333	6.518
0.6133	0.1851	0.2015	1533	4.302	1413	5.412
			1503	4.489	1373	5.951
			1473	4.79	1333	6.409
			1443	5.052	1313	6.635

Table B6
Stein and Spera (1993) [164]

SiO_2	Al_2O_3	FeO	TiO_2	MnO	CaO	MgO	Na_2O	K_2O	P_2O_5	T	log η
0.7189	0.1063	0.0396	0.0046	0.0006	0.037	0.0209	0.0508	0.0206	0.0005	1423	4.860
										1398	5.025
										1373	5.321
										1348	5.432
										1323	5.688
										1293	6.239
										1273	6.423

Table B7
Dingwell (1992) [87]

SiO_2	CaO	Na_2O	K_2O	TiO_2	T	log η	T	log η
0.4632	0.4796			0.0571	1867	−0.777	1793	−0.623
					1842	−0.740	1768	−0.559
					1817	−0.684		
0.4297	0.4456			0.1247	1867	−0.917	1793	−0.764
					1842	−0.873	1768	−0.706
					1817	−0.821	1744	−0.644
0.4082	0.4151			0.1767	1867	−1.056	1744	−0.788
					1842	−1.007	1719	−0.724
					1817	−0.959	1694	−0.656
					1793	−0.903	1670	−0.585
					1768	−0.848		
0.3734	0.3824			0.2441	1867	−1.195	1744	−0.951
					1842	−1.142	1719	−0.893
					1817	−1.107	1694	−0.827
					1793	−1.057	1670	−0.759
					1768	−1.006		
0.3330	0.3372			0.3298	1867	−1.304	1744	−1.089
					1842	−1.272	1719	−1.034
					1817	−1.234	1694	−0.975
					1793	−1.189	1670	−0.910
					1768	−1.140		
0.2872	0.2908			0.4220	1867	−1.463	1744	−1.260
					1842	−1.428	1719	−1.208
					1817	−1.394	1694	−1.146
					1793	−1.354	1670	−1.092
					1768	−1.309		
0.4737		0.4624		0.0639	1424	−0.306	1325	−0.010
					1399	−0.261	1301	0.111
					1375	−0.179	1276	0.161
					1350	−0.096		
0.4420		0.4348		0.1232	1424	−0.460	1325	−0.180
					1399	−0.398	1301	−0.092
					1375	−0.328	1276	−0.025
					1350	−0.255	1251	0.064
0.4030		0.4101		0.1869	1424	−0.656	1350	−0.467
					1399	−0.593	1325	−0.398
					1375	−0.532	1301	−0.332
0.3708		0.3622		0.2670	1424	−0.780	1325	−0.533
					1375	−0.668	1301	−0.458
					1350	−0.604		
0.3348		0.3196		0.3456	1424	−0.896	1350	−0.708
					1399	−0.839	1325	−0.633
					1375	−0.775	1301	−0.553
0.3242			0.3327	0.3431	1424	−0.511	1301	−0.169
					1399	−0.446	1276	−0.091
					1375	−0.381	1251	−0.018
					1350	−0.314	1227	0.079
					1325	−0.244		

Table B8
Tanigushi (1992) [118]

SiO_2	Al_2O_3	CaO	MgO	T	log η	T	log η	T	log η	T	log η
0.5556	0.1111	0.2778	0.5556	1823	0.480	1723	0.950	1173	8.400	1098	11.400
				1773	0.750	1673	1.250	1148	9.300	1073	12.800
								1123	10.600		
0.5479	0.0027	0.2740	0.1753	1773	0.170	1523	1.320	1098	8.400	1023	11.800
				1723	0.360	1473	1.670	1073	9.600	1003	13.000
				1673	0.560	1423	2.190	1048	10.600		
				1623	0.760	1373	2.620				
				1573	1.030						
0.5405	0.0811	0.2703	0.1081	1823	0.330	1623	1.160	1113	8.900	1048	12.000
				1773	0.550	1573	1.440	1073	10.200	1023	13.100
				1723	0.700	1523	1.800				
				1673	0.860	1473	2.240				
0.5128	0.0256	0.2564	0.2051	1723	0.130	1573	0.840	1098	8.200	1023	11.100
				1673	0.280	1523	1.160	1073	9.100	1003	12.300
				1623	0.510	1473	1.520	1048	10.000		
0.5000		0.2500	0.2500	1068	8.600	1048	9.200	1023	10.100	973	12.300
				1053	9.100			998	11.600		
0.5000	0.2500	0.2500		1853	0.680	1673	1.480	1226	8.400	1148	11.500
				1813	0.770	1618	1.760	1198	9.100	1118	12.900
				1773	0.990	1573	2.170	1173	10.300		
				1723	1.170						

Table B9
Nowok and Benson (1991) [46]

SiO_2	Al_2O_3	Fe_2O_3	CaO	MgO	Na_2O	K_2O	TiO_2	T	log η
0.4223	0.1002	0.0456	0.2667	0.0845	0.0625	0.0050	0.0134	1702	0.603
								1682	0.638
								1662	0.648
								1642	0.718
								1622	0.810
								1602	0.934
								1582	1.031
								1562	1.111
								1543	1.261
								1523	1.376
								1503	1.585
								1488	2.343

Table B10
Dingwell (1989) [56]

SiO_2	Fe_2O_3	FeO	MgO	K_2O	T	log η	T	log η
0.5104	0.2528		0.2368		1793	−1.091	1719	−0.997
					1769	−1.088	1670	−0.949
0.7263	0.1339	0.0055		0.1344	1670	2.010	1473	3.090
					1621	2.250	1424	3.310
					1572	2.520	1375	3.760
					1523	2.790		
0.6385	0.1839			0.1776	1719	0.850	1572	1.540
					1670	1.060	1523	1.790
					1621	1.300	1473	2.060
0.4819	0.2692			0.2489	1719	−0.1130	1572	0.540
					1670	0.0900	1523	0.830
					1621	0.2900	1473	1.100

Table B11
Dingwell and Virgo (1988) [165]

SiO_2	Fe_2O_3	FeO	Na_2O	T	log η	T	log η
0.8707	0.0572	0.0099	0.0622	1699	2.510	1592	3.010
				1645	2.750	1540	3.330
0.7573	0.0163	0.0072	0.2192	1674	0.940	1400	1.940
				1619	1.110	1346	2.200
				1560	1.310	1291	2.520
				1504	1.500	1234	2.830
				1452	1.700		
0.7444	0.1166	0.0149	0.1241	1720	1.120	1475	2.160
				1676	1.280	1422	2.440
				1626	1.460	1374	2.770
				1574	1.690	1326	3.140
				1523	1.920		
0.7169	0.0354	0.0088	0.2389	1690	0.730	1354	1.830
				1631	0.800	1300	2.190
				1574	0.980	1248	2.370
				1515	1.190	1195	2.710
				1461	1.370	1133	3.140
				1408	1.580	1082	3.590
0.6612	0.1570	0.0165	0.1652	1681	0.410	1585	0.730
				1635	0.540	1533	0.940
0.6375	0.0757	0.0080	0.2788	1675	0.200	1347	1.300
				1624	0.330	1297	1.520
				1565	0.470	1243	1.800
				1506	0.680	1187	2.120
				1451	0.870	1152	2.340
				1401	1.060		
0.5600	0.1200		0.3200	1665	−0.260	1362	0.760
				1626	−0.160	1292	1.120
				1567	0.020	1235	1.360
				1509	0.220	1179	1.670
				1455	0.400	1117	2.040
				1399	0.620		
0.4784	0.1563	0.0064	0.3589	1681	−0.670	1341	0.410
				1625	−0.530	1284	0.710
				1568	−0.330	1230	0.970
				1512	−0.190	1178	1.270
				1459	−0.020	1124	1.610
				1397	0.210		
0.4000	0.2000		0.4000	1657	−0.930	1392	−0.100
				1605	−0.800	1340	0.110
				1551	−0.630	1285	0.300
				1499	−0.480	1229	0.650
				1445	−0.290		

Table B12
Jones and Lindsey (1987) [60]

SiO_2	Al_2O_3	Fe_2O_3	CaO	MgO	Na_2O	K_2O	TiO_2	SO_3	T	log η	T	log η
0.7663	0.1118	0.0211	0.0398	0.0256	0.0091	0.0110	0.0097	0.0055	1876	1.276	1690	2.157
									1833	1.377	1644	2.419
									1785	1.595	1589	2.793
									1740	1.827		
0.7621	0.0962	0.0249	0.0556	0.0342	0.0049	0.0050	0.0153	0.0018	1777	0.955	1582	2.110
									1729	1.265	1536	2.417
									1679	1.520	1485	2.880
									1633	1.800		
0.7173	0.1257	0.0126	0.0822	0.0293	0.0087	0.0074	0.0154	0.0014	1782	1.038	1631	1.910
									1731	1.319	1588	2.223
									1686	1.571	1542	2.594
0.6977	0.1349	0.0518	0.0515	0.0363	0.0055	0.0118	0.0088	0.0018	1880	0.141	1635	0.801
									1786	0.333	1590	1.037
									1730	0.506	1488	1.679
									1685	0.635	1443	2.510
0.6829	0.1207	0.0301	0.0925	0.0476	0.0068	0.0083	0.0092	0.0019	1760	0.613	1578	1.497
									1725	0.895	1535	1.772
									1678	0.973	1480	2.207
									1622	1.259	1433	2.668
0.5914	0.1312	0.0237	0.1562	0.0647	0.0128	0.0076	0.0099	0.0024	1777	−0.084	1574	0.874
									1720	0.147	1531	1.130
									1680	0.304	1484	1.456
									1620	0.597	1432	1.952
0.5821	0.1640	0.0158	0.1192	0.0358	0.0620	0.0084	0.0107	0.0019	1838	−0.236	1493	1.297
									1830	−0.220	1450	1.589
									1586	0.745	1401	2.189
0.5661	0.1464	0.0198	0.2014	0.0446	0.0038	0.0059	0.0106	0.0015	1794	−0.200	1636	0.409
									1746	0.087	1604	0.602
									1698	0.165	1591	2.005
									1691	0.301	1576	2.990
									1653	0.354		
0.5334	0.1708	0.0993	0.1165	0.0485	0.0094	0.0085	0.0112	0.0025	1833	−0.677	1638	−0.295
									1728	−0.568	1539	0.199

Table B13
Scarfe and Cronin (1986) [124]

SiO_2	Al_2O_3	CaO	MgO	Na_2O	T	log η	T	log η
0.7500	0.1250			0.1250	1873	2.862	1748	3.624
					1848	2.999	1723	3.775
					1823	3.151	1698	3.922
					1798	3.313	1673	4.080
					1773	3.460		
0.6875	0.0938	0.0625	0.0625	0.0928	1873	1.435	1623	2.587
					1823	1.627	1573	2.870
					1773	1.833	1523	3.178
					1723	2.064	1473	3.535
					1673	2.306	1423	3.922
0.6250	0.0625	0.1250	0.1250	0.0625	1823	0.760	1573	1.790
					1773	0.927	1523	2.070
					1723	1.103	1473	2.418
					1673	1.305	1423	2.782
					1623	1.516		
0.5625	0.0313	0.1875	0.1875	0.0313	1863	0.027	1623	0.791
					1823	0.148	1573	1.007
					1773	0.290	1523	1.269
					1723	0.465	1473	1.576
					1673	0.590		
0.5125	0.0063	0.2375	0.2375	0.0063	1823	−0.276	1673	0.211
					1773	−0.116	1623	0.405
					1723	0.040		

Table B14
Vorres et al. (1986) [29]

SiO_2	Al_2O_3	FeO	CaO	MgO	T	log η	T	log η
0.4826	0.0569	0.1211	0.0517	0.2878	1540	1.721	1636	0.214
					1557	1.328	1689	0.075
					1581	0.857	1708	0.022
					1605	0.379		
0.3927	0.1157	0.0411	0.1578	0.2927	1536	1.658	1596	1.051
					1562	1.398	1630	0.790
					1567	1.377	1678	0.474
					1580	1.276	1705	0.158
					1583	1.260		

Table B15
Danêk et al. (1985)

SiO_2	Fe_2O_3 + FeO	CaO	T	log η	T	log η
0.5000		0.5000	1823	−0.542	1723	−0.272
0.6100	0.0780	0.3120		−0.320		−0.066
0.5210	0.0960	0.3830		−0.734		−0.494
0.4720	0.0560	0.4720		−0.674		−0.435
0.4440	0.1110	0.4440		−0.935		−0.704
0.4120	0.1760	0.4120		−1.262		−1.009
0.3530	0.1290	0.5170		−1.387		−1.049

Table B16
Mysen et al. (1985) [83]

SiO_2	Fe_2O_3	FeO	CaO	T	log η
0.4468	0.0159	0.0056	0.5317	1773	0.219
0.4458	0.0136	0.0101	0.5305	1823	0.253
0.4455	0.0128	0.0115	0.5301	1873	0.275
0.4371	0.0343	0.0085	0.5201	1773	0.246
0.4364	0.0327	0.0116	0.5193	1823	0.273
0.4354	0.0304	0.0161	0.5181	1873	0.293
0.5739	0.0132	0.0113	0.4017	1673	0.248
0.5741	0.0135	0.0105	0.4019	1723	0.115
0.5735	0.0126	0.0124	0.4015	1773	0.009
0.5726	0.0109	0.0157	0.4008	1823	0.067
0.5724	0.0105	0.0165	0.4007	1873	0.125
0.5612	0.0318	0.0140	0.3930	1673	0.129
0.5597	0.0290	0.0193	0.3919	1723	0.017
0.5593	0.0282	0.0209	0.3916	1773	0.065
0.5582	0.0262	0.0247	0.3909	1823	0.127
0.5578	0.0254	0.0262	0.3906	1873	0.169

Table B17
Quon et al. (1985) [39]

SiO_2	Al_2O_3	Fe_2O_3	CaO	MgO	Na_2O	K_2O	TiO_2	P_2O_5	T	log η	T	log η
0.7689	0.1303	0.0152	0.0499	0.0186	0.0100	0.0021	0.0038	0.0011	1950	0.185	1758	1.014
									1927	0.287	1741	1.113
									1894	0.407	1731	1.196
									1882	0.479	1701	1.338
									1846	0.585	1684	1.423
									1824	0.676	1664	1.567
									1816	0.746	1651	1.641
									1798	0.853	1623	1.832
									1777	0.916		
0.7676	0.1244	0.0391	0.025	0.0189	0.0062	0.0043	0.0107	0.0039	2014	0.402	1799	1.030
									1938	0.473	1761	1.209
									1917	0.565	1743	1.331
									1894	0.623	1707	1.517
									1868	0.729	1682	1.634
									1852	0.814	1631	1.874
									1820	0.934		
0.7653	0.1476	0.0167	0.0313	0.0152	0.0138	0.0024	0.0060	0.0016	1949	0.793	1852	1.123
									1931	0.808	1792	1.449
									1917	0.891	1761	1.551
									1884	0.988	1733	1.686
									1862	1.087	1685	1.758
0.7629	0.1352	0.0148	0.0503	0.0197	0.0095	0.0022	0.0040	0.0013	1977	0.761	1813	0.194
									1957	0.687	1786	0.309
									1943	0.595	1745	0.529
									1927	0.471	1722	0.692
									1909	0.366	1711	0.823
									1892	0.274	1685	0.886
									1866	0.203	1667	0.984
									1838	0.043		
0.7281	0.1874	0.0174	0.0289	0.0132	0.0081	0.0063	0.0104	0.0001	1960	0.562	1823	0.981
									1934	0.574	1805	1.085
									1911	0.650	1767	1.315
									1893	0.717	1728	1.483
									1871	0.787	1690	1.730
									1850	0.872	1674	1.876
0.7163	0.1335	0.0195	0.0658	0.0201	0.0281	0.0116	0.0027	0.0023	1993	0.384	1915	0.135
									1973	0.352	1895	0.057
									1953	0.265	1871	0.041
									1951	0.204	1860	0.109
0.7116	0.1370	0.0216	0.0740	0.0210	0.0208	0.0081	0.0038	0.0021	1995	0.073	1758	1.125
									1972	0.020	1715	1.383
									1914	0.350	1684	1.568
									1873	0.465	1666	1.651
									1836	0.679	1648	1.760
									1796	0.928	1626	1.955
									1785	0.998		
0.5260	0.1681	0.0198	0.1736	0.0658	0.0284	0.0104	0.0058	0.0021	1859	0.787	1676	0.030
									1772	0.463	1649	0.154
									1752	0.349	1624	0.261
									1722	0.245	1593	0.489
0.5137	0.1591	0.0265	0.1809	0.0670	0.0316	0.0120	0.0074	0.0020	1880	0.777	1721	0.049
									1850	0.628	1695	0.088
									1825	0.473	1674	0.202
									1771	0.258	1649	0.320
									1747	0.143	1618	0.503

Table B18
Schobert et al. (1985) [92]

SiO_2	Al_2O_3	Fe_2O_3	CaO	MgO	Na_2O	K_2O	TiO_2	P_2O_5	SO_3		T	log η
0.6144	0.0808	0.0035	0.1712	0.1183	0.0000	0.0039	0.0070		0.0008	Cooling cycle	1723	0.951
											1674	1.250
										Reducing atm.	1653	1.400
											1644	1.504
										Kemmerer slag	1625	1.623
											1615	1.690
										C crucible	1601	1.785
											1587	1.894
										Mo bob	1576	2.006
											1560	2.499
0.5604	0.1132	0.0527	0.1634	0.0960		0.0058	0.0068		0.0017	Cooling cycle	1748	0.517
											1726	0.626
											1708	0.698
										Reducing atm.	1688	0.797
											1670	0.866
											1659	0.900
										Kemmerer slag	1639	1.011
											1618	1.094
											1601	1.225
										Al_2O_3 crucible	1577	1.344
											1553	1.475
											1518	1.700
										Mo bob	1495	1.878
											1470	2.327
											1463	2.602
0.4376	0.0900	0.0120	0.2842	0.1262	0.0370	0.0007	0.0109		0.0015	Cooling cycle	1621	0.416
											1607	0.478
											1593	0.550
										Reducing atm.	1580	0.602
											1569	0.660
											1555	0.731
										Gascoyne slag	1541	0.758
											1527	0.860
											1513	0.947
										Al_2O_3 crucible	1498	1.026
											1485	1.116
											1473	1.207
										Mo bob	1460	1.470
											1456	1.879
											1450	2.364
										Heating cycle	1527	0.897
											1517	0.964
										Rest as above	1498	1.273
											1481	1.633
											1462	2.285
0.4108	0.1712	0.0386	0.1988	0.0626	0.0837	0.0030	0.0132	0.0005	0.0175	Cooling cycle	1673	0.342
											1650	0.516
											1604	0.675
										Reducing atm.	1588	0.758
											1568	0.893
											1533	1.055
										Baukol–	1517	1.145
										Noonan slag	1502	1.228
											1487	1.323

(*continued on next page*)

Table B18 (*continued*)

SiO_2	Al_2O_3	Fe_2O_3	CaO	MgO	Na_2O	K_2O	TiO_2	P_2O_5	SO_3		T	log η
										Al_2O_3 crucible	1468	1.485
											1451	1.566
											1435	1.810
										Mo bob	1429	2.014
											1428	2.246
0.4010	0.1626	0.0392	0.2061	0.0587	0.0978	0.0044	0.0140	0.0005	0.0157	Cooling cycle	1730	0.264
											1708	0.313
											1687	0.579
										Oxidising atm.	1669	0.780
											1644	0.902
										Baukol–Noonan slag	1627	1.007
											1583	1.233
											1569	1.321
										Al_2O_3 crucible	1545	1.486
											1520	1.637
										$Pt_{90}Rh_{10}$ bob	1492	1.808
											1459	2.030
0.3486	0.1378	0.0398	0.3091	0.1096	0.0400	0.0028	0.0075	0.0005	0.0042	Cooling cycle	1589	0.302
											1578	0.466
											1564	0.719
										Reducing atm.	1556	0.799
											1546	0.945
											1540	1.013
										Indian head slag	1534	1.088
											1529	1.140
											1525	1.205
										Al_2O_3 crucible	1517	1.260
											1507	1.371
											1497	1.457
										Mo bob	1483	1.542
											1476	2.172
0.2473	0.2674	0.0582	0.2252	0.1309	0.0647	0.0008	0.0056			Cooling cycle	1701	0.693
											1682	0.778
										Reducing atm.	1665	0.850
											1650	0.931
										Indian head slag	1634	1.103
											1617	1.285
											1611	1.353
										Al_2O_3 crucible	1610	1.396
											1599	1.557
										Mo bob	1580	1.813
											1560	1.987

Table B19
Hochella and Brown (1984) [32]

SiO_2	Al_2O_3	Fe_2O	CaO	MgO	Na_2O	K_2O	T	log η
0.7903	0.0931	0.0149	0.0201	0.0062	0.0388	0.0365	1477	5.327
							1553	4.689
							1617	4.238
							1671	3.888
							1713	3.590
							1781	3.195

Table B20
Quon et al. (1984) [129]

SiO_2	Al_2O_3	Fe_2O_3	CaO	MgO	Na_2O	TiO_2	BaO	SrO	P_2O_5	SO_3	T	log η
0.7382	0.1655	0.0296	0.0263	0.0207	0.0009	0.0087	0.0028	0.0006	0.0049	0.0018	1902	5.922
											1897	6.110
											1885	6.351
											1871	6.425
											1855	6.529
											1845	6.607
											1821	6.775
											1818	6.823
											1812	6.873
											1805	6.910
											1792	6.935
											1781	7.006
											1775	7.054
											1756	7.100
											1741	7.128
											1727	7.135
											1721	7.156
											1705	7.204
											1686	7.475
0.7233	0.1679	0.0157	0.0442	0.0198	0.0095	0.0098	0.0061	0.0010	0.0025	0.0001	1979	6.321
											1968	6.367
											1934	6.509
											1916	6.549
											1905	6.574
											1886	6.639
											1861	6.726
											1830	6.918
											1826	6.991
0.7106	0.2045	0.0129	0.0355	0.0126	0.0012	0.0132	0.0017	0.0027	0.0026	0.0027	1878	5.955
											1861	6.115
											1819	6.526
											1798	6.636
											1780	6.703
											1740	6.827
											1729	6.945

Table B21
Seki and Oeter (1984) [30]

SiO_2	Fe_2O_3	FeO	CaO	Atm.	T	log η
0.4921	0.0772	0.0938	0.3369	Air	1973	−0.967
0.4307	0.1411	0.1410	0.2872			−1.167
0.3821	0.1791	0.1882	0.2507			−1.292
0.3355	0.2198	0.2226	0.2222			−1.432
0.3316	0.1108	0.0622	0.4954			−1.125
0.2924	0.1753	0.1107	0.4216			−1.398
0.2391	0.2582	0.1634	0.3393			−1.509
0.1807	0.3184	0.2403	0.2605			−1.638
0.5774	0.0276	0.0306	0.3644	Air	1873	−0.291
0.5023	0.0915	0.0798	0.3276			−0.738
0.4341	0.1426	0.1349	0.2884			−1.032
0.4258	0.0879	0.0541	0.4322			−0.951
0.4251	0.0856	0.0570	0.4323			−0.924
0.4215	0.0858	0.0571	0.4356			−0.951
0.3913	0.1939	0.1567	0.2581			−1.187
0.3774	0.1543	0.0903	0.3780			−1.056
0.3436	0.2431	0.1907	0.2226			−1.337
0.3387	0.1199	0.0385	0.5029			−1.032
0.3271	0.2148	0.1158	0.3423			−1.244
0.3191	0.1638	0.0635	0.4525			−1.143
0.3048	0.2819	0.2117	0.2016			−1.387
0.2977	0.1944	0.0923	0.4256			−1.244
0.2888	0.2635	0.1600	0.2878			−1.328
0.2598	0.3177	0.2516	0.1709			−1.444
0.2585	0.2912	0.1790	0.2713			−1.377
0.2504	0.3355	0.2615	0.1526			−1.495
0.2475	0.2712	0.1252	0.3561			−1.367
0.2261	0.3301	0.2111	0.2326			−1.420
0.2182	0.3033	0.1534	0.3251			−1.420
0.1851	0.3497	0.1914	0.2737			−1.456
0.5001	0.0972	0.0548	0.3479	Air	1773	−0.521
0.4417	0.1638	0.0912	0.3033			−0.876
0.3995	0.2276	0.1092	0.2638			−1.097
0.3488	0.2686	0.1483	0.2343			−1.276
0.3390	0.1291	0.0319	0.5000			−0.917
0.2997	0.2096	0.0599	0.4308			−1.143
0.2497	0.3030	0.0891	0.3581			−1.260
0.1866	0.3852	0.1431	0.2852			−1.357
0.4844	0.0616	0.1362	0.3178	CO_2	1873	0.712
0.4168	0.0657	0.1049	0.4125			0.928
0.4085	0.0937	0.2084	0.2894			1.027
0.3711	0.1196	0.1519	0.3573			1.060
0.3419	0.1529	0.2511	0.2541			1.137
0.3310	0.0999	0.0864	0.4827			1.060
0.2973	0.1585	0.3242	0.2200			1.284
0.2891	0.1584	0.1554	0.3971			1.237
0.2707	0.1695	0.2985	0.2614			1.337
0.2365	0.1708	0.2776	0.3150			1.367
04.2111	0.2056	0.3739	0.2094			1.409
0.1707	0.2283	0.3636	0.2373			1.432

Table B22
Streeter et al. (1984) [27]

SiO_2	Al_2O_3	Fe_2O_3	CaO	MgO	Na_2O	K_2O	TiO_2	P_2O_5	SO_3		T	log η
0.5937	0.1188	0.0249	0.1381	0.0690	0.0427	0.0021	0.0108			Cooling cycle	1749	1.165
											1726	1.336
											1706	1.437
											1684	1.575
											1665	1.671
											1649	1.778
											1632	1.891
										Carbon crucible	1613	1.997
											1597	2.112
											1579	2.237
											1564	2.354
											1547	2.462
											1535	2.545
										Heating cycle	1588	2.191
											1581	2.265
										Carbon crucible	1571	2.332
											1560	2.389
											1547	2.477
0.4698	0.1549	0.0099	0.2793	0.0637		0.0035	0.0165		0.0025	Cooling cycle	1745	0.442
											1719	0.564
											1703	0.656
											1686	0.754
											1672	0.861
										Carbon crucible	1655	0.938
											1637	1.044
											1625	1.994
											1622	2.164
											1620	2.247
										Heating cycle	1713	0.675
											1691	0.870
											1679	1.104
										Carbon crucible	1671	1.311
											1663	1.500
											1652	1.798
											1637	2.078
0.4418	0.1216	0.0040	0.2511	0.0689	0.0802	0.0041	0.0186		0.0097	Cooling cycle	1634	0.640
											1609	0.799
											1596	0.860
											1579	0.921
											1566	1.004
											1551	1.086
											1538	1.162
											1512	1.321
										Carbon crucible	1497	1.404
											1484	1.484
											1469	1.583
											1455	1.658
											1444	1.700
											1432	1.834
											1425	2.120
										Heating cycle	1496	1.460
											1490	1.550
										Carbon crucible	1471	1.789
											1453	2.099

Table B22 (*continued*)

SiO_2	Al_2O_3	Fe_2O_3	CaO	MgO	Na_2O	K_2O	TiO_2	P_2O_5	SO_3		T	log η
0.4326	0.1278	0.0186	0.2158	0.0722	0.1056	0.0042	0.0141		0.0091	Cooling cycle	1560	0.999
											1538	1.128
											1520	1.244
											1505	1.364
											1487	1.465
										Carbon crucible	1471	1.561
											1441	1.754
											1432	1.866
											1429	2.076
											1427	2.222
										Heating cycle	1560	1.124
											1550	1.179
											1537	1.230
											1529	1.267
										Carbon crucible	1520	1.360
											1508	1.564
											1495	1.803
											1483	2.099
0.7025	0.1161	0.0229	0.0794	0.0594		0.0113	0.0067	0.0009	0.0008		1772	1.991
											1674	2.528
0.6096	0.0802	0.0035	0.1699	0.1174	0.0079	0.0039	0.0069		0.0008		1720	0.944
											1596	1.770
0.5937	0.1188	0.0249	0.1381	0.0690	0.0427	0.0021	0.0108				1749	1.146
											1530	2.528
0.5723	0.1873	0.0582	0.0861	0.0672		0.0171	0.0073		0.0046	Cooling cycle	1750	0.973
											1664	1.435
0.4932	0.1802	0.0080	0.2188	0.0665	0.0130	0.0085	0.0092		0.0025		1754	0.748
											1639	1.342
0.4862	0.1522	0.0085	0.2385	0.0950	0.0010	0.0007	0.0146		0.0032		1676	0.591
											1624	1.009
0.4698	0.1549	0.0099	0.2793	0.0637		0.0035	0.0165		0.0025	Carbon crucible	1745	0.415
											1634	1.021
0.4576	0.1435	0.0390	0.2061	0.0933	0.0320	0.0015	0.0094	0.0005	0.0171		1671	0.991
											1563	1.625
0.4418	0.1216	0.0040	0.2511	0.0689	0.0802	0.0041	0.0186		0.0097		1633	0.613
											1440	1.683
0.4364	0.0902	0.0121	0.2848	0.1264	0.0371	0.0007	0.0109		0.0016		1621	0.398
											1498	1.009
0.4326	0.1278	0.0186	0.2158	0.0722	0.1056	0.0042	0.0141		0.0091		1557	0.968
											1437	1.739
0.428	0.1314	0.0273	0.2233	0.0698	0.0929	0.0021	0.0176		0.0075		1559	0.699
											1448	1.461
0.4218	0.0967	0.0106	0.3273	0.1038	0.0201	0.0020	0.0156	0.0004	0.0016		1586	0.431
											1468	1.236
0.3234	0.2012	0.0494	0.2084	0.1228	0.0579	0.0038	0.0135	0.0035	0.0161		1592	0.968
											1517	1.512
0.5781	0.1722	0.0900	0.0813	0.0528		0.0161	0.0076		0.0019	Cooling cycle	1754	0.602
											1590	1.384

(*continued on next page*)

Table B22 (*continued*)

SiO_2	Al_2O_3	Fe_2O_3	CaO	MgO	Na_2O	K_2O	TiO_2	P_2O_5	SO_3		T	log η
0.505	0.1663	0.0318	0.1848	0.0698	0.0288	0.0015	0.0120				1680	0.724
											1611	1.057
0.4544	0.1538	0.0509	0.2796	0.0434		0.0074	0.0096		0.0009	Alumina crucible	1744	0.633
											1545	1.803
0.4527	0.1906	0.0394	0.2520	0.0473		0.0030	0.0150				1709	0.398
											1674	0.556
0.4518	0.1969	0.0501	0.2179	0.0691		0.0008	0.0134				1729	0.255
											1655	0.531
0.4144	0.1556	0.0380	0.2239	0.0650	0.0835	0.0015	0.0181				1525	0.839
											1447	1.375
0.3599	0.1735	0.0610	0.2311	0.0977	0.0520	0.0038	0.0161	0.0040	0.0009		1550	0.954
											1465	1.461
0.3025	0.2475	0.0659	0.1929	0.0801	0.0982	0.0016	0.0085		0.0028		1698	0.580
											1577	1.531
0.2473	0.2674	0.0582	0.2252	0.1309	0.0647	0.0008	0.0056				1696	0.681
											1649	0.914

Table B23
Klein et al. (1983) [66]

SiO_2	Al_2O_3	Fe_2O_3	FeO	Na_2O	Atm.	T	log η	T	log η
0.7948		0.0203	0.0083	0.1765	Air	886	7.905	834	9.105
						863	8.113	800	10.127
0.7763		0.0069	0.0043	0.2125		871	8.060	799	9.964
						827	9.218	763	11.291
0.7670	0.0510			0.1820		918	7.788	847	9.859
						901	8.297	826	10.396
						886	8.739	806	10.978
						869	9.203	787	11.781
0.7100	0.1120			0.1780		988	7.871	894	9.999
						970	8.230	861	11.020
						943	8.805	840	11.474
						912	9.456	811	12.274
0.7839	0.0110	0.0017	0.0027	0.2007		926	7.704	842	9.260
						902	7.840	815	10.120
						878	8.189	801	10.733
						864	8.727	782	11.421
0.7781	0.0252	0.0069	0.0044	0.1855		917	7.761	814	10.222
						894	8.096	795	10.925
						870	8.658	776	11.660
						855	9.150	767	11.733
						832	9.662		
0.7312	0.0505	0.0299	0.0123	0.1761		928	7.709	848	9.455
						911	7.908	820	10.581
						885	8.518	794	11.917
						863	9.108		
0.6317	0.0997	0.0725	0.0256	0.1705		926	9.699	871	10.120
						902	9.768	855	10.472
						886	9.873	834	11.189
0.7100	0.0495	0.0319	0.0248	0.1837	Forming gas	908	7.640	853	9.153
						892	8.064	805	10.391
						869	8.468	780	11.506
0.7060	0.0548	0.0133	0.0474	0.1785	w/carbon	917	7.557	818	10.215
						887	8.249	791	11.082
						866	8.764	784	11.419
						838	9.545	770	12.054
						825	9.993		

Table B24
Scarfe et al. (1983) [166]

SiO_2	Al_2O_3	CaO	MgO	T	log η	T	log η
0.3333	0.3333	0.3333		1898	0.333	1748	0.968
				1873	0.433	1723	1.101
				1848	0.513	1698	1.246
				1823	0.625	1673	1.402
				1798	0.711	1648	1.567
				1773	0.841		
0.5000		0.2500	0.2500	1873	−0.535	1723	−0.179
				1823	−0.441	1673	−0.008
				1773	−0.322	1648	0.086
0.4898	0.0203	0.2551	0.2348	1823	−0.352	1673	0.128
				1773	−0.200	1623	0.327
				1723	−0.043	1773	0.539
0.4788	0.0425	0.2606	0.2182	1873	−0.364	1673	0.237
				1823	−0.241	1623	0.442
				1773	−0.102	1573	0.660
				1723	0.057	1523	0.909
0.4505	0.0990	0.2748	0.1757	1873	−0.149	1623	0.721
				1823	−0.010	1548	1.134
				1773	0.146	1498	1.468
				1723	0.329	1448	1.859
				1673	0.518		
0.4386	0.1229	0.2807	0.1578	1873	−0.044	1623	0.854
				1823	0.074	1598	0.989
				1773	0.240	1573	1.132
				1723	0.432	1523	1.457
				1673	0.630	1473	1.846
0.4222	0.1556	0.2889	0.1333	1873	0.029	1673	0.756
				1823	0.194	1648	0.883
				1773	0.370	1623	1.015
				1723	0.553		
0.4039	0.1922	0.2981	0.1058	1873	0.179	1698	0.848
				1823	0.358	1673	0.980
				1773	0.531	1623	1.258
				1723	0.730	1573	1.575
0.3833	0.2334	0.3083	0.0750	1873	0.252	1723	0.836
				1823	0.434	1673	1.098
				1798	0.522	1623	1.384
				1773	0.625	1573	1.730
				1748	0.738	1523	2.140

Table B25
Williams et al. (1983) [138]

SiO_2	Fe_2O_3	FeO	CaO	MgO	T	log η	T	log η
0.3713	0.0087	0.6200			1623	−1.086	1523	−0.959
					1573	−1.022	1473	−0.495
0.3712	0.0039	0.2637	0.3612		1673	−0.839	1573	−0.796
					1623	−0.824	1523	−0.699
0.3082	0.0079	0.5656	0.1183		1673	−1.046	1523	−0.903
					1623	−0.979	1473	−0.854
					1573	−0.939	1423	−0.810
0.3622	0.0026	0.6030		0.0322	1673	−1.046	1573	−1.022
					1623	−1.036	1523	−0.979
0.3542	0.0105	0.4907	0.0242	0.1204	1673	−0.979	1573	−0.439
					1623	−0.854		
0.3489	0.0110	0.5200	0.0245	0.0956	1673	−0.764	1573	−0.602
					1623	−0.740		
0.2746	0.0152	0.4424	0.1710	0.0968	1673	−1.119	1523	−0.939
					1623	−1.076	1473	−0.553
					1573	−1.022		

Table B26
Schobert et al. (1982) [21]

SiO_2	Al_2O_3	Fe_2O_3	CaO	MgO	Na_2O	K_2O	TiO_2	SO_3	T	log η
0.4576	0.1435	0.0390	0.2061	0.0933	0.0320	0.0015	0.0094	0.0171	1517	2.257
									1534	2.093
									1548	1.934
									1575	1.563
									1579	1.510
									1593	1.200
									1607	1.058
									1613	1.138
									1624	1.002
									1640	0.920
									1677	0.752
0.4376	0.0900	0.0120	0.2842	0.1262	0.0370	0.0007	0.0109	0.0015	1445	2.379
									1453	1.884
									1456	1.475
									1483	1.117
									1554	0.735
									1565	0.659
									1579	0.605
									1593	0.547
									1607	0.480
0.4280	0.1314	0.0273	0.2233	0.0698	0.0929	0.0021	0.0176	0.0075	1426	2.434
									1429	2.329
									1431	2.033
									1444	1.502
									1487	1.163
									1506	1.021
									1528	0.860
									1554	0.728
0.4219	0.0967	0.0106	0.3273	0.1038	0.0201	0.0020	0.0156	0.0016	1437	2.336
									1445	1.798
									1453	1.433
									1470	1.217
									1495	1.064
									1540	0.757
									1551	0.673
									1567	0.558
									1585	0.446

Table B27
Shiraishi and Meister (1982) [17]

SiO_2	Al_2O_3	Fe_2O_3	FeO	TiO_2	CaO	MgO	Alk-O	T	log η	T	log η
0.8160	0.0844	0.0016	0.0098	0.0013	0.0095	0.0028	0.0746	1319	7.979	1301	8.140
								1314	8.030	1295	8.213
								1309	8.089	1287	8.303
								1304	8.147	1279	8.365
								1295	8.266	1273	8.433
								1290	8.327	1270	8.488
								1280	8.431	1265	8.534
								1274	8.523	1261	8.609
								1270	8.602	1257	8.671
								1264	8.658	1251	8.726
								1260	8.704	1246	8.810
								1255	8.790	1241	8.885
								1249	8.854	1234	8.968
								1244	8.915	1227	9.059
								1238	8.984	1221	9.122
								1232	9.058	1218	9.188
								1227	9.129	1210	9.285
								1221	9.204	1198	9.448
								1218	9.246	1189	9.504
								1212	9.314	1179	9.708
								1207	9.384	1175	9.752
								1204	9.435	1163	9.836
								1200	9.486		
								1193	9.512		
								1187	9.559		
								1184	9.585		
								1179	9.636		
0.8079	0.0936	0.0071	0.0078	0.0030	0.0142	0.0057	0.0607	1331	7.838	1251	8.926
								1324	7.929	1246	9.016
								1314	8.078	1241	9.082
								1309	8.129	1237	9.164
								1301	8.226	1232	9.206
								1296	8.290	1227	9.278
								1291	8.367	1223	9.336
								1286	8.433	1218	9.411
								1282	8.530	1213	9.457
								1275	8.598	1207	9.523
								1268	8.686	1202	9.642
								1262	8.774	1191	9.750
								1257	8.851	1185	9.763
0.6803	0.1209	0.0191	0.0197	0.0064	0.0699	0.0387	0.0449	1225	7.785	1246	7.633
								1222	7.845	1241	7.713
								1217	7.907	1237	7.794
								1213	7.966	1233	7.871
								1210	8.028	1228	7.983
								1205	8.078	1224	8.058
								1202	8.131	1219	8.170
								1196	8.129	1213	8.311
								1191	8.123	1209	8.395
								1186	8.118	1206	8.446
								1178	8.213	1202	8.529
								1171	8.288	1199	8.604
								1166	8.392	1195	8.661
								1160	8.517	1191	8.730
								1153	8.623	1171	8.745

(*continued on next page*)

Table B27 (*continued*)

SiO_2	Al_2O_3	Fe_2O_3	FeO	TiO_2	CaO	MgO	Alk-O	T	log η	T	log η
								1146	8.757	1166	8.708
								1142	8.865	1161	8.664
								1136	8.977	1153	8.768
								1125	9.116	1187	8.769
								1123	9.182	1178	8.796
								1115	9.286	1143	8.893
								1109	9.391	1136	9.017
								1105	9.446	1133	9.092
								1097	9.517	1128	9.155
										1121	9.266
										1117	9.332
										1111	9.420
										1106	9.486
										1093	9.568
0.5530	0.1093	0321	0.0395	0.0135	0.1083	0.1005	0.0438	1033	9.978	1133	9.584
								1038	9.721	1131	9.428
								1046	9.242	1127	9.340
								1051	8.991	1116	8.931
								1055	9.066	1111	8.771
								1061	9.148	1105	8.754
								1066	9.236	1099	8.793
								1073	9.313	1096	8.892
								1076	9.408	1087	8.996
								1082	9.498	1085	9.042
								1086	9.595	1081	9.111
								1091	9.685	1075	9.168
								1095	9.742	1073	9.236
								1102	9.835	1069	9.287
								1109	9.899	1067	9.326
								1113	9.963	1063	9.381
										1059	9.406
										1056	9.533
										1048	9.602
										1042	9.692
										1036	9.791
								1112	9.143	1056	8.564
								1107	8.958	1052	8.650
								1101	8.626	1049	8.709
								1098	8.450	1044	8.766
								1095	8.332	1042	8.832
								1089	8.275	1041	8.892
								1082	8.246	1037	8.951
								1074	8.297	1035	8.987
								1068	8.372	1029	9.057
								1064	8.440	1024	9.097
								1060	8.506		

Table B28
Urbain et al. (1982) [20]

SiO_2	Al_2O_3	Fe_2O_3	FeO	CaO	MgO	Na_2O	K_2O	MnO	T	log η	T	log η
1.0000									2755	2.526	1925	6.787
									2655	2.924	1872	7.082
									2541	3.365	1711	8.485
									2436	3.803	1648	8.971
									2334	4.246	1579	9.949
									2237	4.789	1523	10.405
									2143	5.362	1465	11.156
									2049	5.901		
0.9380	0.0620								2276	1.995	2076	3.017
									2226	2.230	2026	3.290
									2176	2.480	1976	3.590
									2126	2.732	1926	3.903
0.7980	0.2020								2275	0.431	2076	1.111
									2226	0.586	2026	1.301
									2176	0.751	1976	1.501
									2126	0.925	1926	1.715
0.5000	0.5000								2323	−0.864	2155	−0.516
									2278	−0.775	2153	−0.507
									2228	−0.670	2145	−0.489
									2177	−0.559	2126	−0.445
0.3000	0.7000								2477	−1.354	2276	−1.069
									2427	−1.292	2226	−0.987
									2376	−1.220	2176	−0.903
									2326	−1.145	2126	−0.818
0.4000			0.6000						1713	−1.276	1675	−1.222
									1711	−1.276	1658	−1.194
									1708	−1.268	1645	−1.181
									1705	−1.268	1640	−1.174
									1698	−1.252	1623	−1.143
0.3500			0.6500						1703	−1.469	1518	−1.252
									1675	−1.432	1465	−1.181
									1650	−1.409	1458	−1.168
									1578	−1.328	1443	−1.143
0.3330			0.6670						1685	−1.301	1571	−1.168
									1681	−1.310	1568	−1.161
									1679	−1.301	1566	−1.161
									1669	−1.292	1527	−1.108
									1648	−1.260	1505	−1.071
									1647	−1.268	1476	−1.032
									1601	−1.208	1439	−1.041
									1596	−1.201		
0.3000			0.7000						1688	−1.569	1575	−1.469
									1686	−1.586	1545	−1.432
									1684	−1.569	1541	−1.432
									1655	−1.552	1508	−1.398
									1652	−1.539	1481	−1.367
									1578	−1.482	1478	−1.357
0.2010		0.0040	0.7950						1733	−1.795	1678	−1.743
									1721	−1.769	1660	−1.721
									1710	−1.743	1655	−1.699
									1708	−1.743	1598	−1.656

(*continued on next page*)

Table B28 (*continued*)

SiO_2	Al_2O_3	Fe_2O_3	FeO	CaO	MgO	Na_2O	K_2O	MnO	T	log η	T	log η
									1685	−1.743	1583	−1.656
0.6800				0.3200					2245	−0.400	2084	−0.032
									2172	−0.245	2036	0.090
									2131	−0.146	1990	0.200
0.6240				0.3760					2176	−0.620	1976	−0.174
									2126	−0.520	1926	−0.049
									2076	−0.408	1875	0.076
									2026	−0.290	1825	0.230
0.5000				0.5000					2369	−1.547	2102	−1.141
									2312	−1.452	2038	−1.028
									2262	−1.372	1964	−0.885
									2211	−1.313	1919	−0.788
									2151	−1.219	1858	−0.642
0.4000				0.6000					2393	−1.786	2177	−1.530
									2329	−1.691	2151	−1.469
									2266	−1.621	2118	−1.434
									2240	−1.586	2084	−1.364
									2214	−1.539		
0.5860					0.4140				2220	−0.762	2100	−0.577
									2164	−0.708	2062	−0.491
									2164	−0.706	2047	−0.441
									2121	−0.614		
0.5000					0.5000				2268	−1.201	2104	−0.936
									2265	−1.191	2056	−0.828
									2209	−1.096	2054	−0.810
									2162	−1.020	2031	−0.769
									2157	−1.024	1987	−0.680
									2135	−0.976		
0.3490					0.6510				2461	−1.708	2384	−1.560
									2459	−1.699	2339	−1.604
									2456	−1.664	2335	−1.591
									2411	−1.660	2295	−1.552
									2409	−1.660	2293	−1.547
0.5000								0.5000	2020	−1.013	1969	−0.918
									2013	−1.017	1967	−0.908
									1986	−0.950	1928	−0.846
									1983	−0.936	1925	−0.816
									1977	−0.933	1922	−0.815
									1975	−0.932	1918	−0.812
									1973	−0.931	1864	−0.597
									1971	−0.924		
0.3120								0.6880	1909	−1.886	1766	−1.743
									1907	−1.856	1759	−1.721
									1893	−1.825	1753	−1.699
									1885	−1.856	1742	−1.677
									1867	−1.825	1719	−1.656
									1837	−1.825	1713	−1.656
									1812	−1.795	1705	−1.825
									1799	−1.795		
0.7500	0.1250			0.1250					2456	−0.008	2085	1.145
									2364	0.260	2016	1.416

Table B28 (*continued*)

SiO_2	Al_2O_3	Fe_2O_3	FeO	CaO	MgO	Na_2O	K_2O	MnO	T	log η	T	log η
									2329	0.331	1962	1.650
									2268	0.506	1890	1.991
									2200	0.728	1865	2.132
									2156	0.896	1798	2.469
0.5000	0.2500			0.2500					2449	−1.106	2062	−0.237
									2389	−0.989	2019	−0.098
									2330	−0.903	1972	0.045
									2284	−0.789	1939	0.135
									2233	−0.655	1901	0.293
									2187	−0.551	1868	0.431
									2149	−0.458	1829	0.582
									2089	−0.313		
0.5000	0.2000			0.3000					2176	−0.475	1926	0.152
									2126	−0.359	1875	0.295
									2076	−0.240	1825	0.446
									2026	−0.120		
									1976	0.017		
0.4440	0.1250			0.4310					1997	−0.702	1765	−0.152
									1984	−0.697	1754	−0.130
									1954	−0.639	1682	0.163
									1925	−0.565	1680	0.160
									1894	−0.512	1645	0.330
									1855	−0.404	1640	0.314
									1846	−0.410	1611	0.491
									1812	−0.282		
0.3720	0.2670			0.3610					1937	−0.479	1758	0.124
									1935	−0.480	1733	0.230
									1886	−0.283	1698	0.368
									1856	−0.165	1664	0.504
									1851	−0.158	1648	0.596
									1818	−0.058	1626	0.732
									1782	0.054	1578	0.943
									1764	0.124		
0.2507	0.3736			0.3756					2414	−1.456	2089	−0.898
									2341	−1.361	2041	−0.800
									2296	−1.287	1984	−0.635
									2231	−1.176	1938	−0.502
									2161	−1.069	1881	−0.333
									2110	−0.939		
0.7500	0.1250				0.1250				2388	0.010	2067	1.030
									2346	0.143	2022	1.214
									2285	0.289	1954	1.511
									2242	0.433	1906	1.732
									2188	0.590	1864	1.931
									2143	0.763	1803	2.229
0.5000	0.2500				0.2500				2372	−1.125	2067	−0.451
									2316	−1.020	2017	−0.306
									2256	−0.903	1963	−0.161
									2225	−0.822	1920	0.004
									2163	−0.714	1865	0.185
									2123	−0.585	1810	0.399
0.2500	0.3750				0.3750				2359	−1.412	2248	−1.255

(*continued on next page*)

Table B28 (*continued*)

SiO_2	Al_2O_3	Fe_2O_3	FeO	CaO	MgO	Na_2O	K_2O	MnO	T	log η	T	log η
									2331	−1.378	2214	−1.210
									2291	−1.321		
0.7500	0.1250					0.1250			2003	2.095	1761	3.625
									1993	2.288	1710	3.947
									1940	2.529	1682	4.190
									1924	2.641	1612	4.741
									1887	2.846	1565	5.206
									1856	2.969	1500	5.840
									1811	3.290	1433	6.505
0.7500	0.1250						0.1250		2098	1.884	1848	3.469
									2095	2.013	1818	3.751
									2067	2.072	1761	4.055
									2022	2.245	1716	4.385
									1948	2.702	1655	4.863
									1934	2.964	1615	5.223
									1854	3.412		
0.7610	0.1170							0.1220	2266	0.417	1999	1.402
									2248	0.473	1992	1.403
									2163	0.791	1957	1.537
									2152	0.815	1903	1.859
									2106	0.978	1887	1.880
									2098	0.986	1884	1.889
									2040	1.227	1880	1.900
									2033	1.237		
0.6200	0.1400							0.2400	2068	0.080	1881	0.707
									2063	0.092	1867	0.748
									1994	0.297	1849	0.834
									1971	0.378	1761	1.222
									1946	0.465	1739	1.388
									1939	0.487	1732	1.406
									1920	0.545	1696	1.459
									1915	0.570		
0.5900	0.2900							0.1200	1870	0.486	1826	0.586
									1866	0.451	1824	0.599
									1861	0.500	1820	0.614
									1858	0.500	1803	0.688
									1856	0.499	1802	0.690
									1854	0.504	1750	0.960
									1852	0.525	1745	0.973
									1849	0.548		
0.5490	0.2280							0.2230	2071	−0.523	1887	0.005
									2052	−0.503	1857	0.134
									2032	−0.409	1819	0.279
									2000	−0.328	1786	0.433
									1971	−0.237	1783	0.438
									1939	−0.119	1741	0.604
									1932	−0.114	1739	0.592
									1895	0.001		
0.4260	0.2900							0.2840	2104	−0.815	1902	−0.311
									2092	−0.796	1893	−0.306
									2031	−0.638	1886	−0.259
									2022	−0.622	1882	−0.250
									1964	−0.481	1871	−0.213

Table B28 (*continued*)

SiO_2	Al_2O_3	Fe_2O_3	FeO	CaO	MgO	Na_2O	K_2O	MnO	T	log η	T	log η
									1958	−0.476	1864	−0.193
									1933	−0.419	1836	−0.169
									1910	−0.336		
0.3800	0.1400							0.4800	1876	−0.496	1618	0.345
									1870	−0.487	1590	0.476
									1815	−0.352	1569	0.571
									1752	−0.164	1550	0.670
									1719	−0.032	1525	0.825
									1683	0.080	1493	0.976
									1640	0.273	1473	1.006
									1625	0.299		
0.3894		0.1842	0.0290	0.3974					1810	−1.153	1702	−0.978
									1806	−1.132	1684	−0.875
									1803	−1.062	1661	−0.843
									1784	−1.092	1641	−0.812
									1777	−1.094	1595	−0.732
									1769	−1.072	1567	−0.610
									1753	−1.008	1529	−0.469
									1721	−1.002		
0.3734		0.1191	0.1341	0.3734					1823	−1.235	1707	−1.122
									1802	−1.208	1664	−1.068
									1798	−1.196	1649	−1.003
									1783	−1.191	1595	−0.875
									1753	−1.172	1585	−0.854
									1736	−1.166	1578	−0.728
									1724	−1.159	1559	−0.723
									1717	−1.145		
0.3604		0.0811	0.1982	0.3604					1774	−1.304	1672	−1.037
									1763	−1.205	1658	−1.001
									1750	−1.155	1633	−0.974
									1726	−1.134	1566	−0.846
									1708	−1.151	1543	−0.797
									1698	−1.149	1517	−0.728
									1684	−1.119	1480	−0.640
									1675	−1.102		
0.5140				0.2570	0.2290				2312	−1.292	1945	−0.703
									2204	−1.157	1813	−0.399
									2130	−1.041	1675	0.064
									2054	−0.910		
0.6880	0.1560					0.1080	0.0480		1928	2.127	1821	2.803
									1912	2.308	1820	2.821
									1906	2.299	1808	2.893
									1901	2.316	1796	2.924
									1887	2.320	1784	3.000
									1868	2.476	1768	3.090
									1851	2.646	1762	3.140
									1839	2.731		

Table B29
Cranmer and Uhlmann (1981) [116]

SiO_2	Al_2O_3	CaO	Na_2O	T	log η	T	log η
0.7188	0.1397	0.0447	0.0968	1872	2.159	1529	4.391
				1831	2.389	1180	8.871
				1761	2.758	1157	9.269
				1710	3.081	1127	9.862
				1641	3.561	1109	10.157
				1599	3.875	1095	10.407
				1563	4.096	1075	11.190
0.6439	0.1779	0.1198	0.0585	1865	1.429	1668	2.404
				1848	1.453	1615	2.770
				1780	1.856	1569	3.156
				1756	1.924	1550	3.317
				1714	2.174		
0.5761	0.2085	0.1847	0.0308	1859	1.060	1790	1.353
				1842	1.115		

Table B30
El-Badry et al. (1981) [59]

SiO_2	CaO	MgO	Na_2O	K_2O	Li_2O	T	log η	T	log η
0.6074			0.3926			774	7.849	711	11.245
						747	9.004	698	12.199
						724	10.509	674	13.858
						716	10.998		
0.6541			0.3459			753	9.501	716	11.442
						740	10.374	698	12.579
						732	10.522		
0.7025			0.2975			774	9.507	724	11.803
						757	10.110	713	12.394
						740	10.948	699	13.502
						734	11.147		
0.7443				0.2557		873	7.516	775	11.402
						824	9.512	726	13.032
0.7853				0.2147		873	8.206	775	11.718
						824	10.023	726	13.568
0.8247				0.1753		874	8.441	775	12.051
						825	10.493		
0.6995					0.3005	782	9.318	760	10.399
						775	9.733	740	11.505
0.6795					0.3205	776	9.296	762	9.922
						768	9.588	747	10.726
						766	9.700		
0.6655					0.3345	769	9.354	738	11.009
						763	9.592	735	11.160
0.6381					0.3619	775	8.825	747	10.329
						769	9.079	745	10.473
						751	10.123		

Table B30 (*continued*)

SiO_2	CaO	MgO	Na_2O	K_2O	Li_2O	T	log η	T	log η
0.5823	0.0250		0.3927			870	1.076	709	9.992
						820	3.404	694	10.993
						770	6.058	662	12.297
						723	9.014		
0.5576	0.0499		0.3925			869	0.541	706	9.248
						820	3.009	661	11.460
						770	5.849	644	12.414
0.5321	0.0749		0.3930			871	3.611	725	9.921
						823	5.497	710	10.736
						772	7.639	677	12.691
0.5069	0.1002		0.3929			865	3.309	743	8.920
						812	5.474	676	12.110
						769	7.872		
0.4846		0.5025	0.0130			876	5.169	717	10.778
						828	6.649	711	11.087
						779	8.389	706	11.298
						730	10.258	681	12.444
						726	10.413		
0.4672		0.5065	0.0264			877	4.043	720	9.984
						807	6.960	715	10.398
						731	9.740	701	11.250
0.4496		0.5106	0.0398			874	3.460	718	9.798
						827	5.353	693	10.870
						779	7.263	674	11.715
						728	9.303		
0.4316		0.5148	0.0536			870	3.574	775	7.069
						825	5.232	726	9.125

Table B31
Klein et al. (1981) [65]

SiO_2	Fe_2O_3	Na_2O	Atm.	T	log η	T	log η
0.8000		0.2000	Forming gas	890	8.170	799	10.418
				829	9.578	781	10.941
				814	9.944	751	12.149
0.8026	0.0863	0.1111		905	8.543	813	10.931
				862	9.631	797	11.603
				855	9.714	773	12.413
				844	10.004	768	12.480
0.7903	0.0073	0.2024		866	8.435	765	11.377
				837	9.075	719	13.260
0.7760	0.0187	0.2053		829	8.962	767	10.963
				797	9.892	742	11.956
				772	10.755		
0.7515	0.0404	0.2081		839	8.637	786	10.166
				807	9.433	746	11.809
0.7475	0.0387	0.2139		835	8.615	769	10.622
				794	9.755	725	12.672
0.7409	0.1394	0.1197		896	8.253	813	10.197
				866	8.853	764	11.974
				825	9.877	746	12.809
0.6903	0.0866	0.2231		837	8.006	783	10.612
				822	8.425	771	10.178
				801	9.032	740	11.571
0.6871	0.0832	0.2298		857	8.125	778	10.170
				788	9.752	717	12.897
0.6198	0.1399	0.2403		793	9.037	753	10.597
				775	9.532	716	12.476
0.7903	0.0073	0.2024	Air	853	8.783	775	11.002
				820	9.545	756	11.739
				787	10.598	731	12.877
			Carbon	846	8.669	782	10.487
				831	8.976	743	12.087
				812	9.595	740	12.223
				799	9.934	726	12.668
			Forming gas	865	8.413	764	11.360
				838	9.061	720	13.272
0.7760	0.0187	0.2053	Air	870	8.038	764	11.281
				827	9.095	746	12.103
				800	9.931	736	12.402
			Carbon	816	9.045	720	12.623
				786	10.004	715	12.989
				763	11.017		
			Forming gas	849	8.152	785	10.163
				834	8.599	745	11.882
				805	9.409		
0.7475	0.0387	0.2139	Air	885	7.932	800	10.102
				864	8.165	753	12.037
				833	9.089	740	12.548
			Carbon	840	8.259	768	10.637
				826	8.737	749	11.457

Table B31 (*continued*)

SiO_2	Fe_2O_3	Na_2O	Atm.	T	log η	T	log η
				800	9.296	724	12.666
			Forming gas	834	8.589	775	10.358
				794	9.750	726	12.656
0.6871	0.0832	0.2298	Air	877	8.133	782	10.472
				820	9.172	758	11.567
				801	9.871	745	12.300
			Carbon	835	7.947	745	10.843
				813	8.578	726	12.100
				782	9.276	717	12.340
				764	9.830		
			Forming gas	855	8.100	777	10.154
				789	9.747	717	12.888

Table B32
Piwinskii and Weed (1980) [81]

SiO_2	Al_2O_3	Fe_2O_3	TiO_2	CaO	MgO	Na_2O	K_2O	T	log η	T	log η
0.8381	0.0524	0.0078	0.0044	0.0579	0.0237	0.0054	0.0102	1626	2.571	1485	3.437
								1583	2.782	1422	3.936
								1524	3.171		
0.8246	0.0943	0.0047	0.0023	0.0071	0.0146	0.0261	0.0262	1805	3.168	1627	4.103
								1763	3.294	1579	4.444
								1722	3.540	1543	4.725
								1682	3.798		
0.7978	0.0997	0.0133	0.0044	0.0048	0.0040	0.0508	0.0252	1814	2.561	1632	3.583
								1770	2.778	1585	3.870
								1717	3.120	1567	3.970
								1674	3.360	1512	4.277
0.7611	0.1418	0.0056	0.0027	0.0084	0.0173	0.0321	0.0310	1808	2.992	1689	3.616
								1768	3.283	1648	3.772
								1729	3.447		
0.7436	0.1286	0.0140	0.0088	0.0094	0.0099	0.0563	0.0294	1583	1.825	1431	3.293
								1540	2.091	1390	3.536
								1466	2.785		
0.6484	0.1139	0.0198	0.0133	0.0888	0.0694	0.0363	0.0102	1961	2.820	1844	3.395
								1944	2.870	1808	3.607
								1904	3.142	1761	3.897
								1866	3.351		

Table B33
Krauss (1979) [167]

SiO_2	Al_2O_3	FeO	CaO	MgO	MnO	P_2O_5	T	log η	T	log η
0.2852	0.0059	0.0815	0.4789	0.0404	0.0995	0.0085	1898	−0.557	1751	−0.128
							1879	−0.466	1727	−0.032
							1851	−0.407	1702	0.125
							1825	−0.335	1677	0.353
							1806	−0.257	1657	0.535
							1779	−0.188	1646	0.641

Table B34
Segers et al. (1979) [168]

SiO2	CaO	MnO	T	log η
0.5000	0.3300	0.1700	1773	1.554
	0.1400	0.3600		1.457
	0.0910	0.4090		1.426
0.4500	0.4660	0.0840		1.284
	0.3790	0.1710		1.400
	0.2880	0.2620		1.176
	0.1940	0.3560		1.174
		0.5500		1.004
0.4000	0.4730	0.1270		1.123
	0.3840	0.2160		1.257
	0.3400	0.2600		1.044
	0.3000	0.3000		0.912
	0.2450	0.3550		0.903
	0.1450	0.4550		0.906
		0.6000		0.906
0.3500	0.3440	0.3060		0.962
	0.1960	0.4540		0.773
	0.0940	0.5560		0.649

Table B35
Bodnár et al. (1978) [70]

SiO_2	Al_2O_3	Fe_2O_3	FeO	CaO	MgO	T	log η	T	log η
0.4405			0.5595			1673	−0.886	1523	−0.553
						1623	−0.886	1473	−0.310
						1573	−0.824		
0.4323		0.0754	0.4923			1674	−0.587	1577	−0.210
						1655	−0.572	1516	−0.015
						1621	−0.484		
0.4310		0.0263	0.5426			1573	−0.570		
0.4069		0.0808	0.5123				−0.186		
0.3985		0.0998	0.5017				−0.044		
0.3929		0.1125	0.4946				0.036		
0.3863		0.0701	0.5437				−0.841		
0.3787		0.0884	0.5330				−0.794		
0.3763		0.0939	0.5297				−0.729		
0.3716		0.1053	0.5231				−0.639		
0.3678		0.1146	0.5177				−0.593		
0.3204		0.0544	0.6252				−0.519		
0.3114		0.0808	0.6077				−0.401		
0.3042		0.1021	0.5937				−0.383		
0.3006		0.1127	0.5867				−0.271		
0.2932		0.1346	0.5722				−0.089		
0.2383		0.0740	0.6877				−0.998		
0.2354		0.0850	0.6796				−0.900		
0.2308		0.1031	0.6661				−0.874		
0.2233		0.1321	0.6446				−0.512		
0.2217		0.1384	0.6399				−0.394		
0.4348			0.3242	0.2409		1673	−0.678	1523	−0.398
						1623	−0.638	1473	−0.237
						1573	−0.509		
0.4213		0.0734	0.4798	0.0255		1675	−0.665	1532	−0.480
						1656	−0.656	1512	−0.423
						1616	−0.596		
0.4109		0.0716	0.4679	0.0497		1657	−0.788	1537	0.032
						1608	−0.528	1533	−0.037
						1577	−0.115	1514	0.119
0.4009		0.0699	0.4565	0.0727		1674	−0.905	1576	−0.587
						1652	−1.028	1534	−0.382
						1615	−0.821	1513	−0.344
0.3418		0.0490	0.4647	0.1445		1638	−0.588	1554	−0.481
						1621	−0.589	1532	−0.505
						1606	−0.579	1518	−0.385
						1590	−0.625	1503	−0.302
						1576	−0.629	1478	−0.384
						1563	−0.580		
0.3244		0.0465	0.4411	0.1371	0.0509	1639	−0.479	1563	−0.303
						1618	−0.439	1554	−0.274
						1605	−0.466	1534	−0.150
						1590	−0.434	1521	−0.013
						1576	−0.412	1504	0.176
0.3077		0.0441	0.4184	0.1301	0.0996	1639	−0.263	1566	0.046
						1622	−0.218	1556	0.152
						1608	−0.175	1536	0.285

(*continued on next page*)

Table B35 (*continued*)

SiO_2	Al_2O_3	Fe_2O_3	FeO	CaO	MgO	T	log η	T	log η
						1593	−0.140	1506	0.339
						1575	−0.042		
0.2918		0.0418	0.3967	0.1233	0.1463	1643	0.207	1595	0.266
						1627	0.218	1582	0.296
						1614	0.228	1556	0.327
0.4064		0.3796		0.1124	0.1016	1456	0.368	1533	−0.295
						1476	0.191	1553	−0.597
						1495	−0.071	1572	−1.272
						1514	−0.149	1592	−1.307
0.4041		0.3784		0.1585	0.0591	1593	−0.749	1513	−0.577
						1572	−0.697	1494	−0.169
						1553	−0.662	1474	0.047
						1533	−0.644	1454	0.192
0.3941		0.3682		0.1392	0.0985	1456	0.199	1532	−0.763
						1475	0.068	1552	−0.794
						1494	−0.202	1572	−0.828
						1513	−0.578	1592	−0.840
0.3880		0.3633		0.1522	0.0965	1592	−0.679	1513	−0.529
						1572	−0.630	1494	−0.122
						1553	−0.604	1474	0.183
						1533	−0.588	1455	0.383
0.3880		0.3625		0.1525	0.0970	1457	0.383	1553	−0.638
						1475	0.176	1572	−0.672
						1494	−0.127	1592	−0.714
						1533	−0.594		
0.3820		0.3569		0.1656	0.0955	1457	0.391	1532	−0.416
						1475	0.056	1552	−0.481
						1493	−0.310	1572	−0.493
						1513	−0.417	1593	−0.496
0.3726		0.3488		0.1461	0.1325	1593	−0.360	1535	0.276
						1574	−0.055	1515	0.295
						1554	0.262	1495	0.457
0.3701		0.3458		0.1916	0.0925	1496	0.386	1555	0.123
						1515	0.211	1574	0.123
						1535	0.145	1595	0.122
0.3577		0.3349		0.1403	0.1672	1593	0.017	1555	0.297
						1574	0.112	1535	0.472
0.3011		0.0605	0.5136	0.1224	0.0024	1573	−0.824		
0.2867		0.0576	0.4891	0.1166	0.0500	1573	−0.571		
0.3411		0.0489	0.4638	0.1442	0.0020	1573	−0.617		
0.3251		0.0466	0.4420	0.1374	0.0489	1573	−0.443		
0.3087		0.0443	0.4198	0.1305	0.0967	1573	−0.214		
0.2933		0.0420	0.3988	0.1240	0.1419	1573	0.225		
0.4126		0.0319	0.4050	0.1454	0.0052	1573	−0.638		
0.3948		0.0305	0.3876	0.1392	0.0479	1573	−0.830		
0.3757		0.0290	0.3688	0.1324	0.0940	1573	−0.430		
0.3571		0.0276	0.3505	0.1258	0.1390	1573	−0.088		
0.3274	0.0034	0.0959	0.3502	0.1296	0.0935	1573	−0.539		
0.3141	0.0032	0.1328	0.3359	0.1243	0.0897	1573	−0.424		
0.3126	0.0032	0.1369	0.3343	0.1237	0.0893	1573	−0.451		

Table B35 (*continued*)

SiO_2	Al_2O_3	Fe_2O_3	FeO	CaO	MgO	T	log η	T	log η
0.3113	0.0032	0.1406	0.3329	0.1232	0.0889	1573	−0.354		
0.3110	0.0032	0.1413	0.3326	0.1231	0.0889	1573	−0.291		
0.3097	0.0032	0.1449	0.3312	0.1226	0.0885	1573	−0.138		
0.3093	0.0032	0.1460	0.3308	0.1224	0.0884	1573	0.244		
0.3093	0.0032	0.1461	0.3307	0.1224	0.0884	1573	0.052		
0.3020	0.0031	0.1661	0.3230	0.1195	0.0863	1573	0.411		
0.3434	0.0066	0.0926	0.3163	0.1395	0.1017	1573	−0.581		
0.3280	0.0063	0.1334	0.3020	0.1332	0.0971	1573	−0.653		
0.3254	0.0062	0.1402	0.2997	0.1322	0.0963	1573	−0.249		
0.3254	0.0062	0.1404	0.2996	0.1321	0.0963	1573	−0.476		
0.3241	0.0062	0.1436	0.2985	0.1316	0.0959	1573	0.001		
0.3143	0.0060	0.1696	0.2894	0.1276	0.0930	1573	0.099		

Table B36
Shiraishi et al. (1978) [169]

SiO_2	Fe_2O_3	FeO	Fe	T	log η	T	log η
	0.0585	0.9314	0.0100	1673	−1.721		
0.4176	0.0032	0.5715	0.0078	1673	−1.036	1573	−0.845
				1623	−0.936	1523	−0.742
0.3672	0.0081	0.6162	0.0084	1673	−1.222	1573	−1.076
				1623	−1.131	1523	−1.009
0.3616	0.0077	0.6210	0.0098	1673	−1.301	1573	−1.180
				1623	−1.244	1523	−1.114
0.3579	0.0066	0.6252	0.0102	1673	−1.328	1573	−1.229
				1623	−1.284	1523	−1.180
0.3400	0.0100	0.6393	0.0107	1673	−1.319	1573	−1.222
				1623	−1.276	1523	−1.367
0.3323	0.0098	0.6465	0.0114	673	−1.337	1573	−1.208
				1623	−1.284		
0.3297	0.0086	0.6507	0.0110	1673	−1.328	1573	−1.194
				1623	−1.268	1523	−1.119
0.3232	0.0088	0.6563	0.0117	1673	−1.387	1573	−1.284
				1623	−1.337		
0.3145	0.0058	0.6681	0.0115	1673	−1.432	1573	−1.367
				1623	−1.398		
0.2495	0.0191	0.7192	0.0122	1673	−1.569	1573	−1.523
				1623	−1.538	1523	−1.509
0.1189	0.0300	0.8403	0.0107	1673	−1.658	1623	−1.620

Table B37
Yakushev et al. (1977) [72]

SiO_2	Al_2O_3	CaO	MgO	T	log η	T	log η
0.4380		0.5620		1991	0.585	1822	2.541
				1968	0.744	1796	3.143
				1923	1.127	1764	4.204
				1870	1.722	1750	4.801
				1847	2.106	1736	5.403
0.3039	0.1194	0.4559	0.1208	1970	0.970	1852	2.688
				1941	1.301	1820	3.449
				1901	1.825		
0.3015	0.1036	0.4900	0.1049	1982	0.736	1869	2.230
				1957	0.998	1835	2.887
				1914	1.516	1780	4.490
0.2564	0.1511	0.4396	0.1529	1991	0.753	1871	2.323
				1973	0.861	1833	3.091
				1949	1.136	1815	3.590
				1933	1.331	1792	4.359
				1901	1.778		
0.2514	0.1111	0.5251	0.1124	1989	0.432	1848	1.993
				1960	0.642	1833	2.531
				1931	0.909	1816	3.781
				1901	1.217	1806	4.515
				1877	1.450	1793	5.559
0.2012	0.1347	0.5006	0.1363	1985	0.549	1836	2.439
				1958	0.755	1814	2.898
				1933	1.019	1768	3.842
				1896	1.517	1747	4.662
				1866	1.947		
0.2012	0.1266	0.5971	0.0613	1976	0.604	1882	2.698
				1962	0.723	1873	3.583
				1935	0.996	1865	4.639
				1905	1.402	1859	5.851
				1892	1.987		
0.2012	0.1869	0.4757	0.1261	1988	0.598	1884	1.807
				1967	0.786	1869	2.041
				1939	1.082	1845	2.532
				1919	1.356	1813	3.230
0.2012	0.1185	0.5604	0.1200	1995	0.330	1991	0.312
				1972	0.483	1970	0.482
				1931	0.772	1928	0.771
				1898	1.154	1894	1.118
				1872	1.508	1868	1.472
				1842	3.453	1843	3.474
				1831	4.929	1831	4.931
0.2012	0.1347	0.5006	0.1363	1990	0.370	1870	1.474
				1972	0.490	1841	3.438
				1933	0.787	1830	4.960
				1897	1.124		
0.1880	0.1108	0.5252	0.1761	1987	0.231	1854	1.937
				1959	0.435	1846	4.063
				1921	0.685	1838	5.349
				1873	1.255		

Table B37 (*continued*)

SiO_2	Al_2O_3	CaO	MgO	T	log η	T	log η
0.1855	0.1873	0.5166	0.1106	1992	0.525	1837	2.700
				1974	0.719	1811	3.238
				1952	0.912	1805	3.473
				1916	1.397	1756	5.204
				1873	1.985	1738	6.098
0.1743	0.1027	0.6190	0.1039	1979	0.138	1879	2.312
				1952	0.350	1874	2.981
				1920	0.560	1867	3.673
				1900	0.795	1859	4.752
				1889	1.297		
0.1680	0.2640	0.4679	0.1002	1992	1.076	1879	3.008
				1972	1.350	1857	3.581
				1949	1.687	1817	4.669
				1918	2.242	1785	6.091
0.1509	0.1257	0.5960	0.1275	1985	0.110	1848	1.023
				1952	0.216	1835	1.538
				1910	0.425	1829	2.146
				1863	0.760	1826	4.253

Table B38
Lakatos et al. (1972) [73]

SiO_2	Al_2O_3	CaO	MgO	Na_2O	K_2O	T	log η	T	log η
0.7468	0.0034	0.0834	0.0229	0.1434		1732	1.000	1310	3.000
						1477	2.000	1191	4.000
0.7439	0.0034	0.0953	0.0136	0.1439		1728	1.000	1305	3.000
						1469	2.000	1193	4.000
0.7422	0.0034	0.1140	0.0003	0.1400		1708	1.000	1289	3.000
						1454	2.000	1174	4.000
0.7723	0.0012	0.1087		0.1169	0.0008	1625	1.500	850	11.500
						1021	6.500		
0.7221	0.0130	0.0972		0.1375	0.0302	1564	1.500	817	11.500
						983	6.500		
0.6902	0.0251	0.1239		0.1451	0.0157	1544	1.500	839	11.500
						995	6.500		
0.6857	0.0137	0.1334		0.1246	0.0426	1513	1.500	833	11.500
						985	6.500		
0.7312	0.0120	0.1204	0.0098	0.1261	0.0005	1600	1.500	855	11.500
						1021	6.500		
0.7257	0.0132	0.1099	0.0117	0.1226	0.0168	1596	1.500	839	11.500
						1009	6.500		
0.7236	0.0129	0.1085	0.0298	0.1092	0.0160	1616	1.500	848	11.500
						1024	6.500		
0.7122	0.0142	0.0903	0.0194	0.1192	0.0446	1579	1.500	818	11.500
						989	6.500		
0.6979	0.0131	0.1186	0.0336	0.1365	0.0003	1554	1.500	843	11.500
						1005	6.500		
0.6966	0.0323	0.0961	0.0350	0.1250	0.0150	1617	1.500	848	11.500
						1023	6.500		
0.6938	0.0010	0.1388	0.0163	0.1344	0.0157	1510	1.500	838	11.500
						990	6.500		
0.6920	0.0021	0.1275	0.0324	0.1176	0.0284	1517	1.500	832	11.500
						987	6.500		
0.6914	0.0326	0.1063	0.0189	0.1507	0.0001	1591	1.500	850	11.500
						1014	6.500		
0.6905	0.0441	0.1290	0.0098	0.1264	0.0002	1625	1.500	882	11.500
						1045	6.500		
0.6901	0.0203	0.1168	0.0183	0.1264	0.0281	1554	1.500	838	11.500
						996	6.500		
0.6898	0.0117	0.0964	0.0264	0.1469	0.0286	1522	1.500	809	11.500
						970	6.500		
0.6895	0.0241	0.1431	0.0276	0.1154	0.0001	1581	1.500	876	11.500
						1037	6.500		
0.6880	0.0242	0.1056	0.0330	0.1082	0.0410	1588	1.500	841	11.500
						1012	6.500		
0.6879	0.0365	0.1321	0.0114	0.1058	0.0264	1598	1.500	869	11.500
						1033	6.500		

(*continued on next page*)

Table B38 (*continued*)

SiO_2	Al_2O_3	CaO	MgO	Na_2O	K_2O	T	log η	T	log η
0.6872	0.0439	0.0954	0.0186	0.1145	0.0404	1623 1018	1.500 6.500	842	11.500
0.6868	0.0023	0.1157	0.0082	0.1452	0.0418	1479 956	1.500 6.500	806	11.500
0.6862	0.0000	0.1055	0.0257	0.1258	0.0569	1501 963	1.500 6.500	805	11.500
0.6860	0.0501	0.1158	0.0258	0.1076	0.0147	1660 1057	1.500 6.500	881	11.500
0.6848	0.0136	0.1233	0.0192	0.1048	0.0543	1534 994	1.500 6.500	832	11.500
0.6846	0.0442	0.1056	0.0000	0.1363	0.0293	1596 1006	1.500 6.500	844	11.500
0.6814	0.0220	0.0956	0.0110	0.1356	0.0544	1536 972	1.500 6.500	811	11.500
0.6568	0.0311	0.1168	0.0265	0.1278	0.0411	1537 992	1.500 6.500	834	11.500
0.6519	0.0139	0.1133	0.0334	0.1358	0.0518	1483 962	1.500 6.500	809	11.500
0.6213	0.0414	0.1228	0.0308	0.1331	0.0506	1507 983	1.500 6.500	828	11.500
0.6132	0.0298	0.1015	0.1015	0.1033	0.0506	1565 998	1.500 6.500	835	11.500

Table B39
Skryabin and Novokhatskii (1972) [88]

SiO_2	Al_2O_3	Fe_2O_3	CaO	MgO	$Na_2O + K_2O$	TiO_2	SO_3	Argon		CO_2	
								T	log η	T	log η
0.6437	0.1264		0.2299					1923	0.9861	1923	1.2856
								1898	1.1659	1899	1.4140
								1873	1.2705	1873	1.5434
								1849	1.4460	1849	1.7584
								1824	1.6169	1825	2.0261
								1799	1.7813		
								1774	2.0386		
0.4226	0.1245		0.4528					1924	−0.1353	1923	−0.1980
								1899	−0.0731	1899	−0.1437
								1873	−0.0124	1873	−0.0731
								1823	0.0352	1848	0.0180
								1798	0.1030	1823	0.1078
								1773	0.1573	1798	0.1822
								1748	0.2056	1774	0.2593
								1724	0.2726	1748	0.3306
								1699	0.3529	1722	0.4320
								1673	0.4498	1699	0.5432
										1673	0.6633
0.1929	0.1642		0.6429					1923	−0.7741	1923	−0.5559
								1899	−0.7441	1898	−0.5375
								1873	−0.6582	1873	−0.4474
								1823	−0.5249	1823	−0.3341
								1798	−0.4709	1798	−0.2430
								1773	−0.2603	1773	−0.1260
								1747	0.0373	1748	0.0482
										1723	0.3231
										1698	0.5772
0.7623	0.0019		0.0954		0.1357		0.0048	1924	0.5277	1924	0.3940
								1899	0.5514	1899	0.4806
								1873	0.6229	1873	0.5418
								1848	0.6842	1848	0.6332
								1798	0.9256	1823	0.7974
								1773	1.0922	1799	0.9776
								1748	1.2332	1773	1.1669
								1723	1.3448	1748	1.3193
								1698	1.4757	1723	1.4995
0.7311	0.0118	0.0003	0.0700	0.0625	0.1200	0.0004	0.0038	1924	0.4373	1924	0.3395
								1898	0.5187	1898	0.3597
								1873	0.5767	1873	0.4410
								1847	0.6726	1848	0.5451
								1823	0.7718	1823	0.6474
								1798	0.9568	1799	0.7150
								1773	1.0828	1773	0.8059
								1748	1.2085	1748	0.9835
								1723	1.3364	1723	1.0770
								1673	1.5756	1673	1.3687

Table B40
Shvaiko-Shvaikovskaya et al. (1971) [170]

SiO_2	Na_2O	T	log η	T	log η
0.8500	0.1500	1773	1.250	1473	2.540
		1673	1.610	1373	3.150
		1573	2.010		
0.8240	0.1760	1773	0.960	1473	2.120
		1673	1.290	1373	2.700
		1573	1.640		
0.8020	0.1980	1673	1.120	1373	2.350
		1573	1.460	1273	3.000
		1473	1.850		
0.7490	0.2510	1573	1.160	1273	2.640
		1473	1.580	1173	3.340
		1373	2.080		
0.6900	0.3100	1473	1.260	1273	2.280
		1373	1.680	1173	2.940
0.6640	0.3360	1473	1.130	1273	2.110
		1373	1.560	1173	2.760
0.6380	0.3620	1473	1.000	1273	1.940
		1373	1.400	1173	2.580
0.5930	0.4070	1473	0.700	1273	1.560
		1373	1.080	1173	2.080

Table B41
Taylor and Rindone (1970) [78]

SiO_2	Al_2O_3	Na_2O	T	log η	T	log η
0.7500		0.2500	790	9.405	751	11.401
			790	9.360	750	11.480
			776	10.218	738	12.107
			775	10.317	737	12.161
	0.1250	0.1250	1146	10.769	1100	11.889
			1146	10.735	1097	11.951
			1124	11.228	1086	12.219
	0.1125	0.1375	1041	9.731	998	10.708
			1041	9.692	964	11.696
			1012	10.354	939	12.482
			1011	10.390	937	12.532
			999	10.781		
	0.0938	0.1563	933	9.549	852	12.263
			901	10.473	851	12.303
			879	11.185		
	0.0625	0.1875	874	9.162	845	10.136
			872	9.212	818	11.118
			847	10.085	804	11.681
	0.0313	0.2188	818	9.652	777	11.240
			800	10.303	762	11.969
0.7333	0.0333	0.2333	817	9.413	777	10.811
			815	9.495	777	10.843
			811	9.571	744	12.398
			799	10.039	744	12.448
			798	10.077		
0.7143	0.0714	0.2143	870	9.494	817	11.322
			868	9.435	816	11.284
			836	10.597	802	11.940
0.6970	0.1061	0.1970	921	9.300	867	10.951
			920	9.332	842	12.052
			895	10.194	841	12.096
			892	10.156		
0.6774	0.1452	0.1774	1038	9.390	997	10.237
			1036	9.431	990	10.613
			1003	10.264	987	10.578
			1002	10.310	953	11.501
0.6667	0.1667	0.1667	1193	8.819	1112	10.397
			1193	8.775	1088	10.971
			1141	9.800	1085	11.064
			1140	9.852	1078	11.215
			1114	10.348	1073	11.425
0.6610	0.1780	0.1610	1195	9.466	1111	11.222
			1192	9.518	1101	11.408
			1142	10.354	1100	11.662
			1139	10.692	1086	12.005
			1135	10.645	1084	11.935
			1113	11.292		
0.6552	0.1897	0.1552	1198	9.326	1118	11.178
			1193	9.402	1114	11.143
			1139	10.561	1088	11.970
			1138	10.730	1088	11.900
0.6429	0.2143	0.1429	1192	9.017	1113	10.930
			1192	9.049	1095	11.431
			1135	10.339	1088	11.796
			1115	10.887	1087	11.755
0.6296	0.2407	0.1296	1139	10.182	1088	11.583
			1095	11.300	1086	11.632
			1092	11.347		

Table B42
Boow (1969) [171]

SiO_2	Al_2O_3	Fe_2O_3	CaO	MgO	Na_2O	K_2O	TiO_2	P_2O_5	SO_3	T	log η
0.6247	0.1841		0.1912							1933	1.000
										1353	5.000
										1273	6.000
0.7924	0.1041	0.0572	0.0036	0.0161	0.0104	0.0069	0.0043	0.0013	0.0035	1973	1.000
										1773	2.000
										1613	3.000
										1468	4.000
										1343	5.000
										1253	6.000
										1198	7.000
										1153	8.000
0.6153	0.2159	0.0557	0.0443	0.0236	0.0063	0.0155	0.0109	0.0005	0.0120	1773	1.000
										1433	5.000
0.5587	0.2045	0.0534	0.0611	0.0108	0.0133	0.0038	0.0175	0.0051	0.0718	1713	1.000
										1323	4.000
										1243	5.000
										1173	6.000
										1133	7.000
										1093	8.000
0.5470	0.1646	0.0315	0.0859	0.0445	0.0523	0.0073	0.0168	0.0030	0.0471	1738	1.000
										1538	2.000
										1413	3.000
										1323	4.000
										1253	5.000
										1188	6.000
										1133	7.000
										1083	8.000
0.5374	0.2342	0.0289	0.0749	0.0395	0.0539	0.0112	0.0161	0.0037	0.0002	1723	1.000
										1363	4.000
										1248	5.000
										1163	6.000
										1093	7.000
										1048	8.000
0.5360	0.1789	0.0436	0.1545	0.0431	0.0039	0.0041	0.0105	0.0051	0.0203	1658	1.000
										1518	2.000
										1413	3.000
										1323	4.000
										1253	5.000
										1188	6.000
										1128	7.000
										1073	8.000
0.4976	0.2405	0.0597	0.0439	0.0669	0.0339	0.0047	0.0181	0.0054	0.0293	1718	1.000
										1568	2.000
										1448	3.000
										1353	4.000
										1263	5.000
										1203	6.000
										1153	7.000
0.4288	0.1849	0.0508	0.0981	0.0335	0.0602	0.0019	0.0180	0.0074	0.1163	1613	1.000
										1478	2.000
										1353	3.000
										1263	4.000

(*continued on next page*)

Table B42 (*continued*)

SiO_2	Al_2O_3	Fe_2O_3	CaO	MgO	Na_2O	K_2O	TiO_2	P_2O_5	SO_3	T	log η
										1183	5.000
										1118	6.000
										1073	7.000
										1038	8.000
0.6203	0.1685	0.0299	0.0493	0.0370	0.0336	0.0138	0.0153	0.0047	0.0276	1873	1.000
										1638	2.000
										1493	3.000
										1373	4.000
										1308	5.000
										1203	6.000
										1143	7.000
										1108	8.000

Table B43
Kato and Minowa (1969) [25]

SiO_2	Al_2O_3	FeO	CaO	MgO	MnO	TiO2	XCl_2	T	log η	T	log η
0.5850	0.0624		0.3526					1739	−0.241	1674	0.069
								1705	−0.082	1658	0.139
								1697	−0.048	1652	0.171
								1682	0.021		
0.5589	0.0931		0.3480					1746	−0.175	1682	0.118
								1718	−0.075	1665	0.282
0.5280	0.0880		0.3840					1745	−0.189	1666	0.205
								1726	−0.064	1657	0.270
								1692	0.105	1638	0.413
0.5140	0.0731		0.4129					1624	0.458	1612	0.669
								1622	0.509		
0.4430	0.0840		0.4730					1739	−0.241	1674	0.069
								1705	−0.082	1658	0.139
								1697	−0.048	1652	0.171
								1682	0.021		
0.4170	0.0877		0.4953					1775	−0.585	1726	−0.429
								1748	−0.501	1693	−0.226
0.4150	0.1410		0.4440					1774	−0.145	1677	0.375
								1758	−0.112	1638	0.731
								1708	0.116	1626	0.862
								1690	0.191		
0.4026	0.0764		0.5210					1766	−0.511	1693	−0.274
								1744	−0.431	1685	−0.238
								1716	−0.349	1670	−0.170
0.3841	0.2050		0.4109					1775	−0.080	1709	0.357
								1748	0.062	1694	0.495
								1730	0.156	1678	0.626
0.3681	0.2380		0.3939					1776	0.077	1721	0.329
								1757	0.185	1694	0.562
								1739	0.247	1678	0.805
0.4240	0.1380	0.0140	0.4240					1743	−0.321	1693	−0.044

Table B43 (*continued*)

SiO_2	Al_2O_3	FeO	CaO	MgO	MnO	TiO2	XCl_2	T	log η	T	log η
								1734	−0.280	1665	0.129
								1712	−0.150	1644	0.264
0.4175	0.1359	0.0290	0.4175					1686	−0.205	1653	−0.013
								1678	−0.163	1638	0.079
								1658	−0.050	1624	0.155
0.4081	0.1329	0.0510	0.4081					1724	−0.551	1672	−0.193
								1705	−0.439	1642	0.026
								1691	−0.330		
0.4193	0.1365		0.4193	0.0250				1692	−0.070	1640	0.168
								1665	0.039	1624	0.243
0.4085	0.1330		0.4085	0.0500				1712	−0.203	1651	0.090
								1692	−0.099	1619	0.243
								1673	−0.018	1606	0.300
0.3927	0.1279		0.3927	0.0867				1749	−0.473	1656	−0.029
								1711	−0.276	1635	0.104
								1702	−0.240	1635	0.121
								1689	−0.188		
0.4175	0.1359		0.4175		0.0291			1727	−0.330	1656	0.003
								1703	−0.205	1637	0.102
								1675	−0.083		
0.4080	0.1328		0.4080		0.0511			1727	−0.449	1664	−0.132
								1717	−0.407	1642	−0.001
								1709	−0.363	1618	0.126
								1698	−0.313		
0.4189	0.1364		0.4189			0.0258		1765	−0.439	1701	−0.221
								1756	−0.411	1656	−0.026
								1732	−0.338	1635	0.059
0.4104	0.1336		0.4104			0.0455		1747	−0.505	1677	−0.214
								1725	−0.421	1656	−0.133
								1693	−0.288	1693	−0.429
0.3960	0.1289		0.3960			0.0790		1756	−0.726	1671	−0.332
								1734	−0.612	1654	−0.254
								1716	−0.540		
0.4188	0.1363		0.4188				0.0261	1688	−0.193	1655	−0.081
							(X = Ca)	1676	−0.152	1635	−0.002
0.4116	0.1340		0.4116				0.0428	1676	−0.339	1626	−0.116
							(X = Ca)	1667	−0.291	1605	−0.006
								1648	−0.225		
0.3496	0.1138		0.3496				0.1870	1643	−1.013	1578	−0.522
							(X = Ca)	1627	−0.924	1555	−0.340
								1601	−0.685	1541	−0.211
0.4263	0.1388		0.4263				0.0085	1673	−0.077	1648	0.056
							(X = Na)	1667	−0.035	1637	0.092
								1658	0.022	1617	0.214
0.4223	0.1375		0.4223				0.0180	1615	0.018	1595	0.164
							(X = Na)	1608	0.057	1587	0.246
0.4150	0.1351		0.4150				0.0350	1725	−0.558	1654	−0.122
							(X = Mg)	1685	−0.322	1623	0.097

Table B44
Kovalenko et al. (1969) [90]

SiO_2	Al_2O_3	CaO	Atm.	T	log η
0.6437	0.1264	0.2299	H_2O	1903	0.792
			Ar		0.813
			H_2		0.826
			Prod. gas		0.845
0.4226	0.1245	0.4528	H_2O	1903	−0.398
			Ar		−0.347
			H_2		−0.222
			NH_3		−0.097
			N_2		−0.022
			Prod. gas		−0.187
0.2082	0.1227	0.6691	H_2O	1923	−0.097
			Ar		0.243
			H_2		0.322
			NH_3		0.716
			N_2		0.756
			Prod. gas		0.462
0.0348	0.2940	0.6712	H_2O	1903	−1.398
			Ar		−1.347
			H_2		−1.347
			NH_3		−1.301
			N_2		−1.222
			Prod. gas		−1.301

Table B45
Nemilov (1969) [63]

SiO_2	Na_2O	K_2O	Li_2O	T	log η	T	log η
0.9500	0.0500			1111	8.500	981	11.000
				1082	9.000	956	11.500
				1054	9.500	926	12.000
				1030	10.000	820	15.000
				1005	10.500		
0.9500	0.0400	0.0100		1124	7.500	982	10.500
				1097	8.000	962	11.000
				1070	8.500	941	11.500
				1048	9.000	923	12.000
				1027	9.500	827	15.000
				1002	10.000		
0.9500	0.0300	0.0200		1110	7.500	961	10.500
				1081	8.000	940	11.000
				1053	8.500	921	11.500
				1031	9.000	901	12.000
				1006	9.500	802	15.000
				985	10.000		
0.9500	0.0200	0.0300		1095	7.500	953	10.500
				1069	8.000	931	11.000
				1041	8.500	914	11.500
				1019	9.000	895	12.000
				995	9.500	797	15.000
				975	10.000		
0.9500	0.0100	0.0400		1099	7.500	945	10.500
				1070	8.000	924	11.000
				1042	8.500	905	11.500
				1017	9.000	885	12.000
				991	9.500	783	15.000
				967	10.000		
0.9500		0.0500		1111	7.000	949	10.000
				1080	7.500	926	10.500
				1050	8.000	905	11.000
				1021	8.500	885	11.500
				995	9.000	865	12.000
				971	9.500	765	15.000
0.8700	0.1300			985	8.000	897	10.500
				966	8.500	880	11.000
				948	9.000	866	11.500
				931	9.500	851	12.000
				914	10.000	773	15.000
0.8700	0.1100	0.0200		957	7.500	845	10.500
				935	8.000	830	11.000
				915	8.500	813	11.500
				897	9.000	797	12.000
				879	9.500	719	15.000
				861	10.000		
0.8700	0.0900	0.0400		965	7.000	835	10.000
				939	7.500	816	10.500
				918	8.000	799	11.000
				895	8.500	783	11.500
				874	9.000	766	12.000
				854	9.500	683	15.000

Table B45 (*continued*)

SiO_2	Na_2O	K_2O	Li_2O	T	log η	T	log η
0.8700	0.0700	0.0600		961	7.000	820	10.000
				935	7.500	803	10.500
				910	8.000	784	11.000
				885	8.500	766	11.500
				864	9.000	749	12.000
				841	9.500	660	15.000
0.8700	0.0500	0.0800		966	7.000	830	10.000
				941	7.500	810	10.500
				916	8.000	790	11.000
				893	8.500	772	11.500
				870	9.000	755	12.000
				851	9.500	666	15.000
0.8700	0.0300	0.1000		956	7.000	823	10.000
				931	7.500	803	10.500
				906	8.000	785	11.000
				883	8.500	768	11.500
				862	9.000	752	12.000
				841	9.500	666	15.000
0.8700		0.1300		975	7.000	851	10.000
				953	7.500	836	10.500
				928	8.000	820	11.000
				905	8.500	805	11.500
				885	9.000	790	12.000
				868	9.500	711	15.000
0.8000	0.2000			925	7.000	805	10.000
				902	7.500	790	10.500
				881	8.000	775	11.000
				861	8.500	761	11.500
				844	9.000	746	12.000
				824	9.500	670	15.000
0.8000	0.1800	0.0200		889	7.000	775	10.000
				866	7.500	759	10.500
				844	8.000	745	11.000
				823	8.500	731	11.500
				805	9.000	717	12.000
				790	9.500	647	15.000
0.8000	0.1600	0.0400		873	7.000	766	10.000
				853	7.500	752	10.500
				834	8.000	739	11.000
				816	8.500	722	11.500
				800	9.000	710	12.000
				784	9.500	639	15.000
0.8000	0.1400	0.0600		881	7.000	758	10.000
				855	7.500	744	10.500
				830	8.000	729	11.000
				806	8.500	715	11.500
				790	9.000	702	12.000
				774	9.500	631	15.000
0.8000	0.1200	0.0800		882	7.000	762	10.000
				859	7.500	746	10.500
				836	8.000	731	11.000
				815	8.500	717	11.500
				797	9.000	702	12.000
				779	9.500	630	15.000
0.8000	0.1000	0.1000		878	7.000	766	10.000
				855	7.500	749	10.500
				836	8.000	739	11.000
				816	8.500	724	11.500
				799	9.000	710	12.000
				783	9.500	640	15.000
0.8000	0.0500	0.1500		905	7.000	785	10.000
				880	7.500	766	10.500
				855	8.000	752	11.000
				834	8.500	739	11.500
				816	9.000	724	12.000
				799	9.500	651	15.000
0.8000		0.2000		935	7.000	823	10.000
				914	7.500	806	10.500
				894	8.000	791	11.000
				874	8.500	779	11.500
				856	9.000	764	12.000
				839	9.500	690	15.000
0.8000		0.1500	0.0500	881	7.000	776	10.000
				859	7.500	763	10.500
				839	8.000	749	11.000
				821	8.500	735	11.500
				804	9.000	724	12.000
				790	9.500	657	15.000
0.8000		0.1000	0.1000	897	7.000	786	10.000
				874	7.500	772	10.500
				853	8.000	756	11.000
				835	8.500	744	11.500
				818	9.000	730	12.000
				803	9.500	660	15.000
0.8000		0.0500	0.1500	911	7.000	794	10.000
				885	7.500	779	10.500
				861	8.000	764	11.000
				844	8.500	750	11.500
				825	9.000	735	12.000
				810	9.500	663	15.000
0.8000			0.2000	838	7.000	746	10.000
				820	7.500	734	10.500
				804	8.000	722	11.000
				786	8.500	710	11.500
				773	9.000	699	12.000
				760	9.500	639	15.000
0.7000		0.3000		931	7.000	860	10.000
				916	7.500	850	10.500
				904	8.000	840	11.000
				892	8.500	730	11.500
				880	9.000	721	12.000
				870	9.500	670	15.000
0.7000		0.2500	0.0500	840	7.000	745	10.000
				823	7.500	732	10.500

(*continued on next page*)

Table B45 (*continued*)

SiO_2	Na_2O	K_2O	Li_2O	T	log η	T	log η
				806	8.000	719	11.000
				790	8.500	706	11.500
				775	9.000	693	12.000
				760	9.500	627	15.000
0.7000		0.1500	0.1500	853	7.000	758	10.000
				834	7.500	744	10.500
				816	8.000	730	11.000
				800	8.500	719	11.500
				785	9.000	706	12.000
				773	9.500	640	15.000
0.7000		0.1000	0.2000	835	7.000	746	10.000
				818	7.500	734	10.500
				804	8.000	722	11.000
				788	8.500	710	11.500
				774	9.000	700	12.000
				761	9.500	637	15.000
0.7000		0.0500	0.2500	843	7.000	754	10.000
				825	7.500	741	10.500
				810	8.000	728	11.000
				795	8.500	716	11.500
				782	9.000	704	12.000
				766	9.500	640	15.000
0.7000			0.3000	848	7.000	755	10.000
				826	7.500	744	10.500
				806	8.000	732	11.000
				791	8.500	721	11.500
				779	9.000	711	12.000
				766	9.500	654	15.000

Table B47
Meiling and Uhlmann (1967) [172]

SiO_2	Na_2O	Viscometer	T	log η	T	log η
0.6667	0.3333	Rotating cylinder	1578	0.843	1158	2.843
			1513	1.064	1096	3.344
			1442	1.332	1020	4.090
			1371	1.635	957	4.915
			1295	1.988	896	5.957
			1230	2.360		
		Parallel plates	963	5.320	893	6.061
			953	5.316	882	6.276
			943	5.380	871	6.537
			933	5.535	858	6.707
			923	5.654	847	7.064
			913	5.747	834	7.344

Table B46
Hofmaier (1968) [26]

SiO_2	Al_2O_3	Fe (total)	CaO	MgO	MnO	S (total)	T	log η	T	log η
1.0000							2538	3.351	2077	5.761
							2309	4.472	2057	5.896
							2297	4.585	1930	6.780
							2291	4.538	1904	6.941
							2149	5.323	1878	7.073
							2144	5.360		
0.3373	0.0915	0.0005	0.5021	0.0566	0.0035	0.0085	1773	−0.599	1942	−1.025
							1812	−0.719	1966	−1.084
							1848	−0.822	2013	−1.129
							1889	−0.936		

Table B48
Sage and McIlroy (1959) [104]

SiO_2	Al_2O_3	Fe_2O_3	FeO	CaO	MgO	Na_2O	K_2O	TiO_2	T	log η	T	log η
0.7640	0.1153	0.0099		0.0624	0.0147	0.0128	0.0133	0.0074	1977	1.398		
0.7345	0.1283	0.0051	0.0096	0.0719	0.0213	0.0096	0.0147	0.0050	1977	1.398		
0.7260	0.1245	0.0058	0.0140	0.0707	0.0246	0.0117	0.0168	0.0058	1977	1.398		
0.7100	0.1256	0.0139		0.0694	0.0166	0.0379	0.0199	0.0067	1939	1.398		
0.6860	0.1339	0.0126	0.0349	0.0771	0.0201	0.0142	0.0136	0.0076	1866	1.398		
0.6742	0.1175	0.0158	0.0810	0.0656	0.0203	0.0077	0.0137	0.0043	1827	1.398		
0.6659	0.2088	0.0058	0.0110	0.0571	0.0224	0.0079	0.0140	0.0070	1916	1.000	1855	1.398
0.6554	0.1239	0.0459	0.0664	0.0530	0.0184	0.0060	0.0245	0.0065	1827	0.699	1650	1.398
									1744	1.000		
0.6464	0.0902	0.0526	0.0484	0.0608	0.0220	0.0495	0.0217	0.0085	1800	0.699	1605	1.398
									1700	1.000		
0.6461	0.1122	0.0062	0.0564	0.1344	0.0197	0.0075	0.0133	0.0041	1772	1.398		
0.6437	0.1123	0.0024	0.0122	0.1857	0.0193	0.0073	0.0130	0.0040	1877	1.000	1761	1.398
0.6308	0.1100	0.0021	0.0125	0.1311	0.0896	0.0072	0.0128	0.0040	1739	1.398		
0.6284	0.1792	0.0166	0.1027	0.0331	0.0195	0.0058	0.0076	0.0071	1889	0.699	1719	1.398
									1811	1.000		
0.6212	0.1904	0.0095	0.0758	0.0344	0.0266	0.0046	0.0242	0.0134	1822	1.000	1755	1.398
0.6187	0.1730	0.0087	0.0583	0.0464	0.0349	0.0057	0.0448	0.0097	1872	1.000	1772	1.398
0.6155	0.1846	0.0198	0.1323	0.0052	0.0145	0.0024	0.0139	0.0119	1850	0.699	1739	1.398
									1761	1.000		
0.6134	0.1845	0.0068	0.0369	0.0758	0.0398	0.0034	0.0237	0.0157	1844	0.699	1761	1.398
									1800	1.000		
0.6123	0.1062	0.0260	0.1559	0.0564	0.0192	0.0068	0.0127	0.0044	1811	0.699	1622	1.398
									1722	1.000		
0.6099	0.1545	0.0162	0.1381	0.0216	0.0248	0.0023	0.0174	0.0152	1794	1.000	1661	1.398
0.6054	0.1962	0.0162	0.0973	0.0375	0.0126	0.0047	0.0192	0.0109	1855	1.000	1766	1.398
0.5992	0.1906	0.0099	0.0899	0.0345	0.0302	0.0035	0.0297	0.0126	1780	1.000	1719	1.398
0.5982	0.2103	0.0056	0.0362	0.0675	0.0469	0.0124	0.0141	0.0088	1916	0.699	1758	1.398
									1839	1.000		
0.5939	0.1935	0.0328	0.0870	0.0103	0.0612	0.0070	0.0015	0.0127	1816	0.699	1761	1.398
									1800	1.000		
0.5884	0.2321	0.0175	0.1077	0.0066	0.0148	0.0024	0.0166	0.0140	1866	0.699	1808	1.398
									1816	1.000		
0.5873	0.2241	0.0309	0.0818	0.0417	0.0168	0.0073	0.0016	0.0085	1833	0.699	1816	1.398
									1816	1.000		
0.5818	0.2210	0.0102	0.0816	0.0259	0.0307	0.0035	0.0363	0.0091	1777	1.000	1750	1.398
0.5807	0.2112	0.0077	0.0619	0.0461	0.0356	0.0046	0.0305	0.0216	1777	1.398		
0.5804	0.1783	0.0130	0.0597	0.0590	0.0402	0.0500	0.0097	0.0097	1811	1.000	1711	1.398
0.5789	0.1941	0.0192	0.0989	0.0090	0.0374	0.0463	0.0046	0.0117	1872	0.699	1733	1.398
									1789	1.000		
0.5758	0.2056	0.0051	0.0501	0.0835	0.0520	0.0023	0.0037	0.0219	1866	0.699	1716	1.398
									1789	1.000		
0.5757	0.1669	0.0120	0.0659	0.0721	0.0415	0.0428	0.0126	0.0105	1905	0.699	1722	1.398
									1811	1.000		
0.5743	0.2070	0.0103	0.0786	0.0360	0.0393	0.0093	0.0344	0.0108	1883	0.699	1727	1.398
									1811	1.000		
0.5721	0.2255	0.0294	0.1217	0.0284	0.0038	0.0012	0.0113	0.0067	1789	0.699	1750	1.398
									1755	1.000		
0.5685	0.1942	0.0109	0.0801	0.0227	0.0702	0.0091	0.0293	0.0151	1855	0.699	1705	1.398
									1766	1.000		
0.5641	0.1903	0.0786	0.1186	0.0254	0.0098	0.0026	0.0017	0.0089	1736	0.699	1705	1.398
									1727	1.000		
0.5638	0.2339	0.0120	0.0905	0.0352	0.0272	0.0035	0.0210	0.0128	1866	0.699	1802	1.398
									1816	1.000		
0.5577	0.2559	0.0141	0.0803	0.0202	0.0496	0.0067	0.0071	0.0083	1694	0.699	1641	1.398
									1661	1.000		
0.5569	0.0965	0.0019	0.0113	0.2944	0.0173	0.0061	0.0115	0.0040	1727	0.699	1572	1.398
									1650	1.000		
0.5516	0.2246	0.0123	0.0982	0.0509	0.0218	0.0071	0.0272	0.0064	1816	0.699	1783	1.398
									1789	1.000		
0.5498	0.2172	0.0166	0.0996	0.0326	0.0363	0.0118	0.0279	0.0082	1794	0.699	1664	1.398
									1714	1.000		
0.5396	0.1156	0.0795	0.0349	0.1445	0.0201	0.0440	0.0125	0.0092	1616	0.699	1589	1.398

(*continued on next page*)

Table B48 (*continued*)

SiO_2	Al_2O_3	Fe_2O_3	FeO	CaO	MgO	Na_2O	K_2O	TiO_2	T	log η	T	log η
									1605	1.000		
0.5368	0.0936	0.0027	0.0091	0.1866	0.1503	0.0059	0.0110	0.0038	1727	0.699	1577	1.398
									1650	1.000		
0.5293	0.2510	0.0222	0.1036	0.0189	0.0244	0.0342	0.0032	0.0133	1800	0.699	1733	1.398
									1766	1.000		
0.5277	0.2560	0.0080	0.0641	0.0973	0.0271	0.0012	0.0077	0.0109	1777	0.699	1761	1.398
									1772	1.000		
0.5231	0.1302	0.0145	0.1896	0.0386	0.0208	0.0507	0.0237	0.0087	1600	0.699	1483	1.398
									1527	1.000		
0.5207	0.1381	0.1080	0.1269	0.0600	0.0233	0.0038	0.0183	0.0010	1619	0.699	1614	1.398
									1616	1.000		
0.5204	0.1744	0.0050	0.0101	0.2477	0.0216	0.0065	0.0100	0.0042	1789	0.699	1658	1.398
									1716	1.000		
0.5171	0.2157	0.0191	0.1281	0.0342	0.0348	0.0167	0.0196	0.0148	1716	0.699	1619	1.398
									1666	1.000		
0.5150	0.1851	0.0172	0.0842	0.1264	0.0470	0.0091	0.0037	0.0123	1772	0.699	1616	1.398
									1694	1.000		
0.5150	0.1554	0.1048	0.0644	0.0794	0.0131	0.0414	0.0160	0.0104	1716	0.699	1700	1.398
									1711	1.000		
0.5136	0.1746	0.1061	0.1415	0.0198	0.0157	0.0038	0.0160	0.0089	1705	0.699	1689	1.398
									1694	1.000		
0.5098	0.1425	0.0969	0.0717	0.0784	0.0136	0.0494	0.0267	0.0108	1705	0.699	1683	1.398
									1694	1.000		
0.5093	0.2194	0.0409	0.1907	0.0152	0.0096		0.0033	0.0117	1666	0.699	1650	1.398
									1661	1.000		
0.5063	0.1310	0.0947	0.0430	0.0794	0.0368	0.0838	0.0158	0.0093	1661	0.699	1616	1.398
									1639	1.000		
0.5023	0.1022	0.0139	0.2511	0.0679	0.0339	0.0081	0.0153	0.0054	1494	0.699	1416	1.398
									1466	1.000		
0.4962	0.1840	0.0155	0.0724	0.1435	0.0538	0.0068	0.0163	0.0114	1614	1.398		
0.4890	0.2806	0.0171	0.1029	0.0591	0.0172	0.0162	0.0131	0.0048	1794	0.699	1736	1.398
									1772	1.000		
0.4845	0.2234	0.0038	0.0249	0.1204	0.0837	0.0261	0.0164	0.0167	1777	0.699	1627	1.398
									1705	1.000		
0.4819	0.1270	0.0916	0.0458	0.0516	0.0246	0.1475	0.0194	0.0105	1666	0.699	1622	1.398
									1650	1.000		
0.4805	0.1225	0.0957	0.0237	0.0445	0.0213	0.1889	0.0133	0.0098	1572	0.699	1439	1.398
									1500	1.000		
0.4757	0.0834	0.0024	0.0076	0.3993	0.0124	0.0061	0.0100	0.0031	1589	0.699	1469	1.398
									1527	1.000		
0.4712	0.0997	0.0811	0.0286	0.2330	0.0198	0.0398	0.0185	0.0082	1527	0.699	1500	1.398
									1511	1.000		
0.4651	0.1451	0.1084	0.0559	0.0747	0.0204	0.0928	0.0262	0.0113	1700	0.699	1672	1.398
									1689	1.000		
0.4639	0.1443	0.1026	0.0759	0.0994	0.0269	0.0625	0.0148	0.0097	1705	0.699	1683	1.398
									1694	1.000		
0.4613	0.2711	0.0107	0.1428	0.0604	0.0299	0.0109	0.0016	0.0113	1750	0.699	1639	1.398
									1700	1.000		
0.4459	0.2084	0.0207	0.0984	0.1027	0.0987	0.0080	0.0083	0.0089	1672	0.699	1602	1.398
									1627	1.000		
0.4342	0.1392	0.0236	0.3464	0.0136	0.0170	0.0037	0.0146	0.0076	1555	0.699	1472	1.398
									1536	1.000		
0.4314	0.1570	0.1142	0.0485	0.1332	0.0397	0.0566	0.0089	0.0105	1700	0.699	1666	1.398
									1689	1.000		
0.4310	0.1484	0.0248	0.3314	0.0268	0.0187	0.0036	0.0096	0.0057	1525	0.699	1472	1.398
									1500	1.000		
0.4158	0.1433	0.0080	0.0273	0.2896	0.0955	0.0053	0.0014	0.0139	1577	0.699	1516	1.398
									1527	1.000		
0.3656	0.1390	0.0306	0.1874	0.1264	0.0299	0.0892	0.0196	0.0124	1516	0.699	1411	1.398
									1455	1.000		

Table B49
Bockris et al. (1955) [36]

SiO_2	MgO	Na_2O	K_2O	Li_2O	T	log η	T	log η
0.5570	0.4430				2073	−0.548	1973	−0.334
					2023	−0.444	1923	−0.216
0.5490	0.4510				2073	−0.680	1933	−0.220
					2023	−0.570	1923	−0.340
					1973	−0.513	1823	−0.080
0.5420	0.4580				2073	−0.745	1933	−0.323
					2023	−0.688	1923	−0.450
					1973	−0.580	1823	−0.190
0.5000	0.5000				2073	−0.928	1933	−0.500
					2023	−0.827	1923	−0.609
					1973	−0.747		
0.4860	0.5140				2073	−0.971	1973	−0.821
					2023	−0.907	1923	−0.726
0.9000		0.1000			2023	0.930	1873	1.439
					1973	1.090	1823	1.630
					1923	1.260		
0.8500		0.1500			1873	0.890	1723	1.380
					1823	1.079	1673	1.560
					1773	1.210	1623	1.760
0.8000		0.2000			1773	0.690	1623	1.179
					1723	0.850	1573	1.350
					1673	1.000	1523	1.550
0.7500		0.2500			1773	0.590	1573	1.201
					1723	0.730	1523	1.380
					1673	0.890	1473	1.571
					1623	1.029	1423	1.770
0.7300		0.2700			1773	0.530	1573	1.100
					1723	0.660	1523	1.270
					1673	0.790	1473	1.439
					1623	0.950	1423	1.640
0.7000		0.3000			1723	0.470	1523	1.111
					1673	0.620	1473	1.301
					1623	0.770	1423	1.500
					1573	0.940	1373	1.710
0.6700		0.3300			1723	0.310	1523	0.940
					1673	0.450	1473	1.130
					1623	0.610	1423	1.340
					1573	0.780	1373	1.549
0.6500		0.3500			1773	0.079	1523	0.840
					1723	0.220	1473	1.009
					1673	0.360	1423	1.210
					1623	0.511	1373	1.420
					1573	0.670		
0.9750			0.0250		2023	2.100	1923	2.430
					1923	2.250	1873	2.670
0.9370			0.0630		1973	1.730	1823	2.230
					1923	1.860	1773	2.540
					1873	2.029		
0.8920			0.1080		1873	1.380	1723	1.880
					1823	1.540	1673	2.072
					1773	1.720	1623	2.270
0.8310			0.1690		1673	1.550	1473	2.350

(*continued on next page*)

Table B49 (*continued*)

SiO_2	MgO	Na_2O	K_2O	Li_2O	T	log η	T	log η
					1623	1.850	1423	2.680
					1573	1.920	1373	2.850
					1523	2.140		
0.7770			0.2230		1673	1.360	1473	2.149
					1623	1.530	1423	2.391
					1573	1.730	1373	2.640
					1523	1.930		
0.7440			0.2560		1673	1.061	1473	1.850
					1623	1.230	1423	2.090
					1573	1.430	1373	2.340
					1523	1.511		
0.6660			0.3340		1673	0.780	1473	1.591
					1623	0.920	1423	1.830
					1573	1.161	1373	2.100
					1523	1.350		
0.8000				0.2000	1973	0.439	1773	0.970
					1923	0.560	1723	1.121
					1873	0.690	1673	1.281
					1823	0.860		
0.7500				0.2500	1873	0.330	1673	0.910
					1823	0.459	1623	1.072
					1773	0.600	1573	1.149
					1723	0.750		
0.7000				0.3000	1773	0.201	1573	0.740
					1723	0.320	1523	0.890
					1673	0.450	1473	1.061
					1623	0.590		
0.6700				0.3300	1723	0.179	1523	0.740
					1673	0.301	1473	0.910
					1623	0.439	1423	1.090
					1573	0.590		
0.6500				0.3500	1773	−0.104	1573	0.391
					1723	0.009	1523	0.530
					1673	0.130	1473	0.690
					1623	0.260	1423	0.860
0.6000				0.4000	1773	−0.190	1573	0.190
					1723	−0.110	1523	0.301
					1673	−0.020	1473	0.430
					1623	0.090	1423	0.550
0.5500				0.4500	1773	−0.699	1573	−0.290
					1723	−0.600	1523	−0.180
					1673	−0.510	1473	−0.050
					1623	−0.400		
0.5000				0.5000	1773	−1.018	1623	−0.750
					1723	−0.939	1573	−0.650
					1673	−0.851	1523	−0.541
0.4500				0.5500	1723	−1.347	1573	−1.125
					1673	−1.276	1523	−1.036
					1623	−1.201		

Table B50
Machin and Yee (1954) [173]

SiO_2	Al_2O_3	CaO	MgO	T	log η	T	log η
0.6341		0.3659		1773	0.330		
0.5833		0.4167		1773	−0.046	1723	0.158
0.6868	0.1557		0.1575	1773	1.754	1673	2.369
				1723	2.041		
0.6556	0.1189		0.2255	1773	1.420	1623	2.297
				1723	1.688	1573	2.610
				1673	1.980	1523	3.093
0.6271	0.0853		0.2876	1773	1.100	1623	1.891
				1723	1.334	1573	2.248
				1673	1.593		
0.6180	0.1517		0.2303	1773	1.243	1623	2.117
				1723	1.502	1573	2.483
				1673	1.787	1523	2.917
0.5905	0.1160		0.2935	1773	0.939	1673	1.430
				1723	1.170	1623	1.731
0.5655	0.0833		0.3512	1773	0.610	1673	1.072
				1723	0.836		
0.5424	0.0533		0.4043	1773	0.310		
0.5717		0.3573	0.0500	1773	−0.054	1673	0.281
				1723	0.107	1623	0.481
0.5605		0.3003	0.1393	1773	−0.053	1673	0.286
				1723	0.100	1623	0.479
0.5497		0.2454	0.2049	1773	−0.059	1673	0.260
				1723	0.086	1623	0.442
0.5394		0.1926	0.2680	1773	−0.108	1673	0.228
				1723	0.041	1623	0.428
0.5294		0.1418	0.3288	1773	−0.140	1673	0.253
				1723	0.025		
0.5198		0.0928	0.3874	1773	−0.118		
0.7024	0.1592	0.0579	0.0805	1773	2.013		
0.6845	0.1241	0.1128	0.0785	1773	1.827	1623	2.712
				1723	2.079	1573	3.076
				1673	2.382	1523	3.481
0.6698	0.1214	0.0552	0.1536	1773	1.622	1623	2.479
				1723	1.867	1573	2.839
				1673	2.155	1523	3.243
0.6676	0.0908	0.1651	0.0766	1773	1.410	1623	2.201
				1723	1.647	1573	2.529
				1673	1.914	1523	2.931
0.6535	0.0889	0.1077	0.1499	1773	1.350	1623	2.152
				1723	1.592	1573	2.465
				1673	1.857	1523	2.834
0.6515	0.0591	0.2148	0.0747	1773	1.057	1623	1.762
				1723	1.286	1573	2.049
				1673	1.502	1523	2.394
0.6459	0.1586	0.1153	0.0802	1773	1.543	1623	2.467
				1723	1.824	1573	2.858
				1673	2.130	1523	3.255
0.6400	0.0870	0.0528	0.2202	1773	1.258	1623	2.049
				1723	1.487	1573	2.389
				1673	1.746		
0.6381	0.0578	0.1578	0.1463	1773	0.988	1623	1.703
				1723	1.196	1573	2.004
				1673	1.430		

Table B50 (*continued*)

SiO_2	Al_2O_3	CaO	MgO	T	log η	T	log η
0.6361	0.0288	0.2621	0.0729	1773	0.665	1723	0.820
0.6316	0.1551	0.0564	0.1569	1773	1.358	1623	2.236
				1723	1.616	1573	2.609
				1673	1.911	1523	3.079
0.6295	0.1237	0.1686	0.0782	1773	1.262	1623	2.076
				1723	1.509	1573	2.427
				1673	1.776	1523	2.799
0.6252	0.0567	0.1031	0.2151	1773	0.937	1673	1.373
				1723	1.134		
0.6233	0.0283	0.2055	0.1430	1773	0.600	1723	0.820
0.6160	0.1210	0.1100	0.1530	1773	1.137	1623	1.932
				1723	1.377	1573	2.274
				1673	1.643	1523	2.645
0.6140	0.0905	0.2193	0.0763	1773	0.919	1623	1.620
				1723	1.121	1573	1.920
				1673	1.352	1523	2.260
0.6128	0.0556	0.0505	0.2811	1773	0.873	1723	1.097
0.6110	0.0277	0.1511	0.2102	1773	0.565	1723	0.806
0.6030	0.1184	0.0538	0.2247	1773	0.925	1623	1.691
				1723	1.146	1573	2.013
				1673	1.412	1523	2.367
0.6011	0.0886	0.1610	0.1493	1773	0.839	1623	1.547
				1723	1.049	1573	1.841
				1673	1.288	1523	2.190
0.5992	0.0589	0.2675	0.0744	1773	0.563	1623	1.199
				1723	0.762	1573	1.473
				1673	0.966	1523	1.792
0.5887	0.0867	0.1051	0.2194	1773	0.731	1623	1.436
				1723	0.941	1573	1.724
				1673	1.173	1523	2.072
0.5869	0.0576	0.2096	0.1458	1773	0.512	1623	1.143
				1723	0.702	1573	1.413
				1673	0.901	1523	1.730
0.5851	0.0287	0.3135	0.0727	1773	0.246	1623	0.827
				1723	0.410	1573	1.079
				1673	0.602	1523	1.380
0.5769	0.0850	0.0515	0.2867	1773	0.654	1673	1.083
				1723	0.876	1623	1.373
0.5751	0.0565	0.1541	0.2143	1773	0.455	1623	1.086
				1723	0.630	1573	1.356
				1673	0.851	1523	1.679
0.5734	0.0282	0.2560	0.1425	1773	0.238	1623	0.733
				1723	0.418	1573	0.977
				1673	0.553	1523	1.255
0.5638	0.0554	0.1007	0.2802	1773	0.396	1673	0.794
				1723	0.583	1623	1.045
0.5621	0.0276	0.2008	0.2095	1773	0.167	1623	0.763
				1723	0.367	1573	1.021
				1673	0.559		
0.5529	0.0543	0.0494	0.3434	1773	0.354	1723	0.545
0.5513	0.0271	0.1477	0.2740	1773	0.143	1673	0.501
				1723	0.314	1623	0.716
0.5409	0.0266	0.0966	0.3360	1773	0.134	1723	0.292
0.5308	0.0261	0.0474	0.3957	1773	0.064		

Table B51
Machin et al. (1952) [23]

SiO_2	Al_2O_3	CaO	MgO	T	log η	T	log η
0.3780	0.1591	0.4629		1773	−0.125	1673	0.299
				1723	0.072		
0.4244		0.5053	0.0703	1773	−0.648	1673	−0.351
				1723	−0.511		
0.4162		0.4459	0.1379	1773	−0.650	1673	−0.352
				1723	−0.513		
0.4083		0.3888	0.2029	1773	−0.678	1673	−0.386
				1723	−0.539		
0.4007		0.3339	0.2655	1773	−0.676	1673	−0.402
				1723	−0.547		
0.3933		0.2809	0.3257	1773	−0.712		
0.4915	0.1931	0.2340	0.0814	1773	0.661	1723	0.879
0.4789	0.1568	0.2850	0.0793	1773	0.348	1673	0.757
				1723	0.579	1623	1.025
0.4684	0.1534	0.2231	0.1552	1773	0.305	1623	0.881
				1723	0.480	1573	1.182
				1673	0.621		
0.4669	0.1223	0.3335	0.0773	1773	0.196	1623	0.722
				1723	0.312	1573	1.000
				1673	0.497	1523	1.326
0.4584	0.1501	0.1637	0.2278	1773	0.158	1623	0.791
				1723	0.348	1573	1.100
				1673	0.561		
0.4569	0.1197	0.2720	0.1514	1773	0.124	1623	0.634
				1723	0.236	1573	0.907
				1673	0.420	1523	1.228
0.4555	0.0895	0.3796	0.0754	1773	−0.119	1623	0.459
				1723	0.045	1573	0.706
				1673	0.238	1523	1.009
0.4488	0.1469	0.1069	0.2974	1773	0.111	1623	0.713
				1723	0.301	1573	1.021
				1673	0.501		
0.4474	0.1172	0.2131	0.2223	1773	−0.013	1623	0.556
				1723	0.153	1573	0.825
				1673	0.338		
0.4460	0.0876	0.3186	0.1478	1773	−0.170	1623	0.386
				1723	−0.009	1573	0.627
				1673	0.179	1523	0.914
0.4446	0.0582	0.4235	0.0737	1773	−0.320	1623	0.228
				1723	−0.157	1573	0.471
				1673	0.025	1523	0.763
0.4396	0.1439	0.0523	0.3641	1773	0.025	1673	0.486
				1723	0.230		
0.4383	0.1148	0.1565	0.2904	1773	−0.075	1673	0.281
				1723	0.097	1623	0.508
0.4369	0.0858	0.2601	0.2171	1773	−0.175	1623	0.367
				1723	−0.025	1573	0.614
				1673	0.158		
0.4356	0.0570	0.3630	0.1443	1773	−0.339	1623	0.204
				1723	−0.161	1573	0.439

Table B51 (*continued*)

SiO_2	Al_2O_3	CaO	MgO	T	log η	T	log η
				1673	0.009		
0.4343	0.0284	0.4653	0.0719	1773	−0.419	1673	−0.127
				1723	−0.309		
0.4295	0.1125	0.1023	0.3557	1773	−0.112	1723	0.057
0.4282	0.0841	0.2039	0.2837	1773	−0.224	1673	0.086
				1723	−0.087		
0.4270	0.0559	0.3050	0.2122	1773	−0.390	1693	0.127
				1723	−0.228	1573	0.362
				1673	−0.056	1523	0.660
0.4257	0.0279	0.4054	0.1410	1773	−0.524	1673	−0.183
				1723	−0.378	1623	0.013
0.4199	0.0825	0.1500	0.3477	1773	−0.300		
0.4186	0.0548	0.2492	0.2774	1773	−0.409	1673	−0.076
				1723	−0.268		
0.4174	0.0273	0.3478	0.2074	1773	−0.547	1673	−0.246
				1723	−0.400	1623	−0.044
0.4106	0.0538	0.1955	0.3401	1773	−0.435		
0.4094	0.0268	0.2925	0.2713	1773	−0.554	1673	−0.228
				1723	−0.420		
0.4018	0.0263	0.2392	0.3328	1773	−0.609		
0.3793	0.1916	0.3483	0.0808	1773	0.049	1623	0.683
				1723	0.220	1573	0.966
				1673	0.415		
0.3709	0.1873	0.2838	0.1580	1773	−0.036	1673	0.497
				1723	0.223		
0.3696	0.1556	0.3961	0.0787	1773	−0.187	1673	0.185
				1723	−0.027	1623	0.407
0.3616	0.1522	0.3321	0.1540	1773	−0.252	1623	0.332
				1723	−0.092	1573	0.600
				1673	0.114		
0.3605	0.1214	0.4414	0.0768	1773	−0.319	1673	0.057
				1723	−0.143		
0.3528	0.1188	0.3781	0.1503	1773	−0.387	1673	−0.086
				1723	−0.268	1623	0.137
0.3517	0.0888	0.4845	0.0749	1773	−0.523	1673	−0.155
				1723	−0.337		
0.3455	0.1164	0.3173	0.2208	1773	−0.409	1673	−0.051
				1723	−0.244		
0.3445	0.0870	0.4218	0.1467	1773	−0.569	1673	−0.222
				1723	−0.409		
0.3375	0.0852	0.3616	0.2156	1773	−0.585	1673	−0.276
				1723	−0.444	1623	−0.081
0.3365	0.0567	0.4635	0.1433	1773	−0.638		
0.3298	0.0555	0.4039	0.2107	1773	−0.678		

Table B52
Shartsis et al. (1952) [37]

SiO_2	Na_2O	K_2O	Li_2O	T	log η	T	log η
0.8330	0.1670			1666	1.614	1373	2.856
				1578	1.912	1274	3.488
				1475	2.347	1182	4.194
0.8120	0.1880			1670	1.447	1371	2.774
				1567	1.841	1271	3.365
				1470	2.271	1179	4.124
0.7860	0.2140			1701	1.214	1374	2.578
				1567	1.706	1271	3.190
				1477	2.104	1177	3.957
0.7620	0.2380			1676	1.146	1376	2.481
				1580	1.562	1278	3.095
				1475	2.000	1181	3.840
0.7310	0.2690			1672	1.063	1375	2.402
				1573	1.444	1278	2.998
				1477	1.892	177	3.766
0.7130	0.2870			1673	0.906	1375	2.290
				1571	1.375	1276	2.894
				1473	1.777	1181	3.602
0.6880	0.3120			1661	0.844	1371	2.187
				1561	1.288	1280	2.744
				1477	1.630		
0.6700	0.3300			1679	0.671	1376	2.034
				1578	1.081	1278	2.650
				1481	1.524	1165	3.424
0.8050		0.1950		1665	1.293	1475	1.970
				1563	1.591		
0.8050		0.1950		1681	1.200	1374	2.405
				1568	1.539	1256	3.052
				1477	1.933	1171	3.721
0.6990		0.3010		1676	0.692	1370	1.718
				1573	0.913	1268	2.248
				1468	1.252	1167	2.909
0.6710		0.3290		1677	0.469	1378	1.571
				1576	0.780	1276	2.082
				1478	1.177	1172	2.656
0.6380		0.3620		1673	0.396	1375	1.379
				1571	0.728	1278	1.878
				1473	1.035	1173	2.523
0.7850			0.2150	1663	1.278	1620	1.431
0.7710			0.2290	1676	1.071	1573	1.427
0.7140			0.2860	1673	0.586	1473	1.304
				1569	0.929	1372	1.694
0.6970			0.3030	1664	0.430	1416	1.354
				1561	0.766	1367	1.523
				1515	0.945	1321	1.696
				1466	1.168	1273	1.933

Table B52 (*continued*)

SiO_2	Na_2O	K_2O	Li_2O	T	log η	T	log η
0.6740			0.3260	1675	0.299	1475	0.919
				1575	0.596	1375	1.327
0.6660			0.3340	1663	0.344	1466	0.930
				1563	0.582	1382	1.250
0.6410			0.3590	1674	0.077	1477	0.662
				1580	0.311	1383	1.032
0.6130			0.3870	1659	−0.107	1468	0.555
				1568	0.338	1372	0.818
0.5870			0.4130	1666	−0.207	1473	0.299
				1569	0.017	1368	0.664

Table B53
Machin and Yee (1948) [174]

SiO_2	Al_2O_3	CaO	T	log η	T	log η
0.6341		0.3659	1773	0.356		
0.7568	0.1274	0.1158	1773	1.558	1673	2.029
			1723	1.778		
0.7375	0.0931	0.1693	1773	2.121	1573	3.346
			1723	2.378	1523	3.754
			1673	2.671	1473	4.212
			1623	2.994		
0.7193	0.0606	0.2202	1773	2.597	1623	3.665
			1723	2.918	1573	4.107
			1673	3.260		
0.7187	0.1629	0.1185	1773	2.279	1723	2.598
0.7000	0.1269	0.1731	1773	1.973	1623	2.809
			1723	2.201	1573	3.167
			1673	2.507	1523	3.494
0.6823	0.0928	0.2249	1773	1.493	1623	2.292
			1723	1.759	1573	2.653
			1673	2.017		
0.6654	0.0603	0.2742	1773	0.976	1573	1.931
			1723	1.182	1523	2.250
			1673	1.408	1473	2.619
			1623	1.663	1423	3.045
0.6608	0.1622	0.1770	1773	1.793	1673	2.398
			1723	2.086		
0.6494	0.0294	0.3211	1773	0.625	1723	0.844
0.6437	0.1264	0.2299	1773	1.310	1573	2.403
			1723	1.548	1523	2.760
			1673	1.822	1473	3.167
			1623	2.100		
0.6274	0.0924	0.2801	1773	0.890	1573	1.863
			1723	1.107	1523	2.193
			1673	1.330	1473	2.572
			1623	1.592	1423	3.025
0.6120	0.0601	0.3279	1773	0.513	1573	1.342
			1723	0.713	1523	1.624
			1673	0.912	1473	1.996
			1623	1.100	1423	2.401
0.6033	0.1616	0.2351	1773	1.238	1673	1.820
			1723	1.501		
0.5973	0.0293	0.3733	1773	0.233	1673	0.595
			1723	0.398		
0.5878	0.1260	0.2863	1773	0.789	1573	1.763
			1723	0.994	1523	2.079
			1673	1.233	1473	2.458
			1623	1.490	1423	2.900
0.5833		0.4167	1773	−0.035		
0.5730	0.0921	0.3349	1773	0.456	1573	1.352
			1723	0.651	1523	1.659
			1673	0.865	1473	2.033
			1623	1.083	1423	2.444
0.5590	0.0599	0.3811	1773	0.179	1623	0.784
			1723	0.348	1573	1.068
			1673	0.553		
0.5463	0.1610	0.2927	1773	0.761	1723	0.999
0.5456	0.0292	0.4252	1773	−0.076	1723	0.107
0.5323	0.1255	0.3422	1773	0.480	1623	1.097
			1723	0.626	1573	1.393
			1673	0.851	1523	1.723
0.5190	0.0918	0.3893	1773	0.155	1573	1.021
			1723	0.340	1523	1.320
			1673	0.540	1473	1.671
			1623	0.757	1423	2.097
0.5063	0.0597	0.4340	1773	−0.085	1673	0.283
			1723	0.083		
0.5030	0.1976	0.2994	1773	0.848		
0.4943	0.0291	0.4766	1773	−0.321		
0.4898	0.1603	0.3499	1773	0.420	1673	0.846
			1723	0.613	1623	1.121
0.4773	0.1250	0.3977	1773	0.176	1573	1.097
			1723	0.354	1523	1.435
			1673	0.569	1473	1.829
			1623	0.801		
0.4654	0.0914	0.4432	1773	−0.069	1673	0.288
			1723	0.097	1623	0.520
0.4540	0.0595	0.4865	1773	−0.312	1673	0.064
			1723	−0.121		
0.4433	0.0290	0.5277	1773	−0.467	1723	−0.319
0.4330	0.0000	0.5670	1773	−0.633		
0.4100	0.2762	0.3138	1773	0.396	1723	0.612
0.3988	0.2350	0.3662	1773	0.279	1623	1.037
			1723	0.497	1573	1.394
			1673	0.738		
0.3881	0.1960	0.4158	1773	0.064	1673	0.501
			1723	0.276		
0.3780	0.1591	0.4629	1773	−0.123	1673	0.299
			1723	0.075		
0.3684	0.1241	0.5075	1773	−0.305	1673	0.134
			1723	−0.119		
0.3404	0.2340	0.4255	1773	0.009		

Table B54
Machin and Hanna (1945) [57]

SiO_2	Al_2O_3	CaO	MgO	T	log η	T	log η
0.4453	0.1968	0.3579		1773	0.434	1673	0.841
				1723	0.597	1623	1.112
0.4337	0.1597	0.4066		1773	0.157	1623	0.806
				1723	0.336	1573	1.108
				1673	0.543	1523	1.452
0.4226	0.1245	0.4528		1773	−0.080	1623	0.545
				1723	0.136	1573	0.830
				1673	0.332	1523	1.170
0.4121	0.0911	0.4968		1773	−0.287	1623	0.346
				1723	−0.085	1573	0.605
				1673	0.122	1523	0.933
0.4021	0.0592	0.5386		1773	−0.397	1673	−0.079
				1723	−0.281		
0.4352	0.1923	0.2914	0.0811	1773	0.277	1673	0.711
				1723	0.483	1623	0.982
0.4255	0.1880	0.2279	0.1586	1773	0.167	1673	0.590
				1723	0.364	1623	0.846
0.4240	0.1562	0.3408	0.0790	1773	0.085	1623	0.693
				1723	0.262	1573	0.993
				1673	0.459	1523	1.330
0.4148	0.1528	0.2778	0.1546	1773	0.049	1623	0.600
				1723	0.186	1573	0.877
				1673	0.364	1523	1.200
0.4135	0.1218	0.3876	0.0770	1773	−0.114	1623	0.469
				1723	0.052	1573	0.744
				1673	0.253	1523	1.063
0.4047	0.1192	0.3252	0.1508	1773	−0.159	1623	0.394
				1723	0.002	1573	0.646
				1673	0.180	1523	0.992
0.4034	0.0892	0.4322	0.0752	1773	−0.299	1623	0.292
				1723	−0.092	1573	0.497
				1673	0.075	1523	0.853
0.3963	0.1168	0.2654	0.2215	1773	−0.251	1623	0.317
				1723	−0.077	1573	0.548
				1673	0.108	1523	0.873
0.3951	0.0873	0.3704	0.1472	1773	−0.369	1623	0.213
				1723	−0.187	1573	0.438
				1673	−0.001		
0.3882	0.1144	0.2080	0.2894	1773	−0.267	1673	0.097
				1723	−0.114		
0.3871	0.0855	0.3110	0.2164	1773	−0.429	1623	0.105
				1723	−0.273	1573	0.344
				1673	−0.096	1523	0.773
0.3859	0.0568	0.4135	0.1438	1773	−0.526	1673	−0.194
				1723	−0.370	1623	−0.011
0.3794	0.0838	0.2540	0.2828	1773	−0.416	1673	−0.079
				1723	−0.256		
0.3782	0.0557	0.3546	0.2114	1773	−0.582	1673	−0.279
				1723	−0.439	1623	−0.080
0.3771	0.0278	0.4546	0.1405	1773	−0.650		
0.3720	0.0822	0.1993	0.3466	1773	−0.481		
0.3709	0.0546	0.2980	0.2764	1773	−0.551	1673	−0.26

Table B54 (*continued*)

SiO_2	Al_2O_3	CaO	MgO	T	log η	T	log η
				1723	−0.423	1623	−0.058
0.3698	0.0272	0.3962	0.2067	1773	−0.701	1723	−0.583
0.3638	0.0536	0.2436	0.3390	1773	−0.609		
0.3560	0.0262	0.2861	0.3317	1773	−0.721		
0.1057	0.0078	0.0991	0.7875	1773	−0.719	1723	−0.578
0.0476	0.0070	0.0574	0.8879	1773	−0.483	1673	−0.169
				1723	−0.337	1623	0.012

Table B55
Lillie (1939) [33]

SiO_2	Na_2O	T	log η	T	log η
0.7862	0.2138	1679	1.092	1428	2.015
		1633	1.240	1351	2.385
		1582	1.406	1276	2.812
		1531	1.591	1200	3.339
		1480	1.787	1123	3.968
0.7569	0.2431	1677	0.944	1392	1.986
		1630	1.087	1319	2.357
		1578	1.251	1243	2.801
		1529	1.426	1166	3.349
		1479	1.613	1093	3.974
0.7481	0.2519	1676	0.902	1425	1.778
		1629	1.036	1377	2.003
		1580	1.202	1276	2.535
		1527	1.387	1177	3.197
		1474	1.572	1073	4.108
0.7403	0.2597	1668	0.900	1364	2.034
		1627	1.026	1263	2.582
		1584	1.155	1183	3.129
		1543	1.296	1113	3.698
		1503	1.439	1073	4.085
		1462	1.604		
0.7381	0.2619	1676	0.852	1453	1.616
		1634	0.974	1375	1.960
		1597	1.092	1275	2.476
		1555	1.230	1176	3.142
		1505	1.412	1075	4.021
0.7217	0.2783	1676	0.782	1425	1.659
		1627	0.930	1376	1.884
		1575	1.106	1276	2.391
		1526	1.246	1176	3.042
		1474	1.455	1074	3.926
0.7086	0.2914	1675	0.719	1371	1.822
		1634	0.842	1274	2.315
		1590	0.961	1224	2.629
		1555	1.097	1172	2.985
		1513	1.242	1124	3.371
		1472	1.395		
0.6893	0.3107	1672	0.626	1352	1.805
		1574	0.930	1282	2.154
		1533	1.066	1222	2.511
		1493	1.213	1162	2.916
		1449	1.374	1121	3.243

Table B56
English (1925) [100]

SiO_2	Al_2O_3	Fe_2O_3	CaO	MgO	Na_2O	T	log η	T	log η
0.7618	0.0431	0.0004	0.0783		0.1164	1673	3.742	1268	5.498
						1581	3.936	1193	6.220
						1527	4.097	1131	7.033
						1471	4.295	1075	7.832
						1399	4.665	1043	8.288
						1358	4.864		
0.7557	0.0314	0.0003	0.0863	0.0009	0.1255	1683	3.587	1313	4.920
						1620	3.692	1273	5.199
						1573	3.877	1223	5.597
						1513	3.977	1167	6.075
						1445	4.255	1126	6.742
						1395	4.508	1080	7.320
						1348	4.683	1023	8.248
0.7542	0.0051	0.0003	0.0404	0.0604	0.1397	1684	3.079	1279	4.797
						1578	3.435	1183	5.377
						1485	3.683	1075	6.554
						1373	4.173	1023	7.367
						1333	4.423	984	8.133
0.7475	0.0052	0.0003	0.0331	0.0711	0.1428	1675	3.170	1223	5.307
						1621	3.354	1178	5.608
						1545	3.615	1131	6.093
						1473	3.848	1083	6.754
						1385	4.182	1043	7.501
						1283	4.831	998	8.223
0.7463	0.0024	0.0013	0.0015	0.0997	0.1489	1673	3.255	1271	5.325
						1577	3.651	1175	6.202
						1471	4.095	1069	7.663
						1373	4.626	1015	8.551
0.7459	0.0055	0.0003	0.0804	0.0244	0.1435	1653	3.167	1233	5.086
						1623	3.253	1173	5.680
						1591	3.418	1113	6.324
						1488	3.735	1073	7.049
						1383	4.158	985	8.911
0.7455	0.0158	0.0003	0.1050	0.0013	0.1320	1673	3.450	1253	5.133
						1573	3.638	1205	5.497
						1525	3.806	1163	5.823
						1446	4.114	1118	6.369
						1350	4.579	1073	7.075
						1301	4.851	1017	8.111
0.7447	0.0051	0.0003	0.0579	0.0538	0.1383	1678	2.826	1086	6.339
						1525	3.386	1068	6.763
						1475	3.645	1031	7.346
						1353	4.210	995	7.868
						1263	4.736	973	8.441
						1168	5.436		
0.7428	0.0060	0.0002	0.0685	0.0382	0.1443	1673	2.826	1183	5.585
						1553	3.260	1088	6.846
						1443	3.851	1023	7.881
						1350	4.299	988	8.615
						1266	4.881		

Table B57
English (1924) [15]

SiO_2	Al_2O_3	Fe_2O_3	CaO	MgO	Na_2O	B_2O_3	T	log η	T	log η
0.8045	0.0041	0.0004	0.0013		0.1897		1683	2.846	923	9.508
							1588	3.206	871	10.866
							1467	3.738	828	11.980
							1373	4.272	778	13.790
							1175	4.949		
0.7611	0.0795	0.0018	0.0018		0.1575		1663	3.797	998	8.921
							1581	4.134	973	9.318
							1463	4.658	948	9.906
							1373	5.039	923	10.377
							1273	5.444	898	11.057
							1145	6.717	873	11.522
							1070	7.745	848	12.283
							1023	8.346	823	13.155
0.7491	0.0420	0.0012	0.0012		0.2078		1661	3.269	947	9.193
							1548	3.591	923	9.649
							1453	3.952	897	10.318
							1373	4.310	873	10.872
							1293	4.757	848	11.531
							1182	5.565	825	12.201
							1078	6.802	800	13.097
							1003	7.911	773	13.921
							968	8.883		
0.7477	0.0014	0.0005	0.0023		0.2480		1583	2.886	923	8.796
							1513	2.982	898	9.375
							1409	3.576	873	9.864
							1301	4.250	848	10.585
							1193	5.033	823	11.240
							1093	6.025	797	12.127
							1063	6.433	773	12.893
							1018	7.004	758	13.745
							974	7.702		
0.7466	0.0017	0.0005	0.0411		0.2101		1663	2.806	970	8.190
							1585	2.964	948	9.009
							1473	3.477	923	9.554
							1393	3.851	898	10.121
							1273	4.514	873	10.782
							1173	5.303	848	11.613
							1075	6.468	823	12.444
							1020	7.283	798	12.951
0.7456	0.0012	0.0006	0.0281		0.2244		1673	2.707	966	8.045
							1583	2.919	923	8.984
							1478	3.386	898	9.717
							1393	3.787	873	10.326
							1287	4.428	848	11.124
							1178	5.199	823	11.864
							1074	6.433	798	12.841
							1018	7.201	773	13.498
0.7523	0.0050	0.0050	0.0050	0.1332	0.1096		1698	3.386	1373	5.037
							1677	3.521	1283	5.717
							1578	3.882	1165	6.894
							1468	4.486	1116	7.544
0.7510	0.0018	0.0003	0.0876	0.0039	0.1553		1665	3.187	998	8.924

(*continued on next page*)

Table B57 (*continued*)

SiO_2	Al_2O_3	Fe_2O_3	CaO	MgO	Na_2O	B_2O_3	T	log η	T	log η
							1573	3.373	973	9.447
							1478	3.766	948	10.100
							1367	4.260	923	10.582
							1275	4.802	898	11.117
							1173	5.677	873	11.824
							1071	7.149	848	12.602
							1022	8.000	823	13.522
							999	8.636		
0.7490	0.0051	0.0051	0.0051	0.1084	0.1375		1643	3.324	1266	5.439
							1583	3.709	1165	6.389
							1455	4.223	1088	7.537
							1355	4.831	1023	8.566
0.7486	0.0025	0.0006	0.1001	0.0042	0.1441		1673	3.212	998	9.490
							1578	3.502	973	9.870
							1473	3.814	948	10.522
							1373	4.220	923	11.045
							1268	5.014	898	11.647
							1163	5.971	873	12.318
							1073	7.464	848	13.124
							1023	8.552	823	13.921
							1023	8.917		
0.7480	0.0041	0.0041	0.0041	0.0744	0.1735		1683	3.037	973	9.033
							1573	3.505	945	9.514
							1461	4.140	924	10.017
							1375	4.459	903	10.642
							1273	5.068	868	11.373
							1163	5.973	848	11.906
							1079	7.049	825	12.468
							1021	8.068	798	13.378
							998	8.758		
0.7477	0.0015	0.0015	0.0015	0.0370	0.2138		1671	2.886	951	8.782
							1573	3.238	926	9.245
							1470	3.744	897	9.747
							1363	4.245	873	10.398
							1243	5.009	848	11.121
							1158	5.645	823	11.764
							1079	6.673	798	12.620
							1023	7.459	773	13.444
							963	8.566		
0.7460	0.0018	0.0015	0.0800	0.0036	0.1672		1658	3.146	998	8.790
							1583	3.283	973	9.338
							1457	3.730	948	9.767
							1368	4.187	923	10.279
							1271	4.857	898	10.951
							1182	5.549	873	11.678
							1065	7.124	848	12.602
							1022	7.861	823	13.305
0.7438	0.0026	0.0008	0.1109	0.0045	0.1375		1671	3.269	1040	8.580
							1583	3.638	973	10.117
							1478	3.885	948	10.824
							1391	4.367	923	11.367
							1263	5.243	898	12.068
							1172	6.179	873	12.824
							1077	7.751	848	13.481

Table B57 (*continued*)

SiO_2	Al_2O_3	Fe_2O_3	CaO	MgO	Na_2O	B_2O_3	T	log η	T	log η
0.7433	0.0023	0.0007	0.0486	0.0023	0.2029		1688	2.919	973	8.550
							1583	3.061	948	9.146
							1470	3.591	923	9.655
							1395	3.914	898	10.346
							1273	4.585	873	10.983
							1173	5.346	848	11.745
							1078	6.508	823	12.602
							1023	7.360	798	13.426
							975	8.281		
0.7432	0.0022	0.0006	0.1241	0.0046	0.1252		1681	3.355	973	10.676
							1583	3.803	948	11.362
							1475	4.000	923	11.955
							1375	4.613	898	12.481
							1273	5.251	873	13.346
							998	9.945		
0.7350	0.0034	0.0023	0.0674	0.0031	0.1887		1668	3.143	973	9.045
							1596	3.386	948	9.554
							1504	3.505	923	10.163
							1371	4.068	898	10.750
							1275	4.599	873	11.426
							1180	5.384	848	12.305
							1070	6.772	823	12.867
							1031	7.476	798	13.710
							970	8.607		
0.7579	0.0070	0.0070	0.0070	0.0070	0.1958	0.0393	1686	2.653	1271	4.559
							1577	2.919	1168	5.431
							1478	3.398	1078	6.787
							1368	3.903	1016	7.846
0.7335	0.0069	0.0069	0.0069	0.0069	0.1864	0.0733	1677	2.584	1271	4.255
							1569	2.760	1164	5.248
							1456	3.107	1062	6.935
							1350	3.568	1013	7.894
0.7035	0.0071	0.0071	0.0071	0.0071	0.1887	0.1007	1673	2.408	1270	3.946
							1583	2.505	1164	5.004
							1459	2.760	1065	6.831
							1360	3.310	993	8.623
0.6668	0.0054	0.0054	0.0054	0.0054	0.1993	0.1285	1671	2.350	1177	4.484
							1548	2.458	1066	6.588
							1330	3.107	988	8.901
							1261	3.628		
0.6355	0.0055	0.0055	0.0055	0.0055	0.1903	0.1687	1573	2.423	1178	4.057
							1471	2.550	1076	6.013
							1376	2.723	1003	8.094
							1273	3.143		
0.5257	0.0054	0.0054	0.0054	0.0054	0.2074	0.2615	1489	2.505	1181	3.435
							1361	2.651	1079	5.401
							1253	2.885	973	8.780
0.3774	0.0065	0.0065	0.0065	0.0065	0.2463	0.3699	1378	2.280	1053	4.513
							1273	2.301	973	7.430
							1135	2.763	935	8.888

Table B58
Washburn and Shelton (1924) [18]

SiO_2	Al_2O_3	Fe_2O_3	CaO	MgO	Na_2O	K_2O	T	log η	T	log η
0.7065					0.2935		1616	1.079	1392	2.001
							1605	1.118	1349	2.242
							1598	1.170	1314	2.324
							1509	1.476	1307	2.455
							1504	1.516	1210	3.051
							1479	1.616	1113	3.773
							1451	1.737		
0.6074					0.3926		1721	0.135	1328	1.743
							1657	0.345	1262	2.184
							1598	0.549	1237	2.312
							1525	0.854	1216	2.397
							1457	1.142	1186	2.495
							1371	1.527	1132	2.998
							1345	1.658	1075	3.516
0.7335			0.1069		0.1596		1680	1.171	1508	2.060
							1637	1.402	1469	2.276
							1626	1.454	1466	2.314
							1610	1.533	1408	2.552
							1587	1.623	1388	2.788
							1562	1.855	1254	3.598
0.7249			0.1596		0.1155		1648	1.944	1531	2.396
							1628	1.988	1508	2.628
							1570	2.214	1417	3.228
0.6922			0.2119		0.0959		1730	0.968	1483	2.884
							1694	1.091	1470	2.960
							1629	1.382	1448	3.239
							1581	1.601	1445	3.308
							1545	1.805	1425	3.832
							1542	1.877	1420	3.514
							1520	2.149	1394	4.232
							1498	2.485		
0.6993			0.1070		0.1937		1750	0.699	1409	2.088
							1668	1.009	1360	2.394
							1611	1.201	1299	2.761
							1597	1.362	1251	3.061
							1575	1.367	1237	3.206
							1536	1.509	1189	3.519
							1522	1.394	1123	4.136
							1487	1.736		
0.6807			0.1071		0.2122		1710	0.702	1420	1.880
							1690	0.796	1401	1.990
							1680	0.785	1386	2.081
							1659	0.904	1383	2.106
							1637	0.954	1375	2.155
							1599	1.105	1358	2.259
							1566	1.203	1351	2.289
							1510	1.439	1252	2.914
							1464	1.648	1235	2.964
							1435	1.797		
0.6700			0.1808		0.1492		1688	0.884	1401	2.373
							1670	0.953	1365	2.612
							1625	1.112	1257	3.534

Table B58 (*continued*)

SiO_2	Al_2O_3	Fe_2O_3	CaO	MgO	Na_2O	K_2O	T	log η	T	log η
							1597	1.358	1229	3.815
							1498	1.787	1189	4.300
0.6012			0.1074		0.2914		1608	0.686	1418	1.396
							1481	1.170	1326	1.772
							1430	1.332		
0.6003			0.2073		0.1924		1675	0.329	1406	1.859
							1597	0.659	1343	3.056
							1543	0.857	1299	3.690
							1495	1.057	1289	3.654
							1462	1.215		
0.5458			0.0835		0.3706		1655	−0.035	1390	1.043
							1554	0.075	1375	1.116
							1550	0.309	1366	1.187
							1547	0.387	1335	1.669
							1484	0.616	1265	2.511
							1463	0.735	1214	3.410
							1420	0.907		
0.8323	0.0030				0.1642	0.0005	1757	1.387	1613	1.910
							1742	1.444	1606	1.956
							1731	1.455	1570	2.138
							1704	1.604	1561	2.175
							1689	1.611	1529	2.320
							1677	1.647	1500	2.523
							1648	1.746	1476	2.676
							1631	1.819	1436	2.983
0.7268	0.0042	0.0002	0.13	0.003	0.1358		1710	0.956	1468	2.060
							1638	1.286	1447	2.172
							1587	1.520	1346	2.806
							1571	1.593	1294	3.234
							1549	1.696	1205	4.237
							1510	1.853		
0.6476	0.0029	0.0002	0.1679	0.0012	0.1803		1597	1.048	1375	2.150
							1585	1.162	1305	2.618
							1487	1.519	1251	3.051
							1464	1.644	1227	3.329
							1429	1.879	1115	4.742
							1411	1.958		
0.6259	0.0039	0.0002	0.2467	0.0025	0.1207		1658	0.584	1353	3.061
							1632	0.655	1348	3.142
							1603	0.798	1293	3.861
							1575	0.900	1292	3.915
							1551	0.997	1270	4.222
							1528	1.194		
0.5089	0.0111	0.0002	0.0001	0.0013	0.4769	0.0016	1433	0.037	1263	0.728
							1422	0.132	1224	0.942
							1338	0.289	1218	0.972
							1295	0.511		

Appendix C

The graphical representations of experimental data presented in this appendix are organised according to the scheme outlined in Appendix A.

First is a figure with the results of two studies on pure SiO_2. The legends are attempted organised in the same vertical order as they appear on the chart.

Subsequently binary, ternary, quartenary and quinary systems with the components organised in the order: SiO_2, Al_2O_3, FeO_x, CaO, MgO, Na_2O, K_2O, Li_2O, MnO, TiO_2, B_2O_3, XCl_x are presented. To improve the clarity of the chart titles and legends, molar fractions are simply written as the chemical symbol of the oxide, i.e. $X_{CaO} = CaO$. Whenever there is the basis, an acid-to-base ratio is listed. Most often the following form is used:

$$\frac{SiO_2 + 2(Al_2O_3 + Fe_2O_3)}{FeO + Fe + CaO + MgO + Na_2O + Na_2O + K_2O + Li_2O + MnO + TiO_2}$$

but sometimes another form is used, if this gives a result that is in better agreement with the graphical results (mostly an exclusion of the amphoterics from the ratio). In any case, the precise form of the ratio is given in the sub-title of the chart. The acid-to-base ratio is included to guide the reader in his or hers considerations on the predictablity of viscosity and the trustworthiness of a givens set of measurements.

In each legend text, the molar fraction of SiO_2 as well as the authors of the paper and the publishing year are included as a guide to the experimental procedures in Appendix A and the tabulated data in Appendix B.

All mixtures containing more than six components are categorised as multi-component mixtures and organised separately according to the scheme described above (Table C1).

Table C1

SiO_2	Al_2O_3	FeO_x	CaO	MgO	Na_2O	K_2O	Li_2O	MnO	TiO_2	B_2O_3	XCl_x	Figure
Si												C.1
Si	Al											C.2
Si		Fe										C.3–C.4
Si			Ca									C.5–C.6
Si				Mg								C.7
Si					Na							C.8–C.12
Si						K						C.13
Si							Li					C.14–C.16
Si								Mn				C.17
Si	Al		Ca									C.18–C.27
Si	Al			Mg								C.28
Si	Al				Na							C.29–C.31
Si	Al					K						C.31
Si	Al							Mn				C.32
Si		Fe	Ca									C.33–C.36
Si		Fe		Mg								C.37
Si		Fe			Na							C.38–C.40
Si		Fe				K						C.41
Si			Ca	Mg								C.42–C.43
Si			Ca		Na							C.44
Si			Ca					Mn				C.45
Si			Ca						Ti			C.46
Si				Mg	Na							C.47

Table C1 (*continued*)

SiO_2	Al_2O_3	FeO_x	CaO	MgO	Na_2O	K_2O	Li_2O	MnO	TiO_2	B_2O_3	XCl_x	Figure
Si					Na	K						C.48
Si					Na				Ti			C.49 and C.50
Si						K	Li					C.51
Si						K			Ti			C.50
Si	Al	Fe	Ca									C.52
Si	Al	Fe			Na							C.53
Si	Al		Ca	Mg								C.54–C.64
Si	Al		Ca		Na							C.65
Si	Al		Ca					Mn				C.66
Si	Al		Ca						Ti			C.67
Si	Al		Ca								X	C.68
Si	Al				Na	K						C.69
Si		Fe	Ca	Mg								C.70–C.71
Si	Al	Fe	Ca	Mg								C.72
Si	Al		Ca	Mg	Na							C.73
Si	Al		Ca	Mg	Na	K						C.74
Multi-component systems												
Only major components cited, i.e. mole fractions >5%												
Si	Al											C.75–C.76
Si			Ca									C.77
Si					Na							C.78
Si	Al	Fe										C.79–C.80
Si	Al		Ca									C.81–C.85
Si	Al				Na							C.86
Si		Fe		Mg								C.87
Si			Ca	Mg								C.88
Si			Ca		Na							C.89–C94
Si				Mg	Na							C.95
Si					Na					B		C.96
Si	Al	Fe	Ca									C.97–C.98
Si	Al		Ca	Mg								C.99–C.102
Si	Al		Ca		Na							C.103–C.104
Si			Ca		Na	K						C.105

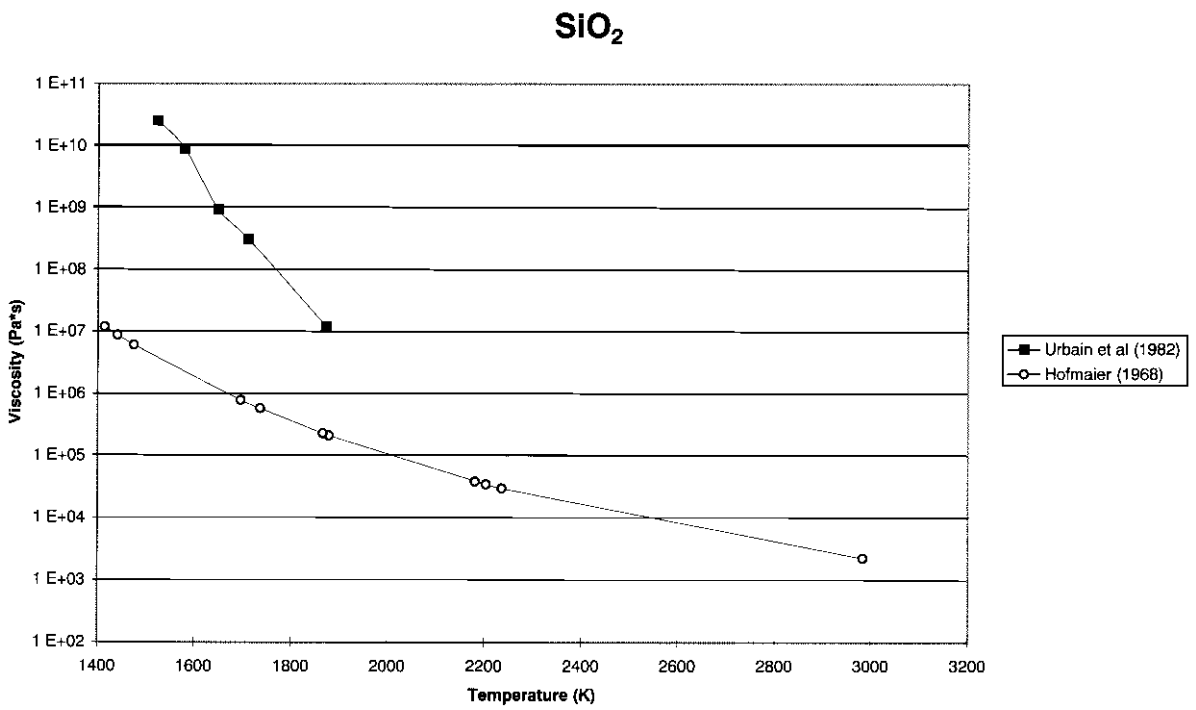
SiO2
1 E+11
1 E+10
1 E+09
1 E+08
1 E+07
1 E+06
1 E+05
1 E+04
1 E+03
1 E+02
Viscosity (Pa*s)
1400
1600
1800
2000
2200
2400
2600
2800
3000
3200
Temperature (K)
Urbain et al (1982)
Hofmaier (1968)

Fig. C.1.

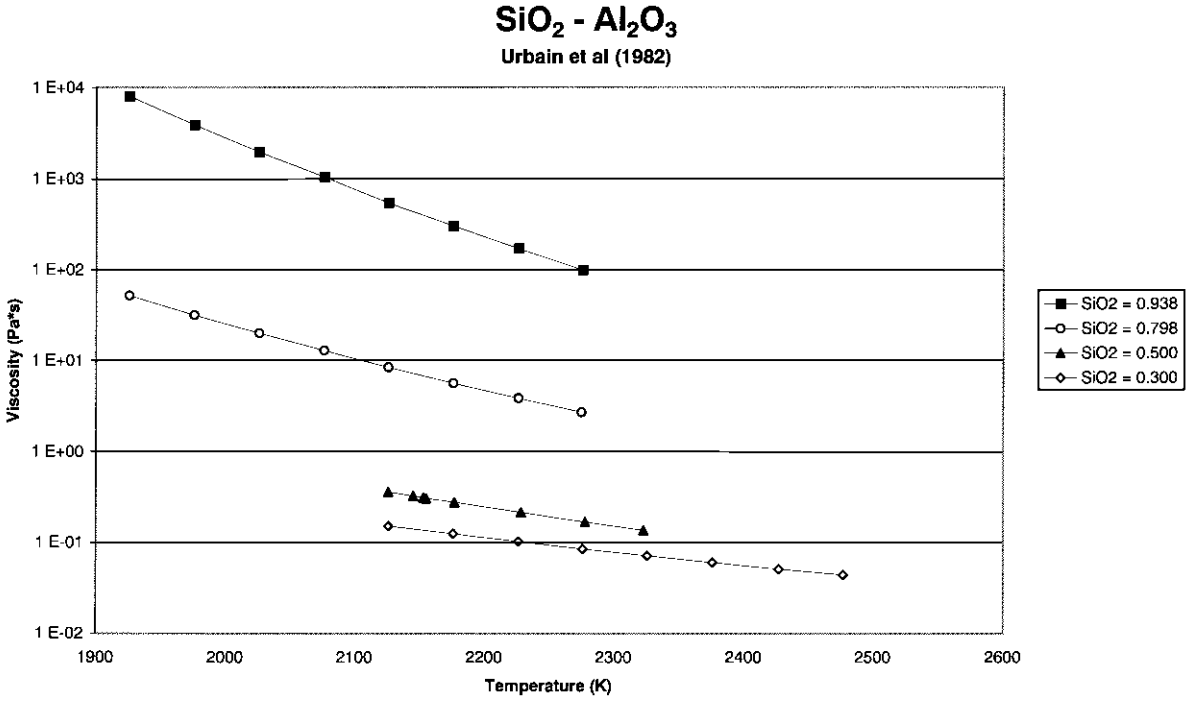
SiO2 - Al2O3
Urbain et al (1982)
1 E+04
1 E+03
1 E+02
1 E+01
1 E+00
1 E-01
1 E-02
Viscosity (Pa*s)
1900
2000
2100
2200
2300
2400
2500
2600
Temperature (K)
SiO2 = 0.938
SiO2 = 0.798
SiO2 = 0.500
SiO2 = 0.300

Fig. C.2.

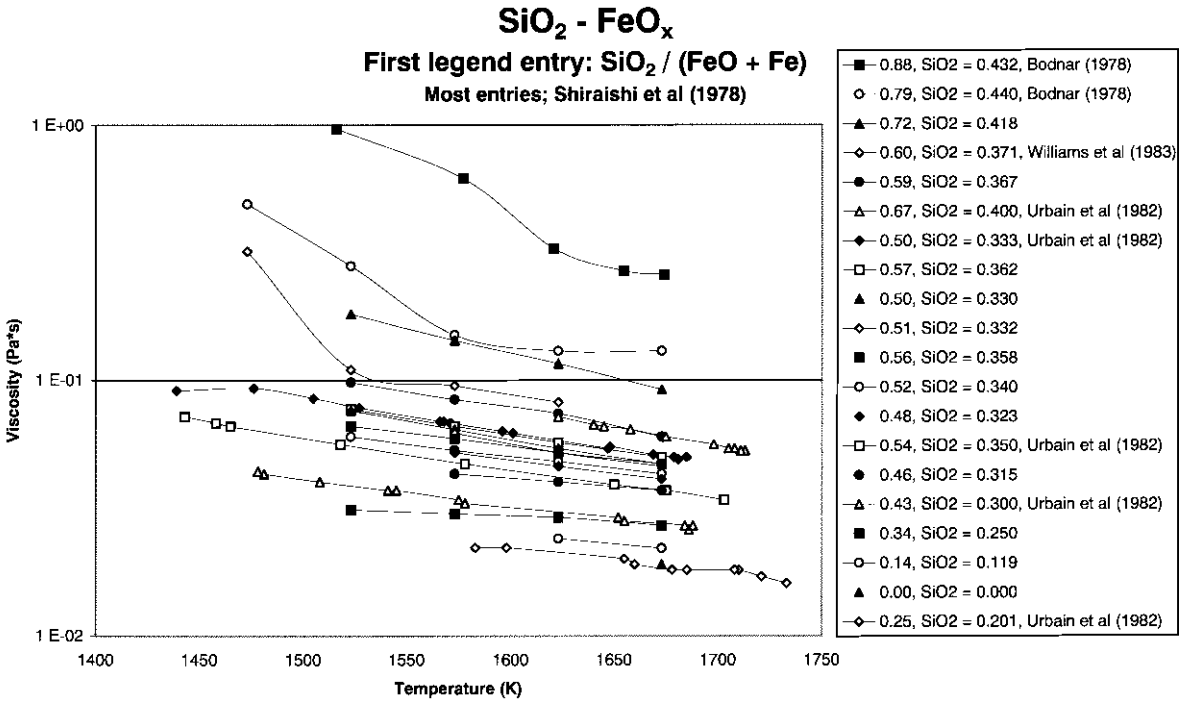
SiO2 - FeOx
First legend entry: SiO2 / (FeO + Fe)
Most entries; Shiraishi et al (1978)
Viscosity (Pa*s)
1 E+00
1 E-01
1 E-02
1400
1450
1500
1550
1600
1650
1700
1750
Temperature (K)
0.88, SiO2 = 0.432, Bodnar (1978)
0.79, SiO2 = 0.440, Bodnar (1978)
0.72, SiO2 = 0.418
0.60, SiO2 = 0.371, Williams et al (1983)
0.59, SiO2 = 0.367
0.67, SiO2 = 0.400, Urbain et al (1982)
0.50, SiO2 = 0.333, Urbain et al (1982)
0.57, SiO2 = 0.362
0.50, SiO2 = 0.330
0.51, SiO2 = 0.332
0.56, SiO2 = 0.358
0.52, SiO2 = 0.340
0.48, SiO2 = 0.323
0.54, SiO2 = 0.350, Urbain et al (1982)
0.46, SiO2 = 0.315
0.43, SiO2 = 0.300, Urbain et al (1982)
0.34, SiO2 = 0.250
0.14, SiO2 = 0.119
0.00, SiO2 = 0.000
0.25, SiO2 = 0.201, Urbain et al (1982)

Fig. C.3.

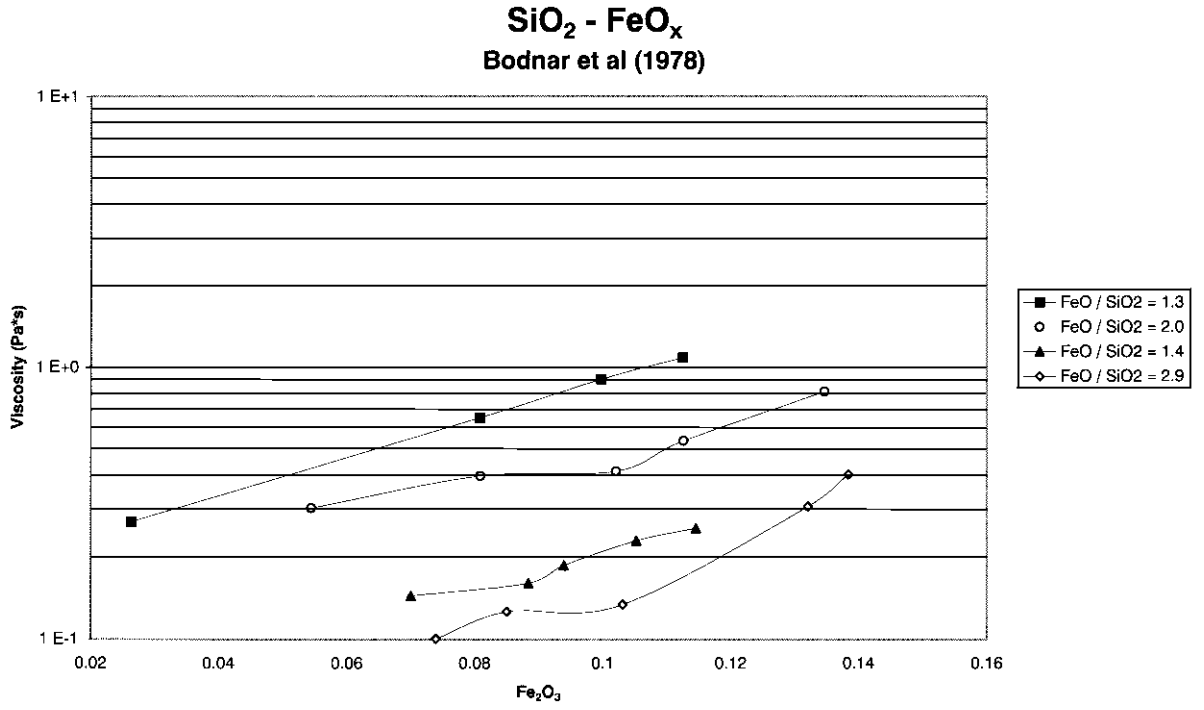
SiO2 - FeOx
Bodnar et al (1978)
Viscosity (Pa*s)
1 E+1
1 E+0
1 E-1
0.02
0.04
0.06
0.08
0.1
0.12
0.14
0.16
Fe2O3
FeO / SiO2 = 1.3
FeO / SiO2 = 2.0
FeO / SiO2 = 1.4
FeO / SiO2 = 2.9

Fig. C.4.

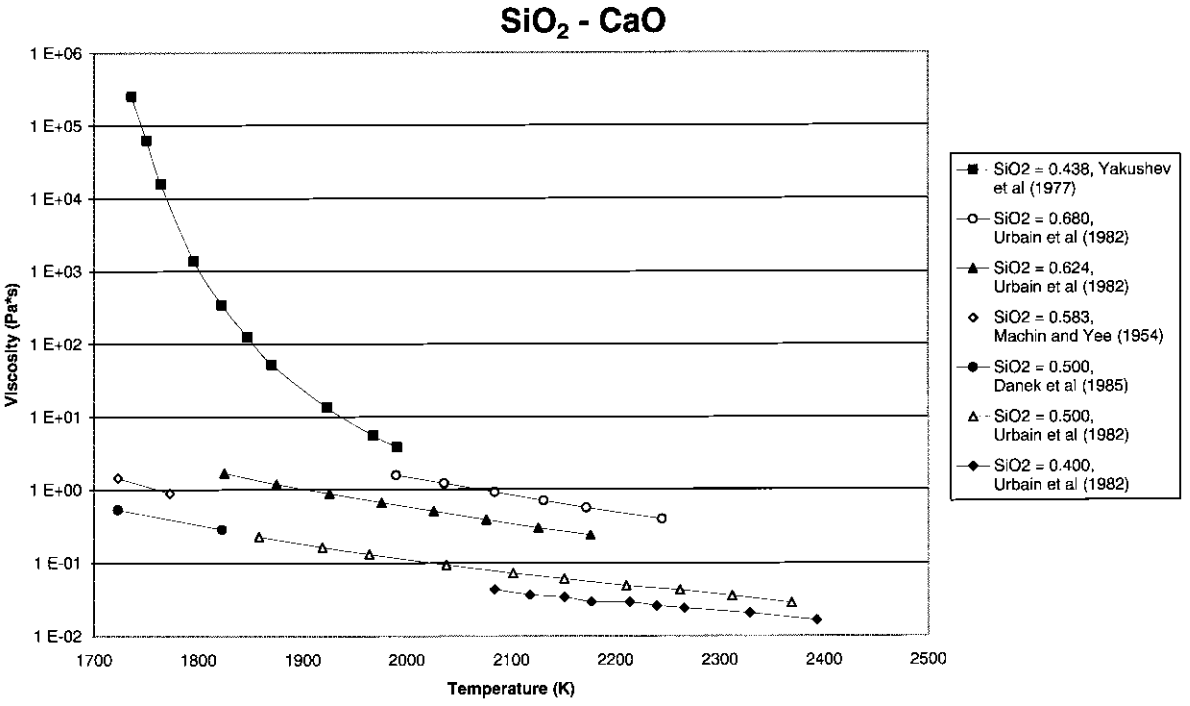
SiO2 - CaO
Viscosity (Pa*s)
1 E+06
1 E+05
1 E+04
1 E+03
1 E+02
1 E+01
1 E+00
1 E-01
1 E-02
1700
1800
1900
2000
2100
2200
2300
2400
2500
Temperature (K)
SiO2 = 0.438, Yakushev et al (1977)
SiO2 = 0.680, Urbain et al (1982)
SiO2 = 0.624, Urbain et al (1982)
SiO2 = 0.583, Machin and Yee (1954)
SiO2 = 0.500, Danek et al (1985)
SiO2 = 0.500, Urbain et al (1982)
SiO2 = 0.400, Urbain et al (1982)

Fig. C.5.

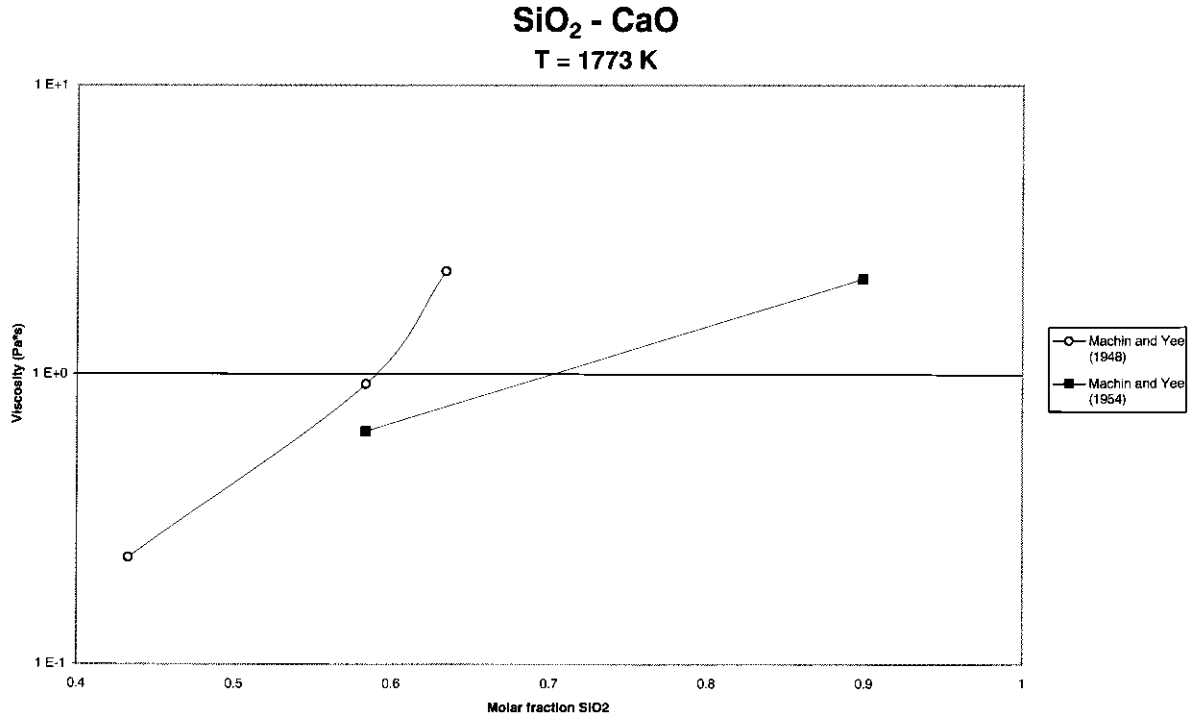
SiO2 - CaO
T = 1773 K
Viscosity (Pa*s)
1 E+1
1 E+0
1 E-1
0.4
0.5
0.6
0.7
0.8
0.9
1
Molar fraction SiO2
Machin and Yee (1948)
Machin and Yee (1954)

Fig. C.6.

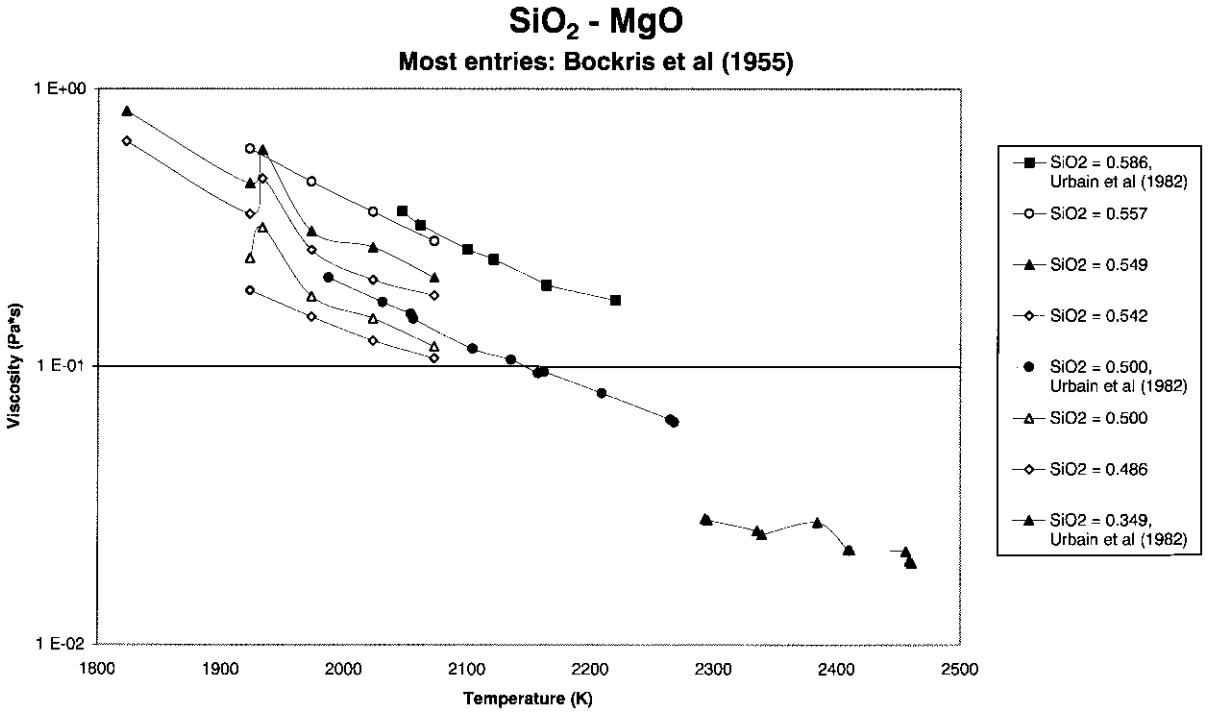
SiO2 - MgO
Most entries: Bockris et al (1955)
Viscosity (Pa*s)
1 E+00
1 E-01
1 E-02
1800
1900
2000
2100
2200
2300
2400
2500
Temperature (K)
SiO2 = 0.586, Urbain et al (1982)
SiO2 = 0.557
SiO2 = 0.549
SiO2 = 0.542
SiO2 = 0.500, Urbain et al (1982)
SiO2 = 0.500
SiO2 = 0.486
SiO2 = 0.349, Urbain et al (1982)

Fig. C.7.

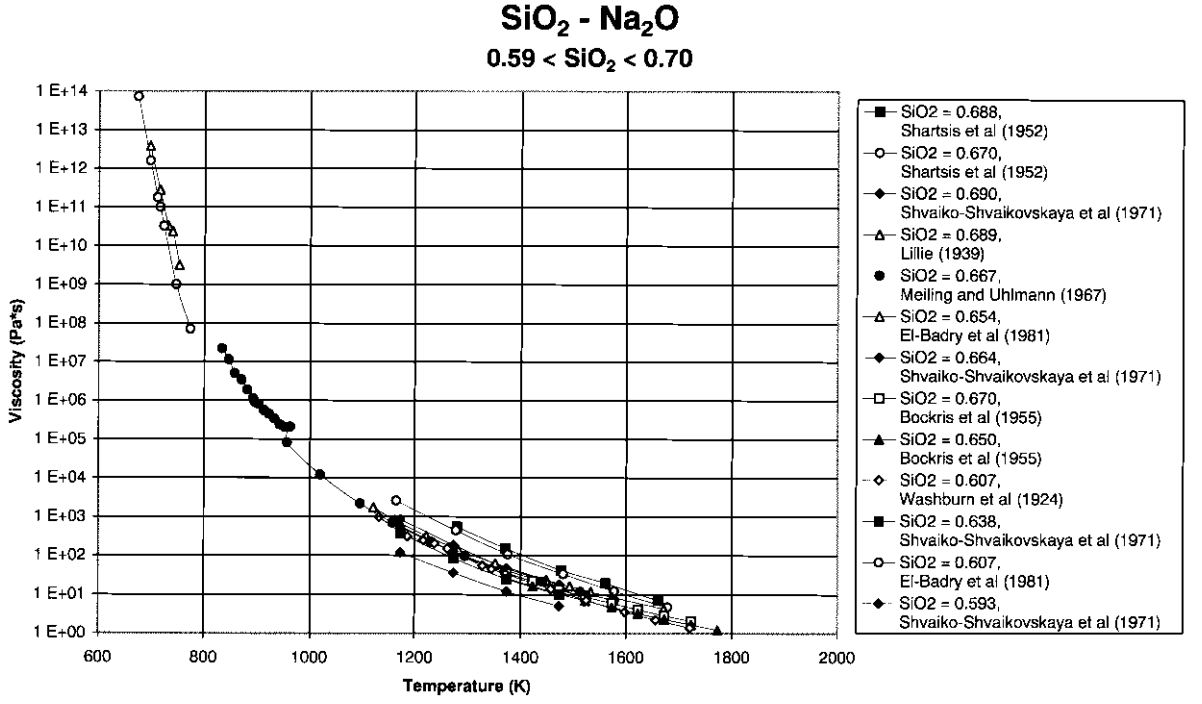
SiO2 - Na2O
0.59 < SiO2 < 0.70
Viscosity (Pa*s)
1 E+14
1 E+13
1 E+12
1 E+11
1 E+10
1 E+09
1 E+08
1 E+07
1 E+06
1 E+05
1 E+04
1 E+03
1 E+02
1 E+01
1 E+00
600
800
1000
1200
1400
1600
1800
2000
Temperature (K)
SiO2 = 0.688, Shartsis et al (1952)
SiO2 = 0.670, Shartsis et al (1952)
SiO2 = 0.690, Shvaiko-Shvaikovskaya et al (1971)
SiO2 = 0.689, Lillie (1939)
SiO2 = 0.667, Meiling and Uhlmann (1967)
SiO2 = 0.654, El-Badry et al (1981)
SiO2 = 0.664, Shvaiko-Shvaikovskaya et al (1971)
SiO2 = 0.670, Bockris et al (1955)
SiO2 = 0.650, Bockris et al (1955)
SiO2 = 0.607, Washburn et al (1924)
SiO2 = 0.638, Shvaiko-Shvaikovskaya et al (1971)
SiO2 = 0.607, El-Badry et al (1981)
SiO2 = 0.593, Shvaiko-Shvaikovskaya et al (1971)

Fig. C.8.

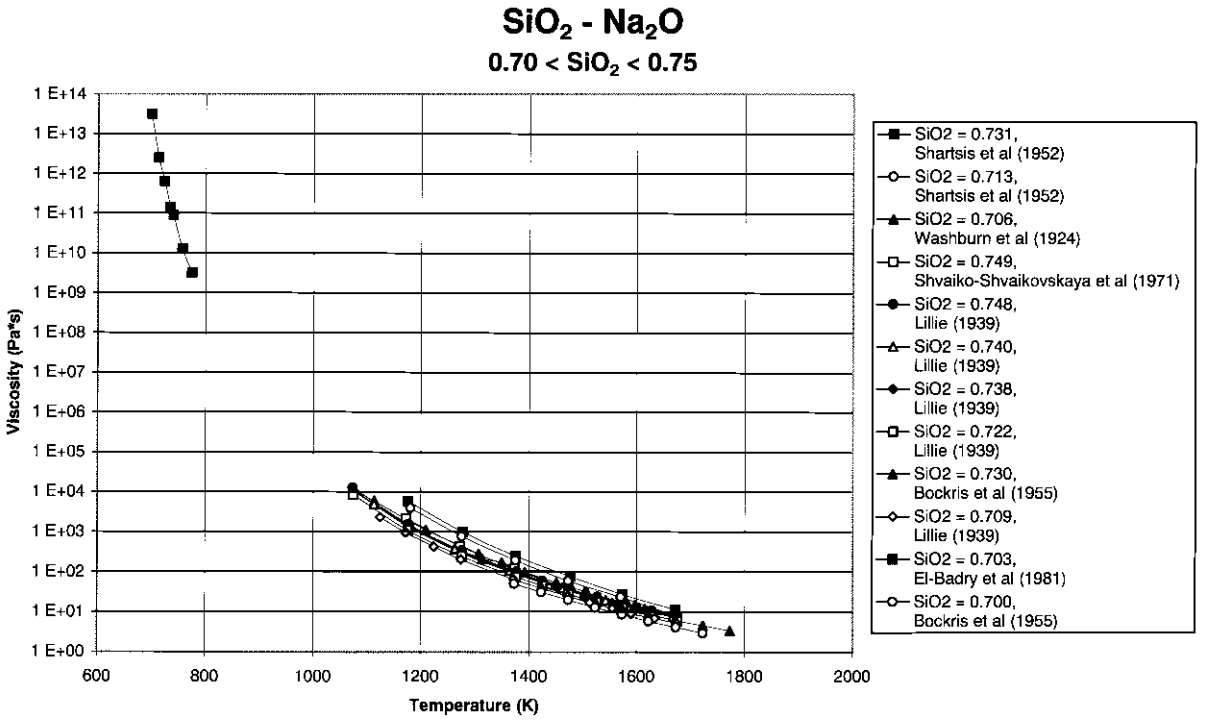

Fig. C.9.

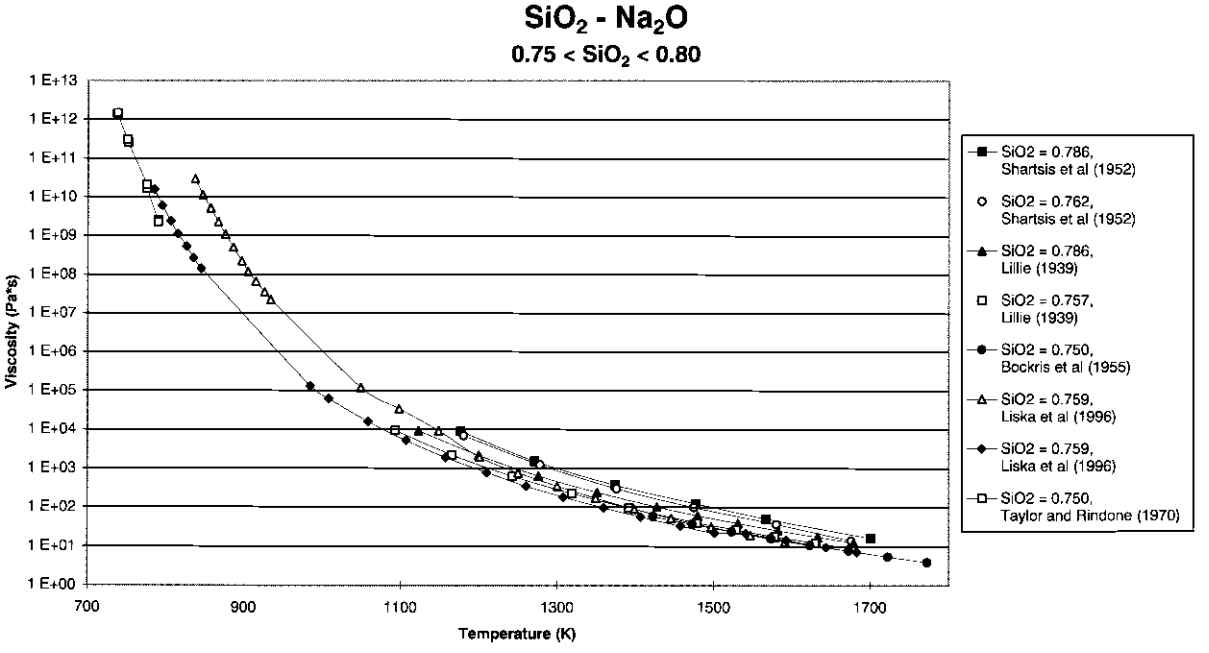

Fig. C.10.

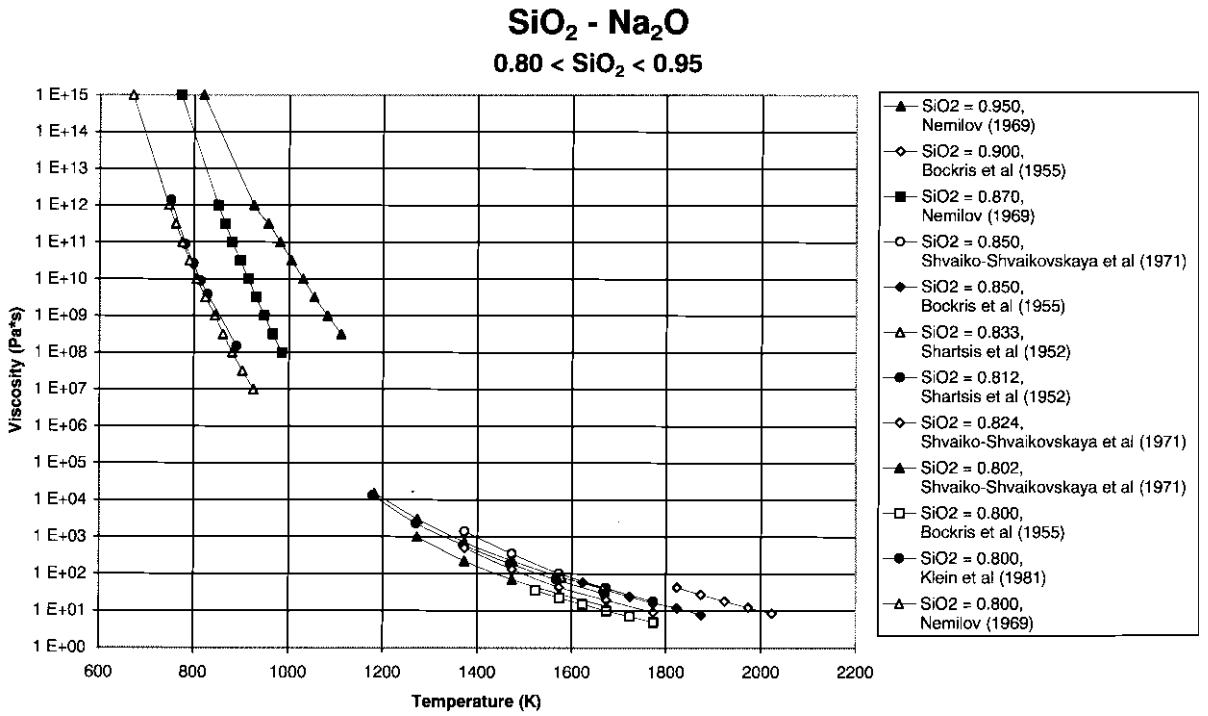

Fig. C.11.

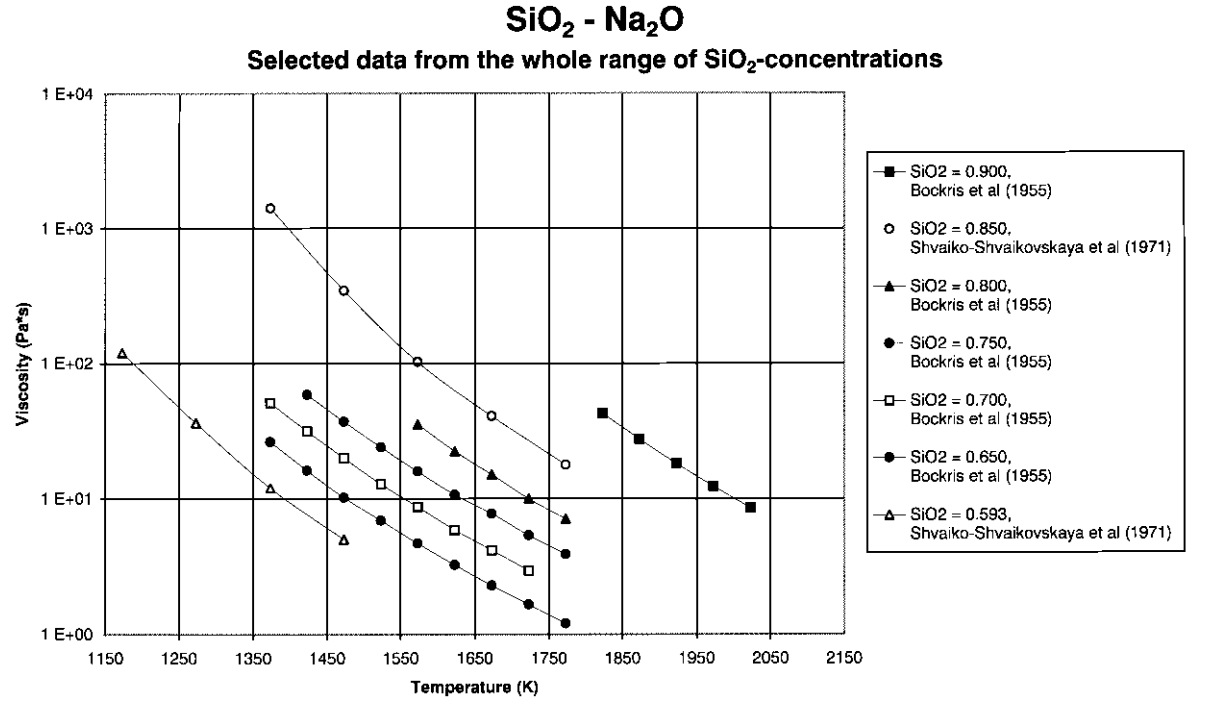

Fig. C.12.

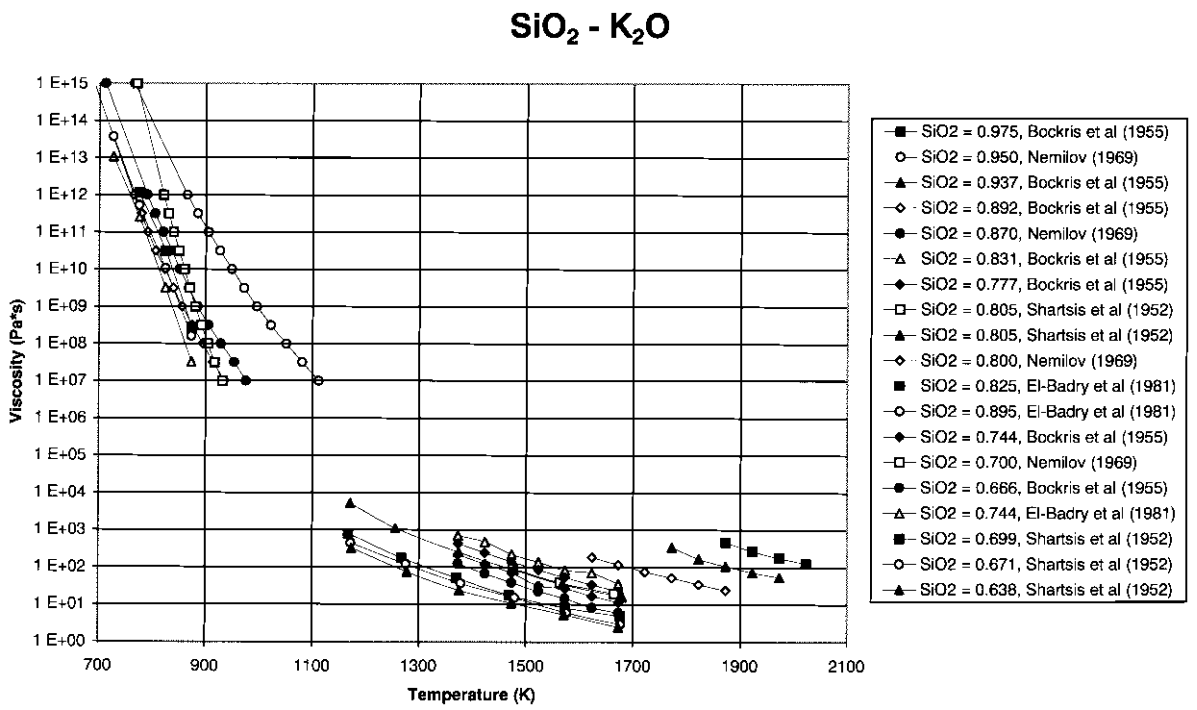

Fig. C.13.

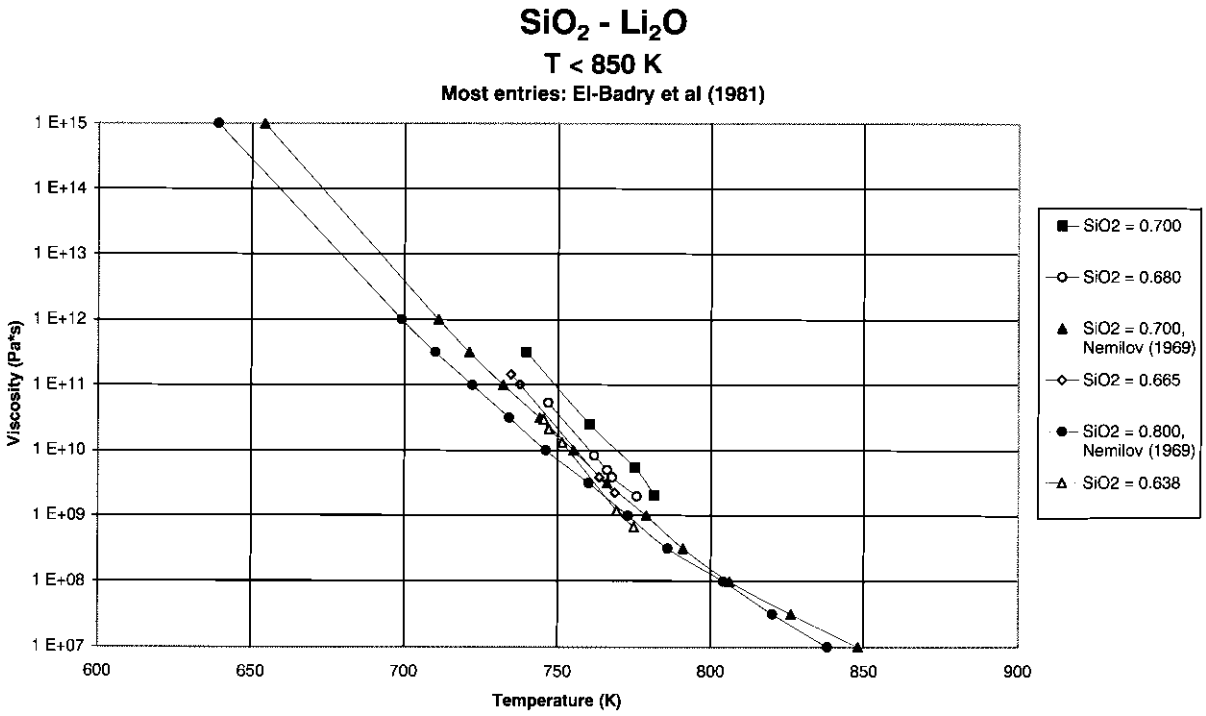

Fig. C.14.

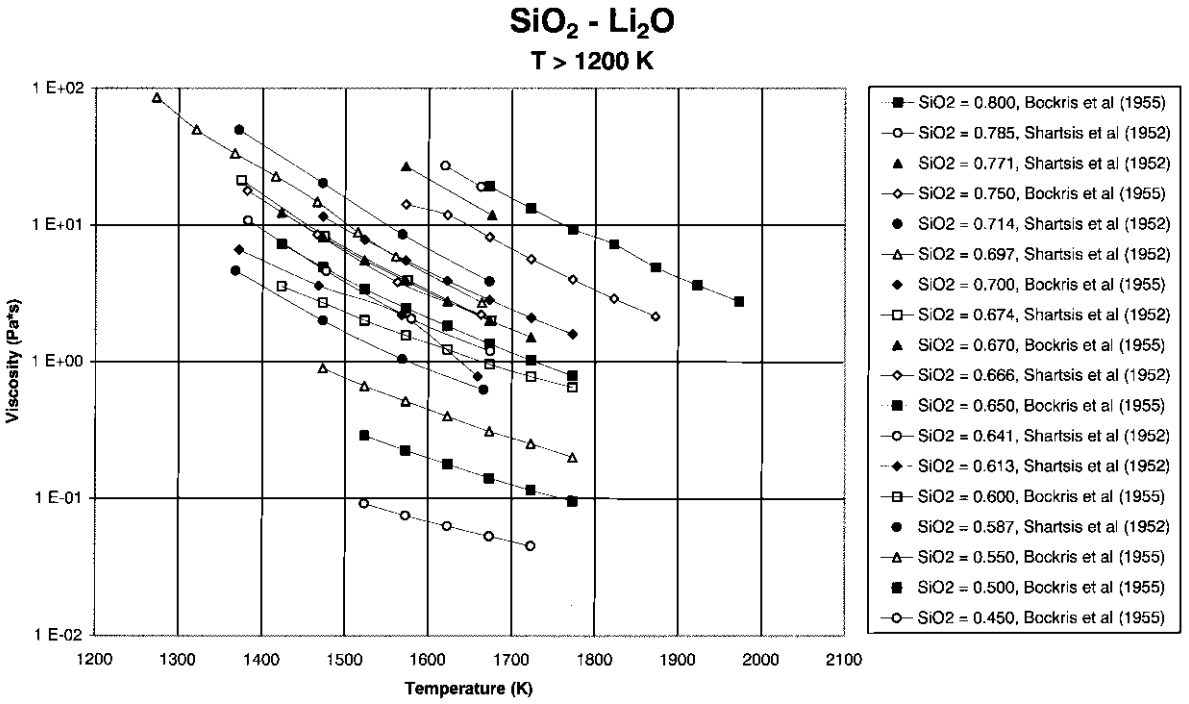

Fig. C.15.

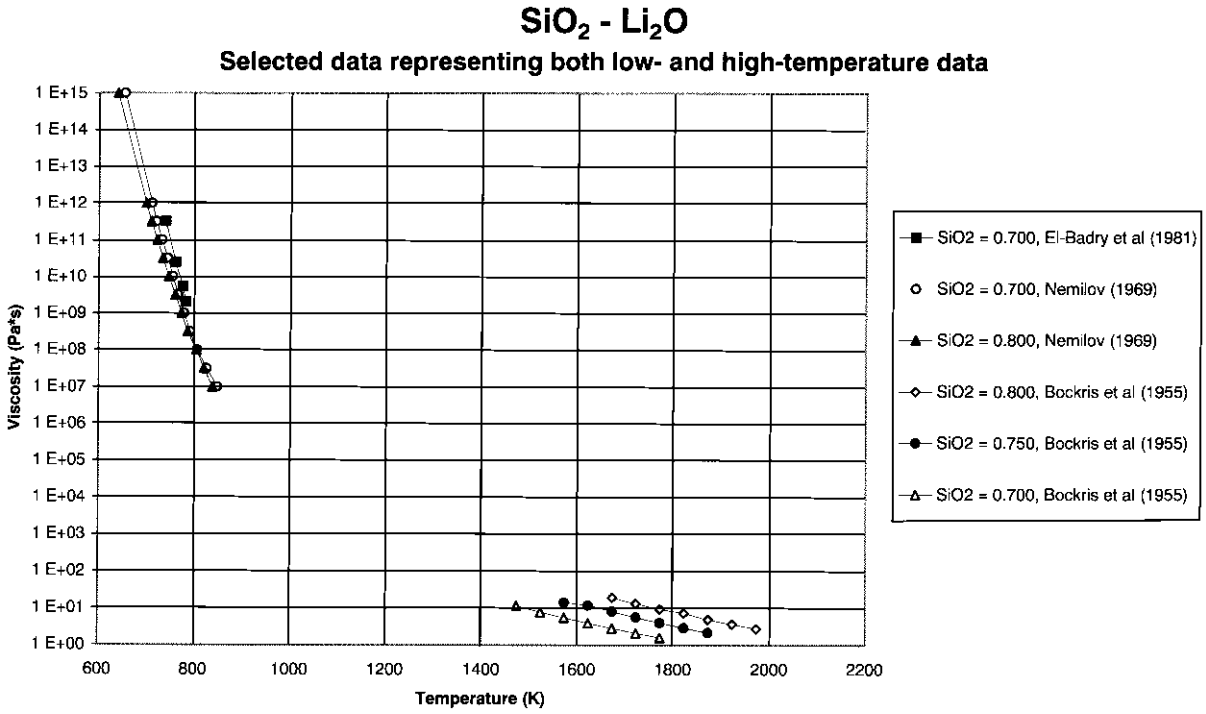

Fig. C.16.

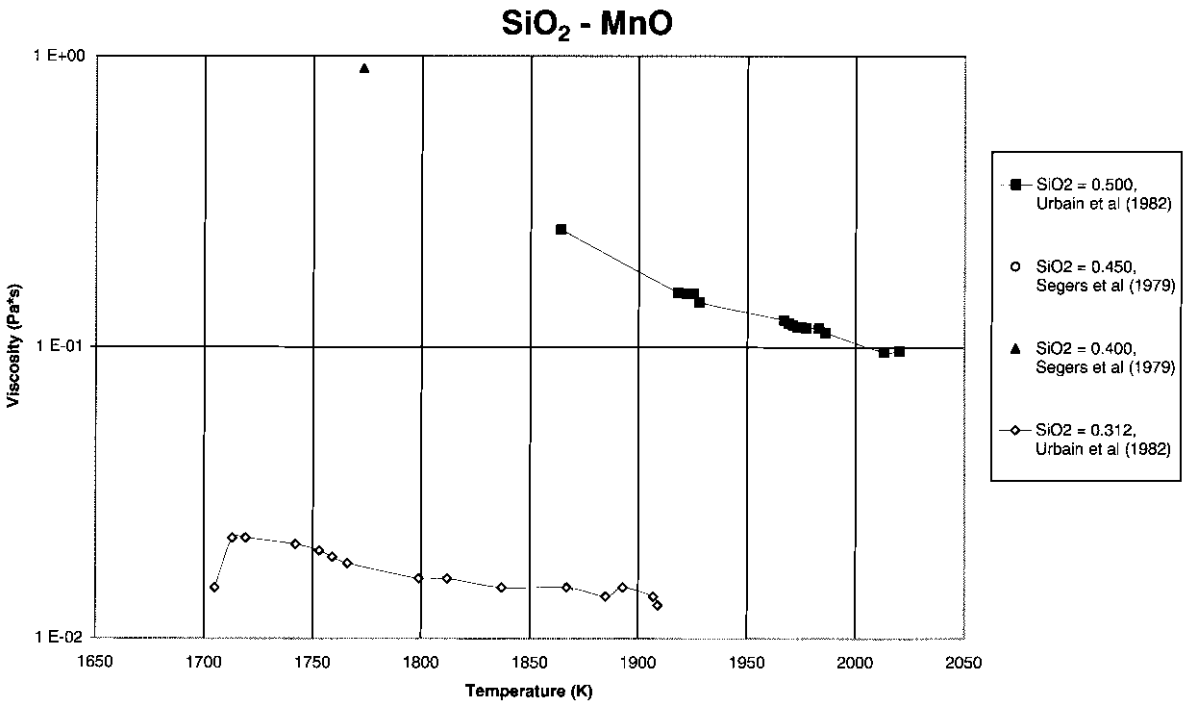

Fig. C.17.

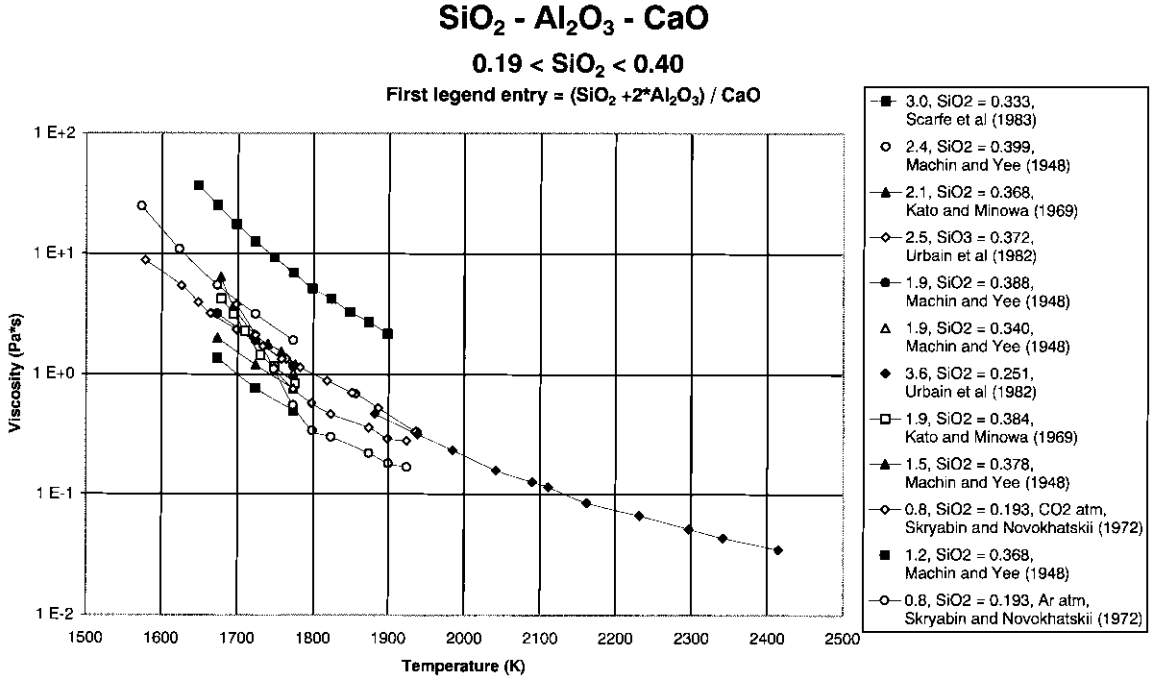

Fig. C.18.

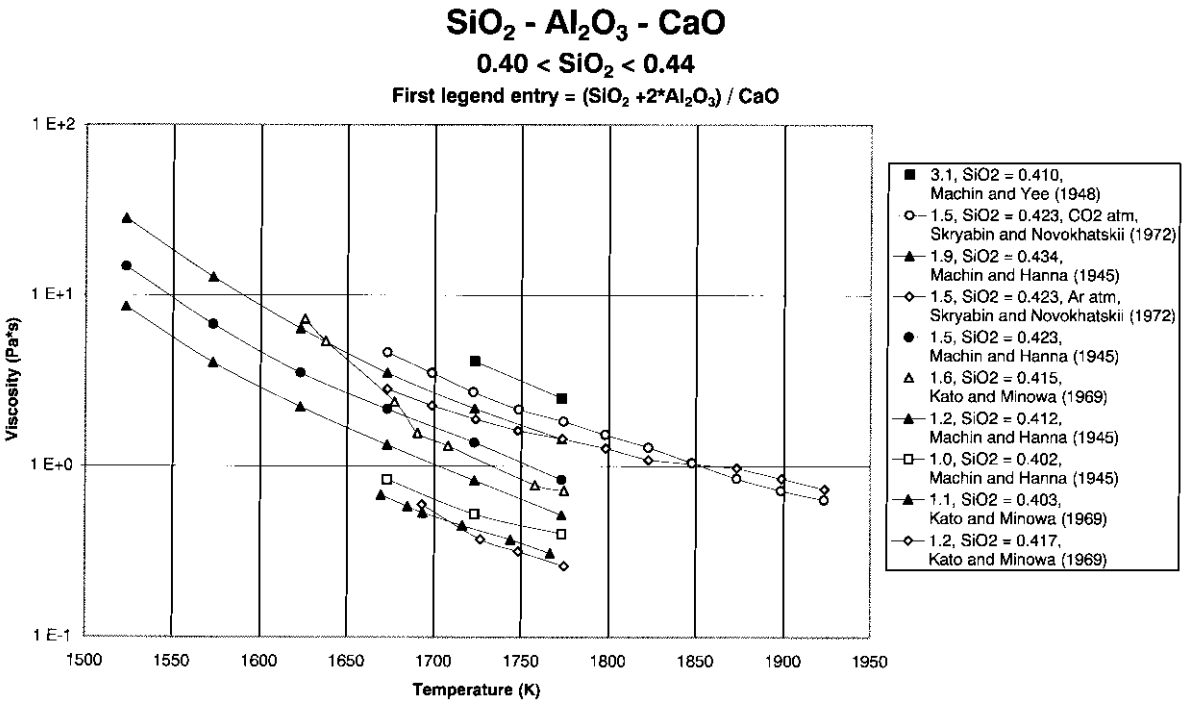

Fig. C.19.

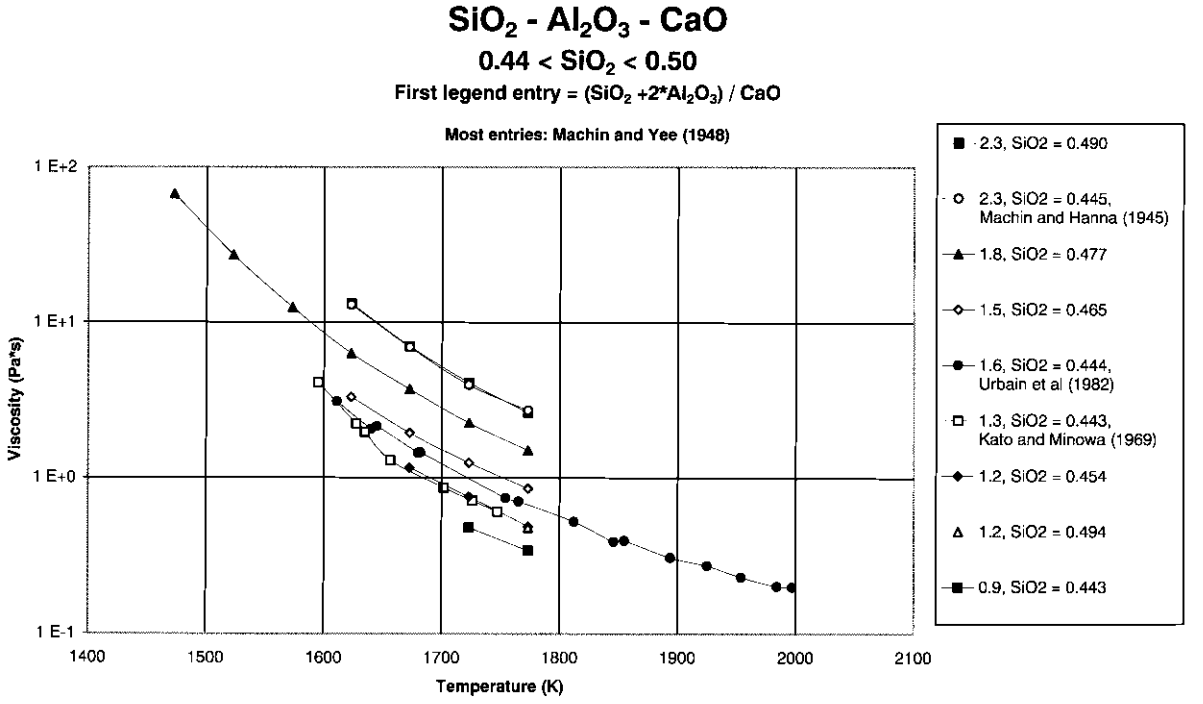

Fig. C.20.

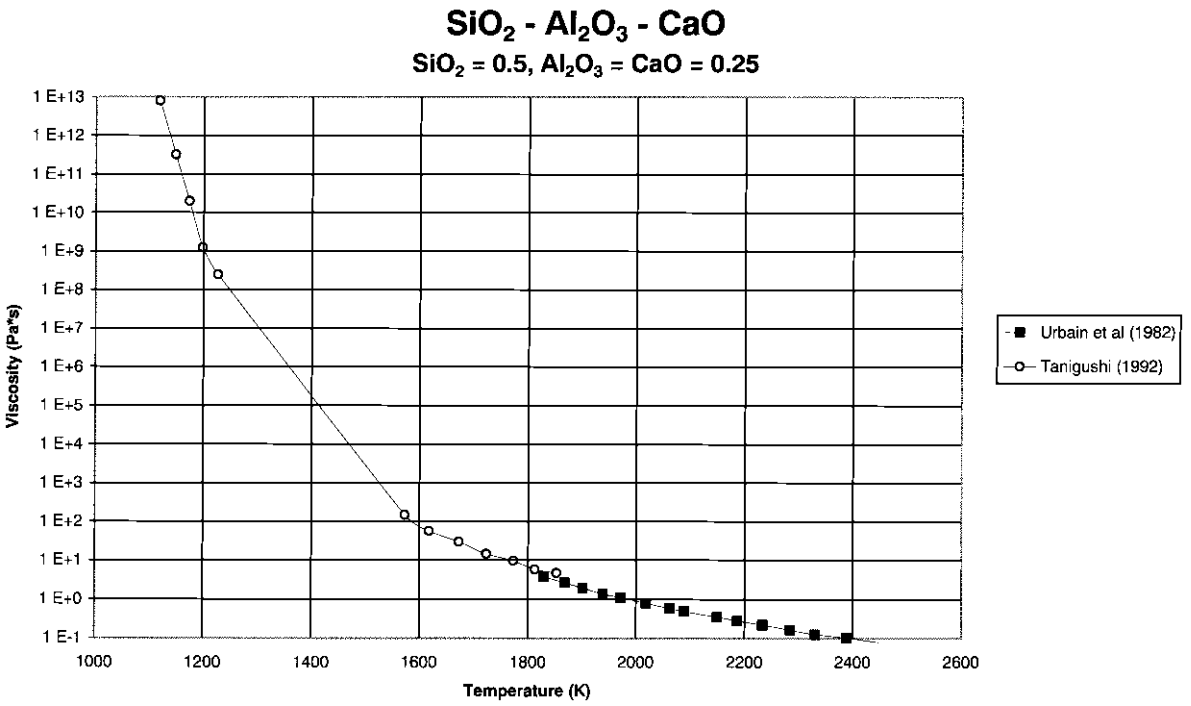

Fig. C.21.

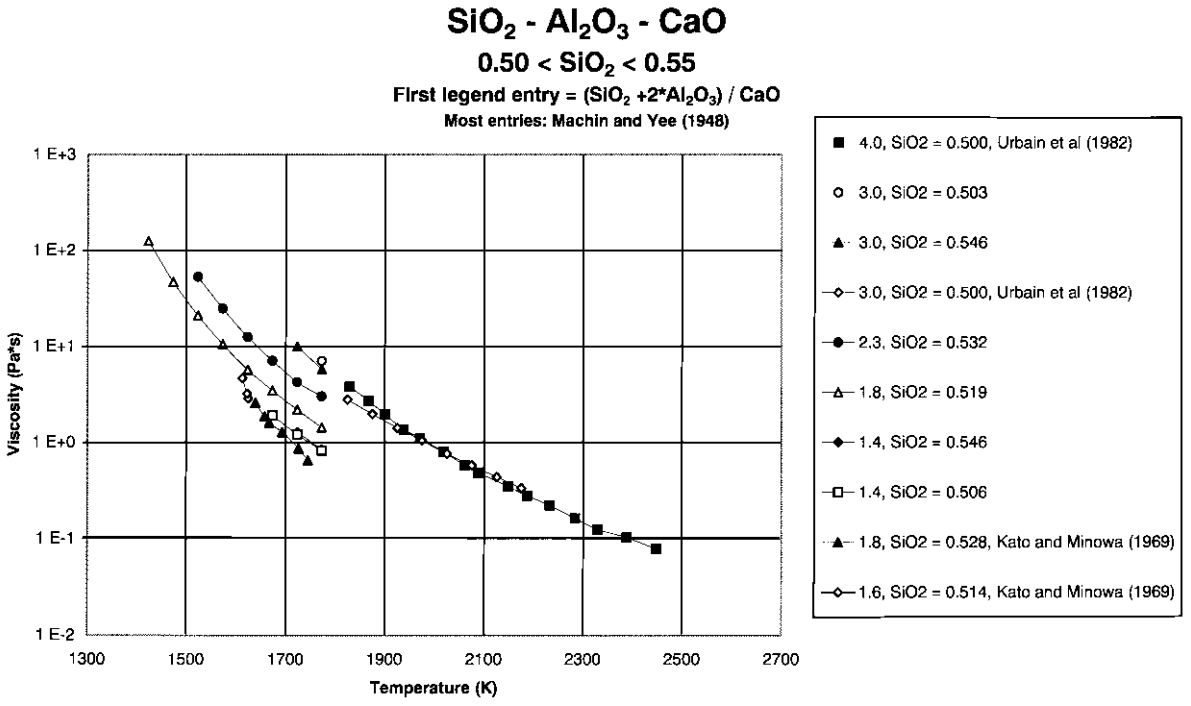

Fig. C.22.

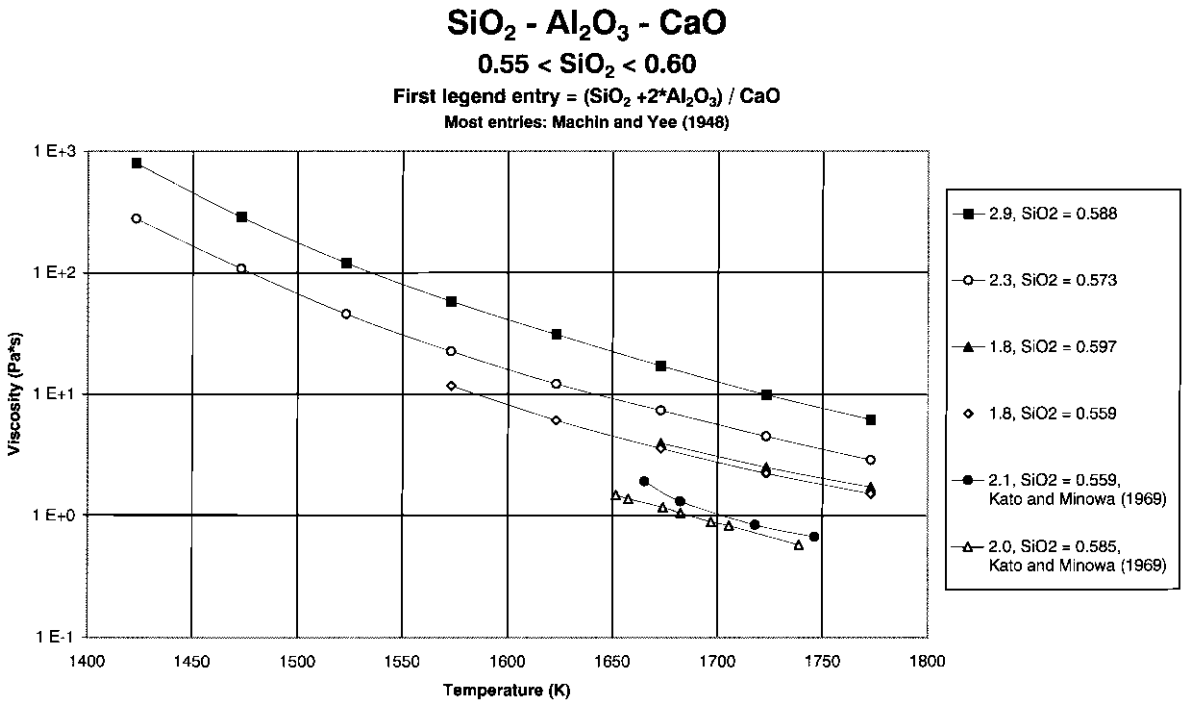

Fig. C.23.

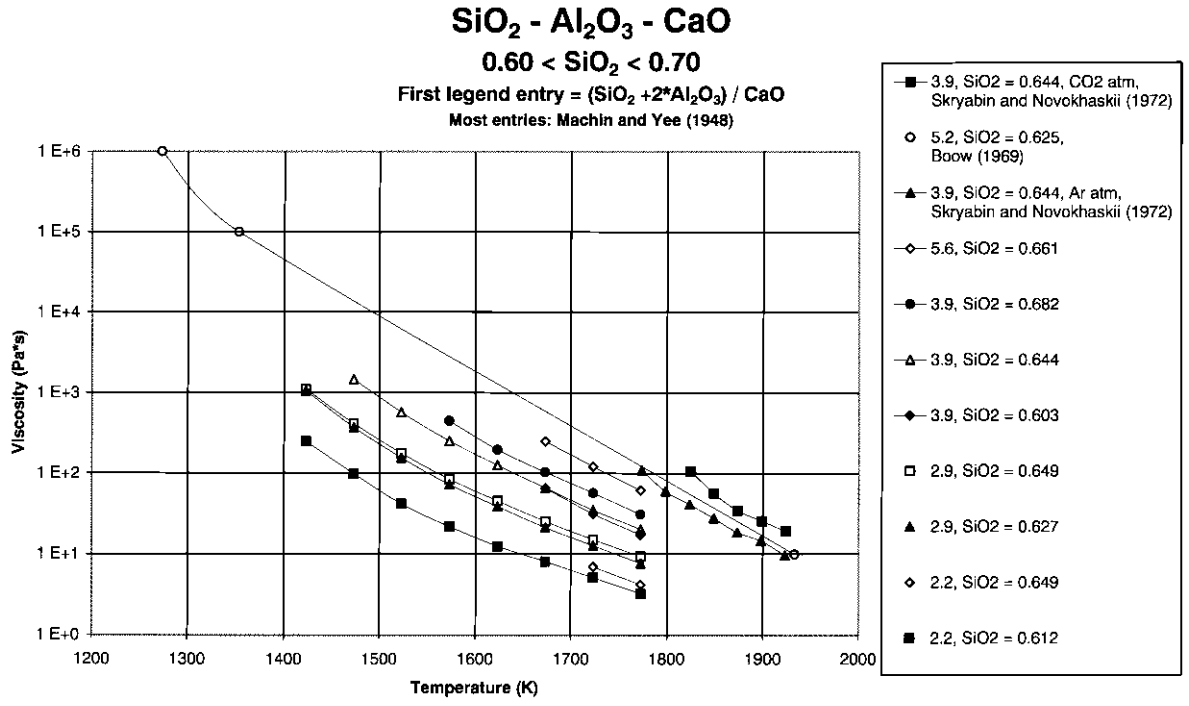

Fig. C.24.

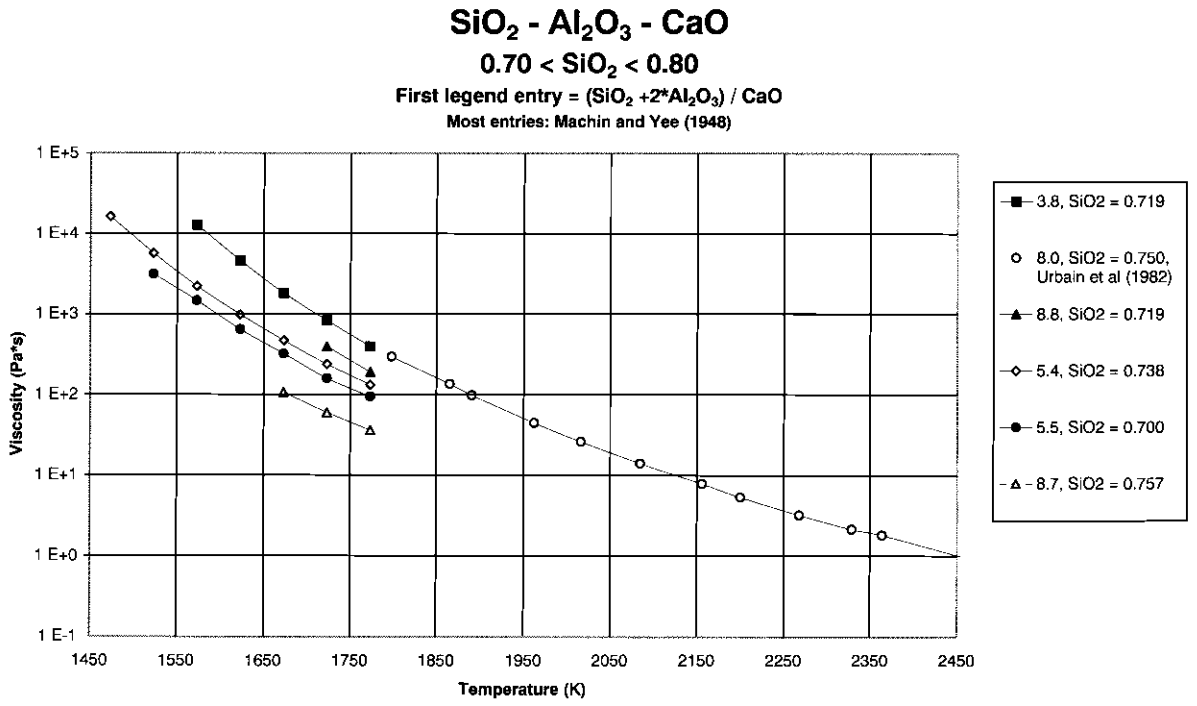

Fig. C.25.

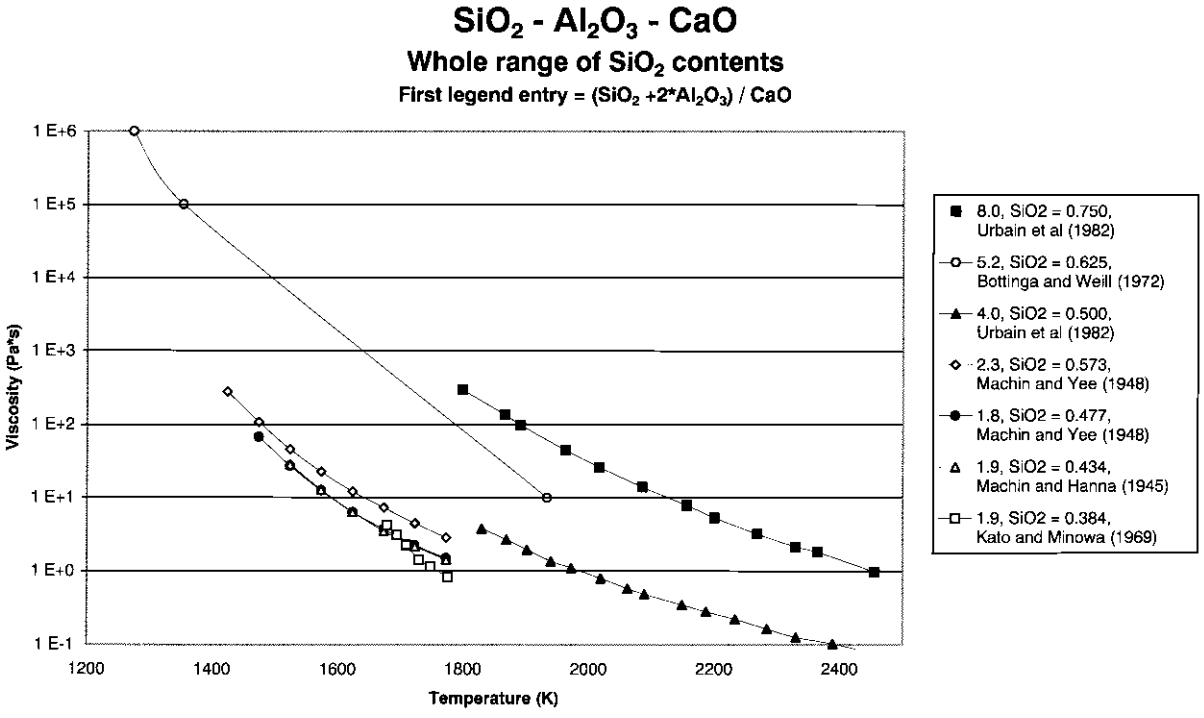

Fig. C.26.

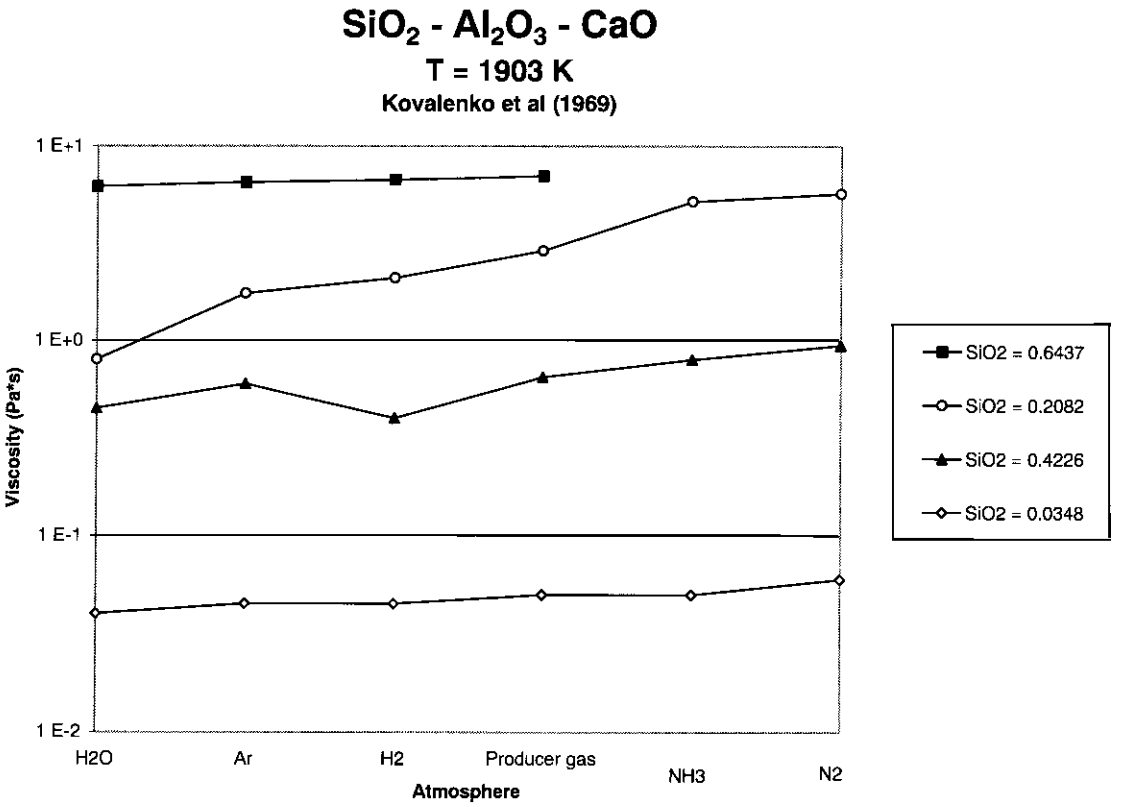

Fig. C.27.

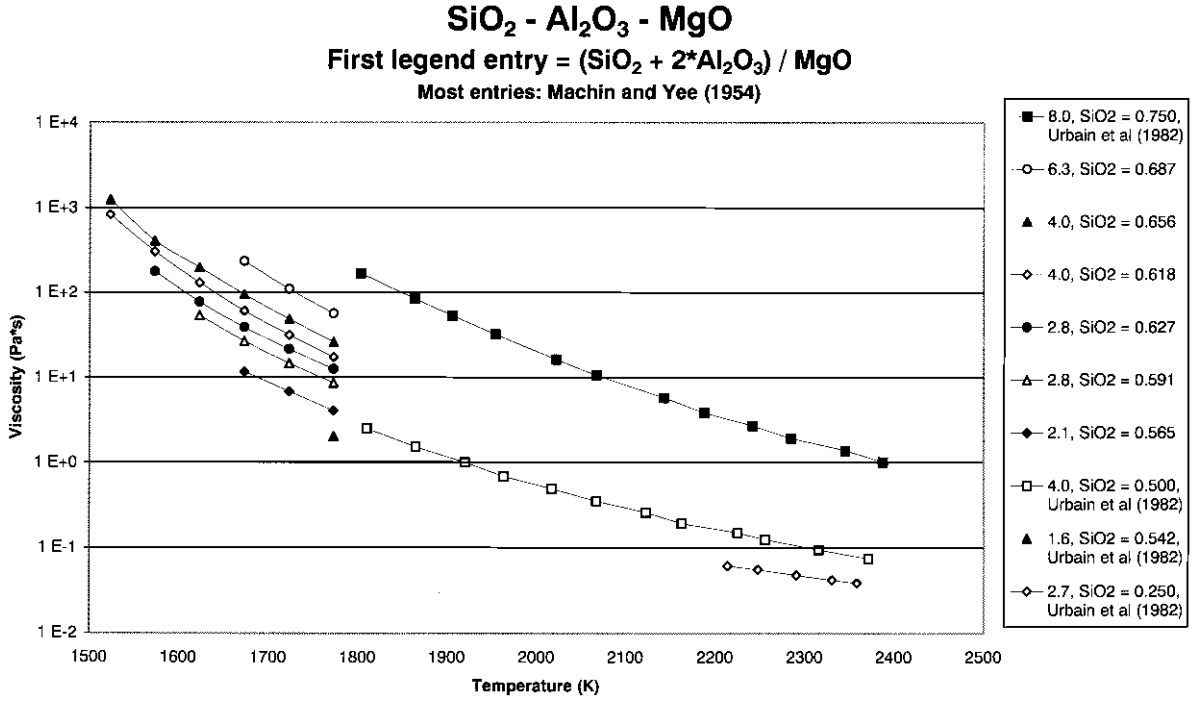

Fig. C.28.

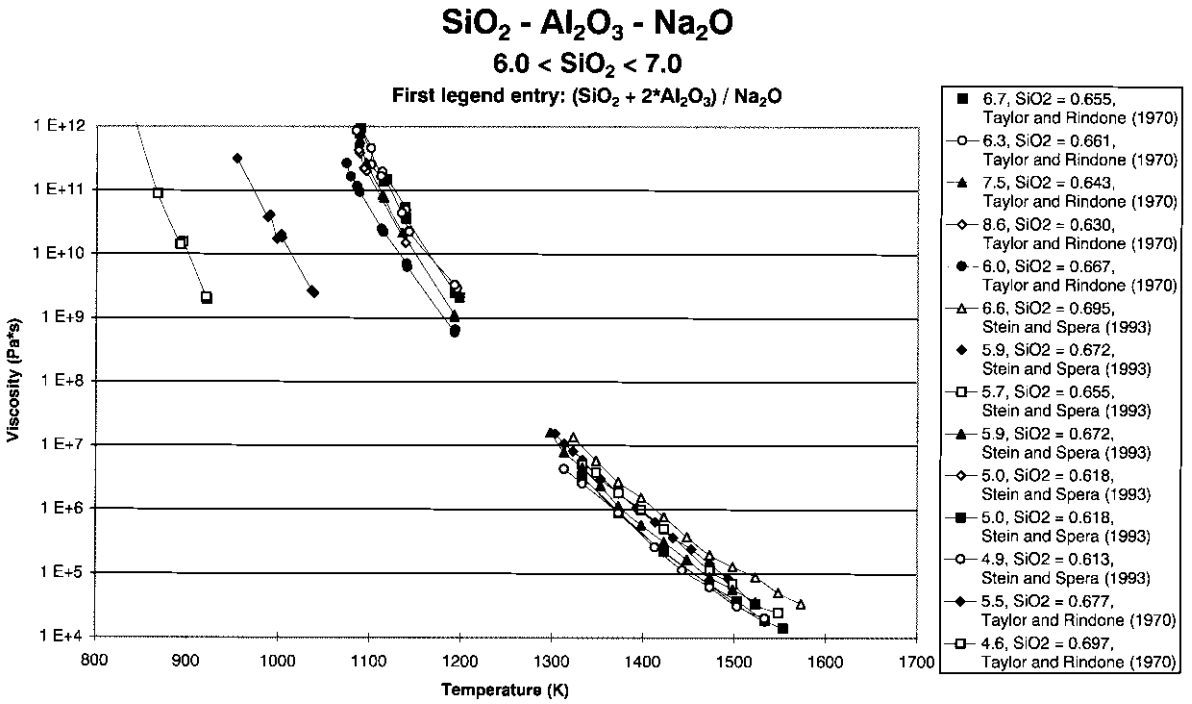

Fig. C.29.

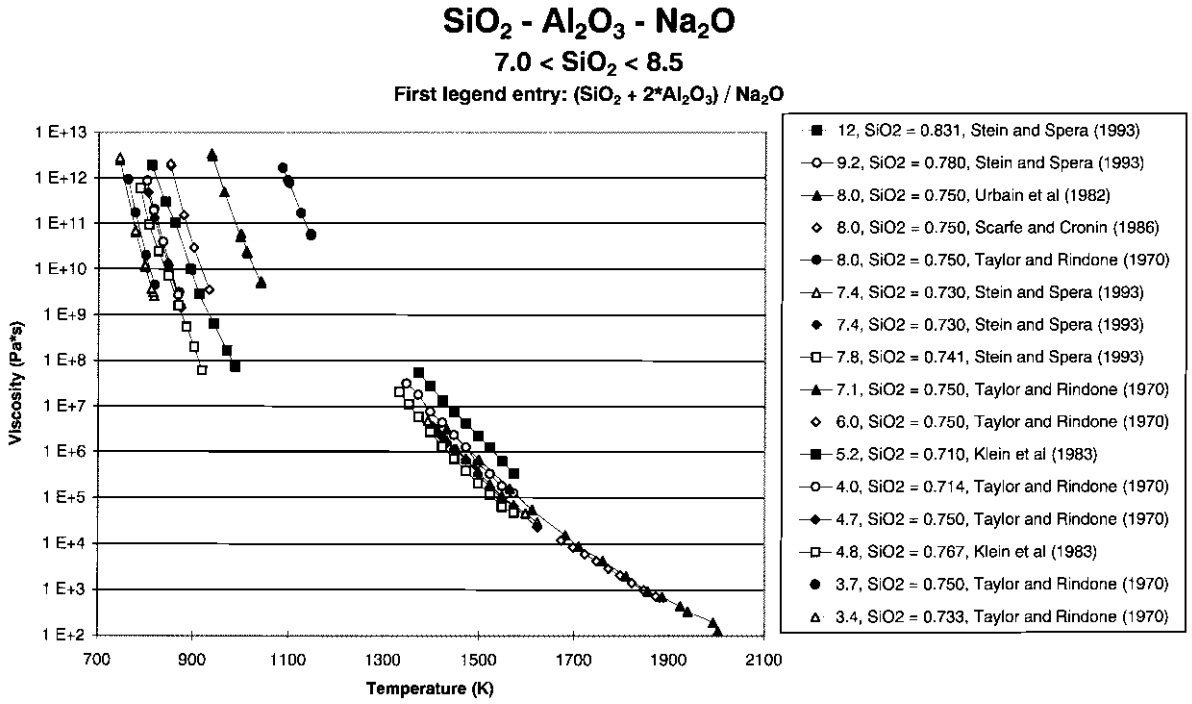

Fig. C.30.

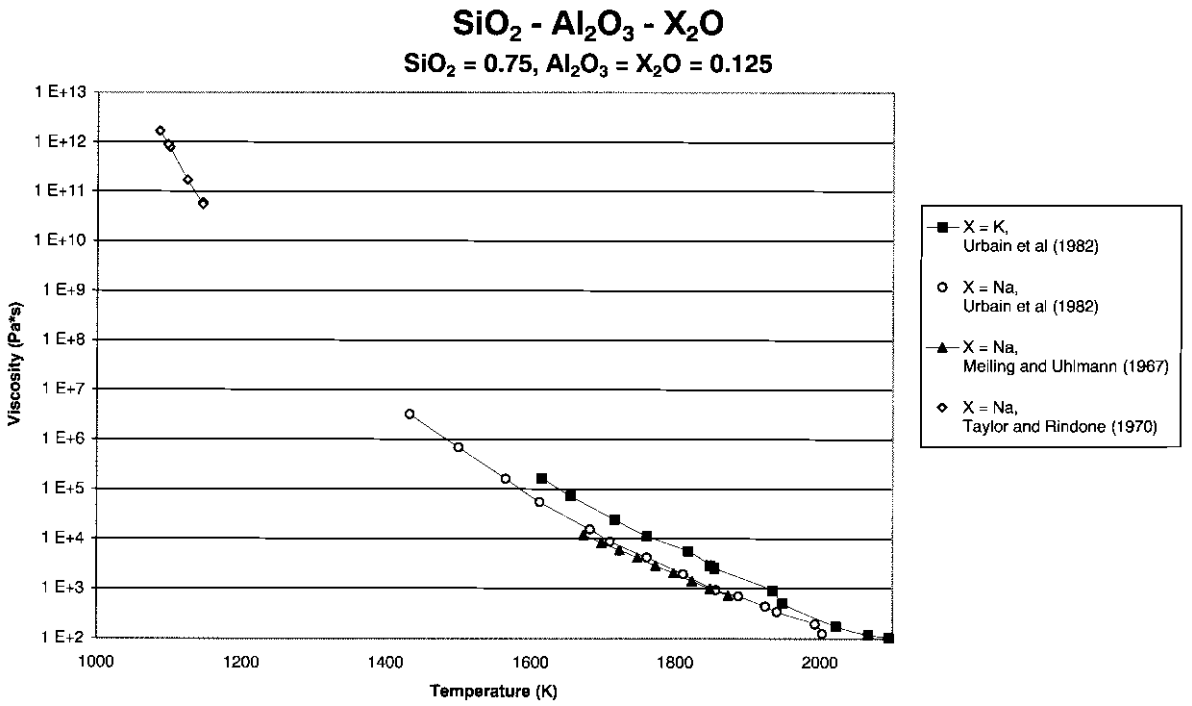

Fig. C.31.

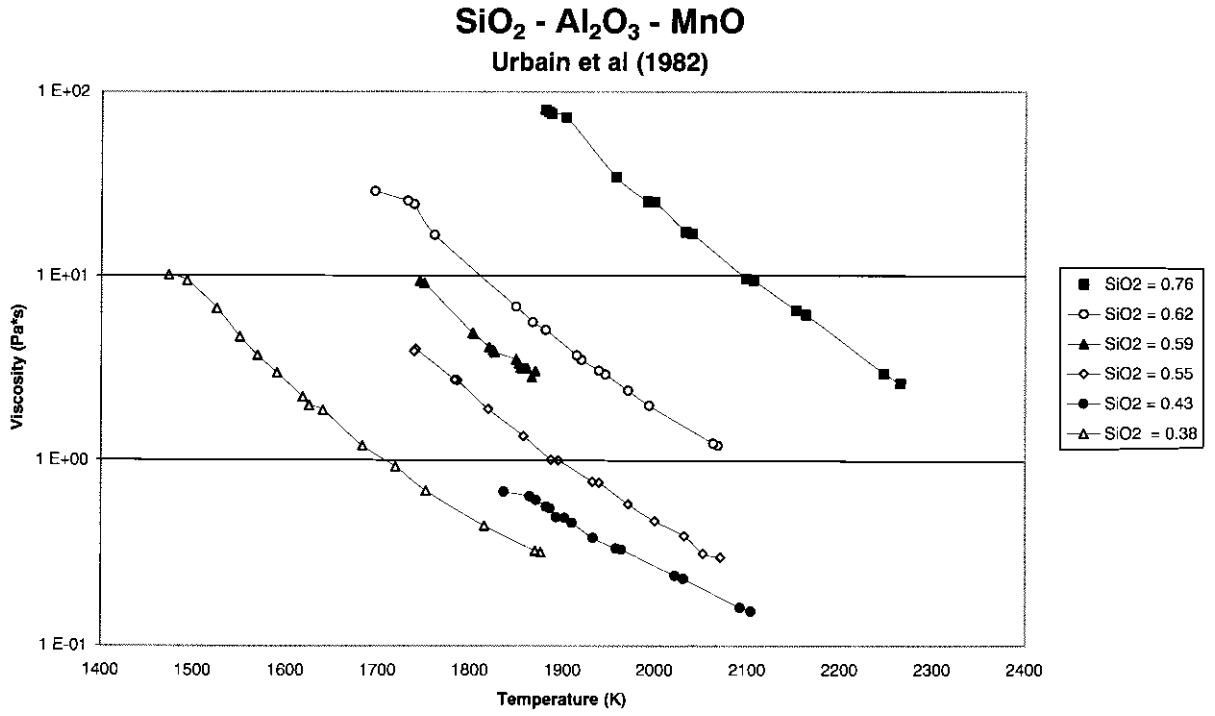

Fig. C.32.

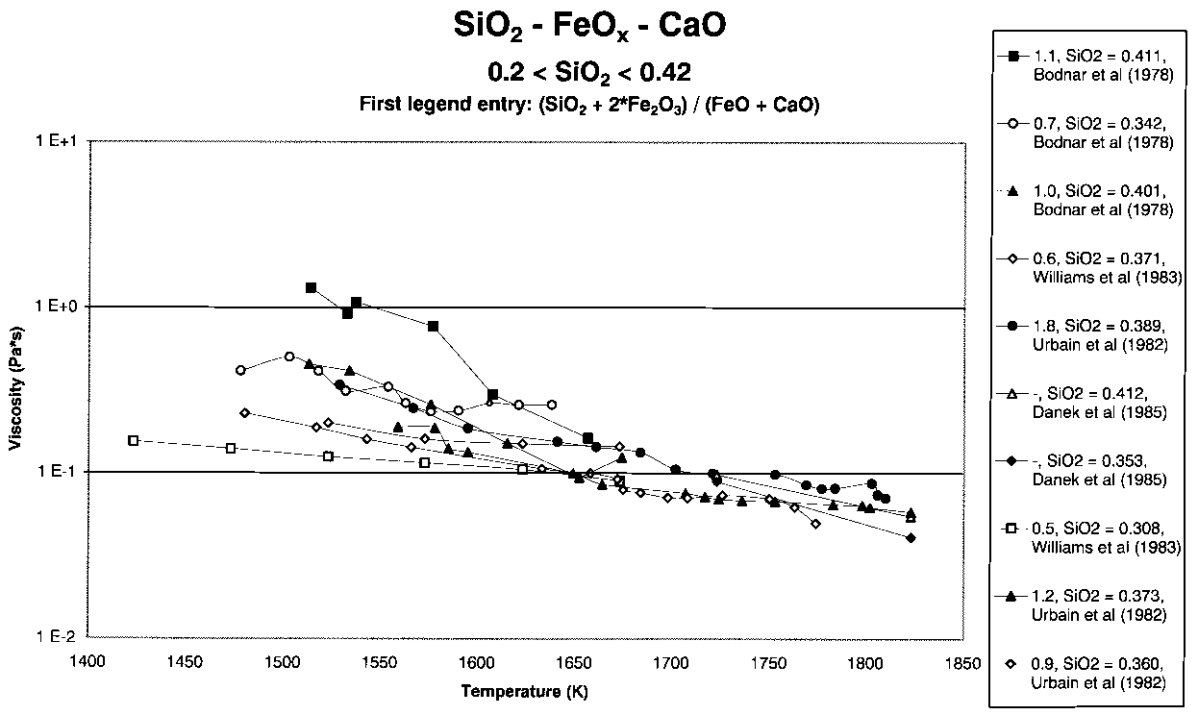

Fig. C.33.

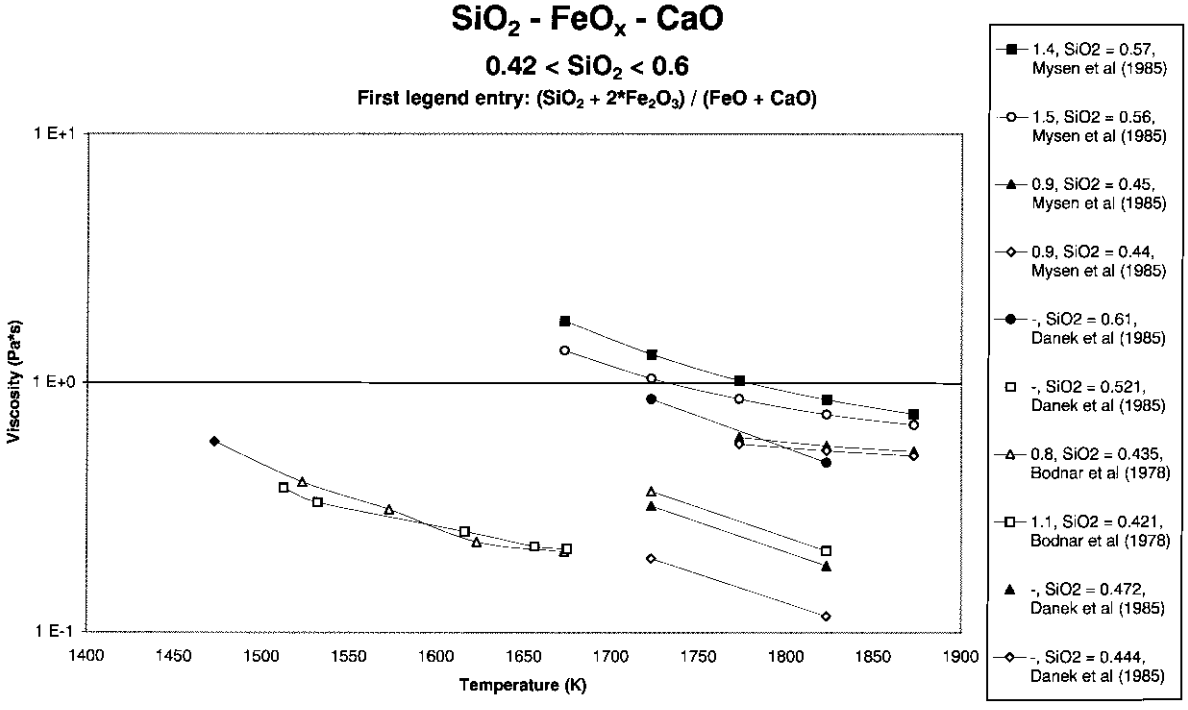

Fig. C.34.

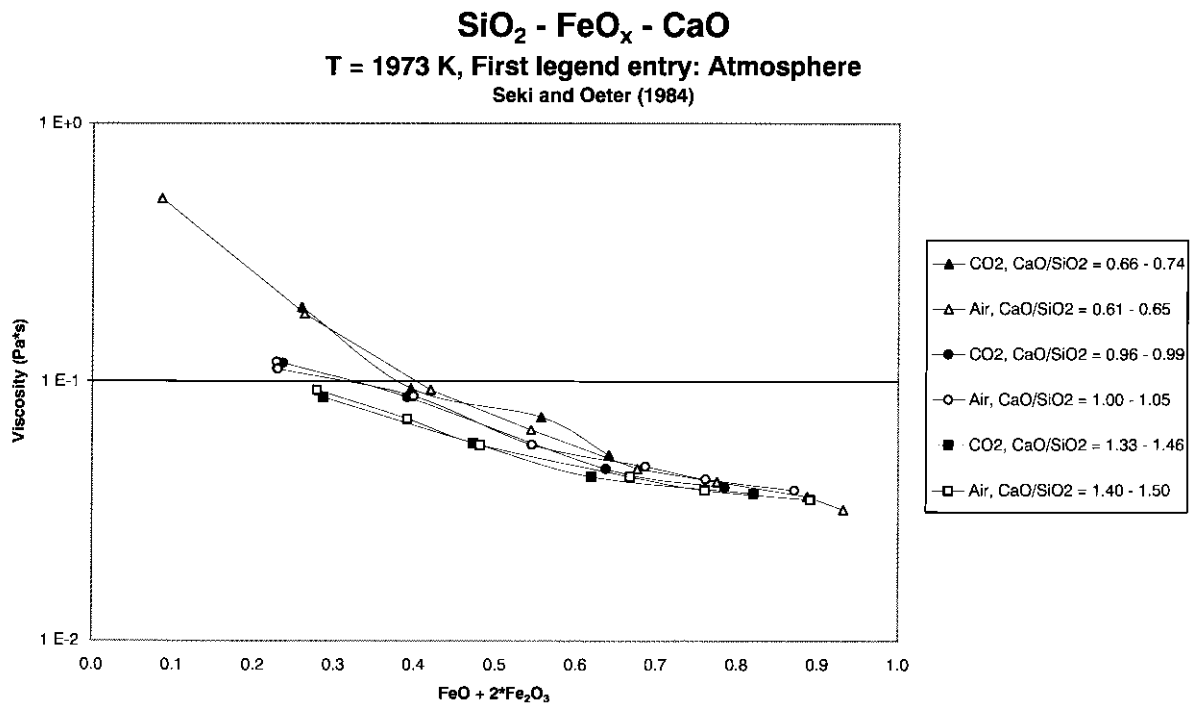

Fig. C.35.

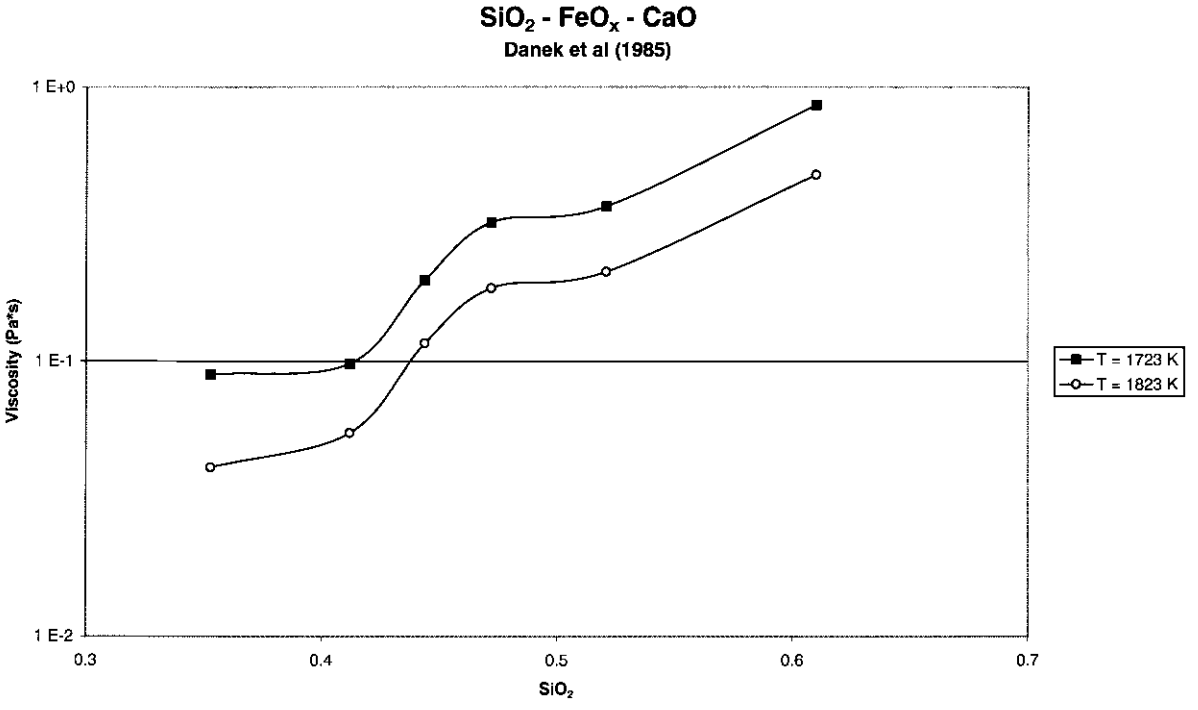

Fig. C.36.

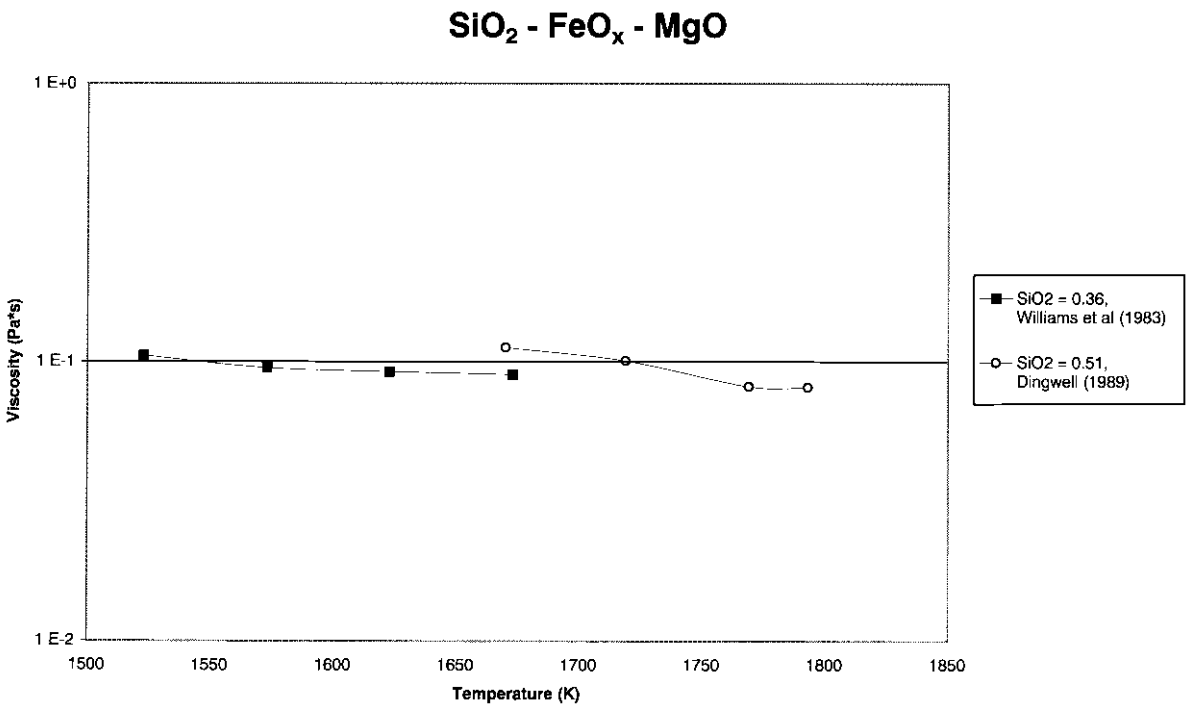

Fig. C.37.

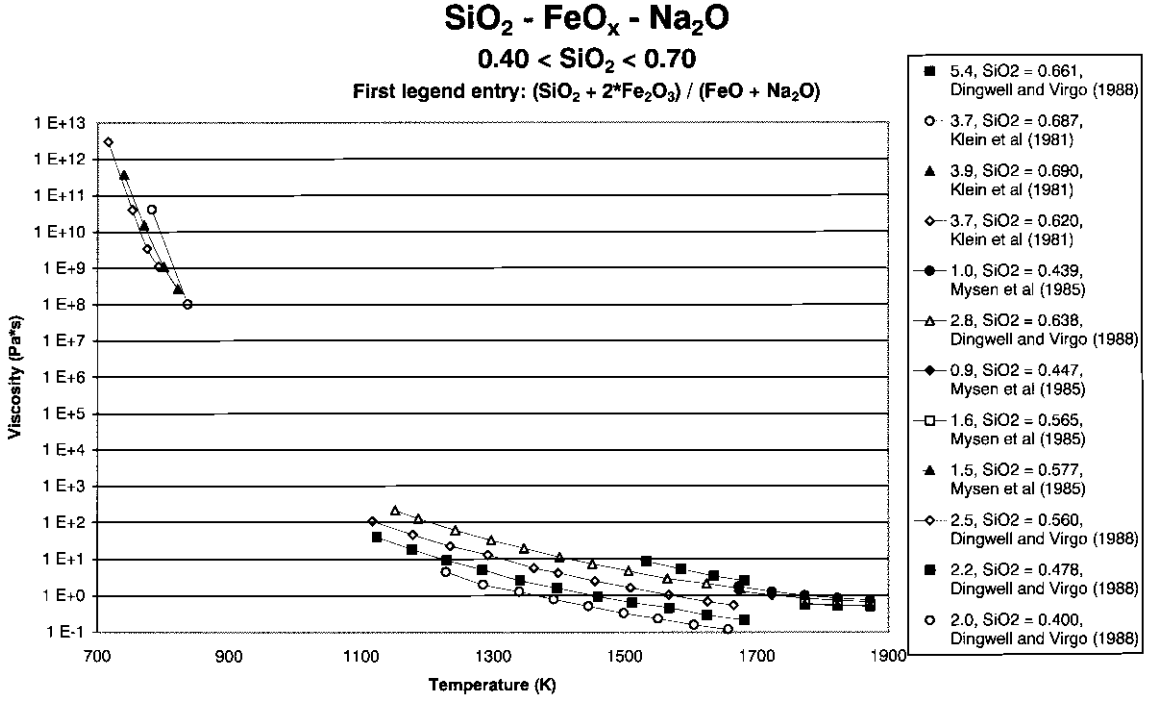

Fig. C.38.

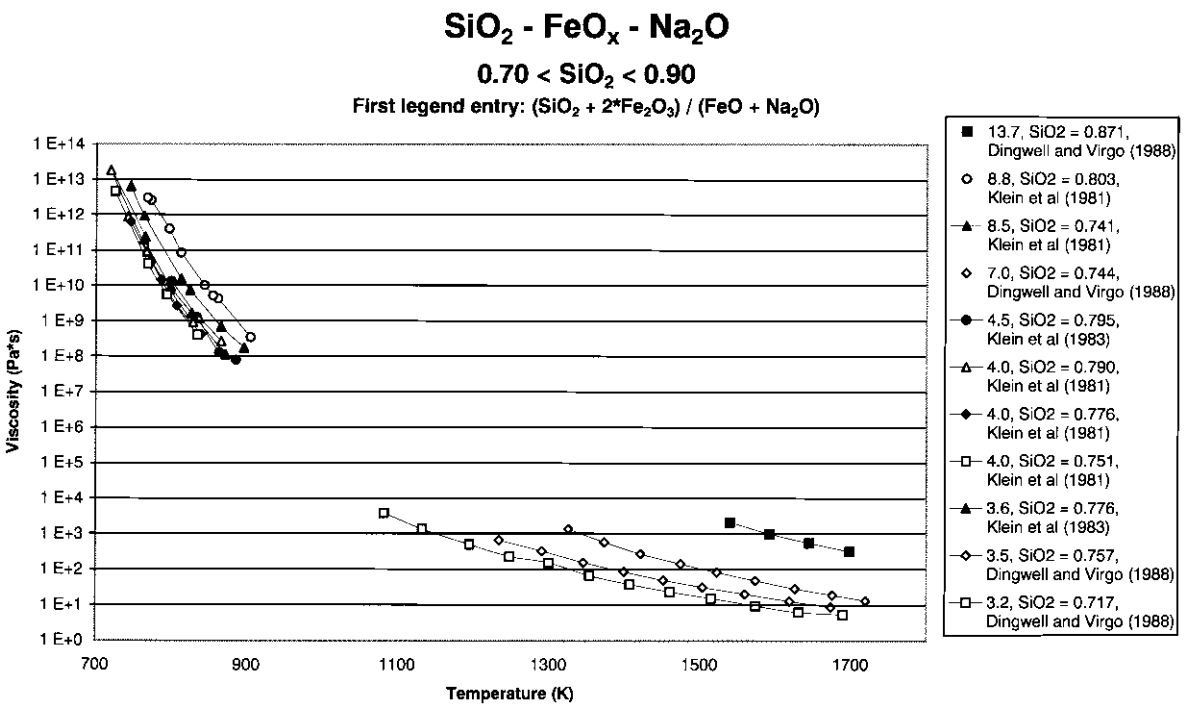

Fig. C.39.

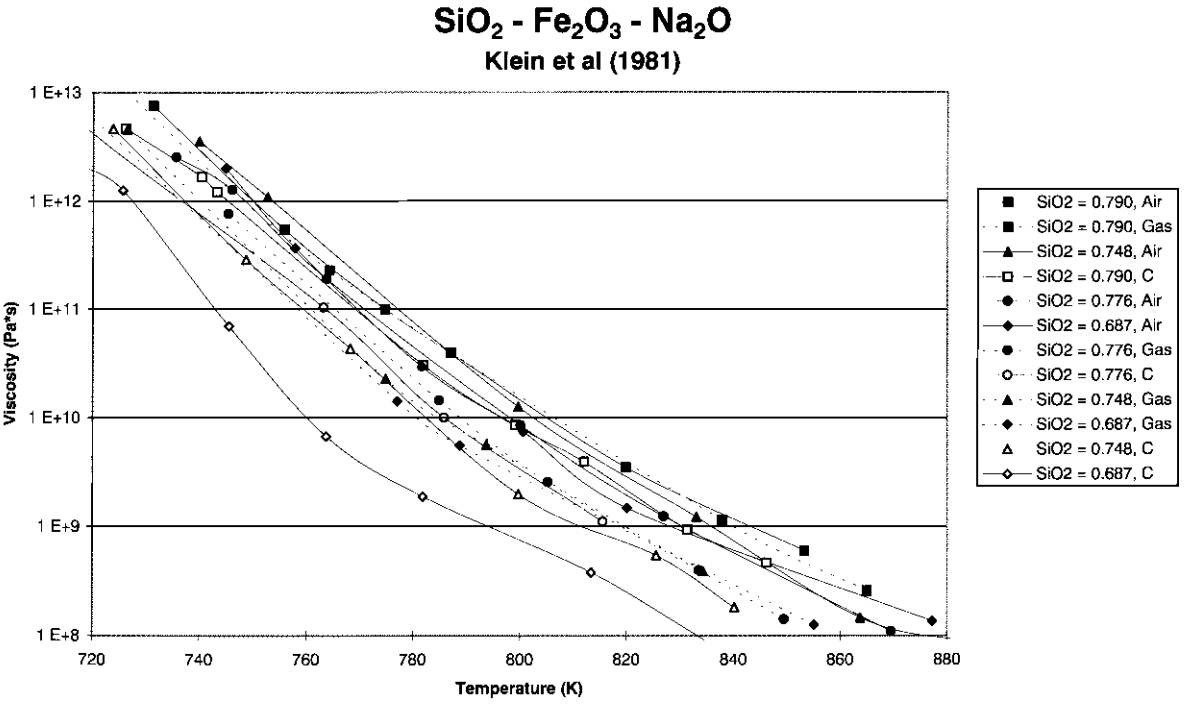

Fig. C.40.

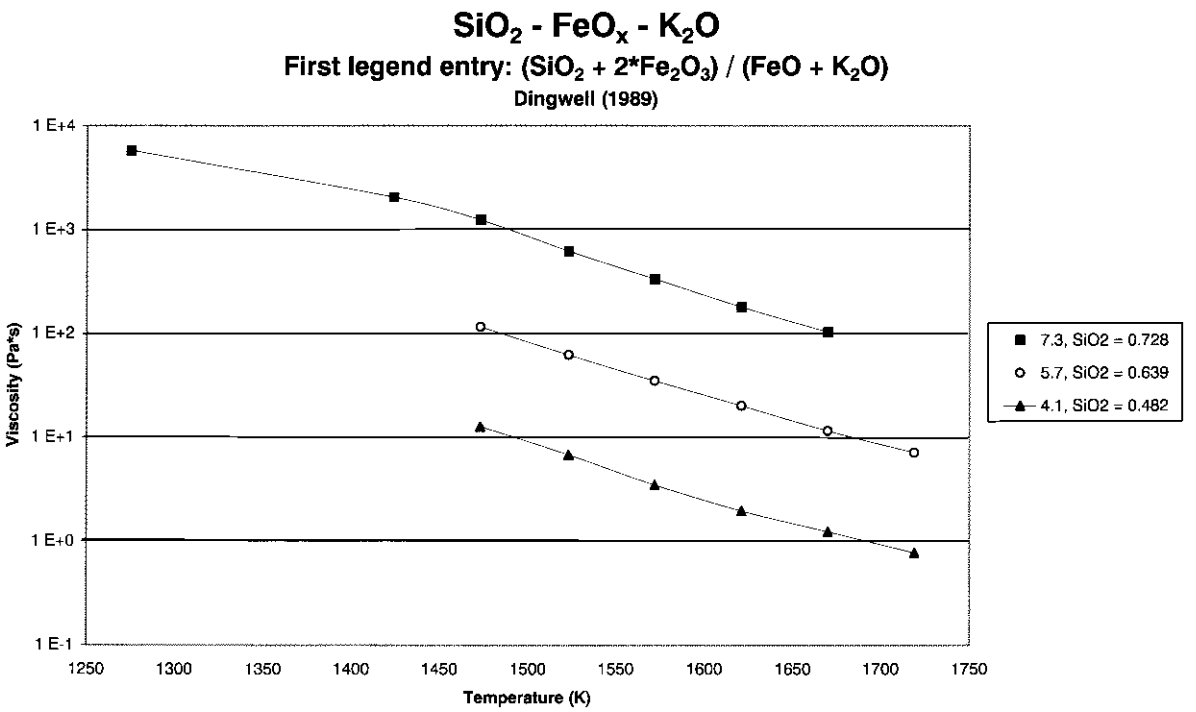

Fig. C.41.

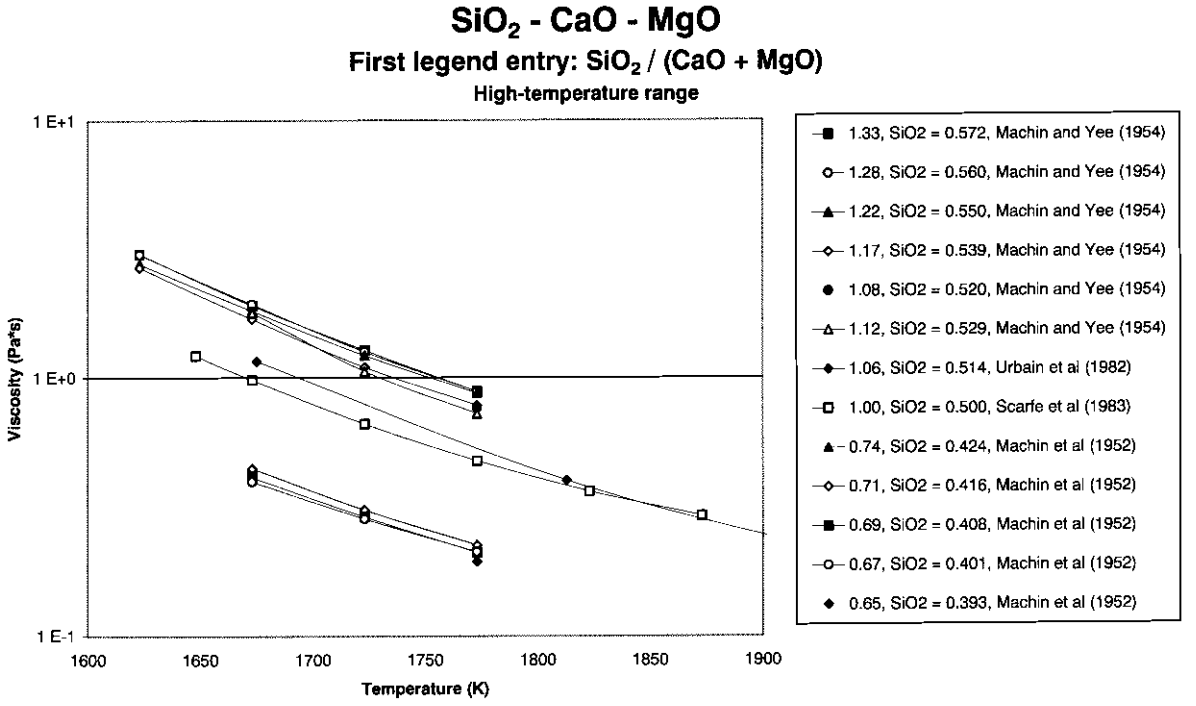

Fig. C.42.

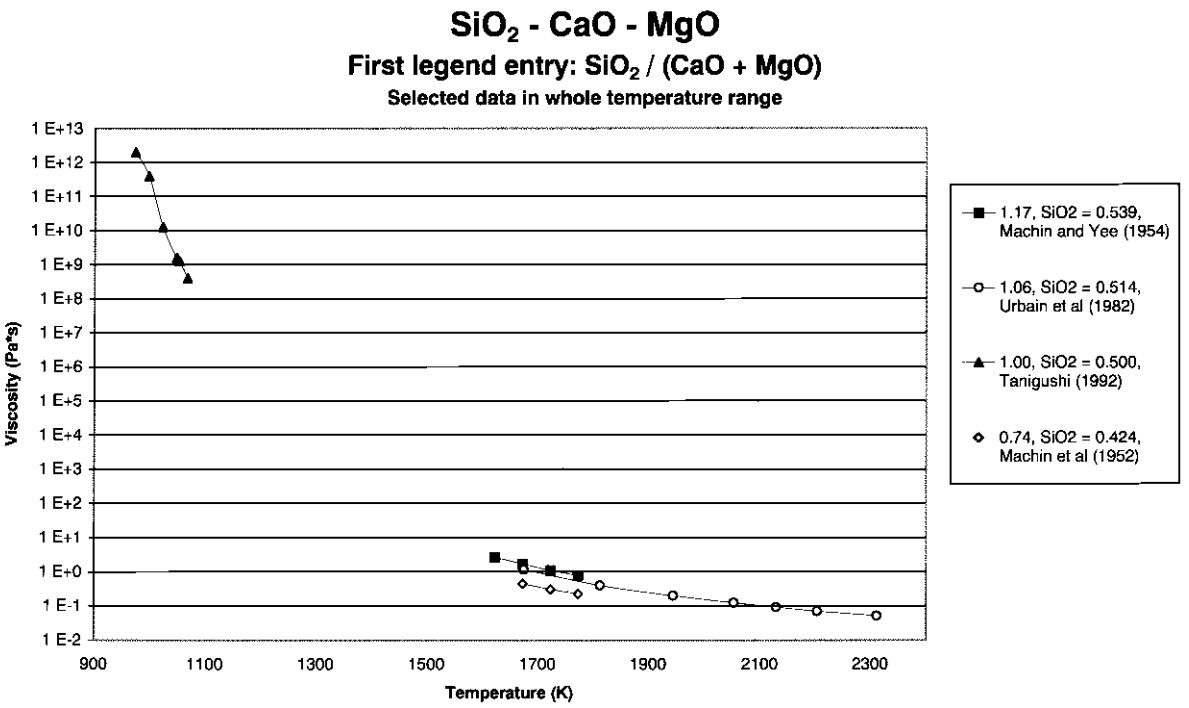

Fig. C.43.

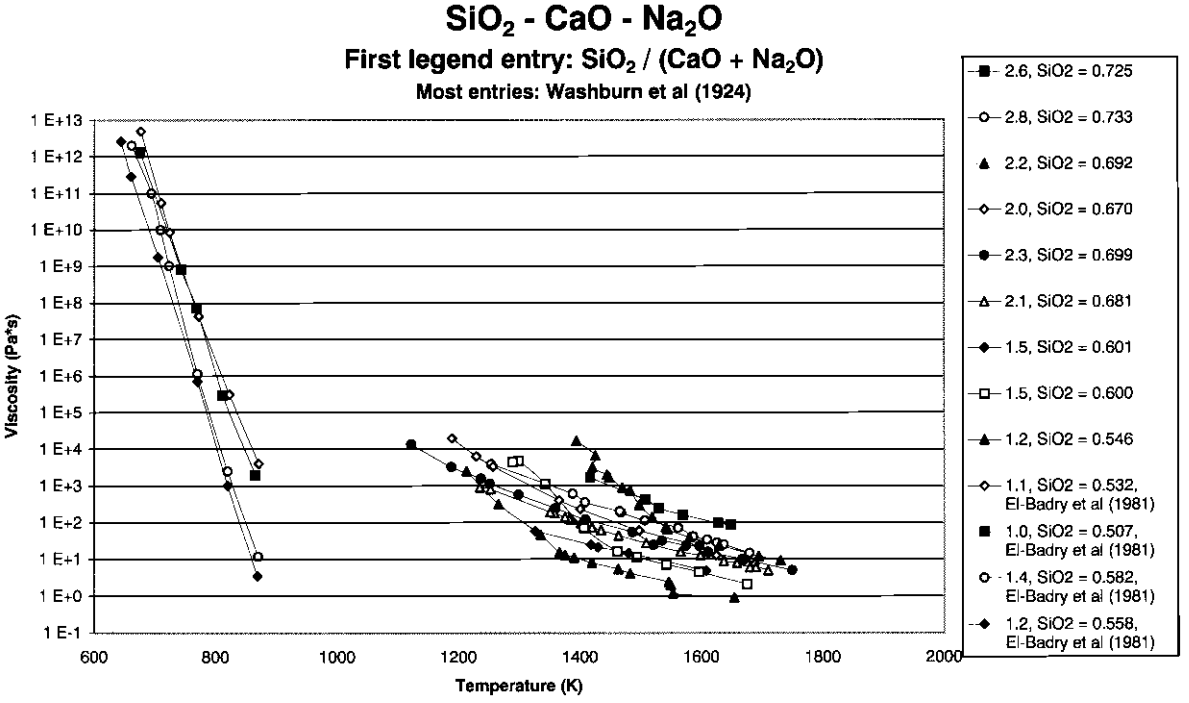

Fig. C.44.

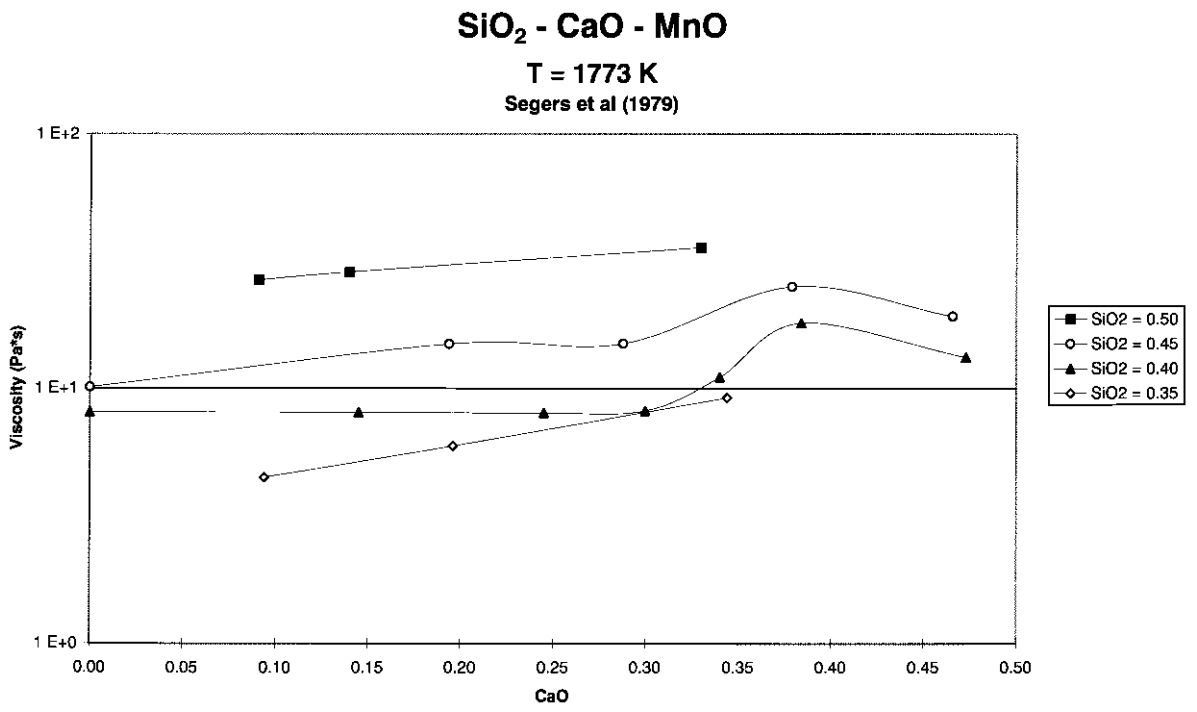

Fig. C.45.

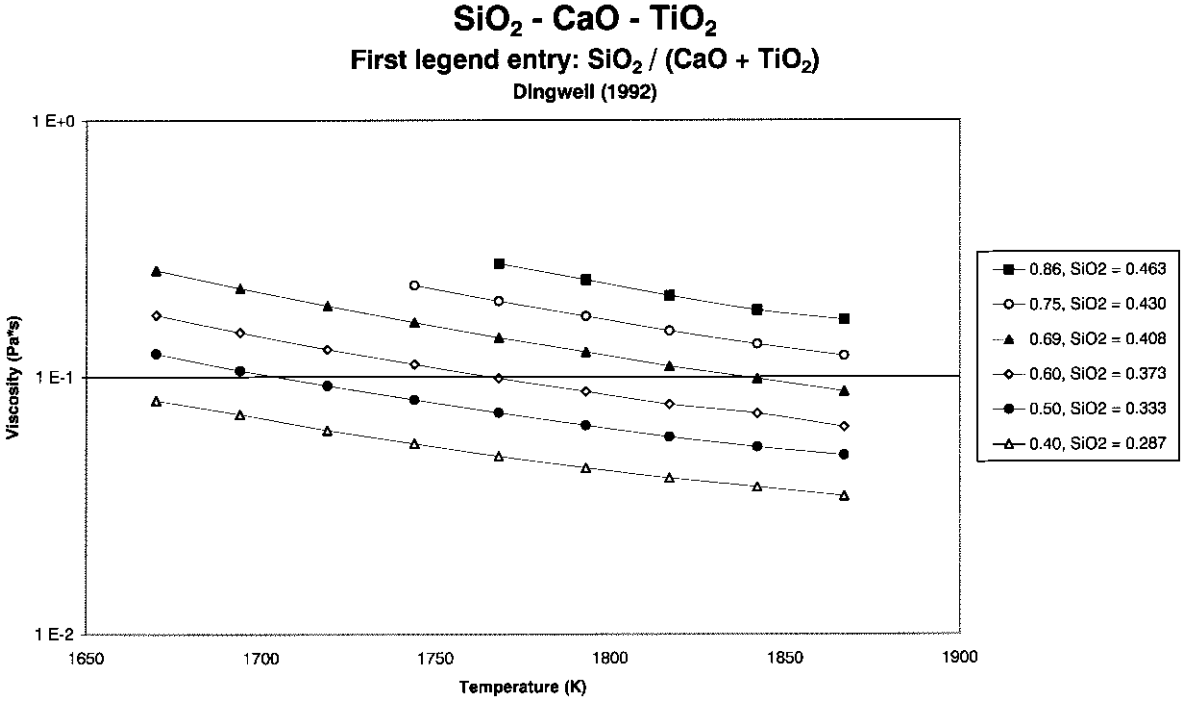

Fig. C.46.

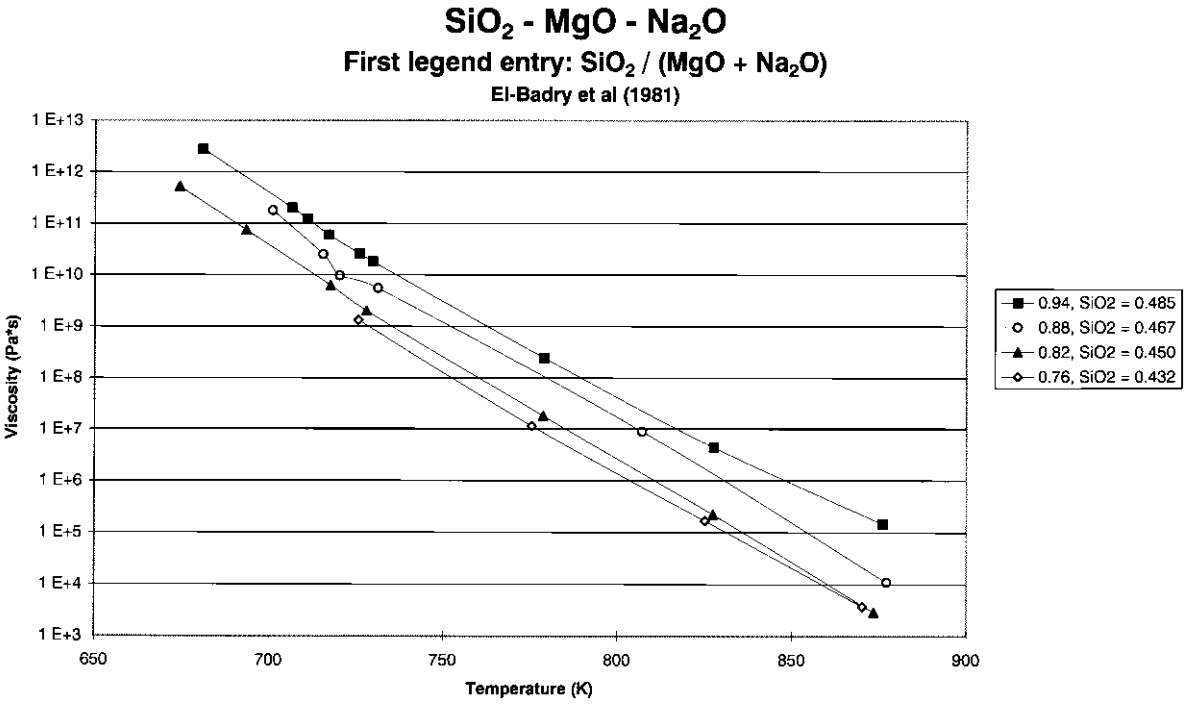

Fig. C.47.

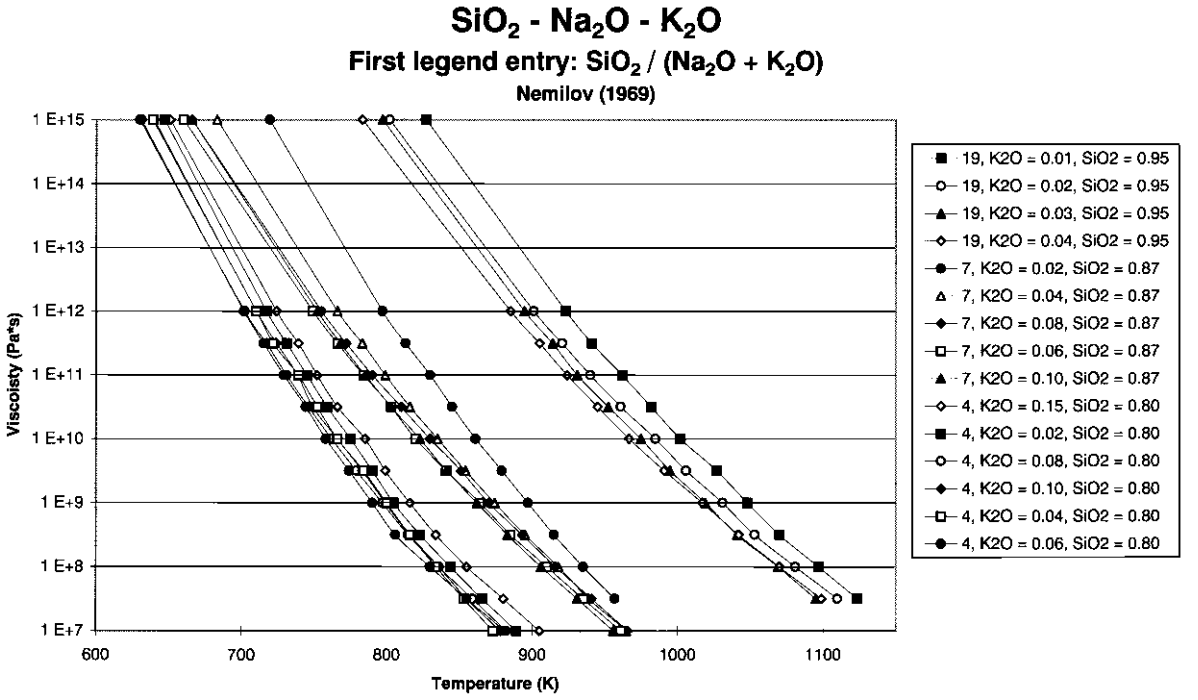

Fig. C.48.

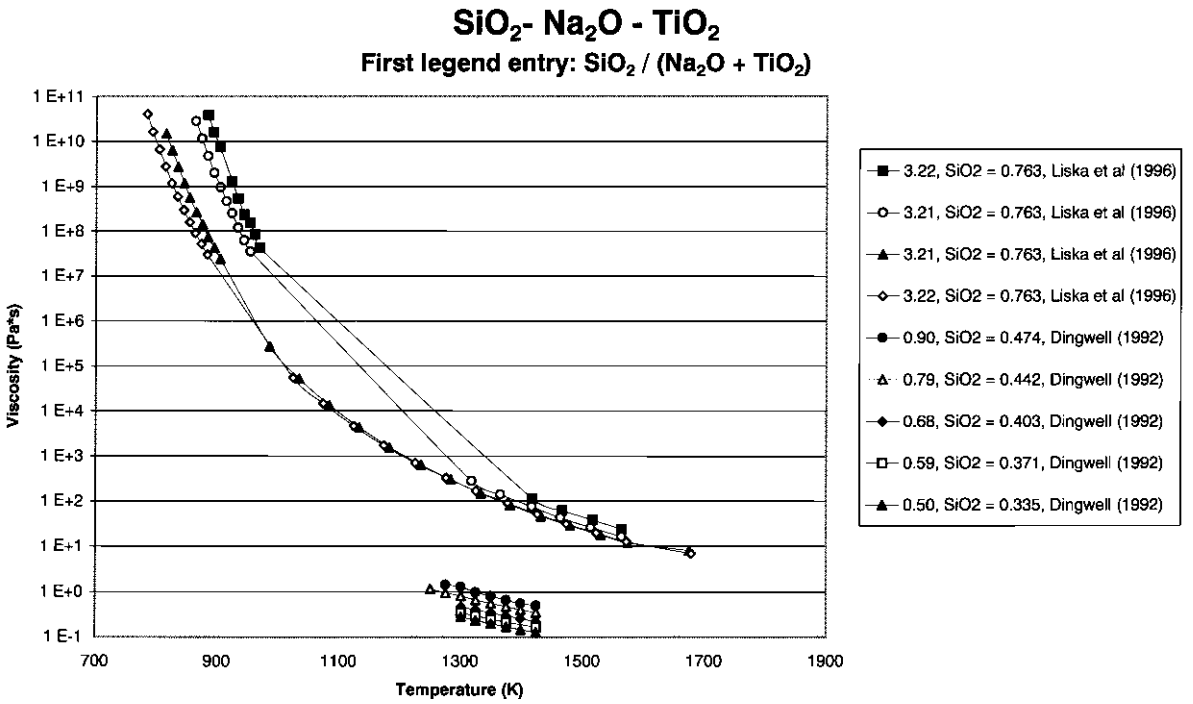

Fig. C.49.

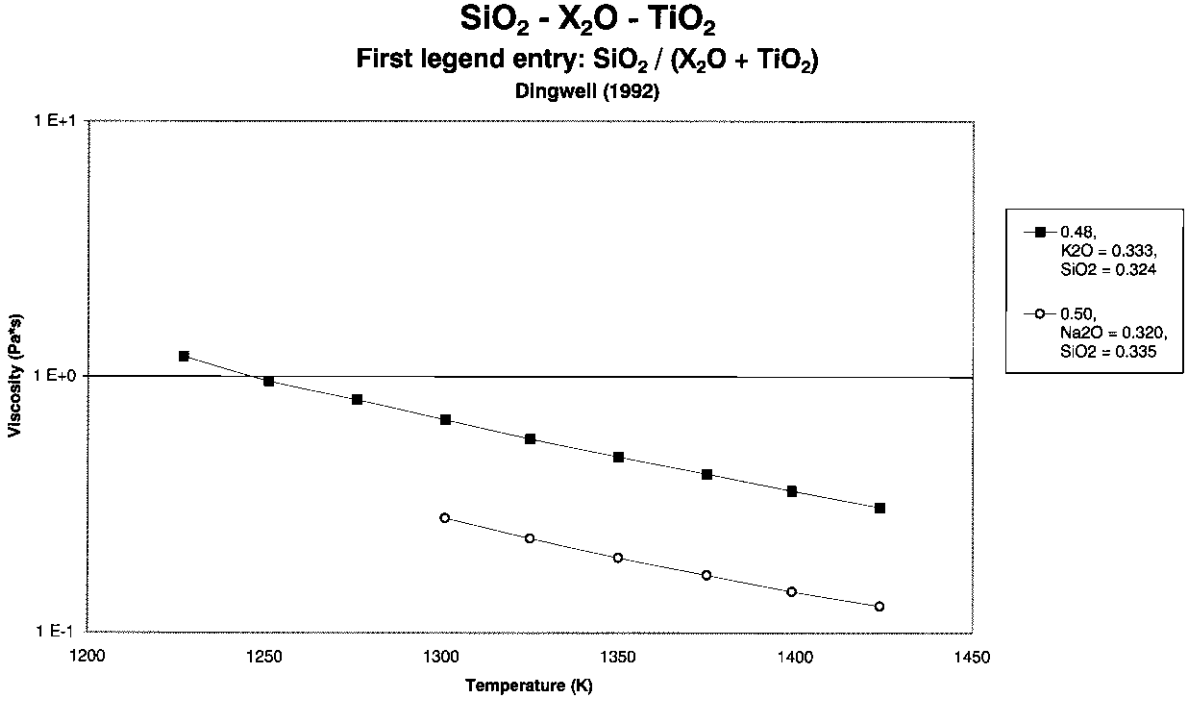

Fig. C.50.

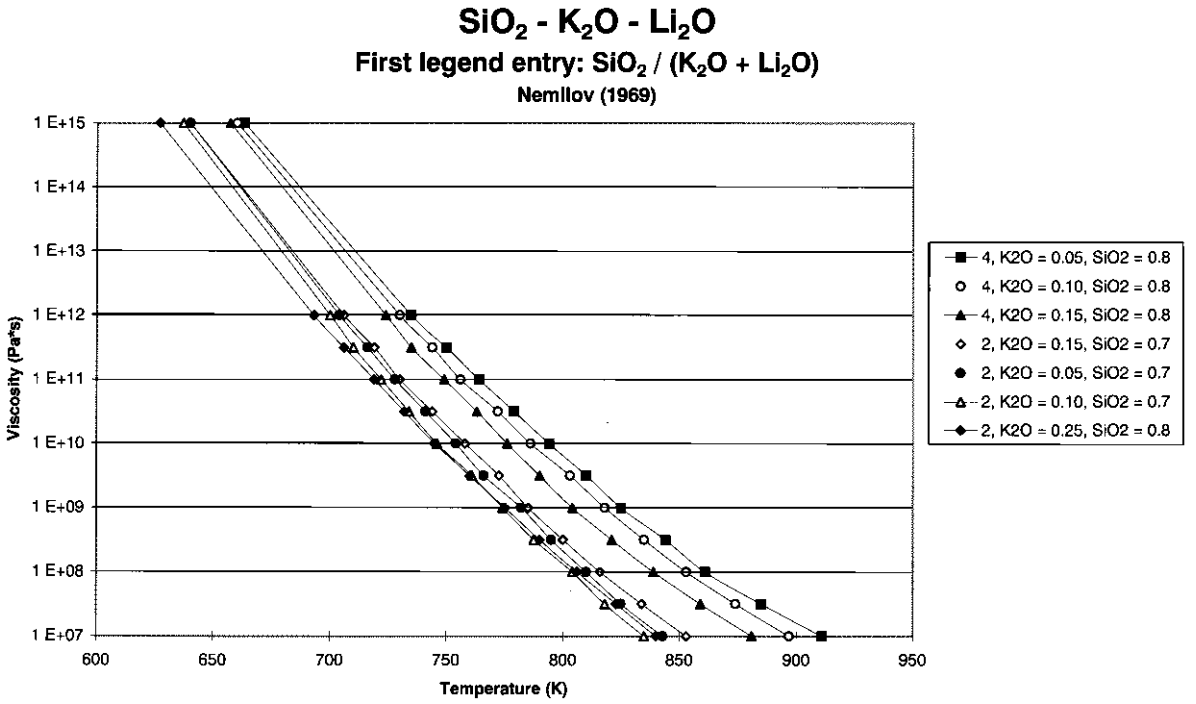

Fig. C.51.

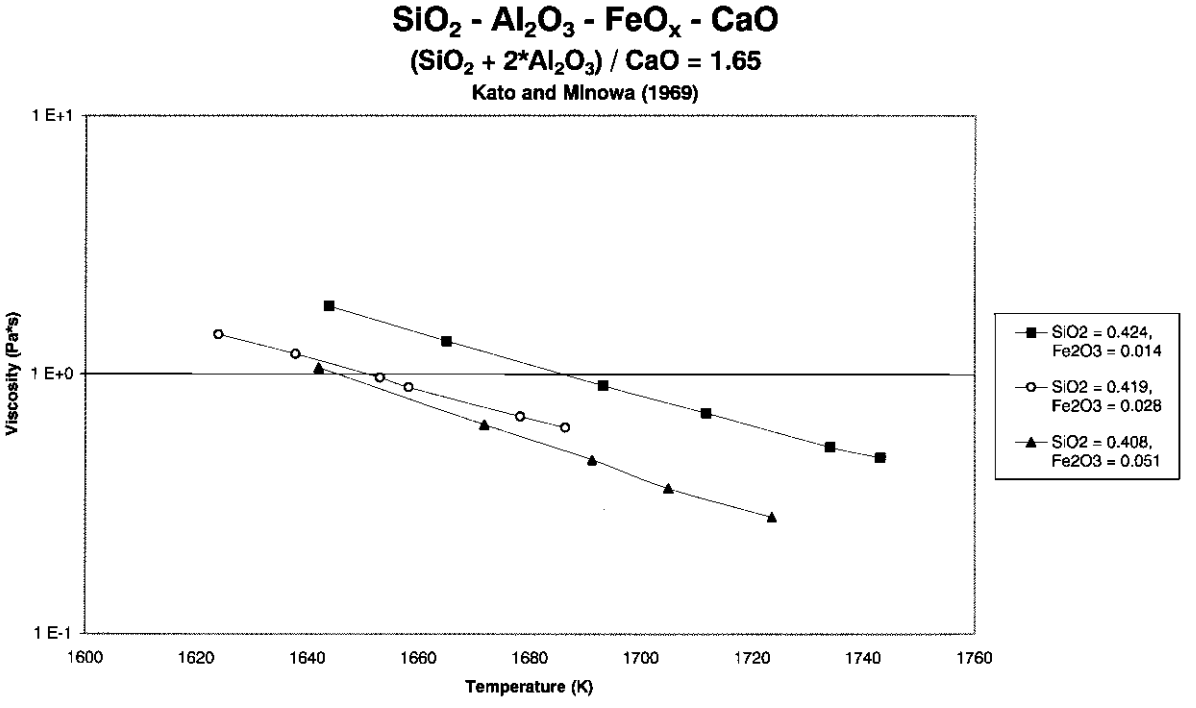

Fig. C.52.

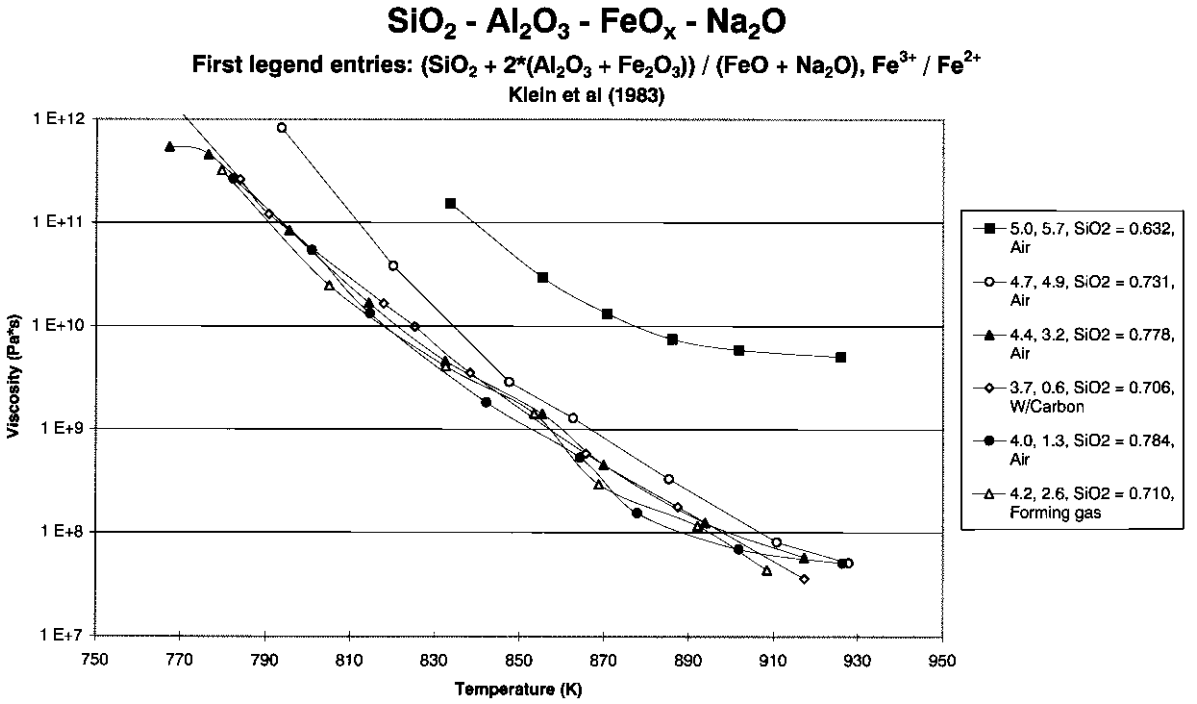

Fig. C.53.

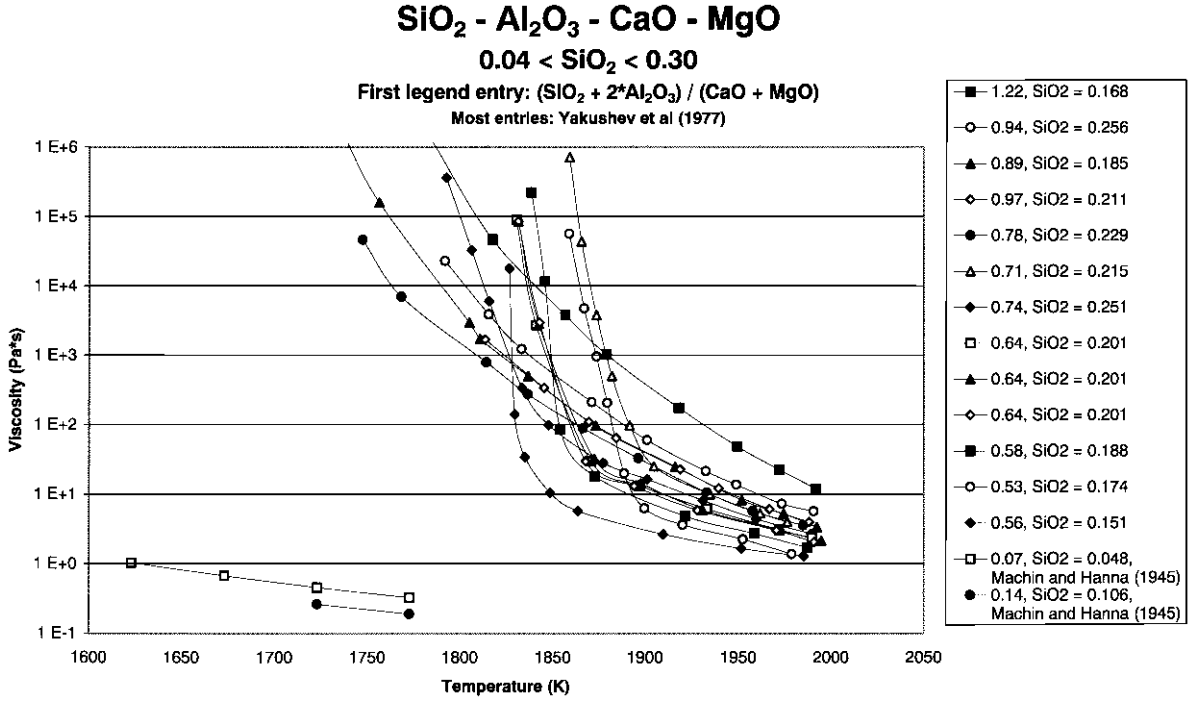

Fig. C.54.

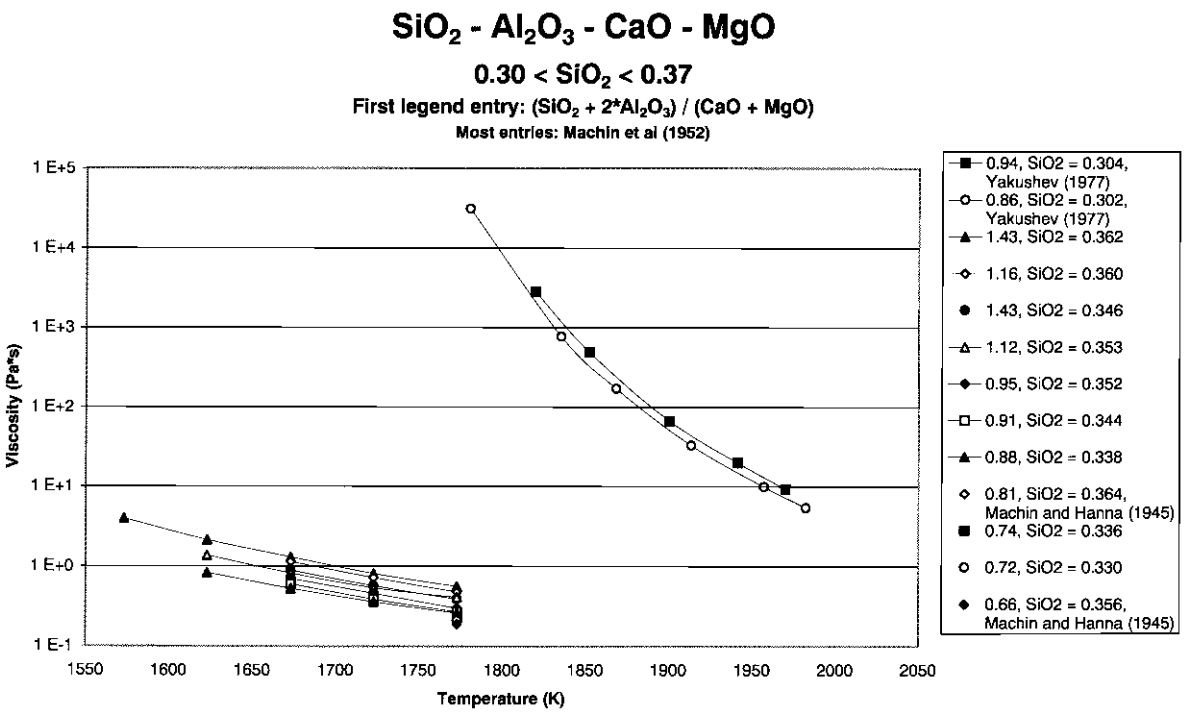

Fig. C.55.

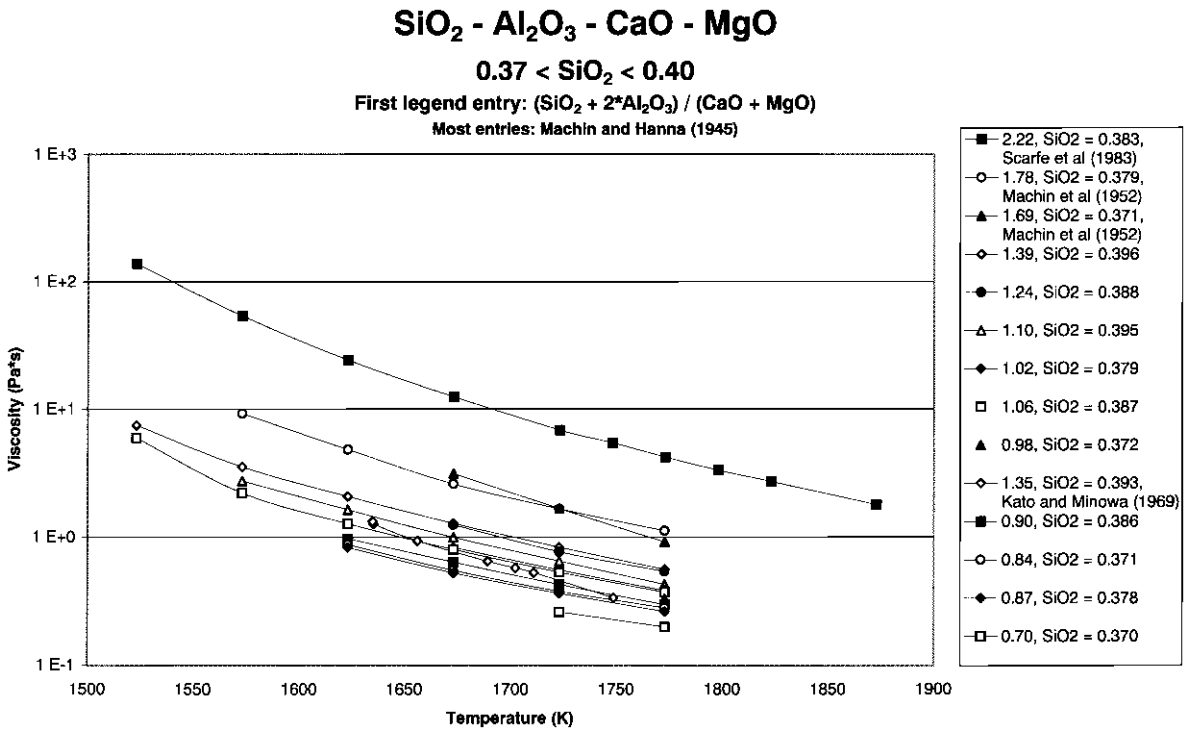

Fig. C.56.

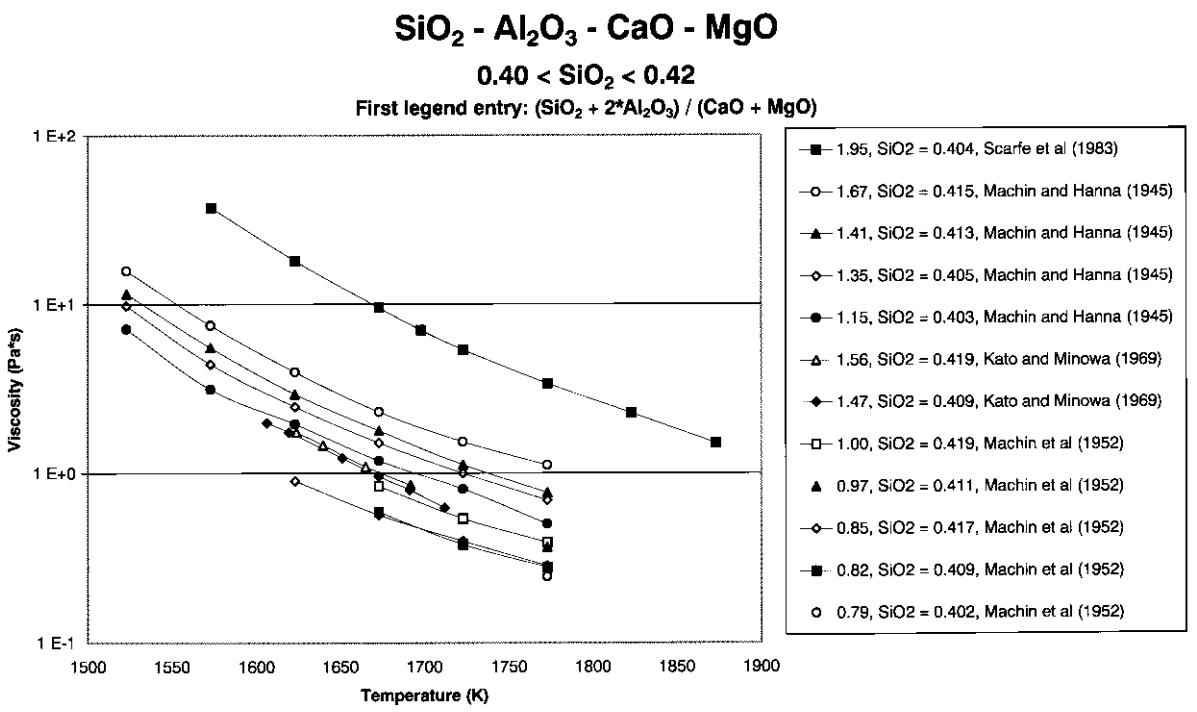

Fig. C.57.

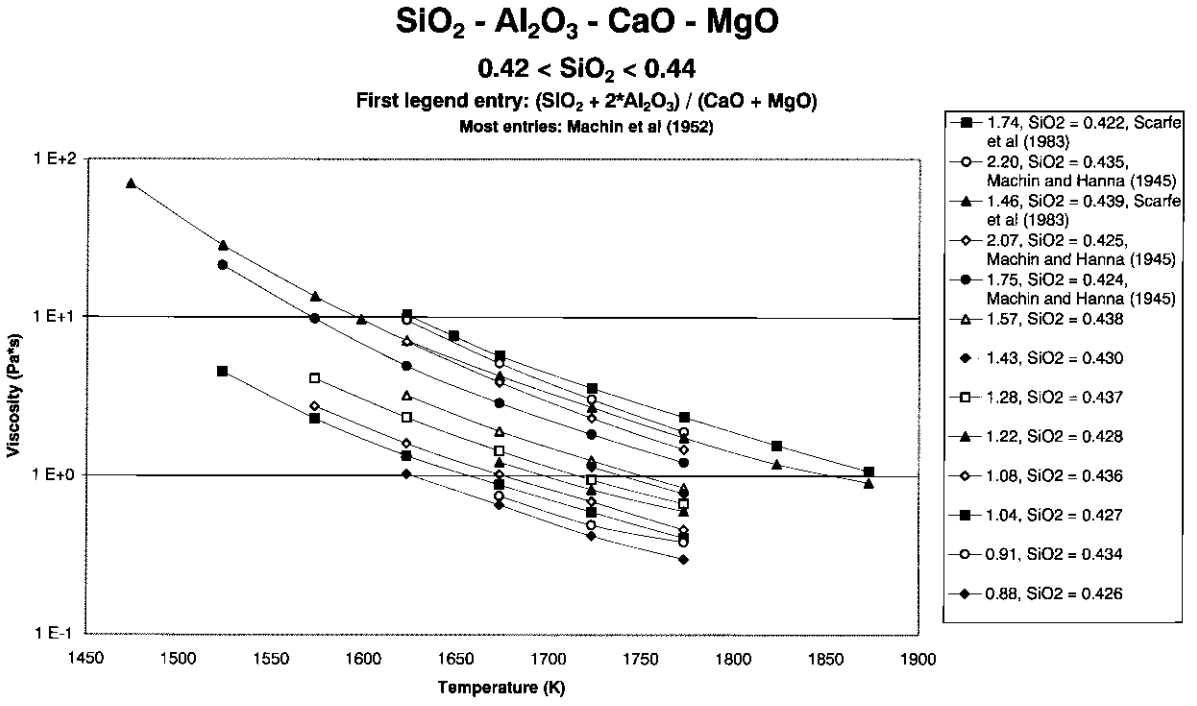

Fig. C.58.

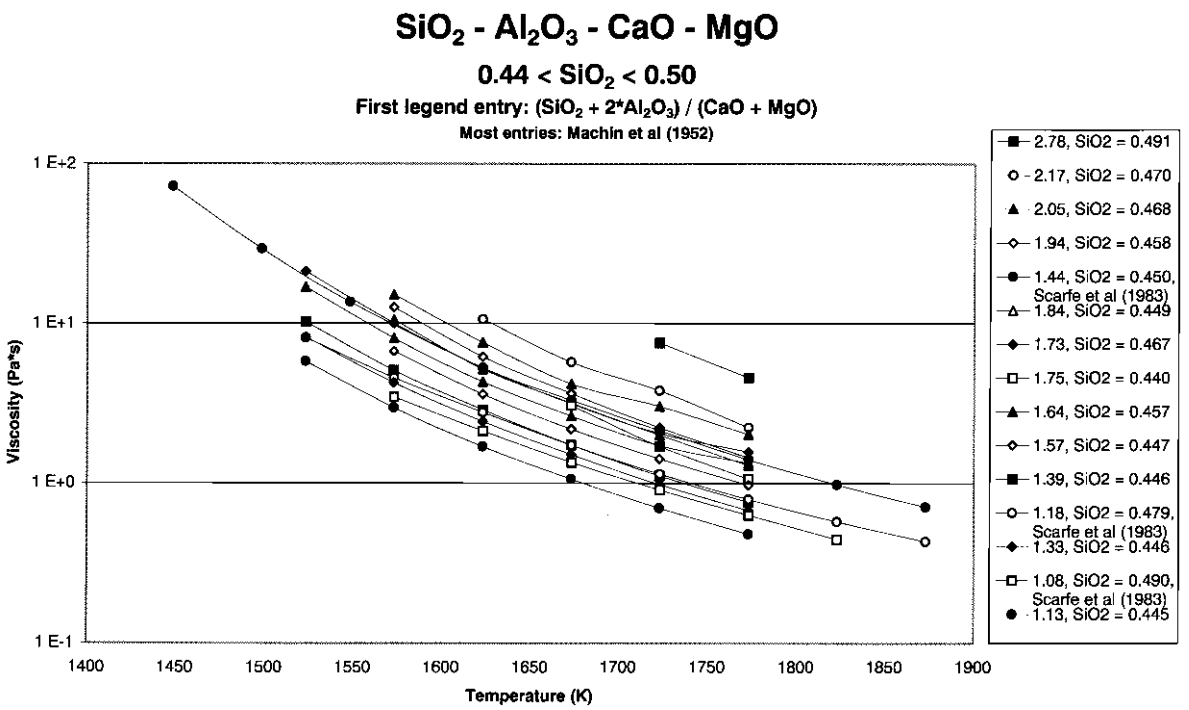

Fig. C.59.

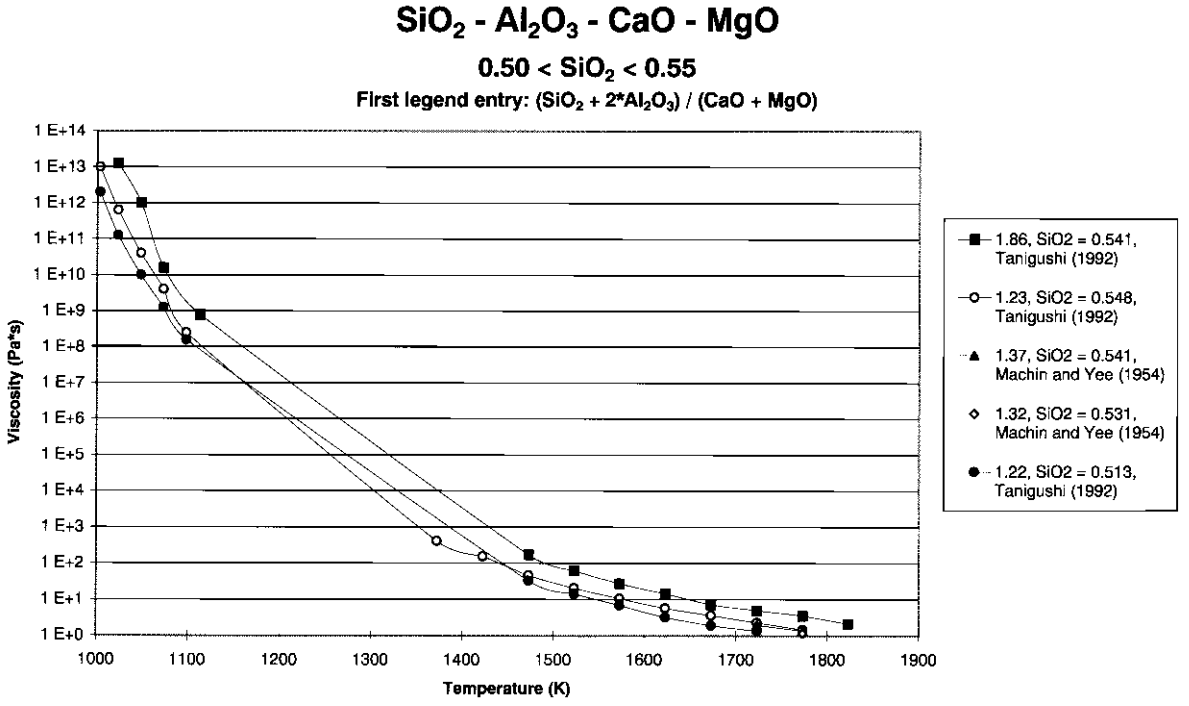

Fig. C.60.

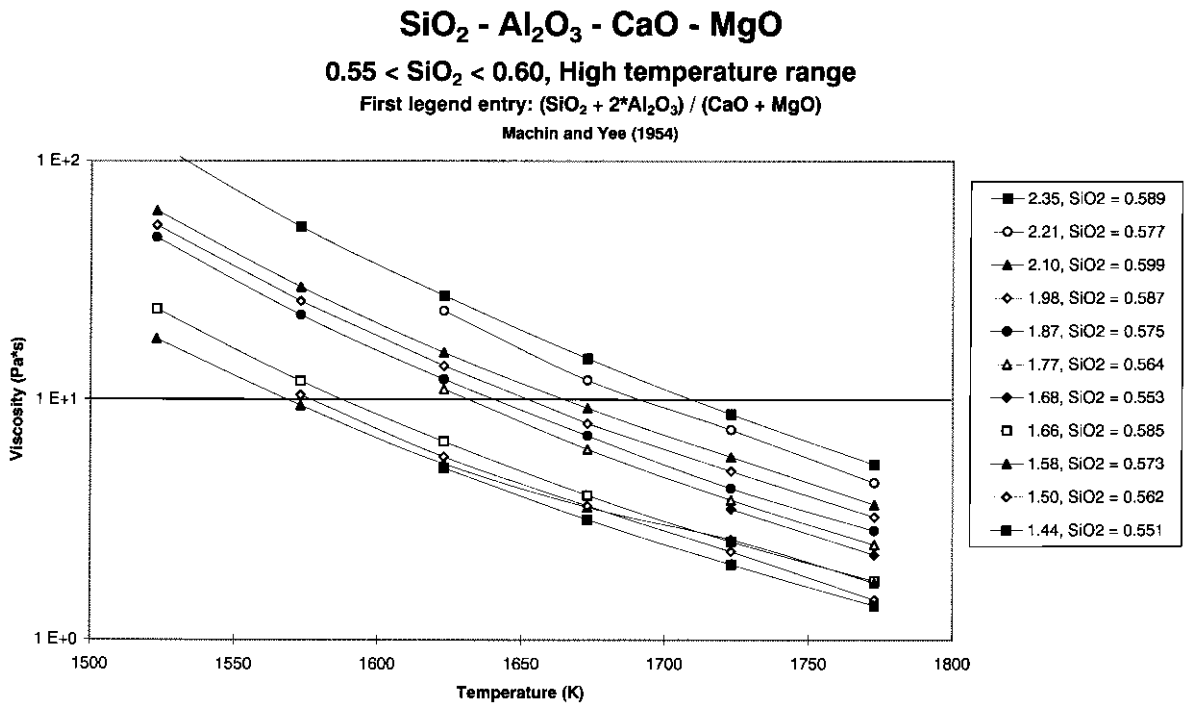

Fig. C.61.

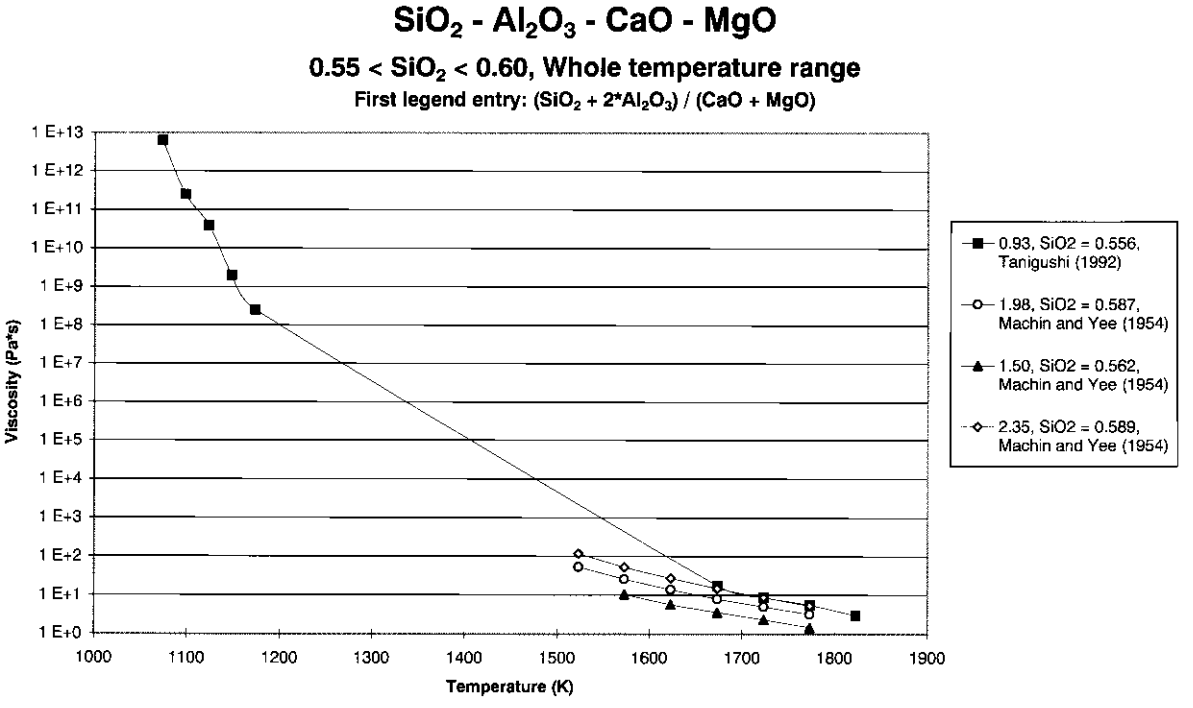

Fig. C.62.

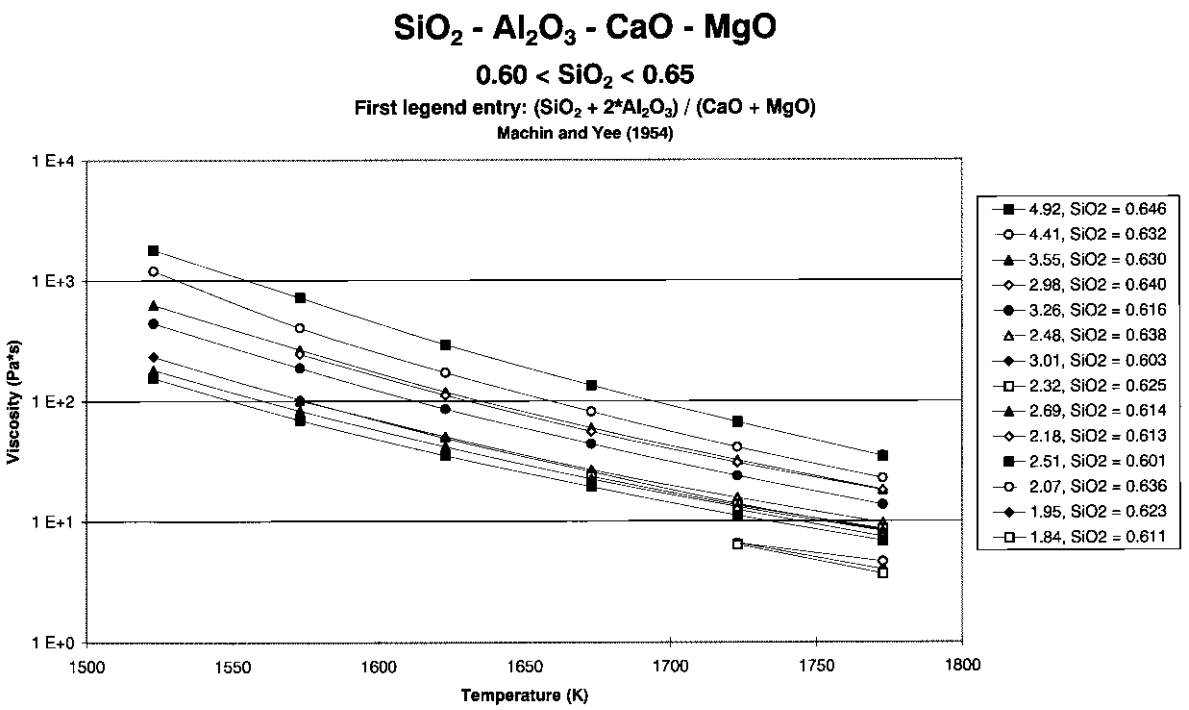

Fig. C.63.

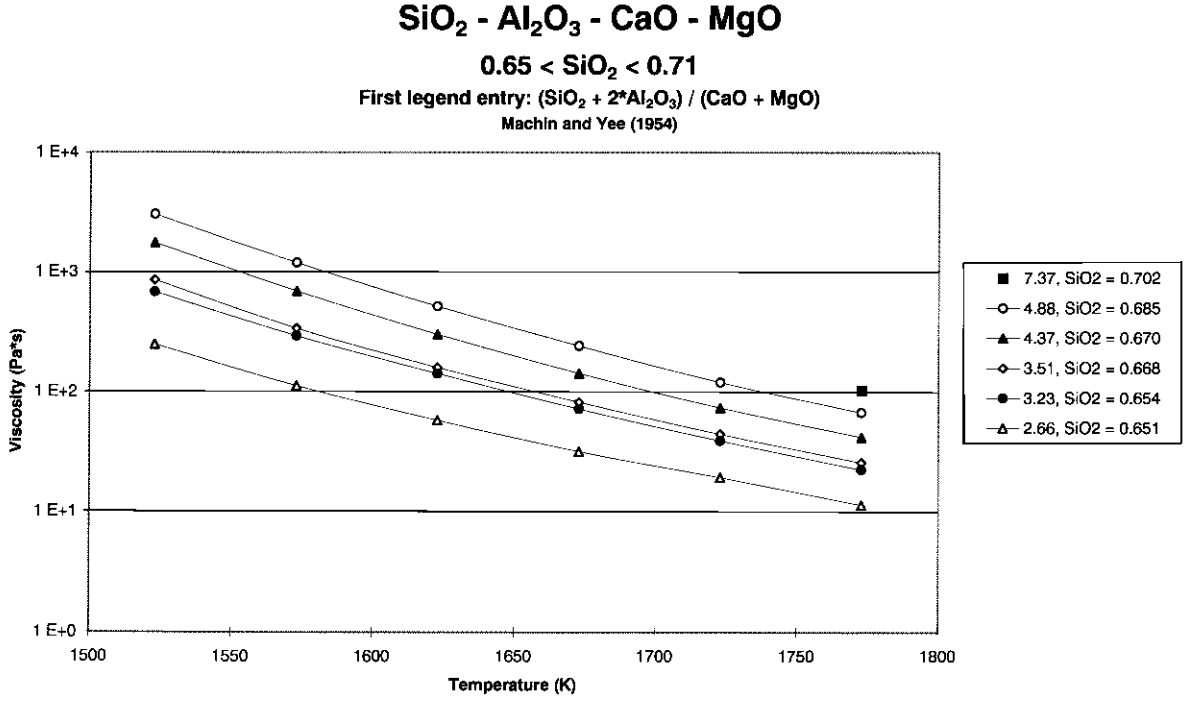

Fig. C.64.

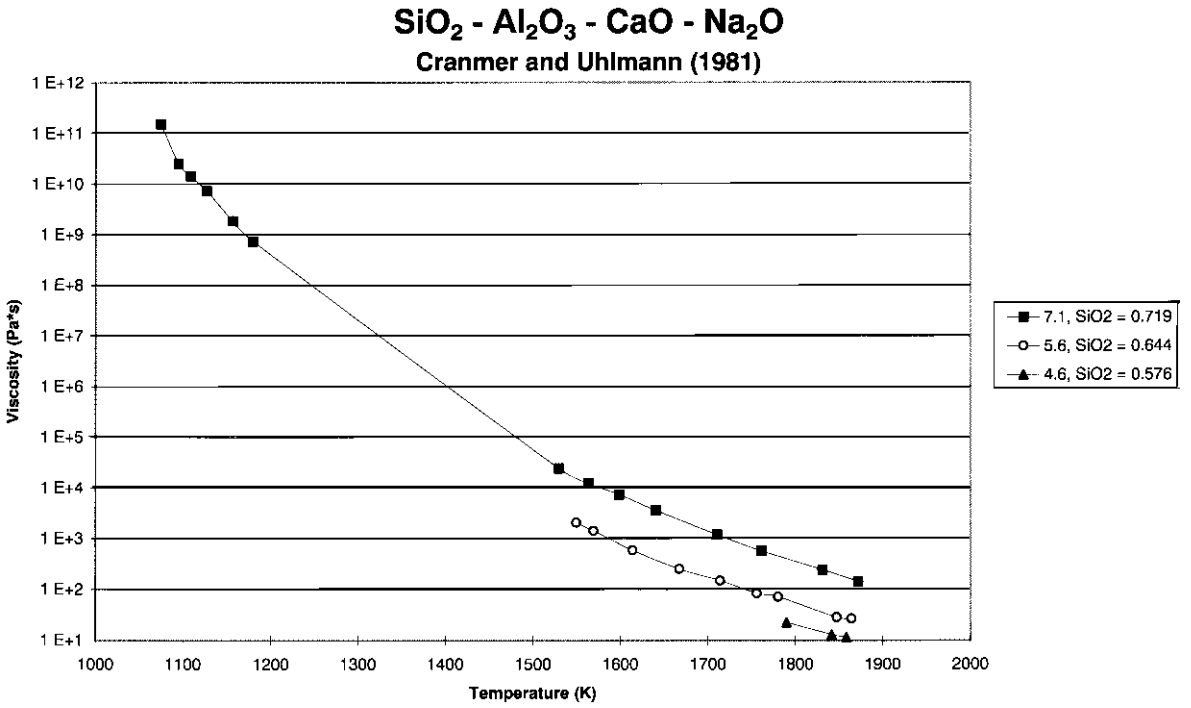

Fig. C.65.

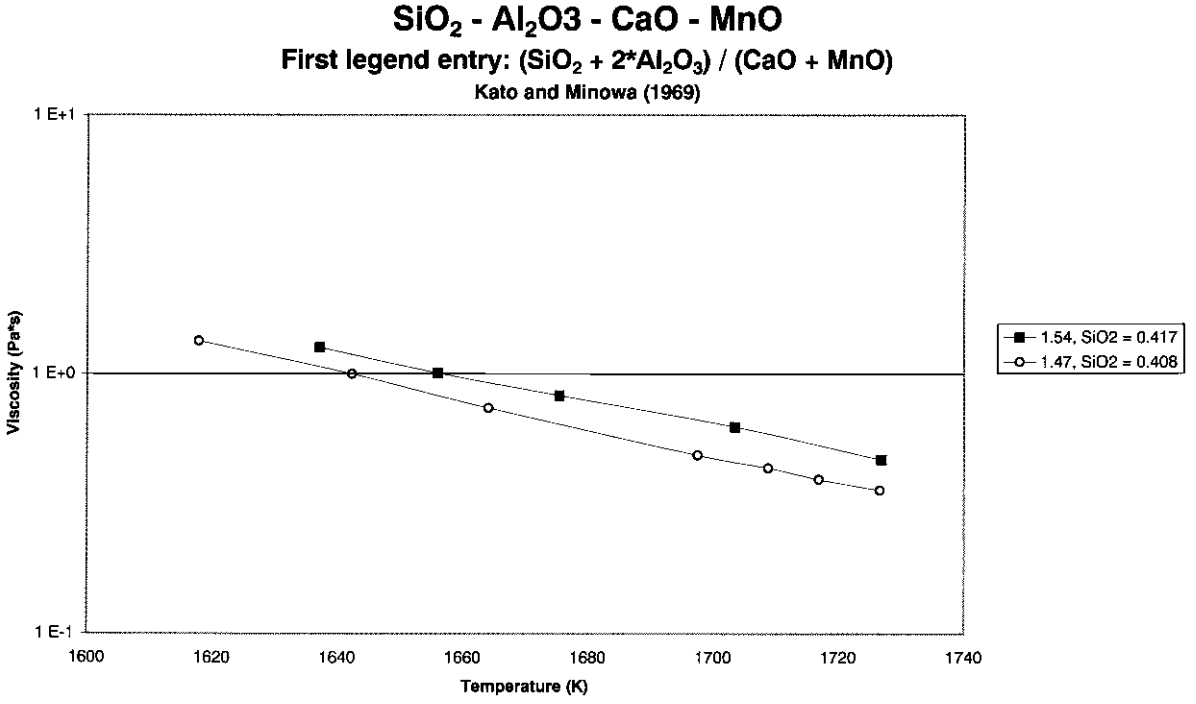

Fig. C.66.

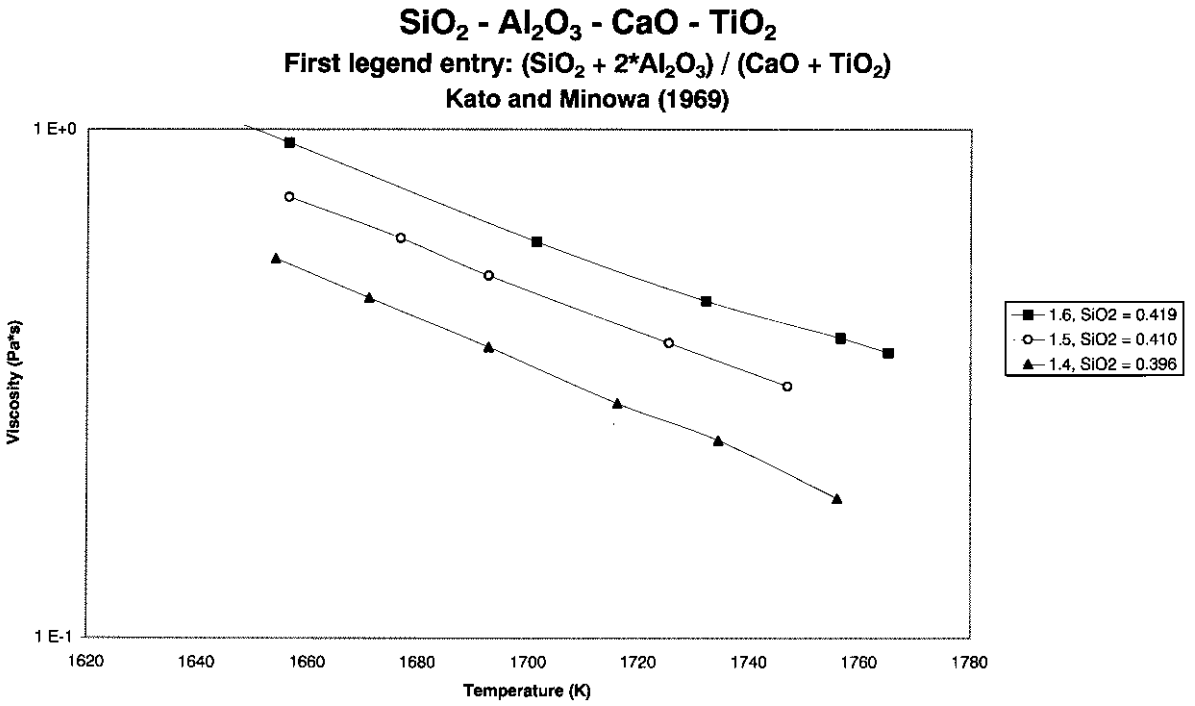

Fig. C.67.

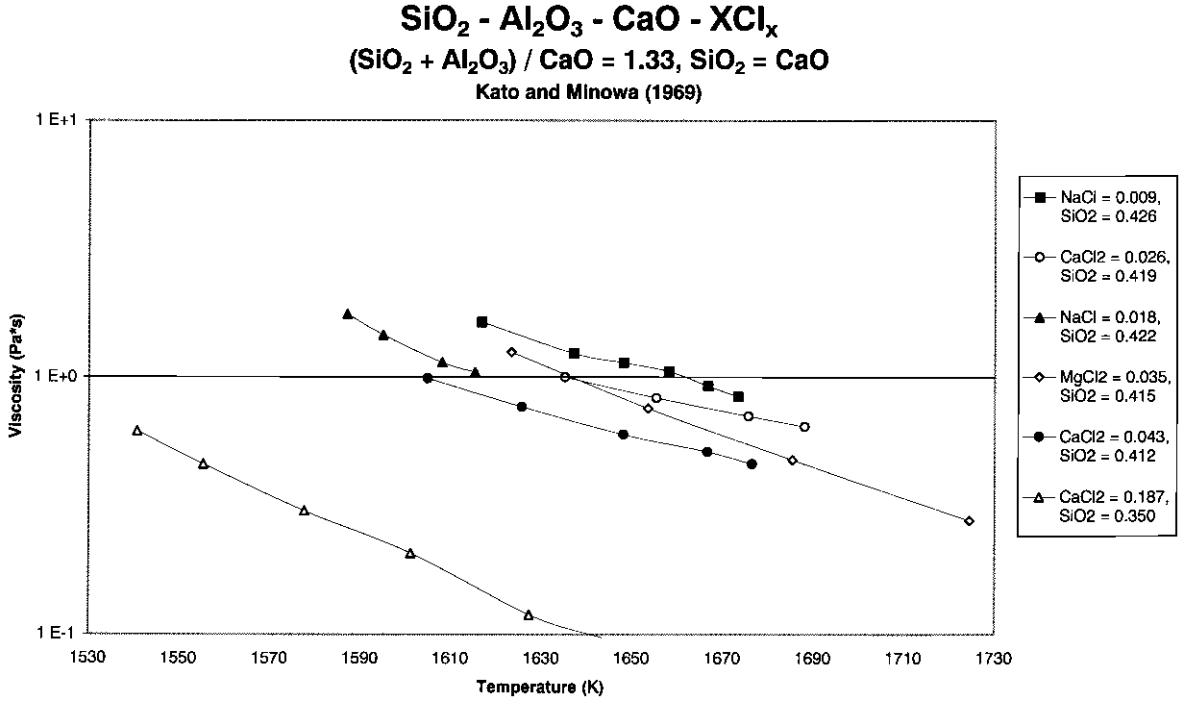

Fig. C.68.

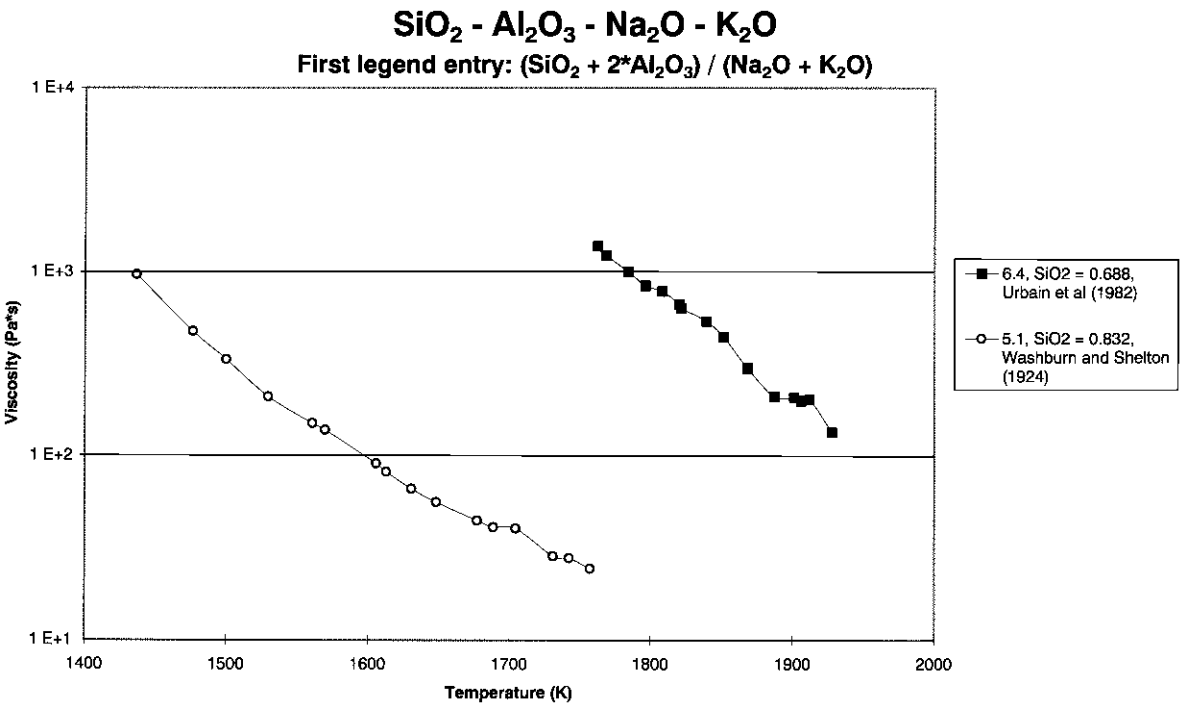

Fig. C.69.

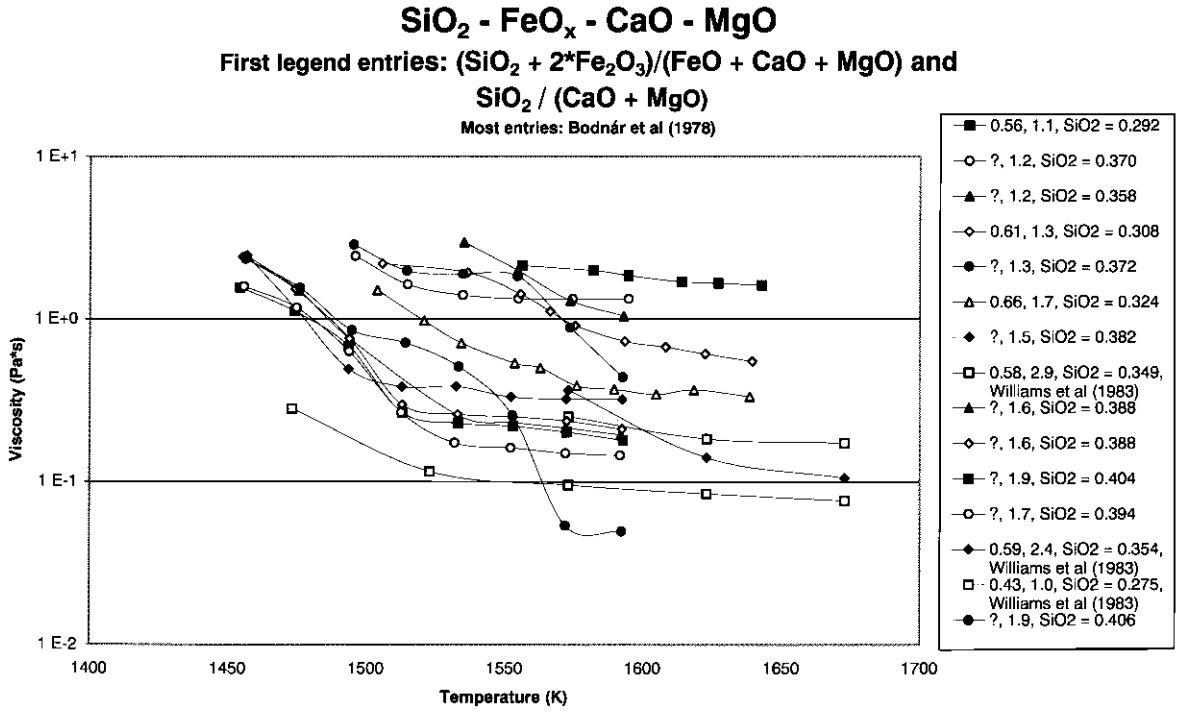

Fig. C.70.

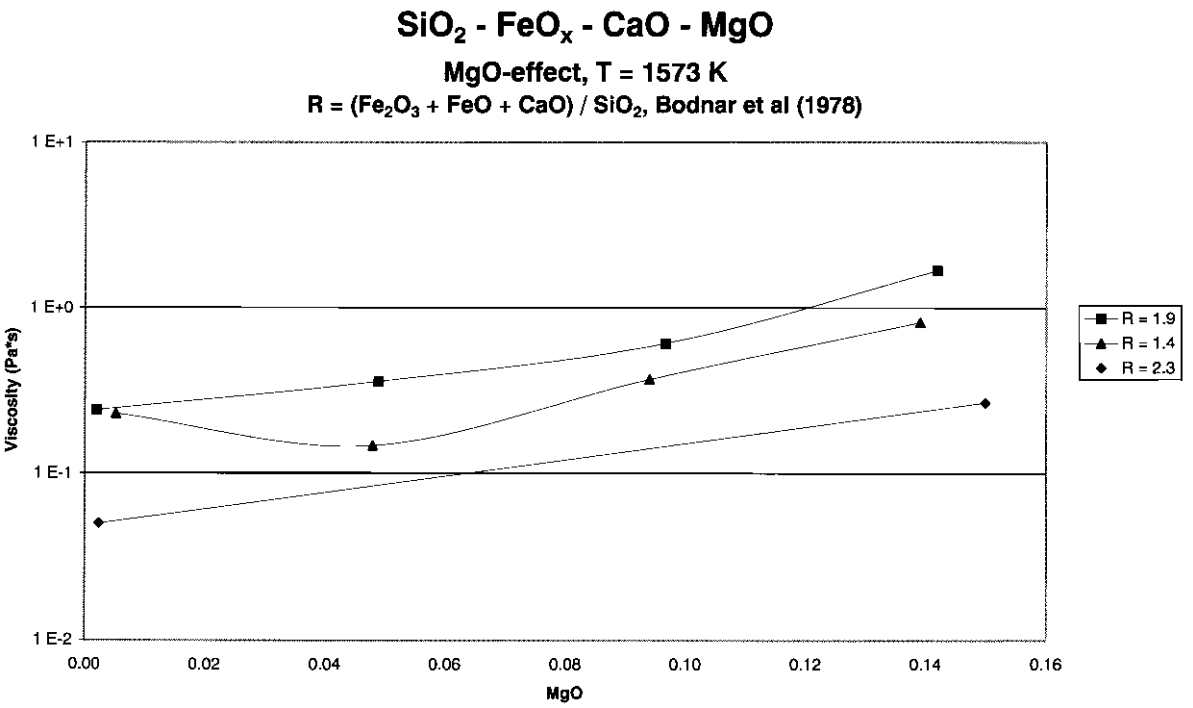

Fig. C.71.

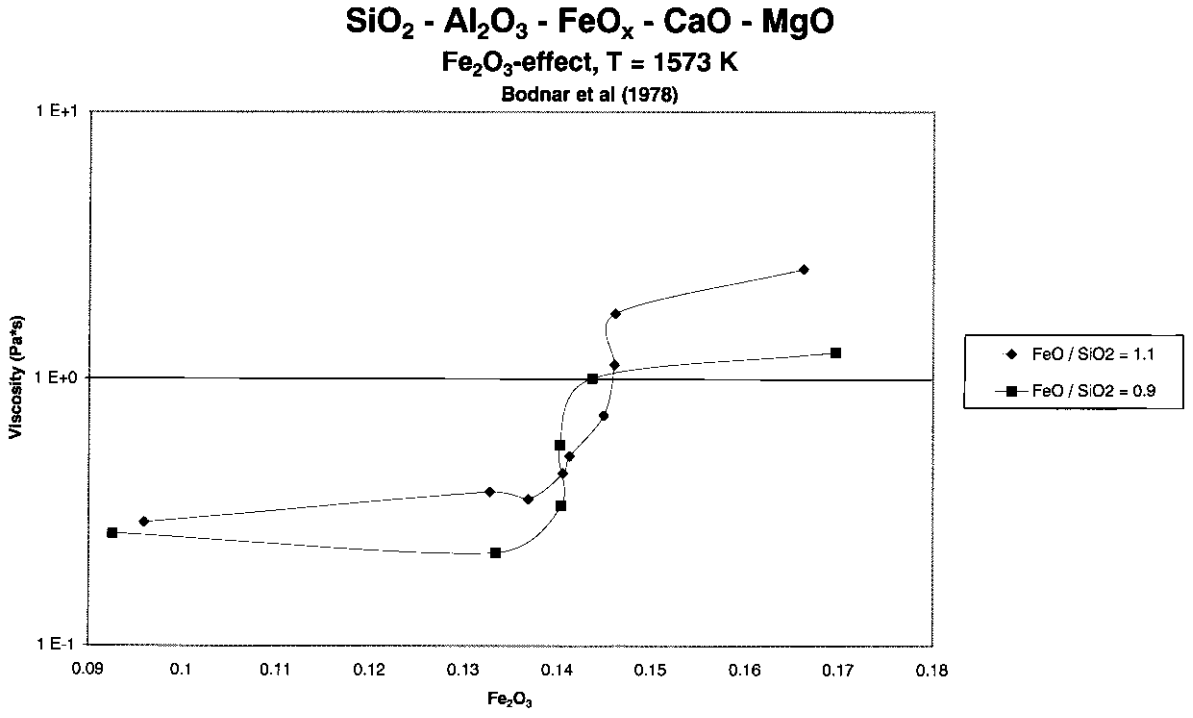

Fig. C.72.

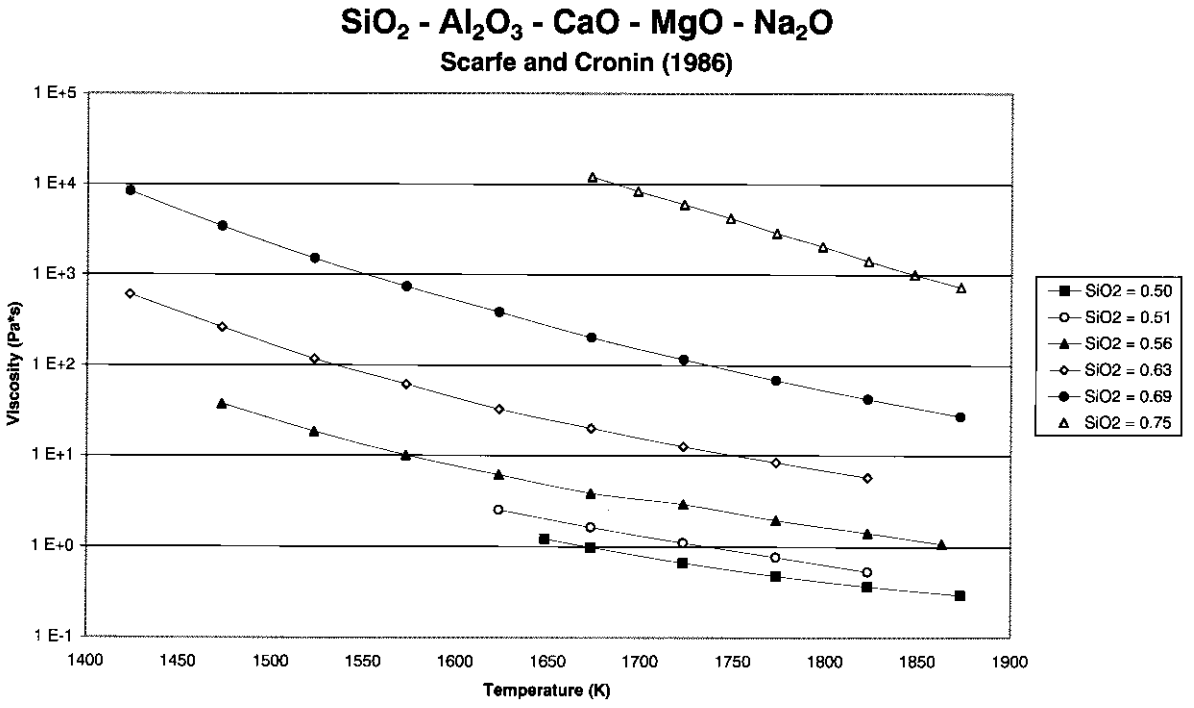

Fig. C.73.

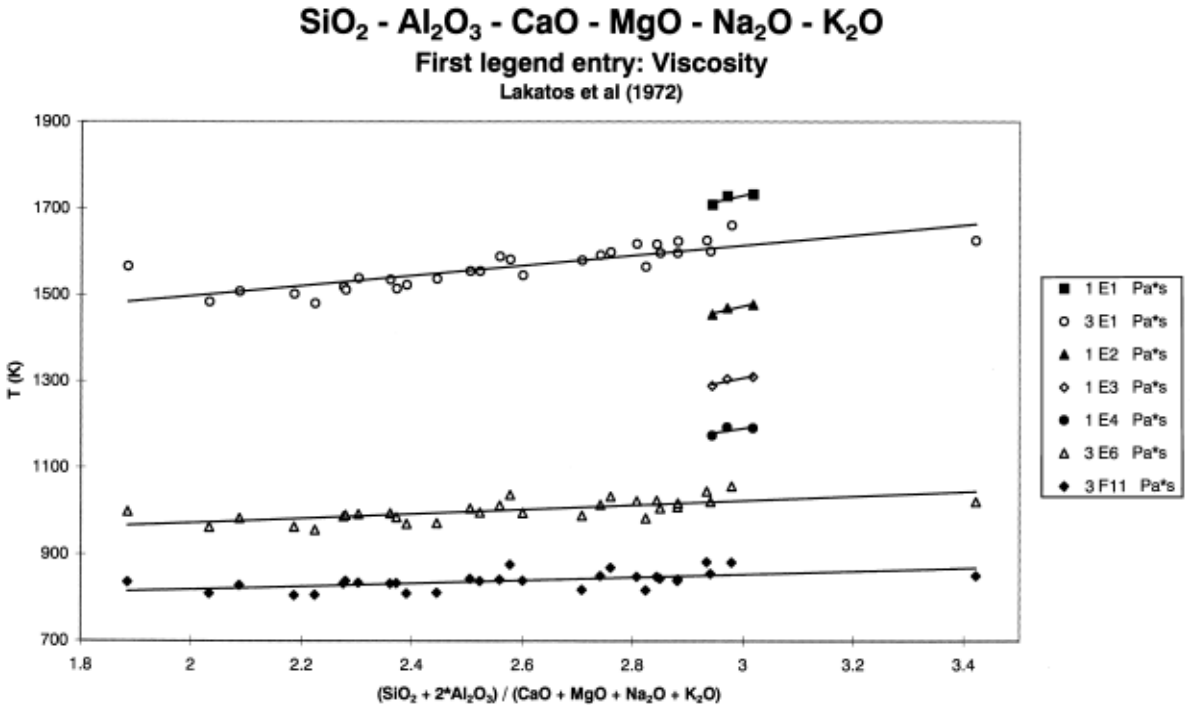

Fig. C.74.

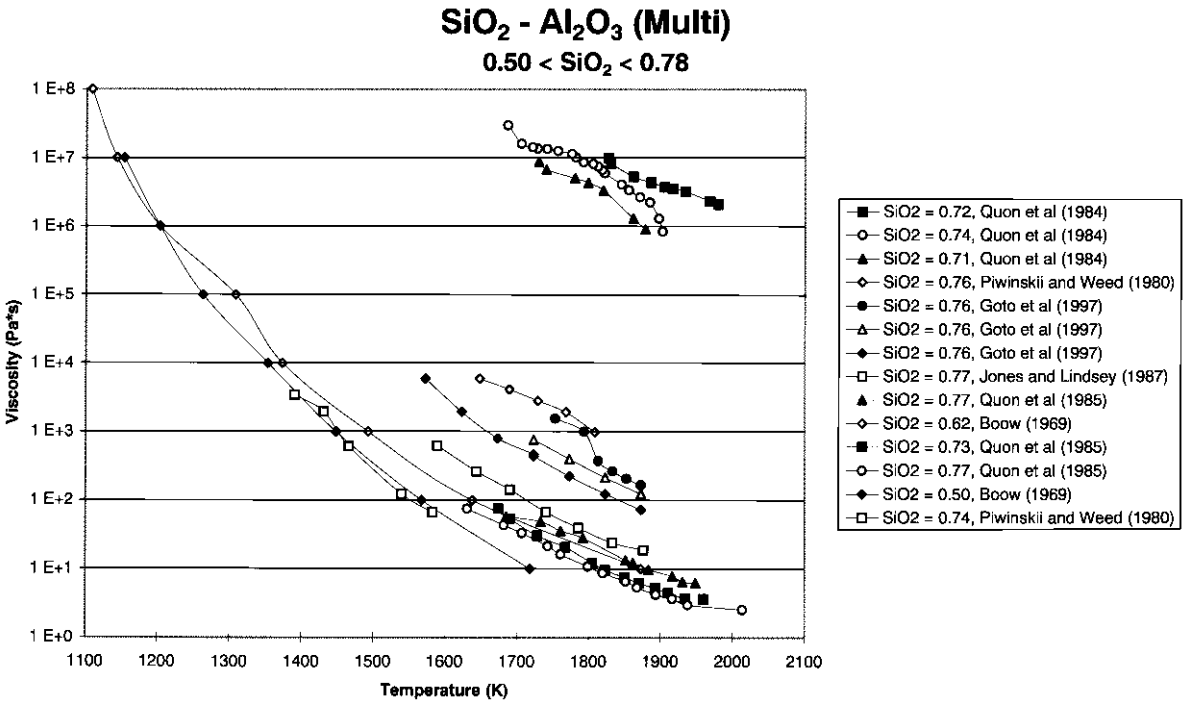

Fig. C.75.

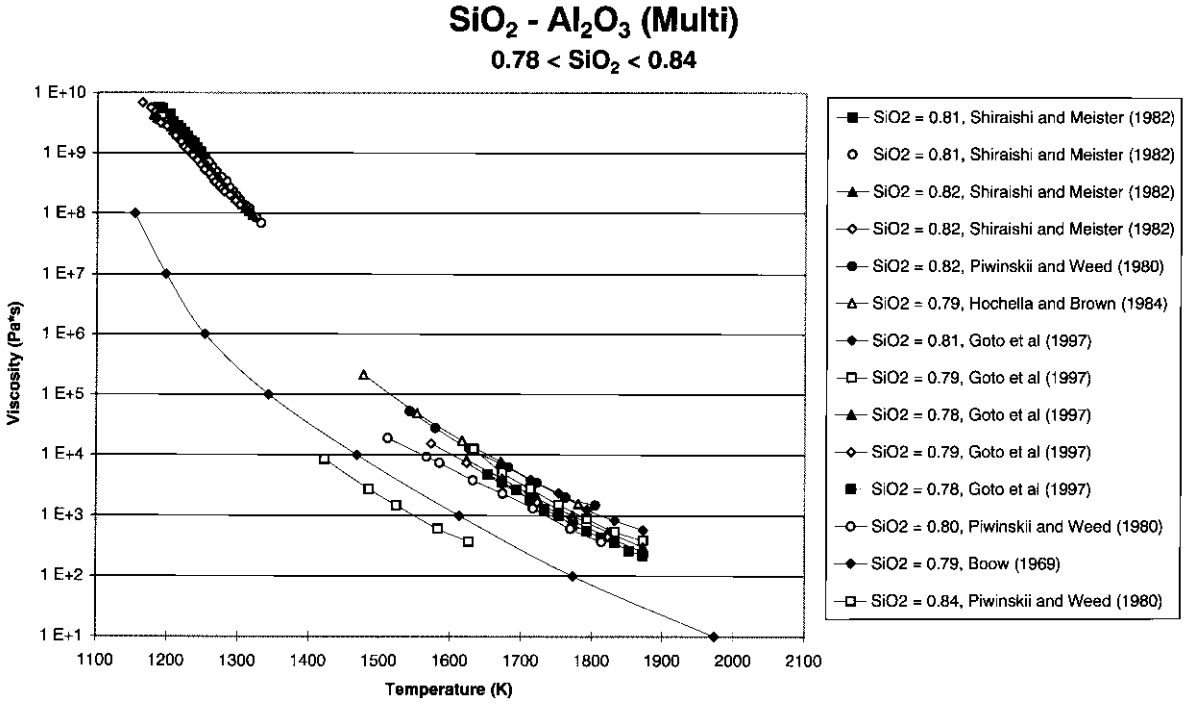

Fig. C.76.

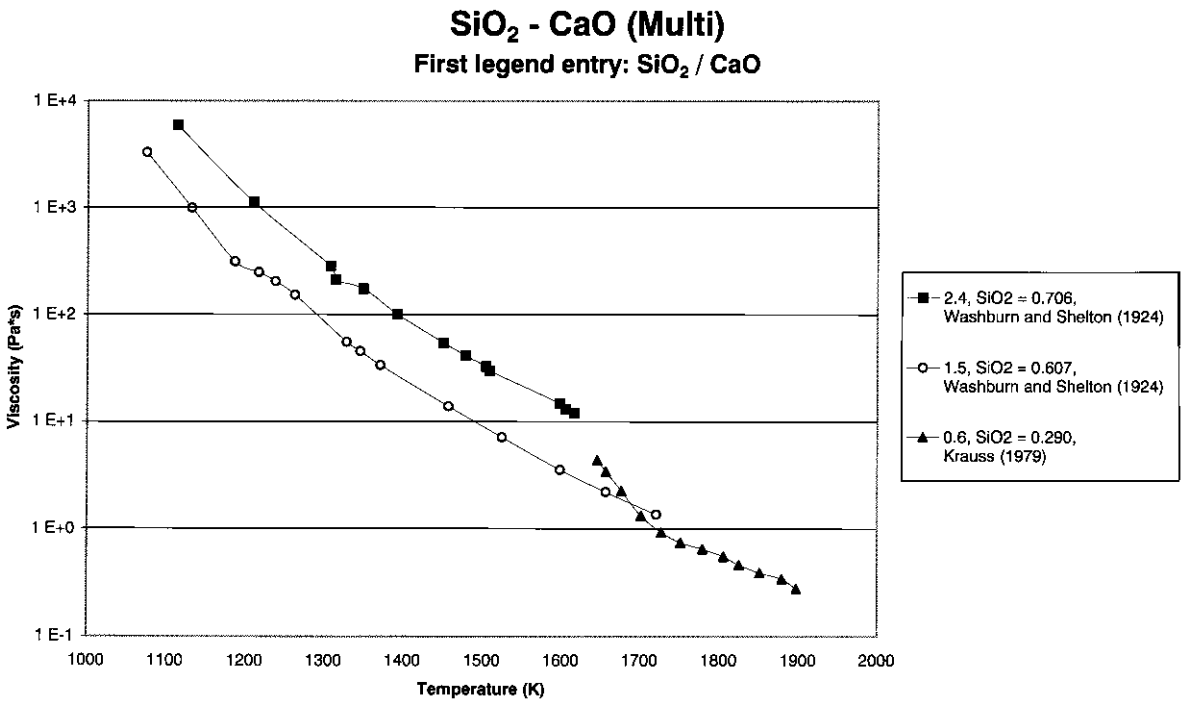

Fig. C.77.

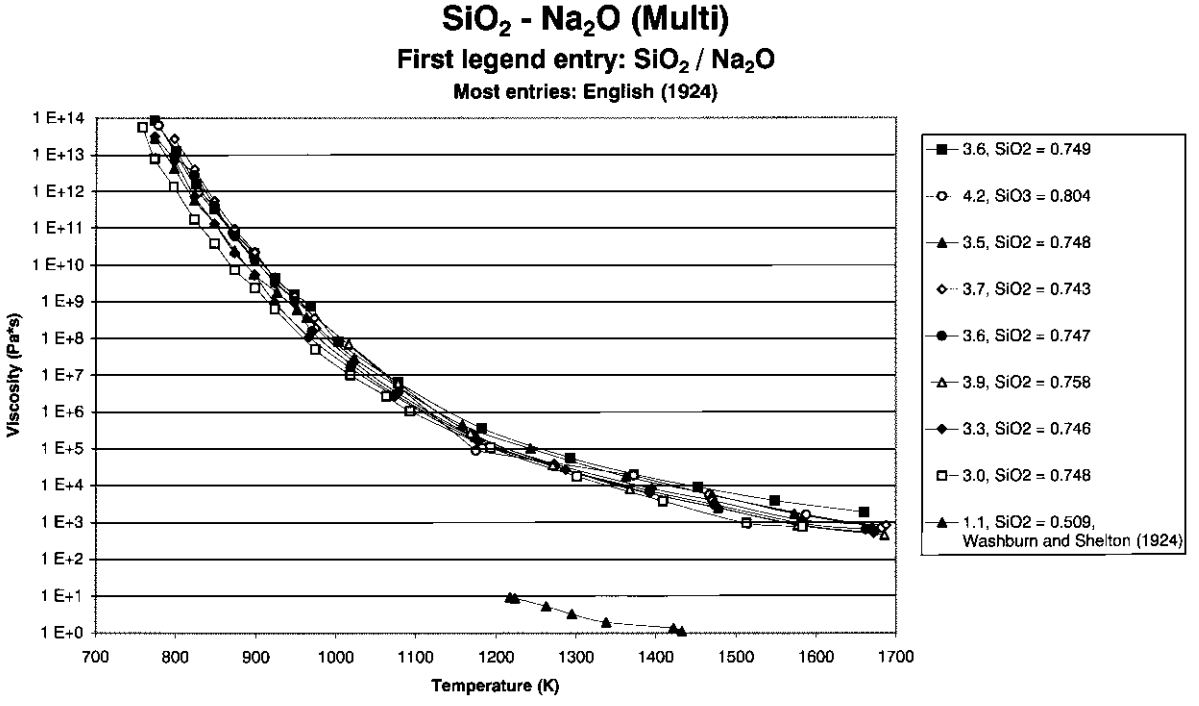

Fig. C.78.

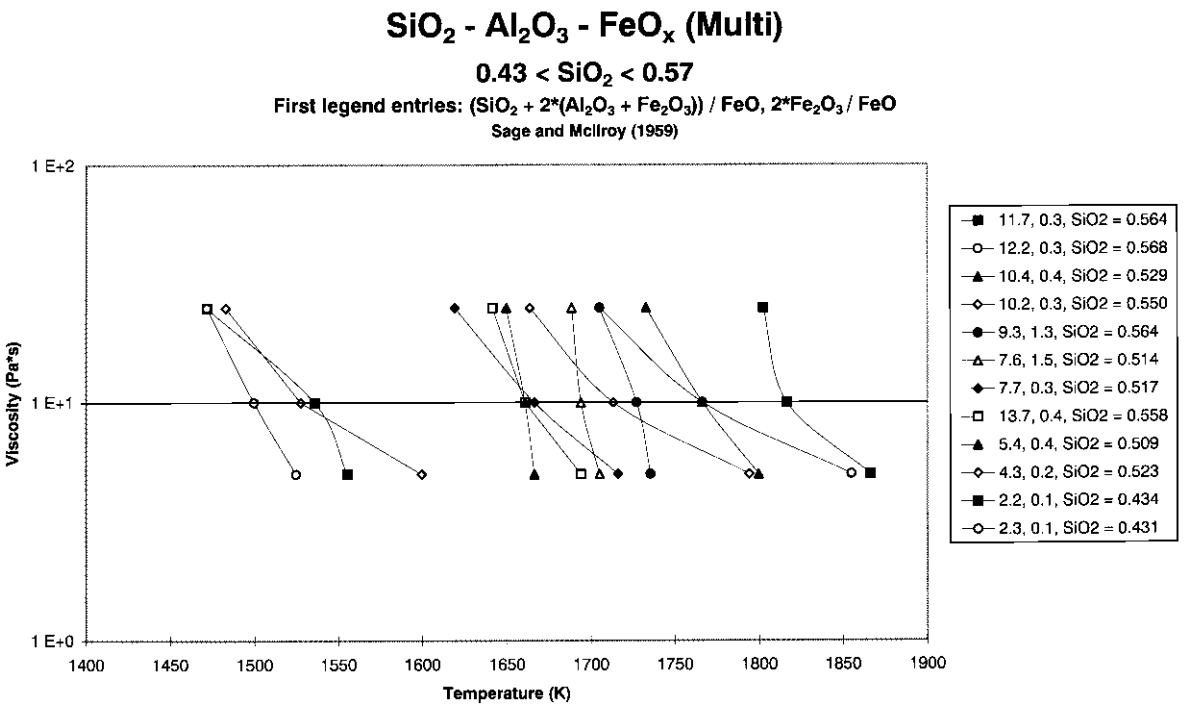

Fig. C.79.

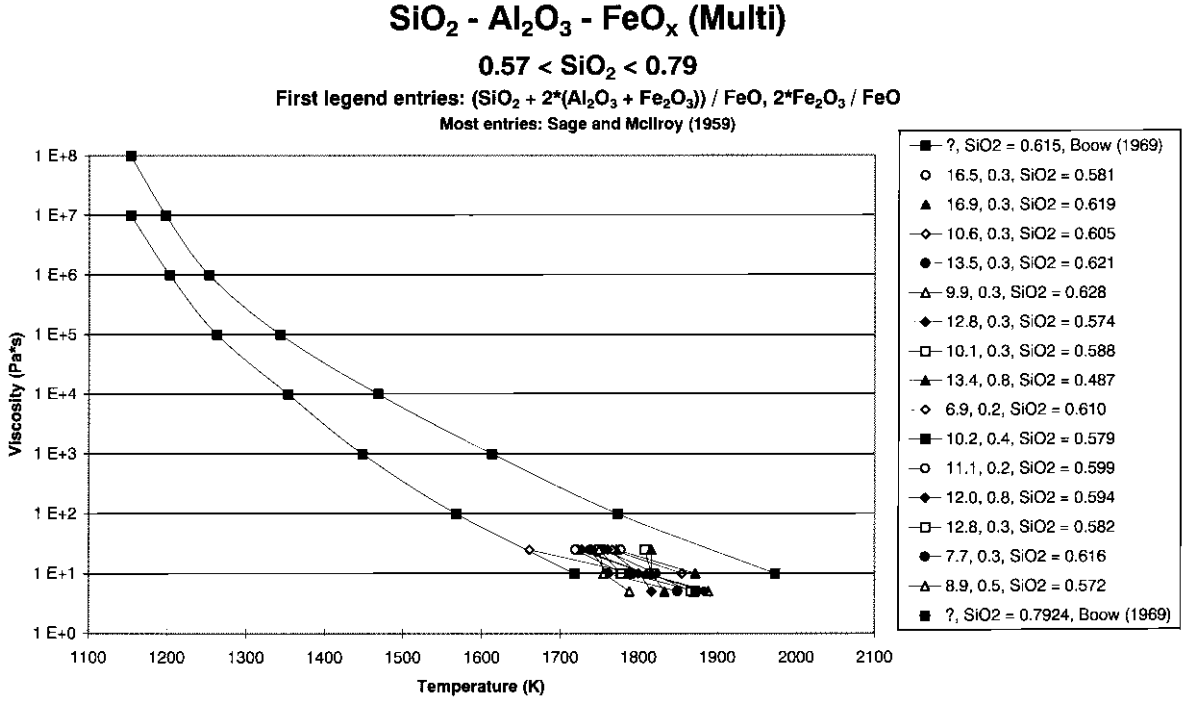

Fig. C.80.

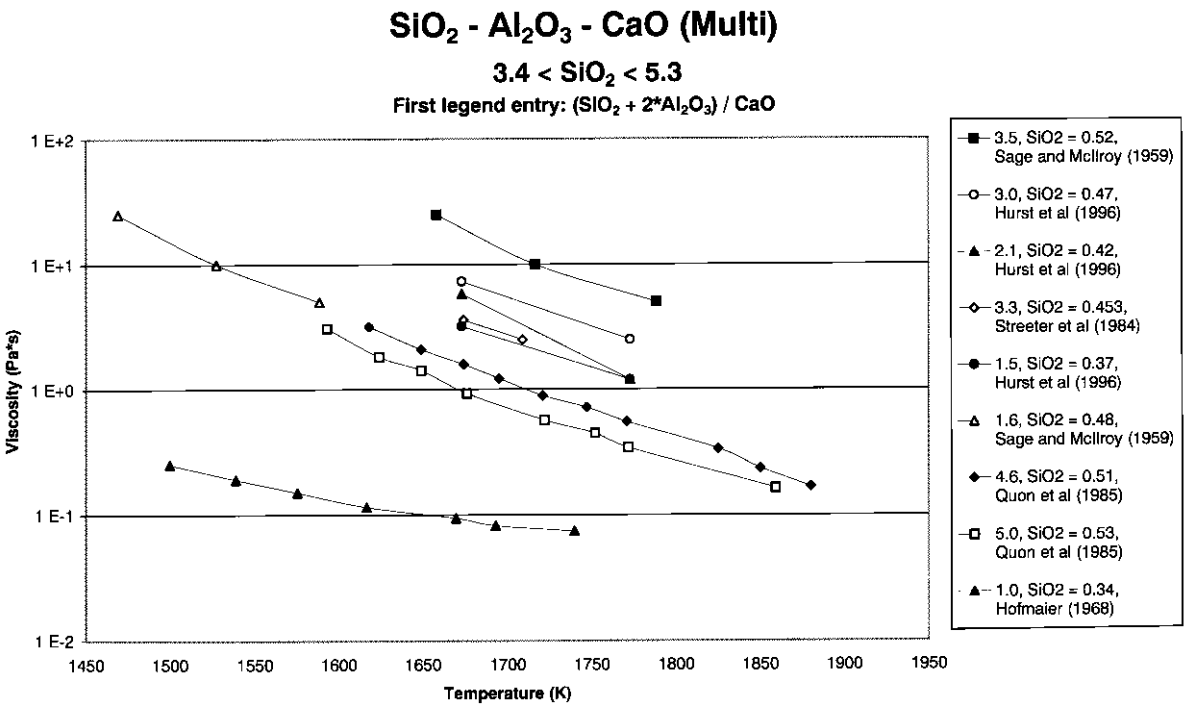

Fig. C.81.

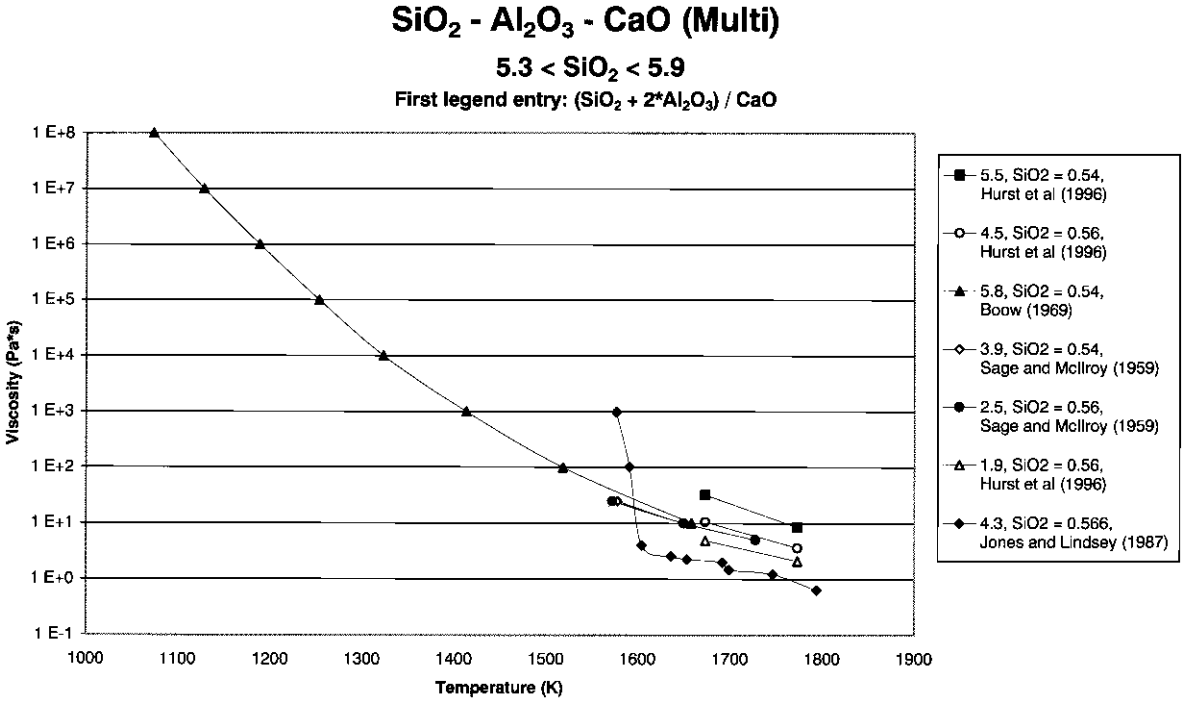

Fig. C.82.

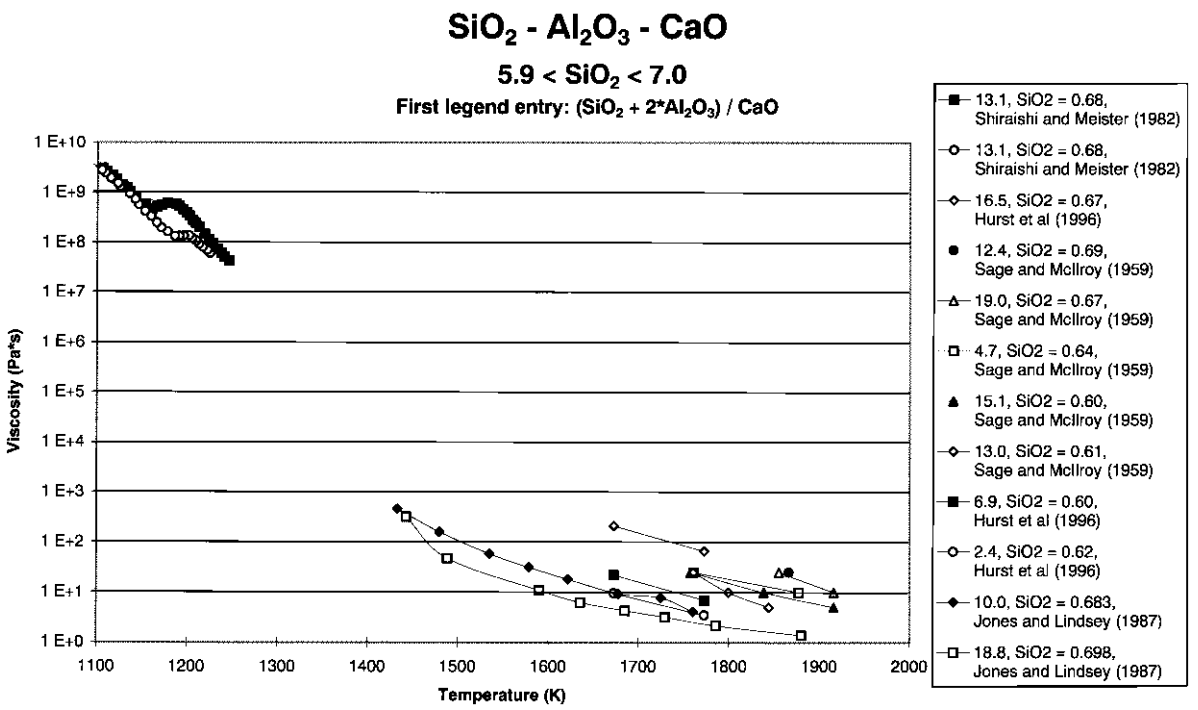

Fig. C.83.

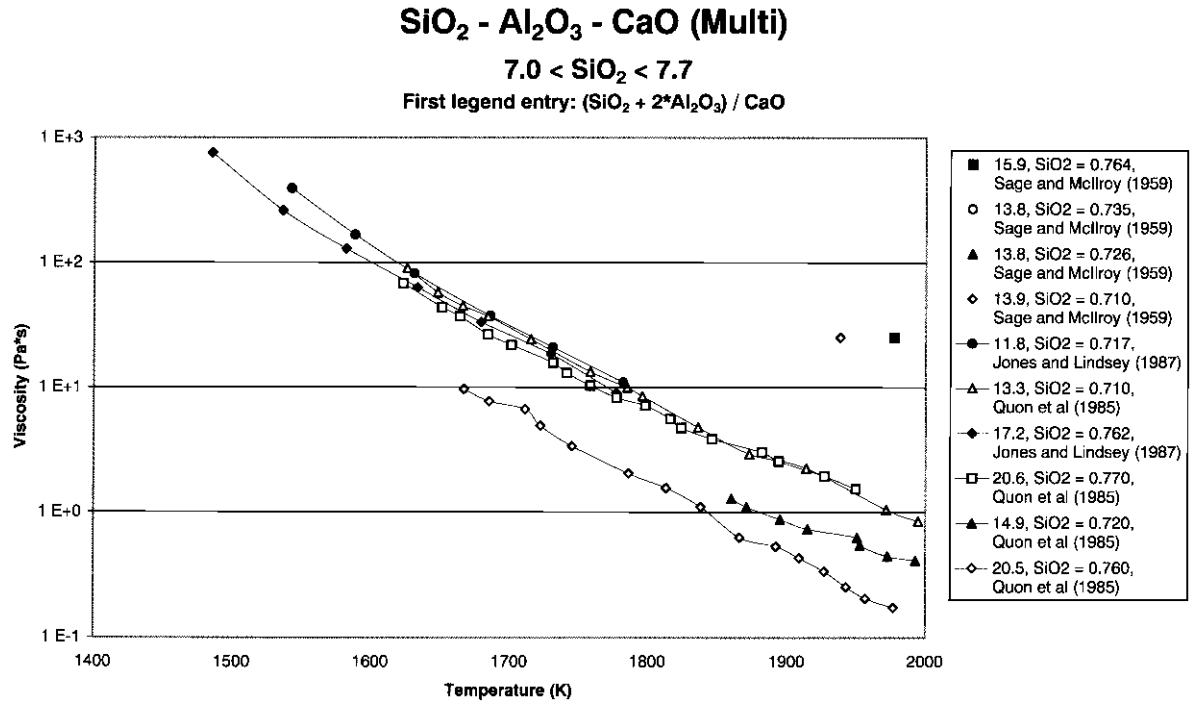

Fig. C.84.

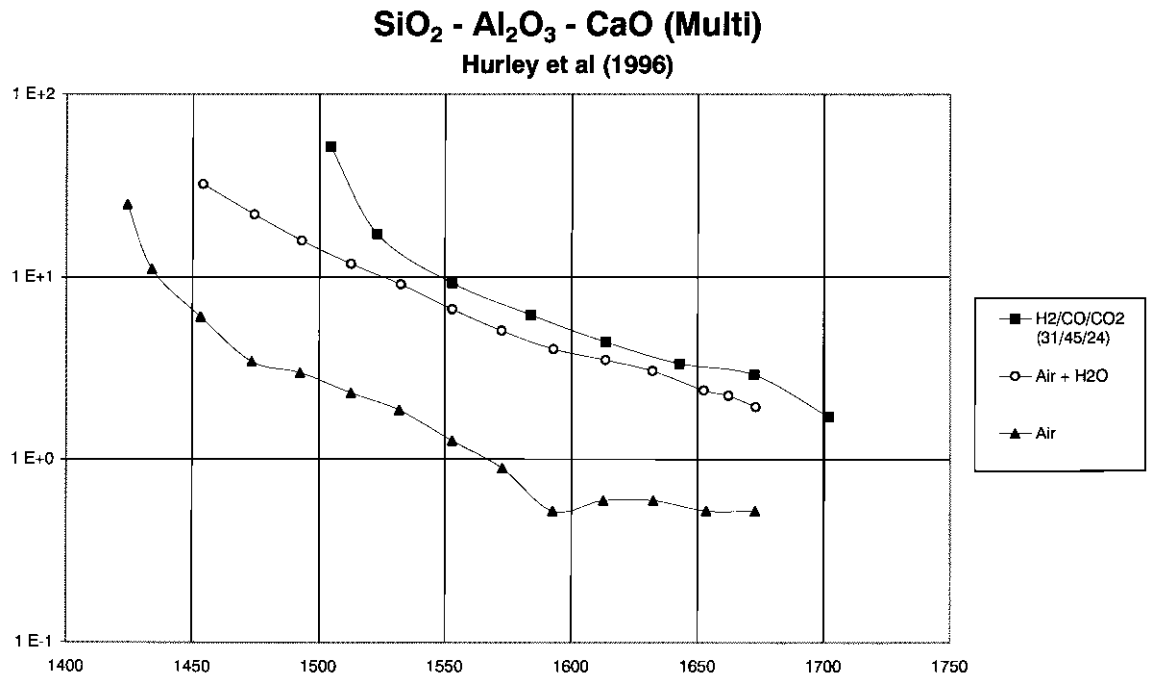

Fig. C.85.

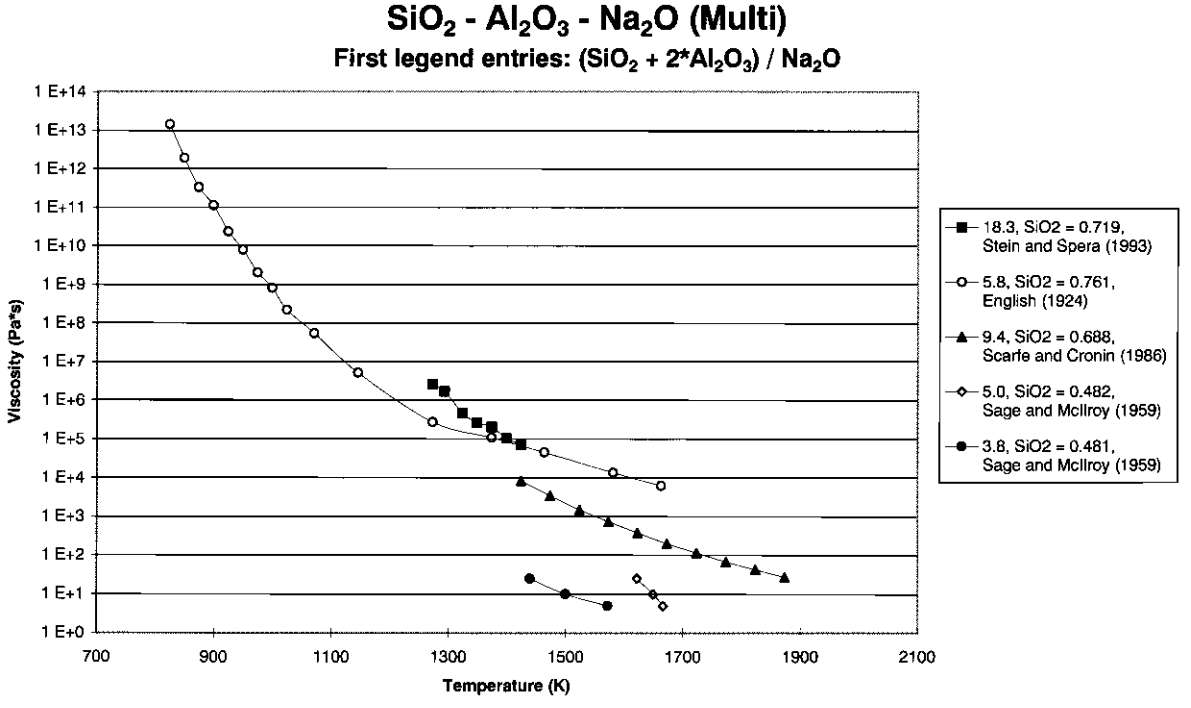

Fig. C.86.

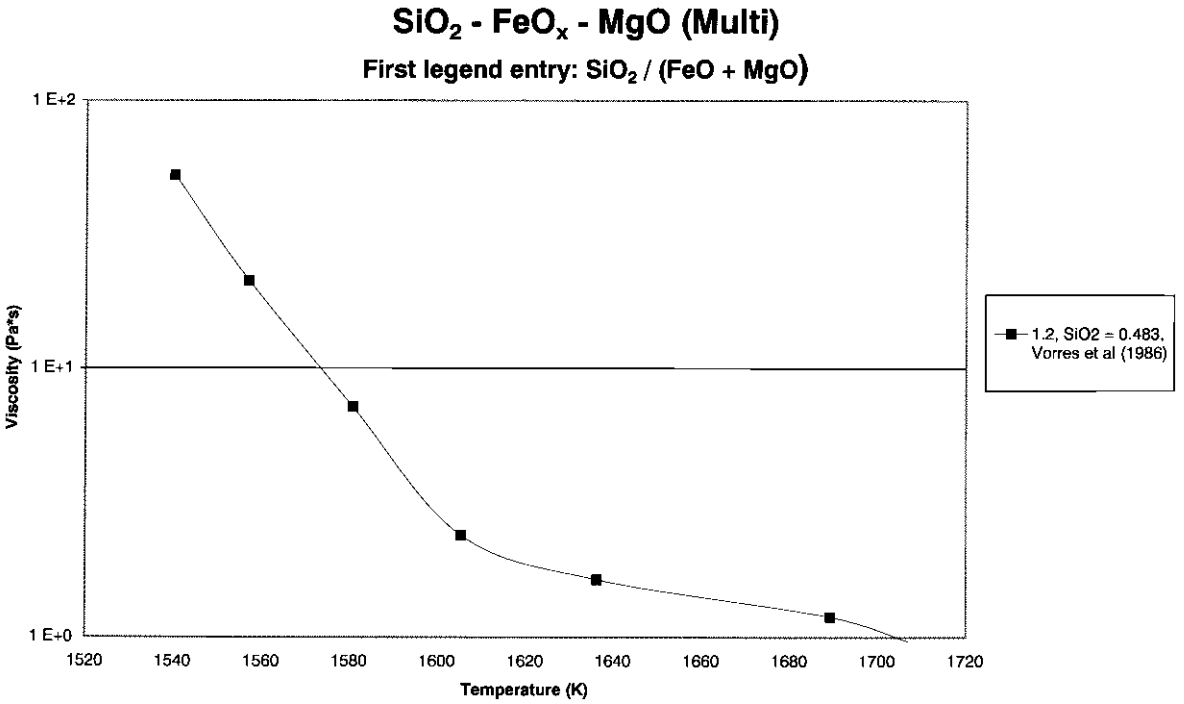

Fig. C.87.

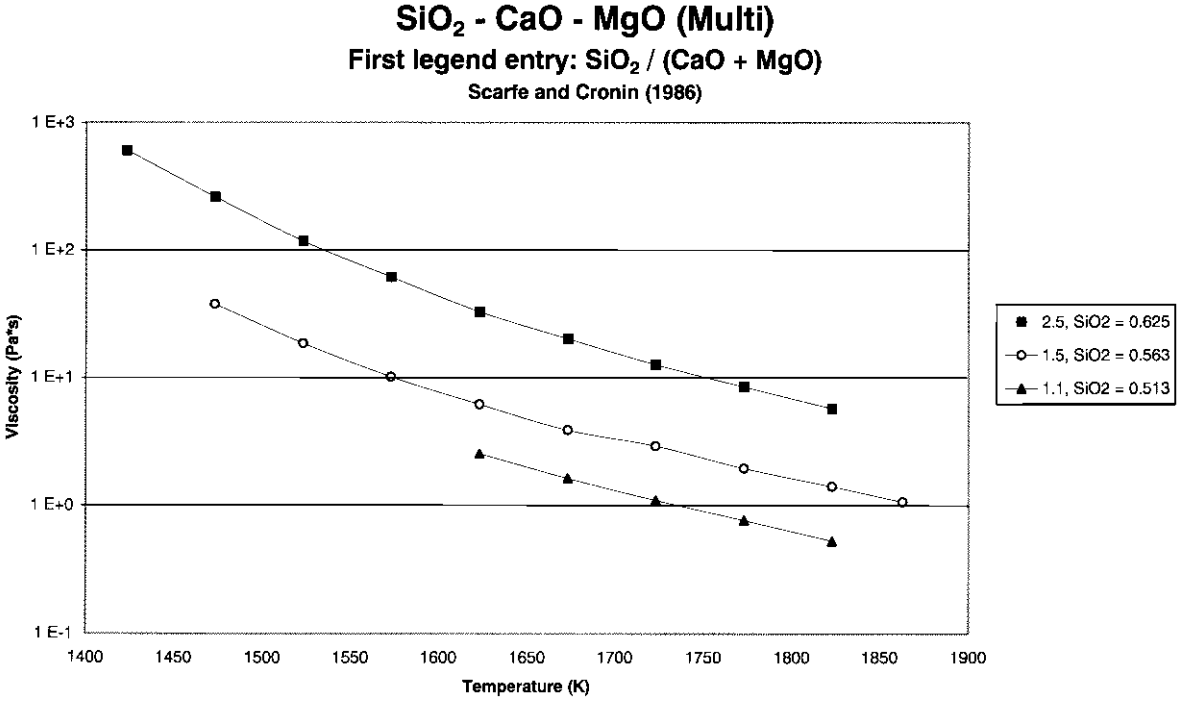

Fig. C.88.

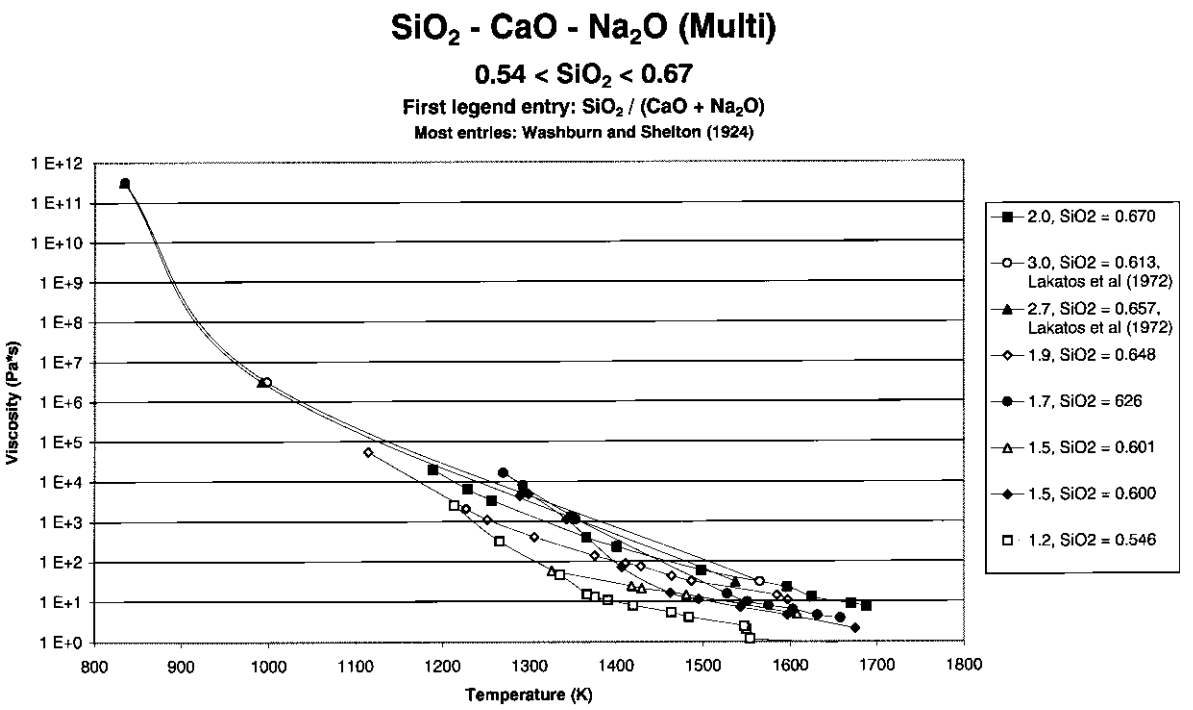

Fig. C.89.

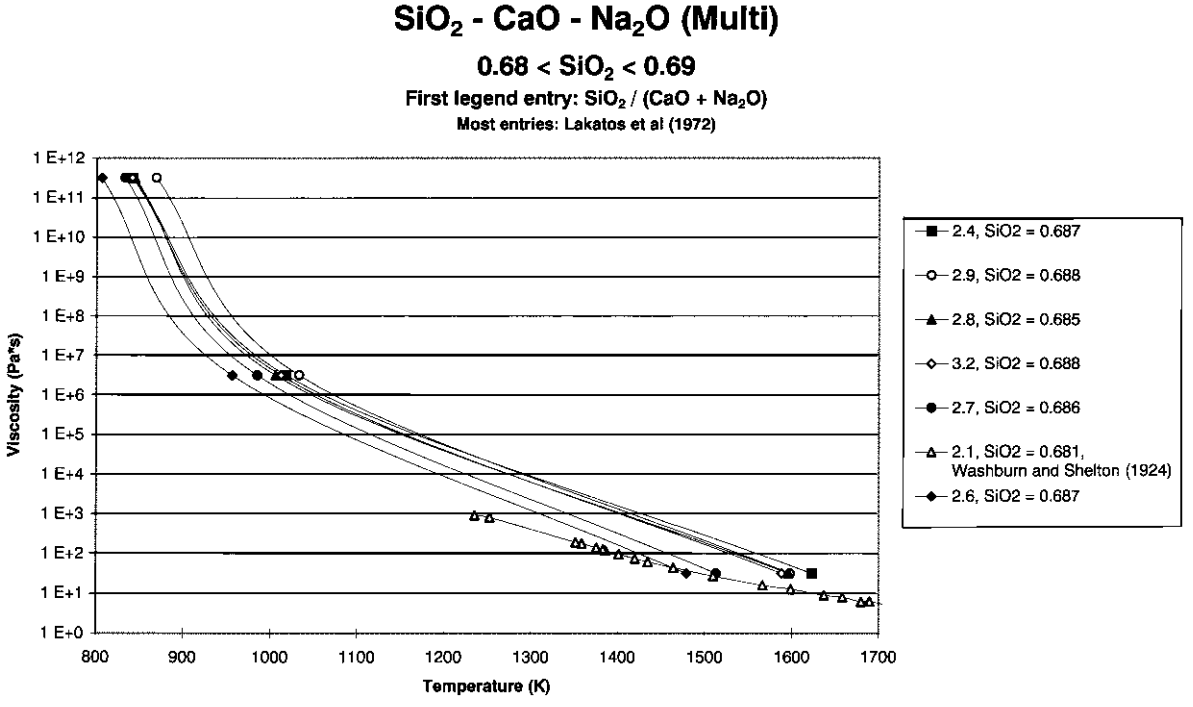

Fig. C.90.

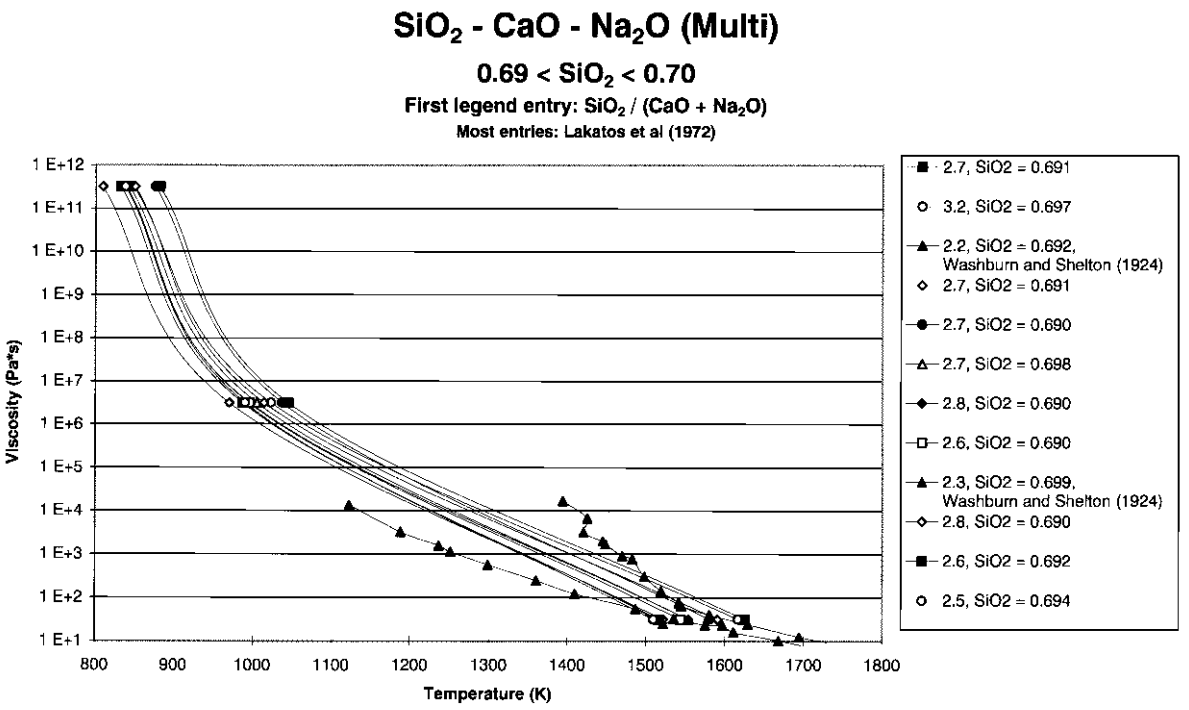

Fig. C.91.

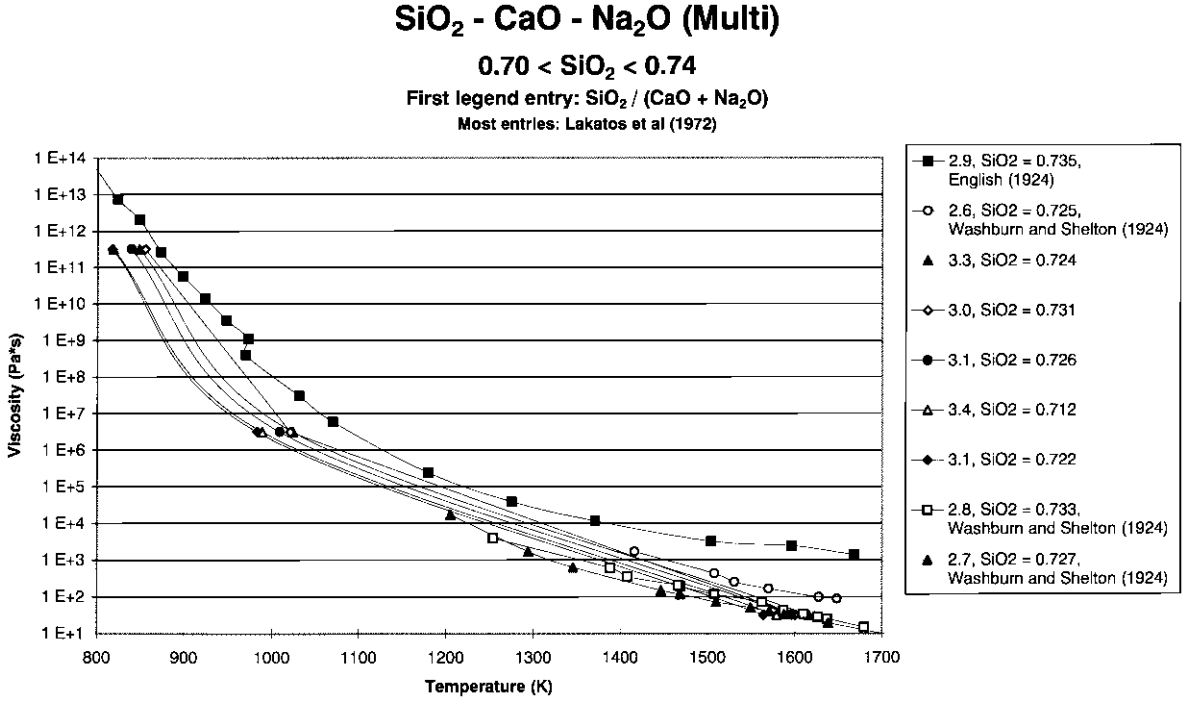

Fig. C.92.

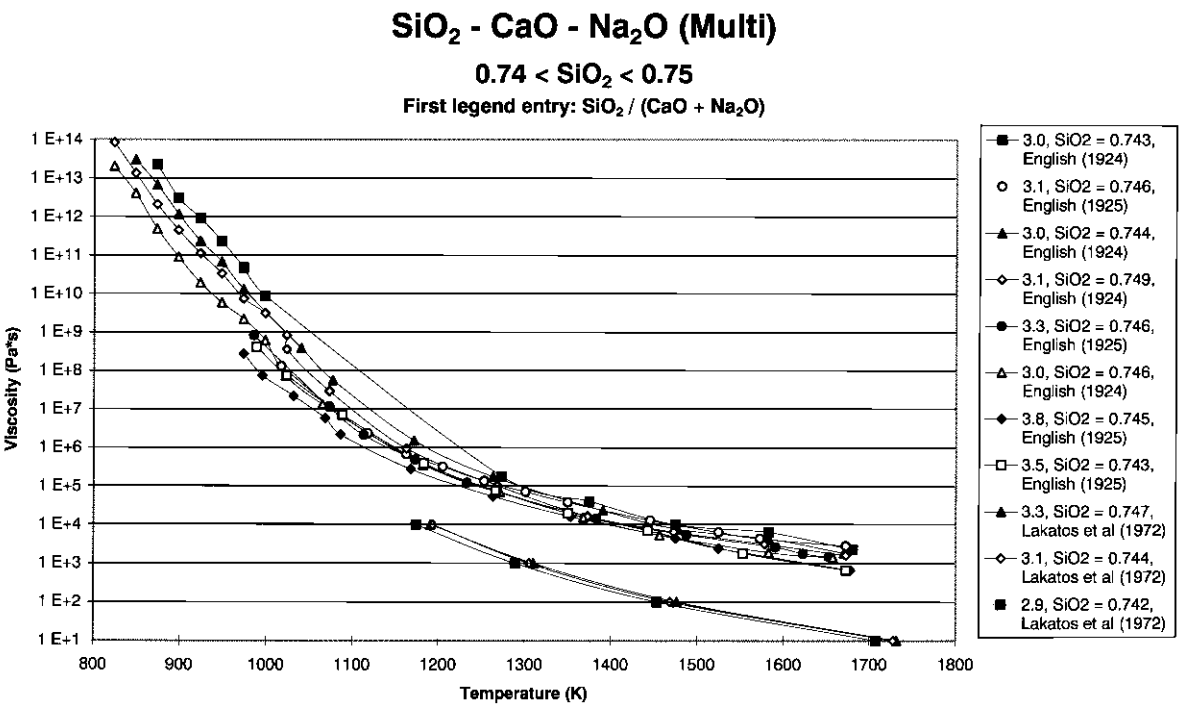

Fig. C.93.

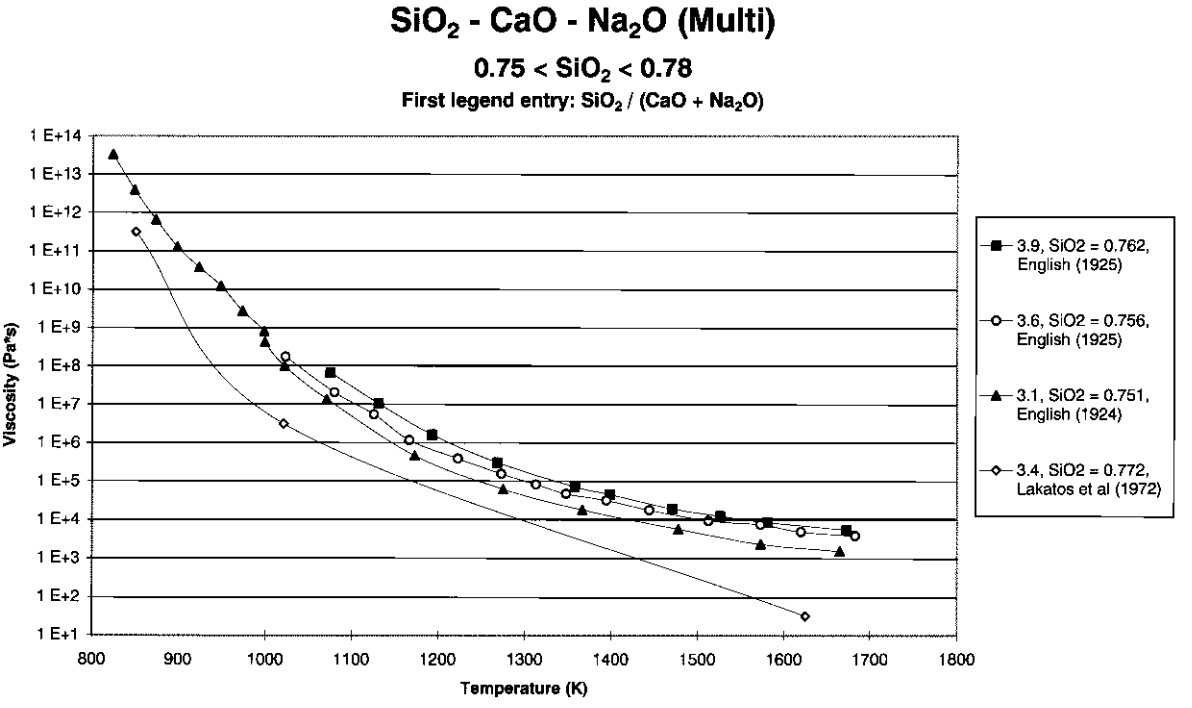

Fig. C.94.

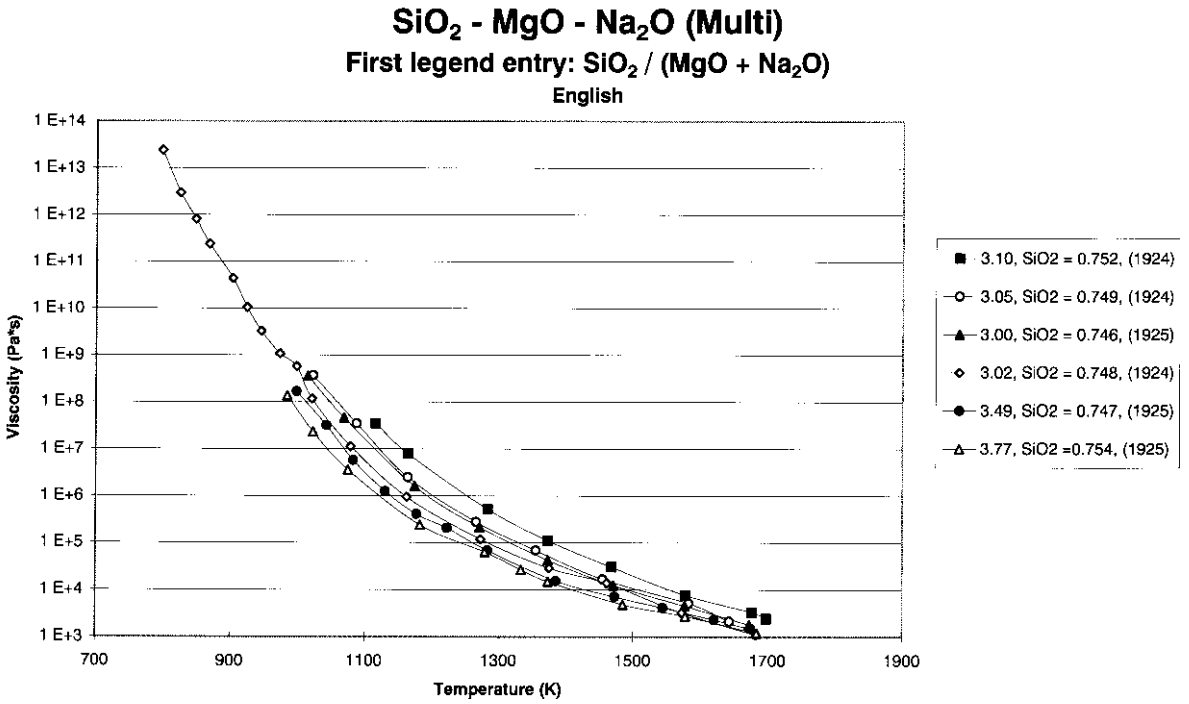

Fig. C.95.

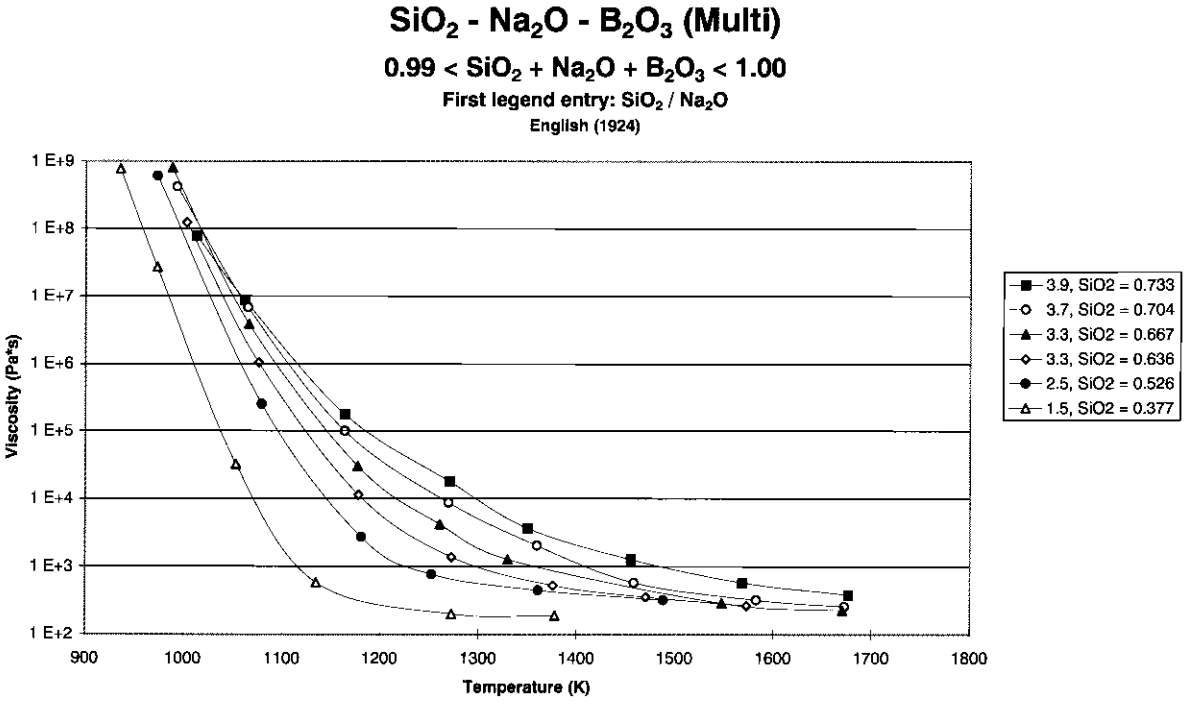

Fig. C.96.

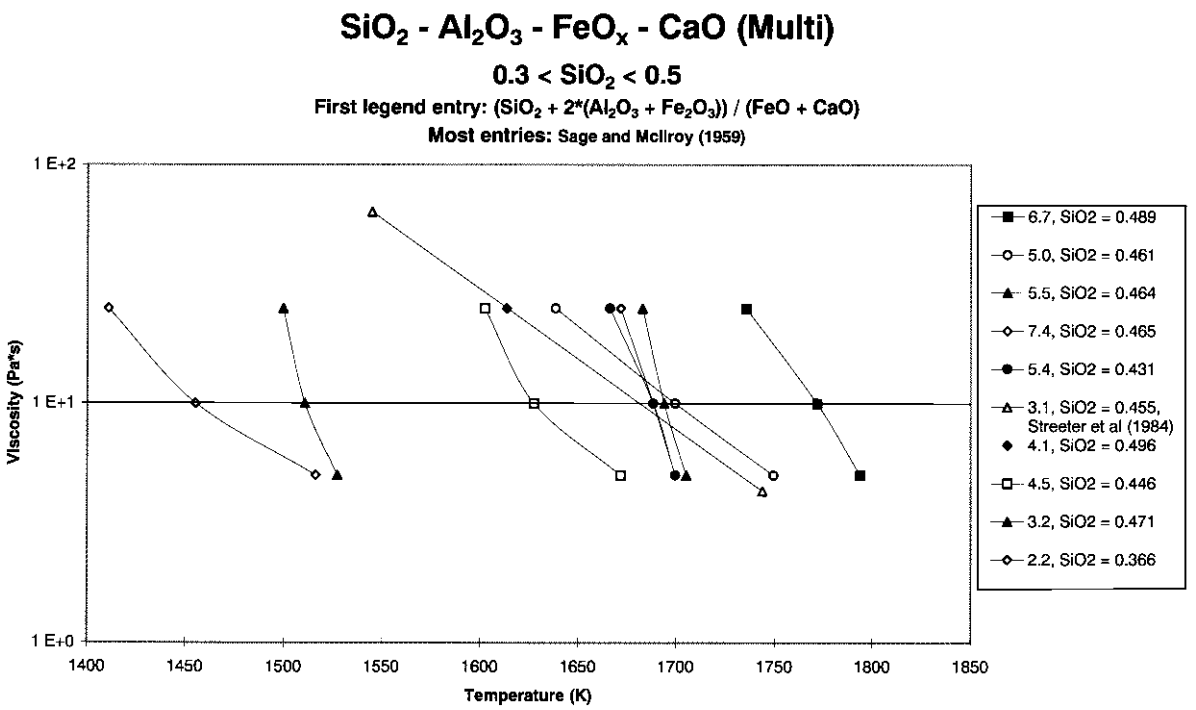

Fig. C.97.

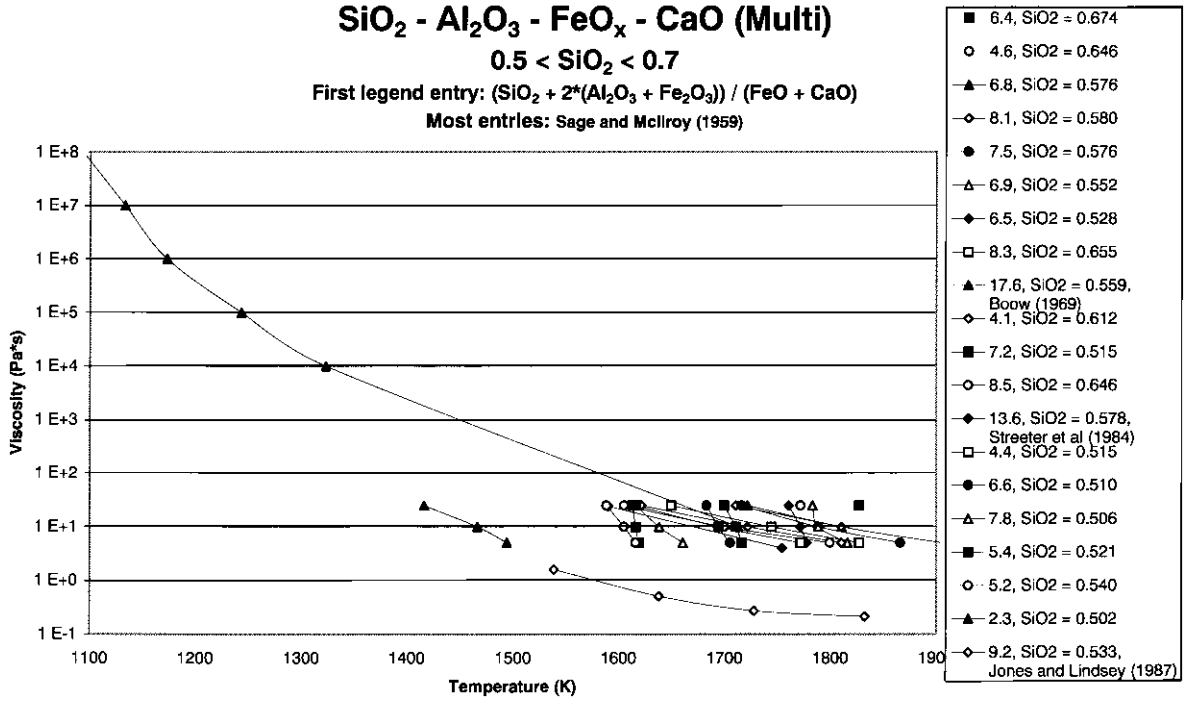

Fig. C.98.

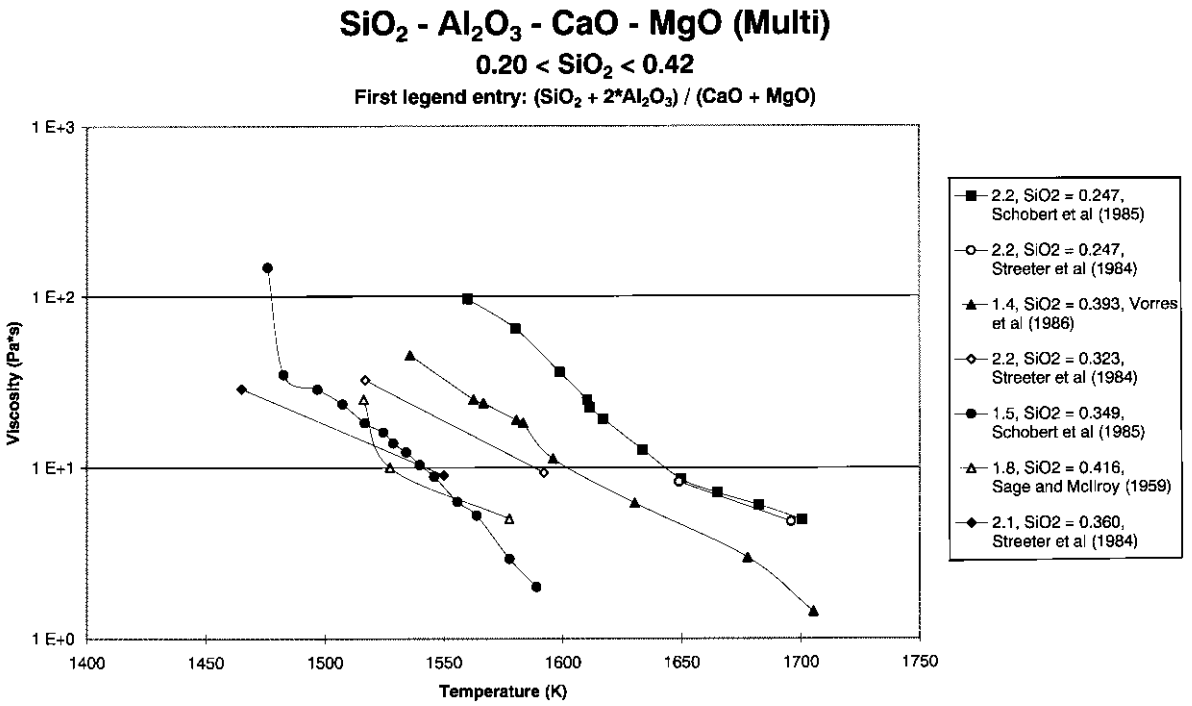

Fig. C.99.

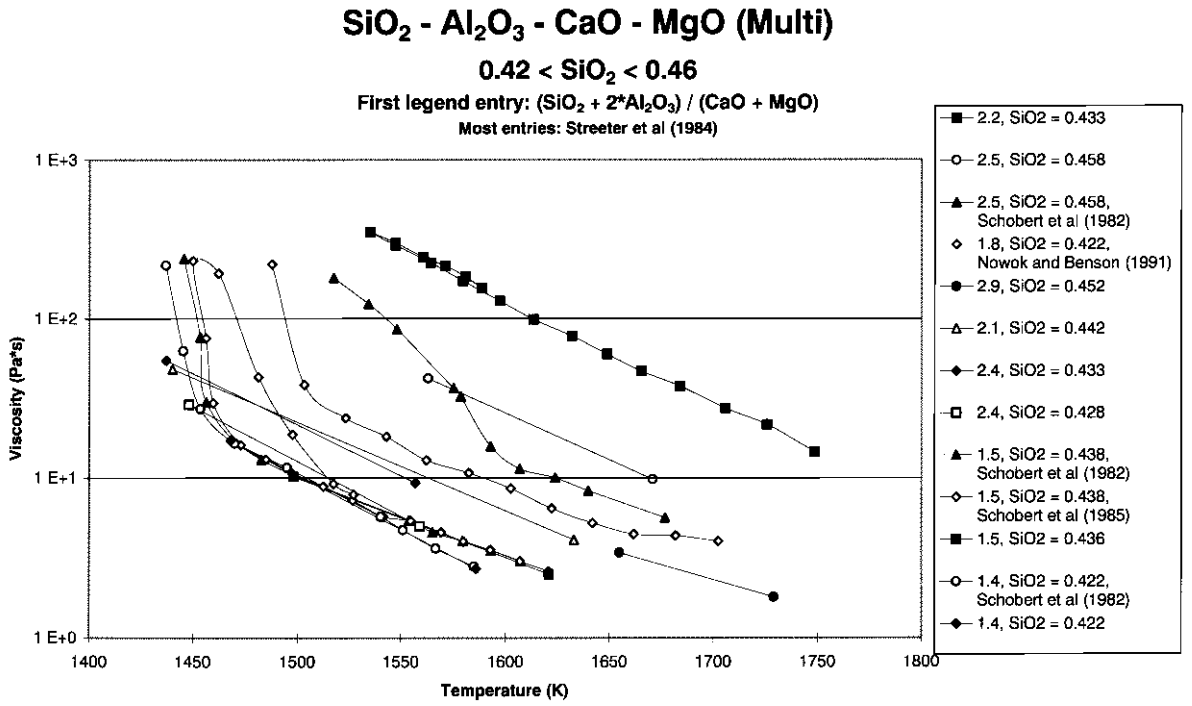

Fig. C.100.

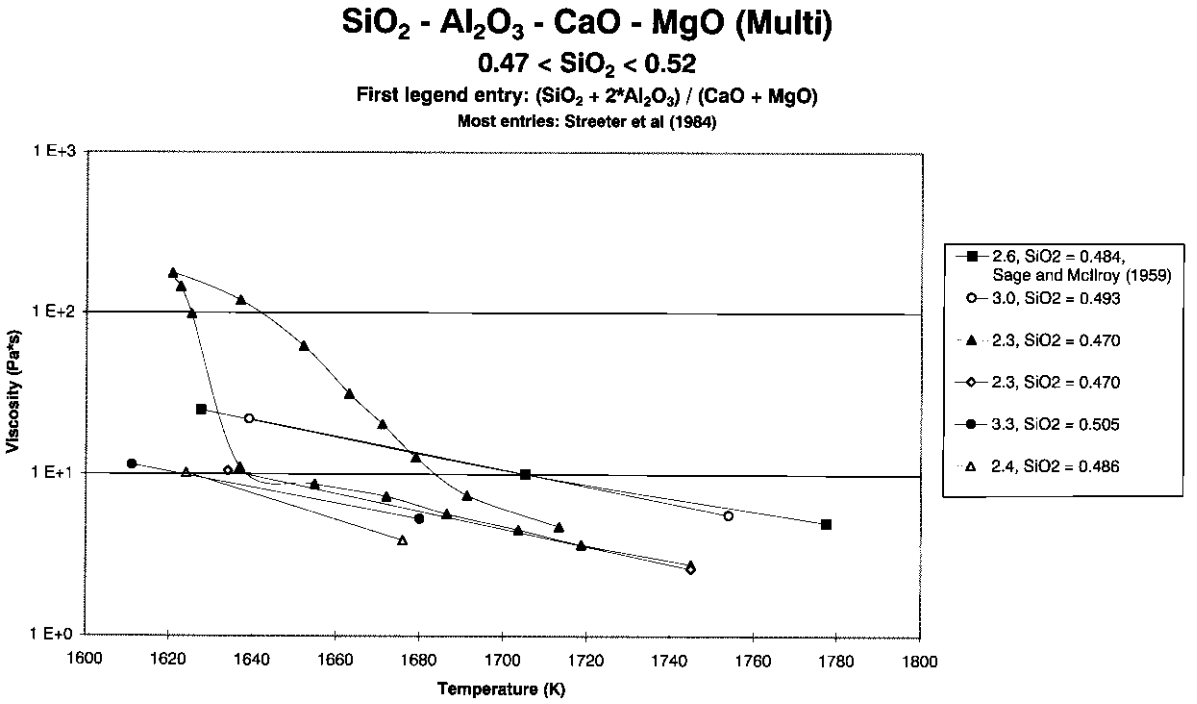

Fig. C.101.

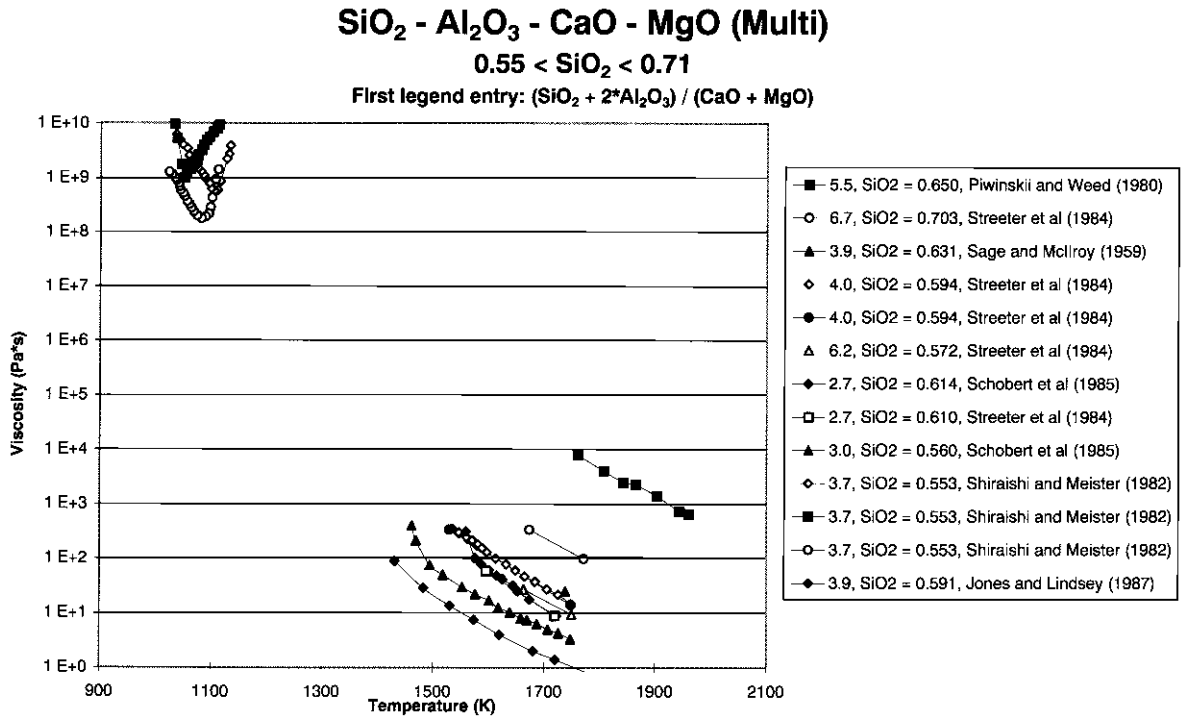

Fig. C.102.

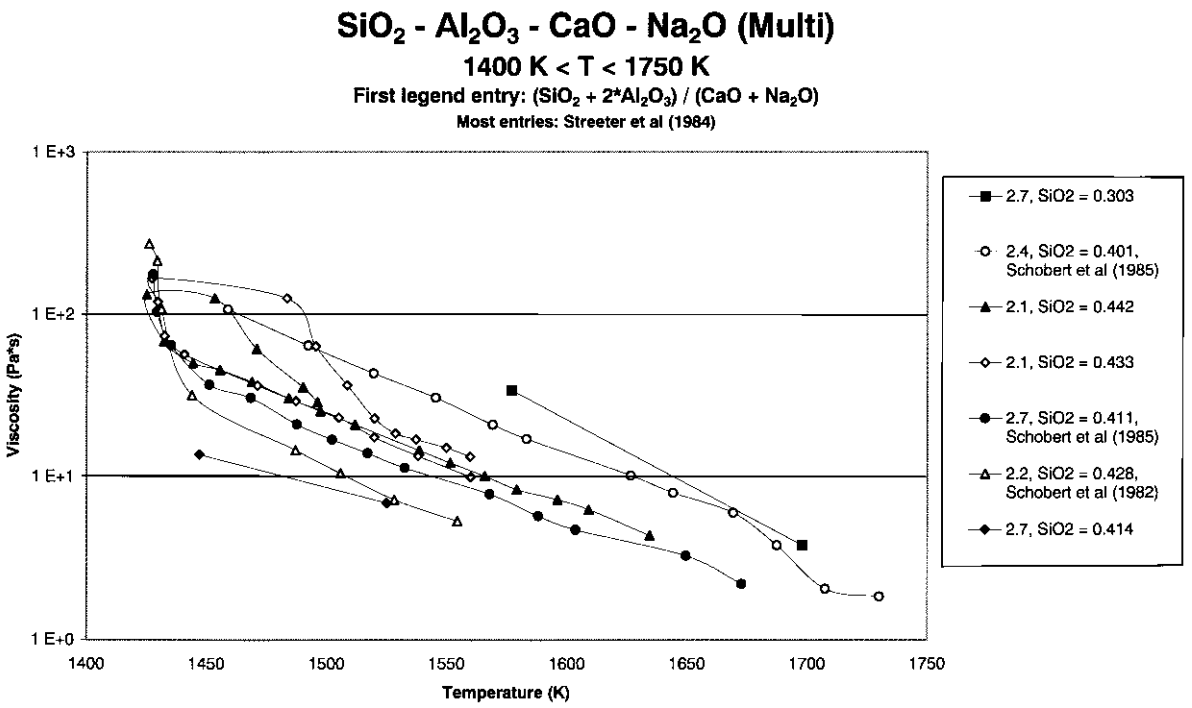

Fig. C.103.

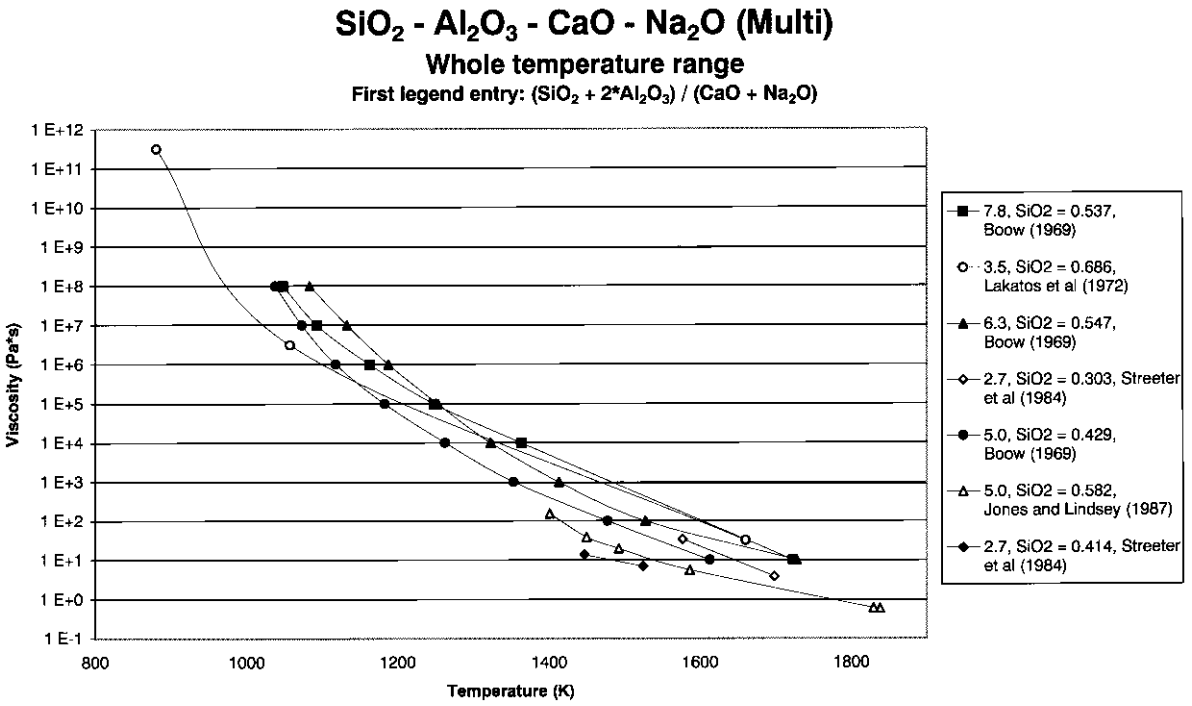

Fig. C.104.

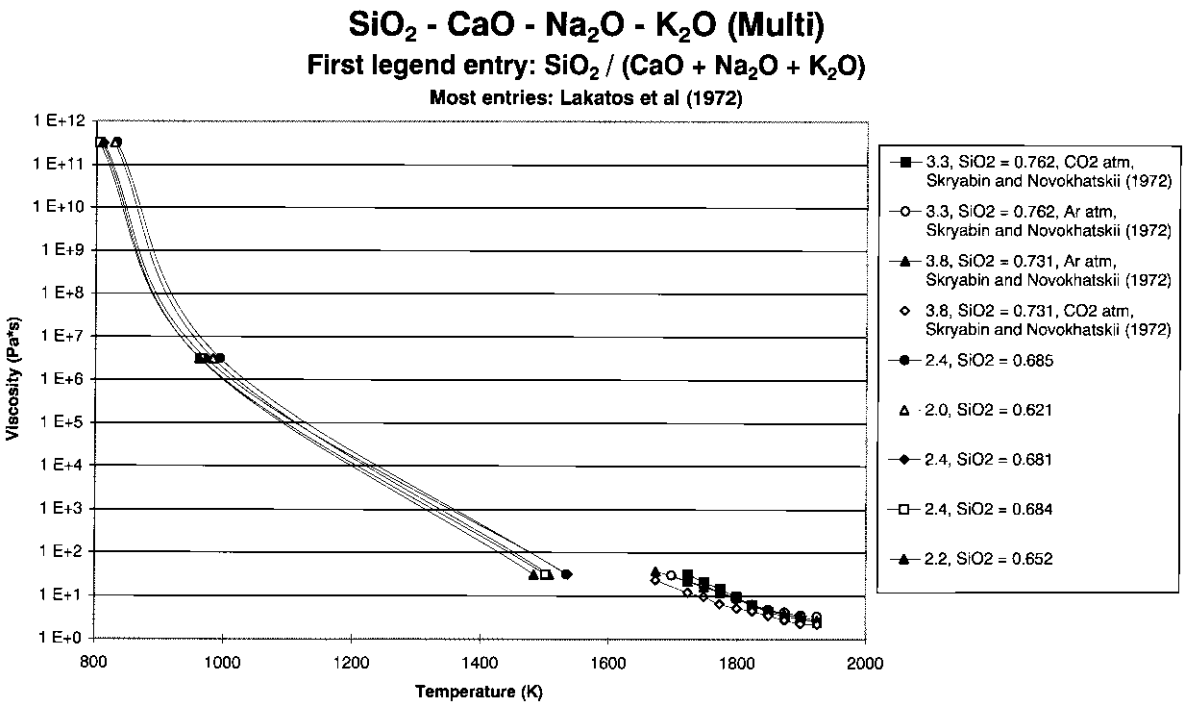
SiO2 - CaO - Na2O - K2O (Multi)
First legend entry: SiO2 / (CaO + Na2O + K2O)
Most entries: Lakatos et al (1972)
Viscosity (Pa*s)
1 E+12
1 E+11
1 E+10
1 E+9
1 E+8
1 E+7
1 E+6
1 E+5
1 E+4
1 E+3
1 E+2
1 E+1
1 E+0
800
1000
1200
1400
1600
1800
2000
Temperature (K)
3.3, SiO2 = 0.762, CO2 atm, Skryabin and Novokhatskii (1972)
3.3, SiO2 = 0.762, Ar atm, Skryabin and Novokhatskii (1972)
3.8, SiO2 = 0.731, Ar atm, Skryabin and Novokhatskii (1972)
3.8, SiO2 = 0.731, CO2 atm, Skryabin and Novokhatskii (1972)
2.4, SiO2 = 0.685
2.0, SiO2 = 0.621
2.4, SiO2 = 0.681
2.4, SiO2 = 0.684
2.2, SiO2 = 0.652

Fig. C.105.

Appendix D

The Bottinga–Weill model for the prediction of silica melt viscosities is of the form:

$$\log \eta = \sum_i x_i D_i - 1 \quad (69)$$

where η is viscosity (Pa s), x_i is the molar fraction of component i, and D_i are tabulated constants reported below as functions of molar fraction of SiO_2 and temperature (K).

Numbers in italics were linearly extrapolated or interpolated from a D_i versus reciprocal absolute temperature plot [68] (Tables D1–D5).

Table D1
D_i constants for $x_{SiO2} \in [0.75; 0.81]$

T	1473	1523	1573	1623	1673	1723	1773	1823	1873	1923	1973	2023	2073
SiO_2	5.92	5.56	5.19	4.87	4.56	4.26	4.00	3.72	3.49	3.26	3.03	2.83	2.62
TiO_2	–	–	–	–	–	–	–	–	–	–	–	–	–
FeO	–	*1.91*	*2.21*	2.48	2.68	2.97	*3.21*	*3.39*	–	–	–	–	–
MnO	–	–	−1.99	−2.05	−2.78	−1.91	–	–	–	–	–	–	–
MgO	*−0.26*	1.66	−0.52	−0.59	−0.97	−0.89	−1.14	*−1.17*	*−1.30*	*−1.39*	*−1.48*	*−1.56*	*−1.65*
CaO	*−1.09*	−1.38	−1.47	−0.81	−1.57	−1.51	−2.25	−1.95	–	–	–	–	–
SrO	–	–	–	–	–	–	–	–	–	*−2.69*	−2.55	−2.48	−2.28
BaO	–	–	–	–	–	*−2.43*	−2.33	−2.25	−2.24	−2.19	−2.07	−2.06	−1.95
Li_2O	–	*−7.17*	−6.94	−6.46	−6.30	−6.02	−5.80	−5.42	−5.28	−5.25	−4.91	−4.65	–
Na_2O	−8.21	−8.10	−7.66	−7.07	−6.69	−5.98	−5.70	*−5.34*	–	–	–	–	–
K_2O	−6.60	−6.39	−6.08	−5.87	−5.63	*−5,39*	–	–	–	–	–	–	–
$NaAlO_2$	*8.47*	*7.99*	*7.51*	*6.99*	*6.56*	6.18	5.75	5.42	5.02	4.66	4.38	4.03	3.78
$BaAl_2O_4$	–	–	–	–	–	–	–	–	–	–	–	–	–
$CaAl_2O_4$	*0.91*	0.34	0.13	−0.54	−0.76	−1.23	−1.78	−2.10	−2.29	−2.45	−2.51	−2.69	−2.74
$MgAl_2O_4$	*0.65*	*−0.09*	−0.69	−1.51	−2.09	−2.62	−2.88	−3.44	−3.52	−3.58	−3.59	−3.66	−3.67
$MnAl_2O_4$	–	–	−5.02	−5.12	−4.99	−4.49	–	–	–	–	–	–	–

Table D2
D_i constants for $x_{SiO2} \in [0.65; 0.75]$

T	1473	1523	1573	1623	1673	1723	1773	1823	1873	1923	1973	2023	2073
SiO_2	5.74	5.39	5.02	4.69	4.36	4.08	3.81	3.53	3.30	3.06	2.82	2.62	2.41
TiO_2	*−2.82*	−2.87	−2.21	−1.98	−1.91	−1.78	*−1.52*	–	–	–	–	–	–
FeO	*−1.69*	−1.85	−1.05	−0.81	−0.90	−0.95	*−0.52*	–	–	–	–	–	–
MnO	–	–	–	–	–	–	–	–	–	–	–	–	–
MgO	*−1.87*	−1.71	−1.19	−1.49	−1.68	−1.55	−1.35	−1.18	−1.17	−1.39	−1.21	−0.96	−0.55
CaO	−1.24	−3.01	−2.84	−2.74	−2.71	−2.63	−2.78	*−2.61*	−1.87	−2.57	−2.59	−2.53	−2.44
SrO	–	–	–	–	–	–	*−2.04*	−3.54	−1.99	−2.01	−2.04	−2.01	−2.00
BaO	–	–	–	–	–	*−3.65*	−3.43	−3.37	−3.36	−3.17	−3.07	−2.95	−2.83
Li_2O	−6.05	−5.83	−5.61	−5.35	−5.09	−4.89	−4.75	−4.76	−4.58	*−4.39*	–	–	–
Na_2O	−5.63	−5.30	−5.05	−4.94	−4.69	−4.49	−4.31	−4.80	−5.39	−4.47	−3.94	*−3.52*	−2.67
K_2O	−4.43	−4.43	−4.21	−4.06	−3.98	*−3.91*	–	–	–	–	–	–	–
$NaAlO_2$	1.45	1.36	1.05	2.14	2.13	2.14	2.12	2.64	2.84	2.75	2.67	1.82	2.73
$BaAl_2O_4$	–	–	–	–	–	–	–	–	–	*−0.61*	−0.74	−0.88	−0.99
$CaAl_2O_4$	*2.08*	*1.30*	0.63	−0.14	−0.53	−1.11	−1.47	−2.27	−2.26	−2.28	−2.33	−2.40	−2.44
$MgAl_2O_4$	*1.56*	0.81	−0.45	−1.04	−1.54	−2.48	−2.79	−2.92	−2.98	−2.99	−3.01	−3.06	−3.09
$MnAl_2O_4$	–	–	–	–	–	–	–	–	–	–	–	–	–

Table D3
D_i constants for $x_{SiO2} \in [0.55; 0.65]$

T	1473	1523	1573	1623	1673	1723	1773	1823	1873	1923	1973	2023	2073
SiO_2	5.35	5.00	4.66	4.33	4.02	3.73	3.46	3.19	2.95	2.72	2.48	2.29	2.07
TiO_2	–	*−1.82*	−1.88	−1.92	−1.85	−1.81	*−1.78*	–	–	–	–	–	–
FeO	−1.34	−2.34	−2.59	−2.69	−2.88	−2.83	−1.99	*−3.13*	–	–	–	–	–
MnO	–	–	–	–	−2.35	–	–	–	–	–	–	–	–
MgO	*−1.35*	−1.39	−1.59	−1.82	−1.85	−1.64	−1.71	−2.03	−1.75	−1.69	−1.61	−1.55	−1.40
CaO	−1.12	−1.86	−1.99	−2.29	−2.41	−2.40	−2.40	−2.46	−2.35	−2.33	−2.25	−2.24	−2.12
SrO	–	–	–	–	–	–	*−2.17*	−2.14	−2.13	−2.11	−2.03	−2.05	−1.95
BaO	–	–	–	–	–	*−2.17*	−2.08	−2.17	−2.17	−2.14	−2.03	−1.98	−1.83
Li_2O	−4.63	−4.45	−4.26	−4.07	−3.91	−3.66	−3.51	*−3.56*	–	–	–	–	–
Na_2O	−3.77	−3.68	−3.61	−3.48	−3.47	−3.41	−3.38	−3.74	−3.53	−2.36	−1.61	–	–
K_2O	–	–	–	–	–	–	–	–	–	–	–	–	–
$NaAlO_2$	2.45	2.31	2.68	2.57	3.25	3.04	2.84	2.82	2.58	2.34	2.14	1.64	*1.61*
$BaAl_2O_4$	–	–	–	–	–	–	–	–	–	–	–	–	–
$CaAl_2O_4$	0.80	1.08	0.32	0.31	−0.10	−0.61	−0.71	−1.26	−1.32	−1.37	−1.39	−1.52	−1.56
$MgAl_2O_4$	*−0.17*	−1.52	−0.79	−0.97	−0.74	−1.52	−1.65	−1.57	−1.95	−2.05	−2.08	−2.16	−2.12
$MnAl_2O_4$	–	–	–	–	–	–	–	–	–	–	–	–	–

Table D4
D_i constants for $x_{SiO2} \in [0.45; 0.55]$

T	1473	1523	1573	1623	1673	1723	1773	1823	1873	1923	1973	2023	2073
SiO_2	4.49	4.13	3.78	3.46	3.15	2.87	2.61	2.34	2.12	1.87	1.64	1.45	1.24
TiO_2	–	–	−0.50	−1.63	−1.76	−1.06	–	–	–	–	–	–	–
FeO	*−1.48*	−1.82	−2.09	−2.35	−2.08	−2.81	−2.34	*−2.87*	–	–	–	–	–
MnO	–	–	−1.78	−0.98	−1.98	–	–	–	–	–	–	–	–
MgO	*−1.22*	−1.18	−1.33	−1.27	−1.25	−1.17	−1.01	−0.76	−0.97	−1.06	−0.93	−0.95	−0.90
CaO	*−0.61*	−0.62	−0.77	−0.96	−1.12	−1.18	−1.25	−1.33	−1.35	−1.47	−1.38	−1.38	−1.30
SrO	–	–	–	–	–	–	*−1.17*	−1.13	−1.12	−1.09	−1.07	−1.08	−1.04
BaO	–	–	–	–	–	–	*−1.22*	−1.22	−1.23	−1.20	−1.15	−1.12	−1.04
Li_2O	−3.37	−3.30	−3.17	−3.04	−2.92	−2.80	−2.58	*−2.61*	–	–	–	–	–
Na_2O	−3.20	−3.13	−2.98	−2.97	−2.88	−2.75	−2.65	−1.68	−1.52	–	–	–	–
K_2O	–	–	–	–	–	–	–	–	–	–	–	–	–
$NaAlO_2$	4.84	4.60	4.33	4.16	3.97	3.54	3.29	2.91	2.67	2.36	2.16	1.94	1.77
$BaAl_2O_4$	–	–	–	–	–	–	–	–	–	–	–	–	–
$CaAl_2O_4$	*3.08*	2.64	2.11	1.52	1.19	0.76	0.32	−0.11	−0.22	−0.46	−0.50	−0.56	−0.56
$MgAl_2O_4$	–	*1.52*	1.12	1.19	1.50	2.75	1.05	−0.52	−0.28	−0.03	−0.07	0.20	0.40
$MnAl_2O_4$	–	–	–	–	–	–	–	–	–	–	–	–	–

Table D5
D_i constants for $x_{SiO2} \in [0.35; 0.45]$

T	1473	1523	1573	1623	1673	1723	1773	1823	1873	1923	1973	2023	2073
SiO_2	2.32	2.18	2.05	1.92	1.81	1.69	1.59	1.48	1.39	1.3	1.22	1.14	1.05
TiO_2	*−0.96*	−0.48	−0.35	−0.57	0.38	0.86	*0.83*	–	–	–	–	–	–
FeO	−0.79	−1.09	−1.22	−1.25	−1.39	−1.30	−1.75	*−1.74*	–	–	–	–	–
MnO	*−1.56*	−1.35	−1.31	−1.38	−1.08	−0.93	*−0.96*	–	–	–	–	–	–
MgO	*0.87*	0.66	1.05	0.23	−0.15	−0.33	−0.53	0.64	0.49	0.46	−0.32	−0.45	−0.49
CaO	0.32	0.32	0.31	0.17	−0.07	0.31	−0.51	−1.51	−1.44	−1.02	−1.12	−1.22	−1.27
SrO	–	–	–	–	–	–	–	–	–	–	–	–	–
BaO	–	–	–	–	–	–	–	–	–	–	–	–	–
Li_2O	*−1.87*	−1.85	−1.90	−1.94	−1.98	−2.02	*−2.04*	–	–	–	–	–	–
Na_2O	−1.93	−2.04	−2.09	−2.14	−2.17	−2.18	−2.22	*−2.26*	–	–	–	–	–
K_2O	–	–	–	–	–	–	–	–	–	–	–	–	–
$NaAlO_2$	–	–	–	–	–	–	–	–	–	–	–	–	–
$BaAl_2O_4$	–	–	–	–	–	–	–	–	–	–	–	–	–
$CaAl_2O_4$	*3.73*	*3.34*	2.91	2.36	2.34	1.87	1.74	2.54	*2.82*	3.07	2.91	2.76	2.42
$MgAl_2O_4$	–	–	–	–	–	–	–	1.51	0.55	−0.99	−0.10	0.11	0.06
$MnAl_2O_4$	–	–	–	–	–	–	–	–	–	–	–	–	–

References

[1] Reid RC, Prausnitz JM, Poling BE. Viscosity. In: Sun B, Fleck GH, editors. The properties of gases and liquids, 4th ed. Singapore: McGraw-Hill, 1988. p. 388–490.

[2] Kestin J, Wakeham WA. The measurement of viscosity. In: Ho CY, editor. Transport properties of fluids, thermal conductivity, viscosity, and diffusion coefficient, New York: Hemisphere, 1988. p. 73–147 [chap. 4].

[3] Viscosity. In: Perry RH, Green DW, Maloney JO, editors. Perry's chemical engineers handbook, 6th ed. Singapore: McGraw-Hill, 1984. p. 3-278–82 [chaps. 3 and 5].

[4] Danek V, Licko T, Panek Z. Silikáty 1985;29:291–9.

[5] De Jong BHWS. Glass. In: Arpe H-J, Biekert E, Davis HT, editors. Ullmann's encyclopedia of industrial chemistry, Würzburg, 1990. p. 365–432.

[6] Clark Jr. SP. Viscosity. In: Clark Jr. SP, editor. Handbook of physical constants, The Geological Society of America, 1966. p. 291–300 [chap. 12].

[7] Bird RB, Stewart WE, Lightfoot EN. Transport phenomena. Singapore: Wiley, 1960.

[8] White FM. Properties of a fluid. In: Beamesderfer L, Morriss JM, editors. Viscous fluid flow, 2nd ed. Singapore: McGraw-Hill, 1991. p. 15–27.

[9] In: Scholze H, Kreidl NJ, Uhlmann CR, Kreidl NJ, editors. Viscosity and relaxation, vol. 3. New York: Academic Press, 1986.

[10] Viscosity. In: Dean JA, editor. Lange's handbook of chemistry, 12th ed. New York: McGraw-Hill, 1979. p. 10–96 [chap. 10].

[11] Rheological measurements. In: Kroschwitz J, Howe-Grant M, editors. Encyclopedia of chemical technology: recycling, oil to silicon, 4th ed. New York: Wiley, 1997. p. 347–404.

[12] Shaw HR. J Petrol 1969;10(3):510–35.

[13] Bacon LR. J Franklin I 1936;221(1322-18):251–73.

[14] Mills KC. Viscosities of molten slags, National Physical Laboratory, 1992.

[15] English S. J Soc Glass Technol 1924;8:205–51.

[16] Stanmore BR, Budd S. Fuel 1996;75(12):1476–9.

[17] Shiraishi Y, Meister R. J Phys, C9 1982;12(43):447–50.

[18] Washburn E, Shelton GR. Illinois Uni Eng Exp Station Bull 1924;140:1–50.

[19] Urbain G, Boiret M. Ironmaking Steelmaking 1990;17(4): 255–60.

[20] Urbain G, Bottinga Y, Richet P. Geochim Cosmochim Acta 1982;46:1061–72.

[21] Schobert HH, Diehl EK, Streeter RC. DOE/METC 1982;82(24):415–31.

[22] Srinivasachar S, Senior CL, Helble JJ, Moore JW. A fundamental approach to the prediction of coal ash deposit formation in combustion systems. PSI Technology Co. Report, No. 24–135, 1992.

[23] Machin JS, Yee TB, Hanna DL. J Am Ceram Soc 1952;35(12):322–5.

[24] Urbain G. J Mater Edu 1985;7(6):1007–78.

[25] Kato M, Minowa S. Trans Iron Steel Inst Jpn ISIJ 1969;9:31–38.

[26] Hofmaier G. Berg-Hüttenmännische Monatshefte 1968; 113(7):270–81.

[27] Streeter RC, Diehl EK, Schobert HH. ACS Symposium Series. 1928 August 1983, 1984. p. 195–209.

[28] Hurley JP, Kay JP. Personal communication, 1998.

[29] Vorres KS, Greenberg S, Poeppel R. Mineral Matter and Ash in Coal, ACS Symposium Series 301. Washington, DC: ACS, 1986 (p. 157–69).

[30] Seki K, Oeter F. ISIJ 1984;24(1–6):445–54.

[31] Morey GW. The viscosity of glass, The properties of glass. 2nd ed. New York: Reinhold, 1960. p. 132–65 [chap. 5].

[32] Hochella Jr. MF, Brown Jr. GE. Geochim Cosmochim Acta 1984;48:2631–40.

[33] Lillie HR. J Am Ceram Soc 1939;22(11):367–74.

[34] Brown Jr. GE, Farges F, Calas G. X-ray scattering and X-ray spectroscopy studies of silicate melts. In: Stebbins JF, McMillan PF, Dingwell DB, editors. Structure, dynamics and properties of silicate melts, Washington, DC: Mineralogical Society of America, 1995. p. 317–410 [chap. 9].

[35] Stein DJ, Spera FJ. Am Mineral 1993;78:710–23.

[36] Bockris JO, Mackenzie JD, Kitchener JA. Trans Faraday Soc 1955;51:1734–48.

[37] Shartsis L, Spinner S, Capps W. J Am Ceram Soc 1952;35(6):155–60.

[38] Nowok JW, Hurley JP, Steadman EN. The impact of ash deposition on coal fired plants 1993, June 21–25, 1994. p. 527–38.

[39] Quon DHH, Wang SSB, Chen TT. J Engng Gas Turb Power 1985;107:803–6.

[40] Bryers RW. Proceedings of a workshop on low-rank coal technology development — 1981, 1982. p. 2-50–2-99.

[41] Nowok JW. Energ Fuel 1995;9:534–9.

[42] Colf JV, Howat DD. J S Afr I Min Metall 1979;79(9): 255–63.

[43] Urbain G. Steel Res 1987;3:111–6.

[44] Kalmanovitch DP, Frank M. Mineral matter and ash deposition from coal, 1988. p. 89–101.

[45] Senior CL, Srinivasachar S. Energ Fuel 1995;9:277–83.

[46] Nowok JW, Benson SA. Inorganic transformations and ash deposition during combustion 1991 March 10–15, 1991. p. 405–24.

[47] Mysen BO. Structure and properties of silicate melts. Amsterdam: Elsevier, 1988.

[48] Nowok JW. J Mater Res 1995;10(2):401–4.

[49] Parker SP, editor. McGraw-Hill encyclopedia of chemistry. New York: McGraw-Hill, 1983.

[50] Castellan GW. Ionization potentials, Physical chemistry. Reading, MA: Addison-Wesley, 1971. p. 548–49 [chap 22-13].

[51] Hess PC. Polymerization model for silicate melt. In: Hargraves RB, editor. Physics of magmatic processes, Princeton: Princeton University Press, 1980. p. 3–48 [chap. 1].

[52] Fyfe WS. Am Mineral 1951;36:538–42.

[53] Nickel EH. Am Mineral 1954;39:486–93.

[54] Badin EJ, Anderson LL, editors. Coal combustion chemistry — correlation aspects. Amsterdam: Elsevier, 1984.

[55] Hess PC. The role of high field strength cations in silicate melts. In: Perchuk LL, Kushiro I, editors. Physical chemistry of magmas, New York: Springer, 1991. p. 152–91.

[56] Dingwell DB. Am Mineral 1989;74:1038–44.

[57] Machin JS, Hanna DL. J Am Ceram Soc 1945;28(11):310–6.

[58] Stebbins JF, Sen S, Farnan I. Am Mineral 1995;80:861–4.

[59] El-Badry K, Ghoneim NA, El-Batal HA, Ammar MM, Gharib S. Sprechsaal 1981;8:599–603.

[60] Jones EE, Lindsey JS. Miner Metall Process 1987:60–64.
[61] Corrales LE, Keefer KD. J Chem Phys 1997;106(15): 6460–9.
[62] Turkdogan ET, Bills PM. Ceram Bull 1960;39(11):682–7.
[63] Nemilov SV. J Appl Chem USSR + 1969;42(1–3):46–51.
[64] Sochor BB. Giessereitech 1965;11(1):14–19.
[65] Klein LC, Fasano BV, Wu JM. 12th Lunar and Planetary Science Conference, 1981. p. 1759–67.
[66] Klein LC, Fasano BV, Wu JM. J Geophys Res 1983;88:A880–6.
[67] Leko BK. Izv An SSSR Neorg Mat + 1967;3(10):1888–91.
[68] Bottinga Y, Weill DF. Am J Sci 1972;272:438–75.
[69] Verein Deutscher Eisenhüttenleute, editor. Slag atlas, Stahleisen M.B.H., Düsseldorf, 1981.
[70] Bodnar L, Cempa S, Tomasek K, Bobok L. Chem Zvesti 1978;6:798–809.
[71] Riebling EF. Can J Chem 1964;42:2811–21.
[72] Yakushev AM, Romashin VM, Amfiteatrov VA. Izv VUZ Cher Metall 1977;11:55–58.
[73] Lakatos T, Johansson L, Simmingsköld B. Glass Tech 1972;13(3):88–95.
[74] Aslanova MS, Chernov VA, Kulakov LF. Steklo Keram 1974;6:19–21.
[75] Goto A, Oshima H, Nishida Y. J Volcanol Geotherm Res 1997;76:319–27.
[76] Nowok JW, Hurley JP, Stanley DC. Energ Fuel 1993;7:1135–40.
[77] Sato RK, McMillan PF, Dennison P, Dupree R. Phys Chem Glasses 1991;32(4):149–56.
[78] Taylor TD, Rindone GE. J Am Ceram Soc 1970;53(12): 692–5.
[79] Potanin VN, Shavrin SV, Panfilov MI. Russ Metall 1976; 1–3:75–78.
[80] Dirken PJ, Kohn SC, Smith ME, Eck ERHv. Chem Phys Lett 1997;266:568–74.
[81] Piwinskii AJ, Weed HC. Thermochim Acta 1980;37:189–95.
[82] Nowok JW. Energ Fuel 1994;8:1324–36.
[83] Mysen BO, Virgo D, Scarfe CM, Cronin DJ. Am Mineral 1985;70:487–98.
[84] Dingwell DB, Virgo D. Geochim Cosmochim Acta 1987;51:195–205.
[85] Liska M, Klyuev VP, Antalik J, Stubna I. Phys Chem Glasses 1997;38(1):6–10.
[86] Liska M, Simurka P, Antalik J, Perichta P. Chem Geol 1996;128:199–206.
[87] Dingwell DB. Am Mineral 1992;77:270–4.
[88] Skryabin VG, Novokhatskii IA. Izv An SSSR Neorg Mat+ 1972;8(7):1334–5.
[89] Lange RA. The effect of H_2O, CO_2 and F on the density and viscosity of silicate melts, Volatiles in magmas. Washington, DC: The Mineralogical Society of America, 1994. p. 331–69 [chap. 9].
[90] Kovalenko AM, Novokhatskiy IA, Petrov AK, Ershov GS. Russ Metall 1969;6:17–22.
[91] Hurley JP, Watne TM, Nowok JW. Am Chem Soc, Div Fuel Chem, Prep paper 1996;41(2):691–4.
[92] Schobert HH, Streeter RC, Diehl EK. Fuel 1985;64:1611–7.
[93] Lejeune A-M, Richet P. J Geophys Res 1995;100(B3): 4215–29.
[94] Pinkerton H, Stevenson RJ. J Volcanol Geotherm Res 1992;53:47–66.
[95] Marsh BD. Contrib Mineral Petrol 1981;78:85–98.
[96] Watt JD. J I Fuel 1969;42:131–4.
[97] Ota R, Wakasugi T, Kawamura W, Tuchiya B, Fukunaga T. J Non-Cryst Solids 1995;188:136–46.
[98] Johnson EK. J Engng Gas Turb Power 1984;106:777–81.
[99] Watt JD, Fereday F. J I Fuel 1969;42:99–103.
[100] English S. J Soc Glass Technol 1925;9:83–98.
[101] Cashman KV. Rev Mineral 1990;24:259–314.
[102] Corey RC. Measurement and significance of the flow properties of coal-ash slag. Washington US Department of the Interior, Bureau of Mines, Report No. 618, 1964.
[103] Appendix B: Determination of coal-ash properties. In: Singer JG, editor. Combustion — fossil power, 4th ed. USA: Rand McNally, 1991. p. B-1–B-18.
[104] Sage WL, McIlroy JB. Combustion 1959;31:41–48.
[105] Hoy HR, Roberts AG, Wilkins DM. IGE J 1965;June: 444–69.
[106] Slag viscosity and properties of fly ash, British Coal Utilization Research Association, 1963.
[107] Bottinga Y, Richet P, Sipp A. Am Mineral 1995;80:305–18.
[108] Arrhenius S. Z Phys Chem 1887;1:285–98.
[109] Wang J, Porter RS. Rheol Acta 1995;34:496–503.
[110] Richet P, Robie RA, Hemingway BS. Geochim Cosmochim Acta 1986;50:1521–33.
[111] Du Sichen, Bygdén J, Seetharaman S. Metall Mater Trans B 1994;25B:519–25.
[112] Doolittle AK. J Appl Phys 1951;22(12):1471–5.
[113] Doolittle AK, Doolittle DB. J Appl Phys 1957;28(8):901–5.
[114] Urbain G. Rev Int Hautes Temp 1974;11(2):133–45.
[115] Tanigushi H. Miner Petrol 1993;49:13–25.
[116] Cranmer D, Uhlmann DR. J Geophys Res 1981;86(B9): 7951–6.
[117] Rosen SL. Fundamental principles of polymeric materials. 2nd ed. New York: Wiley, 1993.
[118] Tanigushi H. Contrib Mineral Petrol 1992;109:295–303.
[119] Richet P. Geochim Cosmochim Acta 1984;48:471–83.
[120] Riboud PV, Roux Y, Lucas L-D, Gaye H. Fachber Hüttenprax Metalweiterverarb 1981;19(10):859–69.
[121] Irving JB. Viscosities of binary liquid mixtures: the effectiveness of mixture equations, Glasgow National Engineering Laboratory, Report No. 631, National Engineering Laboratory Reports, 1977.
[122] Seetharaman S, Du Sichen. EDP Congress, 1994. p. 1171–89.
[123] Seetharaman S, Du Sichen. ISIJ Int 1997;37(2):109–18.
[124] Scarfe CM, Cronin DJ. Am Mineral 1986;71:767–71.
[125] Reid WT, Cohen P. Trans ASME 1944;66:83–97.
[126] Greenberg S. Viscosity of synthetic and natural coal slags, Materials Science and Technology Division Argonne National Laboratory, University of Chicago, 1984.
[127] Huang LY, Norman JS, Pourkashanian M, Williams A. Fuel 1996;75(3):271–9.
[128] Hough DC, Sanyal A, Annen KD, Gruninger JH, Stewart GW. J I Energy 1986;77:77–81.
[129] Quon DHH, Wang SSB, Chen TT. Fuel 1984;63:939–42.
[130] Shaw HR. J Am Sci 1972;272:870–93.
[131] Cukierman M, Uhlmann DR. J Geophys Res 1973;78(23): 4920–3.
[132] Urbain G, Cambier F, Deletter M, Anseau MR. Trans J Br Ceram Soc 1981;80:139–41.
[133] Mills KC. Mineral matter and ash in coal, ACS Symposium Series 301. Washington, DC: ACS, 1984. p. 195–214.

[134] Mills KC, Broadbent CP. Evaluation of slags program for the prediction of physical properties of coal gasification slags. Impact ash deposition coal fired plants, 1993. p. 513–25.
[135] Vargas S, Frandsen F, Dam-Johansen K. ELSAM — Idemitsu Kosan cooperative research project: performance of viscosity models for high-temperature coal ashes, CHEC report No. 9719, Lyngby, 1997.
[136] Deletter M, Cambier F, N'Dala I, Urbain G. Br Ceram Trans J 1984;83:108–12.
[137] Harb JN, Zygarlicke CJ, Richards GH. J I Energy 1993;66:91–98.
[138] Williams P, Sunderland M, Briggs G. Trans Instn Mining Metall Section C 1983;92:105–9.
[139] Malkin AY. Rheol Acta 1995;34:27–39.
[140] Casson N. A flow equation for pigment–oil suspensions of the printing ink type. In: Mill CC, editor. Rheology of disperse systems, Bath: Pergamon Press, 1959. p. 84–104 [chap. 5].
[141] Williamson RV, Patterson GD, Hunt JK. Ind Engng Chem 1929;21(11):1111–5.
[142] Weed HC, Ryerson FJ, Piwinskii AJ. Mineral matter and ash in coal, ACS symposium series 301 — 1984 1986. p. 223–33.
[143] Buscall R. Theoretical and applied rheology. Proceedings of the XIth International Congress on Rheology, Brussels, Belgium, 1992. p. 591–4.
[144] Allen MP, Camp PJ, Mason CP, Evans GT, Masters AJ. J Chem Phys 1996;105(24):11 175–82.
[145] Reddy RG, Yen JY. Extractive metallurgy of copper, nickel and cobalt, 1993. p. 309–23.
[146] Biddle D, Walldal C, Wall S. Colloid Surface A 1996;118:89–95.
[147] Goldsmith HL, Mason SG. The microrheology of dispersions. In: Eirich FR, editor. Rheology, theory and applications, New York: Academic Press, 1967. p. 85–250.
[148] Quemada D. Europhys Lett 1994;25(2):149–55.
[149] Sengun MZ, Probstein RF. Rheol Acta 1989;28:382–93.
[150] Einstein A. Ann Phys (Leipzig) 1906;19:289–306.
[151] Einstein A. Ann Phys (Leipzig) 1911;34:591–2.
[152] Shaw HR. J Am Sci 1965;263:120–52.
[153] Vand V. J Phys Coll Chem 1948;52:277–99.
[154] Roscoe R. Br J Appl Phys 1952;3:267–9.
[155] Sherman P. Rheology of emulsions. In: Sherman P, editor. Emulsion science, London: Academic Press, 1968. p. 217–351 [chap. 4].
[156] Murase T, McBirney AR. Geol Soc Am Bull 1973;84:3563–92.
[157] Quemada D. Lecture Notes in Physics, vol. 164, 1982. p. 210–47.
[158] Ponton A, Quemada D, Lafuma F, Neel O. Colloid Surface A 1996;119:255–9.
[159] Webb S, Knoche R. Chem Geol 1996;128:165–83.
[160] Stott VH. J Soc Glass Technol 1925;9:207–25.
[161] Asbeck WK. Official Digest 1961;33(432):65–83.
[162] Bird RB, Armstrong RC, Hassager O. The generalized Newtonian fluid, Dynamics of polymeric liquids — fluid mechanics. 2nd ed. New York: Wiley, 1987. p. 169–253.
[163] Hurst HJ, Novak F, Patterson JH. Energ Fuel 1996;10: 1215–9.
[164] Stein DJ, Spera FJ. Geophys Res Lett 1993;20(18):1923–6.
[165] Dingwell DB, Virgo D. Geochim Cosmochim Acta 1988;52:395–403.
[166] Scarfe CM, Cronin DJ, Wenzel JT, Kauffman DA. Am Mineral 1983;68:1083–8.
[167] Krauss S. Freiberger Forschungshefte B Metall 1979;212:73–82.
[168] Segers L, Fontana A, Winand R. Electrochim Acta 1979;24: 213–8.
[169] Shiraishi Y, Ikeda K, Tamura A, Saitó T. Trans Jpn Inst Metals 1978;19(5):264–74.
[170] Shvaiko-Shvaikovskaya TP, Mazurin OV, Bashun ZS. Izv An SSSR Neorg Mat + 1971;7(1):143–7.
[171] Boow J. Fuel 1969;48(2):171–8.
[172] Meiling GS, Uhlmann DR. Phys Chem Glasses 1967;8(2):62–68.
[173] Machin JS, Yee TB. J Am Ceram Soc 1954;37(4):177–86.
[174] Machin JS, Yee TB. J Am Ceram Soc 1948;31(7):200–4.

Appendix B
Flow Down a Wall

Introduction

The objective of this report is to give a mathematical description of the flow down a wall of a thick film of varying composition and temperature.

A general model will be deduced. Unfortunately this model can not be solved due to uncertainties about the variation of viscosity and density of the fluid with position.

With a series of assumptions, that divide the fluid into layers of constant viscosity and density, a solution can be found to the general model.

The characteristics of the solution will be examined using experimental data for three coal ash slags.

Generalised mathematical model

Fig 1 shows the flow of a fluid down a vertical wall of infinite height and width. The composition and temperature of the fluid can vary with position.

The layer is constantly bombarded with particles that enter the fluid. The thickness of the fluid changes vertically but is constant horisontally.

In the following a generalised mathematical model will be derived for the system shown in Fig 1.

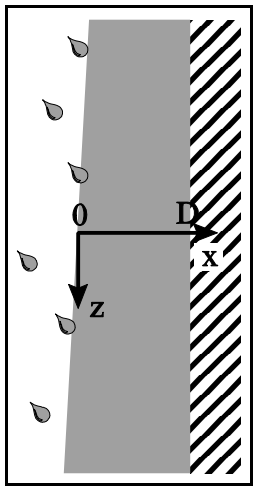

Figure 1 Fluid flow.

Assumptions
The fluid flows straight downwards, there is no turbulence causing macro-mixing across the layer, thus mixing of components is possible due solely to diffusion with no net velocity.

- The velocity of any individual species equals that of the bulk flow ($v_i = v_{bulk} = v$);
- Linear flow: $v = v_z$.

Particles that come from the surroundings and enter the liquid layer do this without affecting

the layer in any other way than by making it thicker and changing the composition.

The fluid sticks to the surface of the wall.

- No slip ($v_{wall} = 0$)

Model deduction

The mathematical model is based on a z-momentum balance over a system of thickness Δx, length Δz, and extending a distance W in the y-direction, as symbolised in Fig 2.

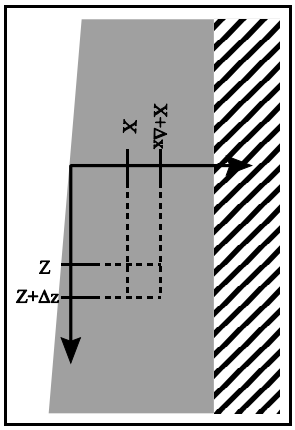

Figure 2 Control volume.

The most obvious orientation of the coordinate system would be to place the origin at the wall with z pointing downwards and x pointing outwards. However the opposite x-orientation has been chosen due to technicalities regarding the solution of the model.

The terms in the steady state momentum balance are:

Rate of z-momentum in across surface at x: $(W\ \Delta z)\ (\tau_{xz})\big|_x$

Rate of z-momentum out across surface at x+Δx: $(W\ \Delta z)(\tau_{xz})\big|_{x+\Delta x}$

Rate of z-momentum in across surface at z=0: $(W\ \Delta x\ v)(\rho\ v_z)\big|_z$

Rate of z-momentum out across surface at z=L: $(W\ \Delta x\ v)\ (\rho\ v_z)\big|_{z+\Delta z}$

Gravity force acting on fluid: $(W\ \Delta x\ \Delta z)\ (\rho\ g)$

These terms are combined in a momentum balance:

In - Out + Sum of forces = Accumulated

$$\Delta z(\tau_{xz} - \tau_{x+\Delta x,z}) + \Delta x(\rho_z v_z^2 - \rho_{z+\Delta z} v_{z+\Delta z}^2) + \Delta x \Delta z \rho g = 0 \qquad (1)$$

This becomes:

$$\frac{\partial \tau_{xz}}{\partial x} + \frac{\partial(\rho v^2)}{\partial z} = \rho g \quad , \quad \begin{matrix} x \in [0;D] \\ z \in [0;L] \end{matrix} \qquad (2)$$

Complete Model

$$\frac{\partial \tau_{xz}}{\partial x} + \frac{\partial (\rho v^2)}{\partial z} = \rho g$$

$$D = D(z) \qquad , \quad \begin{matrix} x \in [0;D] \\ z \in [0;L] \end{matrix} \qquad (3)$$

$$B.C.\ 1: \quad x = 0: \qquad \tau(0,z) = 0$$

$$B.C.\ 2: \quad x = D: \qquad v(D,z) = 0 \quad (No\ slip)$$

Discussion

It is not possible to solve the general model in Eq 4. In the following a series of assumptions will be made, that will facilitate the further calculations.

Simplified Mathematical Model

The general model in Eq 4 contains some very

Assumptions

- The layer can be divided into a series of sub-layers of homogeneous composition and temperature, see Fig 3.
- The sub-layers are Newtonian fluids.

$$Newton's\ law: \qquad \tau_{xz} = \eta \frac{dv_z}{dx} \qquad (4)$$

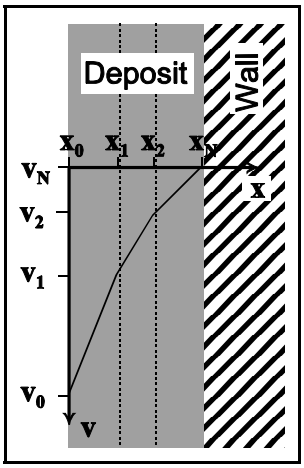

Figure 3 Linear flow.

- Viscosity, η, and density, ρ, are constant for each sub-layer.
- Uniaxial distribution. Conditions are invariant parallel to the wall.

Deduction

The second equation in the generalised model vanishes, since the thickness of the layer is now independent of the vertical position.

Due to the assumption of a uniaxial distribution, the z-derivatives disappear from the first equation in the generalised model, and we get:

$$\frac{d\tau_{xz}}{dx} = \rho g \tag{5}$$

Integration gives:

$$\tau_{xz} = \rho g x + c \tag{6}$$

Due to the separation of the liquid into separate layers, we get:

$$\begin{aligned} &\tau_{xz} = \rho_i g x + c_i \\ &\rho = f(x), \quad c = g(x) \\ &B.C.\ 1: \quad \tau_{xz}(0) = 0 \qquad , \qquad x \in [0;D] \\ &B.C.\ 2: \quad \tau_{xz} \text{ continuous} \qquad\quad z \in [0;L] \\ &B.C.\ 3: \quad v_z(D) = 0 \end{aligned} \tag{7}$$

Layer I

We use B.C. 1 and Newton´s law to get:

$$\tau_{xz} = \rho_1 g x = -\eta_1 \frac{dv_z}{dx} \qquad , \qquad x \in [0;x_1[\tag{8}$$

Rearrangement gives:

$$\frac{dv_z}{dx} = -\frac{\rho_i g}{\eta_i} x \tag{9}$$

By integrating, we get:

$$v_z = -\frac{\rho_1 g}{2\eta_1} x^2 + k_1 \tag{10}$$

The velocity at x_1 is v_1, and in general terms, we get: $v_z(x_i) = v_i$. This gives

$$\begin{aligned} v_1 &= -\frac{\rho_1 g}{2\eta_1} x_1^2 + k_1 \\ \Updownarrow & \\ k_1 &= v_1 + \frac{\rho_1 g}{2\eta_1} x_1^2 \end{aligned} \tag{11}$$

By insertion, we get:

$$v_z = \frac{\rho_1 g}{2\eta_1}(x_1^2 - x^2) + v_1 \quad , \quad x \in [0;x_1[\qquad (12)$$

Layer II

Invocation of B.C. 2 gives:

$$\begin{aligned} \tau_{xz}(x_1) &= \tau_{xz}(x_1+) = \tau_{xz}(x_1-) \\ \updownarrow \quad &= \rho_2 g x_1 + c_2 = \rho_1 g x_1 \\ c_2 &= -(\rho_2 - \rho_1) g x_1 \end{aligned} \qquad (13)$$

Hence:

$$\tau_{xz} = \rho_2 g(x - x_1) - \rho_1 g x_1 = -\eta_2 \frac{dv_z}{dx} \quad , \quad x \in [x_1;x_2[\qquad (14)$$

$$v_z = -\frac{\rho_2}{\eta_2} g x (\frac{x}{2} - x_1) - \frac{\rho_1}{\eta_2} g x x_1 + k_2 \qquad (15)$$

The velocity can be expressed as:In the point x_2, we get:

$$\begin{aligned} v_2 &= -\frac{\rho_2}{\eta_2} g x_2 (\frac{x_2}{2} - x_1) - \frac{\rho_1}{\eta_2} g x_2 x_1 + k_2 \\ \Updownarrow \quad & \\ k_2 &= v_2 + \frac{g}{\eta_2} x_2 \left(\rho_2 (\frac{x_2}{2} - x_1) + \rho_1 x_1 \right) \end{aligned} \qquad (16)$$

Insertion into the general expression for v_z gives:

$$\frac{\eta_2}{g}(v_z - v_2) = \rho_2 (\frac{x_2^2}{2} - x_1 x_2 - \frac{x^2}{2} + x_1 x) + \rho_1 (x_1 x_2 - x_1 x) \qquad (17)$$

Rearrangement gives:

$$\frac{\eta_2}{g}(v_z - v_2) = \rho_2 \left(\frac{x_2^2 - x^2}{2} - x_1 (x_2 - x) \right) + \rho_1 x_1 (x_2 - x) \quad , \quad x \in [x_1;x_2[\qquad (18)$$

Layer III

Again we define the equation constant making use of B.C. 2:

$$\begin{aligned} \tau_{xz}(x_1) &= \tau_{xz}(x_1+) = \tau_{xz}(x_1-) \\ \Updownarrow \quad &= \rho_3 g x_2 + c_3 = \rho_2 g(x_2 - x_1) + \rho_1 g x_1 \\ c_2 &= -\rho_3 g x_2 + \rho_2 g(x_2 - x_1) + \rho_1 g x_1 \end{aligned} \tag{19}$$

The expression for τ_{xz} becomes:

$$\frac{\tau_{xz}}{g} = \rho_3(x - x_2) + \rho_2(x_2 - x_1) + \rho_1 x_1 = -\frac{\eta_3}{g}\frac{dv_z}{dx} \quad , \quad x \in [x_2; x_3[\tag{20}$$

This gives us the following expression for the velocity:

$$\frac{\eta_3}{g} v_z = -\left(\rho_3(\frac{x}{2} - x_2) + \rho_2(x_2 - x_1) + \rho_1 x_1 \right) x + k_3 \tag{21}$$

Assuming $v_z(x_3) = v_3$, we are able to define the constant, k_3:

$$k_3 = \left(\rho_3(\frac{x_3}{2} - x_2) + \rho_2(x_2 - x_1) + \rho_1 x_1 \right) x_3 + \frac{\eta_3}{g} v_3 \tag{22}$$

The final equation becomes:

$$\frac{\eta_3}{g}(v_z - v_3) = \frac{\rho_3}{2}(x_3^2 - x^2) - (x_3 - x)\sum_{i=1}^{2} x_i(\rho_{i+1} - \rho_i) \quad , \quad x \in [x_2; x_3[\tag{23}$$

Model

The velocity equations deduced above show a trend. In combination with B.C. 3 it is now possible to write the following general expression for a film composed of N layers:

$$\frac{\eta_n}{g}(v_z - v_n) = \frac{\rho_n}{2}(x_n^2 - x^2) - (x_n - x)\sum_{i=1}^{n-1} x_i(\rho_{i+1} - \rho_i) \tag{24}$$

Where: $x \in [x_{n-1};\ x_n[$ *and* $v_N = 0$

Discussion

The model consists of three terms that relate velocity on the left-hand side of the equation to position (square and linear) on the right-hand side.

If density is kept constant throughout the film, the second term on the right-hand side of the equations vanishes and the velocity depends only on the position squared.

The velocity of a specific layer depends on the viscosity and the density of the layer. If the viscosity is lowered or the density is raised, then the velocity of the layer is lowered. The effect on the other layers is investigated below.

Computation

A computer program has been written in Fortran to simulate the flow of a film down a wall. A printout of the program is annexed at the end of the report.

The program prompts the user for the number of layers and the width, density, and viscosity of each layer.

The output is shown graphically on the screen, and positions and velocities are written to a file 'Flow.out', situated in the same directory as the program.

Experimental Data

Nowok et al.[1] have measured the temperature dependence of the viscosities and the densities of three different coal ash slags produced from laboratory ashed coals. The viscosities were reported graphically, which enabled the copying of the viscosities at the temperatures where densities had been reported. The results are given in Table 1.

Tempera-ture (K)	Beulah slag		Pittsburgh # 8 slag		Illinois # 6 slag	
	Density (g/cm^3)	Viscosity (Pa·s)	Density (g/cm^3)	Viscosity (Pa·s)	Density (g/cm^3)	Viscosity (Pa·s)
1573	3.08	12	2.80	-	2.51	-
1598	3.13	9	-	-	2.48	-
1648	3.07	5	2.84	57	2.41	132
1698	3.12	3	2.78	16	2.55	60
1748	3.07	-	2.78	-	2.50	41

Table 1 Corresponding densities and viscosities for three different coal ash slags[1].

[1] Nowok, J. W., Bieber, J. A., Benson, S. A., Jones, M. L., Fuel, 1991, Vol. 70.

The experimentally measured density and viscosity data have been used to test the computer program. The results are presented graphically in Figs 4 - 6.

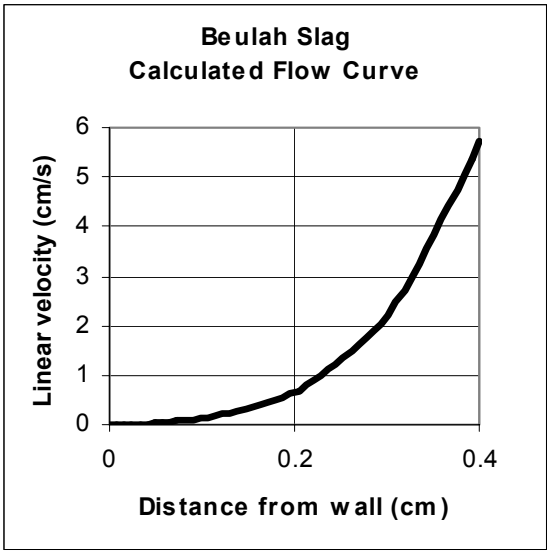

Figure 4 Calculated example with Beulah slag.

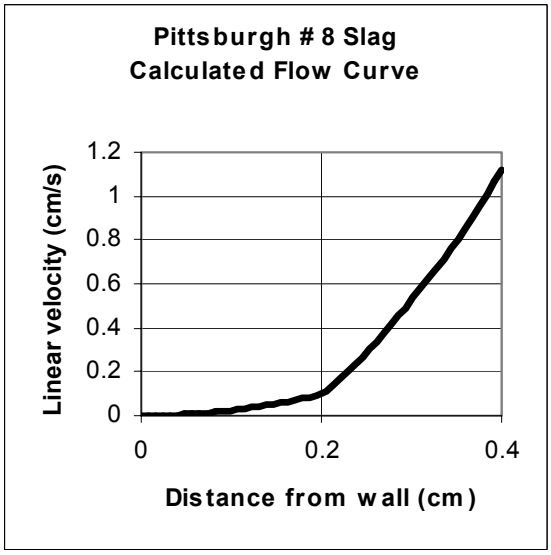

Figure 5 Calculated example with Pittsburgh # 8 slag.

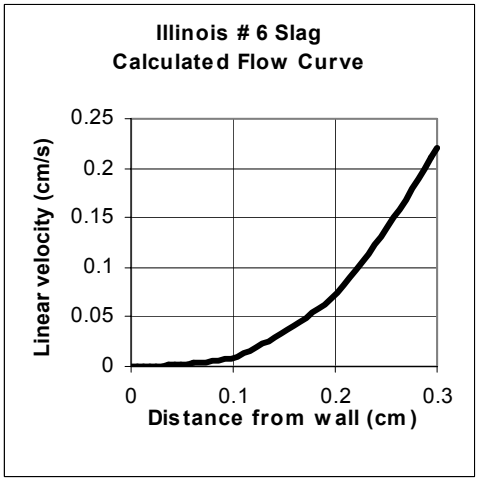

Figure 6 Calculated example with Illinois # 6 slag.

The construction of Figs 4 - 6 will be explained using Fig 4 as an example.

Table 1 contains pairs of density and viscosity at four different temperatures for the Beulah slag. Hence the slag was reported to consist of four layers in the computer program.

The thickness of each layer was arbitrarily set to 1 cm, and the density and viscosity data was entered, starting with the lowest temperature - corresponding to a positive temperature gradient from the wall outwards.

It can be seen from Figs 4 - 6, that the rate of the slag flow down a wall depends strongly on the viscosity of the slag. While the densities of the slags do not differ significantly, the Illinois # 6 slag is more than 20 times more viscous than the Beulah slag at the same temperatures. Correspondingly, the flow in Fig 4 is more than 20 times faster than the flow in Fig 6.

Viscosity

The model shows that the viscosity and the velocity of the fluid are inversely related, thus if

all viscosities are increased a factor 10, then the velocity at any point will be lowered by a factor 10.

If the viscosity of just one layer is raised, the velocity of that layer and all subsequent layers will be affected.

When the viscosity of one layer is multiplied by 10, the velocity increment in this layer is equally lowered, and the velocity profiles of all subsequent layers are shifted downwards.

Fig 7 shows this effect for changes made to the Beulah slag viscosity data.

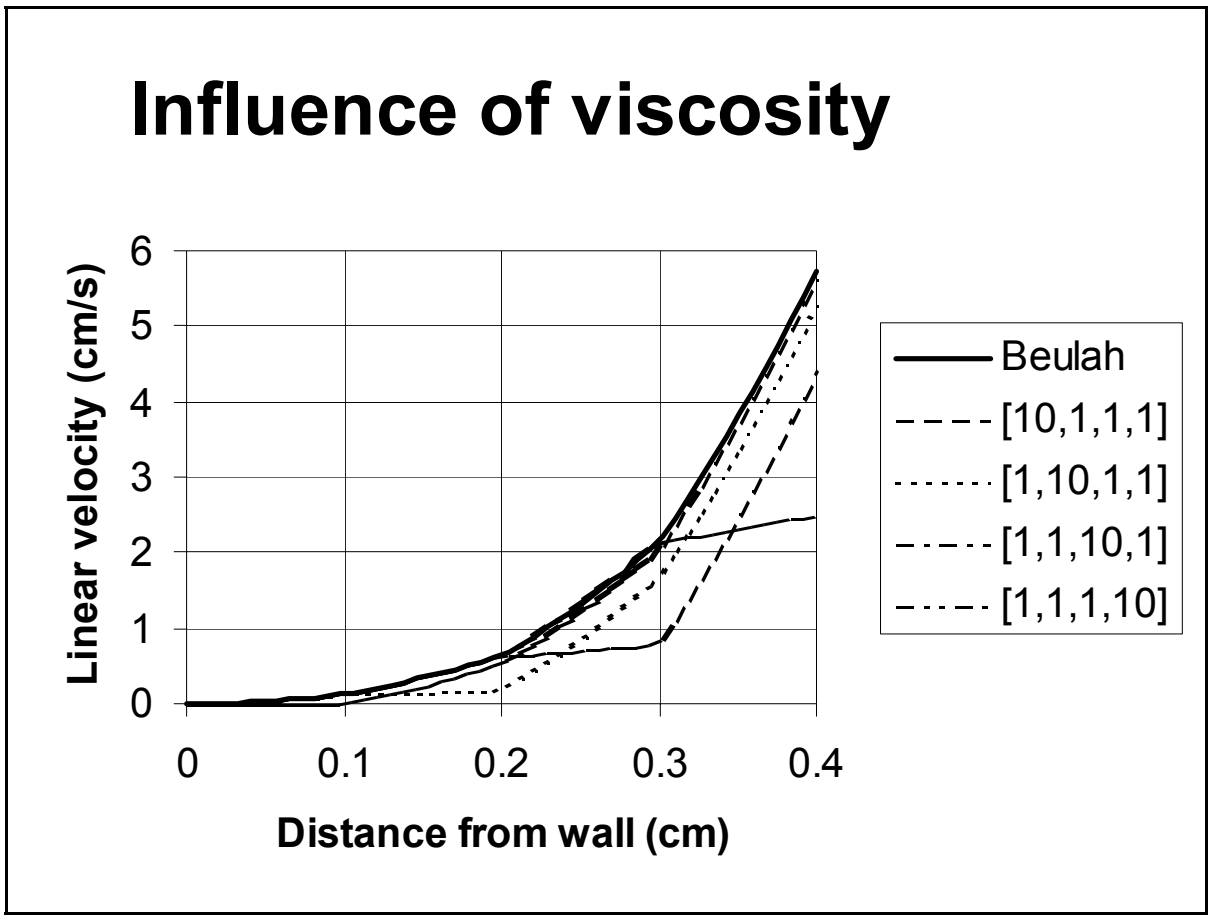

Figure 7 Effect of changed viscosity in one layer (multiplied by 10) on the total velocity distribution. Basis: Beulah slag.

Density

The velocity profile depends linearly on the density of the slag. Thus if all densities are multiplied by 10, so are the velocities.

If the density of the layer i is multiplied by 10, then the velocity profile of the entire film is

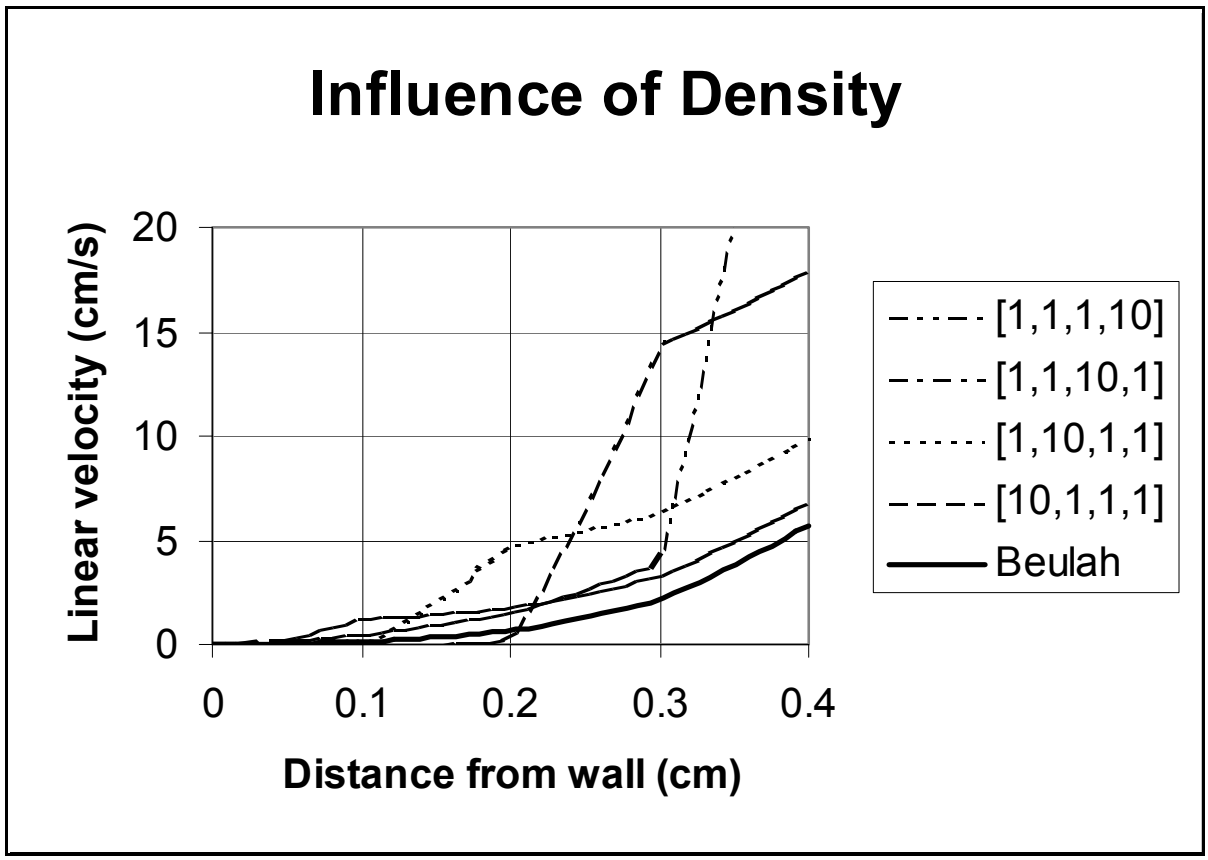

Figure 8 Effect of multiplying density in one layer by 10 on the total velocity distribution of the deposit. Basis: Beulah slag.

affected. Layers 1 through i are affected through the second term on the right-hand side of the equation, and layers i+1 through N are shifted upwards. On close examination, it is possible to see this from Fig 8 that shows layer-wise perturbations performed on the Beulah slag viscosities.

Conclusions

This report contains a theoretical modelling on the flow of ash slags down a vertical wall.

The mathematical model depends on two physical properties of the liquid:

- $v = f(\eta^{-1}, \rho)$.

The effect of viscosity is very simple. The effect of density is slightly more complex.

Program Text (Fortran 77)

```
      PROGRAM FLOW

      PARAMETER (MAXSKAL=5, INT=50)
      IMPLICIT DOUBLE PRECISION (A-H,O-Z)

      DIMENSION XB(MAXSKAL+2), X(INT), V(INT), SUM(MAXSKAL+1),
     1          VKANT(MAXSKAL), GMY(MAXSKAL), RHO(MAXSKAL)

      WRITE(*,50)
   50 FORMAT(/,/,'Number of layers (1 - 5) : ',$)
      READ(*,*) NSKAL

      XB(1) = 0

      DO, I=1,NSKAL
        WRITE(*,51) I
   51   FORMAT(/,/,'Thickness of layer no. ',I1,' (cm): ',$)
        READ(*,*) XB(I+1)
        XB(I+1) = XB(I+1)/100. + XB(I)

        WRITE(*,52) I
   52   FORMAT(/,'Density of layer no. ',I1,' (g/cm^3): ',$)
        READ(*,*) RHO(I)
C Unit conversion of density: g/cm^3 -> kg/m^3.
        RHO(I) = RHO(I) * 1000.

        WRITE(*,53) I
   53   FORMAT(/,'Viscosity of layer no. ',I1,' (Pa*s): ',$)
        READ(*,*) VIS
        GMY(I) = 9.81 / VIS
      ENDDO

C Interpolation points.
      XINT = XB(NSKAL+1) / (INT - 1)
      X(1) = 0
      N = 1
      DO, I=2,INT
        X(I) = XINT + X(I-1)
```

```
      ENDDO

C Edge velocities.
      VKANT(1) = 0
      SUM(NSKAL) = 0
      DO, I=NSKAL-1,1,-1
        SUM(I) = SUM(I+1) + X(I) * ( RHO(I) - RHO(I+1) )
      ENDDO
      DO, I=1,NSKAL-1
        VKANT(I+1) = VKANT(I) + GMY(I) * ( RHO(I) / 2. *
     1       ( XB(I+1)**2 - XB(I)**2 ) - ( XB(I+1) - XB(I) ) * SUM(I) )
      ENDDO

C Internal velocities.
      V(1) = 0
      N = 1
      DO, I=2,INT
 11     CONTINUE
        IF (X(I) .LE. XB(N+1)) GOTO 10
        IF (I .EQ. INT) GOTO 10
        N = N + 1
        GOTO 11
 10     CONTINUE
        V(I) = VKANT(N) + GMY(N) * ( RHO(N) / 2. *
     1        ( X(I)**2 - XB(N)**2 ) - ( X(I) - XB(N) ) * SUM(N) )
      ENDDO

C Unit change.
C Distance from wall: m -> cm, Velocity: m/s -> cm/s
      DO, I=1,INT
        X(I) = X(I) * 100
        V(I) = V(I) * 100
      ENDDO

C Printout to file.
      OPEN (UNIT = 11, FILE = 'FLOW.OUT')
 12   FORMAT(2F15.5)
      DO, I=1,INT
        WRITE(11,12) X(I),V(I)
      ENDDO
```

```
      CLOSE(11)

C Plot.
      CALL AXDRAW(0.D0, X(INT), 0.D0, V(INT), 'Flow', 'Distance (cm)',
     1'Velocity (cm/s)')
      CALL CURVE(INT, X, V, 2, 2)
      CALL PLEND

      END
```